

FORCES ON CYLINDERS
IN
RELATIVE FLUID MOTION

by

Richard Martin / ASHLEY



Thesis submitted in partial
fulfilment of the requirements
for a degree of Master of Philosophy
of the
Council for National Academic Awards

representing work conducted at the National
Maritime Institute and at Thames Polytechnic

July 1980

FORCES ON CYLINDERS IN
RELATIVE FLUID MOTION

by

Richard Martin ASHLEY

ABSTRACT

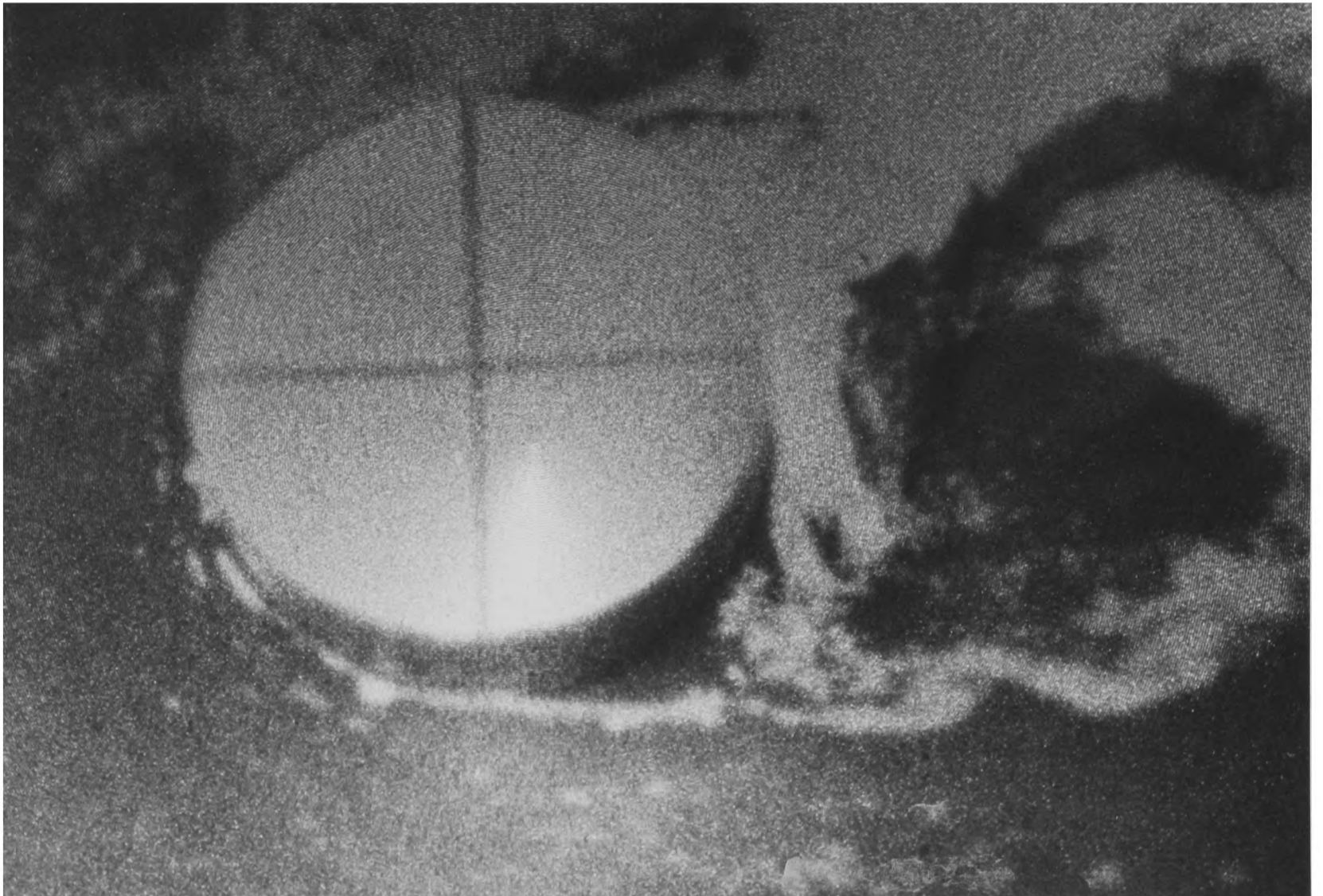
This thesis reviews current knowledge concerning the forces between circular cylinders and relatively flowing fluids. The kinematic conditions considered are those of steady, unidirectional unsteady, oscillatory, and that of monochromatic surface water waves incident upon a vertical surface piercing cylinder. The complicating effects of cylinder surface roughness and freestream turbulence are also considered.

Detailed investigation of an oscillating cylinder experiment carried out by the author, at high Stokes number (Reynolds divided by Keulegan Carpenter number), but covering a low range of Keulegan Carpenter number is presented. Following this, a discussion of wave tank and generator design, culminates in the design of such a facility for the testing of cylinders in progressive waves. These experimental examples are used in conjunction with model theory to explain the deficiencies and similarities between the various kinematic conditions above. The experimental utilization of simpler fluid kinematic conditions to model those that are more complex is shown to be possible within certain limitations. Guidance is given to facilitate selection of the most suitable experimental technique for the investigation of specific fluid-cylinder dynamic problems.

An original picture of vortex behaviour throughout a cycle of relative planar oscillatory motion is postulated based upon recorded circumferential pressure distribution history, and resultant in-line and lift forces.

The Morison equation, considered as a mathematical model which describes the cylinder-fluid dynamics, is shown to be reasonable for Keulegan Carpenter numbers less than 5 (in the inertia dominant regime), or greater than 25 (in the drag dominant regime). The equation is misleading in the intermediate region (5 to 25) where the drag and inertia force components are each of comparable importance. The neglect of the important transverse (with respect to relative flow direction) force component and the effects of flow history, contained in residual vorticity, are also shown to be important deficiencies.

The implications of this work for the understanding of the fluid mechanics of vertical circular cylinders in the sea are also considered.



flow from left to right

VORTEX GROWTH IN STEADY FLOW:
A STILL FROM AN 8mm CINE - SURFACE SPRINKLED
WITH ALUMINIUM DUST, $R_E: 6 \times 10^3$

PREFACE AND ACKNOWLEDGEMENTS

This thesis is the result of work carried out by the author at the National Maritime Institute (NMI) during the latter part of 1977 and of work within the School of Civil Engineering at Thames Polytechnic, during the last five years. My work at NMI was funded by the Department of Energy, to whom, with the Director of NMI, thanks are due for permission to include some of the results herein. Dr Richard Matten was the principal investigator for the NMI work, and special thanks are due to him for his encouragement, assistance, and patience with my difficulties in understanding.

The analysis of the NMI digitized experimental results presented in this thesis is the sole responsibility of the author. This analysis corroborates some of the results of Matten(1979), and enlarges upon the previously published: Matten, Hogben & Ashley(1978).

My supervisor, who has tried to keep me going consistently in one direction, has been Dr W.R.Dickens, to whom a debt of gratitude is expressed. There are many others who have influenced and assisted this work, particularly the staff at NMI, the Technicians of the School of Civil Engineering, and the Central Service Unit at Thames Polytechnic. Patience has been shown by those in the community in which I live, at my recent lack of involvement and neglect of others.

Those principally neglected have been my wife and family: Cate, Charlotte, Ewan, Madeleine, and Elizabeth. To all of these I am greatly indebted.

Special thanks are due to Cate and Mrs Doreen Cooke, who made sufficient sense of my draft to be able to type it so well.

Strood, Kent

July 1980

"Man inhabits two worlds. One is the natural world of plants and animals, of soils and airs and waters which preceded him by billions of years and of which he is a part. The other is the world of social institutions and artefacts he builds for himself, using his tools and engines, his science and his dreams to fashion an environment obedient to human purpose and direction."

Barbara Ward & Rene Dubois
('Only one Earth' 1972)
Andre Deutsch.

"The Lord's is the earth and its fulness"

Psalm 24

CONTENTS

	Page
ABSTRACT	(i)
PREFACE & ACKNOWLEDGEMENTS	(ii)
CONTENTS	(v)
LIST OF SYMBOLS	(viii)
CHAPTER 1 INTRODUCTION	1
(1.1) The basic mechanics of fluid flow relative to solid bodies.	2
(1.2) A smooth circular cylinder in a steady relative flow.	9
(1.2.1) $R_E < 1-5$	10
(1.2.2) $5 < R_E < 40$	11
(1.2.3) $40 < R_E < 150$	12
(1.2.4) $150 < R_E < 2-3 \times 10^5$	15
(1.2.5) $2-3 \times 10^5 < R_E < 3-5 \times 10^6$	17
(1.2.6) $R_E > 3-5 \times 10^6$	18
(1.2.7) Oscillating lift and drag in steady flows.	19
(1.3) A smooth circular cylinder immersed in a relatively unsteadily moving fluid.	25
(1.3.1) An immersed circular cylinder in unidirectional acceleration relative to water.	25
Forces in irrotational flow.	26
The response of viscosity to unsteady flow.	29
(1.3.2) A circular cylinder immersed in relatively oscillating water.	36
(1.3.3) The complications in wave flows.	50
(1.4) Summary	55
CHAPTER 2 MODELLING OF CIRCULAR CYLINDERS IN WAVES	56
(2.1) Introduction.	56
(2.2) Physical models.	57
(2.2.1) Dimensional similarity.	57
(2.2.2) Dynamic similarity and dimensional analysis.	58
(2.2.3) Similitude and model scale.	61
(2.3) Models involving relative motion between a fluid and a structure.	64
(2.3.1) Models where water surface waves are significant.	64
Water waves.	64
(2.3.2) Dimensional analysis.	66
(2.4) Modelling of a smooth vertical circular cylinder immersed in water waves.	69
(2.4.1) Large scale prototype testing in the sea.	75

	Page
CHAPTER 3	
MODELS WITH SIMPLIFIED KINEMATIC FLOW CONDITIONS	78
(3.1) Are waves necessary?	78
(3.2) Planar oscillatory flow models	82
(3.3) Cylinders beneath the node of a standing wave.	85
(3.4) Cylinders in a planar oscillating fluid.	87
(3.5) Cylinders oscillating in a still fluid.	95
(3.6) Unidirectional kinematic models.	102
(3.6.1) Unidirectional or oscillatory?	102
(3.6.2) Relative unidirectional acceleration.	107
(3.6.3) Steady flows.	113
Three dimensional effects.	115
Blockage	118
Freestream turbulence and cylinder roughness.	119
CHAPTER 4	
A TYPICAL APPLICATION OF HYDRAULIC MODEL THEORY	124
(4.1) Introduction.	124
(4.2) A vertical cylinder in planar oscillatory motion.	125
(4.2.1) Background.	125
(4.2.2) PFM Experimental details.	126
End plate design.	126
Kinematic conditions.	128
Instrumentation and data. handling.	129
Experimentation.	130
(4.2.3) Analysis and presentation of results.	130
Fourier Analysis $N_k=17.65$, $T_{pc}=4.334s$.	132
Pressure history.	133
Force history.	134
Pressure distribution.	137
(4.2.4) Discussion and interpretation of results.	137
Wake behaviour.	137
(4.2.5) Further conclusions from the PFM experiment.	147
The effect of end plates.	148
Variation of Stokes and Keulegan Carpenter numbers.	149
(4.2.6) Summary of the PFM experimental findings.	152
(4.3) An introduction to, and an example of, the design of an experimental water wave facility.	154
(4.3.1) Design of a typical wave testing facility.	155
Wave modelling.	156
Wave generators.	158
Selection and design of a wave generator.	159
Wedge angle ψ .	162
Tank design.	165
Possible test ranges.	166
(4.3.2) Summary of wave tank facility design.	166
(4.4) Chapter Summary.	168

	Page
CHAPTER 5 THE RELATIVE SUCCESS OF MODELLING IN UNDERSTANDING FLUID MECHANICS	169
(5.1) The philosophy of this Thesis.	169
(5.2) The representation by simple kinematic conditions of those that are more complex.	171
(5.2.1) Wave-planar oscillatory similarities.	172
(5.2.2) Oscillatory-unidirectional similarities.	175
(5.2.3) Rectilinear steady and unsteady flow similarities.	177
(5.2.4) Summary of relative kinematic similarities.	177
(5.3) Experimental difficulties and analogies.	179
(5.3.1) Three dimensional effects.	179
(5.3.2) Blockage.	180
(5.3.3) The effects of freestream turbulence levels.	181
(5.3.4) Surface roughness, trip wires and splitter plates.	181
(5.4) Wave force model-prototype similarities.	184
(5.5) The Morison equation as a mathematical model.	185
(5.6) Extension into the real sea.	187
CHAPTER 6 CONCLUSIONS AND RECOMMENDATIONS FOR FUTURE WORK	188
(6.1) Summary of conclusions.	188
(6.2) Recommendations for future work.	191
REFERENCES	195
APPENDIX A STEADY AND POTENTIAL FLOW RESULTS.	A1
APPENDIX B WATER WAVE THEORIES.	B1
APPENDIX C FOURIER ANALYSIS.	C1
APPENDIX D INTRODUCTION TO SPECTRAL ANALYSIS.	D1

LIST OF SYMBOLS

SUFFIXES	max	Maximum value
	min	Minimum value
	rms	Root mean square
	spp	Semi peak to peak
	$E[f]$	Mean or 'expected' value of function
1. <u>FLUID</u>	Properties:	
	μ	dynamic viscosity
	ρ	density
	ν	kinematic viscosity
	t_e	temperature
(1.1) STEADY FLOW		
	U_o	velocity
	z_o	depth (if free surface) to still water level (SWL)
	P_o	pressure
	$u_o(\theta)$	particle velocity at angle θ at edge of boundary layer
(1.2) UNSTEADY FLOW		
	t	time
	δt	an time increment
(1.2.1) ACCELERATIVE FLOW		
	a_a	freestream acceleration
	U_a	" velocity
	x_a	particle displacement
	P_a	pressure
	z_a	depth (if free surface) to still water level (SWL)

(1.2.2) PLANAR OSCILLATORY FLOW

x_p	particle displacement relative to mean position
u_p	(absolute) freestream particle velocity
a_p	(absolute) freestream particle acceleration
T_p	period of time taken by a particle to move between successive maximum displacement positions
f_p	particle frequency corresponding to period above $1/T_p$ (Hz)
ω_p	$2\pi f_p$ (rad/s)
p_p	pressure component of particle energy, corresponding to depth (if free surface) to still water level (SWL)
A_p	maximum particle excursion from mean position = x_{pmax}

(1.2.3) WAVES

A_w	wave amplitude relative to mean water level (MWL):- peak, suffix 1, trough, suffix 2
H_w	wave height: crest to preceding trough
Z_1	water depth to MWL
Z_2	water depth to SWL
L_w	wavelength measured between successive zero upcrossings of SWL
C_w	wave celerity
η_w	instantaneous vertical displacement of particles on surface relative to MWL

X	instantaneous wave displacement from origin of record
T_w	wave period between successive zero upcrossings of SWL
f_w	wave frequency corresponding to period above $1/T_w$ (Hz)
ω_w	$2\pi f_w$ (rad/s)
x_w	horizontal component of orbital particle displacement
z_w	vertical component of orbital particle displacement
k	wave number $2\pi/L_w$
u_w	(absolute) horizontal particle velocity
a_w	(absolute) horizontal particle acceleration

2. CYLINDER

d	diameter
R	radius
L	length (may differ from immersed)
D	diameter of end plates
e	thickness of end plates
m	mass per unit length
A	cross sectional area

(2.1) STEADY MOTION (TOWED CYLINDER)

U_t	towing velocity
u_t	particle velocity adjacent to cylinder
z_t	depth (if free surface) to SWL

(2.2) UNSTEADY MOTION

t time

(2.2.1) CYLINDER ACCELERATING UNIDIRECTIONALLY

x_c cylinder displacement from origin
(in X direction)

u_c instantaneous cylinder velocity

a_c cylinder acceleration

z_c depth (if free surface) to SWL

(2.2.2) CYLINDER IN PLANAR OSCILLATORY MOTION

x_{pc} displacement relative to mean position

u_{pc} instantaneous cylinder velocity

a_{pc} " " acceleration

T_{pc} period of time taken by cylinder to
move between successive maximum
positive displacement positions

f_{pc} cylinder oscillation frequency
corresponding to period above $1/T_{pc}(H_z)$

ω_{pc} $2\pi f_{pc}$ (rad/s)

z_{pc} depth (if free surface) to SWL

A_{pc} maximum excursion from mean position = x_{pcmax}

α phase angle

3. CYLINDER - FLUID RELATIVE MOTION

L_z length of cylinder immersed in fluid

V immersed cylinder volume

m_a added mass of fluid associated with
cylinder per unit cylinder length

m_e effective mass of cylinder per unit length

f_n natural frequency of vibration of immersed
cylinder

f_s	frequency of vortex shedding from cylinder
y	characteristic depth of cylinder immersion
z_i	immersed depth from SWL to centre of cylinder

4. DERIVED PARAMETERS

$R_E = \frac{U_{max} d}{\nu}$	Reynolds number
$N_K = \frac{U_{max} T}{d}$	Keulegan Carpenter number
$I_m = \frac{d}{U} \frac{d}{U^2}$	Iversen modulus
$F_r = (g L)^{1/2}$	Froude number
$\beta = \frac{R_E}{N_K}$	Stokes number
$S = f_s d / U$	Strouhal number (steady flow)
$S_t = f_s d / U_{max}$	Strouhal number (oscill. flow)
$R_\delta = \frac{U_{max} \delta}{\nu}$	Roughness Reynolds number
$R_x = \frac{U x}{\nu}$	Boundary layer Reynolds number
$U = \left(\frac{H_w}{L_w} \right) \left(\frac{L_w}{d} \right)^3$	Ursell parameter
$V_r = \frac{U}{f_n d}$	Reduced velocity

5. GENERAL

q	any quantity	
M	mass	} fundamental dimensions
L	length	
t	time	
E	force	
L_r, M_r, t_r	length, mass, time	} scale ratios
V_r	velocity	
E_r	force	
μ_r	dynamic viscosity	
ρ_r	density	
g_r	acceleration due to gravity	

$\phi(\)$	a function of ()
$f(t)$	a function of time
n	an integer
C_n	Fourier coefficient corresponding to the nth harmonic
α_n	phase angle of the nth harmonic
ω	angular frequency (Hz)
$\delta\omega$	increment of angular frequency
T	period $2\pi/\omega$
j	rotation by 90°
k_r	mean roughness height
W	width of water tunnel or channel test section
δ	diameter of roughness particle
p	scalar pressure in fluid
$P\{ \}$	probability distribution of function
\underline{V}	3 dimensional fluid velocity vector
$\underline{i}, \underline{j}, \underline{k}$	unit vectors in X, Y, Z coordinate system
ϕ	potential function
grad or $\underline{\nabla}$	$\underline{i} \frac{\partial}{\partial x} + \underline{j} \frac{\partial}{\partial y} + \underline{k} \frac{\partial}{\partial z}$
div ($\underline{\phi}$)	$\frac{\partial \phi_1}{\partial x} + \frac{\partial \phi_2}{\partial y} + \frac{\partial \phi_3}{\partial z}$
curl ($\underline{\phi}$)	$\underline{\nabla} \times \underline{\phi} = \begin{vmatrix} \underline{i} & \underline{j} & \underline{k} \\ \frac{\partial}{\partial x} & \frac{\partial}{\partial y} & \frac{\partial}{\partial z} \\ \phi_1 & \phi_2 & \phi_3 \end{vmatrix}$
$\frac{D\underline{V}}{Dt}$	$\frac{\partial u}{\partial t} + u \frac{\partial u}{\partial x} + v \frac{\partial u}{\partial y} + w \frac{\partial u}{\partial z}$ in X direction

ω	vorticity
δ_x	boundary layer thickness
x_δ	distance from sharp edge before boundary layer becomes turbulent
h	lateral vortex spacing in a Karman vortex street
v_v	streamwise vortex velocity in a Karman vortex street
s	any distance, <u>or</u> wave generator amplitude of motion
s_s	distance fluid moves relative to cylinder before boundary layer separation occurs
$R()$	correlation coefficient of function ()
E	kinetic energy
Γ	vortex circulation strength
p, q	coordinates defining the position of a vortex
N_v	number of vortices shed in a semi cycle of oscillatory motion
$\Delta R, A_3, A_5, B'_3, B'_5$	Keulegan & Carpenter remainder force constituents
ϵ	Poisson's ratio
E_y	Young's modulus (of Elasticity)
Δ	deflection
q	uniformly distributed load
f_D	sampling frequency
f_N	Nyquist, or folding, frequency

(5.1) WEDGE WAVE GENERATOR

R	wedge wave generator function
W	immersion/water depth ratio

E_1	$\rho g z_2$
ψ	wedge angle
G_1, G_2, G_3, G_4	coefficients
M_1	wedge mass per unit width
E_{RR}	force in phase with velocity
E_{II}	force in phase with acceleration
E_B	buoyancy force

(5.2) FORCES AND COEFFICIENTS

E_{IM}	added mass inertia force per unit length
E_K	Froude Krylov force per unit length
E_I	total inertia force per unit length
E_d	drag force per unit length
E_L	lift, or transverse, force per unit length
E	total in-line (with relative flow direction) force per unit length
E_R	resultant dimensionless force
A_x	potential force component
B_x	separated (vortex independent) force component
C_x	discrete vortex component of force
C_d	steady flow drag coefficient
C_m	potential flow inertia coefficient
$C_D(t)$	unsteady drag coefficient
$C_D'(t)$	time dependent component of (steady) drag coefficient
C_M	real fluid inertia coefficient
$C_L(t)$	unsteady lift coefficient

$C_1(t)$	total in-line force coefficient non-dimensionalized by acceleration
$C(t)$	total in-line force coefficient non-dimensionalized by velocity ²
C_F	$C(t) \times N_k^2$
C_f	maximum in-line force coefficient
C_p	pressure coefficient
C_{pb}	cylinder base pressure coefficient
C_{pk}	Froude Krylov component of pressure coefficient

CHAPTER 1

INTRODUCTION

Fluid movements relative to natural, or man-made structures occur universally. The effect of fluid movement upon a structure depends upon the nature of the fluid and its characteristic motion. A fluid is a substance that cannot sustain shear stresses without significant deformation. Fluids may be compressible or incompressible, viscous or almost inviscid depending upon their deformation behaviour. Generally gases compress significantly under pressure compared to liquids which may be considered virtually incompressible. In this thesis discussion will be concerned with incompressible fluids only, and moreover fluids which may be considered everywhere continuous and homogeneous. The viscosity of a fluid is a measure of its resistance to deformation under the action of a shearing stress, liquids generally exhibiting a higher resistance than gases. There is no fluid that does not have some resistance to shear deformation, but some fluids have very low resistance, and it may be assumed that their viscous resistance is irrelevant, under certain conditions. These are termed inviscid or ideal fluids.

When a fluid comes into contact with a solid at a boundary interface, stresses within the fluid act upon the solid boundary. These stresses are produced by the body and surface forces, envisaged to act upon a fluid particle. Typical of body forces is hydrostatic thrust, due to gravitational attraction on the fluid particle. Surface forces exist at the boundaries of the fluid element and may be normal to the surface (pressure), or parallel to it (shear). In general, fluid motions are caused by normal forces giving rise to a pressure gradient, although a transfer of molecular momentum from one fluid particle to another may be achieved by tangential or viscous shear stresses.

Close to a solid boundary the fluid is retarded by the contact and there is a thin layer of fluid that does not move, but remains stationary relative to the boundary. The relative motion of the fluid remote from the solid surface gradually diminishes as the surface is approached.

This region of kinematic gradient is the 'boundary layer' adjacent to the solid. In this region viscous forces are important, and dominate the transfer of momentum from one fluid particle to another. Outside this retarded layer, if the fluid inertia is sufficiently high compared to the fluid viscosity, viscous forces may be negligible, and motion promoted only by pressure gradients and momentum.

An understanding of the effects of a fluid moving relative to an immersed solid body is therefore based upon a study of the way in which the fluid moves around the body, particularly the behaviour of the boundary layer of limited depth at the interface between the solid and the fluid.

The practical applications of such a study are innumerable. This thesis is concerned only with a fluid, usually water, moving perpendicularly to the longitudinal axis of a circular cylinder. The relative kinematics being either invariant, or variable with time and or position, namely unsteady, steady, uniform, or non-uniform flows, or some combination thereof. Microscopic or molecular fluid behavioural properties and characteristics will not be considered explicitly, although the fundamental influence of viscosity will not be ignored.

(1.1) The basic mechanics of fluid flow relative to solid bodies

The forces created between a relatively moving fluid and an immersed solid body are reasonably well understood for simple kinematic conditions such as steady flows. Many publications endeavour to present explanations and theories pertaining to such cases either for ideal inviscid fluids (the hydrodynamical approach), or for real, viscous fluids in which viscosity exists. Discussion in this Chapter is developed from the presentations of Lamb (1932), Goldstein (1938), Schlichting (1960), Prandtl ^{& Tietjens} (1957), Birkhoff (1960), Rosenhead (1963), Batchelor (1970), Chang (1970), Mehaute (1976), and more recently the excellent review by Lighthill (1979). Experimental results not covered in these references, particularly those concerned with flow visualization will be referred to where appropriate.

Even when stationary a fluid will exert a normal stress, in the form of a scalar pressure, upon its boundaries caused by the hydrostatic pressure distribution due to gravity. This pressure field is everywhere in equilibrium between fluid particles, and is only out of balance at the fluid boundaries, so that the adjacent

boundary provides the reaction to contain the fluid. Consequently a body immersed in a still fluid experiences a hydrostatic pressure upon any point on its surface given by: $p = -\rho g z$ where z is the depth of fluid above that point. Tangential stresses do not exist in static fluids, even if the fluid is viscous.

A fluid in motion possesses inertia which tends to keep the motion steady. In the uniform steady motion of real fluids the fluid inertia resists the retardation caused by viscous resistance. the relative inertia force to viscous force ratio is therefore important in real fluids:

$$\frac{\rho U^2}{L} \div \frac{\mu U}{L^2} = \frac{\rho L U}{\mu} \equiv \frac{L U}{\nu} = R_E \quad \dots \quad (1.1)$$

This is the Reynolds number R_E , and if it is small, viscosity is a dominant parameter in the fluid dynamics. It may be small due to either low velocities or high viscosity, so low viscosity fluids, like air and water, may be viscous in their behaviour at low flow velocities, and virtually independent of viscosity at higher velocities. At low R_E shear stresses are resisted by a microscopic or molecular transfer of heat and momentum; this is laminar flow. At higher R_E the main freestream fluid motion has secondary turbulent and eddying flows superimposed, which are responsible for the transfer of heat and momentum; this is turbulent flow. Due to the difficulties caused by real fluid viscous effects theoretical hydrodynamics evolved based upon the concept of an ideal, inviscid fluid. Fluid dynamic problems could then be solved using the first order non-linear Euler equations. In many cases good agreement has been obtained between the Euler, or potential flow, solution and the observed behaviour of real fluids. Discrepancies between the analysis and reality, are known, the most famous being termed 'paradoxes'. In the context of this thesis the most relevant paradox is that of D'Alembert. This is that according to potential flow theory the force exerted by a steadily moving fluid upon an immersed circular cylinder is zero, which is in contradiction to observation. For incompressible fluids the effects of viscosity have now been incorporated by the non-linear second order Navier-Stokes equations, and it is widely believed that in the solution of these equations lies the answer to any Newtonian fluid dy-

dynamic problem. There are still limitations to obtaining rigorous, or deterministic, solutions using the Navier-Stokes equations, however, particularly where significant freestream turbulence exists. Integration of the complete Navier-Stokes equations is dependent upon the boundary conditions defining a fluid dynamic situation, and exact integrations are rare. Usually approximate, and more recently, numerical solutions are obtained.

The concept of a thin fluid boundary layer adjacent to fluid boundaries, developed by Prandtl and since accepted as a real fluid phenomenon, has enabled analysis to assume that the effects of viscosity are contained within this boundary layer, outside which the fluid behaves as an inviscid, or ideal fluid. The thickness and nature of this boundary layer is principally an inverse function of Re . The equation of Euler may be used successfully in the region outside the boundary layer to determine the fluid dynamic characteristics.

It is not intended here to present a rigorous exposition of hydrodynamic theory, so the Euler and Navier-Stokes equations are simply stated. They are forms of the momentum equation for a fluid particle that may translate, rotate or deform. It is worth noting that in fluid motions the distinction between the energy and momentum methods of analysis that derive from Newton's Inertial Laws is important. In energy methods the internal work done by self equilibrating forces within the body of fluid, which contributes nothing to the gross fluid motion, should be included. Whereas the momentum approach gives larger scale, or fluid body movement solutions, with no reference to the internal individual particle motions.

With reference to Figure (1.1) and the list of symbols (page viii):

(i) Euler equation in 3 dimensions:

$$\underline{F} - \underline{\nabla} p = \rho \frac{D\underline{V}}{Dt} \quad \dots (1.2)$$

(Applied forces = Inertia forces)

\underline{F} is the body force, normally $= \underline{F}_z = -\text{grad}(\rho gz)$

& $\underline{F}_x = 0 = \underline{F}_y$

and $\frac{D\underline{V}}{Dt}$ is the substantive acceleration, composed of local and convective terms.

(ii) Navier-Stokes equation in 3 dimensions:

$$\underline{F} - \underline{\nabla}p + \mu \underline{\nabla}^2 \underline{V} = \rho \frac{D\underline{V}}{Dt} \quad \dots (1.3)$$

(Applied forces = Inertia forces)

$$\text{or } \underline{F} - \underline{\nabla}p + \mu \underline{\nabla}^2 \underline{V} = \rho \left[\frac{\partial \underline{V}}{\partial t} + \underline{\nabla} \left(\frac{\underline{V}^2}{2} \right) + (\text{curl } \underline{V}) \times \underline{V} \right] \quad \dots (1.3a)$$

The term $(\text{curl } \underline{V}) \times \underline{V}$ is the rotational inertia of the fluid element, and this introduces a further simplifying assumption in fluid dynamic analysis: Where fluid velocity gradients are small rotational effects may be ignored and the fluid flow is said to be irrotational. Rotation is often caused by viscous forces, and ideal fluids can frequently be considered irrotational. Generally within the boundary layer of a real fluid the flow is rotational, being considered irrotational outside provided the streamlines are not greatly divergent. For irrotational flows a potential function ϕ may be defined such that

$$\underline{V} = \text{grad } \phi \quad \dots (1.4)$$

The importance of rotational motions is that they are responsible for the vorticity which is seen in real fluids.

$$\text{Vorticity } \underline{\omega} \text{ is defined by } \underline{\omega} = \text{curl } \underline{V} \quad \dots (1.5)$$

and may vary in a real fluid, principally due to the effects of viscosity which is responsible for vorticity diffusion, but also due to the pure strain deformation of the fluid elements. In ideal fluids having vorticity, this vorticity can only be changed by the pure strain deformation of the element.

Vorticity is created at a solid boundary because it is a 'distributed source of vorticity' (Rosenhead). The rate of creation of new boundary vorticity per unit area is approximately equal to the pressure gradient along the boundary per unit fluid mass. This is true for curved as well as flat boundary surfaces. This solid boundary produced vorticity diffuses and convects into the surrounding body of fluid. It is the vorticity convection of the fluid flowing away from the surface that keeps the boundary layer region, in which the vorticity growth is confined, relatively thin at higher R_E .

The convected vorticity creates the downstream 'wake' when an immersed body moves relative to a fluid. This wake is the vorticity that is remote from the body, although the 'near wake' may still be considered effectively attached to the body. In addition to the convection effects the vorticity region may form discrete vortex elements by curling up, and the diffusion will cause the region of vorticity to increase; so broadening the wake.

These effects are usually accompanied by a flow discontinuity if an adverse pressure gradient exists, i.e. if the flow is promoted by viscous transmission of momentum from the freestream velocity and resisted by the solid boundary friction and an increasing pressure gradient. This discontinuity is 'separation' of the boundary layer from the solid boundary, caused by a reversing flow in the boundary layer as shown in Figure (1.2). It occurs when the fluid momentum is insufficient to overcome the adverse pressure gradient near to the wall. Lighthill (1979) explains the separation in terms of the generation of vorticity at the solid boundary: An accelerating, or sympathetic, pressure gradient smoothly increases the boundary layer vorticity, and consequently the shear stress. Figure (1.3). The boundary layer in such a case remains attached to the solid boundary. An adverse pressure gradient, however, creates vorticity of opposite sign, reducing the total shear in the boundary layer. If the vorticity from the accelerating fluid is unable to absorb the vorticity of opposite sign sufficiently then the shear stress distribution changes sign and there is a reversal of flow near the surface impeding the forward motion of the boundary layer, which then has to separate from the surface to get past the reversed flow region. This causes the layer of vorticity to move into the main body of the fluid.

Irrotational, or potential, flow theory is based upon the definition of instantaneous boundary conditions, In potential flows there is no vorticity (by definition) and consequently no convected effects. Any flow memory is contained within the layers of vorticity, either attached to, or shed from the body. Potential flows thus have no memory, or history, effects.

D'Alembert's paradox outlined previously showed that for a potential, steady flow relative to an immersed circular cylinder there was no net force between the fluid and the cylinder. The rotational effects ignored by potential flow theory account for the discrepancy between this result and reality. If a circular cylinder begins to move from rest, in an otherwise still fluid, at the start of the motion the flow tends to potential, because the vorticity has not had a chance to develop, and the non-existent history of the flow therefore makes no contribution to the relative force. The force is then composed only of a potential (irrotational) flow component, which for an accelerative flow is an inertia force. As time increases the 'memory' of the fluid contained in the vorticity and its convection and diffusion also affects the force. The total force can then be considered as the sum of an unchanging irrotational flow and a constantly changing rotational flow. The addition of vorticity rectifies the deficiencies in the assumed boundary conditions of the potential flow solution; the no slip condition, and the disturbances caused to the flow field by separated vorticity. For example the force on an immersed circular cylinder in a steadily flowing fluid is caused by the viscous surface, or skin, friction and the change in pressure of the fluid between the front and rear of the cylinder. Both these effects are vorticity dependent.

The Boundary Layer

The boundary layer on a sharp-edged flat surface with a tangential steady flow is shown in Figure (1.4). If the flat surface is long enough the viscous shear stresses gradually increase the depth of the retarded flow region δ_x in the boundary layer, and the well ordered laminar boundary layer becomes unstable and turbulent after a transition region. The change from laminar to turbulent conditions occurs after the fluid has moved a distance x_δ from the leading edge of the plate, where x_δ may be calculated from the Reynolds number R_x , because it is always in the region $2 \times 10^5 < \frac{U_0 x_\delta}{\nu} < 10^6$, ($R_x = \frac{U_0 x_\delta}{\nu}$), the variation depending upon freestream turbulence. Blasius derived an expression for the thickness of the laminar boundary layer δ_x in terms of x :

$$\delta_x = 5x(R_x)^{-1/2} \quad \dots \quad (1.6)$$

Similarly in a turbulent boundary layer ($R_x > 3.2 \times 10^5$):

$$\delta_x = 0.38x(R_x)^{-1/5} \quad \dots \quad (1.7)$$

Because at the limit of the boundary layer there is not a sudden change to freestream velocity, but rather a gradual one, δ_x is considered as the perpendicular distance from the boundary to the point at which the velocity is within 1% of that in the freestream. Equations (1.6) and (1.7) confirm the frictionless flow case described by $R_x \rightarrow \infty$ for high U_o , where the boundary layer thickness δ_x then tends to zero.

After the transition to a turbulent boundary layer, there is a simultaneous increase in boundary layer thickness and shear stress. This larger shear stress is caused by the turbulence rather than the viscous shear responsible for retardation in a laminar boundary layer. Close to the wall the turbulent particle motions are largely suppressed, resulting in a very thin laminar sub-layer region.

Surface roughness significantly alters the boundary layer effects in turbulent flows. It is the ratio between the roughness size (the mean height) and the laminar sublayer that is important. The flow behaves as a 'smooth' or 'rough' (hydraulically speaking) walled flow, if the laminar sublayer completely covers the roughnesses or they protrude through it, respectively. In the latter case significant turbulence and eddies are generated by the rough surface, and the laminar sublayer is effectively non-existent.

A smooth circular cylinder immersed in a variety of relatively moving fluid kinematic conditions will now be considered in detail. In particular the interaction between the cylinder and fluid, expressed in terms of force, will be discussed.

(1.2) A smooth circular cylinder in a steady relative flow

Steady fluid flows relative to a circular cylinder result in fluid behaviour and effects that are principally a function of the inertia/viscous force ratio: R_E . In this section fluid-cylinder behaviour will be considered in terms of R_E ranges over which the behaviour remains sensibly constant. The discussion presented will relate to either a fluid in steady motion past a stationary cylinder; a steadily moving cylinder immersed in a still fluid; or a slowly accelerating (or decelerating) fluid or cylinder, such that free-stream acceleration effects are too small to affect the fluid behaviour, and at any instant $\underline{u}(t) \approx \underline{u}(t - \delta t)$, where δt is a small increment of time.

All relative motion is perpendicular to the cylinder longitudinal axis (or parallel to a diameter), as shown in Figure (1.5a & b).

Dimensional Analysis of such a situation results in an expression for the drag force on the cylinder in the direction of relative fluid motion (Section 3.6.3):

$$F_d = C_d \frac{1}{2} d \rho U^2 \quad \dots (1.8)$$

Where F_d is the drag force per unit cylinder length.

C_d , the steady flow drag coefficient, is a function of R_E and cylinder-fluid geometry alone if roughness and freestream turbulence are neglected. For boundary layer separation, however, where vortices occur C_d , and hence F_d , are also time dependent as will be shown.

Appendix A gives the steady flow C_d / R_E relationship.

Morkovin (1964) details the process of fluid-cylinder behaviour and consequent interaction:

- (a) Generation of steady and unsteady vorticity at the solid boundary.
- (b) The molecular diffusion of this vorticity.
- (c) Kinematic and dynamic convection of vorticity.
- (d) Vorticity re-distribution downstream.
- (e) Resultant feedback from this process affecting the velocity and pressure fields near the cylinder.

The actual details of this process, and its expression in terms of force interaction will now be detailed for significant Reynolds

number ranges.

(1.2.1) $R_E \leq 1-5$, Figure (1.6a)

In the steady flow of water and air this low R_E range is seldom encountered, or at least sustained for any length of time. For engineering purposes the fluid behaviour would normally be a transient one, and often corrupted by historical effects.

At such a low R_E , particularly for $R_E \ll 1$, the viscous forces predominate over those of inertia. This means that the lateral diffusion of the vorticity created at the cylinder boundary is extensive. This diffusing vorticity extends widely around the cylinder, including upstream. R_E may therefore be regarded as a ratio between the convection and diffusion of the vorticity, because when it is low the diffusion is the principal mechanism for the spread of vorticity from the cylinder into the surrounding fluid, very little vorticity being convected to form a wake.

For a symmetrical upstream-downstream streamline pattern, Stokes (1850 & 1901) theory assuming that inertia effects are negligible, is valid. This really only applies reasonably for $R_E \ll 1$, higher than this ($R_E \rightarrow 5$) Oseen's approximation (Batchelor) incorporates some inertial effects which assume that the streamlines contract further from the cylinder on the downstream side than for the Stokes case.

In this region:

$$C_d \approx \frac{8\pi}{R_E \log(7.4/R_E)} \quad . \quad . \quad . \quad (1.9)$$

Huner & Hussey (1977) review the theories for drag on circular cylinders for $0.23 \leq R_E \leq 2.6$ and present some new experimental results. Interestingly the most significant experimental correction required to their data was that of finite cylinder length, or aspect ratio. This correction is particularly important for low R_E experiments.

Usually low R_E flows are not considered to result in boundary layer separation, however, strictly speaking there is a separation at the rear stagnation point, which in such flows is also the point of minimum normal pressure, (e.g. Chen (1970) cites $C_{pb} = -5.5$ for $R_E = 0.4$). As will be seen from the C_d/R_E graph in Appendix A the value of C_d for this R_E is very high in comparison with the higher R_E range. Skin friction is responsible for virtually the whole of the cylinder-fluid force, because there is no pressure 'defect' between the front and back of the cylinder in the absence of significant convection of vorticity.

(1.2.2) $5 < R_E < 40$, Figure (1.6b)

Laminar flow separation first occurs at an R_E of approximately 5, at the circumferential points where the skin friction is zero. The shear layers come together again further downstream than for (1.2.1) enclosing two weak eddying, or vortex, regions close to the cylinder; so called Föppl vortices. This separation region is termed a 'separation bubble'. The form drag is now substantially increased due to the separation and attendant lower downstream pressure in the base region behind the cylinder. The separation bubble elongates at higher R_E values due to the relative convection of the diffusing vorticity away from the cylinder. The two vortices adjacent to the cylinder first appear at an R_E of approximately 6, and become increasingly elongated and prone to instability as R_E tends to about 40. The greater tendency to instability in higher R_E flows is due to the diminishing effectiveness of viscosity in damping out disturbances, and is therefore prone to turbulence and freestream asymmetry. In this case a slowly varying (sinusoidal) oscillation may begin in the downstream wake behind the separation bubble. The vortices move further away from the cylinder as their vorticity increases, and in theory, if instability did not occur, would continue to move further downstream for higher R_E and convection of vorticity. Batchelor presents results that show a unique dependence of the length of separation bubble compared with cylinder diameter, as a function of R_E . The maximum length of bubble before the separated vorticity layers coalesce downstream, for an R_E of about 40, being $2.4 d$.

The ~~minimum~~ pressure point moves forward on both sides of the cylinder circumference as R_E rises. This means that the base pressure coefficient C_{pb} increases. Chen (ibid) suggests that $C_{pb} = -2.12 R_E^{-1/2}$ for $R_E < 15$. As C_d is directly a function of the pressure defect across the cylinder, this increase in C_{pb} indicates that the drag reduces progressively as R_E rises, however, the reverse flow at the back of the cylinder causes a larger energy drop than if separation did not occur, and the rate of reduction of C_d with R_E reduces due to the greater attendant energy losses.

The C_{pb} / R_E curve shown in Appendix A illustrates the base pressure changes on the cylinder with changing R_E , and because C_d is increasingly composed of form drag for $R_E > 5$, the shape of the C_{pb} graph also indicates salient flow characteristic

changes that affect C_d .

Morkovin (1964) presents numerical results from Kawaguti, Thom, and Apelt that predict the cylinder pressure and vorticity distribution that occurs at an R_E of 40. These results conform to experimental measurements of normal pressure, so the calculated vorticity distribution of Apelt is also shown in Figure (1.6b).

(1.2.3) $40 < R_E < 150$, Figure (1.6c)

The C_{pb}/R_E graph in Appendix A shows a peak at $R_E = 40$ indicating a significant change in the flow field. As R_E increases beyond the critical value at which the laminar wake instability first appears, the wake oscillation gets closer to the cylinder and begins to affect the Föppl vortices. These oscillate transversely to the main flow direction, and start to shed rotating fluid at both extremities of motion. This results in two rows of staggered, out of phase, 'lumps' of vorticity moving downstream from either side of the cylinder, with a speed less than that of the freestream. This is the beginning of a 'laminar vortex street', which is persistent for a great distance downstream from the cylinder, because the mechanism for energy degeneration is totally viscous, and it consequently does not dissipate very rapidly. As R_E further increases, these centres of vorticity in the form of vortices become more individually recognizable. See for example Zdravkovich (1969) for some excellent photographs. At the lower R_E end of this range the two attached vortices are still visible behind the cylinder until about $R_E = 90-100$, when they are no longer present. Berger & Willie (1972) support the proposition by Gerrard that the critical factor concerning the vortex wake and its behaviour is fluid entrainment from the inviscid (outside) region into the rear cylinder region. In the low R_E regime, the vorticity concentrated oscillating wake, streaming from the two attached vortices, does not entrain any of the inviscid fluid. This is the 'Low-speed' mode suggested by Tritton.

At higher R_E the whole flow pattern is asymmetric; a vortex grows behind the adjacent shear layer until its effect is such that it draws the opposite shear layer across behind the cylinder. This vorticity of opposite sign cuts the original supply of vorticity to the vortex, which then can no longer increase in strength. It then detaches from the back of the cylinder, and is moved away downstream.

In this condition the two stable, laminar free shear layers cause a mass defect behind the cylinder by drawing fluid that is close to the cylinder into the wake, which then narrows due to the surrounding inviscid fluid pressure. The curving path of one of the shear layers then curls up into a discrete spiral, entraining the potential fluid into the wake. This behaviour would be expected to happen in one shear layer at a time, and is the 'High-speed' mode of Tritton. With significant time variation of turbulence the Föppl vortices may become re-established with no further inviscid fluid entrainment. This may cause the fluid dynamic conditions to vacillate between the high-speed and the low-speed mode.

Wille (1972) elaborated on the above mechanisms of fluid behaviour, and in particular the feedback from the wake to the drag on the body. He emphasized the effect of the base pressure and the irrotational flow area on producing the alternating vortex wake, which adjusts itself in speed and disposition to produce the minimum drag force on the cylinder for a given R_E .

The asymmetric Karman vortex street produced above an R_E of 40-60 is only clearly defined for $90 < R_E < 150$ approximately, although the alternating vortex pattern does continue in a less 'pure' form to higher R_E . It is observed up to an R_E of 5×10^3 , being stable for a transverse/longitudinal vortex spacing ratio of 0.281 only. By considering the kinetic energy in the growing vortex field; which must be supplied through the relative motion between the fluid and the cylinder, an ideal fluid analysis gives

$$C_d = \frac{2h}{d} \left[2.83 \frac{u_v}{U_0} - 1.12 \left(\frac{u_v}{U_0} \right)^2 \right] \quad \dots (1.10)$$

where h is the transverse vortex street spacing, and u_v is the streamwise velocity of the discrete vortices.

The dimensionless parameter that describes the vortex shedding frequency is the Strouhal number $S = \frac{f_s d}{U_0}$. . . (1.11)

However, this is not an independent dimensionless parameter when used in this context, because it is everywhere a function of R_E , when applied to the spontaneous shedding of vortices from a circular cylinder, as shown in Appendix A. In such a case S is a property of the flow, and not a defining parameter (see Chapter 3). The variation of vortex shedding frequency with R_E is seen to rise rapidly with increasing R_E , up to a maximum S of about 0.21 at an

R_E of approximately 400 when it then levels off.

Mair & Maull (1971) summarize the findings of various experimentalists and theorists, who have noticed that the total circulation, which is the sum of the vorticity shed from one side of a cylinder in each cycle of vortex street production is greater than the intensity of the corresponding vortex. The deficiency is as much as 50%, which is explained by the transfer of circulation between the shear layers across the back of the cylinder. The circulation available to form one vortex is that from the shear layer coming from one side of the cylinder, less approximately 15% which moves across to the other shear layer, less 15% which is destroyed by circulation of opposite sign which moves across from the other shear layer. There is an additional minor loss of circulation which moves into the recirculation region.

It is now apparent that the steady flow conditions that have prevailed up to an R_E of 40, have given way to an unsteadiness which is periodic. This periodicity in the basic flow parameters:

$$p(\theta), \underline{U}_o(\theta), C_p(\theta), C_{pb} = f(t),$$

is within a very narrow frequency range corresponding to that of the shed vortices characterized by S . Consequently the resultant drag force on the cylinder is also unsteady, i.e. C_d now becomes $C_D(t)$. The drag force may be considered to be the sum of a time-invariant mean drag force C_d plus a time dependent component $C_D'(t)$, so that:

$$C_D(t) = C_d + C_D'(t) \quad . . . (1.12)$$

$C_D'(t)$ is periodic at the vortex shedding frequency for this range of R_E . The periodic drag is best considered in terms of the time varying base pressure $C_{pb}(t)$, because this varies markedly throughout a vortex shedding cycle. The C_{pb}/R_E graph given in Appendix A refers only to a time averaged C_{pb} for $R_E > 40$ and should therefore be viewed with caution as an indicator of flow behavioural changes. The front stagnation point pressure, however, remains fairly constant throughout the cycle and has therefore little influence upon the change in C_D , although its position may vary as the circulation velocity around the cylinder circumference oscillates due to the shedding process. The combination of a steady freestream flow and a fluctuating circulation around the cylinder circumference results in a transverse, or lift, force which is perpendicular to the drag force vector and is always unsteady, and for this R_E is periodic at the frequency with which vortices are shed from one side of the cylinder. So that the (unsteady) lift coefficient

$$C_L(t) = \frac{F_L}{\frac{1}{2} \rho d U_0^2} \quad \dots \quad (1.13)$$

The mean value of lift corresponding to the mean drag force would for all symmetrical flow cases, i.e. without a circulation in one sense only, be zero. The fluctuating drag force has twice the frequency of the lift force, and is often obscured by the magnitude of the mean C_d value. This has resulted in less attention being given to this component particularly due to the difficulty of its reliable measurement, and also because it is typically of the order of 10% of the lift force.

Further discussion of the unsteady forces resulting from steady flows past a circular cylinder is postponed until completion of the description of the fluid behavioural characteristics with respect to Reynolds Number. This is because the unsteadiness of fluid force is common above $R_E \approx 60$.

(1.2.4) $150 < R_E < 2-3 \times 10^5$, Figure (1.6d)

This is termed the subcritical range, because above 3×10^5 there is a sudden drop in C_d into the critical R_E range. In the range $150 < R_E < 300-400$ the transition to turbulence in the wake occurs progressively in the shed vortices. Above this the transition occurs in the shear layers before they roll up. As R_E increases the transition point moves further upstream in the shear layers. The intensity of the vortices decrease, with a corresponding increase in C_{pb} and decrease in C_d , until C_d reaches its lowest subcritical value at about $R_E = 2 \times 10^3$, when according to Chen (1970), the transition point has moved so far upstream that it coincides with the point at which the free shear layer breaks down and curls up into a vortex. This means that the vortex is relatively weak because it is now completely turbulent. The wind tunnel results of Bloor (1964) were obtained to investigate the onset of turbulence in the wake behind a circular cylinder, and these confirmed ranges first noticed by Roshko in 1953:

- (1) $R_E < 200$ No turbulence: Stable range.
- (2) $200 < R_E < 400$ Three dimensional wake distortion develops downstream turbulence: Transitional range.
- (3) $R_E \geq 400$ Turbulent vortices: Irregular range.

In region (2) there is a less defined vortex shedding frequency,

the better regularity returning as R_E increases above about 400. The transition to turbulence in the wake moves closer to the cylinder as R_E increases, until about 400, whereupon the length of the laminar region remains fairly constant until $R_E = 1.3 \times 10^3$. Correspondingly the length of the vortex formation region increases to a maximum over the region $400 < R_E < 1.3 \times 10^3$, roughly corresponding to the lowest C_d value at an R_E of approximately 2×10^3 given by Chen. Chen's suggestion that around this point the shear layer breakdown point and the transition point meet in their advances downstream and upstream respectively, fits these findings. As R_E further increases above 2×10^3 the vortex formation region reduces and the shear layer breakdown and transition point both get closer to the cylinder. The turbulent shear layer is more unstable and therefore breaks down sooner. the value of C_d again rises up until an $R_E = 10^4$, when the transition point is very close to the cylinder and the increase in C_d levels off.

Throughout this range as R_E increases the point of separation moves from the rear section of the cylinder to the front, obtaining a minimum angle of approximately 70° from the front stagnation point at an R_E of approximately 10^5 (Appendix A). At the top end of the subcritical range a low frequency modulation of the dominant shedding frequency increases causing the fluctuating force components $C_D(t)$ and $C_L(t)$ to be more random, due to the increasing effects of turbulence on the flow conditions.

Oscillations in the boundary layer around a circular cylinder in a steady flow of air have recently been reported by Dwyer & McCroskey (1973). Using a cylinder with an aspect ratio of 21 they found no lateral variation in fluid behaviour, i.e. conditions were well correlated along the cylinder length, and were assumed to be two dimensional. In the subcritical alternate vortex shedding region, with an $R_E = 1.06 \times 10^5$ the measured oscillation of velocity at the edge of the boundary layer was simple harmonic with a frequency of 28 Hz. This was found to be in phase all around the cylinder circumference in the laminar flow region. In this type of flow the onset of zero wall shear was not a good criterion for definition of the point of separation. A mean flow reversal occurred at an angle of $78^\circ \pm 1^\circ$ from the front of the cylinder, but throughout a cycle of vortex shedding,

separation first occurred around 75° for a brief instant, but the boundary layer then remained attached at this point for the rest of the cycle, only always becoming separated by about 85° . This experiment shows the significant unsteadiness in and around the boundary layer that precedes separation due to the oscillating wake behaviour. Interestingly the effects are seen not just in the boundary layer but also in the adjacent inviscid region.

(1.2.5) $2-3 \times 10^5 < R_E < 3.5 \times 10^6$, Figure (1.6e)

Above an R_E of approximately 2×10^5 the drag coefficient falls dramatically, this is the critical R_E range, which terminates at an R_E of $4-6 \times 10^5$ when C_d again starts to increase in the supercritical region up to an R_E of about $2-3.5 \times 10^6$. The critical and supercritical region are collectively termed the transitional Reynolds Number regime. The actual C_d value for a given R_E being radically affected by the cylinder roughness and freestream turbulence level, see for example: Engineering Sciences Data Unit (1979).

The principal fluid dynamic mechanism altering the value of C_d with R_E is again the transition to turbulence. Up to an R_E of 2×10^5 the boundary layer on the cylinder has been laminar with the wake becoming increasingly turbulence dominated. Above this value of R_E the transition to turbulence in the separated shear layer moves on to the rear of the cylinder. There is still a laminar separation due to the boundary layer momentum being insufficient to overcome the reversed flow on the circumference, but this occurs on the forward semi-circumference of the cylinder; the shear layer springs away from the cylinder, and quickly becomes turbulent, this increases mixing and the exchange of momentum across the shear layer so that it can withstand a greater adverse pressure gradient and hence separation. Under such circumstances the, now turbulent, shear layer re-attaches itself to the cylinder, separating again further back on the cylinder circumference; as far back as 140° for a smooth cylinder in a low turbulent stream. This increased separation angle narrows the separated region behind the cylinder, increasing C_{pb} and reducing C_d . The process of re-attachment of the turbulent boundary layer forms a separation 'bubble', which may only occur on one side of the cylinder at first, causing a flow asymmetry and a lift force, as well as a wider frequency band of vortex shedding; Bearman (1968).

For the supercritical region the transition to turbulence occurs further forward in the shear layer, moving the rear separation point forward on the cylinder circumference, which shrinks the separation bubble and increases the wake width, and with it C_d . At about $R_E = 3 \times 10^6$ the bubble disappears and transition occurs at the forward separation point. Throughout the transition region there is a significant reduction in the correlation of fluid behaviour with cylinder circumference and length due to the increasing complexity of the flow, this results in an increasing randomness in unsteady base pressure, $C_d(t)$, vortex shedding frequency and consequently $C_L(t)$. In this region, therefore, many experimental results fail to agree, particularly where there are significant differences in freestream turbulence levels to complicate the picture even further. Mair & Maull (1971) point out that a change in freestream turbulence level should not be considered as merely equivalent to a change in R_E , because a turbulence change may for example increase drag, but not the lift force. Surry, reported by Mair & Maull, found the correlation of C_d with turbulence for the range $3.4 \times 10^4 < R_E < 4.4 \times 10^4$ to be well described with reference to the Taylor parameter:

$$\frac{v_{rms} d}{U_0 L_x} \left(\frac{d}{L_x} \right)^{1/2} \quad \text{Where } v_{rms} \text{ is the rms longitudinal component of fluctuating velocity, and } L_x \text{ is the lateral integral 'scale of freestream turbulence.}$$

Despite the possible limitations when applied to bluff bodies in the transitional R_E region, the Engineering Sciences Data Unit (ibid) recommend the use of this parameter for practical design purposes in this region.

(1.2.6) $R_E > 3-5 \times 10^6$, Figure (1.6f)

This is termed the **post** critical region, particularly investigated by Rosko (1961). The transition to turbulence now occurs in the boundary layer on the front face of the cylinder, although separation does not necessarily take place until the rear, as the turbulent boundary layer is better able to withstand the adverse pressure gradient. The fluid flow characteristics are again better correlated approaching two dimensional conditions with more regular vortex shedding. The rolling up of the turbulent vortices spreads the vorticity rapidly into the wake, so that at any one time only two vortices will be evident. The position of the separation point is less affected by further changes in R_E , and responds slowly to any in-

crease, widening the wake, until a maximum C_D is achieved at about $R_E = 10^7$. Further increases in R_E reduce the small skin friction component by reducing the boundary layer thickness. Flow is now fully turbulent, and theoretically virtually inviscid. Roughness effects are significant in this region, increasing the value of C_D for a given R_E .

(1.2.7) Oscillating Lift and Drag in steady flows

Earlier in this Chapter it was illustrated that the flow around a cylinder moving relatively to a fluid could be considered in terms of a potential, or irrotational, flow which satisfied boundary conditions, and a viscous flow. In the preceding Sections (1.2) the complexity of fluid-cylinder behaviour in relative steady flow has been shown for the whole practical range of Reynolds numbers. It is apparent that viscous effects are of principal importance in producing a relative fluid-cylinder force, because potential flow theory (Appendix A: D'Alembert's paradox) predicts zero net force. At the initial stages of motion, if relative steady motion is instantaneously applied, the flow field conforms to the potential flow model because the vorticity has not had time to develop and influence the flow, i.e. there is no fluid memory. When steady flow is fully developed, with attendant vorticity convection into a wake, the potential flow model (describing the boundary conditions) is unchanged, but the total input of kinetic energy caused by (say) the body in motion through the still fluid, is expended in increasing the kinetic energy in the wake. Therefore the work done ($\int \underline{F} \cdot d\underline{s}$) by the moving body is transmitted into a rate of increase of kinetic energy in the growing wake, less any energy dissipation in heat (which is proportional to the vorticity, $\nabla \times \underline{v}$). Therefore in steady flows the characteristics of the vorticity components, expressed in separation and wake behaviour, are the effects responsible for the relative forces.

For a cylinder in a relatively moving fluid it has been shown that due to vortex shedding, there is no such thing as a 'steady flow' in normal engineering situations. The wind tunnel tests and boundary layer analysis of Dwyer & McCroskey (1973), already mentioned, determined a 'double zero' wall shear stress occurring within the relative time region 0 to $\pi/2$ (relative to the instant at which the velocity at the edge of the boundary layer was the same as in the freestream).

These double zero shear points were separated by as much as 15° of the cylinder circumference. The other particularly significant result was the simple harmonic oscillation of the stagnation point through $\pm 3.7^\circ$ at the same frequency as the boundary layer edge velocity, but with a phase difference of π . This means that the circumferential/ angular variation between the stagnation point and the separation point varies during a vortex shedding semi-cycle from 70° to 90° , the stagnation point moving towards the separation point as a vortex is shed. Simultaneously on the opposite side of the cylinder the separation point has moved further forward on the cylinder, so that one separation point occurs in front, or earlier, than the other. Figure (1.7) illustrates this postulation, which may, or may not, be characteristic of other R_E regimes in view of the reduction in oscillatory behaviour found for the boundary layer re-attachment condition at an R_E of 3.5×10^5 by Dwyer & McCroskey.

Earlier results of Gerrard (1965) and Son & Hanratty (1969) had shown that the velocity fluctuations in and close to the boundary layer around a circular cylinder in a uniform airflow were sinusoidally periodic in tune with the vortex shedding, at least up to the separation point. Irregular fluctuations with a larger amplitude, were superimposed at, and beyond, the separation point. This fluctuation of boundary layer circulation around the cylinder is equivalent to the potential, inviscid flow model of a cylinder subject to combined steady flow and constant circulation. This 'Magnus effect' is a function of the circulation, but is independent of the cylinder size or shape (i.e. of R_E , because the flow is potential). The circulation is related to the lift force by reducing the pressure on the side of the cylinder where the circulation and freestream velocity are in sympathy. A simple model may therefore suggest that as an attached vortex develops the increased circulation on that side causes a lift in that direction: Figure (1.8). However the position of separation and width of wake region (both functions of R_E) conspire to complicate such a simple model. This point will be taken up again in Chapters 4 & 5. Circulation around the front of the cylinder cannot explain the fluctuating drag force which has a second harmonic periodicity compared to the transverse force. This may be responsible for some of this component, but the principal mechanism must be the base pressure fluctuation when a vortex grows and is separated from the attached region.

Significant investigation of the fluctuating lift and drag forces due to vortex shedding did not begin until the early 1960's and

relevant findings up until then are summarized by Bishop & Hassan (1964). Early experimental work involved indirect measurements of usually the lift force, or the unsteady forces resulting from elastic cylinder response, which are different to the fixed cylinder in a steady fluid flow case. Bishop & Hassan tested a horizontal circular cylinder having an aspect ratio of 8 in a flow of water and measured reaction forces on the central one third section. Their results for the range $3.6 \times 10^3 \leq R_E \leq 1.1 \times 10^4$ showed that both of the fluctuating force components had a variable amplitude, but corresponded to the first harmonic and the second harmonic of the vortex shedding frequency for the lift and drag coefficients respectively. Gerrard (1961) had earlier determined a large variation in C_L over the range $4 \times 10^3 \leq R_E \leq 1.1 \times 10^5$ from tests in a wind tunnel, which was not supported by Bishop & Hassan, who noticed a trend in C_L and $C_D'(t)$ with R_E similar to the type of relationship of C_d (and $1/S$) with R_E . This supported earlier results of Humphreys (1960). The fluctuating drag component was determined by Bishop & Hassan as between $1/12$ and $1/9$ of the lift force: $C_D'(t) = 0.05 - 0.075$ for $R_E = 6 \times 10^3 - 1.1 \times 10^4$. The simple relationship for total drag coefficient postulated by equation (1.12) was found to be inadequate because the mean steady drag C_d was found to oscillate due to beating of the unsteady drag component $C_D'(t)$, which also had a variable amplitude. Significantly they concluded that all the force components C_d , $C_D'(t)$ and C_L were interdependent. Bishop & Hassan's results are included in Figure (1.9) which is compounded principally from King (1977) who summarizes experimentally determined C_L values up until that time. Included in the very scattered Figure are some unsteady unidirectional impulsive results for fixed cylinders, such as those of Schwabe (1935), who shall be mentioned again in the next Section.

It is noticeable that there seems to be very little correlation between C_{Lrms} and R_E for different researchers. Kacker, Pennington & Hill (1974) indicate the reasons for such wide variations:

- (a) Cylinder rigidity; any elastic response results in significant unsteady force changes.
- (b) Surface finish; probably particularly important for the range $4 \times 10^3 < R_E < 7.5 \times 10^5$, and in the transcritical region.
- (c) End conditions; dummy cylinder sections, end plates, air gaps in test cylinder and at boundaries.
- (d) Turbulence levels; freestream, and length scales, water or air experiments.
- (e) Experimental measurement system; pressure transducer circumferential ring, or single rotatable hole, corresponding to an

effective $L_z/d = 0$, or strain gauge reaction measurement of average distributed force, $L_z/d > 0$.

They particularly investigated the discrepancies in comparison of integrated pressure histories and reaction force measurements for the range $10^4 \leq R_E \leq 2.5 \times 10^5$ using both methods. Figure (1.10) shows the significant variation in C_{Lrms} with R_E and L_z/d from this work. As the aspect ratio increases C_{Lrms} decreases, presumably due to a decrease in longitudinal vortex coherence. Any longitudinal phase difference in shed cells of vorticity would reduce the lift force. Similarly as R_E increases into the transitional region the vortex shedding becomes less well defined, and consequently the lift coefficient reduces and tends toward a lower level of C_L which is independent of the aspect ratio and R_E . Jones (1968) using a very large diameter cylinder in a wind tunnel had identified ranges of lift frequency (corresponding to f_s):

- (i) $1.1 \times 10^6 \leq R_E < 3.5 \times 10^6$: wide band random.
- (ii) $3.5 \times 10^6 < R_E < 6 \times 10^6$: narrow band random.
- (iii) $6 \times 10^6 < R_E \leq 18.7 \times 10^6$: quasi-periodic.

Above $R_E = 8 \times 10^6$ the flow was fully turbulent and the C_L results were better defined. These regions correspond to the previously discussed vortex shedding behaviour, particularly in the transitional R_E range, and support the incoherence of vortex shedding as being responsible for low lift force. The C_{Lrms}/R_E diagram from CIRIA (1978) shows a minimum range of C_L in the transitional R_E region, Figure (1.11). In the transitional R_E range Kacker, Pennington & Hill considered three dimensional effects to be particularly prevalent with non-straight boundary separation lines along the cylinder and different shedding zones that move randomly along the length of the cylinder. These zones, being of the same relative size as the cylinder diameter, resulting in less coherence the larger L_z/d .

In the region $0.75 \times 10^4 \leq R_E \leq 1.2 \times 10^4$ Dronkers & Massie (1978) found an upward 'peeling off' of vortices, reducing the coherence of the lift force, when testing a vertical cylinder in a water flow. The addition of end plates and repeating of experimental runs did not alter this condition. However, for $1.2 \times 10^4 < R_E < 2.25 \times 10^4$ the vortices were shed evenly, but in different strength cells, resulting in an increased lift force with a variable longitudinal strength. The aspect ratio used was 30, and the lift force record was found to be an amplitude modulated sine wave, with a frequency

corresponding to f_s .

Pressure tapping records have been used to particularly investigate the influence of turbulence levels and roughness on C_L .

Comprehensive airflow experiments have been reported by Gerrard (1961), Batham (1973), Bruun & Davies (1975), and less comprehensively by McGregor (1957). Results presented in terms of C_p spectra and correlation coefficients from experiments have shown that:

(1) In the subcritical R_E region C_L fluctuates at the vortex shedding frequency. This is noticed at the 90° and 270° angular positions from the front of the cylinder, by a sharp spectral peak at the fundamental frequency. $C_D'(t)$ fluctuates at the second harmonic as shown by a sharp peak in the 180° spectrum at $2f_s$. At the front of the cylinder (0°) the spectra may have double peaks at both frequencies. In this R_E range the increase in pressure level with R_E at 90° was found to be linear by McGregor, but the second harmonic at 180° increased linearly only up to $R_E = 6 \times 10^4$. The spectra recorded between 90° and 135° were similar, indicating similar flow behaviour, although as McGregor used only one pressure tapping there was no phase information. Gerrard integrated his C_p values after checking circumferential correlation, and finding a reasonably 180° phase difference between the 0° - 180° and 180° - 360° sides of the cylinder. The correlation coefficient results presented for this at $R_E = 1.14 \times 10^5$ and 8.5×10^4 , did however, show differences in correlation coefficients, not being so close to +1 and -1 in the latter case. These were unexplained. Gerrard presents a plot of the changes in pressure intensity at the fundamental frequency component at $\theta = 30^\circ, 60^\circ, 90^\circ, 120^\circ$ and 150° with respect to R_E , all of which fall on one curve peaking at $R_E = 7 \times 10^4$. Similarly the angular distribution of pressure intensity at both the fundamental and second harmonic frequency fall on single curves independently of R_E , and correlate well with McGregor's results.

(2) Batham used an array of 24 circumferential and 4 rows of 23 longitudinal pressure tapping points to investigate the influence of turbulence and surface roughness on C_L in the critical R_E region. He found that $C_{L,rms}$ was reduced for increased turbulence and/or surface roughness compared to the uniform flow, smooth cylinder case. He presented axial and circumferential correlations of pressures: e.g. Figure (1.12), showing the circumferential variations in correlation coefficient for a smooth cylinder in a uniform stream. In the trans-

ditional R_E region Bruun & Davies observed a wider spread of energy around the first harmonic as R_E increased, and a 3rd harmonic component at the rear of the cylinder at the 120° and 150° pressure points.

The lower level of $C_D'(t)$ and its dependence upon wake pressure fluctuations make it more prone to be affected by freestream turbulence levels. Most researchers have concentrated on C_L , but Figure (1.13) compiled from available results, shows how $C_D'(t)$ varies with R_E .

This area of fluctuating forces has been little investigated in terms of fundamental fluid behaviour, but with the advent of more sophisticated experimental equipment, experiments such as that of Dwyer & McCroskey should be able to advance understanding in the near future.

(1.3) A smooth circular cylinder immersed in a relatively unsteadily moving fluid.

In this section the relative motion is considered to be either unidirectional or periodic, uniform, or non-uniform acceleration. Whilst the flow behaviour remains relatively constant with respect to the cylinder, whether the fluid or the cylinder are in motion, the relative forces do not, and it is important to consider the two cases individually, Figure (1.5c) & (1.5d). Virtually without exception the reported experiments involving accelerations have been carried out using water as the fluid medium. This is in contrast to the steady flow experiments where the wind tunnel is used extensively. Turbulence levels in water tend to be lower than in air, particularly if the cylinder is towed through still water.

The fundamental correlating parameter in steady flows has been shown to be the Reynolds number, which is defined in terms of the relative freestream velocity. However, in accelerative conditions this is a variable function of time making R_E difficult to define. A possible definition of R_E is therefore its maximum value, which will be achieved at the end of the accelerative period in unidirectional, or periodically, in reversing flows.

(1.3.1) An immersed circular cylinder in unidirectional acceleration relative to water

Schwabe (1935) moved a cylinder impulsively from rest through a tank of still water at a constant velocity to investigate photographically the changes in pressure distribution with time up to the onset of wake asymmetry. The results supported the original photographs of Prandtl (to be seen in many publications, e.g. Prandtl & Tietjens (1957)) which illustrate the development of fluid conditions from the initial potential into the regions of separation, symmetric vortex development, and finally wake asymmetry. There was a continual rise in drag coefficient C_D throughout the wake development up to a maximum of approximately 2 when the cylinder had moved a distance of $2d$ from its starting point. This high value of C_D was maintained until the onset of the wake asymmetry after a distance of $3d$. The Reynolds number for this experiment of 580 corresponds to a C_d of

approximately 1 in a steady flow. The doubling of C_d in this impulsive 'starting' steady flow is considered to be due to the high rate of energy consumption necessary for the symmetrical vortices to develop and grow in as short a time as possible. This experiment was an early example of the importance of flow history. The steadily moving cylinder has to exert a greater force on the still fluid because the kinetic energy necessary to create the wake, which should exist at that particular Re , with a steady transfer of kinetic energy, has to be developed in a relatively short time. The time taken to establish the steady state wake is dependent upon the rate at which vorticity can be generated at the solid boundary, and diffused and convected into the surrounding fluid. In such conditions the relative fluid-cylinder force is no longer a single function of Re , but also a function of time expressed by the dimensionless cylinder displacement S/d where S is the displacement from rest.

Consequently the acceleration, and its rate of change, are important because it takes a fluid a finite time to respond to unsteady conditions. The theoretical distance that the fluid has to move relative to a cylinder in an impulsively started steady flow is $0.16d$ before separation occurs, irrespective of the final value of Re (see page 103). For a uniformly applied acceleration from rest this distance is increased to $0.26d$, although these relative distances do not correspond proportionally to the distances travelled before wake asymmetry begins. This is because the impulsive flow initially develops as quickly as possible (in theory due to the infinite acceleration), but slows after this period has passed, whereas the constant acceleration develops at a more uniform rate. For example the relative distance travelled before the onset of asymmetry was found to be approximately $4d$ by Sarpkaya (1966) for an impulsive motion (Figure (3.4)), and approximately $3d$ by Sarpkaya & Garrison (1963) for a constant acceleration.

Forces in irrotational flow

Before considering the fluid behaviour and its effect on relative fluid-cylinder force it is instructive to compare the force components in steady and accelerative flows. For the steady flow case it was seen that the force is composed of a potential, irrotational, component which is **zero**, because boundary conditions are un-

changing, and a vorticity dependent component which is responsible for the kinetic energy necessary to create the wake, which may fluctuate. In flows where the velocity changes with time, therefore, the irrotational flow component will also change. Consequently even in an ideal fluid with no vorticity this additional force exists. It is different if the cylinder accelerates through the fluid, or the fluid accelerates past the cylinder, but similar in established steady flows.

In a steady flow the kinetic energy required to establish irrotational conditions is a fixed quantity which depends upon the change in the fluid velocity induced by the presence of the cylinder. For a cylinder moving through an inviscid, still, fluid the kinetic energy is comprised of that required to move the cylinder plus an additional amount necessary to induce the motion of the fluid particles around it. The induced fluid velocity decays with distance from the cylinder to zero at infinity, therefore the two dimensional kinetic energy of this part of the system is given by:

$$\frac{1}{2} \int_R^{\infty} \underline{u}_t^2 dm \quad \dots \quad (1.14)$$

where R is the cylinder radius, $dm = \rho 2\pi r dr$, where r is the radial distance from the centre, and \underline{u}_t the particle velocity at a corresponding radial distance, given by: $\underline{u}_t = R^2 / r^2 \underline{U}_t$ (from potential flow theory)

$$\therefore (1.14) \text{ becomes } \frac{\rho \pi R^2 \underline{U}_t^2}{2} = \frac{1}{2} m_a \underline{U}_t^2 \quad \dots \quad (1.15)$$

This equation shows that even for a steady potential flow there is an additional mass of fluid, equal to the mass of fluid displaced, which effectively moves with the cylinder.

The total kinetic energy E is therefore

$$E = \frac{1}{2} m_e \underline{U}_t^2 \quad \dots \quad (1.16)$$

where m_e is the effective, or virtual, cylinder mass per unit length, composed of the actual mass m plus the added mass m_a . This kinetic energy is a constant in relative steady flows remote from fluid boundaries (for the effect of an adjacent fixed boundary, see Duncan, Thom & Young (1972), page 155), and is the work required to stop the cylinder's steady motion through the still fluid, or conversely to produce the steady motion from rest. This conforms to the theoretical model postulated earlier that all the kinetic energy in an established steady flow is expended on producing the viscous wake. In a steady flow the change in kinetic

energy due to the potential flow conditions only takes place at the starting and stopping of the motion.

The force per unit length \underline{F}_{IM} exerted by the cylinder on the fluid if the cylinder is in non-uniform motion may now be determined from the equality of work and energy:

$$\begin{aligned} \underline{F}_{IM} dx &= \underline{F}_{IM} \underline{u}_c dt = dE = m_a \underline{u}_c d\underline{u}_c / dt dt \\ \therefore \underline{F}_{IM} &= m_a d\underline{u}_c / dt = m_a \dot{\underline{u}}_c \quad \dots (1.17) \end{aligned}$$

(assuming the added mass is a steady quantity).

This is termed the inertia force, and it is the same in magnitude whether the cylinder or the fluid accelerates. i.e. $\underline{F}_{IM} = m_a \dot{\underline{u}}_c$ for a fluid accelerating past a stationary cylinder, however, in this case the fluid exerts the force on the cylinder. The corresponding pressure distribution is given from potential flow theory and the unsteady Bernoulli equation as:

$$p(\theta) = \rho d/2 \underline{u}_c \cos \theta \quad \dots (1.18)$$

When a fluid accelerates past a point there is a local inertia of $\rho \frac{\partial \underline{u}_c}{\partial t}$ per unit volume, which is overcome by an equal and opposite pressure gradient. Therefore for a cylinder immersed in an unsteady fluid flow there is an additional force per unit length exerted by the fluid on the cylinder of:

$$\underline{F}_K = \rho A \dot{\underline{u}}_c \quad \dots (1.19)$$

This is the Froude-Krylov force, which is the inertia force that would exist even if the cylinder were not present.

In summary, the (irrotational) inertia force per unit length for both cases of relative unsteady motion is either:

(1) The force exerted by an unsteadily moving cylinder upon a still fluid

$$\underline{F}_I = \underline{F}_{IM} = \rho A \dot{\underline{u}}_c \quad \dots (1.20)$$

or (2) The force exerted by an unsteadily moving fluid past a fixed cylinder

$$\begin{aligned} \underline{F}_I &= \underline{F}_{IM} + \underline{F}_K \\ \therefore \underline{F}_I &= 2\rho A \dot{\underline{u}}_c \quad \dots (1.21) \end{aligned}$$

These forces would be those measured by integrating the normal pressures on the cylinder circumference in an irrotational flow. For arbitrary body shapes, and for generality, equations (1.20) and (1.21) may be replaced by:

$$\underline{F}_I = C_m \rho A \dot{\underline{u}}_c \quad \dots (1.22)$$

where C_m is the inertia or mass coefficient, and is 1 or 2 respectively in the potential flow cases above.

The inertia force in potential flows is consequently only a function of the relative fluid acceleration $\dot{\underline{u}}$, and for a periodic acceleration \underline{F}_I is in phase with $\dot{\underline{u}}$. There are additional complications, even in potential flows, if the pressure gradient is not uniform across the cylinder, this makes the calculation of \underline{F}_K more difficult. If additionally, the fluid flow field is distorted by the body, as in the case of surface waves being reflected or diffracted by a cylinder the added mass term \underline{F}_{IM} will also be different. Analysis of larger diameter cylinders in this context is achieved using diffraction theory when applied to wave loading, and will not be considered in this Thesis, (see Standing (1979) for recent information).

The response of viscosity to unsteady flow

It has been demonstrated earlier in this Section with reference to the work of Schwabe, that 'starting' fluid accelerations quickly exhibit viscous behaviour. The potential flow model developed to obtain an inviscid force (equation (1.20) & (1.21)) only therefore incorporates part of the picture. Sarpkaya (1963) presents a potential flow analysis for an unsteady flow past a circular cylinder using the generalised Blasius theorem and an extension of Lagally's theorem. The model represents the vortex wake by a stream of arbitrarily situated vortices of varying strength and growth rates. The inline and transverse forces were determined as follows:

$$\underline{F} = -\rho \sum_{k=1}^n \Gamma_k \underline{v}_k + \rho \sum_{k=1}^n \frac{\partial}{\partial t} (q_{ki} \Gamma_k) + 2\rho A \frac{\partial \underline{u}_a}{\partial t} \quad \dots (1.22)$$

$$\underline{F}_L = -\rho \sum_{k=1}^n \Gamma_k (\underline{u}_a - \underline{u}_k) - \rho \sum_{k=1}^n \frac{\partial}{\partial t} (p_{ki} \Gamma_k) \quad \dots (1.22a)$$

where n is the number of vortices, \underline{u}_k & \underline{v}_k the velocity components of the real k th vortex, p_{ki} & q_{ki} coordinates of an imaginary k th vortex, and Γ_k the circulation of the k th vortex.

It is apparent by comparison with equation (1.21) that the last term of equation (1.22) is the previously defined inertia force \underline{F}_I , the other two terms incorporating the vorticity effects, which are assumed to perturb this potential flow model.

The potential flow model is a realistic one if applied outside the boundary layer region. For a circular cylinder this is around the front part of the cylinder up to the point of separation, and from there outside the two shear layers delineating the wake region. Potential flow models that approximate viscous wake behaviour do

not predict wake characteristics with great accuracy, but the predicted resultant effects on the external (to the wake) potential flow can give good agreement with observation.

The exact value of the real fluid inertia coefficient C_M is complicated by the additional effects of viscosity. If all measured forces in phase with the fluid acceleration are assumed to be inertial, then C_M has an unsteady value, varying with the fluid kinematics. This was suggested by Iversen & Balent (1951) for example, but this was based upon the assumption of a drag force equivalent to a steady flow, ~~0.16~~ applied to accelerated discs. Because the potential flow solution for added mass is obtained assuming a pressure distribution, and both drag and inertia forces manifest themselves as a pressure distribution in a real fluid, they are inseparable other than by the assumption of a suitable phase relationship.

Sarpkaya & Garrison (1963) accelerated water uniformly past a circular cylinder to compare measured in-line and transverse forces with those predicted by the equations (1.22) & (1.22a), by measuring the characteristics of the shed vorticity. A dimensional analysis similar to that resulting in equation (3.10), (page 106) yielded an in-line force dependence upon R_E and an acceleration modulus, first presented by Iversen & Balent (1951), and now known as the Iversen Modulus (or number):

$$I_m = \dot{U} a d / U_a^2 \quad . . . \quad (1.23)$$

which for the uniform acceleration under consideration reduces to $I_m = d / 2s$. So that the Iversen Modulus is a reciprocal measure of the dimensionless displacement of the fluid relative to the cylinder diameter. The correlation of Schwabe's earlier results with the reciprocal of I_m , which he termed the 'dimensionless time', demonstrates the importance of this parameter in describing accelerative flows.

The physical factors governing the flow around a cylinder in unsteady flow must be principally due to the development of the vorticity. It is apparent from the preliminary description of boundary layer development given in Section (1.1) that the rate of diffusion, or growth, of a laminar boundary layer is a function of $R_x^{-1/2}$, where R_x is a Reynolds Number based upon the distance x travelled by a fluid particle from rest in steady flow with velocity U_0 .

Consequently the time taken for a boundary layer to grow to a thickness of δ_x due to the diffusion of vorticity is of the order (δ_x^2/ν) , termed the 'diffusion time'. For the classes of unsteady flow considered here; impulsive or uniform acceleration, the flow field will develop from an initially potential one into either a steady or quasi-steady state respectively. The relative thickness of the boundary layer after time t is proportional to $(\nu t)^{1/2}$, and its spread into the surrounding fluid may be gauged by the dimensionless distance $y/(\nu t)^{1/2}$, where y is any perpendicular distance from the vorticity generating boundary.

By consideration of the Navier-Stokes equation, important dimensionless groups arise which relate fluid flow parameters to the vorticity and boundary layer development, Rosenhead (1966):

(i) $\nu t/d^2$, where d is a reference length in the direction of flow, in this case the cylinder diameter.

$$\text{As } \delta_x \approx (\nu t)^{1/2} \quad \frac{\nu t}{d^2} = \frac{(\nu/d^2)}{(\nu/\delta_x^2)} = \frac{\text{rate of diffusion through distance } d}{\text{rate of diffusion through distance } \delta_x} \dots (1.24)$$

This is a diffusion ratio which is normally small at the initial instants of motion.

$$(ii) \frac{U_a t/d}{(1/t)} = \frac{(U_a/d)}{(1/t)} = \frac{\text{rate of convection through distance } d}{\text{characteristic time rate of change}} \dots (1.25)$$

$$\text{or} \quad = \frac{(U_c/d)}{(\nu/\delta_x^2)} = \frac{\text{rate of convection through distance } d}{\text{rate of diffusion through distance } \delta_x} \dots (1.25a)$$

In the case of uniform acceleration this is equivalent to the reciprocal Iversen modulus I_m . At the initial instants of motion for small t , the rate of diffusion exceeds that of convection and the boundary layer thickness grows as a function of $(\nu t)^{1/2}$, i.e. at small times the effects of convection are negligible in comparison to diffusion. For steady flows, the rate of convection must balance the rate of diffusion for equation (1.6) to be valid.

$$(iii) \frac{U_a d/\nu}{(\nu/d^2)} = \frac{(U_a/d)}{(\nu/d^2)} = \frac{\text{rate of convection through distance } d}{\text{rate of diffusion through distance } d} \dots (1.26)$$

or, for a longer time interval when the flow is at least quasi-

$$\text{steady: } = \frac{(\nu/\delta_x)}{(\nu/d^2)} = \frac{\text{rate of diffusion through distance } \delta_x}{\text{rate of diffusion through distance } d} \dots (1.26a)$$

This is the Reynolds number, only of importance after a relatively large time interval, when the vorticity has had time to develop and influence the flow.

Rosenhead (ibid) considers the realms of validity, and simplifications of, boundary layer theory using these descriptive parameters. They are included here in order to illustrate the physical meaning of R_E and S/d in unsteady flows.

Sarpkaya & Garrison assumed that the vorticity parameters were functions of R_E and S/d , although by comparing the R_E range used (just less than critical) with steady flows, any correlation of characteristics with R_E was not anticipated, or indeed detected. Dependence of the forces upon one variable only, enables equation (1.22) to be re-written as

$$F = C_D \rho U_a^2 d/2 + C_M \rho A \dot{U}_a \dots (1.27)$$

where C_D and C_M may, or may not, be equivalent to the steady, and potential flow, coefficients of drag and inertia C_d and C_m respectively. It is important to realise that this equation applies only to the case of uniform acceleration,

because $C_D(t), C_M(t) = \phi(S/d)$ only.

This simple formulation, however, does not apply to any other type of motion, particularly because it does not include any term describing the history of the motion, which has been demonstrated to be important in the presence of viscosity.

Due to the relationship between C_M and C_D , expected because of their mutual dependence upon S/d , Sarpkaya & Garrison re-formulated equation (1.27) as:

$$C_1(t) = F/\rho A \dot{U}_a = C_M + \frac{4}{\pi} \frac{S}{d} C_D \dots (1.28)$$

Figure (1.14) shows their results for C_1 , using a variety of cylinder diameters and fluid acceleration (i.e. R_E). The initial potential flow may be clearly seen at low S/d as $C_M = 2$ and $C_D = 0$. The dimensionless circulation of the k th vortex, defined as $\Gamma_k/U_a d = \phi(S/d)$ was determined experimentally and is shown in Figure (1.15), which also shows the relative movement of each vortex with respect to the cylinder. The asymmetric development of one vortex alone is clearly shown above $S/d = 3$. The mechanism of interruption of the shear

layer feeding the larger vortex, thus causing shedding, was identified; caused by flow from the smaller vortex side of the cylinder. This is identical to the behaviour postulated for steady flows. Equation (1.28) led to expressions for C_D and C_M in terms of vorticity, C_D being a function of vortex characteristics and disposition, as would be expected. C_M , however, was also found to be theoretically a function of the circulation of the vortices, disturbing its value from the strictly potential one of 2 by an increasing amount as the vortex circulation increased up to the first asymmetry. Figure (1.16) shows this correlation between C_D and C_M as S/d increases, with a convergence of C_M to 1.3 and C_D to 1.2 postulated for $S/d > 20$. So that for S/d approximately > 3 , C_D tended to C_d .

This experiment and theoretical formulations suggest that for accelerative flows the separation of potential and vorticity dependent components into acceleration and velocity functional terms respectively is inappropriate. The analogy to steady velocity-dependent flows, and the utilization of steady flow C_d for C_D values at corresponding $R_E(t)$ would therefore be erroneous, particularly due to the neglect of flow history effects. Similarly the definition of acceleration-dependent inertia force components, which are history dependent, may not be adequately described by a time invariant added mass.

The conclusions from this experiment of Garrison & Sarpkaya depend upon the initial potential flow model, and the way in which the results have been interpreted. The deviation of the inertia coefficient from the potential value of 2, due entirely to vorticity effects, has evolved from the theoretical formulation. There is no reason to assume that there is in fact a deviation of the added mass from 1, the conclusions are as a consequence of the measured force, and the way the theory has been fitted. An equally valid formulation would be to assume the potential flow value $C_m = C_M$ and calculate C_D , using an equation of the form of (1.27), or simply to adopt a kinematic equation such

$$\text{as: } C(t) = \frac{F}{1/2 \rho d \dot{U}_a^2} \quad \dots \quad (1.29)$$

$$\text{or } C_f(t) = \frac{F}{\rho A \dot{U}_a} \quad \dots \quad (1.29a)$$

where $C(t)$ and $C_f(t)$ are force coefficients based upon a respective velocity and acceleration dependence, e.g. equation (1.29a) equivalent to (1.28), could be used, which would then describe Figure (1.14). Subtraction of the potential flow value for $C_M = C_m$ of 2

would then result in C_D containing all the vorticity, and consequently, history effects. The dotted line on Figure (1.14) shows the variation in C_D with S/d given by equation (1.28), assuming a constant C_M of 2. This line indicates a levelling off of C_D at approximately 1.2.

Keim (1956) used an equation of the form of (1.29) to show a dependence of $C(t)$ upon R_E and I_m for cylinders accelerated with a constant driving force through still water.

Laird, Johnson & Walker (1959) analysed their accelerated cylinder results assuming a $C_M - C_m = 1$ and an equation of the form of (1.29). They found that for R_E below boundary layer transition, C_D conformed reasonably with steady flow C_d values. This work also tested decelerating cylinders, and it was found that a $C_M = 0$ was more appropriate to match C_D to C_d in a corresponding steady flow. Both of these experiments found no force coefficient correlation with R_E from approximately 10^3 up to the transitional region.

In the theoretical analysis developed by Keim (ibid) he suggested that the force was not only a function of R_E and I_m , but also dependent upon higher order kinematic terms of the form:

$$d^n \underline{u}(t)^n \times d^n s/dt^n \quad (\text{see equation (3.14)})$$

For anything other than uniform acceleration, this group of higher order terms may be significant, particularly as they would incorporate the flow history, making an expression of the form of (1.29) or (1.29a) necessary for their inclusion.

For impulsively started steady flows, flow history is particularly important due to the impossibility of creating an infinite acceleration in zero time. An experiment reported by Sarpkaya (1966) concerned the impulsive acceleration of water past fixed cylinders and plates. Figure (3.4) shows the increase in the force coefficient $C(t)$, as defined by equation (1.29) with $2s/d$ for laminar flow separation. Indicating a significant increase in C_D above the steady flow C_d value, similarly to Schwabe, with a maximum of 1.6 at an $S/d = 4$. This was independent of variations in R_E , but for an R_E of 580 Schwabe reported a maximum $C(t)$ of approximately 2 at $S/d = 4$, indicating a probable rate of change of acceleration difference. Sarpkaya's results were produced assuming an inertia force component

$C_M = 4F/\rho g_d d^2$ during the accelerative period, which was subtracted from $C(t)$ to give C_D . This range of C_M is also shown in

Figure (3.14).

The photographic evidence from this experiment showed that the initially formed symmetrical vortices (Höppl vortices by analogy), after the initial potential, unseparated flow period, oscillated longitudinally (in the freestream direction), and also alternately dominated the wake in relative size. Vortex growth was again interrupted by a stream of fluid moving from one side of the wake to the other, causing shedding (vortex capture). Subsequent shedding proceeded at a greater rate from then on.

Hamilton & Lindell (1971) accentuate the importance of the flow history in determining the relative forces on bodies in relative unsteady flows. Their experiments involved the release of spheres in still water after they had been given a constant upward or downward velocity. The added mass coefficient evaluated for the ensuing acceleration, however, showed no tendency to vary with previous flow history.

The relevance of sphere tests applied to circular cylinders is unknown, but the importance of a flow history term, particularly where, for example, a moving immersed body is suddenly brought to rest, would appear to be fundamental.

The transverse force, not commonly reported for unidirectional accelerative flows is, by analogy to the mechanics of its inception dependent upon wake development and behaviour, and is therefore sensitive to rates of change of velocity and acceleration. Notwithstanding these effects the lift force is normally considered formulated in the same terms as the steady flow C_L , because C_L is also time dependent:

$$C_L = \frac{F_L}{1/2 \rho d U_a^2} \quad \dots \quad (1.30)$$

Comparison with the in-line force, equation (1.27), indicates that a possible quadrature term will exist in the lift force in unsteady flows, which will consequently not be in phase with the square of the velocity. The existence of a lift force was noted by Schwabe (ibid) and Sarpkaya & Garrison (ibid), but no details were given. Lift forces in unidirectional unsteady flows may be analogous to limiting oscillatory flows, considered in the next Section.

The interaction of drag and inertia coefficients and their dependence upon velocity and acceleration respectively, and the possible inclusion of a history term in the total force equation, is particularly relevant for oscillatory flows. Dependence of force coefficients may then be expressed in terms of phase relationships, the drag component in phase with the velocity and inertia in phase with the acceleration, any residual being due to a memory, or flow history. Such a theoretical model will depend upon the validity of the relative phase assumptions, and can only be ratified with reference to the flow behaviour.

(1.3.2) A circular cylinder immersed in relatively oscillating water

Periodic, or fluctuating, relative motion between a cylinder and water is considered here to be delineated from the previous sections by a reversal of flow direction. Fluctuating, but not reversing, unidirectional acceleration has been shown to result in fluid-structure behaviour that is principally a function of I_m . For flows starting from rest this has been expressed by a dimensionless displacement. R_E dependence is also weaker in unsteady than steady flows. Any relative flow would be expected to be resolvable into periods of steady and unsteady conditions, whether it were unidirectional or reversing. Fluids, however, have a 'memory' contained in the behaviour of any generated vorticity. Reversing flows, therefore, have to encounter any residual vorticity remaining in the flow history. The degree to which flows may be classed as unsteady, or reversing, is consequently crucial in understanding the potential effects of any higher order rates of change of fluid kinematics, and previously generated vorticity.

The most complicated relative flow is potentially that of the random multi-directional conditions encountered in the sea. Synthesis of such conditions into simpler, more quantifiable kinematics, is essential in order to understand the mechanics of the relative behaviour between the complex sea and an immersed circular cylinder. Consideration of a single repeatable wave shape has led to the development of a number of mathematical models describing the kinematic behaviour of particles within the body of fluid as the wave energy is transmitted, (see for example Appendix B). Such theories, and experimental observation, show that water particles possess vertical as well as horizontal

kinematic components during the passage of a wave. The velocity vector rotates with time about a point in the fluid producing an oscillating horizontal and vertical unsteady flow relative to any immersed vertical cylinder, as shown in Figure (1.5g). This unsteady motion also decays with depth below the water surface. Such regular wave conditions are therefore analogous to a simple harmonically varying horizontal velocity with a vertical shear flow, similar to vertical cylindrical structures in the earth's atmospheric boundary layer. Additionally a vertical irrotational velocity shear would also exist along the cylinder axis, even at the instant of maximum horizontal velocity. Davies (1975) gives this possibility as the reason for investigating the effect of a turbulent sheared axial flow on the base pressure coefficient of a circular cylinder at critical R_E . It was difficult to separate the turbulent and shear flow effects in this experiment but the vortex generation had a pronounced tendency to form into spanwise cells, similarly to that noticed by Dronkers & Massie (1978), discussed earlier. Obviously end conditions are extremely important for this type of flow, and further discussion is continued in Chapters 3 and 5.

The two dimensional effects of shear and axial flows are diminished for two important wave cases:

- (i) Shallow water waves of long wavelength, tending to solitary.
- (ii) Beneath the node of a standing wave.

Work at the U.S. Bureau of Standards in the 1950s utilized both of these simplifications to investigate the forces on submerged cylinders and plates. Kulin (1958) used solitary waves, and Keulegan & Carpenter (1958) standing waves. In both cases the axes of the fixed bodies were horizontal and perpendicular to the direction of wave celerity. The relative size of the cylinders compared to the waves would define the validity of assuming a reversing linear vertical velocity distribution in case (ii), because particle kinematic decay with depth (shear velocity) would still be present, even if the vertical kinematic components were small.

This Section deals with the relative cylinder-fluid dynamics, and so further discussion as to the adequacy of assuming a unidirectional, but periodic, kinematic description, in case (ii) particularly, is postponed until Chapter 3. Discussion will continue devoted exclusively

to relative planar oscillatory motion in which oscillation is linear and reversing only, a 'two dimensional' flow. Such relative flows may be obtained by oscillating the fluid or the immersed cylinder, Figure (1.5e) & (1.5f). Isaacson (1974) showed that the flow pattern and fluid dynamics relative to the cylinder, are identical, with the exception of the existence of a Froude-Krylov irrotational force in the case of a moving fluid. This is correct only provided that there are no solid boundaries within the near vicinity.

The relative force between the fluid and a relatively moving cylinder would be expected to be composed of inertial and drag terms resulting in a combined equation similar to equation (1.27). The original formulation was proposed by Morison, O'Brien, Johnson & Schaaf (1950) for vertical cylinders in waves, and this is now commonly expressed as the linear sum:

$$F = C_D \rho d \underline{u}_p |\underline{u}_p| + C_M A \rho \dot{\underline{u}}_p \quad \dots (1.31)$$

where F is the force per unit length.

The expression is presented for a planar oscillatory flow, the term $\underline{u}_p |\underline{u}_p|$ being necessary to preserve the reversing nature of the drag term. This equation expressed in wave kinematic terms, equation (1.41), is known as the Morison equation.

Dimensional analysis of a two-dimensional periodic flow can be instructive, because more functional groups than the previous R_E and I_m would now be expected. Equation (3.2) shows that the forces due to the irrotational and vorticity effects are apparently dependent upon:

$$\phi \left[R_E, \frac{\underline{u}_{pmax} T_p}{d}, I_m, Fr, \frac{m_e}{\rho d^2}, \frac{t}{T_p}, \frac{f_s}{f_p}, \text{ + geometry} \right]$$

The term $\underline{u}_{pmax} T_p / d$ is a 'period parameter', first presented by Keulegan & Carpenter (1958), and since known as the Keulegan Carpenter number N_k . It is a measure of how far a fluid particle moves in a semi-cycle of period T_p , compared with the relative size of the solid boundary, represented by the cylinder diameter. N_k is the limiting value of I_m in planar oscillatory flows:

$$N_k = 2\pi A_p / d, \text{ therefore } I_{mmax} = 2\pi / N_k. \quad \text{In an oscillatory flow}$$

$$\text{where } \underline{u}_p = \underline{u}_{pmax} \sin \omega_p t, \quad I_m = \frac{d \tan^2 \omega_p t}{x_p} = \frac{2\pi \cos \omega_p t}{N_k \sin^2 \omega_p t} \quad \dots (1.32)$$

Experimental results have been virtually exclusively interpreted in terms of N_k rather than I_m for periodic flows, as will be shown.

N_k may be combined with R_E to give

$$\beta = R_E / N_k = d^2 / T_p v \quad \dots (1.33)$$

β has been used to correlate forces remarkably well in oscillatory flows, particularly by Sarpkaya (page 89). The solution to the problem of the boundary layer on a lamina oscillating in its own plane was developed by Stokes, and reported in Goldstein (1938). The vorticity generated at the solid surface, and diffusing into the surrounding fluid, changes sign periodically. The boundary layer thickness is found to be proportional to $(\nu T_p)^{1/2}$, whether the fluid or the solid surface is oscillating. By analogy to the development of unsteady boundary layer theory in the last Section, and regarding T_p as equivalent to the time t , the relevant dimensionless parameters are seen to be (Rosenhead):

$$(i) \quad d^2 / \nu T_p = \beta \quad \dots \quad (1.34)$$

and

$$(ii) \quad d / T_p U_{pmax} = N_k^{-1} \quad \dots \quad (1.35)$$

These are equivalent to equations (1.24) and (1.25) respectively, therefore equation (1.34), which is also identical to (1.33), expresses the ratio between the rate of diffusion of vorticity through the boundary layer, compared to the rate of diffusion through a cylinder diameter parallel to the oscillating freestream vector. With reference to equation (1.6) for steady flows: $\delta_x \propto d (R_E)^{-1/2}$, similarly for a periodic flow $\delta_x \propto d (\beta)^{-1/2}$, i.e. β in a periodic flow is equivalent to R_E in a steady flow, as a boundary layer thickness parameter, (see also Patten (1979)). β will be referred to as the Stokes number in this thesis, but is also commonly termed the 'frequency parameter'.

The Froude number F_r , which is of the same form as I_m , is a comparison of inertia to gravity forces, and is only of importance where gravitational accelerations exist. This is the case for flows with a free surface, such as an experiment conducted in an open channel, but it is a parameter to be avoided by experiments using planar oscillatory flows. Consequently F_r will hereafter be considered to have a negligible effect upon fluid behaviour. However, it is further considered when dealing with surface waves, and in Chapter 3.

The other dynamic parameter which is given by the dimensional analysis is the effective mass ratio $m_e / \rho d^2$. This is a function of the added mass m_a , the theory of which was developed in Section

(1.2) for potential flows. This parameter is particularly important in vibration analysis, because any hydrodynamic damping is a direct function of this ratio, see Dickens (1976). Application of this dimensionless group in the form of damping is obscure when applied to forced inelastic oscillations, as it corresponds to the inertial term in the linear oscillator equation of motion. The viscous damping term in this equation is however, in phase with the velocity, and would therefore be expected to be a function of the drag force component. In the absence of high frequency response vibration, the mass ratio is therefore assumed to be included in the overall inertia coefficient C_M , of which it forms a principal component.

It is already obvious from a consideration of the unsteady velocity dependent drag, and acceleration dependent inertia forces, that the relative phase of the motion t/T_p will decide the relative force magnitude, particularly for a periodic motion. This dimensionless time is therefore a fundamental force definition parameter.

Vortex generation and shedding has been shown to account for important unsteady effects, and to be responsible for the onset of lift forces. Consequently the rate of shedding per cycle will define the vorticity dependent forces, and affect the unsteady drag and lift coefficients C_D and C_L . Description of vortex shedding in terms of a Strouhal Number can only be approximated using some characteristic cyclic velocity, such as $u_{p,max}$. It is this velocity, however, which is used to define the Reynolds Number in oscillatory flows: $R_E = u_{p,max} d / \nu$

It is not apparent whether the vortex shedding frequency f_s is a function of R_E in oscillatory flows. Defining $S_t = f_s d / u_{p,max}$ means that the ratio $f_s / f_p = S_t N_k$ for oscillatory flows.

From this discussion and previous discussions of steady and unsteady flows the parameters that would seem to influence the relative forces in oscillatory flows are:

$$C_D, C_L = \phi \left[N_k, \beta \text{ (or } R_E), I_m, t/T_p, f_s/f_p, + \text{ geometry} \right] \dots (1.36)$$

$$C_M = \phi \left[N_k, I_m, m/m_d, t/T_p, + \text{ geometry} \right] \dots (1.36a)$$

The subdivision being based upon vorticity dependent, or vorticity free terms respectively. The actual validity of these formulations

will now be considered in the light of considerable experimental evidence.

Numerous experimental studies involving relative planar oscillatory flows have been reported. Some of the most significant are discussed in Chapter 3, with particular emphasis on the experimental techniques. These are also summarized in Tables (3.1) and (3.2). For the sake of brevity a detailed description of the findings from each experiment will not be presented here. An attempt to describe the relative fluid-cylinder dynamics based upon their conclusions will instead be made.

Relative fluid-cylinder oscillation results in a complex viscous reaction producing flow separation and vortex movement. Comparison with uniform acceleration would be expected to give a quantitative picture of the periodic fluid behaviour, however, the discontinuities caused by starting acceleration, deceleration, stopping and relative flow reversal complicate matters. Neulegan & Carpenter (1958), Heinzer & Dalton (1969), Isaacson (1974), Sarpkaya (1976a), Maul & Milliner (1978), Stansby (1978), and Grass & Kemp (1978) have presented flow visualization results which give a description of the fluid behaviour.

The principal correlating parameter for vortex shedding is N_k . The development of vorticity for a starting oscillatory flow for $N_k=10$ was observed by Heinzer & Dalton (ibid):

- (i) Initial potential unseparated flow pattern.
- (ii) $t/T_p = 1/4$ Development of a pair of symmetric attached (Föppl type) vortices.
- (iii) $t/T_p = 1/2$ Pair of symmetrical vortices from both shear layers, with entrained reverse flow between, outside the 'breadth' of the cylinder.
- (iv) $t/T_p = 3/4$ Previously generated symmetric vortices pushed out around cylinder by the reversal of flow direction. Vortices given an induced absolute velocity across the cylinder.
- (v) $t/T_p = 1$ Original two vortices reate from the cylinder, two new symmetric vortices developing on the 'downstream' side of the cylinder, but smaller than the first two at $t/T_p = 1/2$, being within the 'breadth' of the cylinder.

The development of the second vortex pair was seriously inhibited by the convection of the first pair over the cylinder. At this low N_k

the vortex shedding may be attributed wholly to the reversal of the flow direction.

For established oscillatory flows the value of N_k illustrates the number of vortices shed in a semi-cycle:

- (i) $N_k < 1$ No separation- 'acoustic streaming'.
- (ii) $1 < N_k < 4$ Very small discrete vortices close to the cylinder, diffused quickly.
- (iii) $N_k = 4$ Two small attached vortices moved back around the cylinder before diffusing.
- (iv) $N_k > 4$ Vortex asymmetry noticeable and variation in vortex behaviour from cycle to cycle.
- (v) $6 < N_k < 15$ One vortex is separated per semi-cycle, the developing vortex on the opposite side of the cylinder remains attached and is moved back around both sides of the cylinder with flow reversal. It is also affected by the diffusion of the separated vortex. The convection of the vorticity from the attached vortex back around the cylinder causes the sense of the next formed vortex, in the following semi-cycle, to be the same. Consequently the next vortex forms on the same side of the cylinder as the one that previously separated. In this N_k range, therefore, the flow field is very asymmetric.
- (vi) $N_k \approx 16$ Separation of two vortices per semi-cycle, with the attached formation of a third, occurring during some cycles. The attached vortex influences subsequent vortex formation as in (v).
- (vii) $N_k \approx 25$ Separation of at least two vortices per semi-cycle, sometimes also a third.
- (viii) $N_k > 25$ Increasing numbers of vortices shed per semi-cycle.

The effect of increasing R_e is to increase the vortex strength, and at higher N_k to increase the number shed, although only where the shedding would otherwise be 'fractional'. Based upon a characteristic cyclic velocity of $U_p^{max}/2$, for a semi-cycle the theoretical number of vortices shed would be $N_v = N_k/10$ for $S = 0.2$

Consequently if N_k is not a multiple of 10, there would be 'fractional' vortex shedding, or partially developed attached vortices. Isaacson (ibid) considered an instantaneous velocity U_p model for the number of vortices shed per semi-cycle and determined $N_v \approx N_k/8$. This type of formulation would be expected to be valid when the flow is more

quasi-steady. McNown & Keulegan (1959) suggest that for $T_p/T_s \geq 10$ this is the case, this corresponds to an $N_k = 50$ for $S_t = 0.2$, obviously the more vortices shed the closer to the unidirectional condition the flow is. Fractional vortex shedding is particularly noticeable in the region $12 < N_k < 16$, as shown by the discontinuity in the typical S_t/N_k plot taken from Sarpkaya (ibid), Figure (1.17). This graph also shows the significant departure of S_t from the steady flow $S = 0.2$, typical over the range $4 < N_k < 150$, which illustrates the limitations of the simple vortex shedding as a proportion of N_k models proposed above. Because the vortex diffusion rate is an inverse function of R_E , for a laminar shear layer, the Reynolds number will determine the potential influence that the shed diffusing vortices will have on the developing vortices in subsequent semi-cycles. For the lower rates of diffusion, at higher R_E , these vortices will potentially have a greater influence, although the effects of turbulent diffusion will dominate after shear layer transition. The number of shed vortices as a function of R_E and N_k is shown in Figure (1.18), adapted from Isaacson and Sarpkaya.

The dimensionless time t/T_p variation in the angle of boundary layer separation has been presented for an N_k of 38; an $R_E = 2.19 \times 10^4$, corresponding to a laminar boundary layer; and an $R_E = 5.42 \times 10^4$, a transitional boundary layer; and a roughened cylinder, to simulate postcritical R_E conditions, by Grass & Kemp (ibid). This is shown in Figure (1.19); all results are averaged over 10 cycles of motion. Initial separation occurred after the cylinder had moved $0.16d$ and $0.19d$ for the smallest and largest R_E respectively, confirming the flow similarity with gradual acceleration conditions. The reduction in wake width with increase in R_E also indicates a similar reduction in C_D to that in a steady flow, with subsequent increase in the post-critical region for the simulated higher R_E (roughened) condition,

Application of a linear summation of drag and inertia terms resulting in the Morison equation may not necessarily be valid when applied to oscillatory flows. The interpretation of the drag and inertia coefficients C_D and C_M is fundamental with regard to this validity. Mention has already been made of the deficiency of such an equation with regard to history effects. One of the other principal sources of error is in the phasing relationships, complicated by wake formation. The

value of C_M for example would have to vary throughout an oscillatory cycle to preserve the assumption that all forces in phase with the acceleration are inertial, (see for example Keulegan & Carpenter (1958)). Other complications arise from the definition of this term, even in unidirectional unsteady flows negative added mass components may be determined from experimental results, Laird, Johnson & Walker (1959). The deviation of the Morison model from the initially formulated equations for steady and unidirectional, gradually varying, unsteady flows, result from the higher order rates of change of kinematic conditions present in the more complex flows. Understanding, and fitting of this equation to planar oscillatory flows is therefore a prerequisite to its use in wave conditions.

Researchers have, as in the case of unidirectional accelerative flows, been divided into those who use a Morison type of equation to interpret their results, and those who use a combined form with only one force coefficient. Analysis of results has been carried out using accurate equation fitting techniques since Keulegan & Carpenter (1958) presented a harmonic fitting method for determining weighted average values of C_D and C_M over a cycle based upon equating the first harmonic components of the measured force, and the assumed quadrature relationship between drag and inertia forces for the Morison equation. This resulted in a remainder function composed of third and fifth harmonic terms only, assumed because of the anticipated reversing of the hydrodynamic force such that $\underline{F}(t) = -\underline{F}(t + \pi)$. The measure of relative accuracy of the Morison equation fitting the remainder function showed a significant deviation in the range $4 < N_K < 30$, being largest for the third harmonic. Calculation of instantaneous drag and inertia coefficients also showed considerable variation throughout the cycle, the greatest deviation corresponding to the N_K range above. Figure (1.20) shows the remainder force results from this experiment. The other particularly interesting result is that showing the phase and magnitude of the maximum force, Figure (1.21), this differed appreciably from the Morison equation predictions. No R_E dependence was detected for this experiment $4.2 \times 10^3 \leq R_E \leq 2.9 \times 10^4$ and it was not until Rance (1969) investigated higher R_E flows that its' significance was apparent (see Chapter 3). Rance also simultaneously identified the potential magnitude of the lift force in oscillatory flows, thus illustrating the similarities between reversing and non-reversing flows,

particularly as regards force coefficient behaviour in sub and post critical R_E ranges.

Mercier (1973) obtained agreement with Keulegan & Carpenter's results oscillating cylinders in still water. His analysis consisted of least square harmonic equation fitting, and simple spectral analysis to corroborate the harmonic content of force signals. The Morison type of equation was used, and a velocity dependent lift force expression. The frequency structure of the lift force, compared to f_p was observed:

- (i) $A_p/d < 1$ ($N_k < 6$) ; No regular transverse force.
- (ii) $1 \leq A_p/d \leq 2.8$ ($6 \leq N_k \leq 17.6$) ; Second, and to a lesser extent fourth order harmonic.
- (iii) $3 < A_p/d < 3.4$ ($18.8 < N_k < 21.4$); first, and third order harmonic components.
- (iv) $3.5 < A_p/d$ ($\approx 20 < N_k$) ; no definite frequency structure.

Good agreement was achieved with two different diameter cylinders indicating good axial vortex correlation.

Isaacson (1974) reviews experimental analysis in the form of the Morison equation and compares the averaging method of Keulegan & Carpenter (ibid) with that of assuming the value of C_M and C_D that correspond to relative phases of $0(\pi, \dots)$ and $\pi/2(3\pi/2, \dots)$ when the velocity and acceleration respectively are zero. Comparison of Keulegan & Carpenter's data presented both ways indicates an increase in C_M and C_D of the order of 50% when using the latter method of data reduction. However, both indicate significant changes in C_D and C_M that occur for $10 < N_k < 15$. A combined force coefficient, such as given by equation (1.29), expressed as an RMS would, however, not detect such a variation, which is indicative, no doubt, of important fluid behaviour changes.

Isaacson also points out the dependence of C_M upon β for very small N_k as indicated by Rosenhead (ibid), the dependence upon viscosity as well as pressure being due to the influence of viscous forces upon the added mass associated with the cylinder. Rosenhead gives the Stokes correction to potential flow added mass as: $+ 2 \left(\frac{2}{\beta} \right)^{1/2}$ for $A_p \ll d$ only.

The lift force is related to vortex development and shedding by Isaacson. A growing vortex results in a reduced local C_p , and consequently lift in the direction of that vortex. Following shedding this reduced C_p increases in sympathy with a decreased C_p on the opposite side of the cylinder. He assumed a reasonable stationarity of the lift force, so that

where the number of vortices shed per semi-cycle N_v is

(i) odd, $E_L = E_L(t + T_p/2)$

(ii) even, $E_L = -E_L(t + T_p/2)$

Therefore the frequency of the lift force f_L is related to N_v by

$f_L/f_p = N_v + 1$. This figure, however only holds for complete, rather than fractional, vortex shedding, which is more prevalent for higher N_k . A Fourier harmonic representation (see Appendix C) assuming stationarity of the lift force results in the conclusion that for N_v

(i) odd; there are only even harmonic components,

(ii) even; there are only odd harmonic components.

Again this simplistic analysis is based upon a lift force stationarity and integer vortex shedding. It is shown, however, to work well when related to the experimental results of Mercier ($N_k < 25$) and Isaacson ($N_k < 14$).

The effects of flow separation and vortex development on relative forces are given by Stansby (ibid), based on a discrete vortex potential flow solution of Blasius' theorem. This is similar in form to the unsteady formulation previously discussed (equation (1.22)); see Clements & Maull (1975) and Graham (1978) for further details. Due to the difficulty of incorporating the exact point of separation, and behaviour of vorticity, into such a model, complete analytical force solutions are approximate only. The response of drag and lift forces to the presence of vorticity would, however, be expected to be accurately predicted by this approach. The complexity of the behaviour of the generated vorticity makes experimental visualization virtually impossible except for the movement of the main discrete vortices. The component mechanisms of vorticity development, shedding and convection in the reversing flow direction may be considered with reference to Figure (1.22 a-c).

(a) The vortex growing at X and the separated shear layer due to a relative fluid motion from left to right results in an upward lift force, and an in-line force in the flow direction, due to the increased circulation around the cylinder.

(b) After detachment vortex X convects away from the cylinder as shown, the lift and in-line forces are as (a) but reducing in magnitude.

(c) When the flow direction reverses the separated vortex moves back across the shoulder of the cylinder causing an upward lift force, and drag force in the same direction as previous, (b) & (c).
according to Maull & Milliner (1978)

It is the interaction of these basic processes that results in the force variation due to vorticity effects. Maull & Milliner (1978) compare

measured forces with vortex behaviour for a range of N_k at low R_E ($\leq 4 \times 10^3$), which show good agreement, and particularly help to explain the harmonic content of the in-line and lift forces. Figure(1.23a-c) shows the harmonic content of these lift forces determined by spectral analysis (Appendix D) of the force histories. Maull & Milliner comment that the proportion of the third in-line harmonic component (Figure(1.23a)), compared with the fundamental is predicted by the Morison equation with $C_D = 1.45$ and $C_M = 2$. The lift force harmonic peaks are associated with corresponding rms lift force peaks, Figure (1.24), e.g. for $N_k=13$, an rms peak, the frequency content of the lift force is principally of the 2nd order, with a significant 4th order contribution, and similarly for $N_k=18$ a larger 3rd with a smaller 5th harmonic component suggests the validity of the Isaacson model, Table (1.1), at least up to $N_k = 30$.

'Smudging' across harmonics may be attributed to:

- (i) unshed vorticity from a previous cycle, both in the form of fractional shedding (the rolling up of a shear layer) and boundary layer vorticity;
- (ii) the convection of a shed vortex back over the cylinder after flow reversal;
- (iii) a difference in N_v from semi-cycle to semi-cycle, where the shedding rate is close to a boundary line (Figure (1.18)).

Perhaps the greatest contribution to understanding the behaviour of the Morison force coefficients has resulted from the extensive experimental work of Sarpkaya et al (1974-1977c) using fixed smooth and rough circular cylinders in planar oscillatory water flows. Sarpkaya (1976a) marks the break through in the recognition of the correlation of C_D, C_M and C_L with viscous effects, and R_E via β . Re-plotting of Keulegan & Carpenters (ibid) results show a clear correlation with R_E , Figures (1.25a & b), apparent from an initial plotting based upon constant β . The two graphs are antisymmetric with an apparent greater R_E dependence ^{of C_D for $N_k < 15$, and of C_M for $N_k > 15$.} The importance of β as an experimental control parameter, rather than R_E is because of its independence of U_{pmax} , which is also a constituent property of N_k , i.e. Sarpkaya suggests:

$$C_D, C_M = \phi [N_k, \beta, t/T_p, + \text{geometry}]$$

Because the relative magnitude of the drag force as a proportion of the total in-line force is small at low N_k the apparent great variation in C_D with R_E for $N_k < 15$ shown in Figure (1.25a) is quite probably due to experimental errors. This is also true of the apparent effect of R_E upon C_M for $N_k > 15$, where inertial forces are relatively small, Figure (1.25b). Consequently Figures (1.25) should be viewed conceptually only,

particularly as the later results of Sarpkaya contradict some of the trends indicated.

Analysis of forces by Sarpkaya is based upon a Fourier least squares technique, similar to Mercier (ibid), assuming $C_D, C_M, C_L = \phi[N_k, \beta]$ i.e. time invariant in the form of weighted average values. Alternatively results have been presented in the form of combined force parameters C_f either maxima: $C_f = \frac{E_{\max}}{1/2 \rho u_{p\max}^2 d}$, semi peak to peak (spp),

or rms. A similar plethora of presentations has been used for the lift force coefficient C_L , again non-dimensionalized using the kinetic energy term. Figure (1.26a-c) shows the variation of C_D , C_M and C_f with β and N_k found by Sarpkaya for a range of N_k up to 200, and R_E in the steady flow sub and critical range. These graphs indicate that C_D is a maximum and C_M a minimum for the lower β values at an $N_k \approx 15$, C_M being closer to the potential flow value of 2 for higher β (i.e. low N_k). Figure (1.27a & b) shows these same results plotted in terms of an $R_E (= \frac{u_{p\max} d}{\nu})$ dependence at constant N_k values with some higher N_k results from Sarpkaya (1977c). C_D , in accordance with steady flow concepts, apparently experiences a drop at a lower R_E than in steady flows. The explanation that this is due to boundary layer transition effects depends upon the definition of R_E adopted, but would seem likely. The complications caused by relative turbulence and unsteady effects may be inferred from previous sections, but certainly an increased C_D compared with C_D is to be expected at corresponding R_E , as shown. The tendency for C_M toward the potential value is clearly apparent for $N_k < 6$, and also for all N_k above $R_E = 5 \times 10^5$ it appears to stabilize at approximately 1.80. At low R_E , particularly for $10 < N_k < 15$ the digression from potential is the greatest, again as would be expected due to the relative influence of viscosity.

Sarpkaya remarks that there is a definite phase difference between the maximum in-line force and maximum velocity caused by the vorticity history. The C_M variation with R_E , Figure (1.27b) shows a negative added mass ($= C_M - 1$) for $N_k > 9$ and $R_E < 3 \times 10^4$. This is not unexpected because of the averaging of C_M over a cycle of motion, the earlier reported work using decelerative flows of Laird et al (1959) also indicated this trend, which may be a physical reality in this type of relative flow. The overall force coefficient of C_f , Figure (1.26c), demonstrates an independence of β for $N_k < 12$, with an increasing effect as $N_k \rightarrow 200$, the lower β giving the largest force. Again

a peak is observed at $N_k = 15$ for the lower values of β . Therefore detailed flow conditions must differ substantially either side of $N_k = 12-15$ for $\beta < 3000$.

A peak in the maximum lift force coefficient at $10 < N_k < 15$ is clearly shown in Figure (1.28a), with a reduction at higher N_k for all β . The onset of this force corresponding to wake asymmetry at $N_k = 5$. Sarpkaya (1976a) reports that in his experiments the asymmetry had only a 0.05 probability of occurring for $N_k = 4$, and a 0.9 probability for $N_k = 5$; asymmetry being very sensitive to experimental conditions.

Maul & Milliner (1978) used a different formulation when presenting their water oscillation tests for $Re \leq 4 \times 10^3$. Average values over 200 cycles were used to evaluate

$$C_F = \frac{2E T_p^2}{\rho d^3} \dots (1.37)$$

i.e. $C_F = C(t) \times N_k^2$ (equation (1.29))

also $C_{F rms}^2 = \frac{N_k}{2} (\frac{3}{4} C_D N_k^2 + \pi^4 C_M^2)$ if C_D and C_M are assumed constant.

For $\beta = 200$, $C_{F rms}$ was found to be given by the Morison equation with $C_D = 1.45$ and $C_M = 2$. The conclusion drawn therefrom was that the Morison equation predicts rms in-line forces for subcritical Re and $N_k < 30$.

The $C_{L rms}$ given from $C_L = \frac{E_L T_p^2}{\rho d^3}$ is shown in Figure (1.24). At $N_k = 13$ the two values of $C_{L rms}$ are caused by an intermittent lift force which randomly fell to near zero. An attempt to measure the relative force intermittency was made by determining the fraction of time that C_L was outside the range of -0.2 to 0.2 of the maximum; this is indicated on the Figure by the square bracketed numbers. Evidence was presented to reinforce the apparent non-stationarity of the lift force, and consequently any presentation of lift in terms of maxima or rms would be a function of the length of experimental record. Obviously some resort to statistical techniques is therefore necessary for design purposes.

Pressure distributions measured in planar oscillatory flow would be expected to yield a useful picture of fluid behaviour in relation to integrated force histories. Due, however, to the non-stationary nature of the flow field, a larger number of phase related simultaneous circumferential pressure records is required to provide any reasonable information. Pressure plots in the form of the coefficient C_p even for 'steady' flows do not give detailed information, only trends.

Consequently experiments using single rotatable pressure tapping points have little value, see for example Chantranuvatana (1974).

The variation of $C_p(\theta, t)$ for a potential flow has been developed in Appendix A and is given by:

$$C_p = (1 - 4\sin^2\theta)\cos^2\omega_{pt} - \frac{4\pi}{N_k}\sin\omega_{pt}\cos\theta. \quad (1.38)$$

for an oscillating fluid

$$\text{and } C_p = (1 - 4\sin^2\theta)\cos^2\omega_{pct} - \frac{2\pi}{N_k}\sin\omega_{pct}\cos\theta. \quad (1.39)$$

for an oscillating cylinder,

the difference between these is due to the Froude-Krylov force, expressed as a pressure coefficient $C_{pk} = \frac{2\pi}{N_k}\sin\omega_{pt}\cos\theta. \quad (1.40)$

Comparison of this unsteady pressure distribution with that experimentally recorded by a number of circumferentially positioned pressure transducers on an oscillating cylinder is made in Chapter 4. This experiment will also enable comparisons to be made with the conclusions reached by other researchers and presented so far in this Section.

(1.3.3) The complications in wave flows

It has already been shown that even in regular waves, flows past a vertical pile are complicated compared to other kinematic conditions by 'three dimensional' effects, because of

- (i) the rotation of the velocity vector, and
- (ii) the existence of a shear flow.

Consequently both R_E and N_k decrease with depth below the free surface, as well as varying across a cross section with a wave cycle. In the limit a planar oscillatory type of flow is more likely to exist at a greater depth. Full scale testing of cylinders in the sea is even more complicated by wave variability, non-linearity and currents etc. Early experimenters appreciated the invalidity of small scale test extrapolation to full size structures (see Chapter 2) and force histories were recorded at full scale, particularly off the coast of the United States. Correlation of results with any of the basic hydrodynamic parameters such as R_E or N_k was not achieved however, see for example Wiegel (1964), and Wilson (1965). The understanding of the mechanics of wave induced forces has therefore been developed using simplified kinematic models, which may utilize waves or not. The potential for this utilization is further discussed in Chapters 3 and 5, in this section observed fluid behaviour and the fundamental hydrodynamic characteristics discovered in wave flows is considered.

There have been a number of useful reviews relating to wave loading on cylinders, the most comprehensive contemporary report originated from the Offshore Fluid Loading Advisory Group (OSFLAG) Project No. 10: British Ship Research Association (1970). This report resulted in the design paper: Hogben, Miller, Searle & Ward (1977). Hogben (1976a) deals particularly with larger diameter cylinders in the diffraction regime.

A particularly useful photographic flow visualization has been presented by Zdravkovich & Namork (1977) for waves with $kz_2 < 3$ where k is the wave number ($2\pi/L_w$), $3.7 \leq N_k \leq 9.3$ and $1.5 \times 10^2 \leq R_E \leq 5 \times 10^3$, both defined in terms of the maximum horizontal wave particle velocity u_{wmax} . These results are summarized in Figure (1.29 a & b) for $N_k = 5.4$ and 9.3 , based upon surface particle observation.

A falling or a rising surface is seen to significantly alter vortex generation and behaviour. The formation of pairs of vortices only occurs when the surface is falling, this also increases the circulation of individual vortices due to their longitudinal contraction. At lower $N_k = 5.4, 6.1$ and 7.8 asymmetric shedding of the vortex pairs from either side of the cylinder occur following the passage of a wave trough, whereas for $N_k = 9.3$ alternate vortex pair shedding occurred asymmetrically but at both the crest and trough. Consequently any digression from a planar oscillatory flow is caused by the vertical velocity component and free surface, although the bias of a previously formed vortex stimulating new vortex growth is still evident, particularly at low N_k . The Morison equation for the in-line force per unit length on vertical surface piercing cylinders in waves is:

$$F = C_D \frac{1}{2} \rho u_w |u_w| d + C_M \rho A \dot{u}_w \quad \dots \quad (1.41)$$

where u_w is the horizontal component of the wave particle velocity. Again, as in planar oscillatory flows, the relative direction of the non-linear drag term is retained by the drag force component being in phase with u_w (assuming a steady C_D). The kinematic components of this equation are responsible for some of the previous experimental scatter in C_D and C_M because of the impossibility of measuring u_w directly until the last decade. The kinematic inertia force component \dot{u}_w is in fact the substantive acceleration $\frac{D u_w}{Dt}$, composed of local and convective terms. These convective non-linear terms are often neglected in wave force analyses even when the experimental waves are non-linear. It is because of the neglect of any non-linear effects upon the inertia force that all non-linear experimental results are falsely att-

ributed to viscous effects. Lighthill (1979) maintains that the non-linear effects associated with this component are significant in wave flows, and derives second order corrections which also alter the phase relationship of the constituent components of the total force.

Correlation of C_D and C_M with dimensionless groups would be expected to be similar to planar oscillatory flows with the possible addition of wave characteristic groups. No apparent additional force group correlation has been observed, although the Morison equation is not applicable for $d/L_w > 0.2$ due to the disturbing effect of the cylinder upon the incident wave and pressure fields. As regards the waves themselves a dimensionless depth expressed by the kz_2 product (wave number \times still water depth) and a dimensionless steepness kH_w are important. The former classifies the type of wave, whether it is shallow ($kz_2 < \pi/10$) or deep ($kz_2 > \pi$). The Keulegan Carpenter number, now $\frac{U_{wmax} T_w}{d}$, does not describe simply the ratio between fluid particle displacement and cylinder diameter, because it represents a maximum value at the free surface only. The ratio between the maximum drag and inertia forces may be deduced from equation (1.41):

$$\frac{F_{Dmax}}{F_{Imax}} = \frac{2 C_D U_{wmax}^2}{\pi d C_M \dot{U}_{wmax}} = \frac{2 C_D \cdot 1}{\pi C_M I_{mmax}} \dots \quad (1.42)$$

i.e. for deep water linear wave theory, where $N_k \triangleq \pi H_w/d$:

$$\frac{F_{Dmax}}{F_{Imax}} = \frac{C_D \cdot N_k}{C_M \pi^2} \dots \quad (1.42a)$$

Consequently N_k is a measure of the relative magnitude of drag and inertia forces (as in fact is I_m). At high N_k the drag force dominates, and at low N_k the inertia force dominates. The regime of dominance may be summarized on the basis that for $N_k \rightarrow \infty$ and $N_k \rightarrow 0$ flow tends to steady and potential conditions respectively.

- (i) $N_k > 25$ drag dominance.
- (ii) $5 < N_k < 25$ intermediate, drag and inertia.
- (iii) $N_k < 5$ inertia dominance.

Experiments conducted in one force regime would therefore not produce reliable results for the other force coefficient. This point is further pursued in Chapter 2.

The possible correlation of wave force data with I_m as indicated by equation (1.42) has been largely ignored, all work being based upon N_k , with the exception of Crooke (1955) who correlated Morison's original data for cylinders and spheres with I_m . However, interpretation of I_m is difficult in waves because of the variation of the

particle kinematics with depth as well as time. Even throughout a wave cycle the flow conditions may vary from quasi-steady (low I_m) to potential (high I_m) resulting in actual fluctuation of C_M and C_D . Therefore for a vertical cylinder in waves:

$$C(t), C_q(t) = \phi \left[N_k, R_E, t/T_w, kZ_2, kH_w, d/L_w \right] \dots (1.47)$$

This equation may be compared with equation (2.10) and (2.11) resulting from a general dimensional analysis.

As kZ_2 is a representation of relative water depth, the lower its value the closer to a two dimensional planar oscillatory flow the conditions become. Experiments usually consider waves described by small amplitude theory, consequently the kH_w parameter is considered to be small, tending to zero, and its effects are correspondingly ignored. Isaacson (1974) observed the effects of varying kZ_2 upon the shedding of vortices. For an $N_k=10$, he found that at low values of kZ_2 ($\pi/10$) the vortex spanwise correlation was good because the vertical velocity components were small. For high kZ_2 ($>\pi$) vortex shedding was poorly correlated, being dominated by the region near the surface. The intermediate region of kZ_2 , however, exhibited apparently better vortex correlation. The RMS lift coefficient C_{Lrms} was consequently found to be lower for high kZ_2 , although the intermediate depth gave the largest value of C_{Lrms} . This was considered to be due to the increasing wave non-linearities in shallow water.

Figure (1.30) shows the pressure and flow development for a semi-cycle of motion recorded by Isaacson using a single pressure tapping and rotating it, assuming a stationarity of signal. This stationarity assumption is undoubtedly erroneous; it has been shown not to hold even for the simpler kinematic case of planar oscillatory flow, however, the flow visualization is useful to compare with the planar oscillatory experiment detailed in Chapter 4. The conclusion that may be drawn from this Figure is that the vortex behaviour appears to be similar to planar oscillatory flow, although it should also be compared with Figure (1.29b).

The vorticity behaviour may be compared with the earlier work in this area by Bidde (1971), and Wiegel & Delmonte (1972) and related to the development of a lift force. The onset of lift appears to be in the range $N_k = 3.5$ with a relative lift frequency $f_{L/w} = 2$ up to $N_k = 18-20$. Above these ranges it becomes increasingly difficult to distinguish a particularly dominant frequency. However, Sawaragi, Nakamura &

Kita (1976) found that $f_L/f_w = 3$ for $N_k = 12-20$, and $f_L/f_w = 1$ for $N_k < 6$, although this overlapped an $f_L/f_w = 2$ for $N_k = 4-13$. Chakrabarti, Wolbert & Tam (1976) using a spectral analysis of the lift force in waves noticed that there were significant higher order frequency components present, and via a Fourier analysis produced a graph showing the variation of these constituent components of C_L with N_k . Unfortunately there was a wide scatter of results, presumably due to a lack of control of parameters such as kz_2 but one interesting result was the constitution of C_L up to $N_k = 6$, found to be dominated by the first harmonic. Isaacson presented Fourier coefficient content for $kz_2 = 0.77$, Figure (1.31), which may be considered with respect to his presentation of C_{Lrms} , Figure (1.32). In the region $N_k \approx 15$ the relative magnitude of the lift force may be as much as 1.6 times the in-line force. Chakrabarti et al (ibid) recorded resultant force $F_T = (F^2 + F_L^2)^{1/2}$ variation with N_k in the form of polar plots. A selection of these are shown in Figure (1.53) for various surface N_k , from which the significant non stationarity, even of the in-line force may be easily seen. The comprehensive investigation of lift force in waves carried out by Sawaragi et al (ibid) compared the life time of a shed vortex \bar{t}_s with a semi-cycle of wave motion. This ratio was found to exceed 1 only in the region $9 < N_k < 13$, being smallest for low N_k (falling to 0.3 for $N_k = 4$). Above $N_k = 15$, $2\bar{t}_s/T_w$ stabilized around 0.75, at least in the experimental range of $N_k \leq 20$. The ratio gives some measure as to the potential interference between successive semi-cycles due to discrete vortices.

There have been a number of other experiments conducted in waves resulting in the production of graphs showing the variation of C_D and C_M with N_k particularly, and if they are conducted in the appropriate drag or inertia regime (see Chapter 2), and linear waves, the results may exhibit little scatter, however, due to the complexity of the relative flow fields designers frequently utilize the results from planar oscillatory flows to select appropriate values for these coefficients for a particular design wave. Very little understanding of fundamental hydrodynamic behaviour has been gleaned from wave tests, and although much more generalized information could be presented the state of art of wave tank experiments will be left here, although the modelling aspects will be considered further in Chapters 2,4 and 5, particularly because they form a central part of this Thesis.

(1.4) Summary

The Morison equation in reversing flows has been shown to be the linear summation of a non-linear velocity dependent drag term and an irrotational acceleration dependent inertia term. There is assumed to be no interaction between the two components. For high values of N_k the empirical drag coefficient C_D tends to that for steady flows C_{D_s} , while for low values of N_k the empirical inertia coefficient C_M tends to that for potential flows C_{M_p} . Between these extremes it is apparent that viscosity and vortex shedding affect C_M as well as C_D . Determination of time average values of C_M and C_D may be adequate for design purposes, but only for maximum force values. The understanding of fluid behaviour and consequent force variation with time requires the variability of C_M and C_D , particularly where higher harmonic effects are important as in complex vorticity fields.

The Morison equation is further deficient in two obvious respects:

- (i) History effects in complex kinematic conditions, resulting in higher order rates of kinematic change.
- (ii) Ignoring the important transverse force component which may exceed the in-line force. A formulation of this force in terms of a velocity dependence by analogy to the Morison drag term may well be inadequate, particularly in wave flows.

This Chapter has attempted to begin from the simplest possible concepts of fluids moving relatively to immersed bodies and briefly develop the ideas that have led to the present understanding, albeit imperfect, of the relative forces that are generated between them. The accent throughout has been upon the fundamental hydrodynamics, rather than design oriented approximation.

The following Chapters 2 and 3 deal with the possibilities of modelling the fluid mechanic processes observed in relative fluid-cylinder motion, beginning with the complexities of wave flows. Chapter 4 details two experiments that are examples of this modelling, relating experimental observations to previous work summarized in Chapter 1. Chapter 5 brings the information developed in the previous four Chapters together and leads into Chapter 6 with conclusions and suggestions for further work.

CHAPTER 2

MODELLING OF CIRCULAR CYLINDERS IN WAVES

(2.1) Introduction

A model is a three dimensional representation of a proposed structure. The proposed structure is known as the Prototype, and the model is a representation of that prototype. In fluid dynamics, models are utilized to visualize, analyse and measure fluid behaviour and effects.

Models may be considered to be:

(a) Physical, if they are of solid construction,
or (b) Mathematical, if the prototype simulation is attempted by means of a mathematical description. This description may be in either (i) digital, or (ii) analogue form. The simplest of applied mathematical expressions could therefore be termed 'a model'.

Fluid engineering has evolved principally by the observation of natural phenomena, and the adaptation of this observation into empirical investigation. More recently the development by applied mathematicians and physicists of rational theories, without necessarily any recourse to empiricism has led to a hydrodynamic, or purely analytical, approach to understanding and predicting fluid behaviour. Often, in order to model fluid behaviour adequately in this mathematical form, simplifying assumptions have to be made, and this may result in the hydrodynamic model actually bearing little resemblance to the prototype.

Present investigation of fluid flow behaviour attempts to achieve understanding from experimental and mathematical models where appropriate. Reconciliation of the empirical and mathematical modelling of a problem often results in greater understanding.

(2.2) Physical models

Mathematical, or theoretical modelling methods may be limited in their application to real fluid flow situations by:

- a) Non linear effects
- b) Complex boundary conditions
- c) Their representation of turbulence

Foremost among non linear effects is that of convective inertia. This is the part of the total inertia term that is due to changes in velocity with respect to position, or distance (if rotation is ignored) from equation (1.3a):

$$\text{i.e.} \quad \rho \nabla \cdot \left(\frac{V^2}{2} \right)$$

This can be modelled satisfactorily only by using a physical simulation. It may often be neglected, however, and a relevant example of this is in the Stokes first order gravity wave theory (Appendix B). Higher order wave theories account for the convective inertia term with greater success the higher the order. Physical models different in size from the prototype may also be only approximations to complete prototype behaviour. These scale models may be used to investigate particular aspects of fluid behaviour successfully, provided the limitations inherent in scale modelling, and termed 'scale effect', are properly understood.

(2.2.1) Dimensional similarity

The field of fluid mechanics unites the empirical, design by experience approach, with the hydrodynamic, mathematical approximation to reality approach. Within this field physical phenomena can be completely described by four fundamental dimensions:

Mass M, Length L, Time t and Temperature t_e

The use of the English word 'dimension' is rather obscurely applied in this case due to the duality of meaning. Rouse (1961) points out that 'dimension' is used both to define the numerical magnitude of a measurement and its dimensional category. These dimensional categories are termed 'quantities' by Ellis (1966) in a rigorous discussion of the significance of units,

dimensions and quantities and their usage in developing mathematical laws. In this case the word 'dimension' will be used to describe the dimensional category or fundamental 'quantity' of a measurement; this being in accordance with normal engineering usage.

A rigorous discussion on the validity of the assumption that all phenomena may be described by the dimensions M, L, T and t_e is beyond this Thesis, but an interesting view regarding the nature of Time is given by Aked (1977) , in which he demonstrates that whilst we can discern the effects of time, unlike the other dimensions Mass and Length, we cannot define the nature of the property itself.

In the fluid mechanics describing most civil engineering problems the effects of temperature may be ignored. However, in a recent experimental investigation of the effects of temperature on fluid-structure interaction, Marchman (1977) found that the heating of a cylinder immersed in a flow of air had a significant effect upon the fluid behaviour, and consequently on the force exerted on the cylinder. The cylinder had been gradually allowed to cool from a maximum temperature of 1600°F , and noticeable fluid dynamic effects were present only at higher temperatures. Such a large temperature range is extremely rare in practical situations, therefore the temperature dimension t_e will hereafter be neglected.

(2.2.2) Dynamic similarity and Dimensional Analysis

The effects of response due to the flexibility of a structure or its supports cannot be ignored in fluid-structure interaction models. Kolkman and Van Der Weide (1972) discuss the design of such models in terms of their elastic similarity, particularly as related to offshore engineering. This Thesis, however, does not consider responsive structures, other than for occasional specific cases, so that all discussion from now on will be concerned with fixed, rigid structures.

A number of approaches are used to develop the fundamental parameters that relate a prototype to its representative physical model. This representation is one of similitude and may be developed by inspired inspection, dimensional analysis or more rigorously from the Navier-Stokes equation.

The fundamental dimensions L, M and t are combined into a number of quantities derived to describe fluid properties and behaviour; such as density $\rho (M/L^3)$ and velocity $V (L/T)$. Any quantity q has dimensions $[q] = \phi [L^a, M^b, t^c]$ (2.2) where [] denotes 'the dimensions of', and ϕ is a functional representation. The indices a, b and c being appropriate integer values. Quantities are said to be:

- (a) Geometric if they possess only
Length dimensions $[q] = \phi [L^a]$
- (b) Kinematic if they also possess
Time dimensions $[q] = \phi [L^a, t^b]$
- (c) Dynamic if they also possess
Mass dimensions $[q] = \phi [L^a, t^b, M^c]$
- (d) Dimensionless if they have no
dimension $a = 0, b = 0, c = 0$

Yalin (1971) discusses the merits of considering the fundamental dimensions L, M and t or L, \underline{F} and t, where \underline{F} is a Force dimension. Although in common usage Force has hybrid units composed of M, L and t : ML/t^2 , in an absolute system of dimensions \underline{F} may just as reasonably be considered **fundamental**, giving M the units of $\underline{F}t^2/L$. Misunderstanding of this concept is largely caused by terminology, and reference to Rouse (ibid) should be made for further clarification. Any three independent dimensions are adequate for fluid mechanic description.

Conventionally, and in this treatment, L, M and t are used. To develop understanding of fluid mechanics through experimentation the most significant derived quantities describing a prototype, such as fluid velocity V , need to be identified. Laws, or mathematical descriptions of phenomena, can be universal only if they have no reference system of units, otherwise the absolute values would change depending upon the reference system adopted; Ellis (ibid). In engineering the dimensional forms with appropriate units are used to describe phenomena. In order to be independent of units the quantities

must be combined to produce dimensionless numbers. These dimensionless numbers would then relate equally to a prototype or its model.

This appropriate combination of quantities may be achieved by inspection of the relevant quantities or, more formally, by using dimensional analysis. The process of inspection is necessary even when using a method of dimensional analysis such as Buckingham's Π Theorem to ensure the most appropriate grouping of quantities.

This approach theoretically relates a model to a prototype by specifying all the dimensionless groups that should have the same numerical values in the model and the prototype.

Probably the most important of these is the 'Newton inertial force group' which compare inertia forces with the other physical forces in a system.

Dimensional Analysis can never result in fundamental laws. This is because such Laws are independent, i.e. they cannot be derived from any other Laws. The Newtonian inertial laws are implicit in any dimensional analysis relating to moving fluids. The important dimensionless groups that describe either the model or the prototype as derived from dimensional analysis are composed of quantities that are related between the model and prototype by scales. For example, when a typical model length is L_m , the corresponding prototype length L_p is given by:

$$L_p = L_m \times L_r \quad \dots \dots (2.1)$$

then L_r is the scale ratio between those lengths.

If, by this scale, every length in the prototype L_p is related to an homologous length in the model L_m then the model is 'geometrically similar' to the prototype, and L_r is the geometric scale. When describing a model 'scale' as related to a prototype it is this scale that is implied. If a similar relationship also exists for homologous velocity vectors, then the model is said to be 'kinematically similar' to the prototype, and prototype and model velocities are related by the velocity scale V_r as

$$V_r = \frac{V_p}{V_m} \quad \dots \dots (2.2)$$

where V_p and V_m are velocity vectors at homologous points in the prototype and model respectively.

'Dynamic similarity' of the model with the prototype is achieved when homologous model and prototype masses M_m and M_p respectively are also related by a constant scale M_r :

$$M_r = M_p / M_m \quad \dots \dots (2.3)$$

Usually dynamic similarity between model and prototype is expressed by a fixed geometric scale L_r and a consequent constant force vector scale

$$F_r = F_p / F_m \quad \dots \dots (2.4)$$

This force vector scale is obtained upon further combination of the mass and kinematic scales:

$$F_r = M_r \times V_r \times V_r / L_r \quad \dots \dots (2.5)$$

(2.2.3) Similitude and model scale

This condition of dynamic similarity, given by equality of force ratios between a model and a prototype, corresponds with the dimensional analysis which results in a combination of quantities of the same dimensions into dimensionless ratios. Hence these ratios, known as Π s in the Buckingham Π Theorem, may be of forces. For example, one of the Newton inertial force groups (previously mentioned) is the ratio between inertia and gravity forces known as the Froude Number

$$F_r = \rho U^2 / \rho g L = U^2 / g L \quad \dots \dots (2.6)$$

For dynamic similarity therefore:

$$\frac{(\rho U^2)_{\text{prototype}}}{(\rho U^2)_{\text{model}}} = F_r = \frac{(\rho g L)_{\text{prototype}}}{(\rho g L)_{\text{model}}} \quad \text{All other force ratios} \quad \dots \dots (2.7)$$

i.e. Prototype Froude number $F_{rp} = \text{Model Froude number } F_{rm}$ so that the condition of dynamic similarity is satisfied if each of the dimensionless groups, or Π s, is the same for model and prototype. The scale for each quantity is then given by the ratio of forces as in equation (2.7), with reference to the geometric scale from equation (2.1).

e.g. For equality of Froude numbers:

$$\left(\frac{U^2}{g L}\right)_{\text{prototype}} = \left(\frac{U^2}{g L}\right)_{\text{model}}, \text{ hence } U_r = (g_r L_r)^{1/2} \quad \dots (2.8)$$

Any other quantity scale may be determined in this way.

Scale selection is limited by the requirement that all force ratios are simultaneously numerically equal for the model and the prototype. This is most simply explained by reference to the basic quantities involved in describing the fluid mechanical situation. The geometric length scale is usually limited by the space available for the model, so that L_r may only vary down to a limiting value.

For incompressible fluids the scales of viscosity μ_r and density ρ_r are determined when the model fluid is specified. Due to the limited number of fluids practicably available these scales are also limited in range. Additionally if the gravitational acceleration g is an important quantity, as in water surface waves, this implies that $g_r = 1$ due to the relative invariance of gravity on the earth. Yalin (ibid) shows that only three independent scales are sufficient to specify a model completely. So that if a model fluid is selected then two scales μ_r and ρ_r are automatically specified, and if gravity is important a third g_r is also specified due to its uncontrollability. Such a model may be one of water surface waves with water as the model fluid. The basic model scales would thus be: $\mu_r = 1, \rho_r = 1, g_r = 1$ and all of the derived scales would also be unity. Models of the same size as the prototype are of very limited use and some rules for the design of a reduced size model ($L_r > 1$) are required.

A compromise solution is adopted that approximates the constancy of the Π groups between model and prototype. This is achieved

by ignoring the force ratios that have the least significance with regard to the particular fluid dynamic situation.

One of the most important force ratio groups is that between inertia and viscous, or frictional, forces, the Reynolds

Number:

$$R_E = \rho U L / \mu \quad (\text{Chapter 1}) \quad \dots (2.9)$$

If a model is to be built of a prototype where both friction and gravitational forces are of equal importance then this implies that $\mu_r = 1$, and $g_r = 1$, and also that $Q_r = 1$ because Q_r is a measure of the inertia force. This is a full sized model. This irreconcilability is well known, and discussed throughout the literature. It is expressed by the impossibility of achieving Reynolds number similarity (when friction forces are important) and Froude number similarity (when gravity forces are important) simultaneously.

To achieve a reduced sized model in such cases the model scales must be determined based upon the most important of viscous or gravity forces - either a Reynolds, or a Froude model, respectively. The Froude based models are termed non dissipative or fully turbulent by Mehaute (1976). Nondissipative occurring when inertia and gravity forces dominate. Fully turbulent where viscous forces are important outside the particular 'short' section under consideration which is so turbulent that it can be considered independent of friction. Such models would not then reproduce similarity of fluid movement adjacent to solid boundaries or accurate velocity distributions: The 'boundary layer' would not be accurately represented. There are also other force ratios, such as that between inertia and surface tension forces, known as the Weber number, which must often be considered as insignificant.

This approximation to dynamic similarity then results in discrepancies between the model and the prototype known as 'scale effect'. This scale effect limitation means that models may not be constructed to represent the whole of a prototype behaviour, but only to investigate certain aspects of that behaviour. Consequently, often more than one model is necessary to study a prototype completely.

(2.3) Models involving relative motion between a fluid and a structure

The previous section (2.2) may be summarized as follows:

1. The quantities describing a prototype fluid behaviour must be grouped into dimensionless ratios to apply to all sizes of that particular fluid mechanic system.
2. A model of that system should have numerically the same values for those dimensionless groups if scale effect is to be avoided.
3. Due to the impossibility of achieving this condition with reduced size models the equality of the most important dimensionless ratios only is achieved. Scale effect then results from neglect of the other ratios.
4. Dimensional analysis will give guidance as to the most appropriate form of the dimensionless ratios.
5. Any model quantity scale is determined from the equality of force ratios.

These principles are now applied to the present work which involves

- (a) The development of a model water wave facility,
- and (b) an experimental investigation of forces on a relatively moving circular cylinder immersed vertically in water.

As both of these are laboratory model situations their relevance in terms of potential prototype (or indeed other model) behaviour is of paramount interest.

(2.3.1) Models where water surface waves are significant

Waves are required in coastal and offshore engineering models, the possibilities being given comprehensively by Wiegell (1974). Not all of the situations described can, however, be modelled successfully.

A simple description of water surface waves is required in order to consider the modelling difficulties.

Water waves (see also Appendix B)

Waves on the surface of water can be produced naturally by

- (i) Wind
- (ii) Tides
- and (iii) A disturbance in the body of liquid

In (i) and (ii) the wave trains may be considered as pseudo-periodic, effectively continuous. However in (iii) the waves tend to be discontinuous as only a single wave train may be generated. Experimentally the wave train required depends upon the particular problem examined. A continuous wave train is necessary to study the cumulative effects of waves, such as fatigue loading of immersed structures. In such cases a model of the required wave amplitude - frequency spectrum (Appendix D) is often used. This contains waves of many amplitudes and frequencies and is termed random, or irregular, wave modelling. For ultimate load effects, however, a single wave, or a train of monochromatic (single frequency) waves is used with maximum expected conditions represented such as height and steepness. This is regular wave modelling.

The physical representation of surface water waves at model scale is based upon equality of Froude numbers in the model and prototype. Such a simple representation is, however, often inadequate and cannot be separated from the particular situation under investigation. Wave models are always constructed for engineering purposes to investigate the effects of waves on a structure or a natural feature such as a shoreline. Bed movements due to waves or wave-current interaction effects are common examples. Mehaute (ibid) discusses the relative significance of viscosity in the normally encountered situations, and Schoemaker (1970) gives guidance on modelling procedure when the model is to have a mobile bed. Scale distortion, when the vertical scale is different from the horizontal, may be employed only when the waves are non-dispersive, as for tides or long shallow water waves. Mehaute also calculates that model waves should have a period greater than 0.35 seconds and a minimum water depth of 2 cm to avoid surface tension, or capillary, effects. This water depth is also shown to be the minimum to avoid significant viscous damping caused by the solid walls in the model wave basin. Further generalized discussion of wave modelling is here curtailed and continued in Chapter 4. Discussion in this Chapter will continue to determine the dimensionless parameters concerned with

describing the fluid dynamics of a smooth circular cylinder immersed in any relatively moving incompressible fluid.

(2.3.2) Dimensional analysis

The variety of kinematic conditions considered in this Thesis involve a smooth circular cylinder

- (a) (i) immersed in a steady uniformly flowing fluid
- (ii) being towed steadily through a still fluid,
- (b) (i) immersed in a uniformly, or impulsively accelerated liquid,
- (ii) being uniformly or impulsively accelerated through a still liquid,
- (c) (i) immersed in a liquid moving with simple harmonic motion,
- (ii) moving with simple harmonic motion in a still liquid,
- (d) being vertically immersed, or partly vertically immersed, in a regular water wave train.

In each case the relative movement of the fluid is perpendicular to the longitudinal axis of the cylinder, and consequently there is no preferred flow direction, as the cylinder is circular.

These various kinematic conditions are illustrated in Figure (1.5) and discussed in Chapter 1, the symbols being rigorously defined in the List of Symbols (page viii).

The quantities describing each of the above kinematic conditions are similar, with only particular variations in each case. A generalized dimensional analysis combining all of the possible descriptive quantities into dimensionless Π groups is now developed. The resultant dimensionless groups can then be considered specifically for each of the kinematic cases (a) to (d) above, and modelling laws developed therefrom.

The similarity of force ratios may also be clearly seen between the different kinematic conditions.

The pertinent physical quantities are

(i) <u>Fluid</u>			
dynamic viscosity μ		depth Z	
density ρ			
(ii) <u>Unique surface wave quantities</u>			
wave height	H_w	}	unsteady
a characteristic wave amplitude	A_w		
wave length	L_w		
vertical particle displacement	η_w		
wave displacement	X		
(iii) <u>Cylinder</u>			
diameter	d		
immersed length	L_z		
diameter of end plates (if fitted)	D		
thickness " " " "	e		
mass per unit length	m		
natural frequency (immersed)	f_n		
(iv) <u>Relative kinematics</u>			
a velocity	\underline{V}	}	steady
an acceleration	\underline{a}		
time	t		
particle velocity	\underline{u}	}	unsteady
particle displacement	x		
excitation frequency	f		
vortex shedding frequency	f_s		
added mass per unit length of immersed part of cylinder	m_a		
(v) <u>Dynamics</u>			
total force per unit length on cylinder	F	-	unsteady
acceleration due to gravity	g		

Using the M, L and t system and Buckingham's Π Theorem, one result for the dimensionless parameters that generally applies for the variety of kinematic conditions under consideration, is

$$\begin{aligned} \phi \left[\frac{\rho V d}{\mu}, \frac{d g}{V^2}, \frac{f d}{V}, \frac{m}{\rho d^2}, \frac{E}{\rho d V^2}, \frac{m}{m_c}, \right. \\ \pi_1 \quad \pi_2 \quad \pi_3 \quad \pi_4 \quad \pi_5 \quad \pi_6 \\ \left. \frac{f}{f_s}, \frac{f}{f_n}, \frac{g}{g}, \frac{V}{u}, t f, \right. \\ \pi_7 \quad \pi_8 \quad \pi_9 \quad \pi_{10} \quad \pi_{11} \\ \left. \frac{z}{d}, \frac{x}{d}, \frac{A_w}{d}, \frac{H_w}{d}, \frac{L_w}{d}, \frac{\eta_w}{d}, \frac{X}{d}, \frac{L_z}{d}, \frac{D}{d}, \frac{e}{d} \right] = 0 \\ \pi_{12} \quad \pi_{13} \quad \pi_{14} \quad \pi_{15} \quad \pi_{16} \quad \pi_{17} \quad \pi_{18} \quad \pi_{19} \quad \pi_{20} \quad \pi_{21} \end{aligned}$$

.. .. (2.10)

Π groups 1 to 6 are the dynamic, or force, ratios, 7 to 11 the frequency, kinematic and time ratios. Π_{12} to Π_{21} , the geometric ratios, are developed to incorporate the cylinder diameter d in each case. This is because the relative movement considered is perpendicular to the longitudinal axis of the cylinder, i.e. parallel to the cylinder diameter. Fluid quantities, such as particle displacement x , may then be compared with one cylinder property, the diameter.

Some of these groups can be neglected when considering the modelling of a particular kinematic condition.

The constancy of all of the geometric ratios, Π_{12} to Π_{21} , is ensured by adopting a uniform geometric scale, L_r .

The actual formulation of each of the dynamic Π groups depends upon the relative kinematic conditions. In each case a dimensionless combination of these groups results in an appropriate form. These are summarized in Table (2.1), their physical significance having already been discussed in Chapter 1. In the present Chapter discussion will continue regarding the modelling of a smooth vertical circular cylinder wholly or partially immersed in progressive gravity water waves.

(2.4) Modelling of a smooth vertical circular cylinder immersed in water waves

As discussed in (2.2) and (2.3) successful physical modelling is based upon the equality of dimensionless groups, particularly geometric and force ratios. The fluid dynamics of a smooth vertical circular cylinder immersed wholly, or partially, in water waves may be described, with reference to equation (2.10) and Table (2.1), by the following parameters:

$$\phi \left[R_E, N_k, I_m, F_r, \frac{E}{\rho u_w^2 d}, \frac{m_e}{\rho d^2} \quad \begin{array}{l} \text{kinematic and} \\ \text{..geometric terms} \end{array} \right] \quad \dots \dots (2.11)$$

For true dynamic similarity each of these groups must be equivalent for a prototype and a representative physical model. Unfortunately this is impossible with existing fluids and facilities. Various attempts to produce compromise models have been made, and these are claimed to represent particular aspects of the relative fluid dynamics between the cylinder and waves.

As previously mentioned wave models are normally based upon the Froude natural scale law, as the waves are gravitational (see Appendix B). This is the so called 'short model' of Mehaute (ibid), which assumes that viscous effects are sufficiently small to be neglected. However, it was shown in Chapter 1 that the effects of waves when interacting with an immersed cylinder are strongly influenced by viscous forces. This is expressed by the relative magnitude of Reynolds Number; the lower the numerical value of R_E then the more important are the viscous forces. The displacement of the water particles relative to the cylinder diameter gives a measure of the unsteadiness of the flow field, i.e. for a large particle displacement compared with cylinder diameter the relative flow tends to a steady, or rectilinear accelerative, condition. This unsteadiness is described by the Keulegan Carpenter number N_k as discussed in Chapter 1, as it is the ratio between the distance a surface wave particle moves and the cylinder diameter, in half a wave period.

The force parameter $E/\rho u_w^2 d$ is the ratio between the total force exerted on the cylinder by a wave and the force component which is a function of the fluid velocity squared. This velocity squared force term is the drag component of force, and is similar in origin to the drag force experienced by a cylinder in steady flow. Consequently this part of the total force is strongly Reynolds number dependent, as discussed in Chapter 1.

Combination of the Iversen Modulus Im and the force parameter $E/\rho u_w^2 d$ results in a force ratio between the total force experienced by the cylinder and an acceleration proportional component:

$$E/\rho g d^2 \quad \dots \dots (2.12)$$

This acceleration component is termed the inertia force. Both inertia and drag components may be combined to give the total force by some suitable formulation such as the Morison equation, as discussed in Section (1.3).

The Iversen Modulus is therefore the ratio between the inertia and drag force components when they are combined to produce the total force on the immersed cylinder: $\rho g d^2 / \rho u_w^2 d = d g_w / u_w^2$

The mass ratio $m_e/\rho d^2$ compares the effective mass with the mass of fluid displaced per unit length by the cylinder. This parameter is only of separate importance when modelling cylinders that are allowed to respond elastically in moving fluids. In this rigid cylinder case the effect of the added mass of the cylinder is reflected in the composition of the inertia force term (see Section (1.3.2)).

Collier (1972) developed scaling laws for the modelling of marine cables in which all of these dimensionless groups were incorporated. By considering the cable as a cylinder with a large aspect ratio L_z/d , and then distorting the vertical and horizontal geometric scales, equality of the dynamic ratios between a prototype and a model were achieved. Collier allowed for cable dynamic response due to vortex shedding, as defined by the Strouhal number S , in place of the Keulegan Carpenter number N_k and assumed that the response velocity was small compared with the characteristic velocity (towing or current speed).

Unfortunately such large aspect ratios are only practically encountered in such cases, and the similarity laws developed by Collier cannot universally be applied.

Small scale regular wave models in tanks have been used for some time with limited success. The modelling of the waves in conformity to the Froude scaling law has meant low Reynolds numbers.

Some typical prototype regular wave conditions are described in terms of R_E and N_K by Isaacson (1974) and Verley (1977). These are summarized in Table (2.2).

The success of wave tank models in reproducing typical North Sea conditions may be seen from Figure (2.1) taken from Wheatley & Boyle (1975). Typically the Reynolds number range is below critical ($2 \times 10^5 < R_E < 5 \times 10^5$) in the model and above critical in the prototype. With reference to Appendix A it is apparent that there is a significant difference in the drag force exerted on a cylinder immersed in a steady flow of fluid depending upon whether R_E is in the sub-critical or post-critical region. A similar difference in the drag force component also exists for cylinders in unsteady liquid flows such as waves. This scale effect is unacceptably large for the adequate extrapolation of forces other than for limited ranges.

The low value of Reynolds number is a consequence of the small relative wave heights that can be produced in the laboratory. The maximum single wave heights so far produced in laboratory wave tanks ^{in the UK} are of the order of 1 metre and have been created by towing a beam in contact with the water surface: Hogben (1976). Such waves ^{provide} a Reynolds number in the upper critical range, compared with full scale values in the super critical range.

The Morison equation, as shown in Chapter 1, is composed of a drag and inertia term in phase with the wave particle acceleration and velocity respectively. The force parameters $F/\rho g_w d^2$ and $F/\rho u_w^2 d$ developed from the dimensional analysis indicate that for true similitude the relative proportion of inertia to drag force must be the same in the model and prototype, or at least within the same fluid mechanic regime. The

Iversen Modulus gives a measure of this proportion and so does the Keulegan Carpenter number $N_k \propto (I_m \max)^{-1}$. However, the Iversen modulus is more flexibly defined in terms of instantaneous kinematic values, and therefore varies during a wave cycle. Normally modelling in the past has been based upon the Keulegan Carpenter number as a representation of the relative importance of the drag and inertia components of force. However, the Iversen Modulus describes the force component change throughout a wave period, and may be a more useful parameter when considering the complete force history. Due to the difficulties caused by viscosity, represented physically by boundary layer development, flow separation and vortex effects, models of prototypes which are in the viscous drag regime of Figure (2.1) cannot be produced satisfactorily unless they are at full size. The stronger the inertia component of the total force then the smaller size the model may be. This condition is that the Iversen Modulus should be as large as possible, or that the Keulegan Carpenter number should be small, i.e. the displacement of the water particles compared with the cylinder diameter should be small. Mehaute (ibid) has produced a nomograph showing the relative predominance of drag and inertia forces. He assumes a Morison $C_D = 1$ and $C_M = 2$; the mathematical description of the wave kinematics being based upon first order deep water wave theory. This is reproduced as Figure (2.2) and shows the region of larger H_w/d , and small I_m , where drag forces predominate and satisfactory similitude cannot be achieved.

The relative importance of the drag and inertia forces is a function of

- (i) how far the fluid particles move relative to the cylinder diameter:

$$x_{wmax}/d \approx H_w/d \quad (\text{at the free surface}) \dots (2.13)$$

- and (ii) the size of the cylinder compared with the

$$\text{wavelength:} \quad d/L_w \quad \dots (2.14)$$

If the horizontal distance travelled by a water particle is large in comparison with the cylinder diameter then a signi-

ficant, or well developed wake occurs in each half period before the flow direction reverses. This means that viscous effects, and hence Reynolds number, are important and the drag force is at least as important as the inertia force. For $\chi_{wmax} < C$ the drag force component is small and the inertia force predominates. This is because the region of flow separation is small being unable to develop before the flow direction reverses. In this regime small scale modelling is successful: Mehaute recommends an upper limit for χ_{wmax}/d of 1 for reasonable similitude.

If the cylinder diameter is small in comparison with the wavelength then flow is quasi-uniform, and the inertia force tends to become independent of the wavelength. The cylinder diameter should not exceed 0.2 of the wavelength for the assumptions inherent in the Morison equation to remain valid. If $d > 0.2L_w$ the wave slope and pressure gradient will vary across the cylinder diameter, and for increasing d the effects of the cylinder on the incident wave will become more significant, causing reflection and diffraction. For $d > 0.2L_w$ the diffraction methods of analysis discussed by Standing (1979) should be used.

Figure (2.3) reproduced from Standing shows the different regions of force dominance at the free surface for a vertical surface piercing cylinder, based upon the ratio H_w/d & d/L_w .

The appropriate methods of modelling and analysis may be summarized as follows:

- (i) $H_w/d > 1.0$, $d/L_w < 0.2$ Morison equation with drag effects important; small scale physical models not very successful.
- (ii) $H_w/d < 1.0$, $d/L_w < 0.2$ Drag force of less significance, flow tends to potential; physical or mathematical models, either Morison or diffraction, successful.
- (iii) $H_w/d < 1.0$, $d/L_w > 0.2$ Wave scattering important; use diffraction theory, or physical models to investigate non-linear effects.

Figure (2.4) from Hogben (1976a) relates this information to full scale ocean structures, and clearly shows the increase in the drag force component with increasing N_k ;

e.g. for a 0.5m diameter cylinder with a $\frac{d}{L_w} \leq 0.01$ at least 90% of the total force is due to drag, this corresponds to an R_E of 10^6 and an N_k of 22.

The misrepresentation of viscous effects at low Reynolds Numbers has often been overcome in the past for steady flow models by cylinder roughening and/or trip wires attached to the cylinder surface. This can produce similar boundary layer development and flow separation in a small model similar to that occurring in a prototype at higher R_E . This technique has not so far been successfully extended to wave models, but is discussed by Pearcey (1979).

The relative accuracy with which a model may represent a prototype has so far been considered. The typical values mentioned have been the maximum values required, e.g. maximum wave conditions, and their greatest effects on the cylinder, these occurring at or near the free surface. For a surface piercing cylinder the whole range of force dominant regions may be experienced with increasing depth below the free surface, as particle displacements diminish rapidly with depth. This does then indicate that useful information may be obtained from scale models provided it is realised to what degree results from the model may be extrapolated. The use of a scale model either to understand fundamental hydrodynamic behaviour, or as a design tool, must be considered as two entirely different cases.

Millier & McGregor (1978) give a comprehensive review of the major requirements for wave laboratory models for offshore work, and details of facilities available in the UK. The laboratory modelling of actual full size ocean structures is further complicated by

- (i) The size and shape of the structure - i.e. whether it is monolithic or composed of a lattice of structural members.
- (ii) The greater water depths encountered in the oceans. This makes general laboratory wave tanks difficult to design as the modelling of water depth will frequently dictate a model scale, which may be incompatible with the available wave heights. Hogben

(1978) suggests there is a need for wave basin facilities with significantly variable water depths to overcome this difficulty.

- (j.iii) The irregularity of sea waves in form and direction. Many attempts have been made to produce suitable model facilities to generate both unidirectional and multi-directional irregular waves (see Chapter 4) for use in testing both structural components and complete structures. Owing to the above limitations, however, when extrapolating to full scale prototype conditions, great care must be exercised as to the applicability of any results.

Hamilton (1972) suggests that for irregular wave loading simulation the probability distribution of the maximum total force $P\{F\}_p$ for a prototype may be determined by

$$P\{F_{max}\}_p = (\rho g d^3)_p \times P\left\{\frac{F_{max}}{\rho g d^3}\right\}_m$$

where $P\{F_{max}/\rho g d^3\}_m$ is the probability distribution of the measured maximum non-dimensionalized force in the model, provided the model and prototype seas are statistically similar. He did not, however support this recommendation with test results.

- (iv) The presence of multi-kinematic flow conditions, such as currents with waves. Attempts have been made in the laboratory to simulate this usually by towing a cylinder with a wave field present. See for example Matten (1979) .

(2.4.1) Large scale prototype testing in the sea

The integration of physical model testing with computer simulation for actual ocean structures is discussed by Wootton (1978) as applied to specific examples; the integration being necessary to overcome non-linear and complex problems in the analysis of the response of the structures to fluid loading.

There have been several attempts to model at full scale in the sea - the most recent UK experience being the NMI Christchurch Bay Tower; Bishop (1978) . This type of modelling gives a good check on the validity of

the design process, but it is more difficult to decipher fundamental hydrodynamic behaviour than if a small scale laboratory model is used. Careful statistical techniques are required to extract the most reliable and accurate results possible, as pointed out by Holmes (1978) in his discussion of the Christchurch Bay Tower analysis. This experiment had two circular cylinders within different force regimes covering a potential R_E range from 10^4 to 7×10^6 , with a maximum wave height of 6m. Such parameters are only obtainable at full scale. The greatest limitation of full scale models is that the individual parameters cannot be independently varied, so that data extraction cannot be planned to pursue a particular hydrodynamic theory.

Holmes points out that both R_E and N_k are random variables at full scale, so that small scale model tests relating drag and inertia coefficients to maxima of R_E and N_k are of dubious relevance.

Dean (1976) presents a method for planning a model to investigate the fluid dynamic regions where either the drag or inertia forces dominate. This approach can be used for small scale laboratory, or larger scale prototype testing in the sea, and is claimed to give results of the maximum possible reliability. Dean suggests that the large scattering of experimentally determined drag and inertia coefficients in the Morison equation is caused by poorly conditioned data; this being a function of cylinder and wave characteristics. The usefulness of this presentation with regard to the design of an experiment is considered further in Chapter 4, where an experiment designed primarily to investigate fundamental hydrodynamic behaviour is discussed.

This Chapter has been concerned with the limitations of models of cylinders in waves.

To achieve an insight into the fundamental fluid mechanics of relative unsteady flow between water and a circular cylinder a number of different approaches have been developed. These simplify the confused three dimensional flow field in waves by restricting the particle movements to one or two dimensions only. Within this less complex relative dynamic system the fluid mechanics is reasonably well understood, but the validity of extrapolation from two dimensional to three dimensional kinematic conditions in waves depends upon the phenomenon under investigation, and must be carefully considered.

CHAPTER 3

MODELS WITH SIMPLIFIED KINEMATIC FLOW CONDITIONS

(3.1) Are waves necessary?

To understand the fluid mechanics of the complex interaction of full scale waves and vertical circular cylinders, simplified experimental representations of the fluid flow field have been developed. These representations have application to different sized, 'scaled' versions of themselves, and give insight into the more complex fluid kinematic conditions experienced in wave flows. An extreme case may be that of a circular cylinder immersed in a uniformly flowing fluid; it gives information concerning other circular cylinders immersed in flowing fluids by the application of suitable modelling laws, but what can it tell us about a cylinder in a water wave environment? The relative magnitude of the scale effect obviously determines the answer to this question. The natural sea state is complicated hydrodynamically by:

- (1) The randomness of waves in direction, size and frequency, and consequently kinematics.
- (2) Longer term environmental changes, such as the marine fouling of structural members.

The laboratory models so far considered in this thesis have reduced these complications to investigation involving 'regular' small scale waves. However, this reductionist approach needs to be pursued even further if the fundamental hydrodynamics are to be understood.

Regular long crested waves interacting with vertical cylinders result in a three dimensional fluid kinematic structure. Fluid particles move in all three of the orthogonal planes XY, XZ and YZ of Figure (1.1), as a function of time. This is due to the parallel and transverse wave particle velocity components with respect to the cylinder longitudinal axis (Appendix B). The disturbance to the wave caused by the cylinder produces additional effects

such as vortex shedding which convect in the horizontal plane.

Investigation of vortex inception, development and shedding may be simplified if the vortex field is constant along the length of the cylinder. Unfortunately wave particle kinematics decay rapidly with depth below the free surface, so that any model representing a cross section through the longitudinal axis of a cylinder in waves could not adequately represent the spanwise coherence of vorticity in such conditions (Sarpkaya (1976)). Such a representation, in two dimensions only, would also be inadequate to investigate the effects of the vertical wave particle velocity vector.

Notwithstanding these limitations various two dimensional experimental investigations have been carried out, and conclusions for application to wave flows drawn therefrom. Unlike the water wave situation, in two dimensional models either the fluid or the cylinder may be moved, it is the relative motion that is responsible for the development of the fluid mechanics. The possibilities are:

1. Fluid moving perpendicularly to the longitudinal axis of the cylinder with a

(1.1) constant velocity \underline{U}_0 - unidirectional

(1.2) constant acceleration
 $\underline{U}_a = f(t) = \underline{a}_a \cdot t$ - unidirectional

(1.3) variable velocity and acceleration

$\underline{U}_p = f(t)$ - oscillatory

e.g. for simple harmonic motion (SHM)

$\underline{U}_p = A_p \omega_p \cos \omega_p t$ where A_p is the maximum excursion of the fluid from the mean position.

2. Cylinder moving perpendicularly to its longitudinal axis in an otherwise still fluid with a

(2.1) constant velocity \underline{U}_c - unidirectional

(2.2) constant acceleration
 $\underline{U}_c = f(t) = \underline{a}_c \cdot t$ - unidirectional

(2.3) variable velocity and acceleration.

$$u_{pc} = f(t) \quad - \text{oscillatory}$$

e.g. for SHM $u_{pc} = A_{pc} \omega_{pc} \cos \omega_{pc} t$

A_{pc} is the maximum excursion of the cylinder from the mean position.

Within a wave kinematic field the velocity vector rotates completely through 360° in a vertical plane during the passage of the wave past a point. The relative time that this takes in comparison with the vortex 'response' effect determines how 'unsteady' flow conditions are. Based upon the experimental work of Keulegan & Carpenter (1958), McNown and Keulegan (1959) give the following regimes of unsteadiness based upon the excitation period of motion T compared with the time period T_s between the shedding of vortices from the cylinder (Section (1.3)):

- (i) $T/T_s \leq 0.1$ separation and vortex formation unimportant, drag force negligible, potential flow model (Chapter 1) valid.
- (ii) $T/T_s \geq 10$ motion quasi-steady, similar to a cylinder in steady flow, the formation of a Karman vortex street.

The determination of T_s is the same as that resulting from a steady flow at a characteristic velocity; in this case the maximum in the wave cycle. (This may be determined directly from a functional representation of vortex shedding frequency with respect to Strouhal number $S = f_s d / u_{w \max}$ as given in Appendix A).

So that for $T/T_s \geq 10$ the unidirectional models (1.1), and (2.1) above may be adequate to represent the fluid behaviour, and if acceleration effects are significant (1.2) or (2.2) may be used. Conveniently these two categories of unidirectional steady, and unidirectional unsteady accelerative flow, may respectively be used to investigate the mechanisms resulting in velocity dependent drag forces, and acceleration dependent inertia forces.

The other main advantage gained by using unidirectional models is the large Reynolds numbers possible, particularly for cylinders immersed in airflows. For example Roshko (1961) attained Reynolds numbers approaching 10^7 when investigating the drag force on a circular cylinder in a wind tunnel.

For $0.1 < T/T_s < 10$, however, the unsteadiness of the wave field is important and an oscillatory flow model is necessary. This is because the history of the flow field, preserved in the form of shed and convected vorticity during one half of a cycle, affects the fluid mechanics of the next half of the wave cycle. This is in turn carried over into the following half cycle and becomes a regular unsteadiness. It is this 'memory' within the flow field that is claimed to be responsible for the inadequacy of simple flow models such as the Morison Equation. Two dimensional planar oscillatory flow models, usually operating with simple harmonic motion, also produce this residual effect found in waves. Additionally such models have high Reynolds and Keulegan Carpenter Number ranges, approaching those for full scale cylindrical structural members in the sea.

The use of planar oscillatory, and unidirectional experimental models to investigate the fundamental behaviour of unsteady flow about circular cylinders will now be considered in greater detail.

(3.2) Planar Oscillatory flow models

"We believe that the understanding of plane oscillatory flows past bodies is a necessary precursor to the full understanding of flows due to waves. At this stage it holds out more hope of a realistic theoretical treatment which it may be possible to extend to bodies in waves".

Bearman, Graham and Singh (1978)

Three types of planar oscillatory flow, relative to circular cylinder models, have been utilised to study time dependent flow conditions:

1. Moving fluid:

(1.1) Horizontal cylinder submerged beneath the node of a standing wave, and in a solitary wave.

(1.2) Cylinder in a pulsating, or positive displacement, water tunnel.

2. Moving cylinder.

Oscillating a partially or totally submerged vertical or horizontal cylinder in still water.

Most experiments have used a relative simple harmonic motion (SHM) for ease of analysis and periodic continuity. However; Naull and Milliner (1978a) recently oscillated a vertical surface piercing cylinder with a complex motion of the form

$$x_{pc} = \sum_{n=1}^3 A_{pcn} \sin(n\omega_{pc}t + \alpha_{pcn}) \quad \dots (3.1)$$

Without a three dimensional flow component the dimensionless parameters describing the fluid dynamics of a smooth cylinder moving relatively to a fluid may be inferred from equation (2.10): $F/\rho U^2 d$ or $F/\rho g d^2 =$

$$\phi \left[R_E, N_k, I_m, Fr, m_e/\rho d^2, t/T_p, f_s/f_p, \dots \text{geometric terms} \right] \quad \dots (3.2)$$

for a rigidly fixed cylinder.

The actual formulation of the dimensionless force ratios is as summarized in Table (2.1).

In any unsteady two dimensional flow field therefore, the drag and inertia components of the total force \bar{E} expressed by the variable Morison coefficients C_D and C_M respectively (Chapter 1), are functions of:

1. Reynolds number
2. Keulegan Carpenter number
3. Iversen modulus
4. Frequency structure, and phase relationships, described by a type of Strouhal number and the relative time.
5. Froude number (if there is a free surface).
6. An added mass parameter.
7. Geometric effects, such as boundary proximity and three dimensional, or end effects.

It has also been demonstrated that the relative roughness of the cylinder surface (even if it is apparently smooth): k_r/d is important.

Isaacson (1974) suggests a simplified version of equation (3.2):

$$\bar{E}/\rho \underline{u}_{p \max}^2 d = \phi [R_E, N_k, \underline{t}/T_p] \quad \dots (3.2a)$$

The maximum velocity in the cycle of motion $\underline{u}_{p \max}$ corresponds to the limit of the Iversen modulus, which is represented by N_k , ($I_{m \max} = 2\pi/N_k$ for planar oscillatory motion), so that the force corresponding to this condition is independent of I_m . He also considers that the dominant vortex shedding frequency ratio f_s/f_p is a function of R_E and N_k in this type of flow. The Strouhal number is certainly a function of R_E in uniform flow (Appendix A), but the functional assumption of Isaacson will have to be considered further in this thesis. Similarly the added, or effective, mass term is considered to be incorporated by C_M and C_D and invariant with \underline{t}/T_p . Many authors in the literature propose the assumption of a constant value for C_M (usually the C_M potential flow value of 2), particularly to determine

maximum force values, but there is much evidence that this simplification is inadequate to study the fluid mechanics, as discussed in Chapter 1.

Investigation has been directed to discover the effects of these various parameters upon the relative force between the cylinder and fluid, and to achieve some understanding of the fluid behaviour. It has become apparent as experiments have developed that the force transverse to the velocity vector, often termed the 'lift' force by analogy to aerodynamics, is equally as important as the in line force components. This force is not described in the Morison formulation, but as it is considered to be a consequence of separation and vortex formation it is expressed as a velocity dependent term

(Chapter 1):
$$F_L = \rho d u_p^2 \phi[\dots] \dots \dots (3.3)$$

the functional term being as for equation (3.2), but described as the lift coefficient C_L as discussed in Chapter 1. Transverse, or lift forces occur even in steady flows ($u = U_0$) due to asymmetric vortex shedding.

(3.3) Cylinders beneath the node of a standing wave

Sinusoidal, or nearly sinusoidal gravity waves may be produced in a vertical walled tank in such a way that a standing wave condition is set up, see for example McNown (1957). Beneath the node of such a standing wave the particle velocity is given by:

$$\underline{U}_w = \underline{U}_{wmax} \cos \omega_w t \quad \text{horizontally}$$

and $\underline{W}_w \approx 0$ vertically.

The maximum horizontal particle velocity \underline{U}_{wmax} is a function of the geometric conditions, such as water and immersion depth (see Appendix B).

Therefore if a cylinder is mounted horizontally beneath the node of a standing wave, as shown in Figure (3.1a) the experienced vertical component of velocity will be negligible, and only the horizontal velocity vector will be significant. The variation in velocity field across the cylinder diameter, i.e. with depth, is normally small, depending upon cylinder size etc. (Typically $\underline{W}_w < 5\%$ of \underline{U}_w : Keulegan & Carpenter (1958)). A cylinder so mounted experiences a regular, horizontal, planar oscillatory simple harmonic flow, i.e. the three dimensional wave flow is reduced to two dimensions only. With this type of arrangement the vertical velocity component is reduced with higher wave amplitudes and increasing depth of submergence.

Two significant investigations, McNown (1957) and Keulegan & Carpenter (1958), summarised in Table (3.1), have used this method to study the forces on cylinders and plates. That of Keulegan & Carpenter resulted in a significant breakthrough in the theory; the recognition of the 'period parameter' $\underline{U}_{wmax} T_w / d$, now known as the Keulegan Carpenter number, as an important fluid dynamic ratio. They also presented results showing the variation of the in-line force coefficients throughout a cycle of motion, i.e. variation with the phase parameter t/T_w . Many workers have neglected the variation in these coefficients during a period of motion, preferring to develop results in terms of 'best fit' or RMS values, relying upon the variable kinematics to produce the variations in drag and inertia forces in a period.

The application of the results from the standing wave experimental arrangement to that of wave flows is generally the same as for the planar oscillatory flow discussed in the next section, but due to certain limitations, experimenters have rarely used standing waves for this work since that of Keulegan & Carpenter.

These limitations may be summarized as follows:

1. Horizontal particle velocity decays with depth under the node of the standing wave.
2. The vertical particle velocity is never actually zero. Keulegan & Carpenter suggest that for $\pi z/L > 0.9$, w_w 'becomes less significant'. This parameter then relates the length of the tank L to the water depth z , and limits the dimensions of the apparatus.
3. For wave tanks with $L > 2.5\text{m}$ the analysis of the fluid motion is complex.
4. Surface wave-cylinder size relationships can lead to Froude number scale effects.
5. It is impossible to alter Re and N_k independently in any sort of wave flow without also changing the cylinder diameter. This limitation was largely responsible for Keulegan and Carpenter not realizing that the flow induced forces were Reynolds number as well as N_k dependent.
6. Due to the wave, water depth and tank length inter-relationship the Reynolds number range is restricted to model size only.

This last limitation is perhaps the single greatest disadvantage of this experimental arrangement, due to the scale effect discrepancy introduced by the incorrect Reynolds number range, as illustrated in Section (2.4).

(3.4.) Cylinders in a planar oscillating fluid

The development of the understanding of wave forces on cylinders was further advanced when Rance (1969) clearly showed that the forces were viscosity dependent, as described by the Reynolds number. This advance from Keulegan & Carpenter's work, where there was apparently no correlation between the measured forces and Reynolds number, was achieved using a pulsating water tunnel. The ability to unidirectionally oscillate water particles with an amplitude of $\pm 2.5m$ led to large maximum Reynolds, and Keulegan Carpenter numbers, as shown in Table (3.1). For a cylinder in planar oscillatory flow where the displacement

$$\begin{array}{l}
 x_p = A_p \sin \omega_p t \\
 R_E = 2\pi A_p d / T_p \nu \\
 N_K = 2\pi A_p / d
 \end{array}
 \begin{array}{l}
) \\
) \\
) \\
) \dots \dots (3.4, \\
) \\
) \\
)
 \end{array}$$

Rance showed, using a numerical example, that wave force predictions from small scale models at low R_E were of little use for extrapolation to large scale prototypes, particularly in the drag dominant regime in which his tests were reliable. He illustrated that the boundary layer and wake effects were similar in behaviour to steady flow conditions, in that there are different flow regimes based upon Reynolds number. Transverse force measurements were also made, which showed that the magnitude of the force vector transverse to the strictly planar oscillatory velocity vector could be as much as 60% of the in line force.

The advantages of this type of model compared with the standing wave are:

1. More strictly sinusoidal oscillatory flow, and greater control of the variable parameters.
2. No preferred cylinder orientation, i.e. it may be vertical or horizontal: the only requirement is that the longitudinal axis should be perpendicular to the velocity vector at all times.
(There is a hydrostatic gradient causing pressure differences along the length of a vertical cylinder and unless the fluid is gaseous this will be significant.)
3. Ease of measurement of kinematic conditions.
4. No free surface, and hence Froude number, effects.
5. Greater variability in the range of possible flow conditions, i.e. larger potential R_E and N_k
As $R_E \propto A_p d / T_p$ and $N_k \propto A_p / d$ for a given fluid. . . . (3.5)
6. Flow visualization simpler.
7. Ease of introduction of other kinematic conditions e.g. an imposed steady flow, or a non-sinusoidal kinematic field.

These advantages led many investigators to develop planar oscillatory flow water tunnels. The most famous perhaps, being Sarpkaya with water oscillation in large U-tubes. The original apparatus, and its descendents have enabled him to carry out many useful experiments since 1974. Sarpkaya & Tuter (1974) describe the original apparatus which was excited pneumatically to produce simple harmonic water motion, and operated due to the resonant response of the water in the system. Figure (3.1b) shows a diagrammatic U-tube arrangement. The position of the test cylinder may be in either the vertical limbs, or the horizontal section as shown. Other researchers have developed similar apparatus with different exciting force inputs, see for example Lofquist (1977). Oscillation using a solid water surface displacer, such as a piston, has the advantage that a larger range of frequencies, and hence Reynolds

numbers, can be obtained for a particular Keulegan Carpenter number, compared with oscillations that rely on the resonant response of the U-tube system. This is because N_k is independent of the frequency in planar oscillatory flow, unlike R_E (equation (3.4)).

Notable research using U-tube planar oscillatory flow is summarized in Table (3.1). The advancement of understanding of unsteady flow induced forces on bluff bodies due to this work has already been discussed in Chapter 1; in this section the findings relating to the modelling of full scale conditions are considered.

The following is a summary of the conclusions from the work of Sarpkaya that may be directly related to models:

1. All the components C_D, C_M, C_L of the total force exerted on a smooth circular cylinder in an oscillatory flow are functions of R_E and N_k

2. The Stokes number β (Matten (ibid)) given by

$$\beta = R_E/N_k = d^2/T\rho\nu \quad (\text{when applied to oscillatory flow}) \dots (3.6)$$

has a physical significance greater than that indicated by the components R_E and N_k alone. (for a further discussion of this see Chapter 1).

3. There is good correlation of the force coefficients C_D, C_M and C_L , with β in oscillatory flows.

4. Drag force coefficients C_d obtained from steady flow experiments ($\underline{u}(t) = U_0$) on smooth and rough circular cylinders cannot be applied to oscillatory flow conditions, even for loading in the drag dominant regime. (Figure (2.3)). This is because the free stream turbulence which exists in steady flows (fluid moving) experiments cannot accurately represent the reversing vortex street in oscillatory flows, even for a relatively high N_k .

5. Significant lift forces (a function of the velocity squared) occur even in the inertia dominant regime (Figure (2.3)). Care should therefore be taken when applying potential flow theory in the region $4 < N_k < 8$.

6. The spanwise coherence of vorticity is different in planar oscillatory flows compared with wave flows, due to the kinematic structure of the flow, and the disorganised nature of prototype roughnesses in nature and disposition.

Oscillatory flows correspond to the fully correlated case, and therefore to extreme conditions.

Drag coefficients determined in this way are liable to be the maxima for wave flow conditions. Vortex correlation has been extensively investigated in steady flows and is further considered later in this Chapter.

7. Higher Reynolds numbers may be simulated in oscillatory flow by artificially roughening the cylinder in a similar way to the steady flow case. However, the simple description of roughness in terms of average height k_r to cylinder diameter d ratio is inadequate in planar oscillatory, and also wave flows, as different types of roughness with the same k_r/d ratio have resulted in different drag coefficient variations. This means that there is a significant scale effect when attempting to model the effect of roughness on the flow field. It must be remembered that at full scale roughnesses are randomly distributed and may be either hard or soft.

The conclusion then is that the fluid mechanic complications caused by prototype roughness cannot as yet be modelled, but roughnesses may be useful to produce a higher effective Reynolds number in the model. This possibility is further considered later in this Chapter, and in Chapter 5.

8. For roughened cylinders the Strouhal number S describing the relative rate of shed vortices is independent of R_E for $R_E > 2 \times 10^4$, being approximately constant as 0.22.
9. Below an R_E of approximately 2×10^4 C_L, C_M and to a lesser extent C_D , vary little with R_E . This explains why Keulegan and Carpenter found little

correlation with R_E in their work. Subsequent re-analysis of their data by Sarpkaya using β for correlation shows good agreement with his results.

10. Boundary proximity effects are important if the cylinder is within a diameter of the wall. Sarpkaya (1976) says:

"The case of a wavy or oscillatory flow about a cylinder near a plane boundary is not identical to the case of a cylinder oscillating near a plane boundary in a fluid otherwise at rest due to the effect of the bottom boundary layer".

He thus indicates a potential fluid mechanic difference in these two kinematic conditions.

The work of Sarpkaya involved the use of two U-tube water tunnels, the experimental method being to keep the oscillation period T_p constant for a particular diameter cylinder, and to allow the amplitude A_p to diminish gradually, thus varying N_k and R_E , but maintaining a constant β . This obviously had an effect upon the flow history, and could not be strictly defined as sinusoidal planar oscillatory flow. The effect of this neglect of time history changes is unknown, and is everywhere considered negligible by Sarpkaya.

Matten (1979) points out that Sarpkaya's results show that a significant drop in total force occurs as β increases above 3000 indicating substantial changes in the flow field. This shows that there is a limiting value of $N_k (\approx 12)$ above which scale modelling is dubious. This is the same conclusion already derived in Section (2.4), but developed in a different way.

There have been studies of the effect of oscillating a freestream of air in a wind tunnel, as described by

$$u(t) = U_0 (1 + A_p \sin 2\pi\omega_p t) \quad \text{upon the}$$

flow around circular cylinders; see for example Hatfield and Morkovin (1973). Any application of the inconclusive results to water oscillation only cases is doubtful.

Maul & Milliner (1978) used circular cylinders in a sinusoidally oscillating flow (see Table (3.1)) to investigate the changes in force components during a cycle of oscillation, but did not attempt to relate their results to larger scale prototypes.

Bearman, Graham & Singh (1978) and Bearman & Graham (1979) contend that the force dependence upon Reynolds number as shown by small scale planar oscillatory flow experiments is a function of separation and wake effects. The assumption that this dependence may also exist for large scale prototypes at high R_E may be false. Their u-tube experiments employed a series of sharp edged cylinders (triangular, square and flat plates) to fix the separation points and consequently to produce vortex shedding at lower R_E values, and hence to determine the differences in such cases vis a vis circular cylinders. The results showed a definite similarity between shedding behaviour for all the cross sections, including the circular. The drag coefficients were determined as greater than for the equivalent steady flow case. Both the drag and inertia coefficients exhibited different behaviour for each shape as N_k tended to zero, particularly for $N_k < 15$, and C_M tended to the particular potential flow value. Above an N_k of 50 the drag force coefficients tended to become independent of N_k and approached a fairly similar level; slightly greater than that given by steady flow results. The square section was an exception to this due to its greater sensitivity to relative turbulence levels.

Both Maul & Milliner (1978) and Bearman & Graham (1979) have presented results in terms of RMS force values determined over at least 50 cycles. This is because of the large variation of in-line force coefficients between cycles (as large as 20% in 50 cycles), caused by small variations in the relative strengths and phases of shed and convected vorticity. Consequently a uniform sinusoidal motion often results in a less well defined response. This is particularly noticeable in transverse forces, which can tend to random, as discussed in

Chapter 1. Resultant in-line forces expressed in terms of rms values varied by only 6% over 70 cycles in the experiments of Bearman, Graham & Singh (1978). Comparison with the work of Sarpkaya at a particular β value (approximately 450) showed an inexplicable discrepancy for the circular cylinder case. This difference was further supported by unpublished work of Milliner referred to by Bearman, Graham & Singh (1978). Blockage effects alone were not deemed to be the reason for this difference.

The possibility of a, so far unconsidered, scale effect is thus indicated, particularly bearing in mind the high quality of experimentation maintained in all of these experiments.

Blockage is a significant experimental limitation in any water tunnel, forming an upper bound to experiments in U-tubes. Without blockage and wall proximity problems the range of Re could be extended for a given value of N_k simply by increasing the diameter of the cylinder.

In oscillatory flow, Sarpkaya (1976a) and Bearman, Graham & Singh (1978) respectively carried out some simple experiments with circular cylinders, and various sized flat plates, and their conclusions may be compared:

1. The blockage effect on C_D is greater for higher Re .
2. Sarpkaya is dubious about applying steady flow blockage correction factors to oscillatory flow cases, and suggests that for a cylinder diameter to channel width d/W ratio less than 0.18 blockage effects are insignificant for circular cylinders.

Bearman et al, however, apply the steady flow correction of Maskell (1963) to a series of flat plates with a d/W range of 0.04 to 0.125 and reduce their C_D values by as much as 20%, thus indicating significant blockage effects, as the results then correlate better over the range of N_k used.

The maximum correction to be applied to Sarpkaya's results would have been only 6%, but he considered

the blockage correction based upon the condition of maximum velocity to be erroneously applied to any other kinematic condition, such as the maximum acceleration, during the cycle.

End, and aspect ratio L_z/d effects will be discussed at the end of this Chapter.

(3.5) Cylinders oscillating in a still fluid

Isaacson (1974) and Sarpkaya (1976) review the work of Thirriot, Longree & Barthet (1971) who first showed that Keulegan & Carpenter's results could be re-represented in terms of an R_E as well as an N_k dependence of C_D . Their own experiments consisted of oscillating cylinders in a tank of still water, the results from which corroborated their findings relating to Keulegan & Carpenter's results, and consequently supported the conclusions of Rance (1969). The difficulties inherent in such an experimental arrangement were also detailed.

In Chapter 1 it was shown that there is no difference in the relative flow field if the fluid or the cylinder is accelerated, but there is an additional Froude-Krylov inertia force component existing if the fluid is in unsteady motion.

Sarpkaya (1976c) has considered extensively the relative merits of oscillating a fluid around a cylinder or oscillating a cylinder in a still fluid. For a given experiment the choice appears to depend upon the available resources and the information required. The method of measurement to be adopted is crucial. For example forces are usually determined indirectly from reaction measurements (via force transducers) at support points, this makes the oscillating fluid apparatus more attractive because an oscillating cylinder will transmit a high self weight inertia tare force to the support members, which would dominate the force records and mask the hydrodynamic forces.

Reaction force measurements, however, can only measure total forces upon the immersed body, so that no three dimensional effects can be seen. Pressure measurement via tappings around a circumferential ring on the cylinder will give a strictly two dimensional record, and if coupled with simultaneous longitudinal pressure tappings, a detailed investigation of three dimensional effects.

For pressure measurement at enough positions on the cylinder circumference the dimensionless force ratios from the dimensional analysis may be conveniently replaced by the dimensionless pressure coefficient

$$C_p = \frac{p_{pc}(\theta, t) - p_\infty}{\frac{1}{2}\rho U_{pc\max}^2} \quad \dots \quad (3.6)$$

where p_{pc} is the normal pressure on the cylinder with respect to position θ and time t .

p_∞ the ambient undisturbed fluid pressure
and $U_{pc\max}$ the maximum oscillation velocity.

If pressures at enough points (θ) are measured simultaneously the forces can be determined by integration.

The principal limitation of pressure recording, and subsequent integration to determine forces, however, is that for anything other than RMS force values, a number of simultaneous pressure measurements must be recorded. This is due to the non-stationary nature of the force history, even over fairly short periods of time, particularly when the lift force is being investigated, (see Chapter 4). Such recording is normally expensive and requires a significant size of cylinder to accommodate the pressure tappings and/or transducers.

Integration of pressure records to determine force histories also implies interpolation between the tapping points, so that they must be as close as possible to avoid missing any significant effects. Pressure records also neglect the effects of skin friction in the total force composition, but can lead to an easier visualisation of the flow field changes with time.

Apart from these considerations the merits of oscillating the fluid or the cylinder may be summarized as follows:

1. Lower free stream turbulence levels with an oscillating cylinder.
2. Less blockage and wall proximity effects when oscillating the cylinder, but more significant free end effects. Enlarged 'end plates' may be necessary to eliminate three dimensional flows around the ends. Oscillating fluid experiments rely upon large amplitudes of particle motion to obtain high R_E values, this in turn leads to high N_K values. It is therefore difficult to obtain low N_K values for a given R_E . However, by varying the oscillation amplitude only, $\beta (= d^2/T_p v)$ may be kept constant while N_K varies.
3. When oscillating the cylinder, apart from the difficulty of signal conditioning due to the large self weight inertia term as mentioned above, there may be similar difficulties caused by frequency response. The system ; the apparatus and transducers, should have high natural frequencies to avoid resonant excitation, this means that transducer sensitivity will consequently be reduced.
4. Free surface disturbances such as waves occur when oscillating cylinders unless the apparatus is driven by an immersed mechanism. The mechanism itself could, however, create flow field distortions. Yamamoto & Nath (1975) for example, drove fully immersed horizontal cylinders using a cable arrangement that caused very little free surface disturbance. Lamb (1932) develops an expression for horizontal cylinders moving beneath a free surface. Only for an $F_r \rightarrow 1$, where F_r is calculated based upon the depth of submergence, will the wave resistance be significant. The analysis assumes that the cylinder submergence depth/diameter ratio is large. Bishop & Hassan (1964) reported no apparent wave resistance for their horizontal cylinders moving in water, although they tried different submergence depths. The maximum value of F_r in these experiments being 0.375. Surface piercing cylinders obviously produce potentially greater free surface effects, and are often avoided for this reason. (This is further discussed in Chapter 4).

5. Fluid oscillation in U-tubes requires careful avoidance of corner separation effects, and a sufficient length of test section for conditions to become stable. Free surface instabilities in such apparatus when the fluid is accelerating downward are also a problem.

6. High frequency vibration of oscillating cylinders is also common and may need to be removed from the data record using electronic filters. This often leads to phase shifts which are difficult to assess.

An example of significant vibration is given in the discussion of the oscillating cylinder work of Garrison, Field & May (1977) by Sarpkaya & Collins (1978).

7. Oscillating cylinder records produce inertia forces that are a function of the added mass coefficient only, because there is no Froude Krylov component. This can lead to lower experimental errors.

Figure (3.1c) shows a typical arrangement for an oscillating cylinder in otherwise still water.

There have been many experiments reported in the literature where a body has been oscillated in an otherwise still fluid. The limiting condition of small Reynolds number ($\ll 1$) as originally investigated by Stokes (1850), and latterly Schlichting (1960) and Williams & Hussey (1972), have utilized cylinders oscillating in liquids due to simple or compound pendulum action. Such low Reynolds number ranges are of little relevance to the subject under discussion. However, the production of a steady streaming motion at an ever-increasing distance from a circular cylinder oscillating in a liquid is rather surprising, but is predictable using a potential flow model, even though it is a result of viscous forces. Other experiments; King (1971) and Stelson & Mavis (1957), for example, have oscillated cylinders in natural modes and as compound pendula to determine added mass coefficients and viscous damping characteristics. It was the work of Stelson & Mavis that showed experimentally that the virtual mass coefficient C_M , for a circular cylinder oscillating in a water tank, tended to the potential flow value of 2 for high aspect ratios ($L_z/d > 10$).

Another group of experiments has been concerned with the forced oscillation of cylinders in a freestream of flowing fluid, this was Mercier's (1973) principal work, for example. Oscillation can be either in-line or transverse to the freestream. The convection of vorticity away from the cylinder due to the freestream velocity removes any 'history' effect from one cycle to the next, making such experiments incompatible with purely oscillatory flow, other than as a possible limiting boundary. This type of flow is possibly quite relevant to waves, however, and is consequently further considered in Chapter 5.

The planar oscillatory experiments particularly relevant to this work are summarized in Table (3.2).

The experimental limitations of the oscillating cylinder model have been tackled in these experiments in a number of ways:

(i) Surface waves (Froude number effect):

Heinzer & Dalton (1969) had capillary wave problems, so that their maximum oscillation velocity was restricted. Hamann & Dalton (1971), however, installed wave absorbent material at the sides of their tank. Mercier (1973) similarly used vertical surface piercing cylinders, but covered the free surface to prevent waves forming, as did Glass & Kemp (1978), who used a horizontal cylinder. In the absence of surface waves, flow visualization was achieved using buoyant particles on the free surface by Isaacson (1974).

(ii) Boundary effects:

Chung (1976) oscillated horizontal cylinders close to the free surface to investigate the effects upon the added mass and wave damping of the proximity of the boundary. He found that for a depth of submergence to cylinder radius: $Z_{ipc}/r \geq 8$ the fluid dynamics were the same as if the fluid interface were at infinity. These results were only for the region $N_k < 1$, and it is doubtful if the submergence ratio limit derived applies outside this region.

Yamamoto & Nath (1976) oscillated a horizontal cylinder in water near the bed of a tank. Their results indicated that the limit suggested by Sarpkaya (1977b), of one cylinder diameter as the minimum clearance to avoid significant effects upon the force coefficients by the solid boundary proximity, is inadequate for an oscillating cylinder.

This endorses the statement made by Sarpkaya (page 91) that the oscillatory fluid and cylinder cases are fluid mechanically different adjacent to a solid boundary.

(iii) Subtraction of inertia tare of cylinder:

Most investigations reported subtracted this by either initially, or simultaneously, oscillating the cylinder (or a dummy) in air and differencing the strain record signals. There was no discussion as to the distortion of phase information that could result from this process. Bishop & Hassan (1964) show that lift force phase angle relationships are different for oscillation in air and water, and even vary for oscillation in water at different A_{FD} values. This then confirms the danger of subtracting the inertia tare determined by oscillation in air from the oscillation in water record, due to a loss of phase information. Issacson (1974) and Chantranuvatana (1974) both used a single pressure tapping and rotated it to a different angular position for repeated cycles of motion, assuming a certain stationarity of the pressure distribution. This procedure is doubtful, even for average or RMS values, and is certainly inadequate for detailed investigations.

(iv) Three dimensional, end and blockage effects:

A number of experiments used 'active' middle cylinder sections with 'dummy' ends, the strain gauges then recording the reactions of the live portion only. Chung (ibid) varied the dummy lengths to show that there was no effect, but gives no details, other than to confirm that the results agreed. Garrison, Field & May (1977) fitted end plates of a radius 19mm larger than the cylinders tested, as well as keeping the end of the cylinders as close to the wall of the tank as possible. The results of Bishop & Hassan (1964), however, for cylinders in a steady flow of water suggest a difference in forces with and without end plates, even when using 'active' and 'dummy ended' cylinders (Section (3.6.3)).

Barnouin, Mattout & Sagner (1978) and Chantranuvatana (ibid) apparently did not consider three dimensional effects.

Grass & Kemp (1978) give the only reported blockage ratio of 1 : 5.6 for their oscillating 50mm diameter smooth and sand roughened cylinders. There is no discussion, however as to the significance of this figure.

(3.6) Unidirectional kinematic models

(3.6.1) Oscillatory or unidirectional?

Relative simple harmonic planar oscillatory motion between a cylinder and a fluid is shown in Figure (3.2). From Chapter 1 the motion, in this example, of the cylinder, may be considered at each relative time or phase position t/T_p :

- (i) $t/T_p = 0$; Maximum acceleration toward mean position, zero velocity, maximum displacement.
- (ii) $t/T_p = \frac{1}{4}$; zero acceleration, maximum velocity in direction of previous acceleration (i), zero displacement.
- (iii) $t/T_p = \frac{1}{2}$; maximum acceleration toward mean position, zero velocity, maximum displacement (at opposite extreme to (i))
- (iv) $t/T_p = \frac{3}{4}$; As (ii) above, but velocity vector in opposite direction.
- (v) $t/T_p = 1$; As (i), i.e. motion periodic. It is therefore possible, by analogy to steady flow, that:

- (1) If the instantaneous $R_E(t) = \underline{u}_p(t)d/\nu$ is everywhere less than unity potential streamline pattern will exist, and there will be no separation.
- (2) For higher $R_E(t)$; separation will occur, for $30 < R_E(t) < 80$ the laminar wake will be unstable, and for $R_E(t) > 40-80$ an alternate vortex street will occur.
- (3) For $R_E(t) > 10^5$ approximately, the turbulent boundary layer will shift its point of separation farther from the front stagnation point and the drag force on the cylinder will drastically reduce due to the reduction in wake width.

For oscillatory, or wave motion, low values of $R_E(t)$ occur during the oscillation period when $\underline{u}_p(t)$ is close to zero, i.e. near the maximum displacement from the mean position (at the amplitude of motion). The upper limit of $R_E(t)$ will occur at the mean position,

and is a function of x_{pmax} , f_p and d , as well as the fluid properties; so that $R_E(t)$ could be within any of the ranges (1) to (3) above, and the cylinder experience each of them during a period of movement. However, steady flow results do not necessarily represent an oscillatory flow condition. The viscous effects in any fluid moving relative to a cylinder are 'excited' at higher velocities (i.e. after the onset of separation). The relative separation of the excited effect (such as a shed vortex) and the cylinder, a finite time interval after the exciting has occurred, depends entirely upon the relative kinematics. In oscillating flows the excited phenomena in the form of a residual flow 'history' may come into contact with the cylinder again as the flow direction reverses. In unidirectional flows the viscous history is convected away from the cylinder whether the flow is steady or unsteady. In steady flows the 'experience' of the cylinder with respect to time is constant, apart from any vortex shedding, which is periodic. Thus a steady flow may result in a steady non-uniformity, which in turn results in unsteady drag forces and, if the viscous effects are asymmetric, periodic lift forces. For 'starting' steady flows, $\underline{u}(t) = \underline{U}_0$ is achieved after an initial period of large acceleration ($g \rightarrow \infty$), in such cases viscous effects quickly become established. Chang (1970) gives a theoretical expression (after Blasius) relating the distance the fluid moves relative to the cylinder S_s , compared with the cylinder diameter, before separation occurs:

$$S_s/d = 0.16 \quad \dots \dots (3.7)$$

for an 'impulsive starting' motion from rest;

i.e. $\underline{u}(t=0) = \underline{U}_0$, $g(t=0) \rightarrow \infty$, $g(t \neq 0) = 0$

This indicates that there is a finite time required for viscous effects to become established. The conclusion from this that may be related to oscillatory flows is that the instantaneous $R_E(t)$ may not in fact describe the fluid condition at time t due to the 'response' time. So the $R_E(t)$ for an oscillatory flow may not be used to

determine fluid conditions based upon steady flows at the same value of R_E .

Chang (ibid) also gives the corresponding distance for a relative constant acceleration from rest:

$$s_s/d = 0.26 \quad \dots \quad (3.8)$$

$$\underline{u} = f(t), \underline{a}(t) = \underline{a}(t \rightarrow t_\infty)$$

i.e. separation does not occur until the relative movement is 1.6 times that of the impulsive starting motion case.

The oscillating cylinder has a gradually diminishing acceleration from a maximum, which is suddenly applied at the amplitude of motion. Decelerating conditions cannot be the same as accelerating, because the wake is not being convected as far relative to the cylinder. As the cylinder stops at the amplitude of motion, the wake, which is behind it, sweeps past, and there is a residual force, even though the cylinder is no longer in motion. This force is in the opposite direction to that immediately preceding, and consequently reinforces the force at the beginning of the now reversed motion in the next semi-cycle.

The relative strength of the viscous flow history in one semi-cycle decides the residual effects which may persist throughout the following semi-cycle. One measure of relative flow history is the number of vortices shed in a semi-cycle. For a given maximum R_E , this must depend upon the relative distance travelled by the cylinder in the fluid in a half period; obviously the greater distance travelled, then the greater tendency to steady flow conditions (although the motion is gradually decelerating). In steady flow the rate of vortex shedding is predicted by the Strouhal number S , which is a function of R_E . This may be an upper limit for oscillatory flow. Therefore the higher the value of N_k , the more vortices will be shed, up to this limit, although, as already indicated, there is not necessarily any correlation between steady flow R_E

values and oscillatory $R_E(t)$ values as regards viscous fluid behaviour. In Chapter 1 it was shown, based upon Keulegan & Carpenter (1958), that theoretically one vortex will just be shed per semi-cycle if $N_K = 10$, based upon an $S = 0.2$ (for $R_E > 800$).

The other important consideration is the persistence of the vortices. This is expressed by the rate at which they diffuse into the surrounding fluid. If the rate of diffusion is relatively small, the residual vorticity from one semi-cycle can retard the development of vortices in the following. Isaacson (1974) observed this phenomenon at N_K values greater than 20.

For any relative unsteady motion between a fluid and cylinder Hamilton (1972) suggests the following form of equation to determine the in-line force-time history:

$$E(t) = C_d \frac{1}{2} \rho u |u| + C_m \rho \frac{\pi d^2}{4} \ddot{a} + \dots \dots \text{History effects} \quad (3.9)$$

This equation is similar in form to the Morison equation (1.41), but the coefficients C_D and C_M assume their steady and potential flow values respectively. Deviations from this model are catered for by the history term.

He points out that for planar oscillatory motion, or any simply periodic motion, history effects need not be considered explicitly, because force will be simply a function of phase, and may be defined by a harmonic series. Such a simple model, which assumes stationarity of in-line forces for planar oscillatory motion, is naive. The work of Bearman et al (1978) already reported in Chapter 2 indicates that there is a strong history effect which has no apparent periodicity. This will be further pursued in Chapter 4. History effects are then present even in an apparently periodic flow. Hamilton (ibid) has used the results of Sarpkaya (1966) to show that the history term in eq.(3.9) must be non-linear to be generally applicable. Sarpkaya accelerated

water from rest past a horizontal circular cylinder, and then maintained a constant velocity. Figure (3.3) shows the in-line force results, with the calculated drag and inertia terms subtracted. The acceleration part clearly shows that the definition of total force in terms of instantaneous $R_E(t)$ based C_d values, and a potential flow $C_m = 2$ is inadequate because the history term is not zero. Added mass incorporated into the inertia coefficient C_m could be considered as a variable if the history term were neglected in this case. Discussion in the literature concerning the added mass of circular cylinders is confused by the lack of appreciation of history effects. Added mass is either considered as a function, or independent, of time as well as shape, and orientation (Chapter 1).

It is apparent that relative unsteady motion can occur in the form of:

1. An impulsively started motion up to a limiting constant velocity.
2. A constant gradual acceleration.
3. A sudden stopping.
4. A gradual stopping.
5. An oscillatory motion impulsively started.

The relationship between any of these kinematic conditions and a planar oscillatory, and thence a wave, motion must be further considered.

The forces resulting from a relative non-periodic unsteady flow may be described in terms of the following significant quantities, from equation (2.10):

$$\begin{aligned}
 & F(t)/\rho u_d^2 d, \text{ or } E(t)/\rho d_d^2 d^2 \\
 & = \phi \left[R_E(t), I_m, S, F_r \cdot \frac{m_e}{\rho d^2}, \begin{array}{l} \text{kinematic and} \\ \text{geometric} \\ \text{terms} \end{array} \right] \\
 & \dots (3.10)
 \end{aligned}$$

The variation of each dimensionless parameter as a function of time will be considered within the context of the type of unsteady motion.

This leads to the general equation for the total force per unit length:

$$F(t) = C_D \frac{1}{2} \rho d u(t) |u(t)| + C_M \frac{\rho \pi d^2 a(t)}{4} \quad (+ \text{ history}) \quad \dots \dots (3.11)$$

$C_D(t)$ and $C_M(t)$ are now functions of time because they are a function of $\left[R_E(t), I_m(t), S(t), \frac{m_e}{\rho d^2} \right]$ kinematics & geometry (3.12)

Because of this time dependence the history term may or may not now be included. It should be noted that the Keulegan Carpenter number has no meaning for non-periodic flows because it represents a maximum condition (i.e. the limit of $I_m(t)$). The Froude number may also be neglected if there are no free surface effects.

(3.6.2) Relative unidirectional acceleration

For a uniform acceleration such that $a_t = a_{t+\delta t}$, $I_m = d/2s$

where s is the distance travelled by the fluid relative to the cylinder.

Experimental work in this area has been concerned with uniform and impulsively started unidirectional acceleration (or deceleration).

Analysis has considered either equation (3.11) to describe the force, e.g. Sarpkaya & Garrison (1963), or a formulation such as

$$F(t) = C(t) \frac{1}{2} \rho d u_a^2(t) \quad \dots \dots (3.13)$$

$C(t)$ being functionally represented as C_D and C_M are in equation (3.12)

e.g. Keim (1956). Coefficients $C_D(t)$, $C_M(t)$ and $C(t)$ have been considered as independent of, or as functions of, time, and attempts have been made to assign steady flow, or potential flow values to C_D and C_M respectively, and allow for force variations in the variation of the other coefficient, or by means of a history term.

Iversen & Balent (1951) accelerated discs through a still

fluid in a direction perpendicular to their longest surface with a constant driving force, and showed the dependence of $C(t)$ in equation (3.13) upon I_m .

It was also shown that the added mass, which may be expressed by the parameter $m_e/\rho d^2$ in equation (3.12), was a function of u_a and q_a as well as body shape, if the value was calculated assuming a constant (steady flow) value of $C_D = C_d$. This illustrated that the assumption of a steady flow value for C_D and a potential flow value for C_M in equation (3.11) would be incorrect except where the added mass tended to its potential flow value at high I_m , as would be expected. No correlation of these conclusions with R_E was attempted, although the importance of viscous effects at high I_m values was noted.

Prandtl, reported in Prandtl & Tietjens (1957), and Schwabe (1935), moved cylinders impulsively from rest and photographed the unsteady fluid separation growth and behaviour. Schwabe applied the unsteady Bernoulli equation to the velocity field predicted by the movement of buoyant particles to determine pressure distribution changes with time. This technique clearly showed the time rate of change of pressure distribution with vortex development. The experiments covered an S/d range ≤ 3 , by which time asymmetric vortex shedding had begun. Schwabe identified the existence of a lift force, and an increase in in-line force with time, as well as changes in the boundary layer separation point.

Keim (1956) accelerated cylinders with a constant driving force through still fluid, similarly to the Iversen & Balent approach with discs. He concluded that

$$C(t) = \phi [R_E(t), I_m(t), Lz/d]$$

for his work, in the range $0.01 < I_m < 10$ and up to $R_E = 10^3$. Above an R_E of about 10^3 , (a maximum of 4.75×10^5 being achieved), $C(t)$ was apparently independent of I_m and tended to the steady flow value, which is sensibly constant at 0.95 for $10^3 < R_E < 5 \times 10^3$. This corresponded to the higher velocity, or lower I_m range. There were also aspect ratio effects noticed

for $L_z/d = 5$ compared to 15 and 30, similar to steady flow results. He also postulated that the Iversen modulus (or acceleration modulus) alone was inadequate to describe changes in acceleration, and that $C(t)$ should also depend upon the highest order of rate of change of acceleration that exists in the flow:

$$d\underline{a}/u_d^2, (d\underline{a}(t))^2/u_d^3(t), \dots \frac{d^{n-1}}{u^n(t)} \times \frac{d^n s}{dt^n} \dots \dots (3.14)$$

this being an expression of flow history, because similar velocities and accelerations may result in different forces depending upon the way in which the kinematic parameters are changing in time. The lumping of all dimensionless variables in a single coefficient $C(t)$, as in this experiment, avoids the necessity to consider these higher order groups explicitly.

The greatest limitation of these experiments is the inability to control independently the velocity and acceleration.

Laird, Johnson & Walker (1959) in an attempt to understand wave-cylinder fluid dynamics towed horizontal circular cylinders in still water with a range of velocities and accelerations commonly encountered in wave environments. The findings of Keim (ibid), that there is no force coefficient correlation near the early onset of boundary layer transition, which was found to take place in this experiment, were corroborated.

The analysis was carried out using an equation of the form of (3.11), but taking $C_M = C_m = 1$, the potential flow value, and thence evaluating C_D . This allowed a direct comparison with steady flow C_d values, which agreed well for results below transitional conditions for cylinders accelerating and at constant velocities in the I_m range < 0.5 . For decelerating cylinders,

however, the results suggested that C_M tended to zero, compared with unity for the accelerating case. The larger the cylinder diameter, or the smaller the aspect ratio, then the greater difference between the accelerating and decelerating cylinder case; the larger the size, the greater the drag coefficient at lower velocities.

The rigorous work of Sarpkaya & Garrison (1963) involved the measurement of the force due to a uniform acceleration of water past a horizontal cylinder. This was compared to a potential flow model, which had been developed based upon the generalized Blasius theorem. The comparison of a 'starting' acceleration with steady flow conditions at the same R_E was shown to be incorrect due to the finite time taken in a starting flow for separation to occur; equation (3.8), consequently the state of wake development, and hence drag force would be significantly different.

The force per unit length was analysed in terms of

$F(t) = C_1(t) \rho a d^2 / 4$ unlike previous investigators, and $C_1(t)$ was shown to be a function of $s/d (\leq 30)$ alone, as there was no correlation of $C_1(t)$ with R_E in the range tested ($10^4 < R_E < 5.2 \times 10^5$). Considerable discussion as to the functional dependence of vortex characteristics was given, and it was concluded that these were also only a function of s : See Section (1.3.1).

For this uniform acceleration case:

$$C_1(t) = C_M + \frac{4}{\pi} \frac{s}{d} C_D \quad (\text{equation (1.25)})$$

i.e. the force could be considered in terms of drag and inertia components, which were calculated with reference to the photographically examined vortex behaviour. From this there appeared to be a correlation between drag and inertia coefficients, as would be expected from their functional dependence upon s/d . For low s/d values (< 0.5), $C_1(t)$ tended to a value of

2, corresponding to $C_M = 2$ & $C_D \rightarrow 0$, i.e. at initial stages of motion the inertia term exists due to the acceleration, but the drag term does not as the velocity is small. C_D and C_M exhibited large changes, associated with rapid vortex growth, for $s/d \leq 2$, the changes being not so pronounced for $2 < s/d \leq 3.5$. At $s/d \approx 3$ the growing vortices were noticeably asymmetric, and the first was shed at $s/d \approx 4.8$. It was predicted that there is an oscillating convergence of C_M and C_D to steady values of 1.3 and 1.2 respectively over the range $5 < s/d < 25$. Sarpkaya & Garrison also emphasised the importance of the higher order acceleration changes; equation (3.14), which exist in unsteady flows other than uniform accelerations, this being particularly relevant for application to oscillatory motions in which these effects exist. These are the history effects that Hamilton (ibid) has attempted to include in the force equation.

Sarpkaya (1966), in a later experimental study investigated the effects of an impulsively started flow past circular cylinders and flat plates with the long surface normal to flow. This 'starting' accelerating period produced separation of the laminar boundary layer at $s/d = 0.295$ (his assumed theoretical value), and all other relative displacements were referred to this. The drag coefficient, defined as

$C_D = 2E / \rho d u_0^2(t)$ increased rapidly from the start of motion, and carried on increasing after the flow became steady at $s/d \approx 0.75$, up to a maximum value of about 1.6 at approximately $s/d = 4$, when the first asymmetry occurred. The drag coefficient then reduced in value until $s/d > 12$ approximately when it became virtually independent of s/d . Vortex shedding, begun at an $s/d \approx 8.5$, and subsequently continued, did not affect the smooth downward trend of C_D .

Again no correlation with R_2 was detected. Exploratory tests conducted using two trip wires positioned at 80° either side of the front stagnation point, produced

greater scatter in the values of C_D , but did indicate for this turbulent case that the steady condition is virtually instantly obtained after the start of motion. Figures (3.4) and (3.5) taken from this paper show these two cases.

Hamilton & Lindell (1971) measured unsteady fluid forces on a suddenly released immersed buoyant sphere. They defined the basic requirements for an equation to describe the force history, which would equally apply to the forces on cylinders:

- "1. At the instant of acceleration from a long period of rest in a still fluid, it (the equation) must reduce to one acceleration dependent term.
2. After steady motion for a long period, the equation must reduce to one constant-velocity resistance term.
3. After the body has been brought to rest, the force given by the equation must be expressed in terms of the prior motion of the body, and must eventually decay to zero."

Obviously this last requirement indicates the need for a history term. Their experimental work then resulted in the production of an accurate value for the added mass of a sphere moving with an unsteady motion through a still fluid, although a formulation similar to equation (3.11) was suggested for the composition of the total force.

The complexity of fluid dynamics resulting from relative unidirectional unsteady flows can obviously be utilized to model oscillatory flow behaviour, particularly at the starting point of each semi-cycle, when the displacement is a maximum. There will no doubt be a difference between a 'starting' oscillatory flow over the first one or two cycles of motion, compared with a quasi-steady, or established oscillatory flow, where a significant residual, or history effect, will exist.

Few published results relate to the effects when a cylinder is decelerating, important over the second half of a semi-cycle, although the results of Laird et al (ibid) indicate that there will be significant differences compared with the accelerating case. Non-uniform acceleration throughout the oscillatory cycle

$$(\ddot{q}_p(t) = \phi(x_a) \text{ for SHM})$$

suggests the force dependence upon a higher order rate of acceleration change term than the Iversen modulus alone, and that the three conditions suggested by Hamilton & Lindell (page 112) for non-periodic flows should also be fulfilled by any equation describing planar oscillatory, and certainly wave flows. Lack of stationarity in force results reinforces this point. Unidirectional flows allow for easier flow visualization studies because of the relative convection of the separated boundary layer away from the cylinder. Similarity to non-convective flows where appropriate, can therefore assist understanding of the boundary layer behaviour in such cases.

(3.6.3) Steady flows

In the steady flow of a real fluid relative to a cylinder freestream accelerations do not exist, other than in secondary turbulence. Consequently equation (2.10) reduces to:

$$\frac{F(t)}{\rho U_0^2 d} = \phi [R_E, S, Fr, \dots + \text{geometry}] \dots (3.15)$$

If there is no close free surface the scale effect introduced by ignoring the dependence of the force upon

F_r will be negligible.

At low freestream R_E the force between the cylinder and fluid is virtually all skin friction, due to the relatively high viscosity. As R_E increases (> 5) the drag force experienced by the cylinder becomes more as a consequence of form drag due to pressure changes, this is accompanied by flow separation and

$$F(t) = C_d \frac{1}{2} d \rho U_0^2 \dots (3.16)$$

$$\text{where } C_d = \phi [R_E, \dots, \text{and geometry}] \dots (3.16a)$$

Vortex shedding results in an oscillating in-line force

so that $\underline{E} = \underline{E}(t)$. Alternate shedding in the form of a Karman vortex street produces a fluctuating transverse, or lift, force $\underline{E}_L(t)$ due to the asymmetry:

$$E_L(t) = C_L \frac{1}{2} \rho U_0^2 \dots \quad (3.17)$$

C_L is similarly a function of R_E .

Batchelor (1970) discusses the necessity for inclusion of some form of Strouhal number S in the functional dependence of C_L . He concludes that it is not necessary for two dimensional flows where all frequency effects are dependent upon R_E .

As defined here $S = f_s d / U_0$ describes the rate at which vortices are shed from the cylinder in steady flows, particularly in the region where strongly defined shedding occurs. S appears to be uniquely a function of R_E over a wide range $60 < R_E < 10^7$, King (1977), and Appendix A. If this is true then the force coefficients C_D and C_L would be functionally dependent upon R_E and geometry effects alone; equation (3.16a)

The paramount importance of R_E in defining the relative drag and lift forces in steady flows may be expected to reflect in oscillatory and wave flow force dependence. It has already been shown that many experimenters have looked for comparable effects in unidirectional accelerative flows. Batchelor's argument is that unsteady phenomena, particularly periodic flows, will not be expected to be adequately represented by Reynolds based models alone, as some form of frequency parameter which is independent of R_E , will also be required. This is borne out in the previously presented reviews of experimental work involving periodic, and also unidirectional unsteady flows.

Extensive work using steady flows has illuminated the following areas relating to steady or fluctuating lift and drag forces exerted on cylinders immersed in moving air or water:

1. The effects of surface roughness on the boundary layer

behaviour, particularly the early transition from laminar to turbulent.

2. Other geometric effects such as aspect ratio, blockage, three dimensional and end effects.

Conclusions from this work may be expected to give some guidance on unsteady flow behaviour. Self excited in-line or cross flow vibrations of flexible, or flexibly supported, cylinders due to steady flow vortex shedding have been extensively investigated recently, and have led to a better understanding of vortex growth and behaviour. There are many discussions and reviews of circular cylinders immersed in relative steady flows. Particularly useful are those by Marris (1964), Morkovin (1964), Chen (1970), and King (1977).

Three dimensional effects

Mair and Maull (1971) summing up *Euromech 17*, point out the low spanwise vortex correlation lengths on circular cylinders in steady flows, that are nominally two dimensional. This lack of coherence of vorticity has been noticed as a variation in the phase and amplitude of shed vorticity with distance along the cylinder longitudinal axis.

Bursnall and Loftin (1951) measured the circumferential pressure distribution on a circular cylinder in a steady airflow at three longitudinal span positions for an aspect ratio of 18 and noticed a difference, particularly in the base pressure region at the rear of the cylinder. These effects were most significant in the subcritical flow regime. Glenny (1966) summarizes the correlation, or vortex shedding cell, lengths reported up until that time, and the R_E ranges tested. The differences over similar R_E ranges are considerable, particularly for $R_E > 10^4$. The conclusion is therefore that there is no definite correlation length relationship with R_E although freestream turbulence levels may be responsible for some of the differences. Glenny also refers to work of Humphreys

who showed that cells of vorticity exist but move about even in steady flows, and form the basic mechanism for the boundary layer transition from laminar to turbulent.

King (1977) summarizes the many investigations of this phenomenon. He concludes that vortex correlation length is a function of Re , aspect ratio, roughness and freestream turbulence. Figure (3.6) is adapted from Glenny and King and illustrates some currently presented results for correlation length in steady flows. The correlation length in comparison with the cylinder length is fundamental in the production of fluid forces. A small correlation/cylinder length ratio would result in reduced forces due to the vorticity phase difference. Models should consequently represent expected prototype correlations. Vortex correlation may be improved by controlling the three dimensionality of the system, for example by fitting circular discs along the length of the cylinder. The vorticity between discs could then be made coherent and in phase between adjacent sections. This would increase the fluid forces. Cylinder vibration, or oscillation can alter the correlation length considerably, see Chapter 5, so that any extrapolation from the, not well understood, steady flow results to oscillatory flows is not recommended.

Another use of discs attached to cylinders that is extensively utilized, is in the form of end plates. This is necessary to overcome the three dimensional effects resulting from flows around a free end. Significant tests by Stansby (1974) and Gowda (1975), have shown conclusively that there are two types of end effect:

1. Where the cylinder has a completely free end, as when a cantilever dips into water.
2. When the ends of the cylinder are close to boundaries, e.g. a cylinder spanning a tunnel, and the ends either terminate at, or close to the wall.

In the former case flows can take place around the free end of the cylinder, distorting the vorticity pattern near to the end. In the latter case the boundary layer of the adjacent surface affects the fluid behaviour in its proximity. End plates can alleviate both problems, but create additional effects due to the boundary layer behaviour on the plates themselves. In steady flows this may be fairly constant and well established, but in oscillatory flows it will vary, and may create great difficulties if the cylinder is short. Aspect ratios are of equal importance in this respect. Observed uniformity of flow behaviour properties along a cylinder span may be misleading regarding the two dimensional nature of the flow. This argument is advanced by Stansby when measuring base pressure coefficients on cylinders with and without end plates in a wind tunnel: The addition of large enough end plates increases the base pressure even if it is uniform along the cylinder length in their absence. Gowda tested fixed and self excited cylinders in a uniform airflow, and found that reduced aspect ratios affected the Strouhal shedding frequency (for $10^3 < R_E < 10^4$) and consequently response characteristics. He recommended an aspect ratio $L_z/d \geq 45$ as a requirement for two dimensional flows, suggesting that aspect ratio variations in the base pressure coefficient, and vortex shedding frequency would then be eliminated. Even for cylinders fitted with end plates having an end plate/cylinder diameter ratio of 10, the Strouhal number varied over the R_E range of 10^3 to 10^4 for an L_z/d below about 40 (Figure (3.7a)). The minimum end plate size D recommended for an R_E of 2.6×10^3 was at least $10d$ to ensure an invariant S/R_E relationship; (Figure (3.7b)). Figure (3.7c) shows the typical span-wise variation of base pressure coefficient with and without end plates fitted. It also shows that Gowda used a nozzle to produce the airflow, thus creating a greater three dimensionality than would perhaps exist in, say, a tunnel. King (ibid) reports that Benard recommends an $L_z/d \geq 27$ as sufficient to ensure freedom from end effects.

Many experiments have been carried out in the past using 'dummy' cylinder ends with 'live' or active centre sections. This is particularly the case where reaction forces have been measured, rather than pressures. The reaction force has then been considered as uniformly distributed along the active length of the cylinder. Bishop and Hassan(1964) noticed significantly different results, for the lift force particularly, using an 'active' cylinder with dummy ends, compared with the same apparatus fitted with plates at the ends of the cylinder. The lift force frequency structure was considerably more regular with the end plates fitted. With end plates $D=4d$ fitted at the ends of the 'active' cylinder length so that $L/d \approx 3$ the wake was stabilized, and at an R_E of 3×10^3 the lift force was apparently non-existent. This is similar to the wake stabilization that is known to exist at lower R_E for wall confinement; effectively requiring a higher R_E to produce an oscillating wake than without wall proximity.

The application of these results to an oscillating cylinder is further considered in Chapter 4, but King(1977a) in attempting to compare the self excited oscillations of cantilevered cylinders dipping into flowing water with the totally immersed cylinder case, noticed significant end effects depending upon the depth of immersion, and called for more research effort in this area.

Blockage

In confined tunnels blockage effects may be a limiting criterion as to the maximum achievable R_E . Corrections have been derived that may be applied to results from experiments where blockage is significant. Bishop & Hassan (ibid) comment that blockage corrections are now an established part of testing procedures, in order to use cylinders of a large enough size. Blockage effects are caused by a wall proximity in the model, which does not represent the often unlimited flow conditions in the prototype. Recent results from Ramamurthy & Ng (1973) show the effect of blockage ratio d/W upon C_D

and S for a range of R_E , using various bluff body shapes in a wind tunnel. These are shown in Figure (3.8 a&b) for circular cylinders only. It is noticeable that if R_E is calculated from the flow gap velocity rather than freestream velocity then there is closer agreement with the unobstructed results. The higher the blockage ratio then the lower the critical values of R_E . The vortex shedding rate described by S is considerably higher for higher blockages. This paper gives useful guidance on modelling, including the contraction effects caused by blockage, but Ramamurthy & Ng do warn that similarity cannot be adequately achieved by a change in velocity scale due to blockage, because the accelerations approaching separation on bluff bodies are also affected by blockage.

Maskell (1963) in the development of his blockage correction factor defined two types of blockage; that due to the wall restraint, which results in an increase in flow velocity termed solid blockage; and that due to wake distortion, known as wake blockage. Roshko (1961) with his very high R_E flows, and Bishop & Hassan (1964) apply the blockage corrections given by Allen & Vincenti (1944) to obtain corrected velocities and drag coefficients. Different researchers may use either the Maskell, or Allen & Vincenti correction, but in oscillatory flows reference has so far only been made to the Maskell blockage correction, Section (3.4). Strictly speaking the Maskell correction is appropriately applied to subcritical flows where blockage is mostly of the wake type, that of Allen & Vincenti being more appropriate where both solid and wake blockage effects are of comparable importance, in the critical region and above.

Freestream turbulence and cylinder roughness

Freestream turbulence levels in an air flow approaching a stationary cylinder significantly affect the reduction in steady flow drag coefficient in the critical R_E region. Surface roughness and 'trip' wires placed long-

itudinally on the cylinder surface also cause significant changes in the $C_d - R_E$ relationship, through local turbulence effects. Fage & Warsap (1923) tested a number of cylinders to investigate C_d dependence upon these parameters, and discovered for $4 \times 10^4 < R_E < 2.3 \times 10^5$

- (i) The introduction of higher turbulence levels to the freestream displaces the $C_d - R_E$ relationship graph laterally to lower effective R_E values, without significantly altering the shape. Below an R_E of 5×10^4 the relative turbulence level had little effect, because C_d is largely independent of R_E for:

$$10^2 < R_E < 5 \times 10^4$$
- (ii) Increasing the surface roughness level attenuates the fall in C_d over the critical region, and displaces the fall laterally similarly to the increased turbulence case. So that for higher R_E (postcritical) values the value of C_d is greater than the smooth cylinder case. This is because the increased roughness retards the boundary layer, and the separation point effectively moves forward (for a given R_E), so that the cylinder drag increases.
- (iii) Longitudinal wires attached to the cylinder surface just in front of the laminar separation point results in $C_d - R_E$ relationship changes depending upon the relative wire diameter/boundary layer thickness. Wires significantly smaller than the boundary layer promote the drop in C_d values (critical region) at a lower R_E . Wires of the same order of magnitude, or greater than the size of the boundary layer cause the boundary layer to leave the cylinder surface, the actual wire size or value of R_E does not then affect C_d .

The implications from this work for high R_E simulation using turbulence, roughness or trip wires, instead of high flow velocities and/or larger cylinder diameters may be further considered in the light of subsequent experimental work.

A number of researchers have investigated the effects of free stream turbulence in more detail than Fage & Warsap. Bearman (1968) investigated the susceptibility of the fluid behaviour to small disturbances and turbulence using air-flow over a circular cylinder. He confirmed the early reduction in C_D with respect to R_E for higher turbulence levels, but using spectral information about the wake velocity fluctuations suggested that the turbulence altered the boundary layer flow around the cylinder without modifying the vortex shedding mechanism. He concluded therefore, that higher levels of turbulence at a low R_E , were not suitable to model higher smoother flow R_E regions. Bruun & Davies (1975) illustrated that changes in turbulence levels affect the pressure magnitude and correlation along the frontal area of the cylinder, (magnitude and correlation affected for $\psi < \pm 30^\circ$, & $\theta \leq \pm 90^\circ$ respectively), but not for the rear part of the cylinder. So that turbulence is also a three dimensionalizing effect.

Steady flow fluctuating lift coefficients were examined by Ferrard (1965) to investigate the discrepancies in published results as a function of R_E . He concluded that differences were attributable to varying levels of freestream turbulence, the effect of which could not be explained by an effective R_E change. The conclusions from these reports are therefore that:

1. Turbulence levels are significant when investigating steady flow C_D and C_L values.
2. Effective R_E values do not adequately describe the fluid boundary layer behaviour.

and consequently:

3. Simulation of high R_E steady flows cannot be achieved by increasing freestream turbulence.

The important conclusion that would also be expected to apply to oscillatory flows is that the effect of turbulence in the freestream cannot be ignored. The oscillating cylinder experiments should therefore be used if such effects are to be avoided, although the relative turbulence created by the cylinder movement and wake compared with freestream

movement past a stationary cylinder is difficult to assess in comparison.

Batham (1973) extensively investigated the pressure distributions on a circular cylinder in an airflow for an R_E range of 1.11×10^5 to 2.35×10^5 .

He tested smooth and rough cylinders with and without imposed freestream turbulence. The results demonstrated the complexities of the fluid behaviour, and the significant differences in each case.

Szechenyi (1975) used two wind tunnels to investigate the possibility of high R_E simulation using roughened cylinders in an airflow at a lower R_E , ($96 \times 10^4 \leq R_E \leq 4.2 \times 10^6$). He concluded that high R_E fluctuating drag and lift force simulation using low R_E values may be achieved provided that the Reynolds number R_δ (based upon roughness diameter δ), was such that $R_\delta > 200$, the relative roughness size $\delta/d < 2.2 \times 10^3$, and therefore $R_E \geq 10^5$. The 'smooth' cylinder case being equivalent to a relative roughness of $\delta/d \approx 3.5 \times 10^5$. Such simulations only apply to reasonably two dimensional flows. Trip wires, Pearcey (1979), may be used to change the laminar boundary layer to a turbulent one at a lower than usual R_E in a steady flow. This creates apparently supercritical conditions where subcritical would normally exist, although the effect upon the separated wake behaviour is not discussed in this context. Pearcey (ibid) also reports rear splitter plate results which show the clear dependence of the drag force upon vortex behaviour, this in addition to the obvious lift force dependence. In this way he attempts to separate the total drag force into components deriving from a uniform flow with and without vortex shedding. This indicates the important effect of the wake behaviour upon all the forces on a cylinder.

Further comparison of steady with unsteady flows is here suspended until Chapter 5, as this Chapter is particularly concerned with the possibilities and difficulties of simplified kinematic condition modelling.

In summary this Chapter suggests that wave models may be expected to simplify into idealized kinematic representations with varying degrees of success, but such simplifications should only be used with considerable caution. Results from unidirectional steady and unsteady flow models would be expected to predict trends in force and fluid behaviour in oscillatory flows. Particularly important are freestream turbulence levels, the increased roughening of the cylinder surface, and the addition of trip wires. Experimental apparatus limitations applicable to unidirectional flows such as blockage or three dimensional effects would also be expected to apply to oscillatory flow apparatus.

CHAPTER 4

A TYPICAL APPLICATION OF HYDRAULIC MODEL THEORY

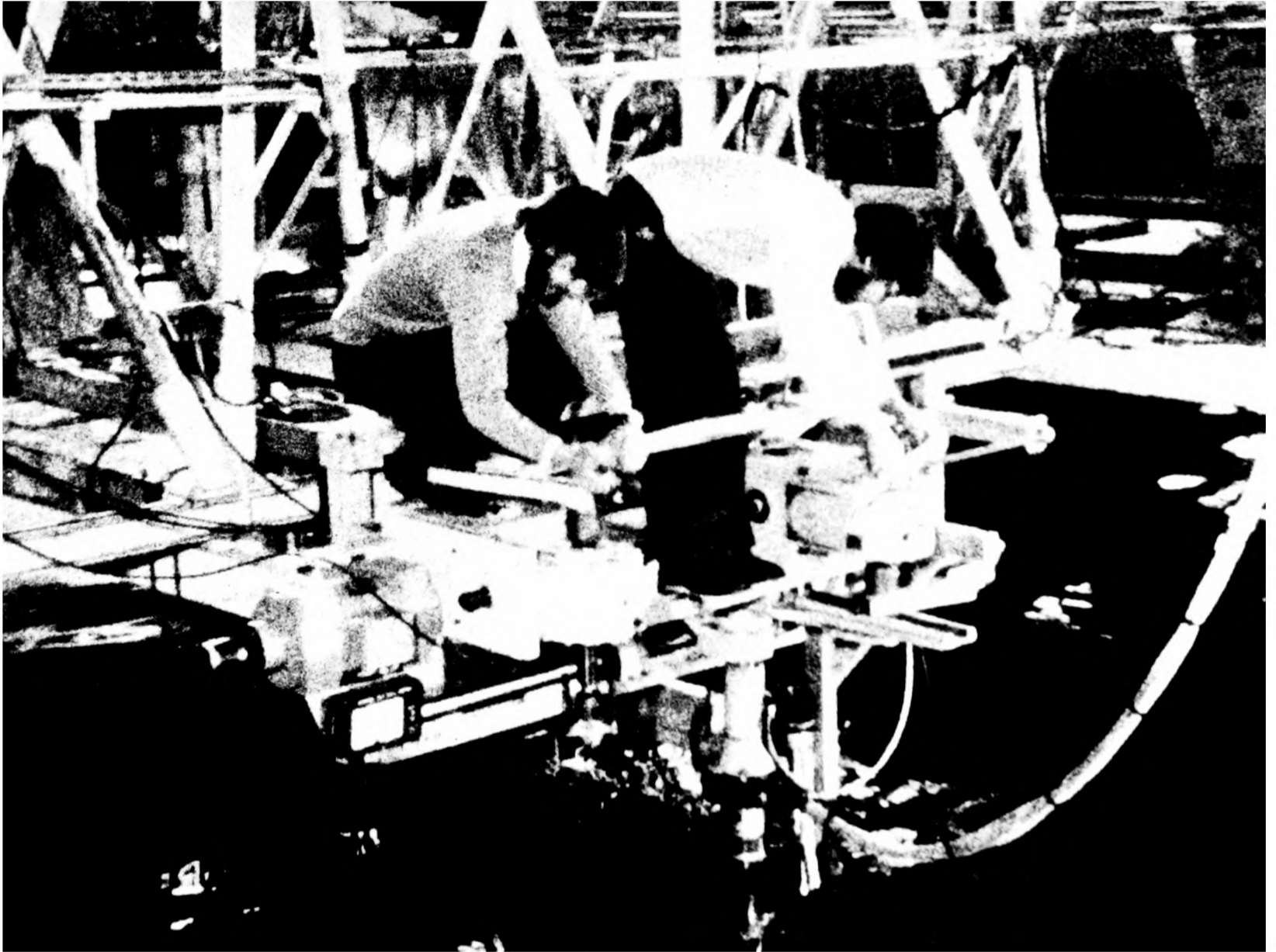
(4.1) Introduction

This Thesis has so far been concerned with a review of previously published work dealing with the relative forces between fluids and immersed, smooth, vertical (in the case of waves), circular cylinders. Intrinsic to this review has been the consideration of the validity of the experimental basis from which conclusions may be drawn relating to

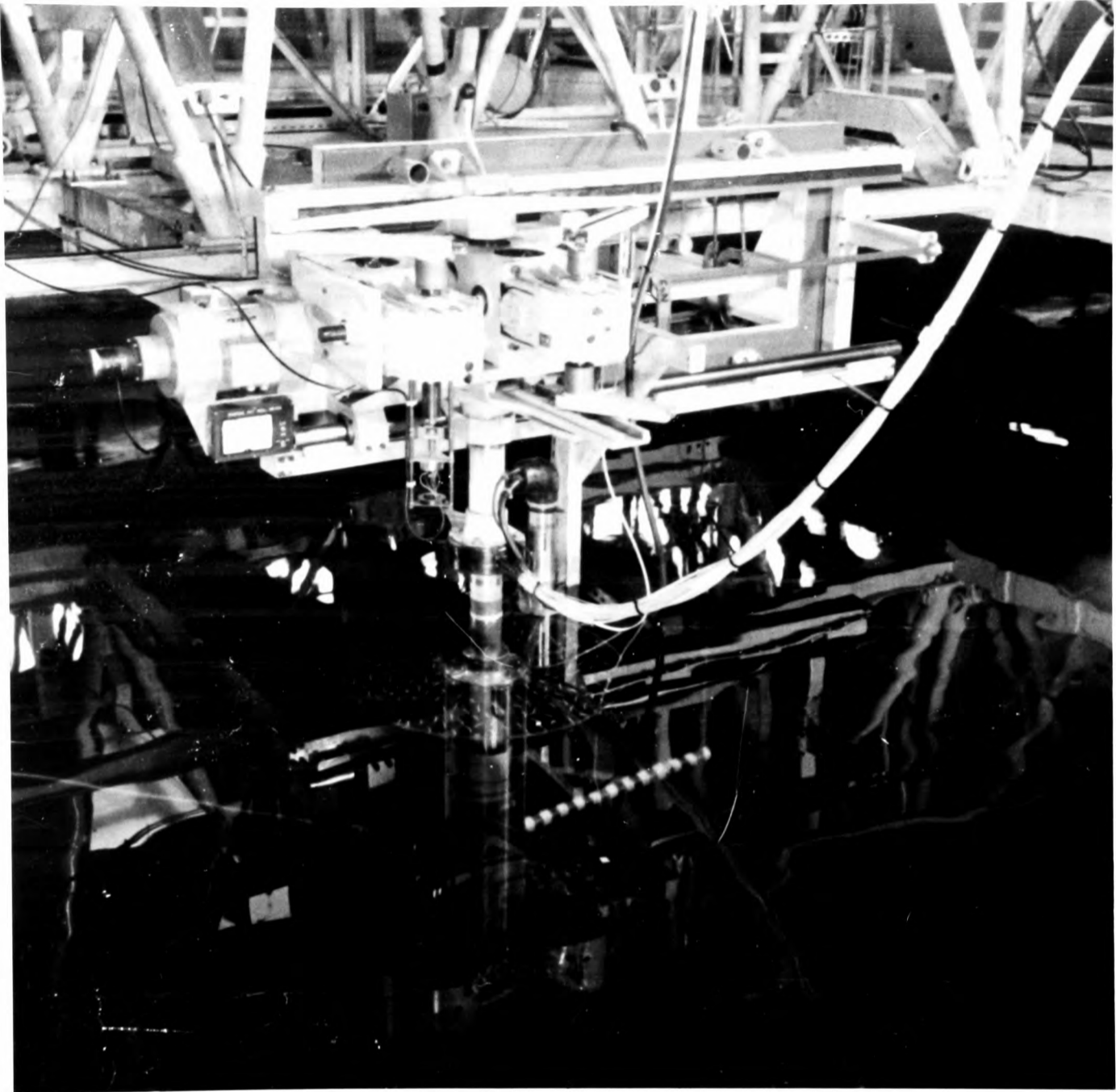
- (i) the detailed fluid mechanics demonstrated by a particular experiment, and
- (ii) the extrapolation of those experimental results to other fluid-cylinder kinematic conditions.

In particular, extrapolation from a model, however idealised, to a larger scale prototype has been discussed.

This Chapter initially describes an experiment conducted to examine basic fluid mechanic behaviour in the case of a large diameter cylinder oscillating sinusoidally in water. The production of surface waves in a laboratory water tank is then considered in relation to a typical design. The potential usage of such a facility is then considered in the light of the foregoing discussion.



PLANAR MOTION MECHANISM EXPERIMENT



THE AEW PLANAR MOTION MECHANISM (PMM) - WITH
CYLINDER ATTACHED

(4.2) A vertical cylinder in planar oscillatory motion

This section describes and discusses an experiment carried out at the National Maritime Institute (NMI) in 1977, for the Department of Energy. The author, together with Richard Matten carried out the experiments, and is grateful to the Director of NMI for permission to include results therefrom in this Thesis.

(4.2.1) Background

The significant contributions of Sarpkaya in the field of planar oscillatory flow, and previously discussed, began about 1974, with the publication of results obtained in an oscillating U-tube water tunnel. This type of experiment simulates high R_E flows by increasing the particle amplitude A_p . Consequently simultaneously with high R_E flows, high N_k values are achieved. Figure (1.27a) for example shows that in the steady flow transitional R_E region Sarpkaya obtained minimum N_k values of around 20, the $N_k=15$ results being limited to the subcritical region. Sarpkaya's contention that boundary layer transition occurs earlier in oscillatory flows is likely to be true, however, and therefore his results could be extrapolated to larger scale cylinders in the critical and subcritical regimes. As is in fact tentatively suggested in design manuals such as CIRIA (1978). Blockage is the cause of this limitation in any enclosed fluid region. Consequently in order to simulate high R_E conditions for low N_k , particularly in the region where drag and inertia are important ($5 < N_k < 25$), a much larger tunnel area free from the effects of blockage is required. Figure (2.1) shows that U-tube experiments, even at high R_E , do not simulate full scale conditions. Such experiments may, however, predict drag force behaviour, and be of invaluable assistance in the understanding of fundamental fluid dynamics. Low N_k with a simultaneously high R_E may be produced by oscillating a larger cylinder in still water, provided it is sufficiently remote from the boundaries. Marine risers used in oil production are typical of prototype structures that experience fluid loading within the transitional R_E region, and also fall within the combined drag and inertia loading region suggested by the Morison equation. Reference to Gamage et al (1976) should be made for further details of marine riser systems, but typically the diameter is of the order of 200-300mm and they are surface piercing and flexible. A larger scale planar oscillating cylinder could therefore be used to directly reproduce a marine riser,

with the advantage of control over the kinematic conditions, if a large enough still water basin were available. Just such an installation was therefore set up in the NMI No.3 Towing Tank, which is 400m long, 20m wide and approximately 8m deep, in September 1977. The experiment, hereafter termed the Planar Motion Mechanism experiment (PMM), utilized the strictly simple harmonic motion provided by the Admiralty Experimental Works (AEW) scotch yoke mechanism, details of which may be obtained from NMI or AEW. A general view of the mechanism with cylinder attached is shown on the frontispiece to Section (4.2).

(4.2.2) PMM Experimental details

Previously reported details of this experiment may be found in Matten, Hogben & Ashley (1978) and Matten (1979).

A polished stainless steel test cylinder 1.6m long and 0.267m in diameter was attached to the PMM with its longitudinal axis vertical, via a smaller diameter cylinder, and immersed in still water, as shown in Figure (4.1). The test cylinder was therefore completely immersed, and surface disturbance caused by cylinder oscillation consequently minimized to that produced by the smaller cylinder. The oscillation direction was aligned with the longest dimension of the tank, and the cylinder situated roughly midway between the side walls. Because of the large depth of No.3 tank the depth of water beneath the cylinder was greater than 5m. Consequently three dimensional effects would be significant if some form of control was not applied, therefore 0.892m diameter perspex end plates were fitted for much of the experiment.

End plate design

Whilst the necessity for fitting end plates has been established (see Chapter 3) rules for their actual design have not been formulated, other than that they should be large enough to contain the flow, which according to Gowda from his tests in subcritical airflows suggests $D/d > 10$. This raises problems of boundary layer growth from the edges of the flat plates (Figure (1.4)), and also dynamic response of the plates themselves, which would be expected to be a function of their size, thickness and material. For this experiment some attempt at a rational design was made using plate theory, in order to establish an optimum plate size. Clear perspex was used as the plate material to allow flow visualization, as will be discussed later, this has an

approximate Poisson's ratio $\epsilon = 0.3$, and Young's Modulus $E_y = 3 \times 10^5 \text{ N/cm}^2$. One plate was idealized as shown in Figure (4.2a) with a uniformly distributed load of $q = 0.5 \text{ N/cm}^2$ over its entire surface. The loading was derived from a consideration of the anticipated C_p range expected from planar oscillatory motion or towing. From Jaeger (1964), the plate equation is $\nabla^4 \Delta = q/K$ The deflection Δ at any radius r is then given by:

$$\Delta = \frac{qr^4}{64K} + \frac{C_1 r^2 (\log r - 1)}{4} + \frac{C_2 r^2}{4} + C_3 \log r + C_4$$

where $K = \frac{E_y \epsilon^3}{12(1-\epsilon^2)}$ and C_1, C_2, C_3 and C_4 are constants determined from the boundary conditions:

$$\Delta \Big|_{r=R} = 0, \quad \frac{d\Delta}{dr} \Big|_{r=R} = 0, \quad \underline{E}_r \Big|_{r=D/2} = 0, \quad \underline{M}_r \Big|_{r=D/2} = 0$$

where \underline{E}_r and \underline{M}_r are the force and bending moments at radius r .

Figure (4.3) lists the (Fortran IV) computer program giving Δ_{\max} for plate thickness $e = 1, 2$ and 3 cm and maximum radii $D/2 =$

$25 - 75 \text{ cm}$ shown in Figure (4.2b). Based on the plate stiffness given by this deflection an approximate natural frequency was also evaluated, however, this seemed much too low because of the uniformly distributed load assumed in the analysis. Figure (4.2c) shows the consequent oscillation mode, which would be unrealistic for the asymmetric loading conditions that actually occur. However, it was decided to adopt an end plate thickness of 25 mm with a diameter of approximately 900 mm . Actual manufacture reduced this diameter slightly to 892 mm . No obvious end plate response was observed during the experiment.

It is appreciated that the relative end plate size used, $D/d = 3.3$, is well below the value recommended by Gowda, and therefore some unwanted end conditions were still expected as this experiment was hoped to represent an infinite cylinder. The same criticism could also be levelled at the small aspect ratio $L_z/d = 6$, so any results will obviously need to be viewed in the light of the discussion in Chapter 3 relating to three dimensional effects.

The end plates were also used to assist with flow visualization. A 50 mm grid of pins was attached to the cylinder side of both end plates and tufts of wool and fibre were fixed to the ends of the pins. It was hoped that the pins would be long enough, of the order of 30 mm , for the tufts to be outside the plate boundary layers, and so respond

to the wake movement around the cylinder. Observation of the tufts was by two immersed television cameras, one remote from, and the other attached to the cylinder mechanism so that it viewed down through the top plate to look at the bottom plate tuft behaviour. Video records were concurrently made of these observations.

Kinematic conditions

The PFM has simple harmonic motion with a possible peak to peak displacement, or double amplitude of motion $2A_{pc}$ of 1.5m at a frequency of 0.23 Hz (4.4s period) displacement being recorded instantaneously via a potentiometer. This meant that a maximum $N_k (= 2\pi A_{pc}/d)$ of 17.65 and $Re (= 2\pi A_{pc}d/T_{pc}v)$ of approximately 2.7×10^5 for $v = 1.07 \times 10^6 \text{ m}^2/\text{s}$, were possible resulting in a maximum β of about 15300. The actual test runs using planar oscillatory motion are illustrated in Figure (4.4) with and without end plates attached. The oscillation of the cylinder in still water could be confidently expected to give a uniform axial velocity, unlike enclosed tunnel water oscillation, apart from any end effects.

Dean (1976) develops an expression for the evaluation of the suitability of oscillatory flow experiments to determine Morison drag and inertia coefficients based upon the ratio between force component maxima. He derives a ratio R between changes in C_M and C_D :

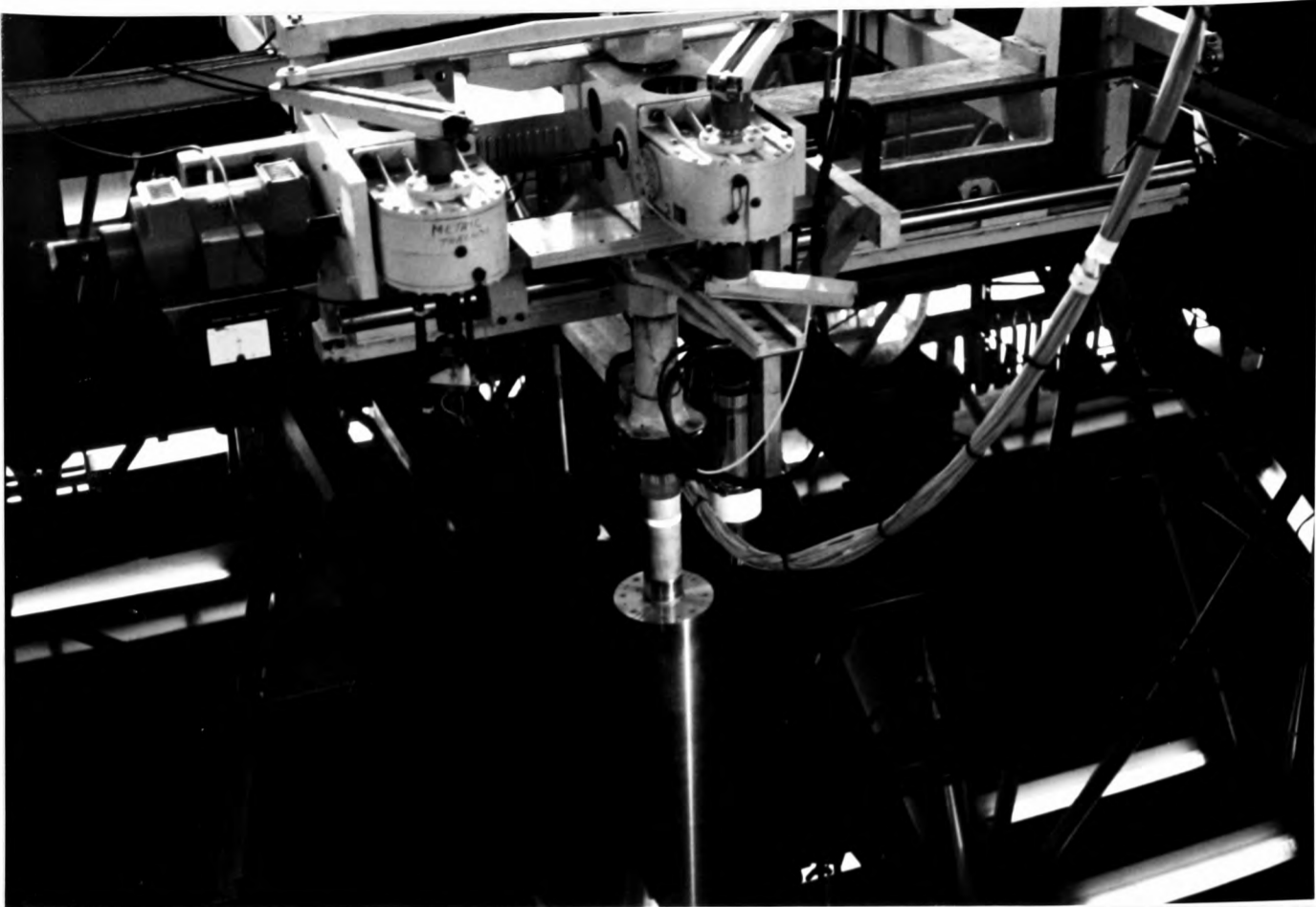
which for planar oscillatory flows reduces to

$$R = 2/\pi d (3/4)^{1/2} (\frac{U_{pcmax}}{\omega_{pc}}) = 0.088 N_k \quad \dots \quad (4.1)$$

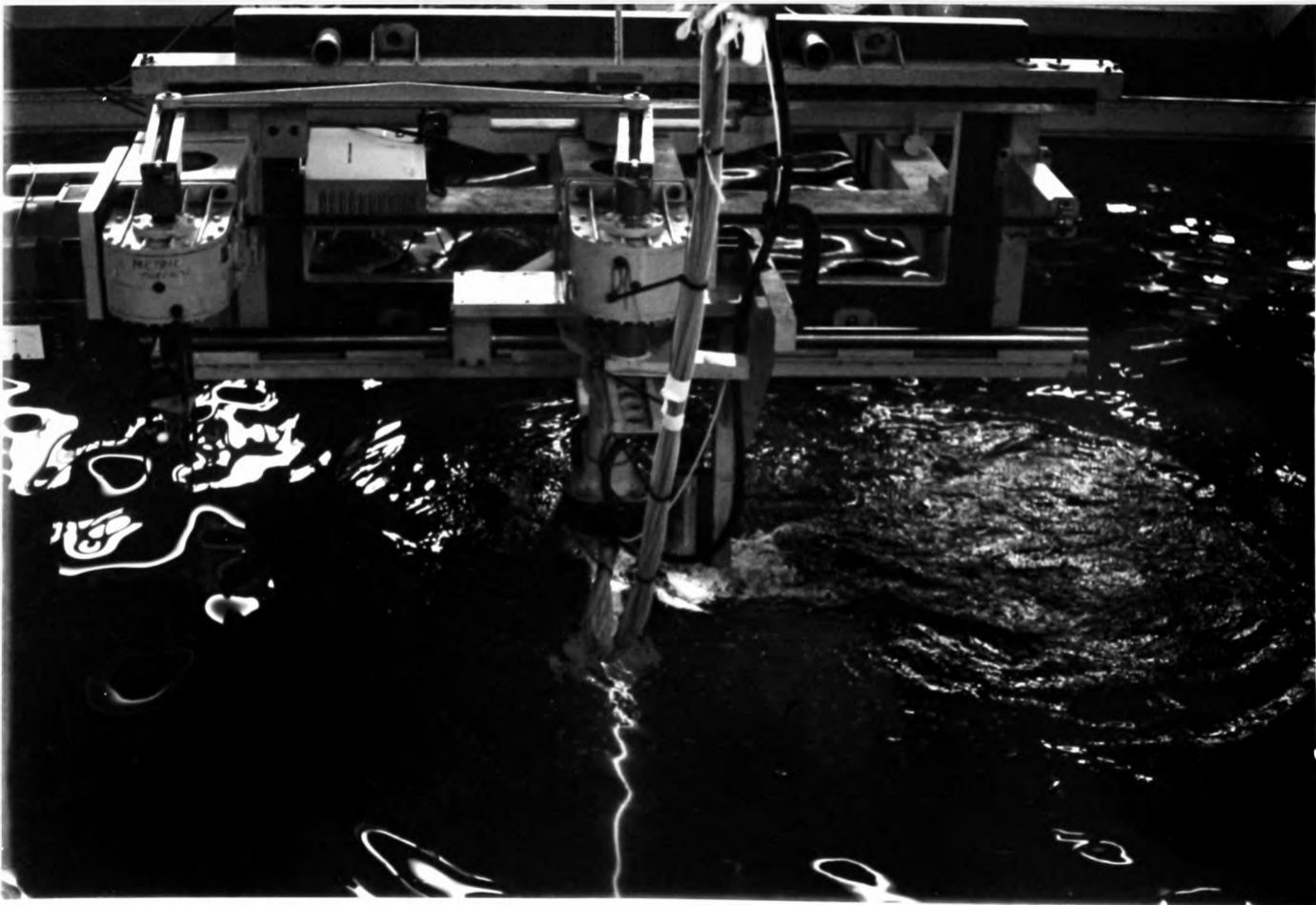
Dean suggests that for $0.25 < R < 4$ data will be reasonably well conditioned for determining both C_D and C_M , i.e. in the range

$3 < N_k < 45$. Above this the drag component dominates such that C_M is unreliable. Consequently the PFM tests, planned on an intuitive basis, are suitable for examination of C_M and C_D behaviour on the basis of this criteria.

The PFM was attached to a towing carriage which could move longitudinally along No.3 tank at a maximum velocity of 2m/s, above which the apparatus unacceptably vibrated. Results from the test runs involving simultaneous towing and in-line planar oscillation have been reported elsewhere by Matten (1979), and related to wave and superimposed current flows.

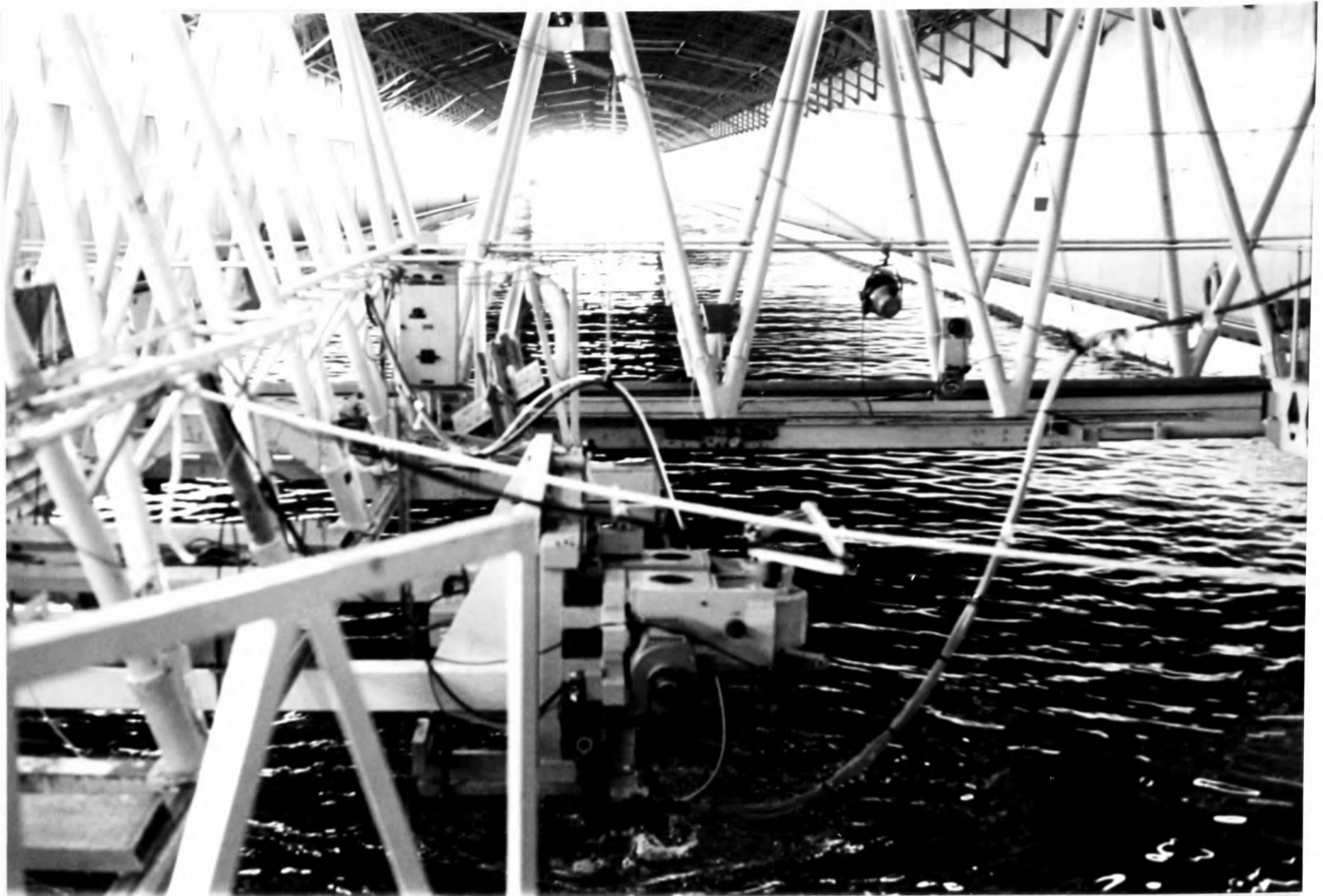


THE PMM WITH CYLINDER ATTACHED - NO END PLATES
PHOTOGRAPH (4.1)



CYLINDER ATTACHED TO PMM - TOWING ONLY

PHOTOGRAPH (4.2)



CYLINDER BEING TOWED AWAY FROM THE WAVE GENERATOR
END OF No.3 TANK - NMI FELTHAM PHOTOGRAPH (4.3)



AN ONCOMING WAVE TRAIN LOOKING FROM THE TOWING
CARRIAGE - No.3 TANK NMI FELTHAM PHOTOGRAPH (4.4)

The other option available in this extensive research facility is that of surface waves, either regular or irregular. Unfortunately the tests involving surface waves were limited because of beach reflection problems, and also the method of data collection was not particularly appropriate for significant water depth changes, as it was in the form of pressure changes.

A range of combinations of in-line planar oscillation, waves and towing (into and away from incoming waves) were used, as well as separate kinematic conditions. In all approximately 200 individual runs were made, but this Thesis will deal only with the conditions of planar oscillatory motion.

Photographs 4.1, 4.2, 4.3 and 4.4 show respectively: The FMM stationary, being towed, being towed away from the wave generator, and the establishment of an incident regular wave train.

Instrumentation and data handling

In Chapter 3 it was shown that the principal weakness in oscillating cylinder experiments is the removal of the inertia tare if reaction forces are measured. The other oft encountered difficulty is due to vibration caused by the dynamic response of the apparatus to the unsteady fluid forces. The latter can only be eliminated using a sufficiently rigid apparatus, but the former may be avoided by measuring pressures. The other advantage of pressure measurement is that the fluid behaviour at a cross section, rather than averaged over the cylinder length, can be recorded. Stationarity of the fluid mechanics cannot be assumed, even in 'steady' flows, consequently a number of simultaneous pressure records is required to adequately investigate the fluid behaviour. In this experiment 24 analogue pressure transducers were circumferentially positioned at the centre cross section of the cylinder. These were situated at 15° intervals of arc, beginning with one at 0° , facing the wave generator end of the tank, and increasing clockwise, (0° is facing left in photograph 4.2). Two additional transducers were positioned at $82\frac{1}{2}^\circ$ and $262\frac{1}{2}^\circ$ for a subsequent check on pressure interpolation between transducers. In order to determine the in-line natural frequency of the experimental equipment an accelerometer was also incorporated at the pressure transducer level. Pressure transducer calibration was carried out by raising and lowering the cylinder and so varying the hydrostatic head. Calibration was particularly important because of the larger hydrostatic head due to the

depth of transducer immersion and so it was carried out around the actual working submergence depth. All calibrations were found to be linear to within a very small error.

Data were recorded on three analogue tape recorders, some of the records being simultaneously recorded by pen recorders. Unfiltered examples of pen records are shown in Figure (4.5a-c), from which it is apparent that noise levels were low. Optional oscilloscope monitoring was also available. The analogue tape records were used for the data analysis and consequently were phase related using reference channels.

Experimentation

Because of the large number of individual experimental runs required (200) to cover the range of kinematic conditions, it was recognised that no statistical reliability could realistically be achieved due to the consequently limited recording time. As the actual record length required to obtain stationarity was unknown the record time for each run varied between 2 and 5 minutes with a median around 4 minutes. Each test run was conducted by setting the PNM controls to the required amplitude and frequency and starting the motion. Data were not recorded until sometime after the motion was started when a 'regular unsteadiness' was judged to exist. Time was allowed between runs for conditions to settle, normally a sequence of tests proceeded by varying the oscillation frequency for a given amplitude setting, i.e. constant N_k and varying R_E .

(4.2.3) Analysis and presentation of results

Analysis will concentrate on one particular experimental run as an example of typical methods of data reduction. Comparison with other runs will then be made so that some general conclusions may be drawn and related to previous work in this field.

Digitization of the analogue data has been reported in Matten (1979) and consequently here only a few general remarks pertaining to analogue to digital conversion will be made.

Without filtering (other than of background noise) data recording in the form of an analogue signal, which is a continuous voltage record of transducer response, is extremely versatile for data analysis because no irreversible decision need be made at the time of the ex-

periment. Data records in the form of magnetic tape may then be perused by visual display, and subsequent conversion to a finite number of digital points representing the function $f(t)$ may be achieved with this hindsight. The conversion sampling rate depends upon the subsequent data analysis, and the required signal resolution. The sampling rate must above all be sufficient to represent the $f(t)$ function reasonably so that the lines between the $f(t)$ points may be assumed either linear or perhaps parabolic. A measure of the 'efficiency' of the sampling rate compared with the original function $f(t)$ is the Nyquist frequency which is the upper limit of the frequency which is resolvable from a record sampled at a rate of f_D Hz. For a record $f(t)$ sampled at f_D Hz, the Nyquist frequency

$$f_N = f_D/2 \quad \dots \quad (4.2)$$

Consequently f_N , and hence f_D should be high enough for the correct resolution of the highest frequencies contributing to the response of the system under investigation. The error introduced by assuming a too high Nyquist frequency is known as aliasing. The potential effects of aliasing may be seen in Figure (4.6), and are removed from a record by suitable filtering of the signal before digitization. Without removal the analysis of $f(t)$, either spectral, or in terms of Fourier coefficients, is contaminated by the higher frequency components; see for example Newland (1975).

Ideally, due to practical electronic filter characteristics it is advisable to filter out frequency components at a somewhat lower level than that given by $f_D/2$, however, this requires even larger amounts of data points to describe $f(t)$, and consequently a larger computer capacity to handle the data if the same maximum resolvable frequency is to be retained. In practice therefore a compromise has to be adopted: In this experiment a sampling rate of 10 Hz was used after filtering at a minimum frequency of 5 Hz. The filters used, however, were such that some aliasing may be present in the range 3-5 Hz, the digitization only being completely reliable for 0-2 Hz, see Matten (ibid). However, as this would ensure uncontamination up to the 9th harmonic of the minimum oscillation period it was considered adequate. The digitization procedure ensured that the information contained on all 3 tapes was not phase distorted by greater than 1°.

The principal data analysis techniques were by Fourier Analysis (short time records) and Spectral Analysis (longer time records). The former

assist in understanding the fluid behaviour during a period of motion, and is the principal tool discussed in this Thesis.

The spectral analysis (see Appendix D) of the pressure, displacement and accelerometer records was achieved by using a Fast Fourier Transform (FFT) computer program developed by M.E. Davies of NMI. The frequency resolution achieved was approximately 0.02Hz up to a maximum frequency of 5 Hz by averaging five blocks of 512 data points for each sample record.

The power spectral densities for the displacement transducer, for an oscillation period of 4.45s, and accelerometer when the cylinder was towed, are shown in Figures (4.7) and (4.8) respectively. The displacement is seen to be sinusoidal and the accelerometer natural frequency response at $f_n = 3.7 \text{ Hz}$. The accelerometer also shows a response at a frequency of approximately 1.9 Hz which is double the Strouhal shedding frequency, for this towed case.

Fourier Analysis $N_k=17.65$, $T_{pc}=4.334 \text{ s}$

Appendix C presents a summary of pertinent theory and application of Fourier analysis to time functions $f(t)$. For this experiment the methods of Fourier analysis were expected to be particularly useful in the interpretation of fluid-cylinder behaviour over a short time period. Because of the obvious non-stationarity of the pressure distributions, and consequent forces, spectral analysis was also necessary for some longer term behavioural understanding. Spectral analysis may be considered similar to Fourier analysis over a frequency range, but at an (effectively) infinite number of multiple frequencies. This results in a continuous line plot, rather than a series of discrete Fourier coefficients. However, where frequency components are expected to exist at integer multiples of the fundamental, in this case the oscillation frequency, Fourier analysis techniques may give as much information at less cost and using less computer time. Fourier analysis is particularly useful where relative phase information is important. The Fourier analysis computer program presented in Appendix C, was written to incorporate not only integer multiples of the oscillation frequency, but also half harmonics. This was particularly because of the findings of Mercier (1973) where components at these frequencies were found for cylinders oscillating in-line with a flowing fluid stream. Consequently the program requires two periods of data to de-

termine the half harmonic component. All results, unless otherwise stated, should therefore be considered as two period averages, which if either two or three vortices are being shed per period may represent two cycles of motion incorporating both possibilities.

For the planar oscillatory motion with end plates attached, one hundred consecutive time intervals were selected at random from the experimental run having a maximum amplitude of 0.75m and the minimum nominal period of 4.4s. The displacement record was analysed using a period averaging program, and a mean period of 4.334s determined. This defined N_k as 17.65, $f_{pc} = 0.231\text{Hz}$ and $\omega_{pc} = 1.450\text{rad/s}$. R_E and β maxima were therefore 2.7×10^5 and 15.3×10^5 respectively.

A Fourier analysis of the displacement $x_{pc}(t)$ in the form of equation (Appendix C) gave the following relationship for these 100 time points:

$$x_{pc} = 0.753 \sin(\omega_{pc}t - 1.358) \quad \dots \quad (4.3)$$

(see Table (4.1a)). This meant that from the start of this record the cylinder was moving in the direction of the 180° pressure transducer with an increasing velocity; the total record covering 2.27 periods of motion.

The cylinder kinematics may therefore be derived from equation (4.3):

$$u_{pc} = 1.093 \cos(\omega_{pc}t - 1.358) \quad \text{and} \quad a_{pc} = -\omega_{pc}^2 x_{pc} \quad \dots \quad (4.4)$$

The displacement and kinematic reference system is illustrated in Figure (4.9) based upon these equations.

Pressure History

The pressure signal records $p_{pc}(t, \theta)$ were normalized, and analysed in the form of the pressure coefficient:

$$C_p(t, \theta) = (p_{pc}(t, \theta) - p_\infty) / \frac{1}{2} \rho u_{pc}^2 \max \quad \dots \quad (4.5)$$

where p_∞ is the hydrostatic head $= \rho g z_{ipc}$.

Fourier analysis of $C_p(t)$ has been carried out at the Thames Polytechnic computer centre using links to the London Polytechnics DEC10 machines. From Appendix C equation (5):

$$C_p(t) = a_0 + \sum_{n=1}^{\infty} c_n \sin(n\omega_{pc}t + \alpha_n) \quad \dots \quad (4.6)$$

for each pressure transducer θ .

Fourier analysis of the $C_p(t)$ records corresponding to the 100 points for each pressure transducer $\theta = 0^\circ \rightarrow 345^\circ$ are summarized in Tables (4.1a-g). C_p Fourier coefficients, up to the 5th harmonic in halves, are only shown where they exceed 0.05. The goodness of 'fit' of this analysis is shown by comparison with the $C_p(t)$ records in

Figure (4.10a-1) for the two complete cycles of motion only. The 'fit' is seen to be reasonable with some higher frequency discrepancies, and an increasing amplitude and phase error towards the end of each record. The higher frequency component errors could be eliminated by extending the analysis to higher harmonics, but this would be misleading in relation to the digitization and the fluid mechanic processes involved. The growing error toward the end of the record is due to the averaging process involved in the program (see Appendix C) incorporated to accommodate any half harmonic components, and also assuming a stationarity of signal over two periods. In view of the lack of any detected half harmonic effects, a Fourier analysis of the two periods separately may be more valid. However, selected Fourier analysis of single cycle C_p histories showed that the Fourier coefficients C_n differed by only ± 0.01 , although the phase angles α_n varied by as much as $\pm 5^\circ$. This result illustrates the non-stationarity of the C_p records from cycle to cycle, which is clearly evident from the time plots Figure (4.10a-1), and emphasises the inadvisability of claiming strict phase relationships between the exciting and response functions. The potential flow C_p -time history is also shown in figures ^(4.10a & b) calculated from Equation (1.39). Again this shows the phase shift away from maximum and minimum kinematic points of the actual record, compared with the irrotational.

As a phase reference for the second and third harmonic components, results from the Fourier analysis of the displacement squared and cubed are also shown in Table (4.1a) and all relative phase information for $C_p(t)$ in subsequent Tables related thereto. Relative phases have been adjusted to angles within the sector $\pm 180^\circ$, as indicated in Appendix C, and are shown for the first, second and third harmonics at each pressure transducer θ , in Figures (4.11a-c).

Force History

In-line and transverse forces have been determined by linear interpolation and integration of instantaneous circumferential pressure distributions:

$$E(t)/\frac{1}{2}\rho d u_{pc}^2 \max = \frac{1}{2} \int_0^{2\pi} C_p(\theta) \cos \theta d\theta \quad \dots \quad (4.7a)$$

$$\text{and } E_L(t)/\frac{1}{2}\rho d u_{pc}^2 \max = \frac{1}{2} \int_0^{2\pi} C_p(\theta) \sin \theta d\theta \quad \dots \quad (4.7b)$$

The force history is shown in Figures (4.12) & (4.13) together with the re-constituted Fourier analysis results, the constituents of which are summarized in Table (4.2).

The various conventionally presented force coefficients may be determined from these results:

(i) The Morison equation coefficients may be determined by inspection of the force at instants of maximum velocity: $C_D = 0.59, 0.53, 0.56, 0.47, 0.78$ (mean 0.57).

Also inspection at maximum acceleration gives:

$$C_M = 0.99, 0.90, 0.81, 0.99 \text{ (mean 0.92)}.$$

More appropriate coefficients considered over the whole record may be determined by 'averaging' in the manner of Keulegan & Carpenter (1958), or by a least squares error minimization as suggested by Sarpkaya (1976a) or Miller & Mattern (1976), using the Fourier coefficients.

Considering the first harmonic only:

$$C_D = \frac{3\pi}{8} \cdot A_n \quad \dots \quad (4.8a)$$

and $C_M = \frac{N_k}{\pi^2} \cdot B_n \quad \dots \quad (4.8b)$

where A_n and B_n are the Fourier coefficients defined in Appendix C:

$C_n = (A_n^2 + B_n^2)^{1/2}$, and $\tan \alpha_n = A_n/B_n$. In this experiment the sampling origin was not coincident with the maximum velocity (or zero displacement) position, and as equations (4.8) have been derived for records originating at that point the in-line force Fourier components given in Table (4.2) need to be phase corrected.

i.e. $E/1/2 \rho d u_{pc}^2 \max = 0.626 \sin(\omega_{pc} t - 0.698)$

for the complete record. From this equation $A_n = 0.402$ and $B_n = 0.479$. Hence $C_D = 0.474$ and $C_M = 0.857$. These values, which are represental of the whole record, have been used to evaluate the in-line force history from the Morison equation, and this re-constituted force is shown in Figure (4.12) for comparison with that measured.

The in-line force behaviour in the two complete individual cycles of motion has also been separately Fourier analysed. This gave the following (phase adjusted) results:

1st cycle: $E/1/2 \rho d u_{pc}^2 \max = 0.626 \sin(\omega_{pc} t - 0.718)$

with $C_D = 0.485$ and $C_M = 0.842$

2nd cycle: $E/1/2 \rho d u_{pc}^2 \max = 0.659 \sin(\omega_{pc} t - 0.697)$

with $C_D = 0.498$ and $C_M = 0.903$

The first cycle also had a significant 3rd harmonic force component, not repeated in the second cycle, (Table 4.5).

The difference in taking these weighted averages over a longer data record is apparent with comparison to the mean values above.

(ii) $C_f (= E_{\max}/\frac{1}{2}\rho d u_{pc}^2)$ for each of the two cycles covered is 0.80 and -0.77, at a relative phase t/T_{pc} of 0.476, and 1.981 respectively. However, to enable comparison to be made with Sarpkaya (1976a), the correction to C_f derived in Appendix A will need to be applied: i.e.

C_f (oscillating cylinder) + $\frac{\pi^2}{N_k} \sin \omega_{pc} t = C_f$ (oscillating fluid)
the correction $\frac{\pi^2}{N_k}$ is in phase with the cylinder displacement, and consequently the in-line force maxima will be moved closer to the maximum cylinder displacement (or acceleration) position. For the first cycle the equivalent $C_f = 1.130$ at $t/T_{pc} = 0.268$, and for the second cycle $C_f = -1.202$ at $t/T_{pc} = 1.791$.

(iii) $C_{L\max} = 1.64$ and 0.82 for each of the two cycles at t/T_{pc} of 0.476 and 1.491 respectively.

The rms lift coefficient for the whole record may be determined using the relationship $C_{Lrms} = (\sum_{n=1}^6 \frac{C_n^2}{2})^{1/2}$ where C_n are the Fourier coefficients of the lift force given in Table (4.2),

i.e. $C_{Lrms} = 0.47$. However, unlike the in-line force there is a significant variation from cycle to cycle; for the first complete period shown $C_{Lrms} = 0.56$, whereas for the second, $C_{Lrms} = 0.38$.

The in-line force coefficients may now be compared with the published results of Sarpkaya (1976a):

from Figure (1.26), and Appendices in Sarpkaya (1976a):

	PLM ($\beta = 15300$)	Sarpkaya ($\beta = 8370$)
C_D	0.474 (0.485, 0.498)	0.65
C_M	0.857 (0.842, 0.903)	0.80
C_f	1.202	1.14

Unfortunately direct comparison at similar β is not possible due to experimental equipment limitations outlined at the beginning of this Chapter. However, despite this difference the results are remarkably similar, considering the significant experimental differences.

The larger variation in $C_{L\max}$ even for these two cycles casts doubt upon its simplistic presentation as a function of β and N_k (e.g. Figure (1.28)); the C_{Lrms} value would seem to have more use as a description, although the number of values averaged would obviously be crucial.

Maul & Milliner (1978), for example, presented details of C'_{Lrms} , defined by $C'_L = E_L T_p^2 / \frac{1}{2} \rho d^3$, as shown in Figure (1.24).

As $C_L = C'_L / N_k^2$ comparison may be made with their 200-run average C_{Lrms} of 0.87 (for a $\beta = 200$), which is approximately double the 0.47 presented here. However, Figure (1.24) has large variations in slope

with N_k and any comparisons are consequently dubious. The large difference in β would also be expected to be significant because this reflects the large R_E difference between the two experiments: 2.7×10^5 compared with 4×10^3 , which by analogy to steady flows represents entirely different separation and wake width conditions. This is also borne out by the large differences in the $C_D:1.45$ for $\beta=200$ (page 48) characteristic of a wide wake, in Maull & Milliner's experiment. The oscillatory flow experiments of Grass & Kemp (1978) reported in Chapter 1 also supported the supposition of a narrowing wake region in the transitional R_E range (Figure (1.19)). Because C_L appears to exhibit some qualitative reduction trends as transitional R_E is approached in steady flows, (e.g. Figure (1.19)), this would also be expected to occur in oscillatory flows, and the difference in C_L or C_{Lrms} at different R_E , and perhaps β , illustrated above is expected.

Pressure distribution

Representational circumferential distributions of pressure coefficient are shown in Figures (4.14a-c) and (4.15a-c). The evolution of the forces resulting from the integrals of these diagrams can be seen: the reversing in-line force direction is noticeable before the cylinder motion is reversed in Figures (4.14a) and (4.15a). The two cycles shown in Figures (4.14) and (4.15) apparently exhibit almost identical trends, the diametrically opposite pressure differences resulting in the in-line and transverse forces are often difficult to see, particularly for the lift force. This seems to indicate that the vorticity and wake behaviour is similar for both cycles, although the lift force histories are considerably different in magnitude.

(4.2.4) Discussion and interpretation of Results

Having shown that the results of this experimental run agree reasonably well with those previously published, some examination of the basic mechanics involved will now be attempted.

Wake behaviour

Any understanding of the forces exerted upon the moving cylinder by the (otherwise) still water must be based upon the relative movement induced in the fluid by the cylinder. Chapter 1 developed the basic picture of the possible fluid behaviour from steady, accelerative and oscillatory flows, and these basic ideas will be applied here particularly with reference to Figures (4.14) and (4.15).

The fundamental parameter correlating the flow conditions is N_k , as has been shown conclusively in Chapter 1. This experiment is an analysis of an 'established oscillatory flow', and so the results of Isaacson (1974) summarized in Chapter 1 should be applicable. The flow visual-

ization attempted in the PFM experiment has proved to be inadequate to infer anything other than the existence of shed vortices, so the conclusions of Isaacson and Sarpkaya: Figure (1.18) indicating the shedding of two vortices per semi-cycle at this N_k will have to be accepted, and considered in the light of the pressure distribution history.

It is difficult to begin at a represental point in the C_p distribution history and fit shear layer separation points and a vortex pattern because of the critical influence of flow history, however, the following principles have been adopted to try to fit a vortex pattern:

- (i) Two vortices are shed per semi-cycle, and perhaps there is also a large developing third vortex which remains attached.
- (ii) Vortex shedding is accompanied by a sudden local increase in C_p (i.e. a collapse in the side lobes).
- (iii) Shed vortices 'convect' along in the wake of the cylinder with an absolute velocity in the direction of cylinder motion.
- (iv) Because of the relatively low diffusion rate at this high R_E , (although turbulence effects may increase this) shed vortices persist until they convect out of the area of cylinder influence.
- (v) Although not previously shown, there is recent evidence that in oscillatory flows, with $5 < N_k < 25$, vortex pairing, in the manner observed by Zdravkovich & Mamork (1977) in waves, Figure (1.29), is responsible for the convection of vortices away from the cylinder.
- (vi) The shedding of vortices will be asymmetric and may occur dominantly upon one side of the cylinder due to the influence of residual vorticity shed during a previous semi-cycle.
- (vii) General trends apparent in steady uniform and unidirectional unsteady flows may be applied to oscillatory flows with caution, e.g. the induced circulation and relative movement of stagnation and separation points: Figure (1.7), and position of the points of separation, which may be inferred from Achenbach (1968), Appendix A and Grass & Kemp (1978), Figure (1.19).

The movement of the stagnation point during the two cycles of motion shown in Figures (4.14) and (4.15) is shown in Figures (4.17a & b), compared with the resultant force $F_R = (F^2 + F_L^2)^{1/2}$. The stagnation point being defined as that where $C_p(t)$ has the largest value. The graph is accurate only to the nearest 15° where pressures were actually measured, but some approximate interpolation has been inferred.

At the maximum excursion $t/T_{pc} = 0.25, 0.75, \text{ and } 1.25 \text{ and } 1.75$ for the first and second cycles of motion respectively. Simultaneously $u_{pc} = 0$ and $a_{pc} = a_{pc}^{max}$. $C_p(\theta)$ would therefore be given by the potential flow solution; the added mass part only thereof, if there were no previous flow history, i.e. for a starting oscillatory flow. In this case, however, the residual vorticity developed in the previous

semi-cycle, and drawn along in the path of the decelerating cylinder, will gradually overtake the cylinder and assist the reversal in direction of the in-line force. For example with the 180° transducer leading: Figure (4.14a) and (4.15a), the stagnation point moves from the front to the back of the cylinder (in the sense of the direction of cylinder motion) as the cylinder decelerates. This may be clearly seen in Figures (4.17a & b) where the stagnation point moves around the cylinder at $t/T_{pc} = 0.14$ and 1.14 , i.e. 0.11 of a cycle before velocity reversal. The in-line force also reversing direction for $t/T_{pc} > 0.1$ and 1.13 . The potential flow solution predicts an initial negative C_p at 180° with the 180° transducer leading for $t/T_{pc} > 0.16$ or 1.16 , however, this mathematical approximation is inadequate when considered in the light of its' prediction of zero in-line force, with perfect C_p symmetry for $t/T_{pc} = 0$ and 1 , with $u_{pc} = 0$ and $u_{pc} = u_{pcmax}$. The potential flow solution therefore appears to be closest to reality where u_{pcmax} and $u_{pc} = 0$ occur, as would be expected due to the assumption of an inviscid fluid. This also fits the starting acceleration results of Sarpkaya (1966) shown in Figure (3.4).

It might be expected that at mid-stroke ($u_{pc} = 0$, $u_{pc} = u_{pcmax}$) an equivalence to steady flow conditions might exist. Unfortunately published C_p results in 'steady' flows (e.g. BSDU (1979)) invariably neglect the significant unsteadiness that occurs, and are in the form of averages, so that direct comparison cannot be made. Indirectly, however, C_D (average 0.57) may be compared with the C_d of 1.20 typical of steady flows at this Re . The implication therefore is that this considerably lower C_D is more typical of a narrower wake than exists in the steady flow case at this Re . This is probably due to the increased turbulence in the water, and conforms to the turbulence in steady flow effects discussed in Chapter 3.

Having considered the conditions at maximum cylinder excursion, where the generation of new vorticity has momentarily ceased, a conjectured flow picture may be postulated from that point onwards; i.e. beginning with Figures (4.14(v)) and (4.15(v)) as the cylinder accelerates in the direction of the 0° transducer. In accordance with the earlier results presented for a 'starting' acceleration, separation would be expected to begin after the cylinder had moved $0.16d$, or around $t/T_{pc} = 0.30$ and 1.30 , however, because this is an established oscillatory flow

the influence of previous vorticity would be expected to enhance the onset of separation. Unfortunately this cannot be identified from the $C_p(t)$ plots, and must remain conjecture only. Grass & Kemp (1978) presented results showing the variation in the average separation angle throughout a semi-cycle for $N_k = 38$. These show, Figure (1.19), a reduction in separation angle as the cylinder accelerates, with a further reduction as it passes the maximum velocity point and decelerates. These results indicate a relatively large wake width with a separation angle of about 86° at maximum velocity, and do not consider any across cylinder asymmetry in the points of separation. It would seem that the $N_k = 17.65$ results under consideration here (with a higher R_E) fit a different picture, with a reduced wake width and a large separation angle ($> 140^\circ$; Appendix A), because of the low value of C_D . Also the difference in N_k may actually represent results on either side of a scaling barrier. For $N_k < 25$ the vortex shedding cannot be considered as resulting in a vortex street, whereas for $N_k > 25$ there is no vortex 'pairing' following shedding and flow reversal, but the establishment of a vortex street which tends to be less of an influence upon following reversed motion, i.e. above $N_k \approx 25$ flow tends more to 'steady'. This figure is actually only one half of that suggested by McNown & Keulegan (1959) of $N_k = 50$, but in the light of recent results may be more applicable.

Sarpkaya (1966) and Sarpkaya & Garrison (1963) for starting impulsive and steady accelerations determined the onset of wake asymmetry from vortex observation after a relative displacement of $4d$ and $3d$ respectively. In this experiment wake asymmetry was virtually perpetual, as illustrated by the asymmetric C_p distributions. Perhaps this is due to the previous vorticity, but it may also show that observation of relative vortex strength may be misleading if applied to pressure distributions even for unidirectional flows. The movement of the stagnation point, which is virtually always on one side or the other of the 0° - 180° line of symmetry would support this contention (Figure (4.17a & b)).

The sequence of vortex formation and shedding may be inferred from the $C_p(t)$ diagrams by considering the previously postulated conditions (i)-(vii) above: Figure (4.14a (iv)) shows the shear layers separated and detached during the previous semi-cycle of motion which

are now moving relatively faster than the cylinder to the right.

The previously formed clockwise rotating vortex moves on to the back of the decelerating cylinder due to its' own momentum. This vorticity then moves around the cylinder, in the direction of the 90° shoulder, interacting with the anti-clockwise vortex there and also assisting the growth of the new vortex of the same sign.

Figure (4.14a(v)) indicates a probable movement of the top (90°) separated vortex across the cylinder shoulder, this increases the relative velocity at this point and in conjunction with the newly separated shear layer creates a low pressure region.

Figure (4.14b(i)) shows a further stage in the development of the new vortices with a vortex pairing on the 90° side.

Figure (4.14b(ii)) has an increasing pressure distribution on the 90° side indicating a sudden change in wake, indicative of the shedding of the vortex pair as shown, and of a reversal in the direction of lift force. This also causes the lower (270°) vortex to be drawn in closer behind the cylinder with consequent base pressure complication. The simultaneous collapse in the suction on the 90° side and the vortex development on the 270° side results in a very large transverse force. Figures (4.14b(iii) and (iv)) show the development and shedding of the lower (270°) side dominant vortex with the simultaneous consequent collapse in suction on that side of the cylinder. The drawing across the back of the cylinder of the vortex from the 90° side again distorts the pressure distribution at the back of the cylinder. Inspection of the force records reveals that both vortices are shed prior to the maximum velocity position.

Figure (4.14b(v)) continues this development with the lift force changing direction as the influence of the shed vortex diminishes and the 90° vortex grows, although this process is attenuated due to the deceleration of the cylinder.

Figures (4.14c(i)-4.15a(iv)) are identical to the above described semi-cycle, only with flow direction reversed. The vortex pairing and subsequent shedding is not obvious during the second semi-cycle, and the flow reversal and subsequent residual vorticity behaviour may be different. This could cause vortex pairing to occur again on the 90° side of the cylinder if the residual vorticity moved over the top shoulder of the cylinder in Figure (4.14c(ii)). However, the behaviour of the lift force vector indicates that fluid behaviour is identical, but on the opposite side of the cylinder, during the second

semi-cycle.

Subsequent C_p distribution appear to follow the same pattern as above, except for Figure (4.15c(iv) & (v)), which have reversed lift force vectors compared with Figures (4.14c (iv) & (v)) indicating a probable switching of influence of the residual vorticity following flow reversal.

It is apparent that this picture of vortex development is highly speculative and founded upon many initial assumptions, however, the complexity of the fluid vorticity behaviour serves to illustrate why the lift force particularly is so variable from cycle to cycle. Recent work at Imperial College by Bearman & Graham indicate that in the range $5 < N_k < 25$ where vortex pairing occurs, there may be as many as eight separate modes of vortex behaviour, even for one particular value of N_k . The movement of the residual vorticity upon flow reversal is an important factor in developing the lift force because of its' interaction with newly developing vorticity in the shear layers. Unfortunately the behaviour of this residual vorticity appears to be pseudo-random, being possibly influenced by a variety of factors. Another possibility not so far considered is the potential perturbation in C_p caused by the cylinder moving back into previously shed discrete vortices following flow reversal. This again may only be considered as a pseudo-random influence, which cannot be quantified in the simple model above. It is the complications that occur at or near the motion reversal points that are responsible for the third harmonic component of the lift force; the two vortex shedding events being responsible for two of the three peaks in the lift force history.

The above postulation of vortex behaviour may be compared with other published explanations. As already stated oscillatory flow experiments have not normally recorded the existence of vortex pairing, perhaps due to it not existing in confined water tunnels, although Maul & Milliner (1978) do show a speculative picture for $N_k = 21$ and it is illustrated by Pearcey (1979). Isaacson (1974) suggests that at low N_k (≤ 16) the residual attached shear layer, e.g. as shown in Figure (4.14a(iii) & (iv)), is turned back against the cylinder in the base pressure/stagnation point region assisting the development of a vortex on the opposite side of the cylinder (which would have the same sense of rotation, or vorticity sign). How this fits into the vortex pairing framework is difficult to assess, and more work is necessary in this area to clarify this point.

Maul & Milliner (1978) present an explanation for the in-line and lift force behaviour based upon vortex growth and movement for $N_k = 7.7$ and 21, this tends to disagree with the explanation so far presented in this thesis, contradicting the postulations in Figures (1.22(a) and (b)). Their explanation is based upon the discrete vortex mathematical model, and may well be true for lower values of R_E . The possible effect of R_E is illustrated in Figure (4.18(a) & (b)). The relative pressures on the cylinder shoulders (90° and 270°) are in fact the result of a complex interaction between the quickly moving separating shear layer, which results in a reduced pressure, and the reverse flow induced into the base region behind the cylinder which ameliorates this reduction in pressure. The net effect is a resultant lift force which may be in either direction, but which must be sensitive to the point of separation and subsequent wake width. This is an R_E dependence, although in oscillatory flows R_E actually changes throughout the cycle, and separation would also appear to be sensitive to t/T_{pc} and, in the light of the remarks made earlier concerning Grass & Kemp's (1978) results, it may also be dependent upon N_k . Consequently during a complete semi-cycle of motion the lift dependence upon the dominant side of vortex growth may invert as the separation points and wake width change.

The force behaviour throughout the two cycles may best be represented in terms of the dimensionless cylinder displacement. In unidirectional accelerative flows this has been shown to be a form of Iversen Modulus I_m . In oscillatory flows, however, I_m is not a particularly useful correlating parameter, tending to infinity at $t/T_{pc} = 0.25$, and 0.75 . Figures (4.19(a) & (b)) and (4.20(a) & (b)) therefore show the variation in in-line and lift forces with $2\pi x_{pc}/d$ for the first and second complete cycles of motion respectively. Figures (4.19(c)) and (4.20(c)) show the variation in the resultant force for each of these two cycles. It is apparent from inspection of each of these Figures that the forces in the two cycles differ considerably. There is a marked difference between the resultant forces, particularly due to the lower level of the lift force during the second cycle. Comparison of the re-constituted Morison equation also shows the semi-cycle asymmetry of the in-line force in both cycles.

From these force figures the point of vortex shedding may be noted, and compared with the C_p history figures (4.14) & (4.15):

Position A corresponds to the maximum cylinder excursion:

$t/T_{pc} = 0.25, 1.25$, Figure (4.14a(iv) & 4.15a(iv)). The lift force is almost zero, and the in-line force varies from the Morison prediction due to previous vorticity moving relative to the (stationary) cylinder. The effects of this vorticity perturb the purely potential flow (theoretical) solution. The first vortex shedding occurs at position B where the transverse force suddenly drops. The action of the in-line force is complex due to the interaction of the gradually diminishing acceleration (the irrotational force component) and the growing vorticity force component. The shedding of the vortex causes a point of inflexion in the in-line force history which is not coincident with the turning point in the lift force. The interaction of pressures across the cylinder in producing forces makes it difficult to exactly define salient points such as those of vortex shedding. Point C indicates a symmetrical C_p distribution about the 0° - 180° axis of the cylinder, this does not occur at the same relative displacement for each cycle. The lift force then increases again up to the second vortex shedding at point D. The in-line force also increasing simultaneously; the effects of the diminishing irrotational force component are now much smaller than earlier in the cycle as relatively this component is a smaller part of the total in-line force. Following D the generation of vorticity is reduced as the cylinder decelerates and the in-line force reduces. The irrotational force component also begins to reverse direction. The lift force reverses direction at E due to the residual vorticity, which causes it to peak at point F. Point G indicates the opposite maximum cylinder excursion compared to position A. The following alphabetical points describe the next semi-cycle in a similar manner to A to G.

The second cycle, however is worthy of further mention. Position L for this cycle, which corresponds to zero lift in the first, falls on the negative side of the $2\pi x_{pc}/d$ abscissa, and the final point for this cycle indicates a discontinuity when joined to the first, on the lift force Figure (4.20(b)). This corresponds to the earlier remarks made concerning the changing lift force direction illustrated in Figures (4.15c(iii)-(v)), and may represent a change in vortex shedding behaviour.

Both resultant force Figures (4.19c & 4.20c) show marked semi-cycle asymmetry, the latter being perhaps the most obvious. The in-line force curves show a 'shift' away from the line of anti-symmetry AG through the Morison equation plot (this line corresponds to $C_M = 1$ and $C_D = 0$), i.e. an increased average in-line force level for the semi-

cycle with the 180° transducer leading, although over much of the cycle the Morison equation seems to represent a 'give-and-take' average.

For the complete record of 100 points the integer Fourier lift force constituents, phase adjusted to the first velocity maximum, are shown compared with similar phase adjusted Fourier components for each of the two complete cycles of motion in Table (4.3). It may be seen from this Table that the harmonic content of the lift force varies from a predominance of the third harmonic in the first cycle to a predominance of the fourth harmonic in the second. This may be due to the different vortex behaviour in the two cycles postulated above, or consistent with the 'fractional' vortex concept introduced in Chapter 1. The phasing of the harmonic components is also reasonably similar where there is a large coefficient C_n , except for the second harmonic which differs by 31° between the first and second cycles.

The difference between the C_p history at 90° and 270° has also been Fourier analysed for the complete sample record, the significant Fourier terms being:

$$0.282 \sin(2\omega_{pct} - 2.012) + 0.574 \sin(3\omega_{pct} + 1.506) \\ + 0.388 \sin(4\omega_{pct} + 1.613) + 0.264 \sin(5\omega_{pct} - 0.979)$$

These may be compared with the lift force results shown in Table (4.2) to illustrate that the lift force frequency structure, which mirrors this equation, is principally composed of this difference. It is also apparent that the relative phases of the harmonics agree closely in the two cases. Individual cycle differencing for the two separate complete cycles of motion also reflect the lift force results shown in Table (4.3). The existence of a large second harmonic component, shown in the 90° and $270^\circ C_p$ histories (Tables (4.1c) & (4.1g)), is because of the pressure response due to the double maximum velocity that occurs in each cycle. This component is well correlated between the two positions, with a phase difference of 11° . This was confirmed by spectral analysis of the difference signal which showed that the signal level at this frequency was severely reduced: Figure (4.16); the third and other odd harmonics dominating. This would indicate that for a longer record, represented by the spectrum, the lift force frequency structure was more typified by the first complete cycle of motion in this shorter sample of 100 time intervals. This is again

evidence of the variability of the vorticity and asymmetric wake structure from cycle to cycle, which are responsible for the lift force.

The relative predominance of the third harmonic component of the lift force may be compared with the results of Maull & Milliner (1978) shown in Figures (1.23a & b), which represent averages of 200 cycles, although at a low β . This comparison is shown in Table (4.4). Except for the first harmonic, each of the coefficients are proportionately larger than those of Maull & Milliner, and even seem to exhibit trends closer to Isaacson's (1974) wave results shown in Figure (1.31). Whether this is a function of the difference between unconfined (oscillating cylinder), and confined (oscillating water in a tunnel) experimental results, it is impossible to say with the limited results presented here.

From the unsteady Bernoulli equation it can be shown that the pressure fluctuations at 90° and 270° are theoretically a function of u_{pc}^2 , where $u_{pc} = 1.093 \cos(\omega_{pc}t - 1.358)$ i.e. $u_{pc}^2 = u_{pc}^{2max} / 2 (1 + \sin(2\omega_{pc}t + 2.00))$ i.e. in phase with the displacement squared signal (Table (4.1a)). Consequently the phase differences recorded of 90° and 270° (Figure (4.11b)) for the 90° and 270° pressure transducers are an illustration of the complexity of the real fluid situation not allowed for in the Bernoulli, or indeed the quasi-steady Morison equation, which also predicts no phase difference. This discrepancy is a consequence of the neglect of the 'history' of the previous flow conditions contained in earlier generated and enduring vorticity.

The in-line force, which is largely composed of the pressure difference between the 0° and 180° pressure transducers, may also be compared with the harmonic structure of the difference between these two records. For the complete record the Fourier analysis gives:

$$1.479 \sin(\omega_{pc}t - 2.526) + 0.127 \sin(2\omega_{pc}t + 0.494) \\ + 0.497 \sin(3\omega_{pc}t + 0.359) + 0.126 \sin(5\omega_{pc}t - 1.558)$$

there are also $\frac{1}{2}$ and $1\frac{1}{2}$ harmonic terms:

$$0.138 \sin(\frac{1}{2}\omega_{pc}t - 1.007) + 0.108 \sin(\frac{3}{2}\omega_{pc}t - 0.804)$$

This does not agree very well with the harmonic structure of the in-line force, Table (4.2), other than for the obvious first harmonic dominance. The half harmonics for example do not constitute any significant part

of the in-line force. It must be concluded, therefore, that the relative contribution of the pressure either side of the 0° - 180° axis, (e.g. 15° and 165°), in making up the in-line force is greater than that either side of the 90° - 270° axis, (e.g. 75° and 285°), when creating the lift force. From the phase angle Figures (4.11a) and (4.11c), for the first and third harmonic terms respectively, it may be seen that the pressures either side of the 90° - 270° axis, (e.g. 60° and 120°), are virtually totally in anti-phase for the first harmonic (producing the in-line force), whereas for the third harmonic the 90° and 270° phase angles are approximately in anti-phase, but this is not reflected in the transducer records compared either side of the 0° - 180° axis further from the shoulder of the cylinder, (e.g. 60° and 300°). As it is the third harmonic that dominates the transverse force, then it is apparent that the pressures causing this force are exerted close to the 90° - 270° axis of the cylinder. The in-line force, however, is affected by the pressure variation all around the cylinder.

The second harmonic difference may be seen to be reasonably in phase all round the cylinder, i.e. about both the 90° - 270° and 0° - 180° axes from Figure (4.11b). This explains why the force component at this frequency is relatively small.

Table (4.5) shows the frequency structure of the in-line force for the complete record of 100 samples, compared with the two individual complete cycles. It is again apparent that the second force cycle is different from the first, and the overall, in not having a third harmonic component. Figure (1.23a) from Maull & Milliner (1978) indicates a relative proportion of third harmonic (to first) component of 0.15. The results shown in Table (4.5) give relative proportions of 0.14 and 0.19 respectively, which are remarkably similar considering the different β and experimental arrangement.

(4.2.5) Further conclusions from the PFM experiment

The previous Section has shown how a set of experimental results may be analysed and interpreted. These results were for $N_k = 17.65$ and $\beta = 15.5 \times 10^3$, recording pressure distributions on an oscillating cylinder with end plates attached. This Section will now deal with the effects of removing the end plates, and also results at different N_k . Reference should be made to Mattern, Hogben & Ashley (1978) and

Matten (1979) for the original publication of these findings.

The effect of end plates

The end plates were designed as explained in Section (4.2.2) to discourage axial flows along the oscillating cylinder and around the ends; to effectively simulate a part of an infinitely long cylinder. The end plates would be expected to be more effective in achieving this at lower N_k , because the relative amplitude of oscillation (expressed by N_k) would be reduced, and the wake would be more contained within the area of the plates. The runs at the maximum N_k used in the experiment would therefore be potentially the least affected by the addition or removal of end plates. Results presented here for comparison are for $N_k = 17.65$ ($\beta = 15.3 \times 10^3$), both with and without end plates.

In Chapter 3 it was postulated that strictly two-dimensional flows (without axial flow) are more axially correlated and result in higher drag forces. Table (4.6) shows that the 5 cycle average C_D is diminished when the end plates are not attached to the cylinder. The equivalent C_M , however, shows an increase, which brings it closer to the potential flow value. The effects of longitudinal vortex correlation (or lack thereof) cannot be seen from this type of experiment with a single ring of pressure transducers (having an aspect ratio of zero), therefore the change in C_D and C_M must be due to the low aspect ratio of the cylinder allowing flows around the free ends to influence the low pressures at the centre section, particularly in the base pressure region. This would be shown particularly in the drag, vorticity dependent, term. The increased inertia coefficient must be due to greater 'boundary condition' changes expressed by the distortion of the streamline pattern.

The overall in-line force coefficient C_f , which has been calculated assuming $C_f = \pi^2 C_M / N_k$, i.e. based upon a maximum Morison predicted force, also shows a slight increase when the end plates are removed. This is because of the change in C_M . This does not necessarily represent the force exerted upon the whole cylinder length, which would be expected to have decreased without the end plates fitted, due to the loss of vortex coherence, which would be reflected in C_D . The in-line force for a complete cycle of motion is shown in Figure (4.22a) for the cylinder oscillating without end plates fitted.

The phase angle at which the (Morison re-constituted) maximum in-line force occurs relative to the zero displacement position is seen to differ substantially between the two conditions, and is a very good illustration of the sensitivity of the Morison coefficients C_D and C_M to changes in phase angle. This phase difference, and the substantially reduced lift coefficient are the most obvious differences when comparing the effect of the end plates. C_L is seen to be 50% lower without the end plates due to the disturbance of the harmonic structure of the pressures around 90° and 270° . The second harmonic component is apparently not affected, but for the 60 cycles considered the C_p variance falls from 1.100 to 0.931 reflecting a change particularly in the third harmonic component, which may be seen in the 90° and 270° C_p spectra, Figure (4.21). The higher frequency peaks are much diminished except for perhaps the fourth, and as the third, and also higher order harmonics are responsible for the lift force it reflects the reduction in C_L . $C_{L\max}$ has also markedly decreased to 0.23, compared with the earlier mean of 0.47 with the end plates attached. The expected significant fourth harmonic structure of the reduced level lift force may be seen in Figure (4.22b) with the end plates removed.

It has been demonstrated that the fitting of end plates to the ends of this oscillating cylinder significantly affected the relative forces between the cylinder and the fluid. At this high N_k the end plates used were possibly too small, but because of the reasonable agreement with other published results for cylinders spanning between side walls, they must have been sufficiently large to reduce most three dimensional effects, at least for the centre section of the cylinder. It is impossible, however, to say whether these results represent those that would be determined using an infinitely long cylinder.

Variation of Stokes and Keulegan Carpenter Numbers

Figure (4.4) shows the range of N_k and β variation obtained in the PEM experiments. Because the period and amplitude of cylinder oscillation were independent, various N_k tests could be carried out for the maximum β of 15.3×10^3 . This was particularly useful because of the large lift forces expected in the lower N_k range, suggested by Sarpkaya (1977a), Figure (1.28a). Figure (4.23) shows a comparison of some of the PEM results of $C_L \max$ (5 cycle averages) for 4 values of N_k with

those of Sarpkaya (1976a). Notwithstanding the significant difference in β between the two experiments there is remarkably good agreement, particularly in the relative increase in C_L as N_k increases. At the lower N_k of 8.9 and 11.3 the lift force was dominated by a second harmonic component, and only one vortex was shed per semi-cycle of oscillation. The relative contribution of higher harmonics to the lift force was small, although there was some fourth order component at $N_k = 11.3$. These results conform to the much lower β findings of Naull & Milliner (1978), Figure (1.23a & b), and considering these results and those reported in Section (4.2.4) for the higher $N_k = 17.65$ case, fit surprisingly well the wave results of Isaacson (1974), Figure (1.31), as do the $C_{L,rms}$ results when compared with Figure (1.32).

Even at this lower N_k the variation in lift force magnitude and relative phase from cycle to cycle, is pronounced. A change in N_k therefore appears to alter the frequency structure of the lift force, but not its variability from cycle to cycle, although at lower N_k the lift force tends to be monochromatic, whilst for higher N_k (possibly > 15) it tends to narrow band random. It could therefore be postulated that the frequency structure of the lift force is uniquely a function of N_k in oscillatory and wave flows, and is independent of β . Any dependence upon Re , would be a function of the shed vortices, which appear to be controlled by the relative cylinder/fluid oscillation expressed by N_k .

For $N_k \geq 8.9$ the number of vortices shed per semi-cycle conformed to the model presented earlier (e.g. Table(1.1)). and boundary layer separation was apparently at a large angle typical of a turbulent shear layer and a narrow wake. This would be expected for the high $\beta = 15.3 \times 10^3$ results, and is supported by the low value of C_D , even at the smallest N_k , Figure (4.24). This Figure also shows the results of Sarpkaya (1976a) over this range of N_k . There is quite a difference in C_D between the two sets of results, as well as for C_M , Figure (4.25), this may be attributable to:

- (i) Different weighting of the results between a 'U-tube' experiment, where there is a Froude-Krylov force component, and an oscillating cylinder experiment, where there is no Froude-Krylov component. This may perturb slightly the calculation of the C_D and C_M coefficients, C_M having to be 'adjusted' for the appropriate Froude-Krylov component.
- (ii) Differences between a confined tunnel environment and a spacious water tank. This may cause relative phase shifts between the two cases, to which C_D and C_M are sensitive, as shown in the last section.

- (iii) The difference between measuring forces by reaction (strain gauged supports), or by integration of pressures; again there may be a phase difference effect.
- (iv) The effectively infinite end plates in a tunnel, and the finite sized end plates on the PIM experiment cylinder. It was shown that for $N_k = 17.65$, C_D decreased and C_M increased if the end plates were removed. In this case the value of C_D is smaller than that with the 'infinite' end plates and C_M larger, indicating a potentially similar condition. However, if this end effect were indeed responsible, then the lower N_k results would be the least affected, due to the relative wake/plate size ratio decreasing, but this is not the case; it would therefore appear to be unlikely that axial and end flows are the cause of the difference in coefficients.

It may actually be that there is a difference in C_D at higher, compared with lower, β . Comparison of Figure (4.24) with Figure (1.26a) indicates a possible reduction in C_D at lower N_k for high β . The low N_k results represent a greater 'unsteadiness' of relative flow and perhaps the greater relative turbulence coupled with high β effectively diminishes C_D by assisting the boundary layer turbulence, analogous to the early onset of transition in turbulent steady flows.

The combined maximum in-line force coefficient C_f shows better agreement with Sarpkaya (1976a) in Figure (4.26) than the component C_D and C_M values, and seems to suggest an independence of β at this level. This is also seen to be probable if Figure (4.26) is compared with Figure (1.26), where C_f is apparently independent of β for $N_k < 50$ and $\beta > 3 \times 10^3$. These Figures indicate some possible fundamental change, such as to postcritical conditions, above a certain β value. There is additional evidence for this supposition in Figures (1.27a & b) where there is a levelling off of C_D (after a decrease), and C_M (after an increase) at progressively lower R_E for smaller N_k , indicating that some fundamental flow characteristic has changed at a particular value of β . The above force coefficient results conform to the trends shown on these Figures, with a reduction in C_f and C_L as β increases.

The in-line force frequency structure is virtually monochromatic at the lower N_k tested (≤ 11.3), without the distinctive kinks around the peaks noticed at $N_k = 17.65$. Matton (1979) suggests that at lower N_k (< 30) the oscillating cylinder and fluid are 'coupled'. The other dominant frequency apart from f_{pc} , is the vortex shedding frequency f_s , which is uniquely a function of N_k in this range, and is therefore coupled to the cylinder oscillation. If N_k were large, however, the vortex shedding frequency would be given by the Strouhal Number S ,

as the relative flow would be quasi-steady. The two frequencies consequently interact, and although there is a dominance by the cylinder oscillation, the Strouhal frequency causes a low frequency modulation, particularly noticeable in the cylinder base pressure and C_L . The closer these two frequencies are, then the greater the lift force will be because it is directly related to the alternate shedding. At higher N_k the two frequencies cause a greater irregularity and reduction in magnitude of C_L because of their greater difference. Figure (1.17) shows a typical variation of $S_c (= f_s d / U_{pc \max})$ with N_k for a particular value of β . As this is equivalent to $f_s / f_{pc} = S_c \cdot N_k$, it indicates the relative constancy of vortex shedding for $N_k < 30$, as observed in oscillatory flows. Above this value S_c tends to 0.2, the steady flow value of S , and f_s increases markedly with increased N_k .

Figure (4.27) and (4.28) show the average in-line force and lift force coefficient variation with $2\pi x_{pc}/d$ for $N_k = 8.9$ and 11.3 respectively. These illustrate the increased magnitude of the in-line force as N_k reduces (by comparison with Figure (4.19a)) and the elimination of two of the lift force reversals, because less vortices are shed (by comparison with Figure (4.19b)). Both Figures exhibit the distinct asymmetry of the forces between successive semi-cycles noticed at higher N_k .

(4.2.6) Summary of the PIM experimental findings

A definite non-stationarity of all the data records was observed. This indicates that Fourier Analysis techniques may be useful for a cycle by cycle analysis of relative flow behaviour, but are inadequate for longer term trends, when Spectral Analysis is necessary. The deficiencies of the Morison Equation outlined at the end of Chapter 1 and further considered in Chapter 3, have been shown to exist when applied to a planar oscillatory flow case. This is particularly apparent when the relative magnitude of the lift force compared with the in-line force is considered.

Flow history, contained in the residual vorticity, is seen to have an important role in developing the wake in succeeding cycles of motion, and therefore strongly affects the force history.

The frequency structure of the forces seems to be uniquely a function of N_k . For $N_k > 25-30$ the relative flow field tends to quasi-steady.

β acts in an analogous way to R_E in steady flows, by defining a significant change in fluid-cylinder behaviour. Above $\beta = 3 \times 10^3$ the fluid

behaviour is typical of post-critical in steady flows.

Any application of the conclusions from this experiment to other relative fluid-cylinder kinematic conditions will be considered in Chapter 5.

(4.3) An introduction to, and an example of, the design of an experimental water wave facility

This Section is included in this thesis as a part of a comprehensive discussion of the problems of investigation of relative fluid-cylinder dynamics. In the previous section a detailed account of an experiment in which a cylinder was oscillated in still water was presented. The experiment was carried out because as previously shown in Section (2.4), the modelling of the fluid dynamics of full scale cylinders in waves may not normally be investigated successfully at a reduced scale. This limitation led, in Chapter 3, to a discussion of the development of alternative experimental methods in order to simulate, at least in part, some of the relative fluid-cylinder behaviour. Notwithstanding the deficiencies of small scale wave-cylinder models, it may still be desirable to experiment using small waves in a controlled environment such as a laboratory.

In Section (3.1) it was indicated that for a relatively oscillating flow, the ratio of oscillation period T to vortex shedding period T_s determined the relative unsteadiness of the flow field. For

$0.1 < T/T_s < 10$, there is a significant contribution from each of the potential and viscous force components, and in addition the effects of the flow reversal are important. This range corresponds roughly to $N_k \leq 50$ (for deep water waves); as N_k increases the relative proportion of the total force which is composed of the viscous dependent, or drag, term also increases. Section (2.4) and Figure (2.3) give the relative regions of force dominance, and illustrate that for $H_w/d > 1$, (approximately $N_k > 6$) small scale models will not reproduce prototype conditions because of the relative dominance of this drag force, and the corresponding scale effects at different R_g , which pose the principal difficulty in constructing a suitable hydraulically similar wave-cylinder scale model.

The construction of a small scale wave-cylinder model should only therefore be considered either where inertia forces dominate (at low N_k), or when it is not expected to represent prototype conditions. Much useful information, however, concerning the fluid dynamics of relative fluid-cylinder interaction has been obtained in the past from such models, particularly where they are of a relatively large physical size, such as in the NMI No.3 Tank mentioned in the previous Section.

Wave experiments are unique in the incorporation of a vertically oscillating velocity vector simultaneously with that oscillating horizontally, and all planar oscillatory experimenters must consider this deficiency when extrapolating to wave flows. The effects of the decay of the resultant velocity vector with depth under waves must also be considered as fundamental. Wave flows are invariably multi-harmonic. Due to the complexity of a water surface wave, very rarely may one be considered as monochromatic, or even then, be adequately described mathematically. This multi-harmonic condition of waves leads to complications in wave modelling either for:

(i) The development of a wave model with monochromatic waves only. This may easily be compared with a 'simple' wave theory, but is hampered by many complicating factors, (to be mentioned later) which make a single harmonic wave structure virtually impossible to achieve.

or

(ii) The reproduction of a prototype wave train with a known harmonic structure, i.e. an amplitude-frequency spectrum. This is also hampered by the same complicating factors.

These two possibilities represent extremes of the same problem, which exists even without the additional complication of an immersed, or partly immersed structure.

Wave-cylinder modelling must therefore be considered in two parts:

- (i) The modelling of an adequate wave train.
- (ii) The modelling of the wave train in conjunction with the structure to be investigated.

(4.3.1) Design of a typical wave testing facility

Wave generators are designed to fulfill particular specifications, within the constraints of available space and resources. This thesis will continue with a discussion of the evolution of a design for a wave tank, and generator, at Thames Polytechnic, London, in the Hydraulics Laboratory of the School of Civil Engineering. Resources and space were both restricted, but it was hoped that the specified requirements could be achieved. The original specification, associated with a research project, was altered, and may now be summarized as follows:

- (i) A wave tank to produce (a) regular, and (b) random, waves of controllable characteristics.
- (ii) The provision of a current superimposed upon the progressive wave

field.

(iii) This facility to be jointly useful for:

(a) Undergraduate teaching.

(b) Research:- particularly in the fluid-structure interaction area.

(c) Consultancy for industry.

Coupled with these requirements was the simultaneous development of appropriate data recording and handling facilities.

The Hydraulics Laboratory was at the conception of this Project a severely congested area, and an allocation of space of approximately 10m in length by 3m in width was all that was available. In addition it was stipulated that the water containing tank must be raised above floor level to allow for equipment storage underneath. Despite these limitations it was hoped to be able to achieve at least some of the specifications, with perhaps the exception of (iii) (c), the attraction of consulting work.

The design of such a facility may be approached in two ways:

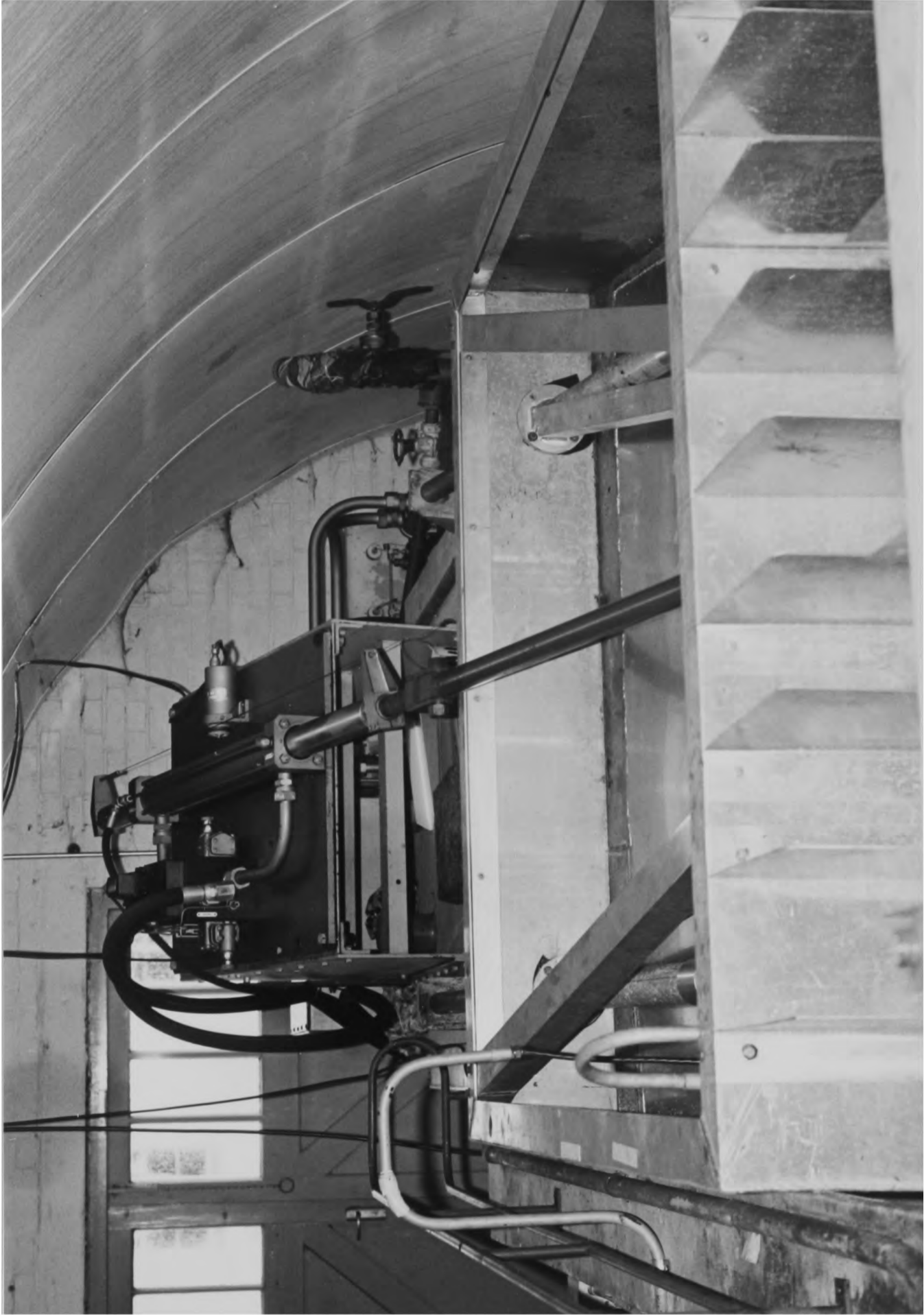
Either (i) Attempt to develop equipment that will produce exactly specifiable wave characteristics; such as amplitude- frequency spectra, steepness, shape etc.

or (ii) Design to the maximum limits available, and concentrate on obtaining desired wave characteristics when these maximum limits have been attained.

Because of the limited space available it was decided to try to produce the largest feasible wave height within a realistic model frequency range for a regular progressive wave train, i.e. approach (ii) above. This was also deemed to be the most realistic approach due to the virtual impossibility of designing such apparatus in the hope of achieving (i) above.

Wave Modelling

Any discussion of wave modelling, or production in a laboratory, must begin with the simplest possible wave. A unidirectional, monochromatic, progressive train of waves, with long crests (perpendicular to the direction of wave advance) are termed 'regular waves'. It is the production of such regular waves in a laboratory tank that will now be considered.



WEDGE WAVE GENERATOR - HYDRAULICS RESEARCH STATION

PHOTOGRAPH (4.5)



BATTERY OF WEDGE WAVE GENERATORS TO PRODUCE A MULTI-DIRECTIONAL RANDOM SEA - HRS WALLINGFORD

PHOTOGRAPH (4.6)

There are significant differences between waves in shallow and deep water. The former 'feel' the bottom and may have a different form to the latter. For irrotational gravity waves of small amplitude (Appendix B) the distinction may be characterised by the relative water depth

Deep water $kz_2 > \pi$

Intermediate $\pi/10 < kz_2 < \pi$

Shallow $kz_2 < \pi$

where k is the wave number $2\pi/L_w$, first introduced on page 51.

It has already been shown in Figure (1.32) that this dimensionless depth is a significant correlating parameter for fluid-cylinder interaction for a surface piercing cylinder. From equation (2.10) and (2.11), the dimensionless groups pertaining to wave conditions only (without an immersed cylinder) may be obtained:

$$\phi \left[F_r, z_2/L_w, H_w/L_w + \begin{array}{l} \text{additional kinematic and} \\ \text{geometric terms} \end{array} \right] = 0 \quad \dots \quad (4.9)$$

These first three are the most important, because the quantities contained therein may be used to evaluate others, such as wave celerity c_w or horizontal particle velocity u_w . This is apparent with reference to the small amplitude (Airy) wave theory (Appendix B):

$$c_w = L_w/T_w = (g/k \tanh kz_2)^{1/2}$$

and
$$u_w = \pi H_w/T_w \frac{\cosh k(z_2 + \eta_w) \cos(kX - \omega_w t)}{\sinh kz_2}$$

because the F_r group may be combined with z_2/L_w to give $T_w(g/L_w)^{1/2}$ i.e. a group linking the wave period and length. The z_2/L_w grouping is $kz_2 \times (2\pi)^{-1}$, that of fundamental importance in characterising the relative water depth. The inclusion of the third group, the wave height/wavelength ratio H_w/L_w , the wave steepness, is then sufficient to describe this simple wave. The modelling of gravity waves is based upon these three dimensionless groups. A model therefore must have a water depth/wavelength ratio such that the waves are within the appropriate region of deep, intermediate, or shallow. Appendix B introduces the common linear, and non-linear wave theories used, the approximate regions of validity of which are shown in Figure (B.1) in terms of H_w/gT_w^2 and z_2/gT_w^2 , dimensionless groups which may be derived from equation (4.9). A model wave which is scaled in

accordance with the three quantities detailed above will consequently automatically be within the same area of this figure as the prototype.

Wave generators

The production of water waves in a long tank may be achieved using a variety of methods:

- (i) Wind blowing over the water surface: A wind-wave generator.
- (ii) A mechanical device driven so as to periodically displace water in the tank.
- (iii) A pressure difference on part of the water surface, created pneumatically.

Wind-wave generation has many advantages, because it simulates the actual mechanism by which most prototype progressive waves are produced in the oceans. However, because the wave height is a function of the distance for which the wind is blowing over the surface, the 'fetch', it requires a very long tank in order to obtain a reasonable wave height. Wind-wave tanks are also virtually impossible to control if a specified wave amplitude-frequency spectrum is required, and consequently the mechanical displacement type of wave generator is now the most frequently used, although to produce more realistic sea state conditions, 'hybrids' containing both mechanical displacers and wind are often used, such as at Delft Hydraulics Laboratory in the Netherlands, described by D'Angremond & Oorschot (1969). The pressure difference type of wave generator produces waves that cannot be significantly varied, and unless this type of generator has been constructed in order to produce only a specified limited range of waves, it is not as versatile as the mechanical displacement types.

In view of the restricted fetch available (maximum 10m) it was decided to use a mechanical displacement device for wave creation. It was not expected that the apparatus would be of very much use for the study of 'pure' wave mechanics such as refraction or diffraction, other than as associated with immersed structures, and so an approximate channel cross sectional size of 1m x 1m was adopted, as being the largest practically possible. One way of achieving larger amplitude waves than may normally be created by a mechanical generator is to taper the channel inwards as the waves move away from the generation area, this would cause the progressive waves to steepen as the channel section narrows. This idea was rejected, however, due to the difficulty of constructing a smoothly tapering section, and also the increased mass, and driving power, requirement for the mechanical generator itself. Also Caldwell

(1955) reported that tests using a parabolically tapering channel resulted in standing waves being set up in the region between the generator and the narrowed channel section for some wave periods. The eventual solution proposed by Caldwell required the introduction of two longitudinal dividing walls in the narrowing section of tank.

Selection and design of a wave generator

There have been many ingenious mechanical devices for creating water waves in a tank, a fair selection being reviewed by Biesel & Suquet (1951). This is the earliest attempt to assess the typical characteristics of principal types. For practical design, Gilbert, Thompson & Brewer (1977) is now the best starting point, particularly where random waves are also required. This publication provides design charts for hinged, piston and wedge generators, but it does not, however, consider all the possible waves generators, and reference should be made to Hyun (1976) for the vertically plunging wedge type of wavemaker which is also commonly used. Dedow, Thompson & Fryer (1976) give the only contemporary comparison of these four types of generators; they may be considered in two categories:

- (i) Flat plates: Figure (4.29a & b)
- (ii) Wedges : Figure (4.30a & b)

The plate types produce waves in the region behind the wavemaker as well as in front, unlike the wedges which are usually hollow box structures, and have a considerably higher inertia and buoyancy than the plates. Motion is created by connection to a suitable ram, which may be oil hydraulic powered via a servo-valve, or transmitted from a rotating gear system. Intuitively the hinged plate and plunging wedge would seem to impart the same type of motion to the water particles; one that varies markedly with depth. This type of distribution of particle displacement is approximately in accord with the actual particle motions within a ^{deep water} wave, which decay exponentially with depth, and would be expected to produce reasonably 'stable' waves (i.e. waves that do not alter significantly as they progress) fairly close to the generator. Both generators would also impart some direct vertical particle motion to the fluid. The plunging wedge would have a variable depth of immersion s , but a fixed face angle, whereas the hinged plate would have a variable face angle ($= \tan^{-1} S/z_2$), but a fixed depth of immersion. The piston wave generator would impart no variable particle displacement with depth, and would only give a direct horizontal thrust to the fluid particles. For these reasons the piston wave generator alone

is less frequently used, as the waves generated travel a greater distance before achieving stability, although Dedow, Thompson & Fryer (ibid) suggest that when generated monochromatic waves have travelled a distance greater than three times the water depth away from the generator, their form becomes stable, irrespective of the type of generator used. No information is available, however, for multi-harmonic waves, often a combination of piston and hinged plate is used with two separate driving rams, one for the piston motion, and the other for the rotational motion. The University of Bristol, Department of Civil Engineering, and Delft Hydraulics Laboratory (D'Angremond & Oorschot (ibid)) have both successfully developed this type of wave generator to produce random (specifiable amplitude-frequency spectra) waves. Wedge types are used extensively by the Hydraulics Research Station (HRS) and the National Maritime Institute (NMI). The sliding wedge by HRS, Photographs 4.5 & 4.6, and the plunging wedge by NMI. The sliding wedge pushes the water in a similar way to the piston, but the particle displacement imparted varies with depth. The depth of immersion Z_d may be varied for a given wedge slope by varying s . There is also a small direct vertical particle motion caused by the vertical motion of the front vertical face of the wedge.

The piston wave generator was quickly rejected as a possibility for the Thames Polytechnic wave tank because of the lack of particle motion variation with depth, and consequent greater distance of travel required for the generated waves to become stable. The complications caused by the waves created behind the piston were also instrumental in this rejection. Small scale pilot tests using a hinged wave maker in a 150mm wide tank illustrated the problems of waves behind the oscillating plate, as well as a tendency for wave breaking to occur on the front face of the plate at higher frequencies and oscillation amplitudes s . Comparison with a sliding wedge in the same tank showed that larger amplitude waves were created in the latter case, because the tendency to break was reduced. It was decided following these tests to proceed with some type of wedge generator.

Because of the large number of variables involved in wedge-wave generation it is virtually impossible to produce a coherent comparison between the plunging and sliding types, even theoretically based upon Gilbert, Thompson & Brewer (ibid) and Hyun (ibid). Unfortunately these two theoretical approaches produce rather different design aids, that

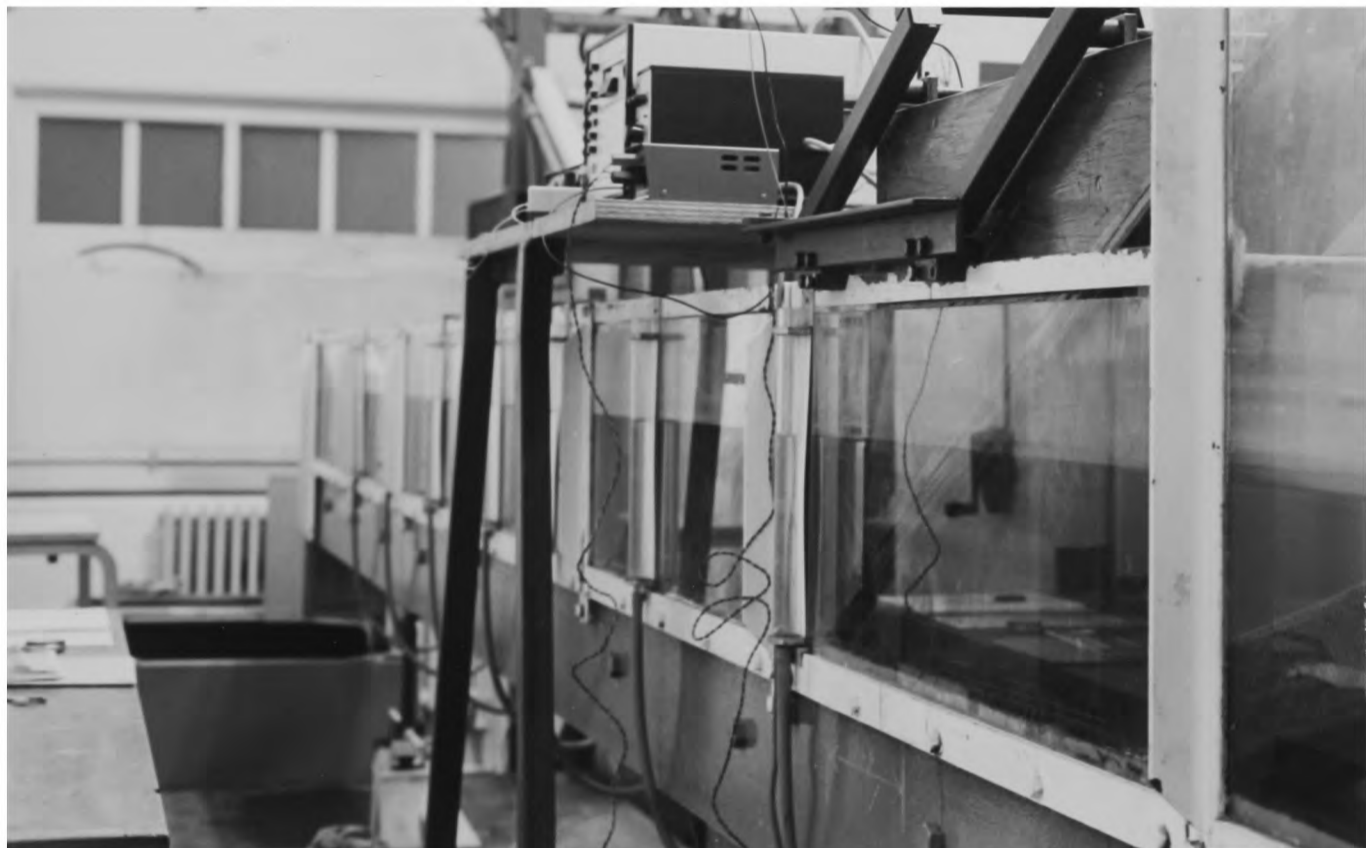
of Gilbert et al is in the form of design curves for wave and wedge operating characteristics for both regular and random wave generation, whereas Hyun's are in equation form for regular waves only. Due to these differences a direct comparison is extremely difficult, and it was decided to adopt a sliding wedge based upon the reasonable results seen in the smaller tank tests, and also because of the extension to random wave generation possible using the recommendations of Gilbert et al. It was recognised, however, that the sliding wedge would be more difficult to construct, and would also occupy more laboratory space. It was hoped that using the sliding wedge, larger waves could be produced without breaking than if the sloping front faced plunging wedge was used.

Despite the apparent simplicity of design using the graphs from Gilbert et al, these represent theoretically exact solutions for first order or random waves produced by an oscillating wedge. To attempt to predict maximum and minimum achievable wave characteristics, and moreover a whole range as represented by a spectrum, from these graphs would be naive. There are many problems which perturb this simple theoretical approach, particularly as a result of wave-tank interaction; those commonly occurring being:

- (i) Water leakage around the sides of the wedge.
 - (ii) Slight imperfections in wedge motion.
 - (iii) Effects of wave shape, steepness, and breaking.
 - (iv) Wave reflection.
 - (v) Cross waves.
 - (vi) Wave shape instability and variation with progression along the tank.
- Such problems have often been considered in the past following the construction of a particular wave generator and tank, see for example: Warren (1977). However, there seems to be no reported information for sliding wedge generators, although some of the results from piston generator experiments may well be applicable, e.g. Hansen & Svendsen (1975) or Keating & Webber (1977). Because of these indeterminable effects it was decided to design the sliding wedge generator for regular wave production only, based upon Gilbert et al, and by suitable testing to determine the potential range of use to avoid the above problems (i)-(vi), taking suitable measures to eliminate these where possible. It was also decided to simultaneously construct a smaller scale version of the wedge in a 150mm wide channel.



SMALL SCALE WEDGE WAVE GENERATOR - THAMES POLYTECHNIC
PHOTOGRAPH (4.7)



SMALL SCALE WAVE TANK - THAMES POLYTECHNIC
PHOTOGRAPH (4.8)

wedge angle ψ

The maximum anticipated water depth in the wave tank Z_2 was assumed to be 0.6m, allowing approximately 0.3m freeboard. The maximum amplitude of wedge motion was also limited to 0.225m. Assuming that the wedge will operate to full depth in certain circumstances, i.e. down to point B in Figure (4.29c), the corresponding minimum usable water depth Z_2 has been taken to be 0.2m to allow for wave formation. Gilbert et al (ibid) recommend that for

$$R = s \tan \psi / 4Z_2 \ll 1 \quad \dots \quad (4.10)$$

second order buoyancy effects will be negligible, and that R should be ≤ 0.05 as a working limit. Preliminary calculations based upon the space available and these recommendations suggested a wedge angle of $27\frac{1}{2}^\circ$. This, combined with an assumed $W = Z_d/Z_2 = 0.8$ as recommended for a full depth stroke, gives $Z_d = 0.8$ and $R = 0.065$, for $s = 0.18\text{m}$ (slightly less than the maximum available of 0.2m). The theoretical wave amplitude A_w may now be determined using Figure (4.30) from Gilbert et al for a range of frequencies up to 3.5Hz. Figure (4.32a) is derived from Figures (4.30) and (4.31) which give the relative waveheight/frequency and wavelength/frequency possible for the range of stroke and water depths available. The other restriction to increased waveheight, apart from wedge stroke and water depth, is the limiting wave steepness, assumed as $(H_w/L_w)_b = 0.142 \tanh kz_2$, a theoretical limit developed by Miche for a Stokes intermediate wave. Silvester (1974) suggests that a more realistic limit, however, should be $(H_w/L_w)_b = 0.12 \tanh kz_2$. Figure (4.32b) shows the potential relative wave/water depth ranges available, the majority being within the intermediate (Airy) range $\pi/10 < kz_2 < \pi$. Comparing the two Figures (4.32 a & b), it is apparent that the highest waves will occur in the intermediate region. There are only a relatively small range of possible frequencies for shallow water waves, resulting in long period waves; these will be particularly susceptible to wave tank characteristics, such as reflection. Deep water waves are possible for frequencies greater than approximately 1Hz, but these will have a smaller amplitude than the intermediate depth waves available at the lower frequencies.

This analysis was deemed inadequate for complete design purposes, and a small scale model wedge was constructed to see if the theoretical predictions conformed to reality. Figure (4.33) shows diagrammatically the apparatus used for these small scale tests. A $\psi = 27\frac{1}{2}^\circ$ sliding

wedge was oscillated with approximately simple harmonic motion over a range of wedge displacement s from 47 to 115mm, in water depths from 143 to 240mm. The wedge stroke could be adjusted so that it just touched the bed of the channel at maximum forward stroke, or be adjusted to stop at some position on the sloping base plane. Rubber wipers were attached to the sides of the wedge face to prevent any leakage around the sides. Fins were also fitted to the face to discourage cross wave formation. Photographs 4.7 & 4.8 show the small scale wedge and channel.

Data were recorded using two twin wire wave probes and an accelerometer attached to the wedge.

The results are shown plotted on Figures (4.30), (4.31) and (4.32), and may be summarized as follows:

- (i) All waves generated were 'peaked', i.e. not monochromatic, mostly being of the Cnoidal or Stokes 3rd order type (Appendix B), see for example Figure (4.34).
- (ii) All waves were in the intermediate depth range.
- (iii) There were no significant alterations in wave characteristics along the tank length.
- (iv) It was only possible to produce waves up to a maximum steepness of 76% of the theoretical maximum. However, this actually represented 91% of the breaking criterion suggested by Silvester of $(H_w/L_w)_b = 0.12 \tanh kZ_2$.
- (v) The longer wavelengths produced greater wave reflection from the beach, e.g. for $L_w = 2.22\text{m}$ ($f_w = 0.60\text{Hz}$). The theoretical and experimental wavelengths were well correlated.
- (vi) The range of $W (= Z_d/Z_2)$ covered was 0.67 to 0.83. No definite correlation of A_w/s with Z_2/gT_w^2 for a particular W was observed in this range, although the actual waveheights obtained were slightly lower than predicted for the larger water depths (Figure (4.30)). There is, however, a reasonable agreement with the ranges of $A_w/s - Z_2/gT_w^2$ at this relatively high W .

Conclusions from (i)-(v) above may now be drawn relating to the larger prototype wedge:

- (vii) Although the theory was developed for monochromatic waves, none were in fact generated. Consequently monochromatic waves may be difficult to produce.
- (viii) The majority of waves generated will be of the intermediate depth

type. This means that in order to generate shallow water waves the water depth will have to be significantly reduced, and the wedge operated close to the bed of the wave tank. To produce deep water waves, a larger depth of water will be required with a small wedge stroke at higher frequency.

The conclusion from this is that the prototype wedge should be able to oscillate about a specifiable position with respect to the bottom of the wave tank, i.e. variable Z_m (Figure (4.29c)) independent of Z_2 .

- (ix) Although the waves will achieve stability fairly soon after generation it is advisable to consider the wave field at one (longitudinal) position only in the tank for test purposes. This is particularly important for non-monochromatic wave trains, and would need to be carefully considered.
- (x) Because of the wave breaking criterion, and also some observed turbulence at the generator, the theoretically possible waveheight of 0.38m is unrealistic, and more realistically should be expected to be approximately 0.28m. This may be further reduced by around 10% in accordance with the observations of Dedow et al (ibid) who report that turbulence at the generator reduces the waveheight below the theoretical
- (xi) The small scale tests did not attempt to test the theoretical frequency range (0 - 3.5Hz). However, nothing was observed to contradict these predictions, although the lower frequencies (longer wavelengths) could encounter beach reflection problems, which could only be overcome by special beach design and the higher frequency waves may also be affected by surface tension. The theoretical wavelengths are expected to predict reasonably well those that will actually be produced.

The larger wedge is shown diagrammatically in Figure (4.35), and as constructed in Photograph 4.9. The wedge is hollow, made of varnished marine plywood internally braced with timber. It was considered necessary for it to be deep enough to accommodate the greatest water depth plus the maximum anticipated wave amplitude, which requires a front face depth of 1m. Due to space limitations, the inclined sloping base up which the wedge runs, has been curtailed at the maximum expected still water level, this means that the length of the wedge need only be 825mm. In order to eventually generate random waves it was decided to use an oil-hydraulic powered ram via a servo-valve. The maximum theoretical thrust required may be determined using

Figure (4.30). The thrust will need to be sufficient to overcome the worst combination of bearing friction, wedge and water inertia, viscous and buoyancy effects. Gilbert et al (ibid) consider these forces (parallel to the wedge incline) separately:

(i) A force in phase with the wedge velocity:

$$E_{RR} = E_1 G_3 \cos \psi$$

(ii) A force in phase with the wedge acceleration:

$$E_{II} = E_1 G_4 \cos \psi + 4\pi^2 M_1 \sec \psi \frac{a_w}{T_w^2} - W E_1 \sin \psi$$

(iii) A buoyancy force E_B necessary to hold the wedge at mid-stroke position.

In this case the condition requiring the greatest thrust is that for maximum oscillation frequency, assuming a full depth immersion: For a wedge of nominal mass 100kg the maximum thrust required is 3.47kN, neglecting the bearing friction. In comparison the thrust required to produce the greatest wave height is 1.6kN. The largest force component is that of wedge inertia and buoyancy, in this case the wedge has not been considered neutrally buoyant. The bearing friction was indeterminable until after wedge construction, however, four linear roller bearings were specified to support the wedge upon two stainless steel shafts (Photograph 4.9). It was hoped that these would keep the bearing friction to a minimum.

Details of the power supply equipment are specified in Figure (4.36), as supplied by Hi-Power Ltd to provide a maximum thrust of 3.56kN (800lbf), and a stroke amplitude of 0.229m (9"). Using a sine wave generator and a suitable amplifier to control the servo valve, and hence the ram, a series of tests will be carried out to compare the input command signal with the resultant waves generated by the wedge. In this way a transfer function may be derived so that any specified regular waves may be generated. This is a pre-requisite necessary before considering random wave generation, as it is a form of wave generation 'calibration',

Tank design

As mentioned earlier the wave tank was designed to have a cross section of 1m x 1m. The maximum attainable length, measured from the bottom of the wave generator slope, of 8.7m was used. A hammer headed section has been constructed having a width of 1.2m and a length of 3m (1.5m either side of the tank centre line) at the end of the tank. This is

to broaden the wave dissipating beach, in the hope of being able to make it as steep as possible and thereby retain the maximum possible working area within the tank.

The introduction of a current superimposed upon progressive waves is planned using a pump connected between inlet and outlet tanks admitting and withdrawing water from the main tank, at the hammer head end and along its length. The complete tank is shown diagrammatically in Figure (4.37).

Possible test ranges

The potential experimental ranges for a vertical surface piercing cylinder may now be examined when it is immersed in the waves generated in the wave tank designed above.

Figure (4.32a & B) gives the possible wave heights, lengths and frequencies, assuming a maximum still water depth of 0.6m: However, practically the waveheights shown should be reduced by at least 10% (in the deep water range) and by as much as 30% in the shallow range. To avoid possible blockage effects, Sarpkaya (1976a) (page 93), suggests a maximum cylinder diameter-channel width ratio d/W of 0.18 for planar oscillatory flow, thus by analogy limiting the cylinder diameter to 0.18m unless some blockage correction is applied. Therefore for the maximum cylinder diameter and wave height conditions $d/L_w = 0.066$ and $H_w/d = 2.1$ with reference to Figures (2.1) to (2.4) the possible experimental conditions may be seen to be:

- (i) Within the combined viscous and inertia force region, or the inertia force region alone.
- (ii) Always at subcritical R_E .

These conclusions could have been anticipated following the discussion presented in Chapter 2 pertaining to models in wave tanks.

Possible extension of this range using cylinder roughening, or trip wires etc will be considered in Chapter 5, where the earlier relevant discussion in previous Chapters is correlated,

(4.3.2) Summary of wave tank facility design

This Section (4.3) has developed and applied some of the ideas relating to the design of model wave test equipment. Regular wave generation has been considered as a pre-requisite for eventual random wave modelling, about which little has so far been said. Space precludes discussion in this area and reference may be made to Dedow, Thompson & Fryer (1976) for model random wave design philosophy, or to Christian

(1973) for design example.

Some assessment of the potential fulfillment of the original specification may now be made (page 155):

- (i) (a) Controllable regular waves within the limited range above are expected.
- (b) Extension to random waves would seem to be possible once the transfer function between the control signal and the wave output has been determined. Reference to Christian (ibid) indicates that a maximum model frequency of 3.5 Hz would be adequate for modelling (intermediate water depth) full scale wave amplitude-frequency spectra. A typical model geometric scale of the order of 45 could be used. The servovalve/oil hydraulic generation system is suitable for developing a controllable 'random' output.
- (ii) The superimposed current will be produced, and generally used to steepen the waves by opposing their direction of progression, using a pumping system.
- (iii) (a)&(b) Within the constraints above this will be a useful undergraduate teaching and postgraduate research facility.
- (c) It is obvious with reference to Chapter 2, particularly due to the low potential R_E simulation, that industrial consultancy using this wave tank will be minimal.



THAMES POLYTECHNIC WEDGE WAVE GENERATOR

PHOTOGRAPH (4.9)



THAMES POLYTECHNIC WAVE TANK

PHOTOGRAPH (4.10)

(4.4) Chapter Summary

This Chapter has considered two experimental approaches, that of a relative planar oscillatory flow between a fluid and a circular cylinder, and the possibility of using a progressive wave flow past an immersed circular cylinder. Some of the experimental difficulties have been discussed, particularly relating to the experimental ranges and procedures. Any similarities between the two cases will be considered in Chapter 5 with reference to Chapters 1.2 and 3.

CHAPTER 5

THE RELATIVE SUCCESS OF MODELLING IN UNDERSTANDING FLUID DYNAMICS

(5.1) The philosophy of this Thesis

"The difficulties in stepping straight from studies of physical mechanisms to the Morison Coefficients, or from small scale, idealised models to large scale structures in real seas, should not obscure the importance of the fundamental studies. In the quest for design-data, they provide routes that can usefully be followed in parallel to measurements at sea and empirical formulations".

Pearcey (1979)

This quotation encapsulates the philosophy of this thesis: To consider the possibility of modelling complex fluid-cylinder kinematic conditions in a simpler form, and the validity of that modelling as a representation of

(i) the relative fluid-cylinder dynamics of different kinematic models,

and

(ii) larger scale prototype fluid-cylinder dynamics.

Both of these cases may lead to information relevant to the design of cylindrical structures constructed in a moving fluid environment, either by an understanding of the fundamental force producing mechanisms, or simply by a gross scaling up of measured model forces to prototype size.

Chapter 1 traced the understanding of the mechanics of relative fluid force from the simplest, kinematically, to the more complex, only stopping prior to considering the greater complexities involved in kinematic randomness, which occur, perhaps more commonly, in nature. The development of the theory of modelling in Chapter 2 led into a discussion of the difficulties of modelling cylinders in a water wave environment, although the emphasis was again upon deterministic conditions, rather than random. Following these two Chapters, Chapter 3 considered the types of simplified, or otherwise, kinematic experimental models that have evolved to investigate fluid-cylinder dynamics. The emphasis here was on the experimental techniques, difficulties and limitations. A thorough discussion of the reported results from cylinder in water wave experiments has not been presented, principally because of the

analogy to planar oscillatory flows, but also because of the limited usefulness of much of the early experimental wave-cylinder work. Further consideration of wave-cylinder experiments is included in the present Chapter.

By way of example, Chapter 4 examined in detail the setting up of, and results from, a relative planar oscillatory flow experiment, and the difficulties and limitations of water wave experiments.

This Chapter will be concerned with the philosophy outlined in (i) and (ii) above, rather than a rigorous exposition of the fluid-cylinder dynamics so far presented, except where the two approaches inevitably coincide. The questions that may now be answered (at least in part) as a result of Chapters 1-4 are:

- (1) As to what extent simpler kinematic conditions may be used to represent those that are more complex.
- (2) The important experimental conditions which are a pre-requisite for that representation.
- (3) The extension of this representation to other scales, expressed in terms of ratios, such as R_E or N_K .
- (4) The usefulness of simple mathematical models, such as the Morison equation.
- (5) The relevance of (1)-(4) for
 - (a) the investigation of fundamental fluid dynamics,
 - (b) design purposes.

(5.2) The representation by simple kinematic conditions of those that are more complex

Bernitsa (1979) describes an oscillating cylinder immersed in flowing water experiment for which a dimensional analysis is presented. The relevant dimensionless groups that influence the in-line force are considered in terms of an instantaneous $R_E(t)$ and a flow history, $C(t) = \phi [R_E(t), \text{history}]$. The application of this representation becomes increasingly more complex as the relative cylinder-fluid kinematic complexities increase. This thesis has shown this to be true, although such a reduction into an $R_E(t)$ and history dependence alone may be too simple.

Equation (2.10) was an attempt to bring together all of the physical quantities affecting the fluid dynamics of vertical circular cylinders in waves. This equation was produced without any recourse to available knowledge in this area. In the light of subsequent discussion, and indeed earlier discussion in Chapter 1, a more useful formulation for a rigid vertical circular cylinder immersed in a fluid moving with the relative kinematic conditions specified in Section (2.3.2), remote from a solid boundary, would be:

$$C(t), C'(t), C_L = \phi \left[R_E \text{ or } \beta, N_k \text{ or } I_m, N'_k \text{ or } I'_m, Fr, m/m_d, f/f_s, f/f_n, \right. \\ \left. d/W, t/T, L_z/d, e/d, H_w/L_w, d/L_w, kz_2 + \text{history} \right] \dots \quad (5.1)$$

The higher order rates of kinematic change specified by equation (3.14):

$$d^{n-1}u(t)/dt^{n-1} \times d^n s/dt^n$$

are important for kinematic conditions that are more complex than planar oscillatory motion. Maull & Milliner (1978a) and Matten (1979), have shown that this equation may be incorporated into the functional form of the force coefficients as higher order forms of N_k or I_m ; N'_k or I'_m .

Subdivision of equation (5.1) into purely oscillatory or rectilinear terms gives:

(i) Relative oscillatory motion

$$C(t), C'(t), C_L = \phi \left[\beta, N_k, N'_k, Fr, m/m_d, f/f_s, f/f_n, t/T, \right. \\ \left. D/d, e/d, L_z/d, d/W, H_w/L_w, d/L_w, kz_2 \right. \\ \left. + \text{history} \right] \dots \quad (5.2a)$$

The terms $Fr, H_w/L_w, d/L_w$ and kz_2 would apply in wave flows only, if the effects of unwanted surface waves caused by

relative fluid-cylinder movement may be neglected.

(ii) Relative rectilinear motion

$$C(t), C'(t), C_L = \phi \left[R_E, I_m, I'_m, m/m_d, S, \xi/f_n, L_z/d, D/d, e/d, d/W, \right. \\ \left. + \text{history} \right] \dots \quad (5.2b)$$

In this case S is included to incorporate the vortex shedding frequency, and may be a function of R_E , if the relative motion is steady, for example. These equations (5.2a) and (5.2b) can be used as the basis for the conclusions regarding the realms of similarity between the different types of motion.

(5.2.1) Wave- planar oscillatory similarities

Chakrabarti (1980) extends the range of results of Chakrabarti (1976), using a larger diameter cylinder in waves, up to $N_K = 85$ ($R_E : 2 \times 10^4 - 3 \times 10^4$). Comparison of these results for C_D and C_M in this range with those of Sarpkaya (reported in Chapter 1) show fair agreement, particularly for $N_K < 40$. Although there is some difference, particularly in C_M around $N_K = 12$, as shown in Figure (5.1). The good agreement is surprising because the results were evaluated using 5th order Dean's Stream Function wave theory (Appendix B), and not obtained by measuring the actual wave particle kinematics. There was comparatively little scatter, however, in the experimentally recorded values of C_D and C_M with respect to N_K , except in C_D at low N_K , as expected due to the relatively low proportion of the drag component in this region. It was shown in Chapter 1, (Figure (1.32), for example) that kZ_2 is significant when determining the vorticity dependent forces (at least) in waves. It would be expected that if kZ_2 were large then the planar oscillatory flow and wave flow cases would differ. In Section (1.3.2) a discussion of cylinders immersed in waves, using equation (1.43), which is a simplified version of equation (5.2a), considered the effects of kZ_2 , ignoring any wave non-linearities as expressed by H_w/L_w , and assuming negligible wave diffraction (i.e. $d/L_w < 0.2$). It was shown that the shallow water waves (low kZ_2) tended more to planar oscillatory conditions. The experiment reported by Chakrabarti involved non-linear waves (as illustrated by the use of 5th order wave theory) and therefore the effects of H_w/L_w must also be considered in relation to planar oscillatory flows. The differences between non-linear (or finite amplitude) water wave conditions and planar oscillatory have been given by Isaacson (1974) and may be summarized

in relation to kZ_2 :

- (i) The Ratio between higher order wave particle velocities compared with first order: U'_{Wmax}/U_{Wmax} are important. As kZ_2 increases the effects of this decrease.
- (ii) The wave steepness: H_w/L_w , indicates increasing non-linearities as it becomes larger (see for example, the model wave tank results in Section (4,3)). As kZ_2 increases this effect will also increase.
- (iii) H_w/Z_2 , the relative wave height/water depth, is a measure of the asymmetry of the horizontal 'flow' in one semi-cycle compared with the next (in the opposite direction). This is manifest by an increased vorticity dependent force during the 'forward' motion compared with the 'backward' motion, e.g. the lift force maximum will be larger during the passage of a wave crest than during the passage of the trough. kZ_2 does not affect this ratio, but the greater H_w/Z_2 the more the conditions will differ from those of planar oscillatory.
- (iv) The relative proportion of W_w to U_w will increase with kZ_2 (e.g. $W_w/U_w = \tanh(kZ_2)$ even for first order waves).

This last effect has been compared with the planar oscillatory case by Pearcey (1979), and formerly considered in Chapter 1 from Davies (1975): Vortex shedding behaviour is significantly affected by an axial or shear flow, not only by affecting the vortex correlation length, but also by destabilizing the laminar boundary layer and promoting transition to turbulence at a lower R_E . This suggests that the critical R_E may be lower in wave flows than in planar oscillatory flows, which in turn have a lower critical R_E than cylinders in a steady flow. Obviously the value of kZ_2 would therefore be of fundamental importance here.

Chakrabarti (ibid) indicates a correlation of in-line wave force coefficients with planar oscillatory flow for all results recorded at three separate depths below his wave surfaces. There appears to be no obvious scattering of the results which would confirm any velocity-depth gradient effects, when compared with the planar oscillatory case. Details of the actual wave heights used are not given, but if a large kZ_2 condition (deep water waves) is assumed:

$N_k \propto \pi H_w/D$, i.e. an increase in N_k is obtained in wave flows by increasing the wave height. In such conditions, as shown in

the discussion above, the wave nonlinearity and its deviation from the planar oscillatory analogy, would also be expected to increase. The divergence of the two flow conditions for an $N_k > 40$, shown in Figure (5.2), is therefore to be expected.

Another important difference between wave and planar oscillatory flows is the rising and falling of the free surface, indicated by Zdravkovich & Namork (1977) to affect the relative vortex strength and shedding, by longitudinal compression or expansion of vortex 'tubes'. Comparison of the number of vortices shed in a wave semi-cycle with those shed at similar N_k in a planar oscillatory flow would be expected, therefore, to illustrate differences. However, no significant difference in the numbers of vortices shed in wave flows has been reported, even in the extensive tests of Sawaragi, Nakamura & Kita (1976), who compared their wave test results with those of Sarpkaya for an oscillating water tunnel. Sawaragi et al also refer to the importance of kZ_2 in wave flows, but contend that if an $rms N_k$ is used, corresponding to the water depth, rather than a maximum (surface) N_k , then the effects of kZ_2 are included in N_{krms} . They found that the probability distribution of the maximum lift force fitted a Rayleigh distribution. Comparison of the ratio between the 1/10 significant value of the maximum lift forces and the mean value of the maximum in-line forces with Sarpkaya's results and correlated with N_{krms} , was good for $N_k < 15$ ($N_{krms} < 14$), as shown in Figure (5.2a). This was similar to the 1/10 significant C_L comparison, and correlation with N_{krms} ; Figure (5.2b). This Figure also shows the results of a potential flow solution using the Blasius equation, in a similar way to equation (1.22), and assuming planar oscillatory flow, but utilizing the observed vortex pattern for N_{krms} less than, and greater than 9. These fit the observed C_L measurements quite well, apart from the inevitable scatter, and for $N_{krms} < 5$. The phase angle of the maximum in-line and lift forces compared with wave crest phase for the N_k (1-30) range tested was also presented. The significant variation in phase from 0° or 90° in the intermediate (drag and inertia) N_k (5 to 15) range found in planar oscillatory flows (Figure (1.21)) was repeated with a large scatter in maximum lift force phase angle. The digression of these results from those of Sarpkaya for larger N_k (in the drag dominant region) are explained as actual experi-

mental differences between wave and planar oscillatory flow experiments, however, without a simultaneous presentation of the β values actually obtained in this experiment it is impossible to comment upon this statement, particularly in view of the previously postulated differences that exist for experiments with β less than, or greater than, 3×10^3 in oscillatory flows.

In summary it may be said that planar oscillatory flows may be expected to represent wave flows provided:

- (i) The waves are not significantly non-linear, i.e. H_w/L_w and also H_w/z_2 are small.
- (ii) The waves tend to shallow water, i.e. kz_2 is small.
- (iii) The relative cylinder size d/L_w is small.

In the case of non-linear waves, the many reported experiments using an oscillating airstream in a wind tunnel, of the form of $u(t) = U_0(1 + A_p \sin 2\omega_p t)$, see for example Hatfield & Morkovin (1973), may be applicable due to the inequality of the fluid kinematics from semi-cycle to semi-cycle, similar to that found under non-linear wave crests and troughs. However, these would suffer from the other deficiencies mentioned, particularly a lack of longitudinal vortex stretching and compressing.

Unfortunately no evidence is so far available as to the exact numerical definition of the limits (i) to (iii) above, and the statements must remain general. It is also expected that because β is a correlating parameter in planar oscillatory flows, being a basic boundary layer parameter, equivalent to R_E in steady flows, it would also be important in wave flows. Consideration should therefore be given to simulation of wave flows using planar oscillatory flows at equivalent β .

(5.2.2) Oscillatory-unidirectional similarities

The obvious difference here is due to flow history contained in the residual vorticity. Even a significant freestream turbulence level will not simulate the effects of a reversing flow (Pearcey (1979)), although it may go some way to eliminating the difference, by hastening the onset of boundary layer transition. The principal effect of residual vorticity, however, is to influence the development of vorticity in subsequent semi-cycles. At higher R_E the ^{viscous} diffusion of vorticity will be diminished, and the effects from one semi-cycle will

be expected to persist longer, influencing that following. The 'degree of unsteadiness' in an oscillatory flow has been shown to depend upon N_k ; the larger N_k the more the flow conditions tend to steady. An $N_k > 50$ has been determined from the $T/T_s \geq 10$ suggestion of McHown & Keulegan (1959) as a minimum value above which flows may be considered quasi-steady, and for which an oscillatory flow may be modelled using a unidirectional steady flow. Below this N_k , parts of the oscillation cycle may be compared with unidirectional experiments, but care must be exercised due to possible differences such as the increased vortex correlation lengths recorded in oscillating flows (see for example, Feng (1968)), and the earlier boundary layer transition found by Sarpkaya for oscillatory flows.

The $N_k \approx 50$ suggested as a limit, may in fact be higher than necessary, as it is based upon an equivalent steady flow Strouhal number, which may not be generally applicable to oscillatory flows (see Figure (1.17), for example) and some reduction in N_k may be possible, particularly as there is evidence that a vortex street is established in oscillatory flows for $N_k > 25$. However, in the absence of further evidence the original suggestion remains that N_k should be greater than 50 before an oscillatory flow can be represented by a steady flow.

There is obviously significant differences between decelerative and accelerative flows, and this should be borne in mind when comparing unidirectional conditions with those during deceleration of a relatively oscillating cylinder. The deceleration part of the cycle for example experiences a reversal of the in-line force vector before the velocity vector reverses at the amplitude of motion (Chapter 4). Decelerative flows are therefore similar to oscillatory in that they are influenced by residual vorticity. Unfortunately experimentation using this type of unidirectional flow has so far been too limited to reach any definite conclusions.

In unidirectional unsteady flows the Iversen modulus, in the form of S/d , is the appropriate correlating parameter, being a more general form of the Keulegan Carpenter number. Unfortunately cross-correlation between unidirectional accelerative and oscillatory conditions cannot be achieved using I_m , because of its tendency to zero or infinity where kinematic quantities tend to zero, at the maximum and minimum oscillatory displacement positions.

(5.2.3) Rectilinear steady and unsteady flow similarities

The two cases of relative unidirectional unsteady flow considered were gradual and impulsive acceleration, the fluid dynamics of which were shown to correlate with S/d . Shear layer separation and asymmetry were seen to develop as a function of S/d alone, and to be independent of $R_E(t)$ in each case up to a limiting S/d . This is in contrast to steady flows, which correlate exclusively with R_E . Although lift forces have not been investigated in unsteady flows, the drag and inertia in-line force components tend to fixed values at relatively large S/d after vortex shedding has been established, e.g. the results of Sarpkaya & Garrison (1963) show that C_D tends to C_{D_s} for $S/d > 3$ for a gradual acceleration, whereas Sarpkaya (1966) suggests an $S/d > 12$ for an impulsive acceleration. The implications of this are that only for an S/d greater than 12, may steady flow conditions be considered to represent unidirectional accelerative, although the possible effects of the higher order rates of change of the kinematic conditions, expressed by I'_n , and suggested in these two experiments, should also be considered. Comparison of Figures (3.5) and (3.6) shows that the incidence of boundary layer transition is also important, because it affects the rate at which steady conditions are attained

(5.2.4) Summary of relative kinematic similarities

The fluid dynamics of relative motion between water and an immersed vertical circular cylinder may be understood by reducing the more complex relative flows to simpler ones within certain limitations. Taking advantage of this reduction, Pearcey (1979) considers the relative in-line fluid forces to be composed of three parts:

- (i) A potential component, A_x , which is completely independent of viscous effects.
- (ii) A separated (vortex independent) component, B_x , which may be determined using a wake splitter plate to suppress vortex formation and wake oscillation.
- (iii) A discrete vortex component C_x .

Using a steady flow, component (iii) may be determined by measuring the total in-line force and subtracting component (ii). These components for wave, planar oscillatory, and steady flows are shown in Figure (5.3), taken from Pearcey (1979), and based upon published C_D/R_E results. This simple picture assumes that these effects are mutually exclusive and may be linearly summed, similarly to the pre-

sentation in Chapter 1.

From the previous Sections it would seem that relative steady flows may represent unsteady flows experimentally only provided that the 'degree of unsteadiness' is small. That rectilinear unsteady flows may represent oscillatory unsteady flows only for parts of the oscillation cycle. Relative oscillatory flows may be represented by steady flows when the oscillation period or amplitude is large. More experimental investigation of the oscillating force components in steady flows may assist in the understanding of more complex kinematic conditions, particularly as there is evidence of similarity between the various harmonic effects. Planar oscillatory may be employed to represent wave conditions provided the waves are not steep or non-linear.

(5.3) Experimental difficulties and analogies

A great deal of experimental effort has been directed in the past to understanding the fluid dynamics involved in relative steady flows. This has resulted, for example, in the universally accepted $C_d - R_E$ relationship shown in Appendix A. The problems of experimentation in relative steady flows have also been extensively investigated, as summarized in Chapter 1; the effects of blockage, turbulence, roughness, aspect ratio, and three dimensional problems, for example have been reported, and guidance as to their avoidance or utilization, has often been given. Much of this work has been carried out in uniform airflows, in order to obtain a high R_E . There have been occasional comments in the literature, and reported experimental results, (see Dickens (1976) for example), which appear to indicate differences between relative air and water flow results, particularly pertaining to vorticity behaviour and effects. Whether this is only because of, say, different turbulence levels rather than any other neglected scale effect it is impossible to say. This possible difference is particularly relevant to the present discussion because of the extension of steady flow (in air or otherwise) results to other kinematic conditions. However, there appears to be no conclusive evidence for postulating a difference between relative water and airflows, or suspicion of the existence of any additional correlating parameter other than those previously mentioned. On this basis, the extension of steady (airflow) experimental experience to the non-uniform relative water flow conditions, which are particularly relevant to this thesis, may be included within the context of Section (5.2) above, when considering experimental analogies.

The various experimental problems which may affect the relative cylinder-fluid dynamics are now considered.

(5.3.1) Three dimensional effects

These will be grossly comparable for all of the kinematic conditions considered, in that the problems will be similar, i.e. vortex correlation lengths, aspect ratios, end effects, and shear flows etc. However, previous discussion has indicated that there will be large differences between steady, unidirectional unsteady, planar oscillatory, and wave flow conditions. There is evidence to suggest that the planar oscillatory case represents an extreme, or fully vortex

correlated, wave flow condition. The avoidance of end effects, and the simulation of an infinitely long cylinder can only be approached using the steady flow criteria, due to the complexity of the other types of relative flow, apart from wave flows, where an axial kinematic component exists. There is conflicting evidence as to the effectiveness of simulating an infinite cylinder by using an increased (dummy) cylinder length, or end plates, which themselves cannot be rigorously designed. The method of relative fluid force measurement to be used in an experiment is fundamental in this context due to the difference in measuring either the cylinder support reactions, giving a total force resulting from a finite aspect ratio, or a circumferential ring of pressures, and integrating to determine the forces, resulting in a zero aspect ratio, and a neglect of the skin friction force component. In the latter case flow visualization studies, and the understanding of vorticity behaviour cannot adequately represent a full scale, or design situation, where the behaviour of vorticity would be expected to be confined to longitudinal 'cells' of activity, by analogy to its behaviour, even in 'steady' flows. The pressure measurement method would, however, be less affected by end effects than the reaction force measurement technique.

(5.3.2) Blockage (neglecting solid boundary proximity effects)

The employment of steady flow blockage corrections for oscillatory conditions, in order to use as large a size cylinder as possible, is attractive. However, the validity of so doing is inconclusive; conflicting arguments being presented in the literature reviewed. The gross effects created by an over-sized cylinder may be considered to be similar in oscillatory compared with unidirectional conditions, but the additional problems created by residual vorticity and wake reversal are unknown. Without additional corroboration, the claims of Bearman et al (1978), based upon flat plate 'bluff body similarity' tests in oscillatory flows; that the Maskell steady flow correction may also be used in oscillatory flows, must be considered unsubstantiated. Sarpkaya's recommendations of $d/W \leq 0.18$ should therefore be accepted as the limiting condition to avoid blockage effects, and hence to determine the limiting cylinder diameter in oscillatory flows.

(5.3.3) The effects of freestream turbulence levels

Like the previously considered effects, results from steady flow tests would be expected to be generally applicable to more complex kinematic conditions. It was shown in Chapters 1 & 3 that an increase in freestream turbulence in a relative steady flow induces an early onset of boundary layer transition with respect to R_E , and a consequent narrowing of the wake and reduction in C_d for a given subcritical R_E . In the postcritical R_E region relative turbulence levels have less effect upon C_d . The simulation of higher R_E flows by increasing turbulence levels is, however, not possible even in 'steady' flows because the vorticity behaviour is more complicated than as would be suggested merely by an equivalent R_E . Consequently the utilization of turbulence levels to simulate higher R_E flows in more complex kinematic conditions is inadvisable, despite the apparent similarity between the early onset of transition in turbulent steady flows, with that in planar oscillatory flows.

(5.3.4) Surface roughness, trip wires and splitter plates

The detailed fluid dynamics of roughened surface cylinders in a relative fluid flow has not so far been considered in this thesis for other than steady flows (Section (3.5.3)), and obliquely, when reviewing the work of Sarpkaya in Section (3.4). Experiments and discussions particularly relevant to the effects of roughness in wave and planar oscillatory flows are presented in Miller (1976), Matten (1977) and Lighthill (1979). A summary of the relevant conclusions from these papers are:

- (i) The effects of relative surface roughness are different in the subcritical, critical, super and postcritical shear layer regions for all types of relative kinematic flow conditions: In the subcritical region the drag may be reduced by increasing the surface roughness, despite the increased overall size of the cylinder. In the super and postcritical region the drag will be increased by increasing the cylinder surface roughness.
These regions may be defined approximately for steady flows (Miller (ibid)):
(i) Super critical: $R_E \geq 6 \times 10^3 (kr/d)^{-1/2}$
(ii) Postcritical: $R_E \geq 2 \times 10^3 (kr/d)^{-1}$ for $kr/d > 10^{-3}$
- (ii) The lift force coefficient in planar oscillatory or wave flows appears to be unaffected by surface roughness. However, the in-line force is altered by the relative roughness in both cases. It appears that roughnesses in wave flows coupled with the effects of the axial flow component conspire to effect a boundary layer transition at a lower R_E than in the planar oscillatory flow case, which, as mentioned earlier, occurs earlier than in steady flows. See for example Figure (5.4) from Matten (ibid).

The conclusions that may be drawn from these findings are that post-

critical steady, planar oscillatory and wave flows exhibit similar behaviour for an increase in surface roughness, although the actual value of $R_E(t)$ (say) at which the boundary layer transition occurs is substantially different, being lower for the more complicated relative kinematic conditions, which are found in wave flows. The employment of the scaling limits of Szechenyi (1975), reported in Section (3.5.3) for steady flows, to simulate high R_E oscillatory flow conditions must, however, be reviewed with suspicion until further research has been carried out in this area.

Trip wires, unlike surface roughness, do not occur at full size, but are used to experimentally induce boundary layer transition at low R_E , and so simulate high R_E conditions. In Chapter 3, steady flow trip wire experiments were mentioned. Extension of the technique to planar oscillatory flows has been attempted recently by Bushnell (1979), using a pulsating water tunnel apparatus at HRS. The trip wires were positioned at all four 45° radial positions, with respect to the oscillating flow vector, on the 7.62cm diameter cylinders used, and were 3.2mm in diameter. For both the in-line and transverse forces any R_E force dependence disappeared with the trip wires fitted, as shown in Figures (5.5a & b), thus indicating that the trip wires correctly created high R_E analogous conditions. However, a much larger in-line force coefficient was obtained with the trip wire simulation than was expected at high R_E and N_k , which leads Bushnell to conclude that this simulation technique may not be applicable to oscillatory flows. He does not attempt to correlate these results with β , however, which does seem to be a striking omission in view of Sarpkaya's extensive results illustrating its' importance in oscillatory flows. No discussion as to the size or disposition of the trip wires around the cylinder is presented either, and in view of the importance of this in steady flows, as illustrated in Chapter 3, this is also an unfortunate omission. Despite Bushnell's pessimism regarding this type of high R_E simulation, it would seem that there is scope for further investigation into the use of trip wires in planar oscillatory flows. Their use in wave flows, however, is not recommended until the simpler planar oscillatory condition is better understood.

The introduction of a splitter plate positioned on the dividing streamline behind a circular cylinder in a steady flow can suppress vortex

shedding in both the sub and postcritical flow regions. This may significantly reduce C_d , as reported by Pearcey (1979), except in the transcritical region. The reduction of a complex flow into constituent vorticity dependent components due to separate vortex shedding and flow separation effects has already been considered in Section (5.2.4) and illustrated in Figure (5.4), but this has been derived from a steady flow analogy condition. To the author's knowledge no unsteady, or oscillatory flow tests using splitter plates have been reported. The extension of this experimental technique for isolating the vortex shedding force component into planar oscillatory flow, and even into wave flow experiments, would provide information to corroborate, or dispute, the simplistic model suggested by Pearcey (ibid).

(5.4) Wave force model- prototype similarity

The functional dependence of the drag, inertia and lift force components in relative oscillatory and rectilinear relative flows is given by equations (5.2a) and (5.2b) respectively. As shown in Chapter 2, these equations are the starting point for developing a small scale model which accurately represents a full sized prototype. Because of the vorticity dependence of each of the constituent forces in oscillatory flows, scale modelling in waves has been shown to be possible only where the relative inertia/drag force ratio, expressed by I_m^{\max} is large. In waves this is a dependence upon the ratio x_w^{\max}/d (approximately $= Nk/2\pi$), for wave-cylinder conditions that are not in the diffraction regime ($H/L_w < 0.7$), as illustrated in Figure (2.3). For $x_w^{\max}/d < 1$ the total wave force upon an immersed cylinder is dominated by the inertia component, and the R_E scaling problems, that particularly affect C_D are reduced. Prototype scale modelling is therefore possible only in the region of Nk approximately less than 6, depending upon the relative water depth and wave non-linearity. The application of the possible difference in fluid dynamic conditions postulated either side of $\beta \approx 3 \times 10^3$, for planar oscillatory flows, has so far not been considered, or observed, in wave flows. Indeed the significance of β in wave flows, as distinct from R_E and Nk , has not been identified. β may be expected to have a similar significance in all oscillatory flows, as it has been demonstrated to be the parameter that describes the relative boundary layer thickness. In this respect it is equivalent to R_E in steady flows.

The range of application of wave model testing may be extended by employing the simplified kinematic models where possible, and described above, or by using one of the experimental techniques for enhancing the effective experimental R_E such as cylinder surface roughening, the attachment of trip wires, or the fixing of separation points using sharp-edged bodies. Unfortunately insufficient information is available at present to explicitly recommend and detail the possibilities, and until further work is reported these techniques must remain purely conjectural when applied to wave conditions.

In summary, Figure (5.6) gives a flow chart which illustrates the possible physical models available to obtain information about the fundamental fluid dynamics in a full sized prototype.

(5.5) The Morison equation as a mathematical model

It has been repeatedly demonstrated in this thesis that the quasi-steady Morison equation may only be considered as an adequate description of the relative fluid dynamics in an unsteady flow where either the inertia forces ($N_k < 5$) or the drag forces ($N_k > 25$) predominate. In the drag and inertia force regime the Morison equation gives a misleading picture of fluid-cylinder dynamics. This is because the equation has evolved from an individual consideration of the two force components, as demonstrated in Chapter 1. The omission of the vorticity effects upon the 'irrotational' component C_M , and the neglect of a history term have been illustrated in previous discussion, but perhaps the most significant omission in the equation is that of the very large lift force which exists above an N_k of about 4. Formulation of C_L in terms of the kinetic, non-linear term also appears to be inadequate. Some recourse to a simpler formulation, which does not attempt to constrain the force components into strictly vorticity and potential terms would appear to make more sense in this region of both drag and inertia force importance. It has been suggested by a number of authors that a force equation in the form of a harmonic series

$$\underline{F}' = \sum_{n=1}^m c_n \sin(n\omega t + \alpha_n) \quad \dots \quad (5.3)$$

may be more appropriate, where \underline{F}' is the dimensionless resultant force, which includes both in-line and lift components, and the harmonic series is of sufficient order (m) to include all significant harmonic components. Alternatively equation (5.3) may be formulated after deducting either the irrotational, or steady force component, assuming respectively either a potential flow $C_M = 2$ (in waves), or a steady flow C_D , based upon a characteristic instantaneous $R_E(t)$. An equation of the form of (5.3) has been used to fit the forces obtained in the oscillating cylinder experiment described in Section (4.2). The harmonic and phase composition for $\underline{F}' = \bar{F}_R / 1/2 \rho U_{pc}^2 \max$ for the two complete cycles of motion recorded are shown in table (5.1). This Table reflects the non-stationary nature of the fluid dynamic forces, particularly shown by the variation in the higher than fundamental frequency components. Consequently for anything other than, say a gross maximum value of cyclic force, the general description of wave forces in the drag and inertia regimes would be expected to be only

possible using a statistical formulation, even for first order,
small amplitude, regular waves.

(5.6) Extension into the real sea

In comparison with the fluid dynamic conditions discussed in this thesis the additional complications arising in real seas are legion. The effects of wave randomness, in direction as well as characteristics, currents, marine growth and accretion, all serve to significantly perturb the simple(?) fluid dynamic conditions discussed in this thesis. The extension of the 'idealised' conditions presented herein into that sort of environment may seem to be unrealistic, but the understanding of the simpler quantifiable conditions is surely a pre-requisite for any understanding of structures in the sea environment.

Recent work such as the NMI Christchurch Bay research tower, mentioned in Chapter 2, will aid our understanding of the deficiencies between the laboratory, mathematics and reality

CHAPTER 6
CONCLUSIONS AND RECOMMENDATIONS
FOR FUTURE WORK

(6.1) Summary of Conclusions

The following summary of conclusions relates to a vertical (where appropriate), smooth, circular cylinder immersed in a relative fluid flow:

- (1) The fluid dynamics of a cylinder in a relative steady flow are reasonably well understood. This includes the effect of surface roughness and freestream turbulence.
- (2) The fluid mechanic processes observed in steady flows are grossly applicable to unsteady and periodic flows, in that the growth and development of vorticity is a controlling factor.
- (3) The relative fluid dynamics between a cylinder and an unsteadily moving fluid may be considered in two parts: as a vorticity dependent, and a vorticity free, irrotational, component. However, the extension of this fluid dynamic perspective to more complex flows, such as those that are reversing, should be made with caution, because the two components may no longer be independent, particularly for N_k between 5 and 25.
- (4) Reversing, or decelerating rectilinear flows, have important history effects contained in the vorticity, which affect the structure and magnitude of the fluid forces between the fluid and an immersed cylinder.
- (5) Even for steady flows there are unsteady force components, particularly in the direction transverse to the relative flow direction. In oscillatory flows these lift forces may be of a comparable magnitude to the in-line force, particularly for $4 < N_k < 25$. The oscillating forces have a basic harmonic content that is a function of vortex development and shedding, and consequently a function of N_k .
- (6) Cylinder boundary layer oscillation, observed in steady flows, has also been observed in an oscillatory flow. A picture of vortex behaviour in a relative oscillatory flow has been built up from the history of the pressure distribution around a circular cylinder. This pressure distribution has been used to show the importance of the residual vorticity, or history effects, in decelerative flows.
- (7) There are definite analogies between relative planar oscillatory

flows around a cylinder, and a vertical cylinder immersed in a wave field, provided the wave height and water depth to wavelength ratios are small. The simple kinematic conditions in planar oscillatory flows may therefore be used to simulate wave flow conditions, with the advantage of a higher potential R_E , and greater experimental control, such as in the accurate measurement of the fluid particle kinematics.

- (8) Steady, or rectilinear, flows may be used to simulate oscillatory conditions provided the oscillatory conditions tend to quasi-steady, i.e. for $N_k \geq 50$. Parts of the oscillatory cycle may also be simulated if they tend to quasi-steady conditions, as indicated by a low I_m , unless history effects are significant, in which case it may be possible to simulate oscillatory conditions using a decelerative unsteady flow.
- (9) Generally, the more complex the kinematic conditions then the less stationary are the relative forces exerted upon an immersed cylinder. This is particularly so for the lift force component.
- (10) The relative size of the cylinder boundary layer in planar oscillatory flows is a function of the Stokes number β , which is comparable to R_E in steady flows. β is found to be a useful correlating parameter in such flows. There appears to be significant change in fluid dynamic conditions above a $\beta = 3 \times 10^3$ approximately. Whether this corresponds to a boundary layer transition effect, similar to critical R_E in steady flows is unknown. The relevance of β to wave flows is similarly unproven.
- (11) There is no universally applicable mathematical formulation which describes the forces upon a cylinder in a relatively moving fluid. However, the Morison equation is a very good approximation, with the exception of the lift force component, for all relative flows, except those having an N_k between about 5 and 25. Even in this region, however, the Morison equation gives a sufficiently good approximation to the maximum in-line force for design purposes.
- (12) The scaling up of small scale experimental to full sized prototype conditions is restricted by the viscous scale effect which separates subcritical boundary layer conditions from post and supercritical. For wave flows this restricts models to an N_k below a value of approximately 6. 'Enhancement' of R_E , or boundary layer transitional conditions may be achieved by roughening the surface of the cylinder or by fitting longitudinal trip wires.

These techniques, however, have not been sufficiently investigated in either planar oscillatory, or wave flows, for their total effects to be adequately understood.

(6.2) Recommendations for future work

- (1) Despite the reasonable understanding of the fluid mechanics of circular cylinders immersed in a relative steady fluid flow, there is much detailed information that is lacking. In particular the relationship between the oscillating lift and drag forces and the behaviour of the separated shear layers has not been established for the range of R_E in which separation takes place. Detailed investigation of the boundary layer oscillation, in the manner of Dwyer & McCroskey (1973), and/or measurement of oscillating force components simultaneously with flow visualization studies of vortex shedding for sub, trans, and supercritical R_E , will provide answers to the detailed fluid mechanic processes involved. Simultaneous circumferential pressure records would also be useful for correlation with the other recorded information.

This requirement is a pre-requisite of any advancement of understanding in more complex kinematic flow conditions, and may also be linked with an investigation of the possible differences between air and water steady flow experiments.

- (2) The other obvious area for future experimental research, is that of decelerative unidirectional flows. These are unique because they possess a simple flow history. Such experiments, which have not proved to be very successful in the past, would respond to the sort of effort being applied to the more complicated flow cases, and provide invaluable information about the oft mentioned, but poorly understood, effects of residual vorticity. The formulation of a semi-empirical Morison type of equation would benefit from work in this area, being particularly extendable to periodic flow conditions.
- (3) The experimental effects of cylinder roughening, trip wires, and splitter plates need to be further investigated in all cases of unsteady flow, the kinematically simplest would provide basic information for extrapolation to the more complex. Also the blockage criteria for unsteady flows in tunnels, and the efficient design of end plates, particularly for oscillating cylinder experiments, are both needed. These will probably develop from a concerted programme investigating planar oscillatory flows in U-tubes, and by cylinder oscillations, at similar β and N_k .

- (4) Comparison of the range of fluid kinematic conditions in steady, unsteady and periodic flows, relatively incident upon a rigid circular cylinder, with the extensive literature dealing with flow induced vibration of flexible, or flexibly supported cylinders may yield useful correlations. A possible analogy of the dynamically responding in-line vibrating cylinder to that of the forced oscillating cylinder for example, should be investigated, and particularly the oscillating freestream case compared with that of a cylinder in non-linear waves. The coupling effects reported by Mattern (1979) indicate the importance of the frequency structures involved in relative fluid-cylinder dynamics.
- (5) Finally, some investigation as to the importance of β in wave flows would seem to be necessary, as well as further work in planar oscillatory flows to determine whether it is a more useful correlating, and scaling, parameter than R_E or N_K alone.

- Aked, C.K. (1977)
The Engima of Time. Jour. Nautical Sci.
Vol.3 No.3 July.
- Allen, H.J. & Vincenti, W.G. (1944)
Wall interference in a two-dimensional wind tunnel.
with consideration of the effects of compressibility.
Nat. Adv. Comm. Aero. Wash. Rep. 782.
- Barnouin, B. Mattout, M. & Sagner, M. (1978)
Experimental study of the validity domain of some
formula e for hydrodynamic forces for regular and
irregular flows. Proc. Conf. Mechanics of wave
induced forces on cylinders. Bristol 1978, Pub.
Pitman 1979.
- Batchelor, G.K. (1970)
An introduction to fluid dynamics.
Cambridge Univ. Press.
- Batham, J.P. (1973)
Pressure distributions on circular cylinders at
critical Reynolds Number.
Jour. Fluid Mechanics, Vol.57,2
- Bearman, P.W. (1968) The flow around a circular cvlinder in the crtiical
Reynolds Number regime.
NPL Aero. Rep No.1257
- Bearman, P.W. Graham, J.M.R. & Singh, S. (1978)
Forces on cylinders in harmonically oscillating flow.
Proc. Conf. Mechanics of wave-induced forces on
cylinders. Bristol 1978. Pub Pitman Ed. T.L. Shaw 1979
- Bearman, P.W. & Graham (1979)
Hydrodynamic forces on cylindrical bodies in oscill-
atory flow.
Proc. 2nd Conf. Behaviour of Offshore structures.
London
- Berger, E. & Willie, R. (1972)
Periodic flow phenomena.
Annual Review of Fluid Mechanics Vol.4
- Bernitsas, M.M. (1979)
Analysis of the hydrodynamic forces exerted on a
harmonically oscillating circular cylinder in any
direction θ with respect to a uniform current.
Proc. 2nd Int. Conf. on Behaviour of offshore
structures. Imperial College (BOSS 79)
- Bidde, D.D. (1971)
Laboratory study of lift forces on circular piles.
ASCE WW4 November.
- Biesel, F. & Suquet, F. (1951)
Les appareils generateurs de houle en laboratoire.
La Houille Blanche, March-April
- Birkhoff, G. (1960 revised edition)
Hydrodynamics, a study in logic, fact and similitude.
Princeton Univ. Press
- Bishop, J.R. (1978)
Aspects of large scale wave force experiments and
some early results from Christchurch Bay.
Paper 6 SUT Seminar: 'Models and their use as design
aids in offshore operations'. May
- Bishop, R.E.D. & Hassan, A.V. (1964)
The lift and drag forces on a circular cylinder in
a flowing fluid.
Proc. Roy. Soc. Series A Vol.227
Also: The lift and drag forces on a circular cylinder
oscillating in a flowing fluid. Proc. Roy. Soc. 1964

- Blevins, R.D. (1977)
Flow-induced vibration.
Van Nostrand Reinhold.
- Bloor, M.S. (1964)
The transition to turbulence in the wake of a circular cylinder.
Jour. Fluid Mechanics 19,2
- British Ship Research Assoc. (1976)
A critical evaluation of the data on wave force coefficients.
Contract Report No. W278.
See Also: Hogben, Miller, Searle & Ward (1977).
- Bruun, H.H. & Davies, P.O.A.L. (1975)
An experimental investigation of the unsteady pressure forces on a circular cylinder in a turbulent cross flow.
Jour. Sound & Vib. 1975 40(4)
- Burnsall, W.J. & Lottin, K. (1951)
Experimental investigation of the pressure distribution about a yawed circular cylinder (in the critical Reynolds Number range).
Nat. Adv. Comm. Aero. (NACA) Tech. note 2463. Sept.
- Bushnell, M.J. (1977)
Forces on cylinder arrays in oscillating flow.
OTC 2903.
- Chakrabarti, S. Wolbert, A. & Tam W. (1976)
Wave forces on vertical circular cylinder.
Proc. ASCE WW2 May.
- Chakrabarti, S.K. (1980)
Inline forces on fixed vertical cylinder in waves.
Proc. ASCE WW2 May (15403)
- Caldwell, J.M. (1955)
The design of wave channels.
Proc. 1st Conf. ships & waves Eng. Foundation Council on wave res.
- Chang, P.K. (1970)
Separation of flow.
Pergamon.
- Chantravattana, B. (1974)
Angular distribution of pressure on a cylinder oscillating sinusoidally in water.
M. Sc. Thesis Univ. Houston. December.
- Chen, Y.N. (1970)
The relationship between the Von Karman vortex street and the drag of a single circular cylinder.
Flow-induced vibration in heat exchangers. Winter annual meeting of ASME New York, December 1st.
- Christian, C.D. (1973)
The development of a programmable wave generator for the simulation of sea state.
Ph.D. Southampton Univ.
- Chung, J.S. (1977)
Forces on submerged cylinders oscillating near a free surface.
Jour. Hydronautics Vol. 11,3 July.
- CIRIA (1978)
Dynamics of marine structures
Report UR8 2nd Ed.

- Clements, R.R. & Maull, D.V. (1975)
The representation of sheets of vorticity by discrete vortices.
Proc. Aerospace Sci. Vol.16,2
- Collier, M.L. (1972)
Dynamic similarity scaling laws applied to cables.
Jour. Hydronautics Vol.2
- Crooke, R.C. (1955)
Re-analysis of existing wave force data on model piles.
U.S. SERB Tech Memo No.71 April
- D'Angremond, & Oorschot J.H. (1969)
Generation of irregular waves on model scales.
Proc. Symp. Research on wave action, Delft Hydraulics Laboratory.
- Davies, M.E. (1975)
The effects of turbulent shear flow on the critical Reynolds Number of a circular cylinder.
NPL Mar. Sci. Tech. Memo TM 108, Nov.
- Dean, R.G. (1976)
Methodology for evaluating suitability of wave and wave force data for determining drag and inertia coefficients.
Proc. Conf. Behaviour of offshore structures. Trondheim.
- Dedow, H.R.A. Thompson, D.M. & Fryer, D.K. (1976)
On the generation, measurement & analysis of random seas.
Proc. Central water and power research station. Diamond Jubilee symp. Poona, India. November.
(HRS reprint)
- Dickens, W.R. (1976)
Self-induced vibration of a cylinder-in line with a fluid flow.
Ph.D. Univ. of London
- Dronkers, M.E.L. & Massie, W.W. (1978)
Lift forces on circular cylinders.
Proc. Conf. Mechanics of wave-induced forces on cylinders. Bristol. Pub. Pitman 1979.
- Duncan, W.V. Thom, A.S. & Young, A.D. (1972)
Mechanics of fluids.
Edward Arnold 2nd Ed. 1972.
- Dwyer, H.A. & McCroskey (1973)
Oscillating flow over a cylinder at large Reynolds Number.
Jour. Fluid Mech. (1973), 61, part 4.
- Ellis, B. (1966)
Basic concepts of measurement.
Cambridge Univ. Press.
- Engineering Sci. Data Unit (1970) with amendments 1979
Fluid forces acting on circular cylinders for application in general engineering. Part 1: long cylinders in two-dimensional flow.
Item No. 70013
Part 11: Finite-length cylinders Item No. 70014 1971 (with amendments)
- Fage, A & Warsap, J.H. (1929)
The effects of turbulence and surface roughness on the drag of a circular cylinder.
ARC Memo 1203.

- Feng, C.C. (1968) The measurement of vortex induced effects in flow past stationary & oscillating circular & D-section cylinders.
M. Thesis Univ. of British Columbia.
- Gammage, W.F. Ortloff, Peers & Caldwell (1976)
Design, fabrication & installation of a prototype multiline marine production riser system.
ASME Conf. Petrol mech. eng. & pressure vessels & piping. September.
- Garrison, C.J. Field, J.B. & May, M.D. (1977)
Drag & inertia forces on a cylinder in periodic flow.
Proc. ASCE WW2 12913, May.
- Gerrard, J.H. (1961)
An experimental investigation of the oscillating lift and drag of a circular cylinder shedding turbulent vortices.
Jour. Fluid Mechanics 11, 244.
- Gerrard, J.H. (1965)
A disturbance-sensitive Reynolds Number range of the flow past a circular cylinder.
Jour. Fluid Mechanics 22, 1.
- Gilbert, G. Thompson, D.M. Brewer, A.J. (1977)
Design curves for regular and random wave generators.
HRS Report No. INT 81, 2nd impression July.
(first published in the Journ. of Hydraulic research 9, 1971 no.2)
- Glenny, D.E. (1966)
A review of flow around circular cylinders, stranded cylinders and struts inclined to the flow direction.
Australian Defence ARL Mech. Eng. Note 284
- Goldstein, S. (Editor) (1938)
Modern developments in fluid dynamics.
Oxford (Clarendon Press) Vol 1 & 11. 1st Ed.
- Gowda, B.H. L. (1975)
Some measurements on the phenomenon of vortex shedding and induced vibrations of circular cylinders.
Technische Universitat Berlin.
- Graham, J.M.R. (1978)
Analytical methods of representing wave-induced forces on cylinders.
Proc. Conf. Mechanics of wave-induced forces on cylinders. Bristol. Pub. Pitman 1979. (Ed. T.L. Shaw)
- Grass, A.J. & Kemp, P.H. (1978)
Flow visualization studies of oscillatory flow past smooth and rough circular cylinders.
Proc. Conf. Mechanics of wave-induced forces on cylinders. Bristol. Pub. Pitman 1979 Ed. T.L. Shaw.
- Hamann, F.H. & Dalton, C. (1971)
The forces on a cylinder oscillating sinusoidally in water.
Trans ASME Jour. Eng. for Indus. November.
- Hamilton, W.S. & Lindell, J.E. (1971)
Fluid force analysis and accelerating sphere tests.
Proc. ASCE HY6 paper 8195 June.

- Hamilton, W.S. (1972)
Fluid force on accelerating bodies.
Proc. 13th Conf. Coastal Eng. Chapter 99.
- Hansen, J.B. & Svendsen Ib.A. (1975)
Laboratory generation of waves of constant form.
Scholten Series Paper 9 Tech. Univ. Denmark.
Previously published Proc. 14th Conf. Coastal Eng.
1974.
- Hatfield, R.M. & Morkovin, M.V. (1973)
Effect of an oscillating free stream on the un-
steady pressure on a circular cylinder.
Trans ASME Jour, Fluids Eng. June.
- Heinzer, A. & Dalton C. (1969)
Wake observations for oscillating cylinders.
Trans ASME Jour. Basic Eng. December.
- Hogben, N. (1976)
The 'Wavedozer': A travelling beam wavemaker.
Proc. 11th Symp. Naval Hydrodynamics University
College.
- Hogben, N. (1976a)
Wave loads on structures.
Proc. Conf. Behaviour of offshore structures.
Trendheim.
- Hogben, N. (1978)
Aspects of ocean engineering which are relevant for
the ITTC: A review with emphasis on the modelling of
sea conditions.
Proc. 15th Int. Towing Tank Conf.
- Hogben, N. Miller, B.L. Searle J.W. & Ward, G. (1977)
Estimation of fluid loading on offshore structures.
NMI R11 April
- Holmes, P. (1978)
Analysis of data from the Christchurch Bay experiment.
Proc. Seminar 'Models and their use as design aids
in offshore operations'. Paper No.7
- Humphreys, J.S. (1960)
On a circular cylinder in a steady wind at transition
Reynolds Number.
Jour. Fluid Mechanics 9, 603.
- Huner, B. & Hussey R.G. (1977)
Cylinder drag at low Reynolds Number.
Physics of fluids, Vol.20,8. August.
- Hyun, J.M. (1976)
Simplified analysis of a plunger-type wavemaker
performance.
Jour. Hydronautics, Vol.10, 3, July.
- Isaacson, M. de St.Q. (1974)
The forces on circular cylinders in waves.
Ph.D. Cambridge Univ.
- Isaacson, M. de St.Q. (1978)
Wave induced forces in the diffraction regime.
'Mechanics of wave-induced forces on cylinders'.
Pub. Pitman, Ed. T.L. Shaw. 1979
- Iversen, H.W. & Balent, R. (1951)
A Correlating modulus for fluid resistance in acc-
elerated motion.
Jour. Appl. Phys. Vol.22,3, March.
- Jaeger, I.G. (1964)
Elementary theory of elastic plates.
Pergamon.

- Jones, G.W. (1968) Unsteady lift forces generated by vortex shedding about a large, stationary, and oscillating cylinder.
ASME Pub. 68-FE-36
- Kacker, Pennington, Hill (1974)
Fluctuating lift coefficient for a circular cylinder in cross flow.
Jour. Mech. Eng. Sci. I.Mech. E. Vol.16,4.
- Keating, P. & Webber, N.B. (1977)
The generation of periodic waves in a laboratory channel: a comparison between theory and experiment.
Proc. ICE,2, Paper 7985 December 819-832.
- Keim, S. (1956)
Fluid resistance to cylinders in accelerated motion.
Proc. ASCE Jour. Hyd. Div. paper 1113
- Keulegan, G.H. & Carpenter, L.H. (1958)
Forces on cylinders and plates in an oscillating fluid.
Jour. Nat. Bur. Standards Vol.60 No.5 May.
- Kim, Y. & Hibbard, H.C. (1975)
Analysis of simultaneous wave force and water particle velocity measurements.
OTC 2192
- King, R. (1971)
The added mass of cylinders.
BHRA TN 1100 April.
- King, R. (1977)
A review of vortex shedding research and its application
Ocean Engng. Vol.4 pp 141-171.
- King, R. (1977a)
Vortex excited oscillations of a cylinder dipping into water.
Unpublished BHRA report.
- Kinsman, B. (1965)
Wind waves.
Prentice Hall
- Kolkman, P.A. & Van Der Weide, J. (1972)
Elastic similarity models as a tool for offshore engineering development.
Delft Hydr. Laboratory, April.
- Kulin, G. (1958)
Solitary wave forces on submerged cylinders and plates.
U.S. Nat. Bur. Standards. Report 0603-11-3546.
- Laird, Johnson & Walker (1959)
Water forces on accelerated cylinders
Proc. ASCE WW1, 1982, March.
- Lamb, H. (1932)
Hydrodynamics.
Cambridge Univ. Press 6th Ed.
- Lighthill, J. (1979)
Waves and hydrodynamic loading.
Opening address 2nd Int. Conf. on behaviour of offshore structures. Imperial College.
- Lofquist, K.E.B. (1977)
A positive displacement oscillatory water tunnel.
U.S. Army CERC Misc. Rep. No.77-1 February.
- Mair, W.A. & Maull, D.J. (1971)
Bluff bodies and vortex shedding. (A report on Euro-mech 17).
Jour. Fluid Mechanics 45,2.

- Marchman, J. (1977)
Effective Reynolds Number for heated spheres and cylinders.
AIAA Jour. Vol.15, No.7 July.
- Marris, A.W. (1964)
A review on vortex streets, periodic wakes, and induced vibration phenomena.
Trans. ASME Jour. of basic Eng. June.
- Maskell, E.C. (1963)
A theory of the blockage effects on bluff bodies and stalled wings in a closed wind tunnel.
ARC Rep. & Memo No.3400, November.
- Matten, R (1977)
The influence of surface roughness upon the drag of circular cylinders in waves.
OTC 2902.
- Matten, P.B. (1979)
Loads on a cylinder in waves, currents and oscillatory flow.
Ph.D. Univ. Cambridge.
- Matten, R.B. Hogben, N. & Ashley R.M. (1978)
A circular cylinder oscillating in still water, in waves and in currents.
Proc. Conf. Mechanics of wave-induced forces on cylinders. Bristol. Pub. Pitman 1979 Ed. T.L. Shaw
See also NMI R63 July 1979.
- Maul, D.J. & Milliner, M.G. (1978)
Sinusoidal flow past a circular cylinder.
Coastal Eng. 2: 149-168.
- Maul, D.J. & Milliner, M.G. (1978a)
The forces on a circular cylinder having a complex fluid motion.
Proc. Conf. Mechanics of wave-induced forces on cylinders. Bristol. Pub. Pitman 1979 Ed. T.L. Shaw.
- Mehaute, B. le (1976)
An introduction to hydrodynamics and water waves.
Springer-Verlag.
- Mehaute, B. le (1976a)
Similitude in coastal engineering.
Proc. ASCE WW3 12293. August.
- Mercier. J.A. (1973)
Large amplitude oscillations of a circular cylinder in a low speed stream.
Ph.D. Diss. Stevens Inst. Tech.
- Miller, B.L.P. (1976)
The hydrodynamic drag of roughened circular cylinders.
NPL Rep. Mar. Sci. R147 April.
- Miller, B.L.P. & Matten, R.B. (1976)
A technique for the analysis of wave loading data obtained from model tests.
NPL Mar. Sci. R136, June.
- Miller, N.S. & McGregor, R.C. (1978)
The problem of scale in model testing for offshore work.
SUT Proc. Seminar: Models and their use as design aids in offshore operations.
- Morison, J.R. O'Brien, M.P. Johnson, J.W. Schaaf, S.A. (1950)
The force exerted by surface waves on piles.
Petroleum Transactions AIME Vol.189.

- Lorkovin, N.V. (1964)
Flow around circular cylinder- a kaleidoscope
of challenging fluid phenomena.
ASME Symp. on fully separated flows.
- McGregor, D.M. (1957)
An experimental investigation of the oscillating
pressure on a circular cylinder in a fluid stream.
Inst. of Aerophysics Univ. of Toronto. UTIA Tech
Note No.14 June.
- McNown, J.S. (1957)
Drag in unsteady flow.
Proc. 9th Congress Applied Mech. Brussels.
- McNown, J.S. & Keulegan, G.H. (1959)
Vortex formation and resistance in periodic motion.
Proc. ASCE EM1 January.
- Newland, D.E. (1975)
Random vibrations and spectral analysis.
Longman.
- Prape, A. & Breusers, H.N.C. (1966)
The influence of pile dimension on forces exerted
by waves.
Delft Hydr. Laboratory Pub. No.41 October.
- Pearcey, H.H. (1978)
Discussion of paper by Miller & McGregor, 1978.
- Pearcey, H.H. (1979)
Some observations on fundamental features of wave-
induced viscous flows past cylinders.
NMI R60 OT-R-7940 August.
- Prandtl, L. & Tietjens, O.G. (1957)
Applied hydro and aeromechanics.
Dover Pub.
- Ramamurthy A.S. & Ng C.P. (1973)
Effect of blockage on steady force coefficients
Proc. ASCE EM4 August.
- Rance, P.J. (1969)
Wave forces on cylindrical members of structures.
HRS Annual Report.
- Rance, P.J. (1969a)
The influence of Reynolds number on wave forces.
Proc. Symp. Res. on wave action. Delft.
- Rosenhead, L. (Editor) (1963)
Laminar boundary layers.
Oxford, (Clarendon Press) 1st edition.
- Roshko, A. (1961)
Experiments on the flow past a circular cylinder
at very high Reynolds Number.
Jour. of Fluid Mechanics Vol.10
- Rouse, H. (1961)
Fluid mechanics for hydraulic engineers.
Dover Pub. Inc. New York.
- Sarpkaya, T. (1963)
Lift, drag and added mass coefficients for a circular
cylinder immersed in a time dependent flow.
ASME Jour. Appl. Mech. Vol.30 March.
- Sarpkaya, T. (1966)
Separated flow about lifting bodies and im-
plusive flow about cylinders.
AIAA Jour. Vol.4,3

- Sarpkaya, T. (1976a)
 Vortex shedding and resistance in harmonic flow about smooth and rough circular cylinders at high Reynolds Number.
 Naval Postgrad. School, Monterey, California
 NPS-59SL76021 2nd February.
 In-line and transverse forces on cylinders on oscillatory flow at high Reynolds Number.
 Offshore Technology Conf. OTC 2533 (1976).
- Sarpkaya, T. (1976b)
 Forces on cylinders near a plane boundary in a sinusoidally oscillating fluid.
 Trans. ASME Jour. Fluid Eng. September.
- Sarpkaya, T. (1976c)
 In-line and transverse forces on smooth and sand roughened cylinders in oscillatory flow at high Reynolds Number.
 Naval Postgrad. School Monterey, California.
 Rep. NPS-69SL76062 4th June.
 Forces on rough-walled circular cylinders in harmonic flow.
 Proc. 15th Conf. Coastal Eng. (Hawaii) 1976.
- Sarpkaya, T. (1976d)
 Vortex shedding and resistance in harmonic flow about smooth and rough circular cylinders.
 Proc. Conf. Behaviour of offshore structures.
 Trondheim 1976.
- Sarpkaya, T. (1977a)
 The hydrodynamic resistance of roughened cylinders in harmonic flow.
 Royal Inst. Naval Arch. Spring meeting, paper No.4
- Sarpkaya, T. (1977b)
 In-line and transverse forces on cylinders near a wall in oscillatory flow at high Reynolds Number.
 Proc. 9th Offshore Technology Conf. OTC 2898.
- Sarpkaya, T. (1977c)
 In-line and transverse forces on cylinders in oscillatory flow at high Reynolds Number.
 Jour. Ship Res. Vol.21,4 December, pp 200-216.
- Sarpkaya, T. Collins N.J. Evans (1977)
 Wave forces on rough-walled cylinders at high Reynolds Number.
 Proc. 9th Offshore Technology Conf. OTC 2901.
- Sarpkaya, T. & Collins, N.J. (1978)
 Discussion of: Garrison, Field & May(1977)
 Proc. ASCE WWI February.
- Sarpkaya, T. & Garrison C.J. (1963)
 Vortex formation and resistance in unsteady flow.
 Trans. ASME Jour, Appl. Mech. March.
- Sarpkaya, T. & Tuter, O. (1974)
 Forces on cylinders and spheres in a sinusoidally oscillating fluid. (Periodic flow about bluff bodies part 1).
 Tech. Rep. NPS-59SL74091 Naval Postgrad. School, Monterey, California. September.
 Forces on cylinders and spheres in a sinusoidally oscillating fluid,
 ASME Jour. Appl. Mech. Vol.42,1. March 1975.

- Sawaragi, T. Nakamura, T. & Kita, H. (1976)
 Characteristics of lift forces on a circular pile in waves.
 Coastal Eng. in Japan Vol.19.
- Schlichting, H. (1960)
 Boundary layer theory.
 McGraw Hill 4th Ed.
- Schoemaker, H.J. (1970)
 Some pitfalls in scaling hydraulic models.
 Delft Hydr. Laboratory Pub.79. April.
- Schwabe, M. (1935)
 Pressure distribution in non-uniform two-dimensional flow.
 NACA Tech, Memo 1039, Pub.1943.
- Silvester, R. (1974)
 Coastal Engineering 1.
 (Developments in Geotechnical Eng., 4A)Elsevier.
- Son, J.S. & Hanratty, T.J. (1969)
 Velocity gradients at the wall for flow around a cylinder at Reynolds Number from $\times 10^3$ - 10^5
 Jour. Fluid Mech. 35,2.
- Standing, R.G. (1979)
 Numerical prediction of wave loads and response motions of offshore structures.
 NMI R56, May.
- Stansby, P.K. (1974)
 The effects of end plates on the base pressure coefficient of a circular cylinder.
 Aero. Jour. January.
- Stansby, P.K. (1978)
 Mathematical modelling of vortex shedding from circular cylinders in planar oscillatory flows, including effects of harmonics.
 Proc. Conf. Mechanics of wave-induced forces on cylinders, Bristol 1978. Pub. Pitman 1979.
 Ed. T.L. Shaw.
- Stelson, T.E. & Mavis, T. (1957)
 Virtual mass and acceleration in fluids.
 ASCE Trans. 2870 Vol.122.
- Stokes, G.G. (1850)
 On the effect of the internal friction of fluids on the motion of pendulums.
 Trans. of Cambridge Phil. Soc. 9. and
 Mathematical & Physical papers Cambridge Press 1901
- Szechenyi, E. (1975)
 Supercritical Reynolds Number simulation for two-dimensional flow over circular cylinders.
 Jour. Fluid Mech. Vol.70
- Thirriot, C. Longree, W.D. & Barthet, H. (1971)
 Sur la perte de charge due a un obstacle en mouvement periodique.
 Proc. 14th Congress IAHR.
- Tickell, R.G. & Holmes, P. (1979)
 Approaches to fluid loading, probabilistic and deterministic analyses.
 Chapter 2 of 'Numerical Methods in offshore engineering'. Ed. Zeinkewicz, Lewis & Stagg.
 Pub. Wiley, April.

Verley R. (1977)

On the estimation of drag and inertia coefficients for smooth and rough cylinders in steady currents and in waves for $N_k > 10$ and Reynolds Number $>$ critical.

Univ. Trondheim, Norway.

Warren J.G. (1977)

The development and use of a wave facility to investigate the dynamic response of circular cylinders to wave action.

Ph.D. Salford Univ.

Wheatley, J.H.W. & Boyle, H.B. (1975)

Proceedings of seminar on fluid loading of offshore structures.

Paper No.7: A review of progress-Part III measurement. NPL September.

Wiegel, R.L. (1964)

Oceanographical Engineering.

Prentice-Hall.

Wiegel, R.L. (1974)

Engineers concern with waves, and their measurement. Proc. Conf.

Ocean wave measurement & analysis 'Waves 74'

ASCE. Appendix 'Scope of Coastal & Offshore Engineering'

Wiegel, R.L. & Belmonte, R.C. (1972)

Wave induced eddies and 'lift' forces on circular cylinders.

Univ. California Hydr. Eng. Lab. HEL9-19 July.

Wille, R. (1972)

Generation of oscillatory flows.

Proc. Symp. on Flow-induced structural vibrations Karlsruhe (IUTAM- I AHR) Pub. Springer-Verlag 1974.

Williams, R.E. & Hussey, R.G. (1972)

Oscillating cylinders and the Stokes Paradox.

Physics of fluids Vol.15, No.12 December.

Wilson, B.W. (1965)

Analysis of wave forces on a 30" dia pile under confused sea conditions.

U.S. CERC Tech. Memo No.15.

Wootton, L.R. (1978)

The integration of model tests with the design process.

SUT Proc. Seminar: Models and their use as design aids in offshore operations.

Yalin, M.S. (1971)

Theory of hydraulic models.

Pub. MacMillan 1971.

Yamamoto, T. & Nath, J.H. (1976)

High Reynolds Number oscillating flow by cylinders.

Proc. 14th Coastal Eng. Conf. (Hawaii).

Zdravkovich, M.M. (1969)

Smoke observations of the formation of a Karman vortex street.

Jour. Fluid Mech. Vol.37,3.

Zdravkovich, M.M. & Namork, J.E. (1977)

Formation and reversal of vortices around circular cylinders subjected to water waves.

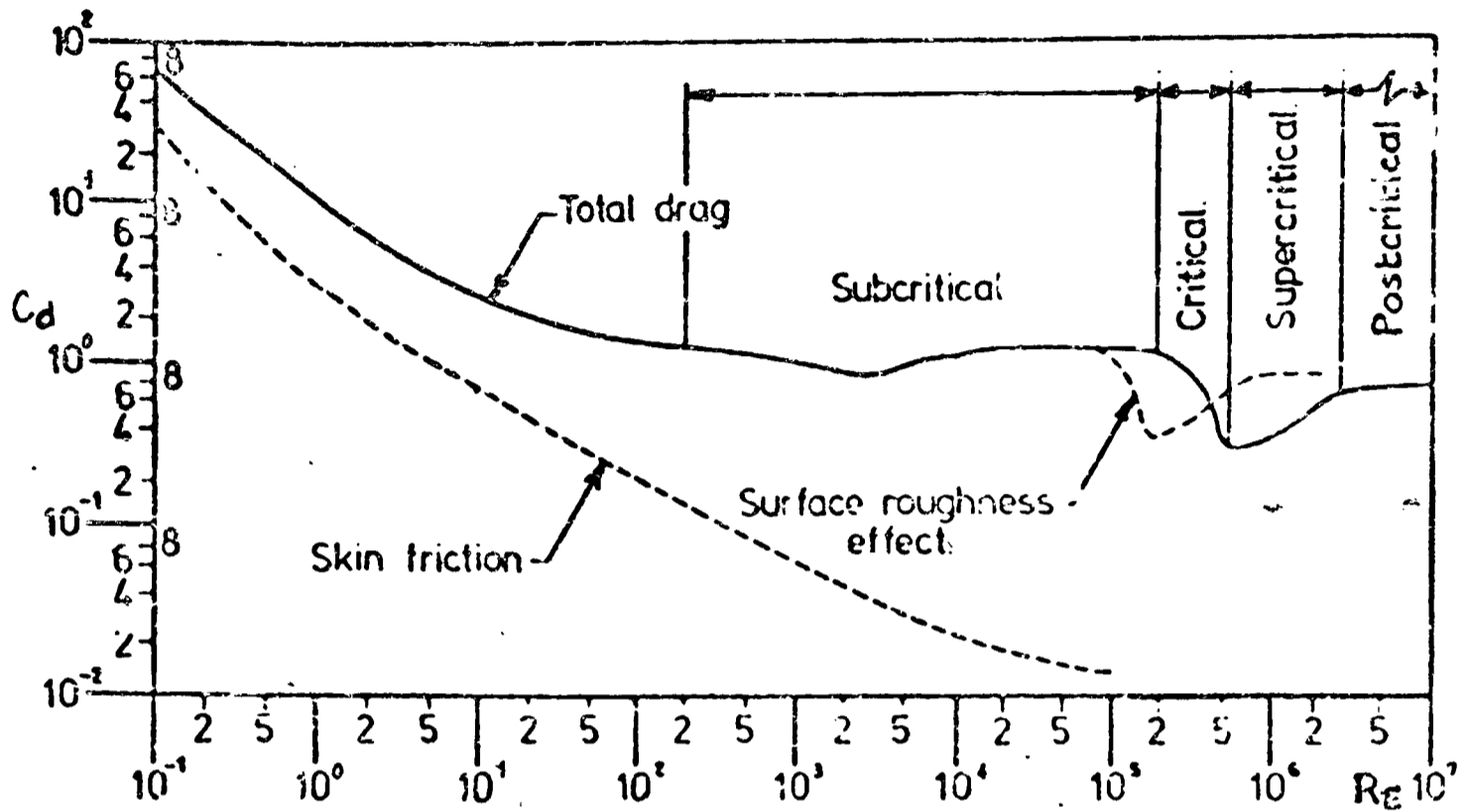
Proc. ASCE WW3, August. Tech. Note

APPENDIX A

STEADY AND POTENTIAL FLOW RESULTS

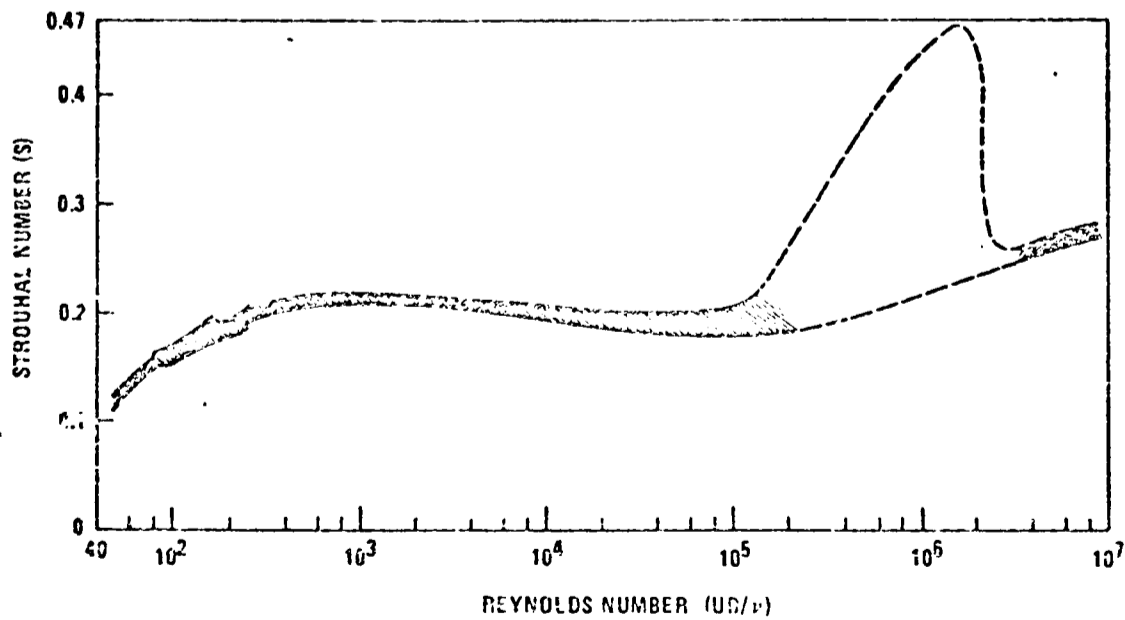
(A.1) Steady flow experimental results

These all correlate with Reynolds number:



• STEADY FLOW DRAG COEFFICIENT
VARIATION WITH R_E

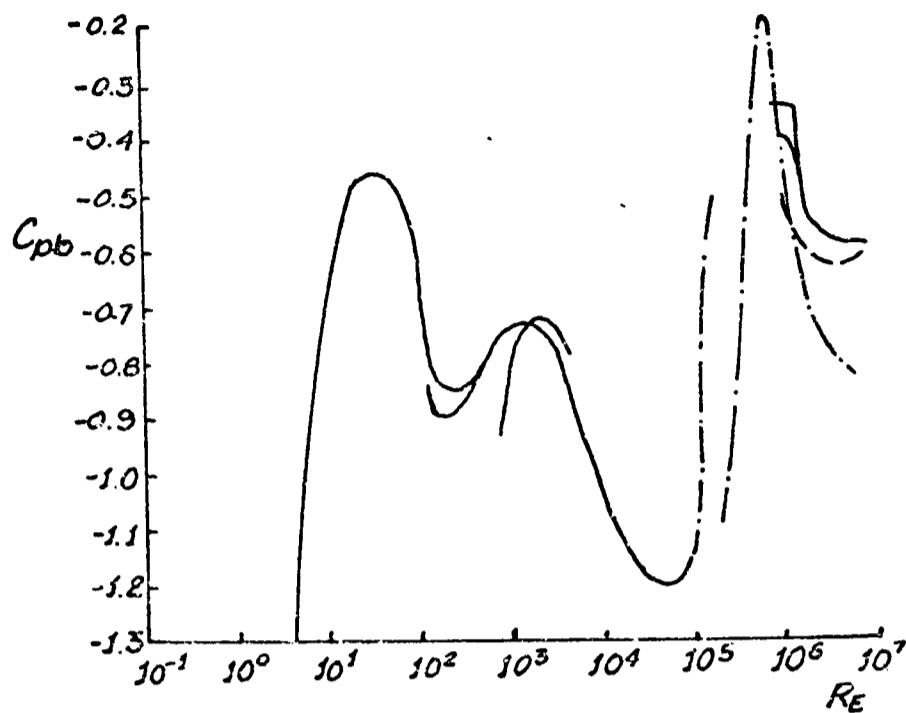
FIGURE (A.1)



STROUHAL NUMBER VARIATION
WITH R_E

FIGURE (A.2)

(from: Blevins(1977))

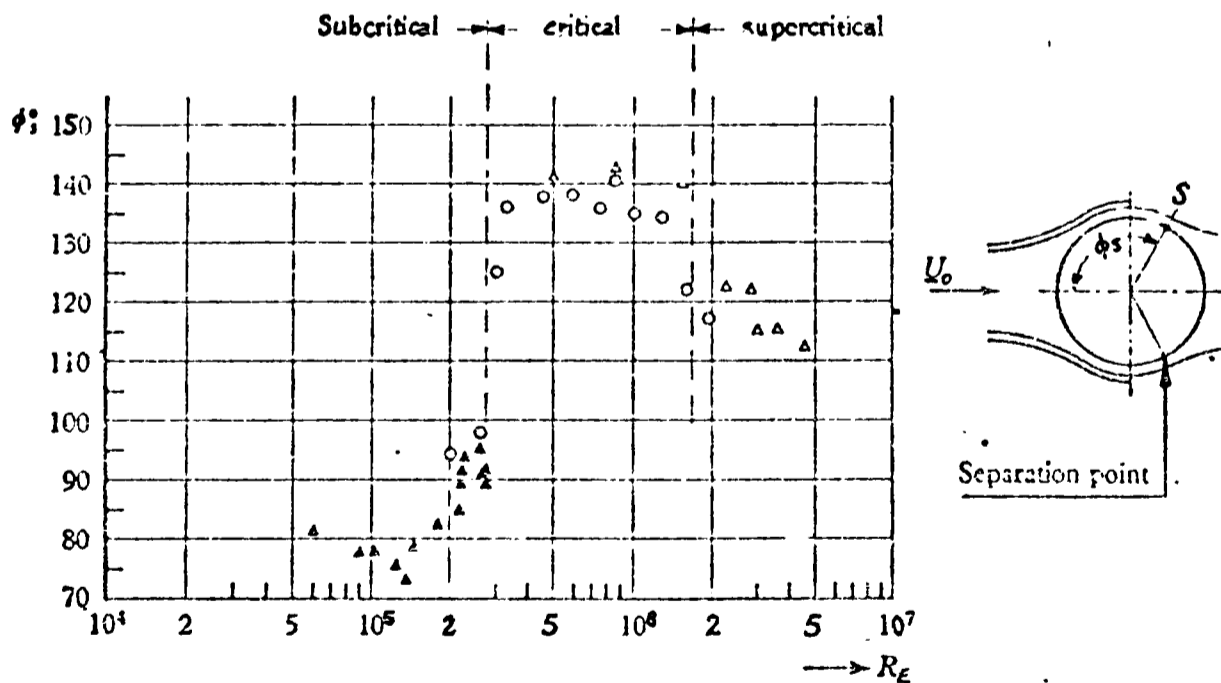


N.B. For key to individual researchers see original ref.

VARIATION OF CYLINDER BASE PRESSURE COEFFICIENT WITH Re

(From: CHEN(1970))

FIGURE (A.3)



Circular cylinder: position of the separation point as a function of the Reynolds number. Δ , $L/d = 3.33$ channel; \triangle , $L/d = 3.33$ channel; \circ , $L/d = 6.66$ channel.

(From: Distribution of local pressure and skin friction around a circular cylinder in cross-flow up to $Re = 5 \times 10^6$ Achenbach, E. Jour. Fluid Mech. 34,4 1968)

VARIATION OF ANGLE OF BOUNDARY LAYER SEPARATION POINT IN A STEADY FLOW

FIGURE (A.4)

(A.2) Potential flow analysis of relative (sinusoidal) motion between a cylinder and fluid

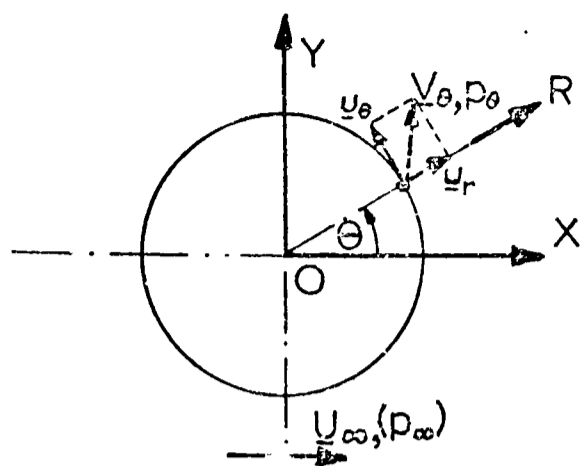


Figure (A5)

Coordinate reference system

The unsteady form of the Bernoulli equation:

$$\frac{p}{\rho} + \frac{U(t)^2}{2} + \frac{\partial \phi}{\partial t} = F(t) \quad \dots (1)$$

may be applied to a point on the cylinder circumference (r, θ) and the far flow field: U_∞, p_∞ to give the pressure coefficient:

$$C_p = \frac{p_\theta - p_\infty}{\frac{1}{2} \rho U_\infty^2} = \left[1 - \left(\frac{V_\theta}{U_\infty} \right)^2 \right] - \frac{2}{U_\infty^2} \frac{\partial \phi}{\partial t} \Big|_{r=d/2} \quad \dots (2)$$

This equation may be solved for any deterministic kinematic condition, being uniquely defined by the boundary conditions.

A doublet at the origin O is given by the complex stream function:

$$F(r) = \frac{U(t) d^2}{4r} (\cos \theta - i \sin \theta) \quad \dots (3)$$

For $r = d/2$ this equation describes a circular cylindrical (in three dimensions) surface. This flow pattern is therefore equivalent to a cylinder moving through a still fluid, with origin translating at a rate $U(t)$.

Superposing a uniform flow on the doublet of equation (3):

$$F(r) = U(t) \left[\frac{d^2}{4r} (\cos \theta - i \sin \theta) + r (\cos \theta + i \sin \theta) \right] \quad \dots (4)$$

The real and imaginary parts of equation (4) describe the potential and stream functions respectively:

$$\phi = U(t) \left(\frac{d^2}{4r} + r \right) \cos \theta, \quad \psi = U(t) \left(r - \frac{d^2}{4r} \right) \sin \theta \quad \dots (5)$$

This kinematic flow field is also equivalent to that of a stationary cylinder in a fluid moving with a velocity of $U(t)$.

Solutions of equation (2)

(i) Fluid moving with absolute velocity $U(t)$ past a stationary cylinder

Boundary conditions: $U_{\infty} = U(t)$
 $V_{\theta} = (U_{\theta}^2 + U_r^2)^{1/2}$

For $r = d/2$, from equations (5):

$$\therefore U_r \Big|_{r=d/2} = \frac{\partial \phi}{\partial r} = U(t) \left(1 - \frac{d^2}{4r^2}\right) \cos \theta = 0$$

$$\text{and } U_{\theta} \Big|_{r=d/2} = \frac{1}{r} \frac{\partial \phi}{\partial \theta} = -U(t) \left(1 + \frac{d^2}{4r^2}\right) \sin \theta = -2U(t) \sin \theta$$

$$\text{also } \frac{\partial \phi}{\partial t} \Big|_{r=d/2} = \frac{\partial U(t)}{\partial t} d \cos \theta$$

Substituting equations (6) in equation (2):

$$C_p = (1 - 4 \sin^2 \theta) - \frac{2}{U^2(t)} \frac{\partial U(t)}{\partial t} d \cos \theta \quad \dots (7a)$$

For a planar oscillatory flow: $U(t) = U_{pmax} \cos \omega_p t$

$$\therefore C_p = (1 - 4 \sin^2 \theta) \cos^2 \omega_p t - \frac{2}{U_{pmax}} \omega_p \sin \omega_p t d \cos \theta$$

For $N_k = U_{pmax} \cdot 2\pi / d \omega_p$:

$$C_p = (1 - 4 \sin^2 \theta) \cos^2 \omega_p t - \frac{4\pi}{N_k} \sin \omega_p t \cos \theta \quad \dots (7b)$$

(ii) Cylinder moving with absolute velocity $U(t)$, fluid stationary

Boundary conditions (i), but axes now translating with the cylinder, i.e. from equation (4):

$$\phi = U(t) \frac{d^2}{4r} \cos \theta \quad \dots (8)$$

$$\therefore \frac{\partial \phi}{\partial t} \Big|_{r=d/2} = \frac{\partial U(t)}{\partial t} \frac{d}{2} \cos \theta$$

For a planar oscillatory cylinder oscillation:

$$C_p = (1 - 4 \sin^2 \theta) \cos^2 \omega_{pc} t - \frac{\omega_{pc}}{U_{pcmax}} \sin \omega_{pc} t d \cos \theta$$

i.e.

$$C_p = (1 - 4 \sin^2 \theta) \cos^2 \omega_{pc} t - \frac{2\pi}{N_k} \sin \omega_{pc} t \cos \theta \quad \dots (9)$$

(iii) Comparison of the two planar oscillatory conditions
(i) & (ii)

Although the flow patterns are similar when the fluid and the cylinder move with simple harmonic motion (equations (4), (5) and (8)), the pressure distribution, and hence forces, are different by a factor of:

$$\frac{F}{\frac{1}{2} \rho u_{p \max}^2} = \frac{1}{2} \int_0^{2\pi} \frac{2\pi}{N_k} \sin \omega_p t \cos^2 d\epsilon = \frac{\pi^2}{N_k} \sin \omega_p t \dots (10)$$

This is the Froude Krylov component, caused by the pressure required to accelerate the moving fluid.

(iv) Cylinder, or fluid, moving with absolute velocity U_0

This condition may be obtained from either (i) or (ii) above for

$$U_\infty = U(t) = U_0 \quad , \text{ e.g. from equation (7a):}$$

$$C_p = 1 - 4 \sin^2 \theta \dots (11)$$

APPENDIX B

WATER WAVE THEORIES

Appendix D shows how sea waves may be represented by amplitude-frequency spectra. Because the sea surface is composed of many progressive wave trains interacting in all directions, this unidirectional spectrum is an approximation. The analysis of deterministic, or regular unidirectional waves has evolved based upon various approximations, and is here briefly considered in terms of the principal types.

A useful summary is presented in Mehta (1976), which, although not as rigorous as Kinsman (1966), is much easier to understand. Water waves are either translational or oscillatory, depending upon whether there is an actual translation of fluid particles in the wave direction or not. Progressive waves are those commonly encountered, and would appear stationary to an observer moving with them at the wave celerity c . There is no universal mathematical solution for surface waves, but a number of different approximate solutions have been developed based upon the relative importance of the nonlinear, or convective inertial, effects (Chapter 1). For large H_w/L_w , H_w/z_2 and L_w/d the nonlinear effects are significant. (Reference may be made to Section (4.3) for some discussion of nonlinear effects). In deep water the wave steepness H_w/L_w is important, whilst in shallow water H_w/z_2 is important, however, a more general grouping is $(H_w/L_w)(L_w/z_2)^3$ which is known as the Ursell parameter, denoted as U . Although not completely definitive, the Ursell parameter gives a good first approximation for the relative importance of the nonlinear wave effects. In general linear wave theories apply for $U \leq 1$. The commonly used oscillatory wave theories are termed 'small amplitude' although they may also apply to waves of significant amplitude.

If an irrotational incompressible flow is assumed, with reference to Figure (1.5g), in two dimensions:

$$\text{Continuity:} \quad \frac{\partial u}{\partial x} + \frac{\partial w}{\partial z} = 0 \quad \dots (1)$$

$$\text{Vorticity:} \quad \frac{\partial u}{\partial z} - \frac{\partial w}{\partial x} = 0 \quad \dots (2)$$

Substitution of the velocity potential ϕ gives:

$$\nabla^2 \phi = 0 \quad \dots \quad (3)$$

the Laplace equation.

Application of the boundary conditions are now required to formulate the solutions of this equation.

At the free surface, for any particle distance η above the x axis:

$$\left. \frac{\partial \phi}{\partial z} \right|_{z=\eta} = \frac{\partial \eta}{\partial t} + \left. \frac{\partial \phi}{\partial x} \right|_{z=\eta} \frac{\partial \eta}{\partial x} \quad \dots \quad (4)$$

this is the nonlinear kinematic free surface condition.

Application of the unsteady Bernoulli equation to the free surface results in:

$$\frac{1}{2} \left[\left(\frac{\partial \phi}{\partial x} \right)^2 + \left(\frac{\partial \phi}{\partial z} \right)^2 \right] - \left. \frac{\partial \phi}{\partial t} \right|_{z=\eta} + g\eta \quad \dots \quad (5)$$

This is the dynamic free surface condition, which is also nonlinear.

The third boundary condition is linear:

At the bed:
$$\left. \frac{\partial \phi}{\partial z} \right|_{z=-z_2} = 0 \quad \dots \quad (6)$$

These boundary conditions are then applied to the Laplace equation, and a solution of the form $\eta = f(x-ct)$, which describes a progressive wave moving with celerity c , may then be obtained.

However, the Laplace equation cannot be solved for the complete forms of the nonlinear boundary conditions. Solution is obtained by taking only a finite number of terms of the series expansions of these conditions. This results in solutions for ϕ and η of 1st, 2nd, 3rd... and practically, up to the 5th order. These solutions, attributed to Stokes, are harmonic and possess harmonics of frequency order up to the number of significant series terms used. The first order, or linear wave theory, is frequently used, even to describe non-monochromatic waves, because of its simplicity, particularly in deep water. The Stokes first order theory conforms to the Airy small amplitude wave theory.

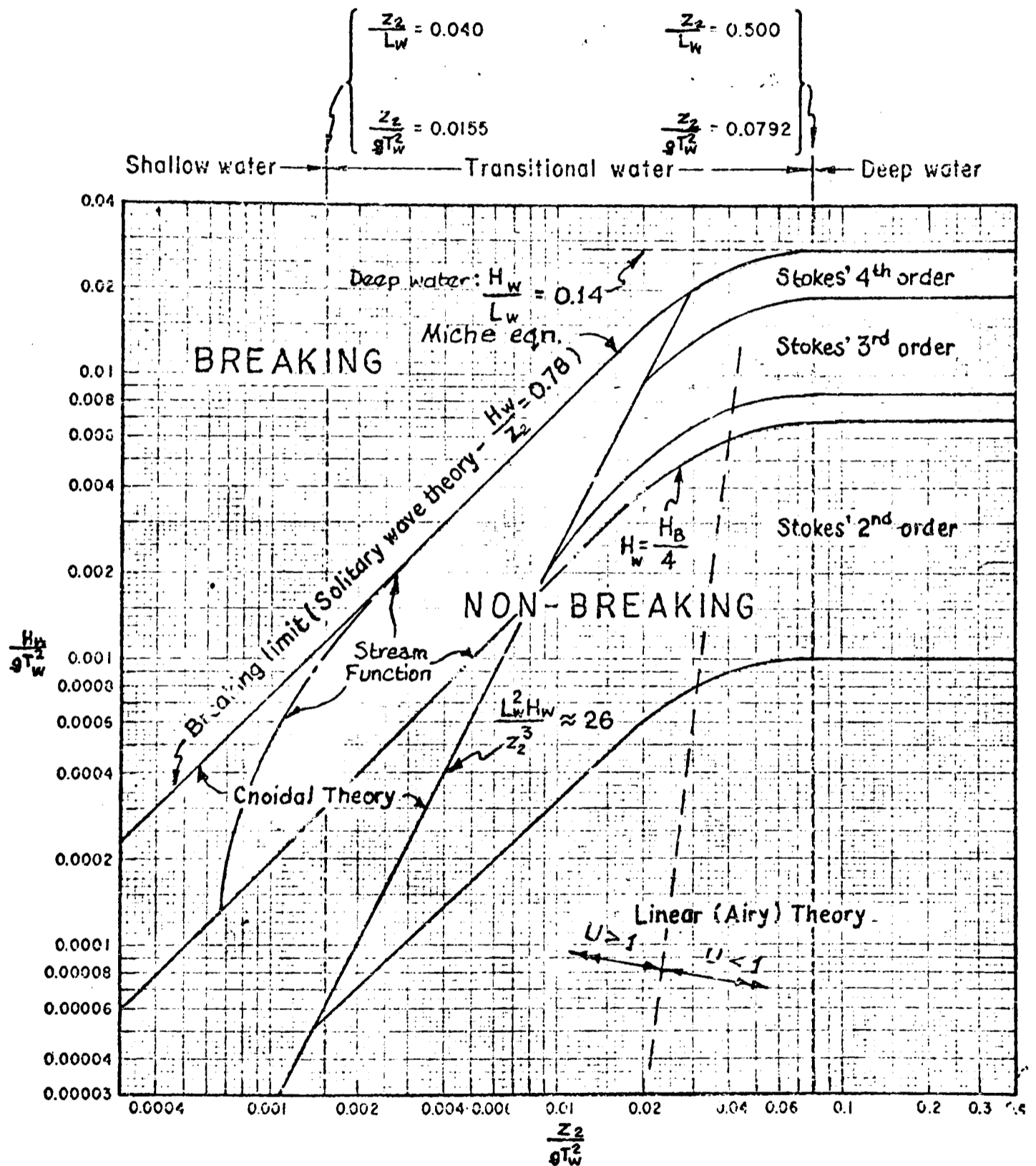
To first order:
$$\phi = \frac{g A_w}{\omega_w} \frac{\cosh k(z+z_2)}{\cosh k z_2} \sin(kx - \omega_w t)$$

$$\eta = H_w/2 \cos 2\pi \left(\frac{x}{L_w} - \frac{t}{T_w} \right)$$

and
$$L_w = \frac{g T_w^2}{2\pi} \tanh k z_2$$

The expressions for ϕ and L_w may be abbreviated for shallow or deep water, because of the hyperbolic functions of $k z_2$.

There are other useful wave theories for particular relative wave heights and water depths, notably the Cnoidal group, which are shallower water elliptical function theories, and the extensively used stream function, numerical theory developed by Dean. A useful approximate determination of the relevant wave theory may be obtained from Figure (B.1), based upon a dimensionless wave height H_w/gT_w^2 and water depth z_2/gT_w^2 . The waves are limited by the breaking criterion discussed in Chapter 4.



APPROXIMATE REGIONS OF VALIDITY OF WATER WAVE THEORIES
 (From: Shore Protection manual, US Army CERC 3rd Ed. 1977)

FIGURE (B.1)

APPENDIX C

FOURIER ANALYSIS

(C.1) Introduction In the same way that any number of points relating a function $f(t)$ say, to t can be related by a polynomial over a discrete range, so for a function that is periodic in nature the polynomial may be replaced by a harmonic series.

For periodicity of 2π : $f(t) = f(t+2\pi)$

$$f(t) = c_0 + c_1 \sin(t+\alpha_1) + c_2 \sin(2t+\alpha_2) + \dots + c_n \sin(nt+\alpha_n)$$

$$f(t) = c_0 + \sum_{n=1}^{\infty} c_n \sin(nt+\alpha_n) \quad \dots \dots (1)$$

This is a Fourier Series,

2π in this case is the fundamental period.

The $\sum_{n=1}^{\infty}$ terms are harmonics; for $n = 1$ the term is the first harmonic, or fundamental. For $n = 2$ the 2nd harmonic, etc. The α_n functions represent the phase differences between the harmonics, and the integer n in the nt term defines the frequency, e.g.

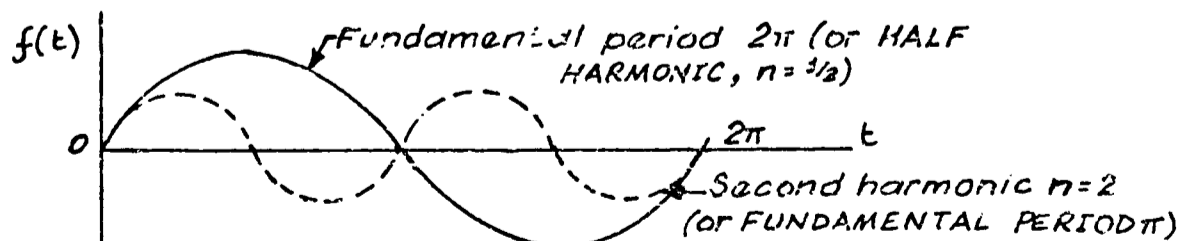
$$n=1: f = 1/2\pi \text{ etc.}$$

By substituting $c_n \sin\alpha_n = a_n$ and $c_n \cos\alpha_n = b_n$ in the expansion of (1)

$$f(t) = a_0 + \sum_{n=1}^{\infty} a_n \cos nt + \sum_{n=1}^{\infty} b_n \sin nt \quad \dots \dots (2)$$

(1) and (2) hold if the function is single valued, and has a finite number of discontinuities in range 2π .

Each of the functions $\cos nt$ or $\sin nt$ have fundamental periods of $2\pi/n$ (See Fig. C.1)



HARMONIC STRUCTURE OF WAVEFORMS

FIGURE (C.1)

Integrating (2): $a_0 = \frac{1}{2\pi} \int_{-\pi}^{\pi} f(t) dt$ i.e. mean value of $f(t)$ for range $-\pi$ to π (3)

Similarly $a_n = \frac{1}{\pi} \int_{-\pi}^{\pi} f(t) \cos nt dt$)
 $b_n = \frac{1}{\pi} \int_{-\pi}^{\pi} f(t) \sin nt dt$) (4)
 These coefficients from (3) and (4) are "Fourier Coefficients".

If $f(t)$ is an 'even' function, $b_n = 0$
 i.e. if $f(t) = f(-t)$

and

If $f(t)$ is an 'odd' function, $a_0 = 0 = a_n$
 for $f(t) = -f(-t)$

If a function is not periodic but only defined over a range, then a new function must be defined that is repeated with period equal to the range of the first function.

(C.2) Expansion of a function, period T

Such a function is defined as $f(t + T) = f(t)$, and is more commonly occurring than period 2π functions.

Putting $2\pi t / T = \omega t$

where ω is frequency in rad /s.

Then ωt increases periodically as 2π when $t = T$.

Therefore:

$$f(t) = a_0 + \sum_{n=1}^{\infty} c_n \sin(n\omega t + \alpha_n) \quad \text{from (1)}$$

$$f(t) = a_0 + \sum_{n=1}^{\infty} a_n \cos \frac{2\pi n t}{T} + \sum_{n=1}^{\infty} b_n \sin \frac{2\pi n t}{T}$$

$$\text{or } f(t) = a_0 + \sum_{n=1}^{\infty} (a_n \cos n\omega t + b_n \sin n\omega t) \quad \dots (5)$$

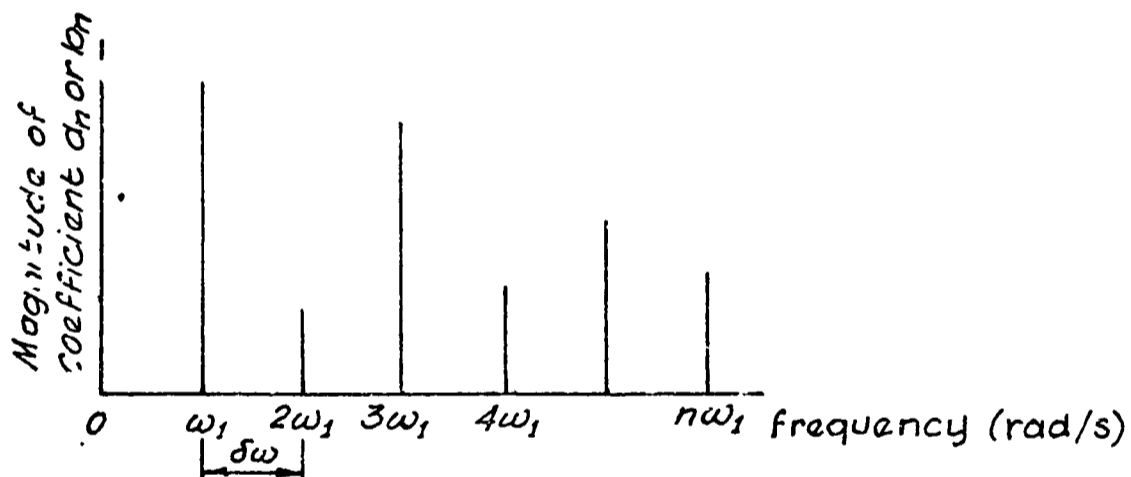
$$\begin{aligned}
 a_0 &= \frac{1}{T} \int_{-T/2}^{T/2} f(t) dt &) \\
 & &) \\
 a_n &= \frac{2}{T} \int_{-T/2}^{T/2} f(t) \cos n\omega t dt &) \\
 & &) \\
 b_n &= \frac{2}{T} \int_{-T/2}^{T/2} f(t) \sin n\omega t dt &) \\
 & &) \\
 & &) \dots \dots (6)
 \end{aligned}$$

These are the most general Fourier Coefficients. The limits are between any two corresponding period points - as long as the interval is one complete period.

These coefficients may be represented graphically as shown in Fig. (C.2.)

(Assuming the average $E(f(t)) = 0 = a_0$)

Such graphs give a measure of the predominant frequency components of $f(t)$.



GRAPHICAL REPRESENTATION OF
FOURIER COEFFICIENTS

FIGURE (C.2)

$$\delta\omega = \omega_1 = 2\pi/T \dots \dots (7)$$

Hence for large T , $\delta\omega \rightarrow 0$ and the line becomes continuous, i.e. $f(t)$ is no longer periodic if $T \rightarrow \infty$

If this does occur then the basic Fourier Series (5) no longer holds.

(C.3) Fourier Integral

To analyse a function $f(t)$ where $T \rightarrow \infty$ into basic harmonic components (hence to investigate frequencies) a Fourier Integral must be used:

(For $E(f(t)) = 0$)

By substituting (6) into (5), and substituting (7):

$$f(t) = \sum_{n=1}^{\infty} \left[\frac{\delta\omega}{\pi} \int_{-T/2}^{T/2} f(t) \cos n\omega t \, dt \right] \cos n\omega t - \left[\frac{\delta\omega}{\pi} \int_{-T/2}^{T/2} f(t) \sin n\omega t \, dt \right] \sin n\omega t$$

for $T \rightarrow \infty, \delta\omega \rightarrow d\omega$

$$\text{and } f(t) = \int_{\omega=0}^{\infty} \left[\frac{d\omega}{\pi} \left(\int_{-\infty}^{\infty} f(t) \cos \omega t \, dt \right) \cos \omega t + \frac{d\omega}{\pi} \left(\int_{-\infty}^{\infty} f(t) \sin \omega t \, dt \right) \sin \omega t \right]$$

defining:

$$\begin{aligned} A(\omega) &= \frac{1}{2\pi} \int_{-\infty}^{\infty} f(t) \cos \omega t \, dt \\ B(\omega) &= \frac{1}{2\pi} \int_{-\infty}^{\infty} f(t) \sin \omega t \, dt \end{aligned} \quad \dots \dots (8)$$

then:

$$f(t) = \int_0^{\infty} [A(\omega) \cos \omega t + B(\omega) \sin \omega t] \, d\omega \quad \dots \dots (9)$$

This equation is the Fourier integral, or Inverse Fourier Transform of $f(t)$.

$A(\omega)$ and $B(\omega)$ are components of the Fourier Transform of $f(t)$. They are 'even' and 'odd' functions respectively.

Eqn (9) holds generally only for functions such that

$$\int_{-\infty}^{\infty} |f(t)| \, dt < \infty, \text{ i.e. for } |f(t)| \rightarrow 0 \text{ as } t \rightarrow \infty$$

A Fourier Integral is the limit of a Fourier series as $T \rightarrow \infty$ for function $f(t)$.

It is used to determine the frequency composition of aperiodic functions.

(C.4) Complex Fourier Analysis

(i) Complex Fourier Series

Basic eqn.

$$f(t) = a_0 + \sum_{n=1}^{\infty} (a_n \cos n\omega t + b_n \sin n\omega t) \quad (\text{eqn.5})$$

$$\left. \begin{aligned} \text{now } \cos n\omega t &= (e^{jn\omega t} + e^{-jn\omega t}) / 2 \\ \text{and } \sin n\omega t &= (e^{jn\omega t} - e^{-jn\omega t}) / 2j \end{aligned} \right\} e^{j\theta} = \cos\theta + j\sin\theta \\ (\theta - \text{any angle})$$

$$\therefore f(t) = a_0 + \sum_{n=1}^{\infty} (p_n e^{jn\omega t} + q_n e^{-jn\omega t}) \quad \dots \dots (10)$$

$$\text{where } p_n = 1/2 (a_n - jb_n),$$

$$q_n = 1/2 (a_n + jb_n) \quad \dots \dots (11)$$

$$\text{or } f(t) = \sum_{n=-\infty}^{\infty} g_n e^{jn\omega t} \quad \dots \dots (12)$$

Where $p_n = g_n$ & $q_n = g_{-n}$ (a_0 is replaced by $a_0/2$ in (10))

Hence $a_n = 2 \cdot \text{Real}(g_n)$

$b_n = 2 \cdot \text{Imag}(g_n)$

It can be shown that:

$$g_n = \frac{1}{T} \int_{T/2}^{T/2} e^{-jn\omega t} f(t) dt \quad \dots \dots (13)$$

(ii) Complex Fourier Transform

$$\text{From (9): } f(t) = \int_{-\infty}^{\infty} [A(\omega) \cos \omega t + B(\omega) \sin \omega t] d\omega$$

(The inverse Fourier Transform of $f(t)$)

$$\text{Now } e^{j\omega t} = \cos \omega t + j \sin \omega t$$

and putting $X(\omega) = A(\omega) - jB(\omega)$

$$\text{from (8) } A(\omega) = \frac{1}{2\pi} \int_{-\infty}^{\infty} f(t) \cos \omega t dt$$

$$\& B(\omega) = \frac{1}{2\pi} \int_{-\infty}^{\infty} f(t) \sin \omega t dt$$

$$\therefore X(\omega) = \frac{1}{2\pi} \int_{-\infty}^{\infty} f(t) (\cos \omega t - j \sin \omega t) dt$$

$$\therefore X(\omega) = \frac{1}{2\pi} \int_{-\infty}^{\infty} f(t) e^{-j\omega t} dt \quad \dots \dots (14)$$

This is the Fourier Transform of $f(t)$

As eqn. (9) is totally an 'even' function

then:
$$\int_0^{\infty} \dots = \int_{-\infty}^{\infty} \dots$$

So that (9) may be re-written:

$$f(t) = \int_{-\infty}^{\infty} [A(\omega) \cos \omega t + B(\omega) \sin \omega t] d\omega \quad \dots \dots (9a)$$

As $A(\omega)$ is 'even' and $B(\omega)$ 'odd' (eqns. (8))

$$\therefore \int_{-\infty}^{\infty} A(\omega) \sin \omega t d\omega = 0 = \int_{-\infty}^{\infty} B(\omega) \cos \omega t d\omega \quad \dots (15)$$

Summing (15) + (9a)

$$f(t) = \int_{-\infty}^{\infty} [A(\omega) - jB(\omega)] [\cos \omega t + j \sin \omega t] d\omega$$

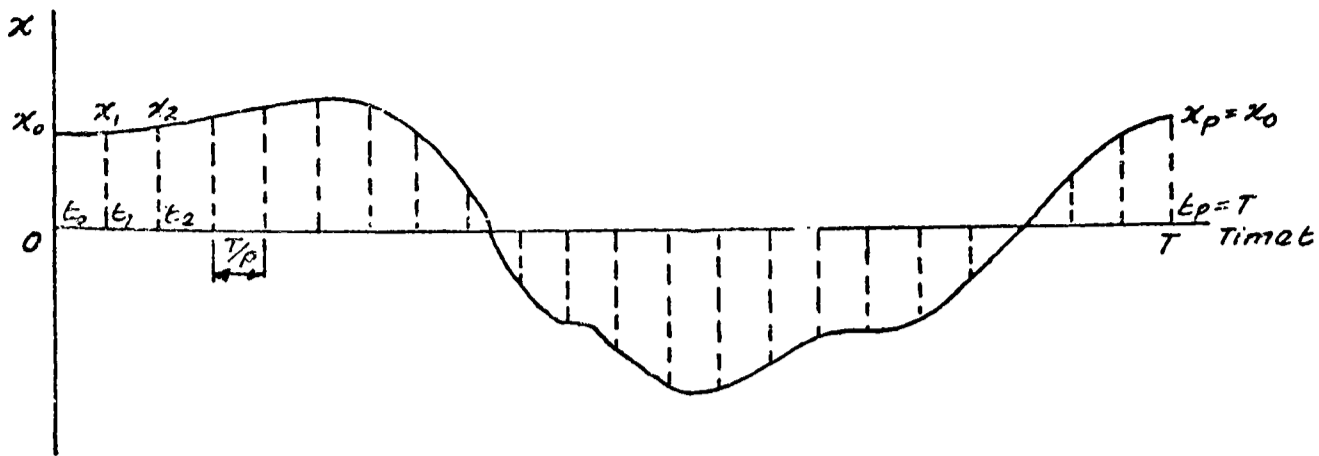
$$\therefore f(t) = \int_{-\infty}^{\infty} X(\omega) e^{j\omega t} d\omega \quad \dots \dots (16)$$

Together with equation (14) the above are known as a Fourier transform pair, and only strictly hold if:

$$\int_{-\infty}^{\infty} |f(t)| dt < \infty$$

(C.5) Numerical Integration (of recorded functions)

If the function $x = f(t)$ is in analogue form, approximation to a Fourier series can be made using an appropriate numerical integration formula.



NUMERICAL FOURIER COEFFICIENT APPROXIMATION

FIGURE (C.3)

Fig. (C.3) shows a typical function assumed to be periodic over the time interval T . This period T can be divided into p equal parts as points t_1 to t_p . The corresponding values of x are then x_1 to x_p .

i.e. $x_r = r \cdot \frac{T}{p}$ (where $r=1, p$)

From equations (6)

the Fourier Coefficients are:

$$a_0 = \frac{1}{T} \int_0^T x(t) dt$$

$$a_n = \frac{2}{T} \int_0^T x(t) \cos n\omega t dt, \quad b_n = \frac{2}{T} \int_0^T x(t) \sin n\omega t dt$$

$$\therefore a_0 \approx \frac{1}{T} \cdot \frac{T}{p} \sum_{r=1}^p x_r = \frac{1}{p} \sum_{r=1}^p x_r \quad \dots \dots (17)$$

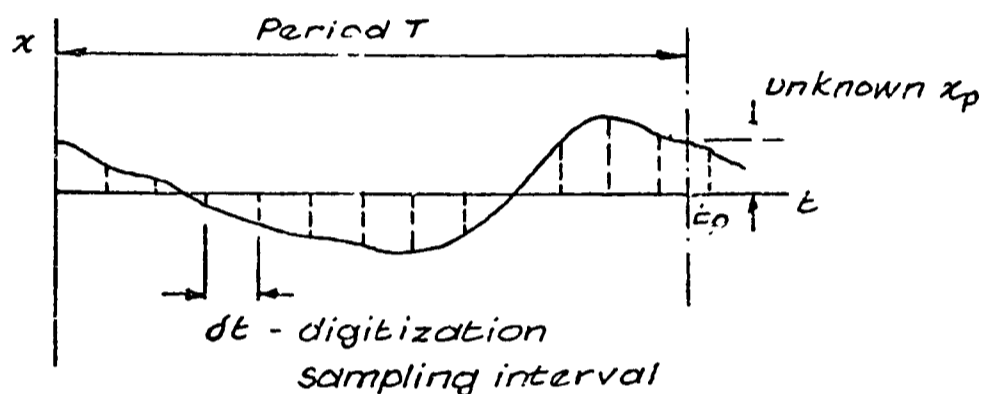
$$a_n \approx \frac{2}{T} \cdot \frac{T}{p} \sum_{r=1}^p x_r \cos n\omega t_r$$

but $n\omega t_r = n \cdot \frac{2\pi}{T} \cdot r \cdot \frac{T}{p} = \frac{n2\pi r}{p}$

$$\underline{a_n = \frac{2}{p} \sum_{r=1}^p x_r \cos \frac{2\pi nr}{p}} \quad \& \quad \underline{b_n = \frac{2}{p} \sum_{r=1}^p x_r \sin \frac{2\pi nr}{p}} \quad \dots \dots (18)$$

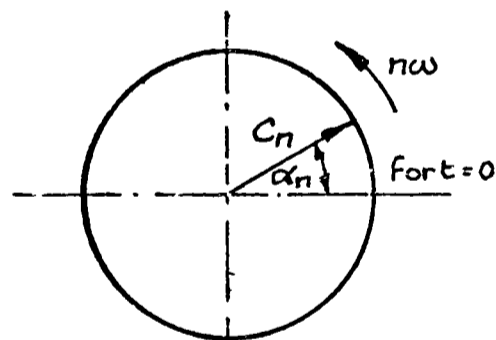
(C.6) Application of equations (18) to analysis of recorded
time functions

It is impractical to digitize a record so that there are an exact number of sampling time intervals per cycle, or period. Consequently the analysis using equation (18) needs to be modified. The relative accuracy of such analysis will depend upon the method of numerical integration used, the sampling time interval and the interpolation of the value of $x(t)$ at the exact period point, illustrated in Figure (C.4). This interpolation particularly affects the higher harmonic values.



INTERPOLATION FOR $ndt \neq T$

FIGURE (C.4)



ROTATING VECTOR REPRESENTATION
OF HARMONIC FUNCTIONS

FIGURE (C.5)

Selection of the fundamental period depends upon the periodicity of the function. As discussed in Chapter 4 there may be significant effects at the half harmonic (relative to the exciting motion) so that determination of the Fourier coefficients is always relative to the excitation. This is particularly important when considering the relative phase information contained in these coefficients.

A simple linear interpolation has been assumed in this analysis between the last digitized point in the period (or period multiple for higher harmonics) and that following. Consequently the program developed, and listed following, requires one extra data point outside the fundamental period selection. It is written to evaluate harmonic components in halves from one half up to any specified integer. Any number of averages may also be specified; the analysis considers the next frequency 'window' starting from an origin displaced by one sampling interval δt for each degree of averaging specified. For this analysis 10 averages were stipulated because 100 data points were available with 88 of these coming within the first two periods. The program listing is included at the end of this Appendix.

Interpretation of coefficient and phase angle results have been based upon the rotating vector concept shown in Figure (C.5).

$$\text{From } x(t) = a_0 + \sum_{n=1}^r c_n \sin(n\omega t + \alpha_n)$$

$$= a_0 + \sum_{n=1}^r (A_n \cos n\omega t + B_n \sin n\omega t)$$

i.e. $\alpha_n = \tan^{-1}(A_n/B_n)$

and $c_n = A_n/\sin\alpha_n$

This last equation differs from the usual calculation of $c_n = (A_n^2 + B_n^2)^{1/2}$ because it retains the relative phase of c_n , allowing it to be either positive ($\alpha_n = \alpha_n$) or negative (in which case $\alpha_n = \alpha_n - \pi$). This is illustrated in Figure (C.6). All phase angles are therefore recorded as less than 180° ; this is because it is impossible to define whether one vector leads or lags another in this type of flow situation.

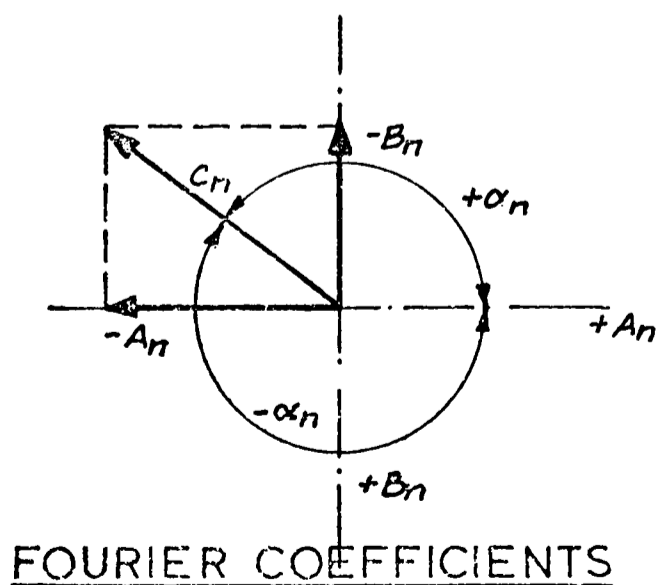


FIGURE (C.6)

NUMERICAL FOURIER ANALYSIS PROGRAM

This program has been developed for use on small core size computers. This was a requirement to enable on line data processing using the Thames Polytechnic, School of Civil Engineering COMPULOG machine, (supplied by INTERCOLE). Although this is not relevant for this thesis, it explains why the program uses a relatively large amount of computer time.

The program may be used to determine harmonics in halves, or integers, up to any specified limit. The numerical integration approximations and the presentation of the coefficients and phases has been explained in the previous section. For 'averaging' by the shifting of the record origin the standard deviation is given bracketed, following the coefficient.

```

      DIMENSION X(100),Y(100),Z(100),XX(100),XR(100)
      DIMENSION SDAH(50),SDBH(50),AL(50),C(50),H(50),AH(50),BH(50)
C   DIMENSION Y - NO. OF DATA POINTS
C   DIMENSION SDAH ETC - NO. OF HARMONICS (TOTAL)
C   F=1 - INTEGER HARMONICS ONLY
C   F=2 - ALSO HALF HARMONICS
      PI=3.1415926536
      READ(20,997)KK,DP
      READ(20,998)IP,N1,AVJ,NA
      WRITE(50,981)KK,DP,N1,AVJ,NA
      READ(20,999)(X(I),I=1,KK)
      READ(20,983)ANGLE
      WRITE(50,982)ANGLE
      IF(IP .LT. 2)AVJ=AVJ/2.
      INTEGER Q,O,E,G,M
      FF=1./AVJ
      FJ=FF/2.
      IF(IP .LT. 2)WRITE(50,996)FJ
      IF(IP .GT. 1)WRITE(50,996)FF
33  AVP=2.*AVJ
      M=AVP/DP
      S=FLOAT(KK)
      IF(NA .EQ. 0)NA=M
      U=FLOAT(NA)
      IF((DP*(S-1.)) .LT. (AVP+(U-1.)*DP))GO TO 700
      V=FLOAT(M)
      SUMXA=0.
      O=M+1
      K=M-1
      G=1
      IF(ABS(DP*V-AVP) .LT. .001)WRITE(50,995)
800  N2=N1
```

```

C IF N1 INPUT = 0 MEAN VALUE ONLY REQD
IF(N1 .EQ. 0)N2=1
DO 600 N=1,N2
H(N)=FLOAT(N)
DT=AVP-(V*DP)
SUMAA=0.
SUMAN=0.
SUMBN=0.
SUXAH=0.
SUXBH=0.
DO 300 I=1,NA
FI=FLOAT(I)
J=1+M
DO 200 Q=1,KK
200 XX(Q)=X(Q)
CONTINUE
XL=XX(J)
XG=XX(J+1)
CX=XG-XL
DX=CX*DT/DP
XP=XL+DX
AA=(XX(I)+XX(J))*DP/2.
AB=(XL+XP)*DT/2.
IF(ABS(DP*V-AVP) .LT. .001)AB=0.
SUMA=0.
J=I+1
L=I+M-1
DO 310 Q=J,L
310 SUMA=SUMA+XX(Q)
CONTINUE
SUMA=SUMA*DP
A00=(AA+AB+SUMA)/AVP
IF(N .GT. 1)GO TO 315
IF(G .EQ. 1)GO TO 315
XA=(A00-A0)**2
SUMXA=SUMXA+XA
315 SUMAA=SUMAA+A00
IF(N1 .EQ. 0)GO TO 300
C NORMALIZE TO MEAN LEVEL
XP=XP-A00
DO 320 J=1,KK
320 XX(J)=XX(J)-A00
CONTINUE
WP=H(N)*PI*(AVP+DP*(FI-1.))*2./AVP
YP=XP*COS(WP)
ZP=XP*SIN(WP)
L=I+M
J=0
DO 330 Q=I,L
330 FQ=FLOAT(Q)
T1=DP*(FQ-1.)
T2=DP*(FI-1.)
W=H(N)*PI*T1*2./AVP
J=J+1
Y(J)=XX(Q)*COS(W)
Z(J)=XX(Q)*SIN(W)
CONTINUE

```



```

AAA=(Y(1)+Y(M+1))*DF/2.
ABA=(Y(M+1)+YP)*DT/2.
BAB=(Z(1)+Z(M+1))*DF/2.
BBB=(Z(M+1)+ZP)*DT/2.
SUMACA=0.
SUMBCB=0.
DO 350 J=2,M
SUMACA=SUMACA+Y(J)
SUMBCB=SUMBCB+Z(J)
350 CONTINUE
ACA=SUMACA*DF
BCB=SUMBCB*DF
A=(AAA+ABA+ACA)/AVJ
B=(BAB+BBB+BCB)/AVJ
C S.D. EVALUATED 2ND TIME ROUND
IF(G .EQ. 1)GO TO 355
XAH=(A-AH(N))**2
XBH=(B-BH(N))**2
SUXAH=SUXAH+XAH
SUXBH=SUXBH+XBH
355 SUMAN=SUMAN+A
SUMBN=SUMBN+B
300 CONTINUE
IF(N1 .EQ. 0)GO TO 400
H(N)=H(N)/2.
AH(N)=SUMAN/U
BH(N)=SUMBN/U
IF(G .EQ. 1)GO TO 400
SDAH(N)=SQRT(SUXAH/U)
SDBH(N)=SQRT(SUXBH/U)
400 A0=SUMAN/U
600 CONTINUE
IF(G .EQ. 1)GO TO 610
SDA0=SQRT(SUMXA/U)
610 G=G+1
IF(G .EQ. 2)GO TO 800
IF(N1 .GT. 0)GO TO 1000
C IF MEAN VALUE ONLY REQD:
AH(1)=1000000.
BH(1)=1000000.
WRITE(50,991)A0,SDA0
GO TO 1000
700 H(N1)=0.
WRITE(50,994)
1000 WRITE(50,993)U
IF(AH(1) .EQ. 1000000)GO TO 5000
IF(H(N1) .EQ. 0)GO TO 5000
WRITE(50,990)
WRITE(50,989)A0,SDA0
DO 3000 N=1,N1
IF(IP .LT. 2)H(N)=2.*H(N)
WRITE(50,992)H(N),AH(N),SDAH(N),BH(N),SDBH(N)
IF(IP .LT. 2)H(N)=H(N)/2.
3000 CONTINUE
C DETERMINE PHASE & RECONSTITUTE X(T)
DO 4000 N=1,N1
R=AH(N)/BH(N)
AL(N)=ATAN(R)
C(N)=AH(N)/SIN(AL(N))
4000 CONTINUE

```

```

DO 4500 I=1, KK
J=I-1
SUM=0.
DO 4250 N=1, N1
EX=C(N)*SIN(N*2.*J*DP*PI/AVP+AL(N))
SUM=SUM+EX
4250 CONTINUE
XF(I)=SUM+A0
4500 CONTINUE
WRITE(50,987)
DO 2000 N=1, N1
IF(IP .LT. 2)H(N)=2.*H(N)
WRITE(50,988)H(N),AL(N),C(N)
IF(IP .LT. 2)H(N)=H(N)/2.
2000 CONTINUE
WRITE(50,986)
WRITE(50,985)
TIME=0.
DO 1500 E=1, K1
WRITE(50,984)TIME,X(E),XR(E)
TIME=TIME+DP
1500 CONTINUE
5000 STOP
999 FORMAT(F)
998 FORMAT(I,I,F,I)
997 FORMAT(I,F)
996 FORMAT(/10X,'FUNDAMENTAL FOURIER FREQUENCY =',
1F8.4,' HZ',/)
995 FORMAT(/10X,'EXACT NO. OF INTERVALS PER CYCLE:',
1'SD NOT CALCULATED',/)
994 FORMAT(/10X,'INSUFFICIENT DATA POINTS, NOT 2 CYCLES')
993 FORMAT(10X,'HARMONICS AVERAGED OVER ',F3.0,' WINDOWS')
992 FORMAT(9X,F4.1,8X,F8.4,'(',F6.4,')',6X,F8.4,
1'(',F6.4,')')
991 FORMAT(/10X,'MEAN VALUE (ONLY):',F8.4,'(',
1F6.4,')')
990 FORMAT(/10X,'H',16X,'AH',16X,'BH')
989 FORMAT(10X,'O',9X,F8.4,'(',F6.4,')')
988 FORMAT(8X,F4.1,13X,F8.4,9X,F8.4)
987 FORMAT(/10X,'H',16X,'PHASE',13X,'CH')
986 FORMAT(/15X,' COMPARE DAT: (X) WITH OUTPUT (XR)')
985 FORMAT(20X,'T',7X,'X',11X,'XR')
984 FORMAT(15X,F5.2,5X,F8.4,4X,F8.4)
983 FORMAT(F)
982 FORMAT(10X,F8.4,1X,'DEGREE PRESSURE TRANSDUCER')
981 FORMAT(5X,'INPUT: K=',I3,2X,'DP=',F5.3,2X,'NO.H=',I3,
12X,'PER.=',F7.4,2X,'NO.AVERAGE=',I3,/)
END

```

EXAMPLE OF OUTPUT FROM PROGRAM

Planar oscillatory motion: T_{pc} of 4.334s, PDM experiment.
Displacement transducer digitized record X for 100 data points,
time interval 0.1s.

DISPLACEMENT TRANSDUCER FOURIER COEFFICIENTS PMM105

INPUT: K=100 DP= .100 NO.H= 10 PER.= 4.3340 NO.AVER.= 10

FUNDAMENTAL FOURIER FREQUENCY = 0.2307 HZ

HARMONICS AVERAGED OVER 10 WINDOWS

H	AH	BH
0	0.0012(0.0000)	
0.5	-0.0004(0.0000)	0.0001(0.0000)
1.0	-0.7361(0.0000)	0.1587(0.0000)
1.5	0.0004(0.0000)	-0.0001(0.0000)
2.0	0.0020(0.0000)	0.0007(.0001)
2.5	0.0005(.0001)	-0.0005(.0001)
3.0	0.0019(.0001)	0.0006(.0001)
3.5	-0.0003(.0001)	-0.0000(.0001)
4.0	-0.0007(.0001)	0.0013(.0001)
4.5	-0.0003(.0001)	0.0000(.0001)
5.0	-0.0004(.0002)	-0.0021(.0001)

H	PHASE	CH
0.5	-1.3614	0.0005
1.0	-1.3584	0.7530
1.5	-1.4318	-0.0004
2.0	1.2281	0.0022
2.5	-0.7835	-0.0008
3.0	1.2454	0.0020
3.5	1.4538	-0.0003
4.0	-0.5181	0.0015
4.5	-1.5060	0.0003
5.0	0.1810	-0.0021

COMPARE DATA WITH OUTPUT (XR)

T	X	XR			
0.00	-0.7330	-0.7322			
0.10	-0.7010	-0.7020			
0.20	-0.6550	-0.6565			
0.30	-0.5960	-0.5969			
0.40	-0.5260	-0.5247			
0.50	-0.4440	-0.4422			
0.60	-0.3530	-0.3514			
0.70	-0.2540	-0.2541			
0.80	-0.1500	-0.1519			
0.90	-0.0440	-0.0459			
1.00	0.0600	0.0625			
1.10	0.1720	0.1714			
1.20	0.2770	0.2782			
1.30	0.3800	0.3798			
1.40	0.4740	0.4728			
1.50	0.5540	0.5543			
1.60	0.6210	0.6224			
1.70	0.6760	0.6761			
1.80	0.7170	0.7152	5.60	0.3460	0.3465
1.90	0.7420	0.7401	5.70	0.4430	0.4420
2.00	0.7490	0.7508	5.80	0.5290	0.5272
2.10	0.7450	0.7473	5.90	0.5970	0.5999
2.20	0.7290	0.7291	6.00	0.6580	0.6587
2.30	0.6970	0.6955	6.10	0.7040	0.7031
2.40	0.6470	0.6465	6.20	0.7350	0.7333
2.50	0.5830	0.5827	6.30	0.7500	0.7492
2.60	0.5060	0.5059	6.40	0.7470	0.7508
2.70	0.4180	0.4182	6.50	0.7400	0.7376
2.80	0.3220	0.3223	6.60	0.7080	0.7092
2.90	0.2200	0.2205	6.70	0.6660	0.6654
3.00	0.1150	0.1148	6.80	0.6060	0.6064
3.10	0.0040	0.0070	6.90	0.5350	0.5337
3.20	-0.1010	-0.1014	7.00	0.4490	0.4491
3.30	-0.2000	-0.2086	7.10	0.3550	0.3552
3.40	-0.3150	-0.3122	7.20	0.2530	0.2545
3.50	-0.4140	-0.4098	7.30	0.1490	0.1491
3.60	-0.5010	-0.4984	7.40	0.0410	0.0410
3.70	-0.5740	-0.5756	7.50	-0.0660	-0.0681
3.80	-0.6370	-0.6396	7.60	-0.1750	-0.1761
3.90	-0.6880	-0.6892	7.70	-0.2820	-0.2809
4.00	-0.7240	-0.7241	7.80	-0.3820	-0.3799
4.10	-0.7450	-0.7441	7.90	-0.4720	-0.4707
4.20	-0.7500	-0.7490	8.00	-0.5490	-0.5507
4.30	-0.7410	-0.7389	8.10	-0.6160	-0.6184
4.40	-0.7130	-0.7135	8.20	-0.6730	-0.6724
4.50	-0.6710	-0.6730	8.30	-0.7130	-0.7123
4.60	-0.6170	-0.6181	8.40	-0.7380	-0.7377
4.70	-0.5500	-0.5500	8.50	-0.7490	-0.7484
4.80	-0.4720	-0.4707	8.60	-0.7460	-0.7440
4.90	-0.3830	-0.3821	8.70	-0.7230	-0.7242
5.00	-0.2870	-0.2863	8.80	-0.6880	-0.6890
5.10	-0.1840	-0.1851	8.90	-0.6370	-0.6389
5.20	-0.0780	-0.0799	9.00	-0.5740	-0.5751
5.30	0.0260	0.0279	9.10	-0.5010	-0.4994
5.40	0.1370	0.1365	9.20	-0.4160	-0.4140
5.50	0.2430	0.2436	9.30	-0.3220	-0.3209
			9.40	-0.2190	-0.2219
			9.50	-0.1130	-0.1183
			9.60	-0.0090	-0.0114
			9.70	0.1000	0.0974
			9.80	0.2080	0.2060
			9.90	0.3120	0.3115

APPENDIX D

INTRODUCTION TO SPECTRAL ANALYSIS

This Appendix is not a rigorous exposition of spectral analysis theory and its application to digitized records, only an introduction to the continuation of the Fourier Analysis concepts of appendix C. For problems where there are many frequency components making up a time function, or if the function may be considered as effectively extending for an infinite time, with period tending to infinity, the discrete Fourier Series concept cannot be successfully applied.

Particularly useful sources which describe the techniques of frequency analysis are: Newland (1975), CIRIA (1978) and Tickell & Holmes (1979). The first of these is particularly concerned with the theory and analysis of analogue and digitally recorded time functions, whereas the latter two apply these and probabilistic concepts to fluid loading conditions specifically. Christian (1973) should also be referred to where guidance is sought on the spectral analysis of wave records.

Equations (14) and (16) of Appendix C allow the transformation of a time function into a frequency function, or the reverse. These two equations, the Fourier Transform pair, therefore relate a 'time domain' to a 'frequency domain'. Actual recorded time functions will not, however, extend over an infinite time, and consequently equation (14) cannot be solved even for a stationary function. Note also that the condition expressed by equation (16a) in Appendix C is not met by recorded time functions either. There are two approaches used to determine the solution of equation (14), both of which result in the spectral density function $S_f(\omega)$. The common approach used nowadays is to evaluate the Fourier transform of $f(t)$ using the Fast Fourier Transform directly from $f(t)$. This technique is particularly useful for computer analysis of digitized data. For a comprehensive discussion of this method, however, reference should be made to Newland (ibid). In this Appendix the alternative method using the autocorrelation function will be introduced as it usefully illustrates the meaning and significance of the processes involved and the functions evaluated.

Depending upon the way in which sampling of a random process $f(t)$ is carried out, if it is random, then for records at different

times, or over different timespans, $f(t)$ will be represented by different $f(t)$ records:

$f_1(t), f_2(t), f_3(t), \dots, f_n(t)$, as shown in Figure (D.1)

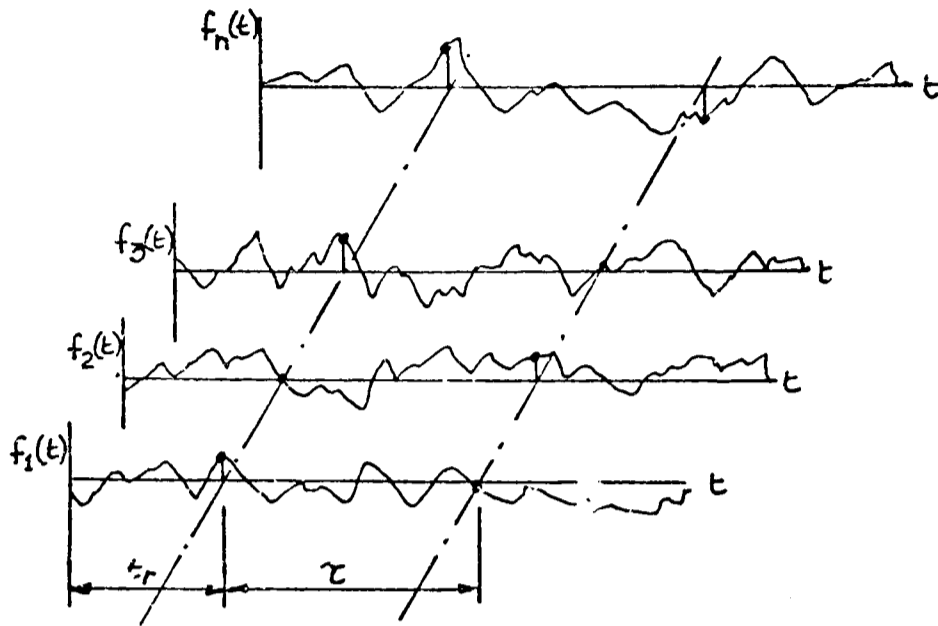


Figure (D.1)
Ensemble

Such a collection representing $f(t)$ is termed an 'Ensemble', and for $n \rightarrow \infty$, an infinite ensemble. The average value of $f(t)$ may then be defined by the average of $f_n(t)$ with t , or the average across the ensemble records at a certain time t_r i.e. the ensemble average of $f(t)$ is calculated from $f_n(t_r)$; if both averages are the same then $f(t)$ is termed 'ergodic'. Similarly this approach may be extended to other statistical properties of $f(t)$. The probability distribution function

$$P(f) = p_r \{ f(t) \leq f \} \quad , \text{ i.e. the probability that}$$

$f(t)$ is less than some specified value f can be determined from $f(t_r)$.

If a second time point is taken t_{r2} the second order probability density function may also be determined from $f(t_{r2})$ across the ensemble. This process may be extended to determine any order of probability distribution function. The complete time function, or random process $f(t)$, is said to be 'stationary' if the higher order probability distribution functions are a function of the sampling interval τ alone, and not of absolute time. The implications of this are that for a stationary process the mean, mean square and variance are time invariant. Ergodic functions are also stationary, and in many engineering situations the recorded, finite length, time function is assumed to be represental of the whole record, and hence ergodic and stationary.

For a random function of time $f(t)$ the autocorrelation function $R_f(\tau)$ is defined as the mean, or expected, value of the product $f(t) \times f(t+\tau)$, where τ is the time interval between any two sample record points $f(t)$ and $f(t+\tau)$. For a stationary process:

$$R_f(\tau) = E[f(t), f(t+\tau)] \quad \dots \quad (1)$$

will therefore be only a function of τ . $R_f(\tau)$ is normally presented graphically as a function of τ . Where it is impossible to Fourier analyse the function $f(t)$, say due to the limitations mentioned above, the autocorrelation function may be Fourier analysed: Normalizing $R_f(\tau)$ by first subtracting the mean value $E[f(t)]$, and because for $\tau \rightarrow \infty$, $R_f(\tau)$ will tend to zero, for the random function $f(t)$, the condition for Fourier transformation

is substituted by $\int_{-\infty}^{\infty} |f(t)| dt < \infty$ is satisfied if $f(t)$ is substituted by $R_f(\tau)$.

Therefore from equation (14), Appendix C:

$$S_f(\omega) = \frac{i}{2\pi} \int_{-\infty}^{\infty} R_f(\tau) e^{-j\omega\tau} d\tau \quad \dots \quad (2)$$

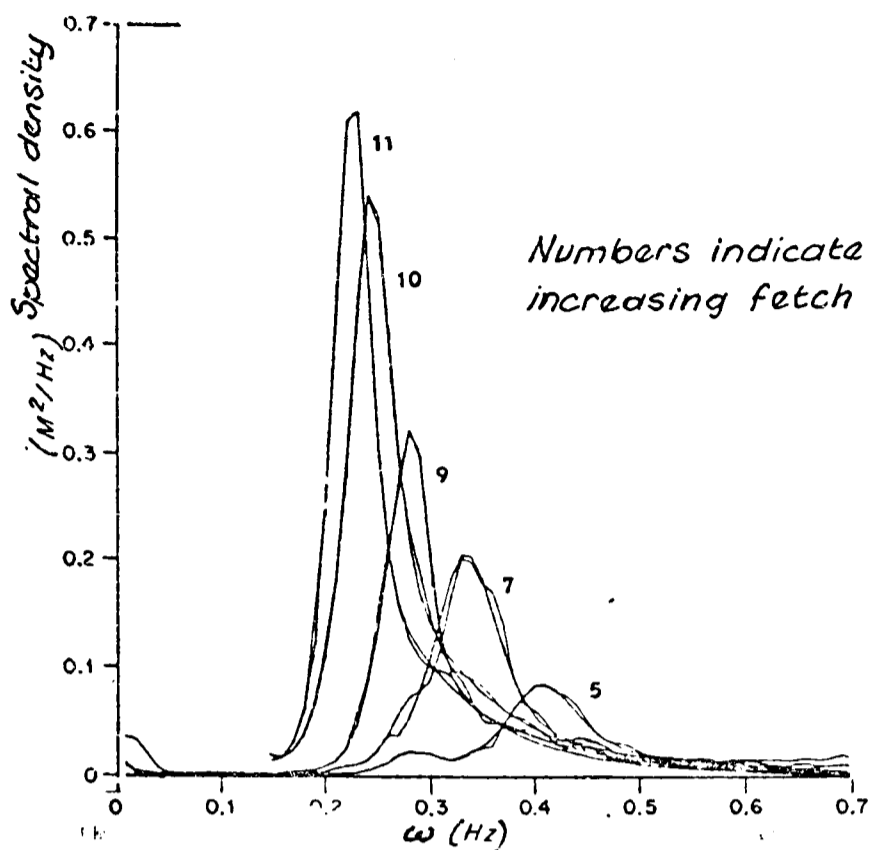
i.e. the Fourier Transform of the autocorrelation function of a time function $f(t)$ is the spectral density of $f(t)$. This sounds relatively simple, but there are many limitations to this apparently straightforward approach when dealing with actual records.

For $\tau = 0$ the autocorrelation function for the stationary random function $f(t)$:

$$R_f(0) = E[f^2(t)] = \int_{-\infty}^{\infty} S_f(\omega) d\omega$$

i.e. the mean square value is the area of the spectral density/frequency graph. This property is particularly important because of the derivation of the statistical properties of $f(t)$ that are possible using the mean square, which for a zero mean function, is equal to the variance. The spectral density is therefore useful not only in describing the frequency content of a function $f(t)$, but may also be used to obtain statistical information concerning the probability of the value of the function in time.

The representation of sea wave heights and frequencies in the form of spectral density illustrates the energy content-frequency structure for small amplitude deep water waves, because the wave energy is proportional to H_w^2 , Figure (D.2).



WAVE SPECTRA MEASURED DURING OFFSHORE WINDS-
ILLUSTRATING THE FETCH DEPENDENCE OF ONE -
DIMENSIONAL WAVE SPECTRA

(From: 'Some results from the Joint North Sea Wave Project of interest to engineers' Ewing, J.A. Proc. Int. Symp. Dynamics of marine vehicles and structures in waves Univ. Coll. 1974)

FIGURE (D.2)

Such representations of the sea surface may be used to determine wave particle kinematics, or wave induced forces, using suitable transfer functions.

This extremely simplified introduction to spectral analysis ignores many of the difficulties encountered when analysing actual records, problems occur due to finite record length, non-stationarity, wave non-linearity and the actual interpretation of digitized records. For a more rigorous treatment and discussion of actual application see the references cited at the beginning of this Appendix.

N_k [@]	N_v	f_L/f_p	No. of Zero Crossings	Harmonic content of Lift force
8 - 16	1	2	4	2,4....
16- 24	2	3	6	(1),3,5...
24- 32	3	4	8	2,4....
32- 40	4	5	10	(1),3,5...
$8n \rightarrow 8(r+1)$	n	$n+1$	$2(n+1)$	$n+1$

@ based upon a varying characteristic velocity, i.e.
 $N_v = N_k / 8$ (see page 42).

NUMBER OF SEED VORTICES AND HARMONIC CONTENT OF LIFT FORCE FOR
A PLANAR OSCILLATORY FLOW (FROM: ISAACSON (1974))

TABLE (1.1)

RELATIVE MOTION	π_1	π_2	π_3	π_4	π_5
STEADY (For cylinder moving in a still fluid \vec{U}_0 becomes $\vec{U}t$)	$\frac{\rho d}{\mu} = RE$ Reynolds No.	$\frac{U_0}{(gd)^{1/2}} = Fr$ Froude No.	$\frac{U_0}{fd} = Vr$ Reduced Velocity also: $\frac{fsd}{U_0}$ Strouhal No.	$\frac{m}{\rho d^2}$ Mass parameter	$\frac{F}{\rho d U_0^2}$ Force parameter
UNIDIRECTIONAL ACCELERATION (For cylinder moving in still water \vec{U}_0 becomes $\vec{U}c$)	$\frac{\rho d}{\mu} = RE(t)$ Reynolds No. (instantaneous)	$\frac{U_d}{(gd)^{1/2}} = Fr$ Froude No. (instantaneous) also: $\frac{d \rho g}{U_d^2} = Im$ Iversen No. (or modulus)	$\frac{fsd}{U_d} = S$ Strouhal No. (instantaneous)	$\frac{m_e}{\rho d^2}$ Mass parameter	$\frac{F(t)}{\rho d U_d^2}, \frac{F(t)}{\rho g d^2}$ Force parameters
PLANAR OSCILLATORY MOTION (i) Fluid moving (For cylinder in standing waves replace suffix p by w)	$\frac{\mu_{max} d}{\mu} = RE$ $= \frac{2\pi A p d}{l p \nu}$ Maximum Reynolds No.*	$\frac{d \rho p}{U_p^2} = Im$ $= -\frac{d}{X_p}$ Iversen No.	$\frac{U_{max} p}{d} = Nk$ $= \frac{2\pi A p}{d}$ Keulegan - Carpenter No.*	$\frac{m}{\rho d^2}$ Mass parameter	$\frac{F(t)}{\rho d U_p^2}, \frac{F(t)}{\rho g d^2}$ Force parameters (instantaneous)

(See also next page)

TABLE (2.1)

RELATIVE MOTION	π_1	π_2	π_3	π_4	π_5
PLANAR OSCILLATORY MOTION (ii) Cylinder moving	$\frac{\bar{u}_{pc} \max d}{\nu} = RE$ $= \frac{2\pi A_{pc} d}{T_{pc} \nu}$ Maximum Reynolds No. *	$\frac{d g_{pc}}{\bar{u}_{pc}^2} = Im$ $= -\frac{d}{X_{sc}}$ Iversen No.	$\frac{\bar{u}_{pc} \max T_{pc}}{d} = Nk$ $= \frac{2\pi A_{pc}}{d}$ Keulegan - Carpenter No. *	$\frac{m_e}{\rho d^2}$ Mass parameter	$\frac{F(t)}{\rho d \bar{u}_{pc}^2}, \frac{F(t)}{\rho g_{pc} d^2}$ Force parameters (instantaneous)
LONGITUDINAL WATER WAVES (Cylinder stationary)	$\frac{\bar{u}_w \max d}{\nu} = RE$ Reynolds No. (maximum)	$\frac{S_w}{(g z)^{1/2}} = Fr$ Froude No. also: $\frac{d g_w}{\bar{u}_w^2}$ Iversen No. $\cdot Im$	$\frac{\bar{u}_w \max T_w}{d} = Nk$ Keulegan - Carpenter No.	$\frac{m_e}{\rho d^2}$ Mass parameter	$\frac{F(t)}{\rho d \bar{u}_w^2}, \frac{F(t)}{\rho g_w d^2}$ Force parameters (instantaneous)

* combining π_1 & π_3 gives $Re/Nk = d/T_{pc} \nu = \beta$ Stokes No.

Cylinder diameter c (m)	Water depth z (m)	Wave height H_w (m)	Wave length L_w (m)	relative $1/z$	d L_w	$R_{1/2}$		H_k	
						surface	%Cm below	surface	%Cm below
0.075	deep	16	300	deep	25×10^{-5}	2.8×10^5	7.6×10^4	660	100
	deep	10	150	water waves	5×10^{-4}	2.5×10^5	-	410	-
0.25	deep	16	300	" "	8×10^{-4}	1×10^6	2.7×10^5	200	60
	deep	10	150	" "	1×10^{-3}	3.5×10^5	-	125	-
1.00	deep	16	300	" "	3×10^{-3}	4×10^6	1.1×10^6	50	14
	deep	10	150	" "	6×10^{-3}	3.2×10^6	-	31	-
	130	30	500	inter-	2×10^{-3}	1.5×10^6	-	100	-
	130	10	100	mediate	0.01	"	-	30	-
	130	5	40	deep	0.025	"	-	15	-
	30	5	40	water waves	0.025	"	-	15	-
2.50	deep	16	300	" "	8×10^{-3}	1×10^7	2.7×10^6	20	5.5
	deep	10	150	" "	0.016	3.5×10^6	-	12.5	-
3.00	130	30	500	inter-	6×10^{-3}	0.5	-	30	-
	130	10	100	mediate	0.03	to	-	10	-
	130	5	50	deep	0.075	2×10^7	-	5	-
	30	5	40	" "	0.075	-	-	5	-

TABLE (2.2) TYPICAL FULL SCALE VALUES OF $R_{1/2}$ & N_k IN WAVES AT THE SURFACE, AND AT A DEPTH OF 80m

AUTHOR	RELATIVE FLOW CONDITION	$L \frac{z}{d}$	N_k	R_E	NOTES
McNown 1957	Cnoidal standing waves (but assumed sinusoidal)	31.6	2.5 to 9	400 to 1400	Horizontal lenticular cylinder at mid water depth. Ends close to walls. Reaction forces measured.
Keulegan & Carpenter 1958	Sinusoidal standing waves	6.8. to 43.3	2 to 120	4×10^3 to 3×10^4	Horizontal circular cylinders. Ends close to walls. Reaction forces measured.
Rance 1969	Pulsating water tunnel	0.6 to 12.0	60 to 230	$*4 \times 10^3$ to 7×10^5	Horizontal circular cylinders. Dummy end sections attached to walls. Reaction forces measured.
Businell 1977	Pulsating water tunnel	6.5	12.6 to 170	2×10^4 to 8.6×10^4	"
Sarpkaya 1974-77	Water oscillating in U-tubes. Motion allowed to decay.	2 to 20	up to 200	up to 1.5×10^6	Horizontal cylinders. Ends close to walls. Reaction forces measured.
Mull & Lilliner 1978	Water oscillating in a U-tube	11.8 & 17.7	5 to 28	up to 4×10^3	Horizontal cylinders attached to walls. Reaction forces measured.
Bearman, Graham & Singh 1978-79	Water oscillating in a U-tube.	-	3 to 75	up to 4×10^5	Horizontal sharp-edged and circular cylinders attached to walls. Reaction forces measured.

* R_E calculated using velocity at instant of maximum force

FLUID OSCILLATING RELATIVE TO A STATIONARY CYLINDER

TABLE (3.1)

AUTHOR	$\frac{L}{d}$	N_k	R_E	NOTES
Paape & Brausers 1966	16.7	1 to 17	1.5×10^3 to 1.8×10^5	Unspecified submerged oscillating cylinder. Reaction forces measured on central part of cylinder.
Heinzer & Dalton 1969	-	2 to 28	up to 6×10^4	Vertical surface piercing cylinders. Flow visualization only (on surface of water).
Hamann & Dalton 1971	-	4 to 58	up to 4×10^5	Vertical surface piercing cylinders. Reaction forces measured.
Mercier 1973	7.5	up to 22	10^3 to 10^4	Vertical cylinder, no end plates. Reaction forces measured.
Chantran- uvatana 1974	10	4 to 23	10^3 to 3.5×10^4	Vertical cylinder, end conditions unspecified. One rotatable pressure tapping.
Isaacson 1974	-	up to 14	up to 3×10^3	Surface piercing vertical cylinder. Effectively a large bottom end plate. Reaction forces measured.
Yamamoto & Math 1975	12	30 to 120	10^5 to 10^6	Horizontal cylinder oscillating near boundary. Reaction forces measured on central part of cylinder.

All motions approximately Simple Harmonic

CYLINDER OSCILLATING IN OTHERWISE STILL WATER -- I

TABLE (3.2)
(continued overleaf)

AUTHOR	$\frac{L^2}{a}$	N_k	R_E	NOTES
Chung 1977	12	less than 1	up to 3×10^3	Horizontal cylinders oscillating near free surface. Reaction forces measured.
Garrison, Field & May 1977	5.1 to 11.5	6 to 33	10^4 to 5×10^5	Horizontal cylinder with small end plates, close to sid, walls. Reaction forces measured.
Barnouin, Mattout, & Sagner 1978	-	4 to 20	2×10^3 to 7×10^4	Horizontal cylinders without end plates. Reaction forces measured. R_E less than 1.2×10^4 results unreliable.
Grass & Kemp 1978	8.4	38	2.2×10^4 to 5.4×10^4	Smooth and rough horizontal cylinders. Flow visualization only.
Mauil & Milliner 1979	24	5 to 35	-	Vertical cylinder oscillating with a complex motion. Reaction forces measured.

All motions approximately Simple Harmonic, unless otherwise specified.

CYLINDER OSCILLATING IN OTHERWISE STILL WATER - II

SIGNIFICANT FOURIER COEFFICIENTS & PHASES

(Up to 5th harmonic with $c_n \geq 0.05$, except forces)

For $f(t) = c_n \sin(n\omega t + \alpha_n)$

where c_n amplitude

and α_n phase - at start of analysed record -
adjusted to an angle $< 180^\circ$

Relative phases of 1st, 2nd and 3rd harmonics
determined by comparison to displacement,
(displacement)² and (displacement)³ phase angles.

FUNCTION	HAR- MONIC	c_n	α_n		PHASE RELATIVE TO DISP. TRANS. ($ \alpha_n < 180^\circ$)
			(rad)	(degree)	
Displace- ment Trans- ducer	1	0.753	-1.358	-77.8	/
(Displace- ment Trans- ducer) ²	2	0.283	2.000	114.6	
(Displace- ment Trans- ducer) ³	1	0.320	-1.356	-77.7	
	3	0.105	-0.926	-53.1	
<u>PRESSURES:</u>					
$\frac{C_p}{0^\circ}$	$\frac{1}{2}$	0.052	-1.334	-76.4	
	1	0.736	-2.639	-151.2	-73.4
	2	0.250	0.083	4.8	-109.8
	$2\frac{1}{2}$	0.078	2.568	147.1	
	3	0.216	0.345	19.8	72.9

Table (4.1a)

FUNCTION	HAR- MONIC	C_n	α_n		PHASE RELATIVE TO DISP. TRANS.
			(rad)	(degree)	
15°	$\frac{1}{2}$	0.053	-0.340	-19.5	-64.4 -145.3
	1	0.631	-2.483	-142.2	
	2	0.057	-0.535	-30.7	
	$2\frac{1}{2}$	0.072	2.330	133.5	82.4
	3	0.294	0.511	29.5	
	$3\frac{1}{2}$	0.075	-1.118	-64.1	
	4	0.148	1.463	53.8	
	$4\frac{1}{2}$	0.054	1.574	90.2	
	5	0.153	-1.231	-70.5	
30°	1	0.259	-2.308	-132.2	-54.4
	2	0.109	3.010	172.5	57.9
	$2\frac{1}{2}$	0.066	2.700	154.7	59.9
	3	0.220	0.119	6.8	
	4	0.268	1.660	95.1	
	$4\frac{1}{2}$	0.053	1.030	59.0	
	5	0.228	-1.675	-95.9	
45°	1	0.209	-0.279	-16.0	61.8
	2	0.441	2.803	160.9	46.3
	3	0.132	-0.360	-20.6	32.5
	4	0.351	1.628	93.3	
	5	0.192	-1.992	-114.1	
60°	1	0.446	-0.087	-5.0	72.8
	$1\frac{1}{2}$	0.055	-2.220	-127.2	43.6
	2	0.880	2.760	158.2	
	$2\frac{1}{2}$	0.052	2.314	132.6	-138.2
	3	0.050	2.944	168.7	
	4	0.446	1.444	82.7	
	$4\frac{1}{2}$	0.057	-0.174	10.0	
	5	0.100	-1.981	-113.5	

Table (4.1b)

FUNCTION	HAR- MONIC	c_n	α_n		PHASE RELATIVE TO DISF. TRANS.
			(rad)	(degree)	
75°	1	0.409	0.055	3.2	81.0
	1½	0.067	-2.604	-149.2	
	2	1.219	2.903	166.3	51.7
	3	0.156	2.628	150.6	-156.3
	4	0.418	1.702	97.6	
5	0.109	-0.800	-45.8		
90°	1	0.052	2.818	161.4	-120.8
	1½	0.065	2.705	-155.0	
	2	1.380	2.664	152.6	38.0
	3	0.235	1.396	80.0	133.1
	4	0.178	1.355	77.6	
5	0.120	-1.102	-63.1		
105°	1	0.489	-3.087	-176.9	-99.1
	1½	0.071	3.006	172.2	
	2	1.102	2.569	147.2	32.6
	2½	0.105	-1.954	-112.0	
	3	0.515	1.242	71.2	124.3
	3½	0.085	0.028	1.6	
	5	0.267	-0.886	-50.8	
120°	1	0.695	3.085	176.8	-105.4
	2	0.709	2.533	145.1	30.5
	2½	0.053	-1.878	-107.6	
	3	0.609	1.111	63.7	116.8
	3½	0.074	0.000	0.0	
	4	0.090	-0.541	-31.0	
	5	0.269	-0.866	-49.6	

Table (4.1c)

FUNCTION	HAR-MONIC	C_n	α_n		PHASE RELATIVE TO DISP. TRANS.
			(rad)	(degree)	
135°	1	0.416	2.480	142.1	-140.1
	2	0.434	1.909	109.4	-5.2
	3	0.474	0.657	37.6	90.7
	3½	0.059	-0.081	4.7	
	4	0.174	-0.784	-44.9	
	5	0.226	-1.556	-89.2	
150°	1	0.327	1.265	72.5	150.3
	2	0.249	1.106	63.4	-51.2
	3	0.308	0.956	54.8	107.9
	3½	0.054	0.596	34.1	
	4	0.092	-0.323	-18.5	
	5	0.159	-1.930	-110.6	
165°	½	0.087	1.948	111.6	
	1	0.574	0.891	51.05	128.9
	1½	0.098	2.835	162.4	
	2	0.159	-0.115	-6.6	-121.2
	2½	0.057	-2.900	-165.6	
	3	0.063	1.478	84.7	137.8
	4	0.118	0.358	20.5	
180°	½	0.090	2.321	133.0	
	1	0.753	0.728	41.7	119.5
	1½	0.062	2.573	147.5	
	2	0.143	-0.280	-16.0	-130.6
	3	0.281	2.772	158.9	-148.0
	3½	0.080	2.158	123.6	
	4	0.083	0.173	9.9	
	4½	0.060	2.317	132.8	
	5	0.114	1.353	77.5	

Table (4.1d)

FUNCTION	HAR- MONIC	C_n	α_n		PHASE RELATIVE TO DISP. TRANS.
			(rad)	(degree)	
195°	1	0.710	0.723	41.4	119.2
	2	0.111	-0.450	-25.8	-140.4
	3	0.351	-2.830	-167.1	-109.0
	4	0.087	1.622	92.9	
	5	0.136	1.324	75.9	
210°	1	0.422	0.932	53.6	131.4
	1½	0.067	-0.154	-8.8	
	2	small com- ponent			
	2½	0.080	0.271	15.5	
	3	0.276	-2.616	-149.9	-96.8
225°	4	0.129	2.061	118.1	
	5	0.154	1.400	80.2	
	1	0.228	1.809	103.7	-178.5
	1½	0.077	-0.653		
	2	0.232	2.508	143.7	29.1
240°	2½	0.106	0.199		
	3	0.208	-2.126	-721.8	-68.7
	3½	0.085	2.587	148.2	
	4	0.099	1.968	112.8	
	5	0.161	1.472	84.3	
240°	½	0.071	1.940	113.3	
	1	0.300	2.436	139.6	-142.6
	1½	0.073	-0.285	16.3	
	2	0.768	2.693	154.3	39.7
	2½	0.118	0.139	8.0	
	3	0.393	-1.255	-71.9	-18.8
	3½	0.075	2.934	168.2	
	4	0.075	1.469	84.2	
	5	0.209	2.537	145.3	

Table (4.1e)

FUNCTION	HAR- MONIC	C_n	α_n		PHASE RELATIVE TO DISP. TRANS.
			(rad)	(degree)	
255°	$\frac{1}{2}$	0.114	1.986	113.8	
	1	0.253	2.458	140.8	-141.4
	2	1.248	2.576	147.6	33.0
	$2\frac{1}{2}$	0.140	-0.463	-26.5	
	3	0.450	-1.410	-80.8	-27.7
	4	0.123	-0.753	-45.1	
	5	0.172	2.113	121.0	
270°	$\frac{1}{2}$	0.110	2.105	120.6	
	1	0.039	2.593	148.6	-133.6
	2	1.419	2.405	141.2	26.6
	$2\frac{1}{2}$	0.143	-0.410	-23.5	
	3	0.342	-1.560	-89.4	-36.3
	$3\frac{1}{2}$	0.060	2.933	168.3	
	4	0.223	-1.326	-76.0	
5	0.145	2.265	124.8		
285°	$\frac{1}{2}$	0.113	2.361	135.3	
	1	0.072	-1.207	-69.2	8.6
	2	1.282	2.409	138.0	23.4
	$2\frac{1}{2}$	0.160	-0.219	12.5	
	3	0.246	-1.733	-99.3	-46.2
	$3\frac{1}{2}$	0.077	3.134	179.6	
	4	0.330	-1.348	-77.2	
$4\frac{1}{2}$	0.053	-2.908	-166.6		
5	0.181	2.458	140.8		
300°	$\frac{1}{2}$	0.104	2.237	128.1	
	1	0.179	-0.786	-45.0	32.8
	2	0.852	2.050	117.5	2.9
	$2\frac{1}{2}$	0.179	-0.281	-16.1	
	3	0.224	-2.314	-132.6	-79.5
	$3\frac{1}{2}$	0.054	3.009	172.4	
	4	0.389	-1.782	-102.1	
$4\frac{1}{2}$	0.089	-2.958	-169.5		
5	0.195	1.983	113.6		

Table (4.1f)

FUNCTION	HAR- MONIC	c_n	α_n		PHASE RELATIVE TO DISP. TRANS.
			(rad)	(degree)	
315°	$\frac{1}{2}$	0.055	1.994	114.2	16.6 -9.3 -104.5
	1	0.217	-1.069	-61.2	
	$1\frac{1}{2}$	0.050	-1.955	-112.0	
	2	0.369	1.839	105.3	
	$2\frac{1}{2}$	0.096	-0.149	-8.5	
	3	0.183	-2.751	-157.6	
	$3\frac{1}{2}$	0.067	2.126	121.8	
	4	0.335	-1.510	-86.5	
	$4\frac{1}{2}$	0.077	-2.377	-136.2	
	5	0.122	1.724	99.3	
330°	1	0.376	-2.318	-132.8	-55.0
	2	0.215	0.911	52.2	-62.4
	3	0.057	2.839	162.7	-144.2
	$3\frac{1}{2}$	0.070	2.410	138.1	
	4	0.298	-1.246	-71.4	
	5	0.091	1.552	88.9	
345°	1	0.657	-2.565	-147.0	-69.2
	2	0.284	0.144	8.2	-106.3
	3	0.088	0.643	36.8	89.9
	4	0.197	-1.197	-68.6	
	5	0.069	1.786	102.3	

Table (4.1g)

FUNCTION	HAR- MONIC	C_n	α_n		PHASE RELATIVE TO DISP. TRANS.
			(rad)	(degree)	
<u>FORCES:</u> IN LINE	$\frac{1}{2}$	0.029	-0.939	53.8	-40.0 5.0 52.3
	1	0.626	-2.056	-117.8	
	$1\frac{1}{2}$	0.007	-1.676	-96.0	
	2	0.024	2.087	119.6	
	$2\frac{1}{2}$	0.022	2.793	160.0	
	3	0.085	-0.014	-0.8	
	$3\frac{1}{2}$	0.024	-1.794	-102.8	
	4	0.033	-2.334	-133.7	
	$4\frac{1}{2}$	0.016	2.333	133.7	
	5	0.015	-2.023	-116.2	
TRANS- VERSE	$\frac{1}{2}$	0.068	-1.006	-57.6	-94.6 121.6 121.5
	1	0.024	-3.009	-172.4	
	$1\frac{1}{2}$	0.056	2.958	169.5	
	2	0.178	-2.161	-123.8	
	$2\frac{1}{2}$	0.139	3.069	175.9	
	3	0.466	1.194	68.4	
	$3\frac{1}{2}$	0.096	-0.181	-10.3	
	4	0.311	1.579	90.5	
	$4\frac{1}{2}$	0.064	0.669	38.3	
	5	0.303	-1.205	-69.0	
	$5\frac{1}{2}$	0.042	2.399	137.4	
6	0.108	-0.685	-39.2		

Table (4.2)

Harmonic	Complete record		1st cycle		2nd cycle	
	C_n	α_n	C_n	α_n	C_n	α_n
1	0.024	-1.65	0.014	-0.50	0.030	-2.21
2	0.178	0.56	0.203	1.01	0.191	0.46
3	0.466	-1.02	0.568	-1.02	0.285	-1.04
4	0.311	0.73	0.261	0.98	0.341	0.77
5	0.303	-0.70	0.352	-0.86	0.194	-0.63
6	0.108	1.18	0.108	1.52	0.069	1.44

Comparison of Fourier components of lift force for complete record and individual cycles of motion

Table (4.3)

Harmonic	Fourier coefficient as a proportion of 3rd harmonic			
	Maul & Milliner (1978)	Complete record	1st cycle	2nd cycle
1	0.24	0.050	0.025	0.11
2	0.18	0.38	0.36	0.67
3	1	1	1	1
4	0.2	0.67	0.46	1.20
5	0.54	0.65	0.62	0.6 ^a

Relative harmonic dominance of lift force

Table (4.4)

Harmonic	Complete record		1st cycle		2nd cycle	
	C_n	α_n	C_n	α_n	C_n	α_n
1	0.626	-0.698	0.626	-0.718	0.659	-0.697
2	-	-	-	-	-	-
3	0.085	-2.221	0.121	-2.084	-	-
4	-	-	-	-	-	-
5	-	-	0.064	-1.332	-	-

Harmonic structure of in-line force

Table (4.5)

PARAMETER	WITH END PLATES		WITHOUT END PLATES	
	Range	Mean	Range	Mean
Drag Coefficient	0.43 — 0.56	0.49	0.31 — 0.39	0.36
Added Mass Coefficient	0.81 — 0.92	0.88	0.93 — 0.98	0.95
Overall Force Coefficient	1.01 — 1.07	1.05	1.08 — 1.11	1.09
Phase Angle between Max. Fluid Accn. and Max. Force	54° — 66°	60°	31° — 47°	41°
Lift Coefficient	0.73 — 1.50	1.30	0.47 — 0.71	0.59

Effect of end plates: $N_k = 17.65$

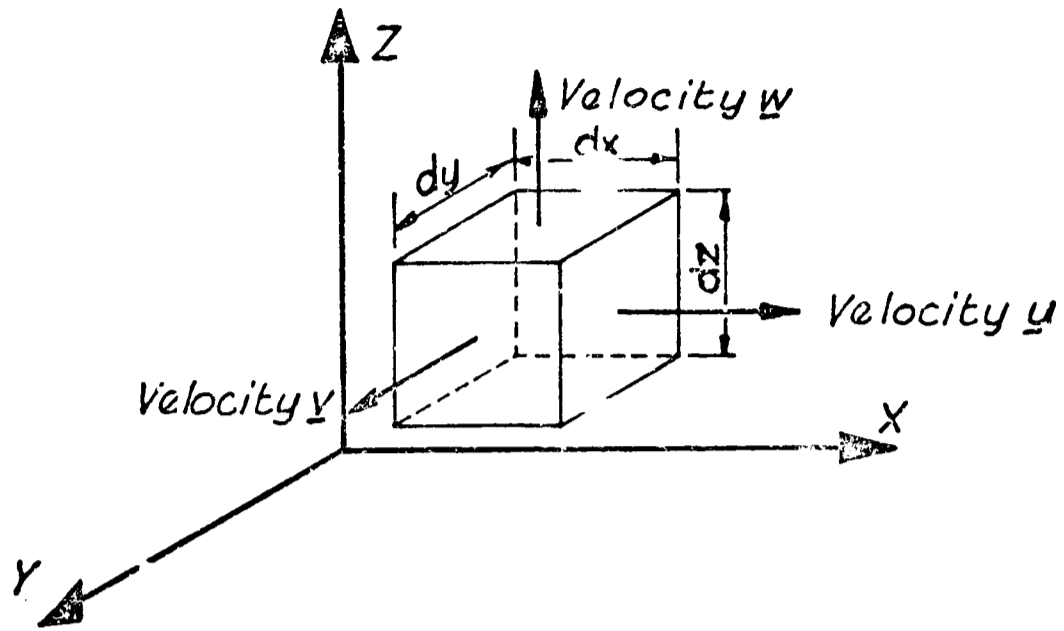
Table (4.6)

Harmonic	1st cycle		2nd cycle	
	C_n	α_n	C_n	α_n
1	0.867	-0.936	0.815	-0.929
2	0.116	1.248	-	-
3	0.250	-2.000	-	-
4	-	-	-	-
5	0.146	-2.393	-	-
6	0.167	2.011	0.143	0.684
7	-	-	-	-
8	0.227	1.551	0.118	0.483
9	0.145	-0.180	-	-
10	0.150	-1.045	-	-

N.B. only $C_n > 0.1$ results recorded

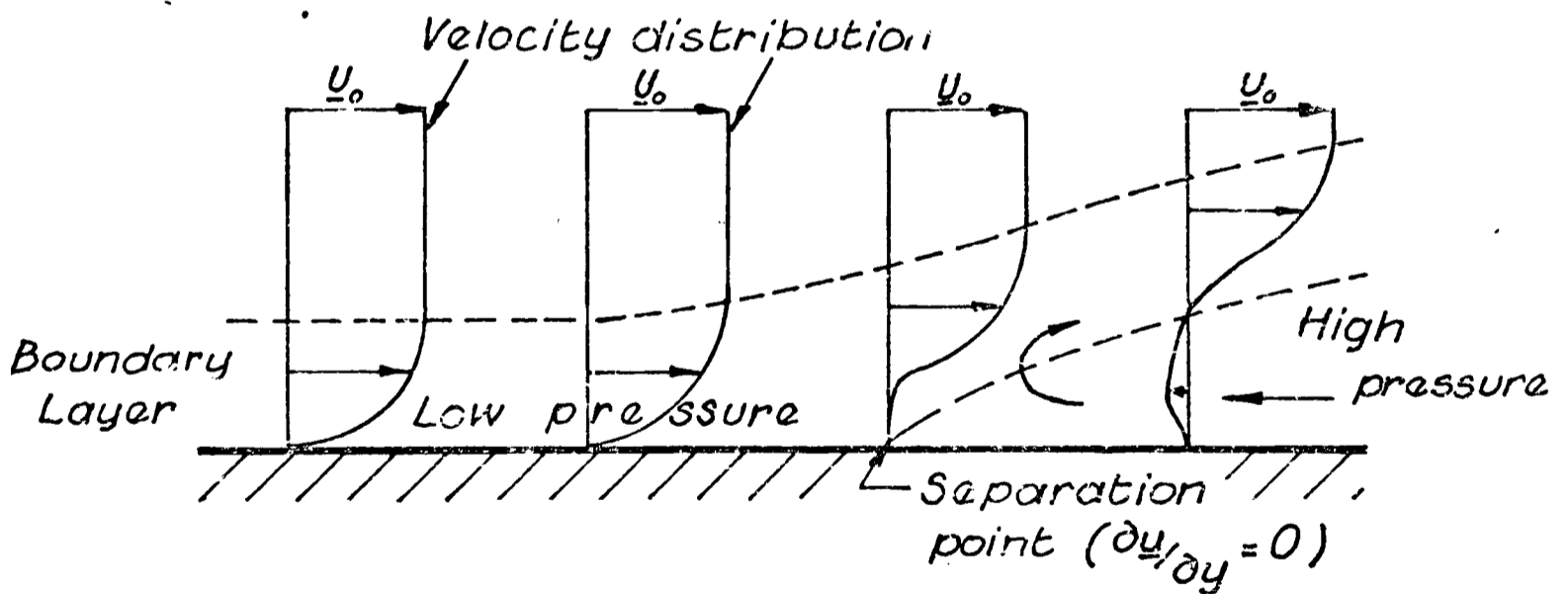
Resultant force harmonic composition- PWM experiment

Table (5.1)



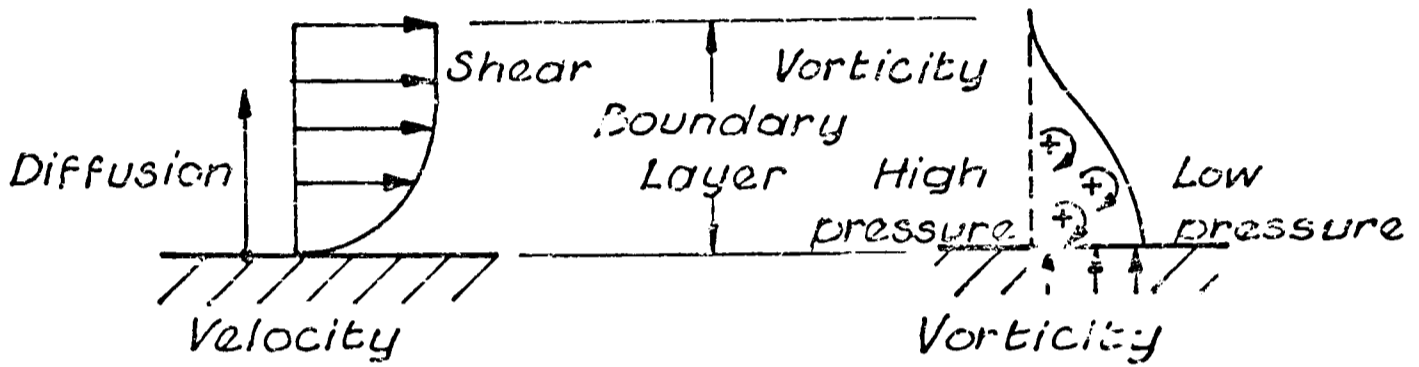
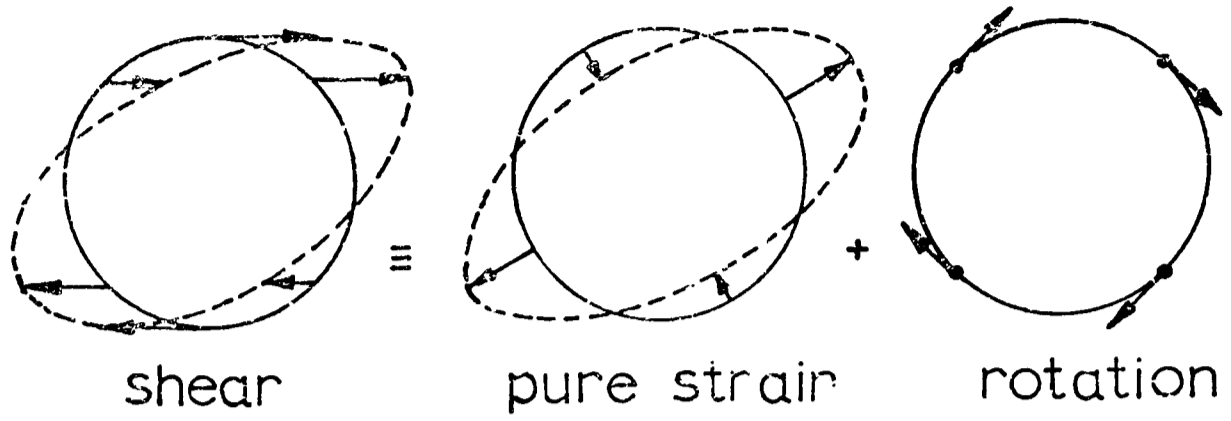
RECTANGULAR CO-ORDINATE SYSTEM

FIGURE (1.1)

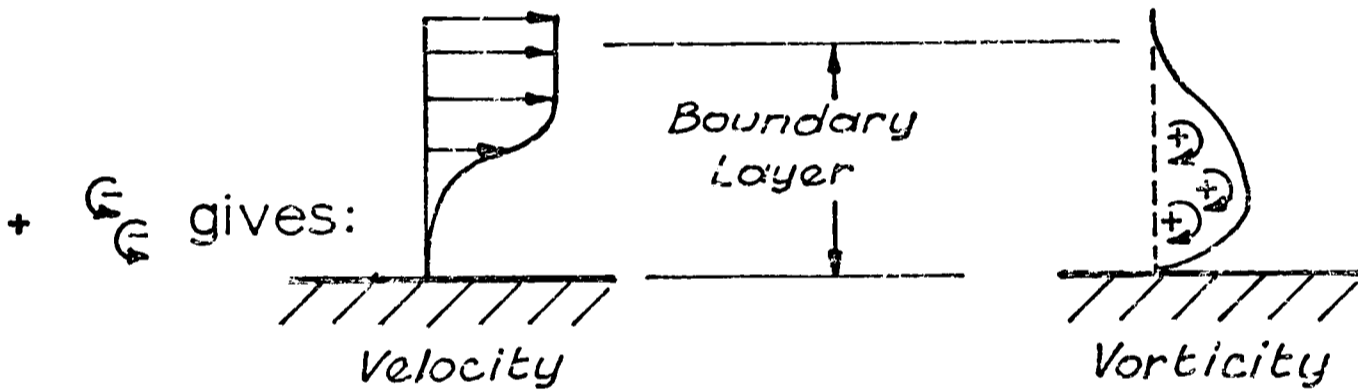


BOUNDARY LAYER SEPARATION

FIGURE (1.2)

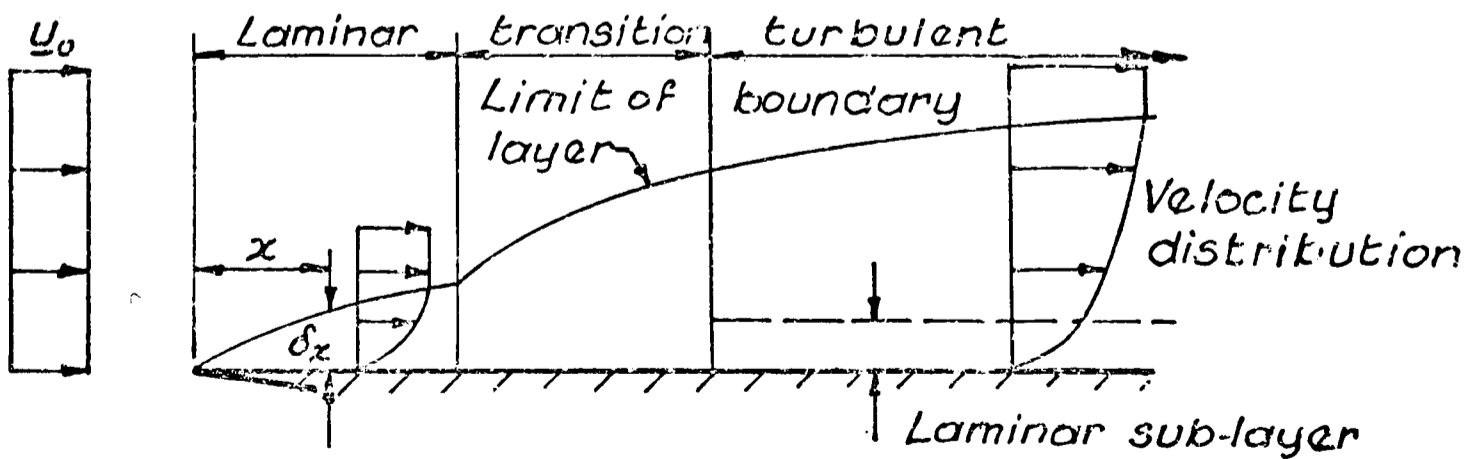


Distributions



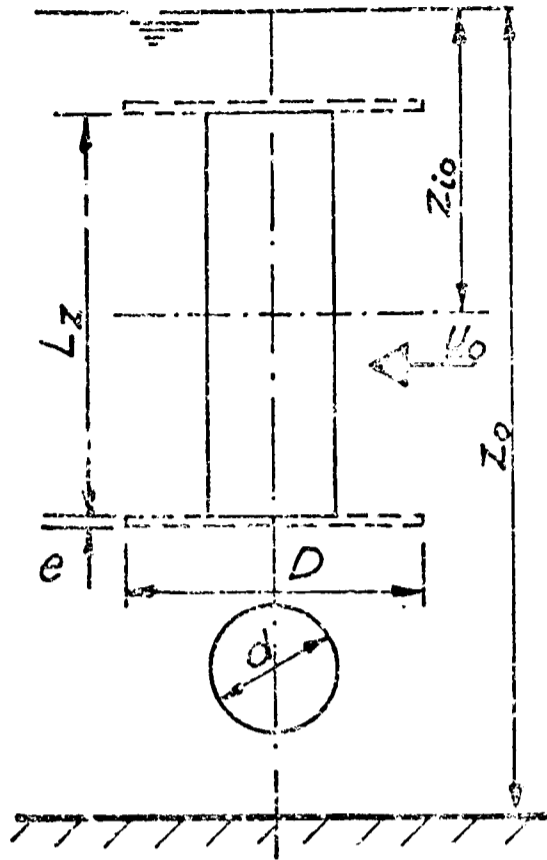
ADDITION OF REVERSE VORTICITY
RESULTING IN FLOW SEPARATION
 (From LIGHTHILL(1979))

FIGURE (1.3)

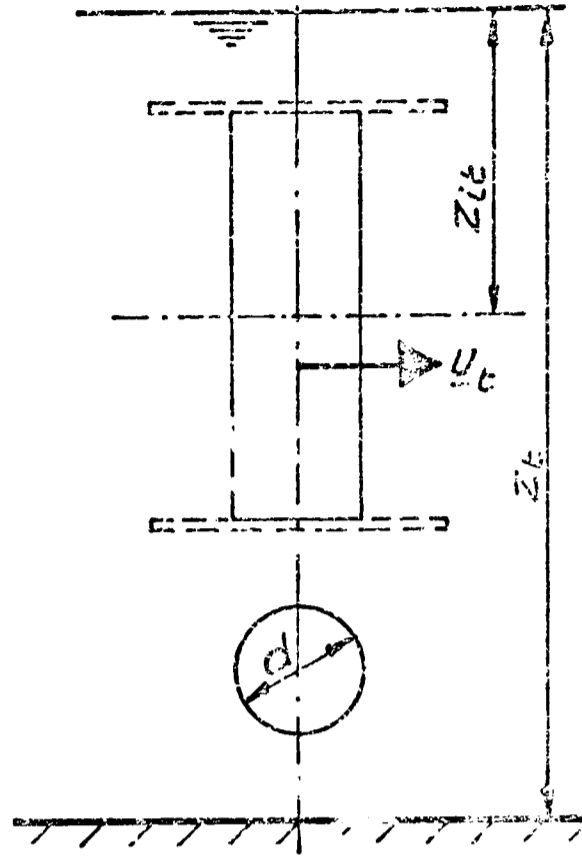


BOUNDARY LAYER DEVELOPMENT

FIGURE (1.4)

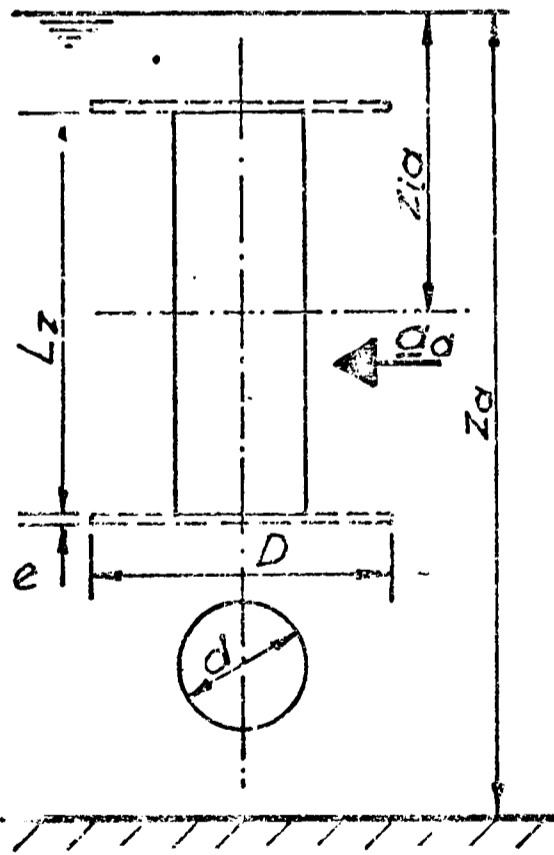


Fluid moving
(a)

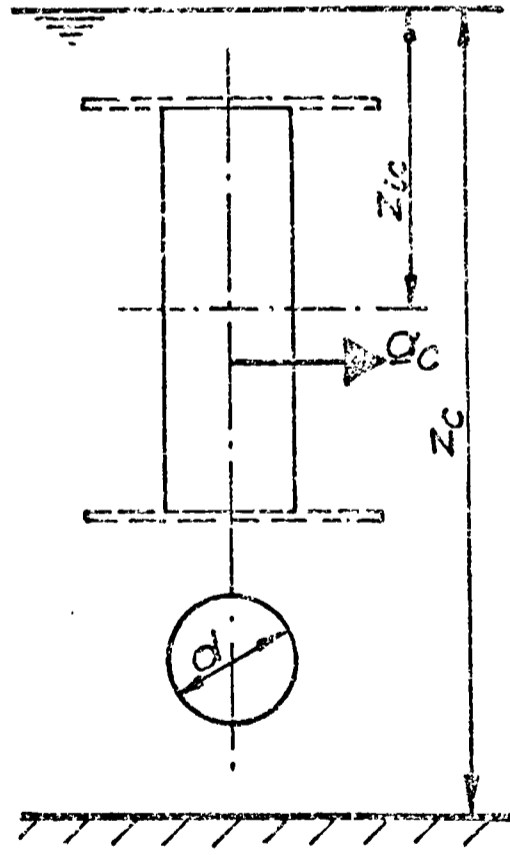


Cylinder moving
(b)

STEADY RELATIVE MOTION



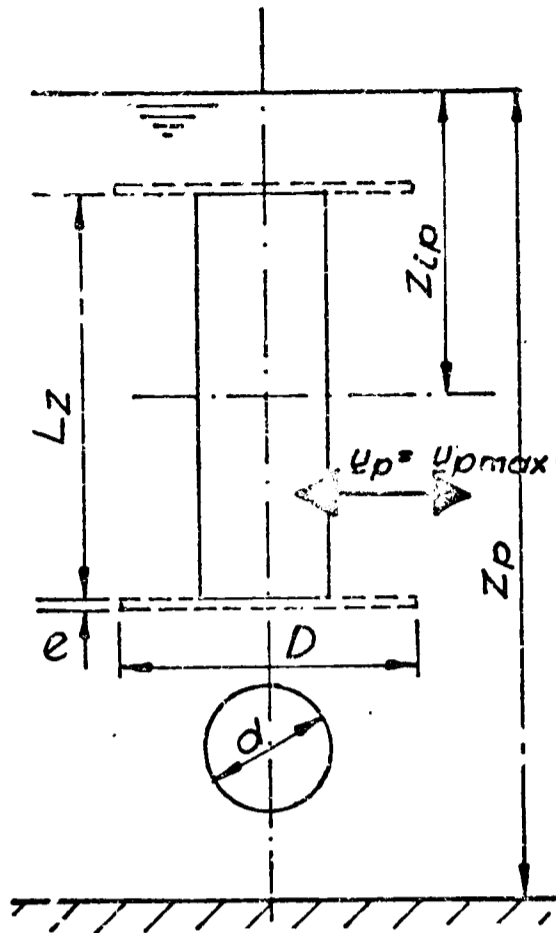
Fluid accelerating
(c)



Cylinder accelerating
(d)

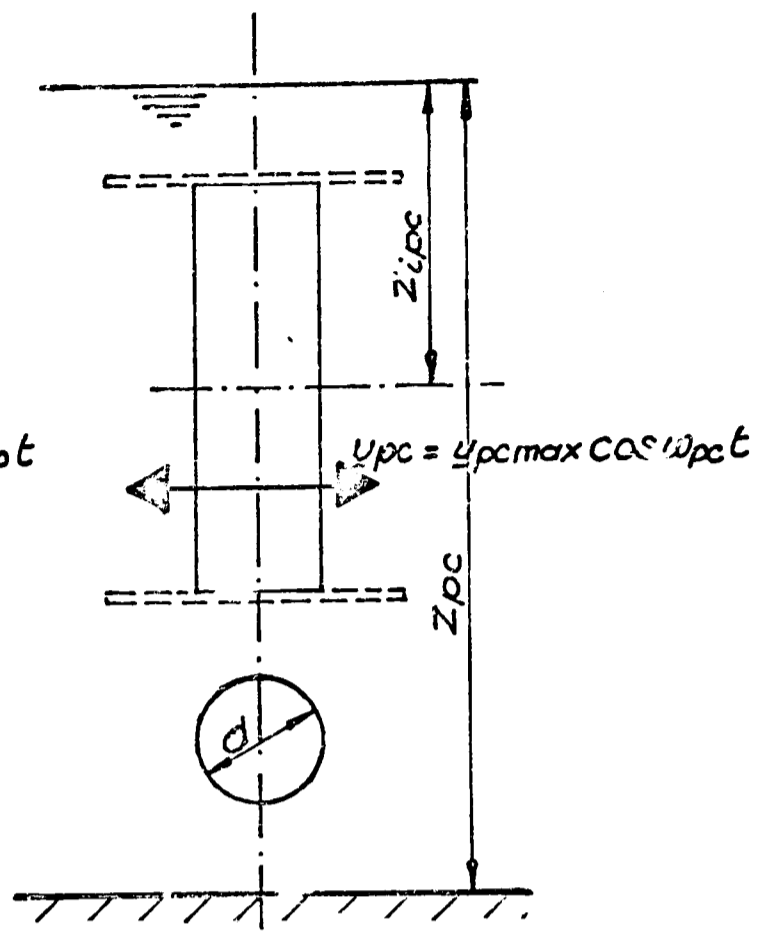
UNIDIRECTIONAL RELATIVE UNSTEADY
MOTION

FIGURE(1.5a-d)



Fluid moving with SHM

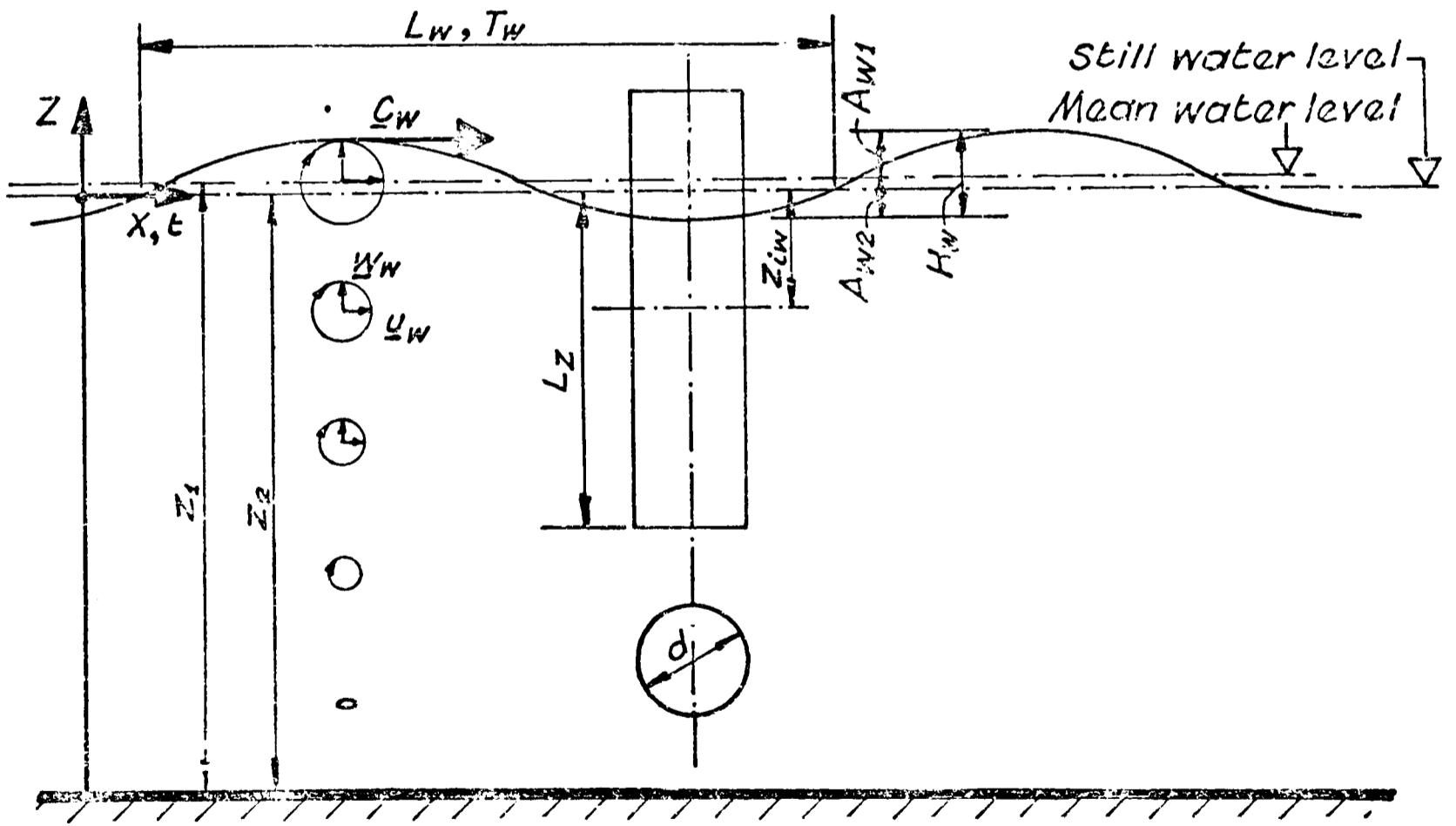
(e)



Cylinder moving with SHM

(f)

RELATIVE PLANAR OSCILLATORY MOTION

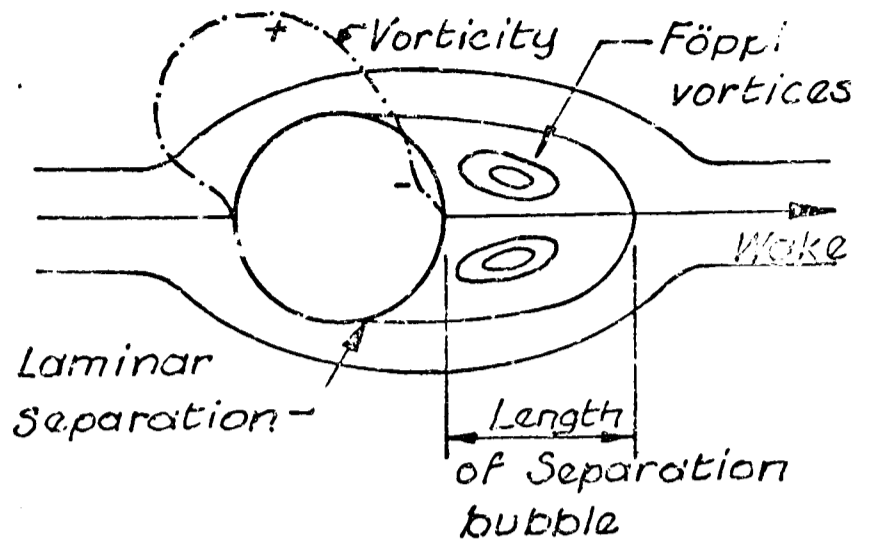
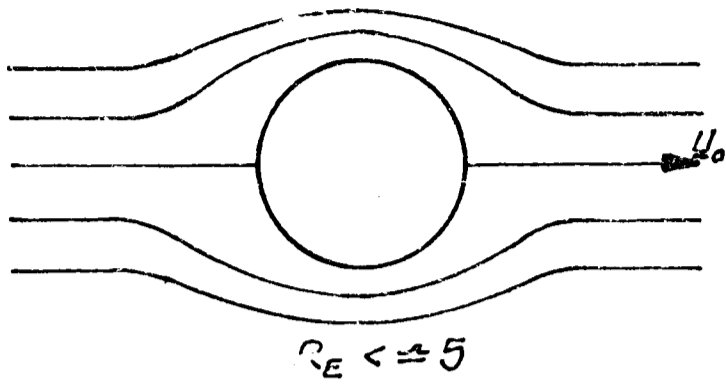


Cylinder in waves

(g)

THREE DIMENSIONAL OSCILLATORY MOTION

FIGURE (1.5e-g)

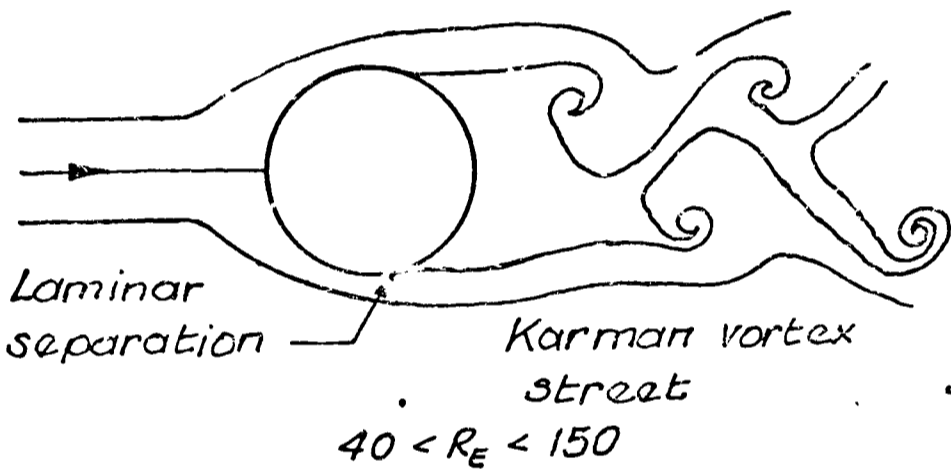


N.B. Vorticity plotted with cylinder surface as origin.

$5 < R_E < 40$

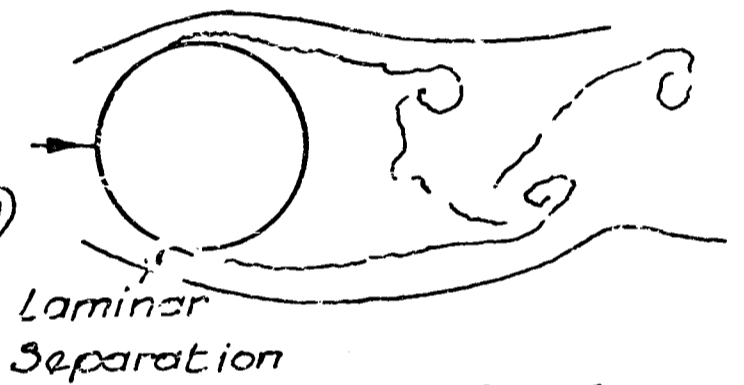
(a)

(b)



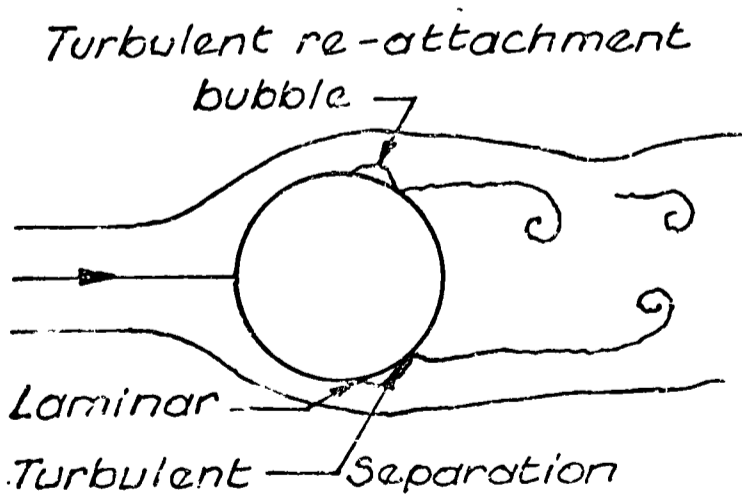
$40 < R_E < 150$

(c)



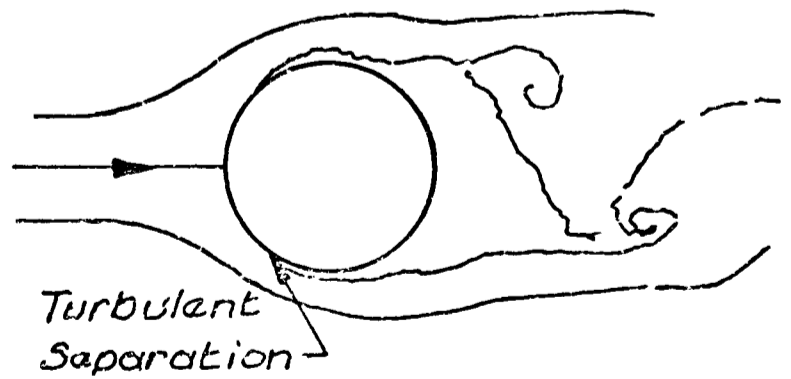
$150 < R_E < 2-3 \times 10^5$

(d)



$2-3 \times 10^5 < R_E < 3.5 \times 10^6$

(e)

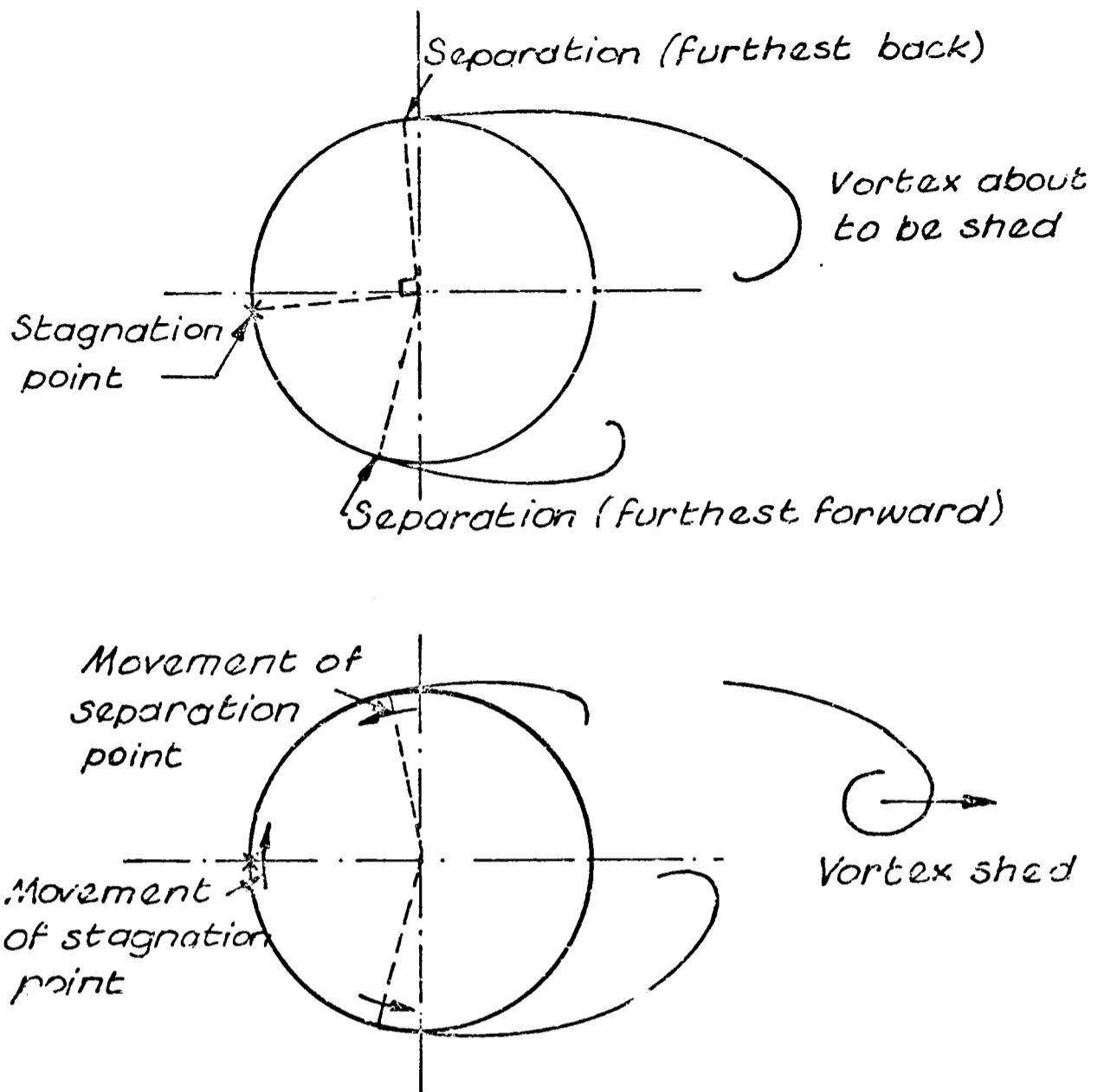


$R_E \geq 3.5 \times 10^6$

(f)

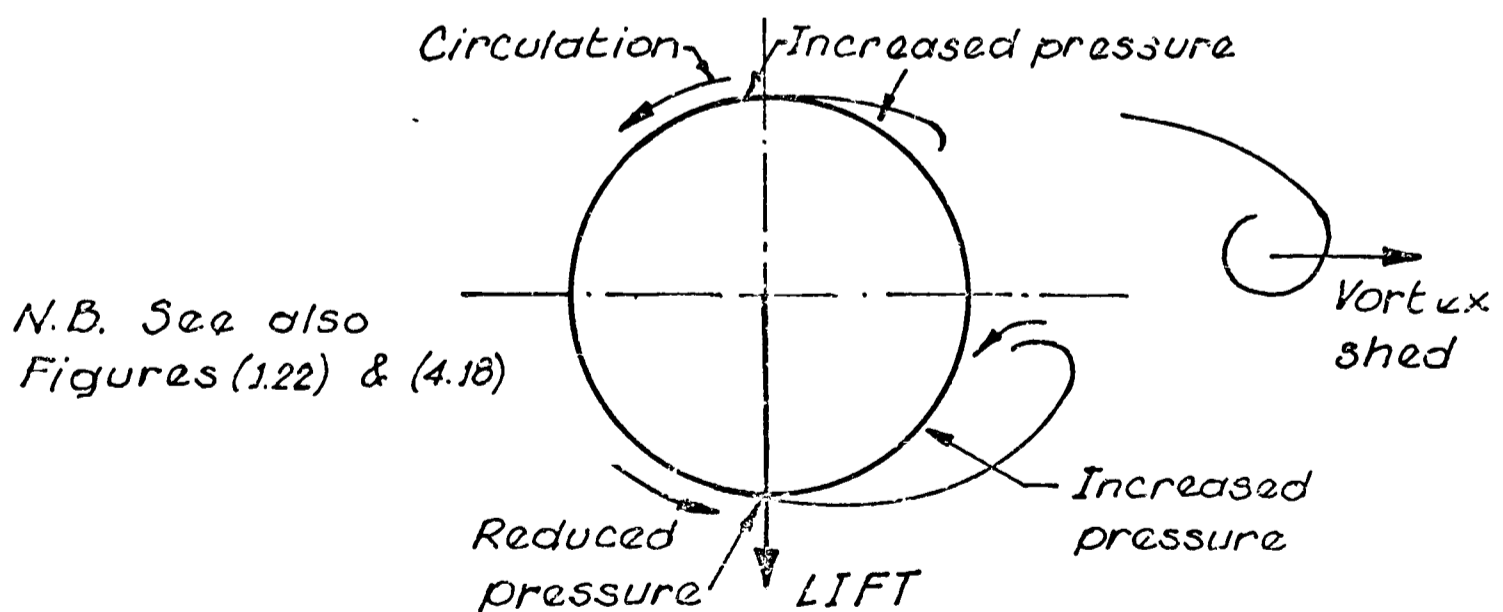
STREAKLINES IN STEADY FLOW WITH RESPECT TO R_E

FIGURE (1.6)



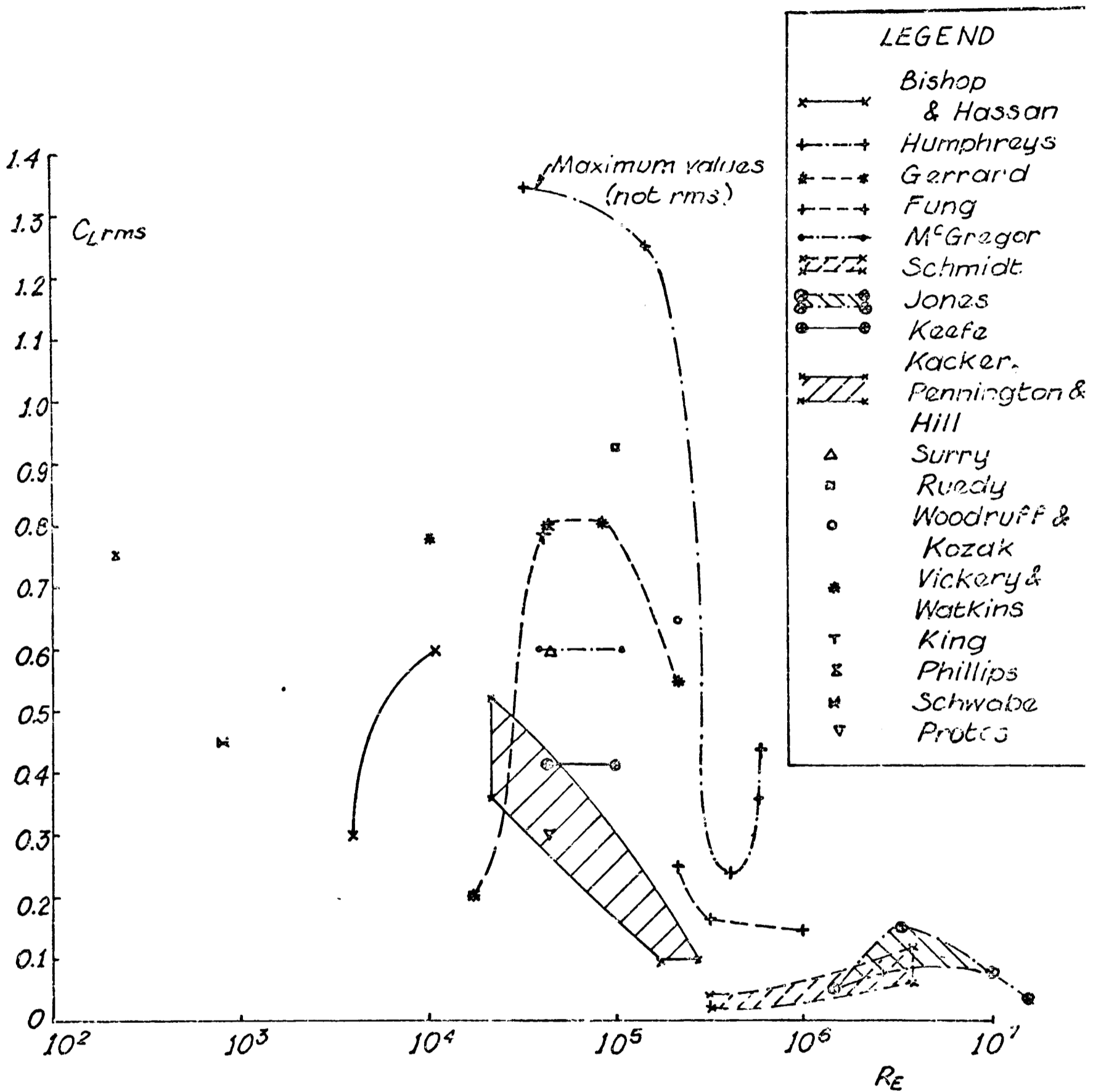
POSTULATED MOVEMENT OF STAGNATION AND SEPARATION POINTS IN STEADY FLOW BASED ON DWYER & McCROSKEY (1973)

FIGURE (1.7)



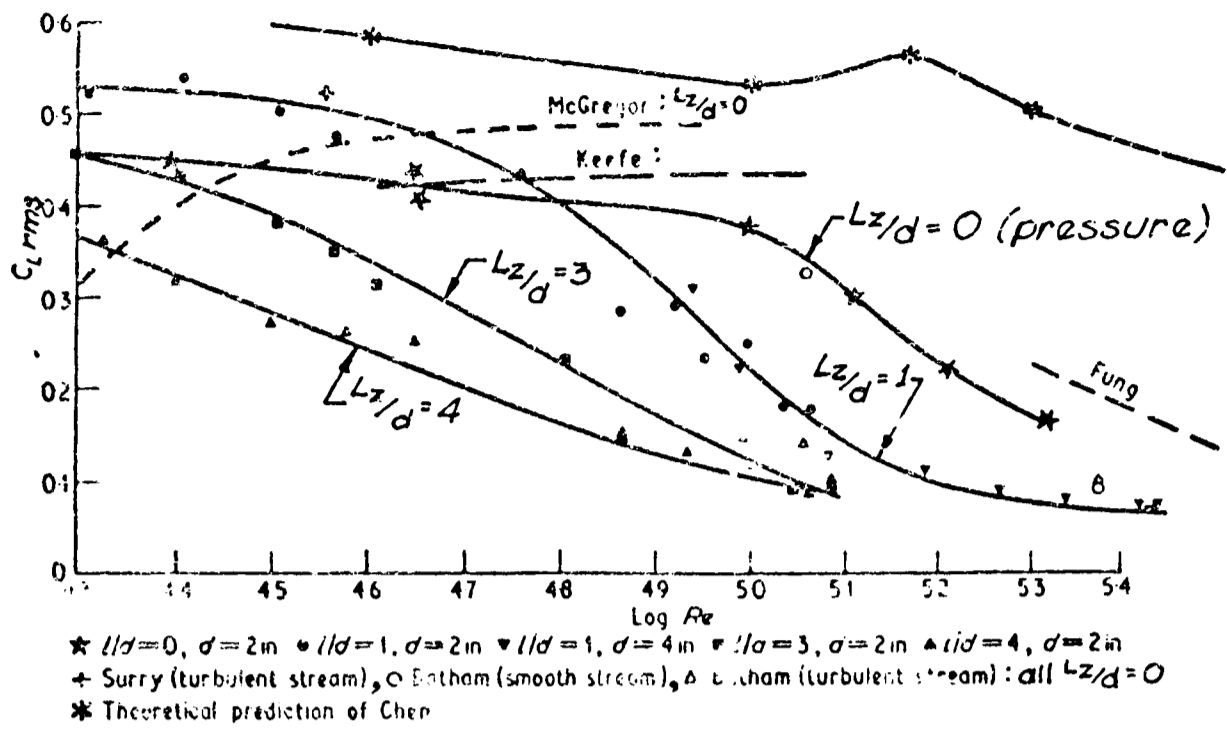
DIRECTION OF LIFT FORCE AS A CONSEQUENCE OF BEHAVIOUR IN FIGURE (1.7)

FIGURE (1.8)



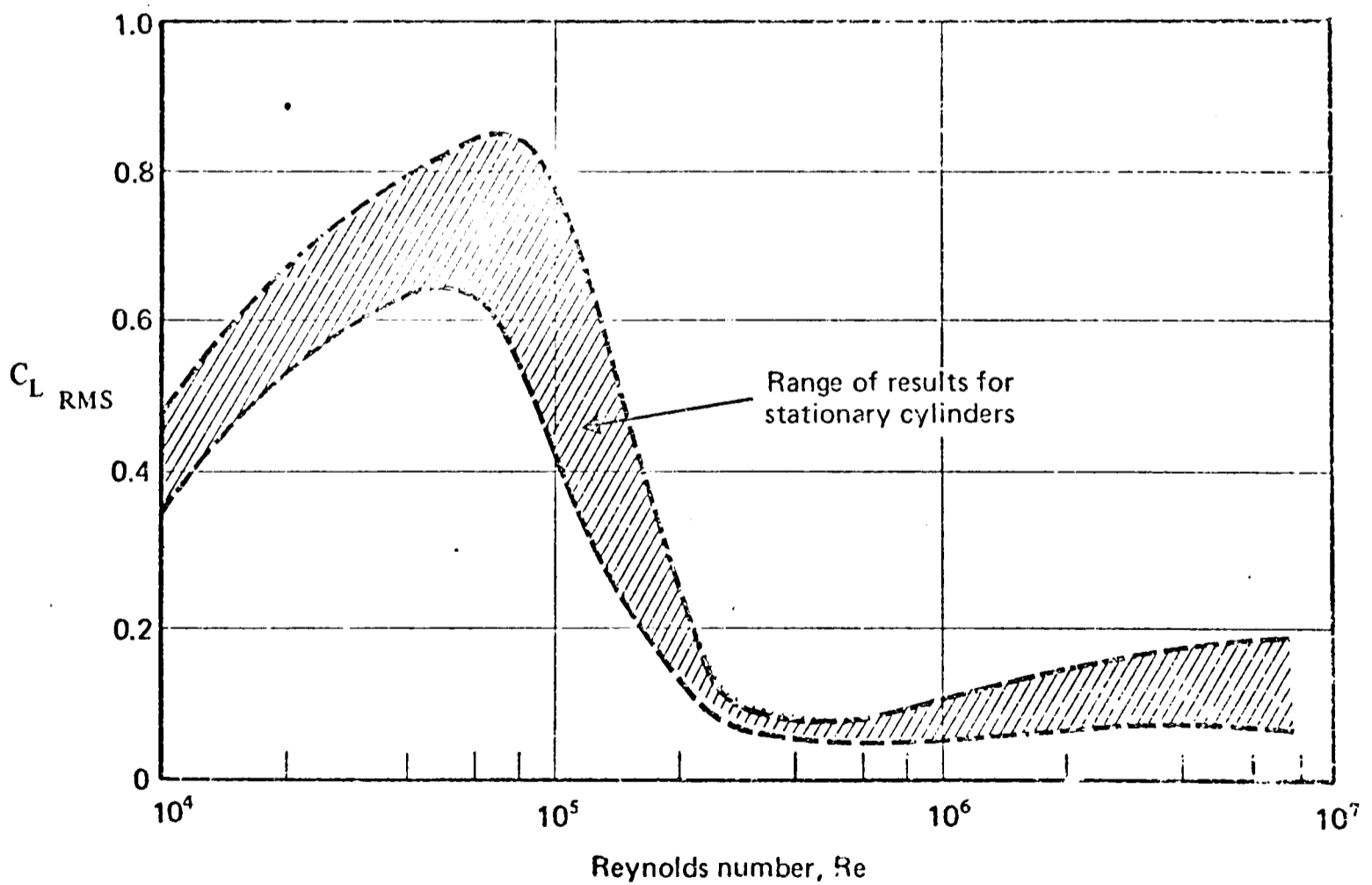
RMS FLUCTUATING LIFT COEFFICIENT VARIATION WITH Re

FIGURE (1.9)



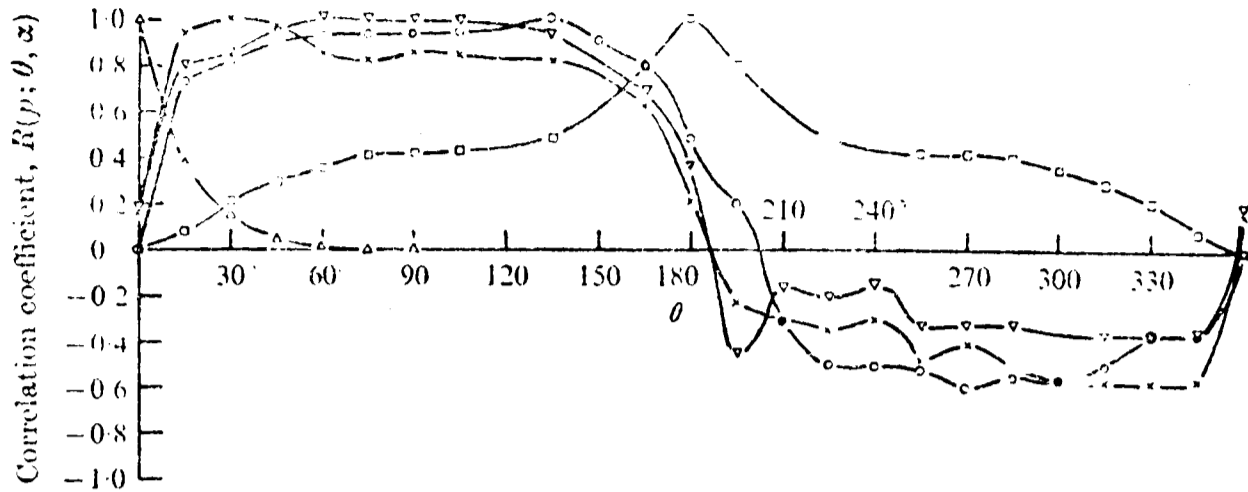
EFFECT OF Lz/d ON $C_{L\text{rms}}$
 (FROM: KÄCKER et al (1974))

FIGURE (1.10)



$C_{L\text{rms}}$ VARIATION WITH Re
 (FROM: CIRIA (1978))

FIGURE (1.11)

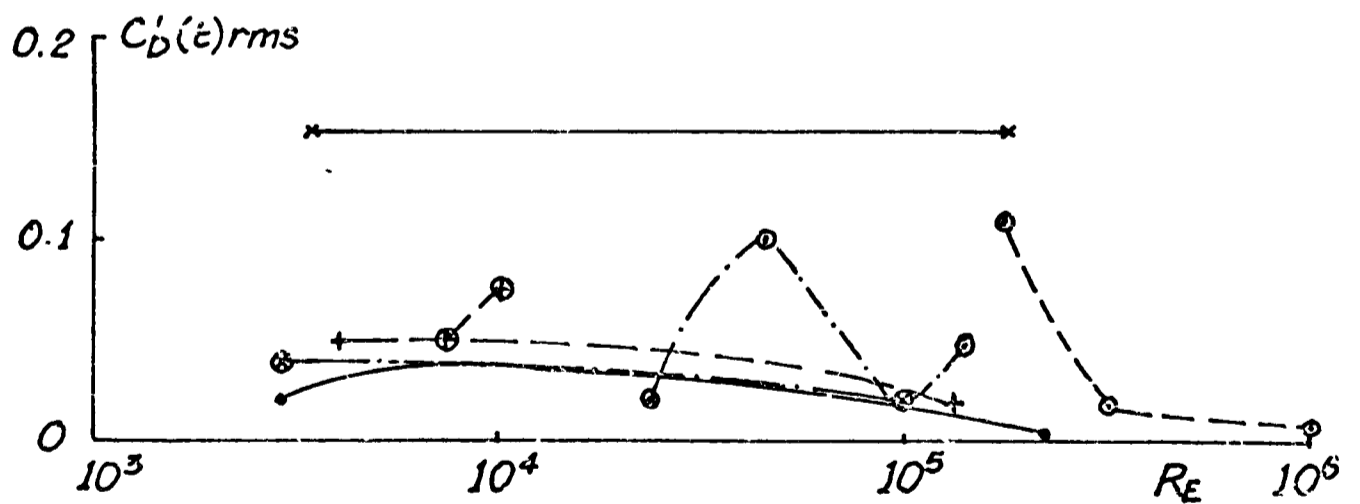
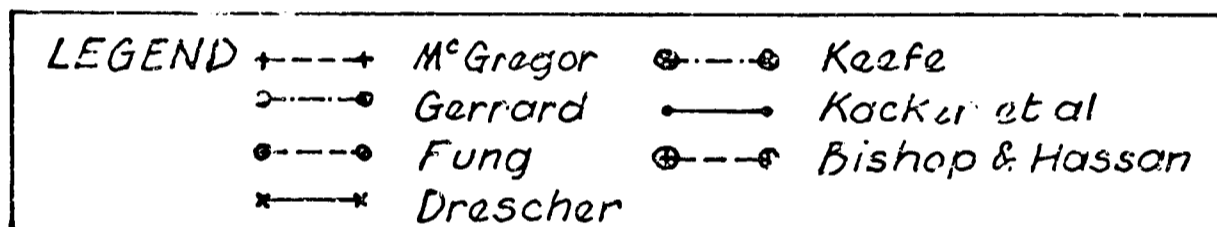


Distribution of $R(p; \theta, \alpha)$ for smooth cylinder in uniform stream at $Re = 1.11 \times 10^5$. Δ , $\theta = 0^\circ$; \times , $\theta = 30^\circ$; ∇ , $\theta = 60^\circ$; \circ , $\theta = 135^\circ$; \square , $\theta = 180^\circ$.

CIRCUMFERENTIAL PRESSURE CORRELATION IN STEADY FLOW

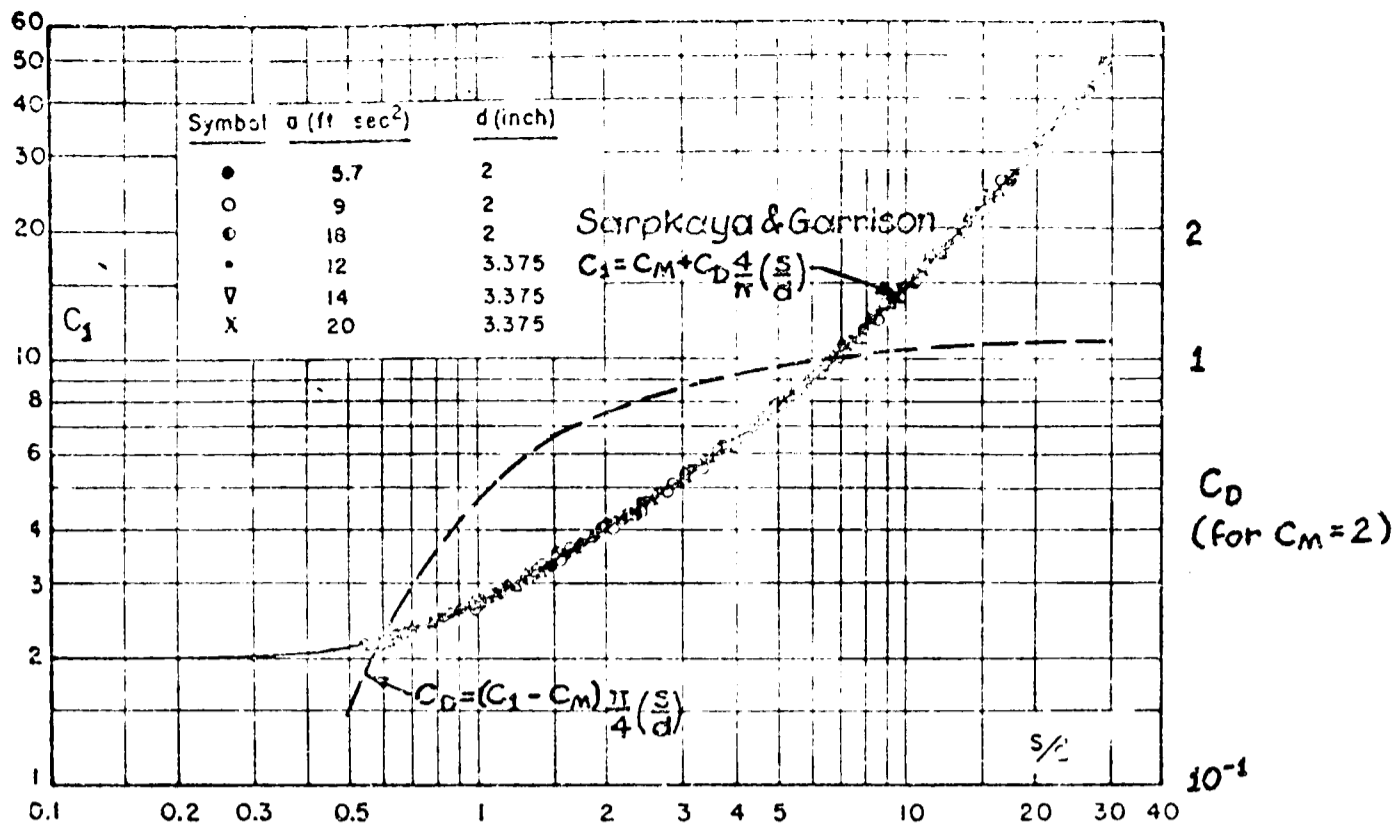
(FROM: BATHAM (1973))

FIGURE (1.12)

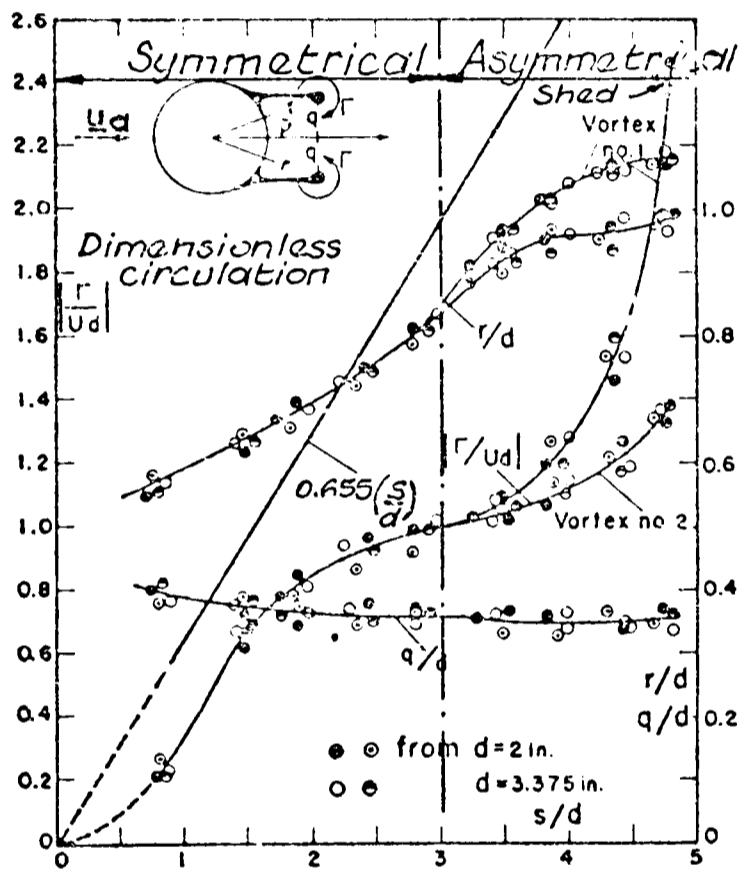


RMS FLUCTUATING DRAG COEFFICIENT VARIATION WITH Re

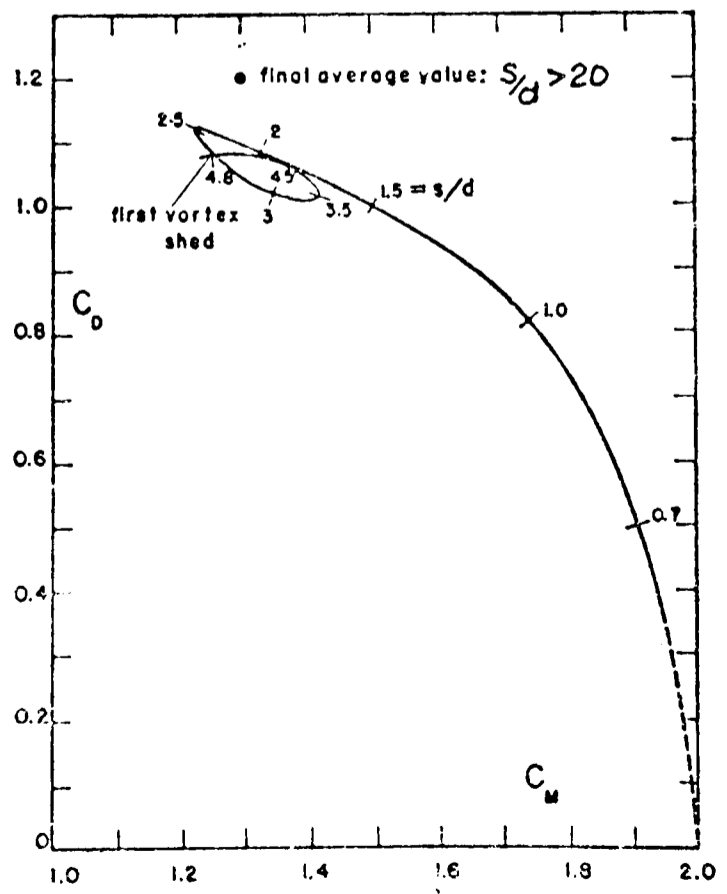
FIGURE (1.13)



CORRELATION OF C_1 WITH s/d FOR A UNIFORM ACCELERATION OF WATER PAST A CYLINDER
FIGURE (1.14)

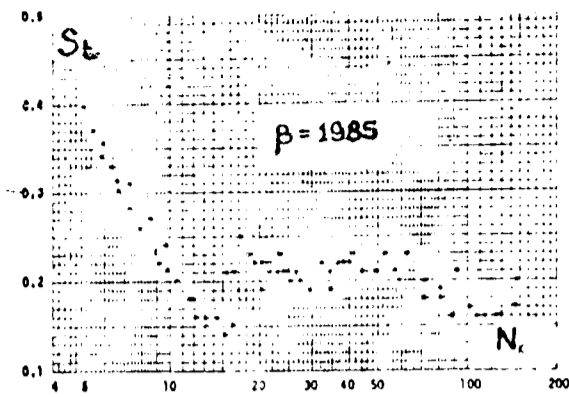


DIMENSIONLESS VORTEX CIRCULATION AND DISPOSITION
FIGURE (1.15)



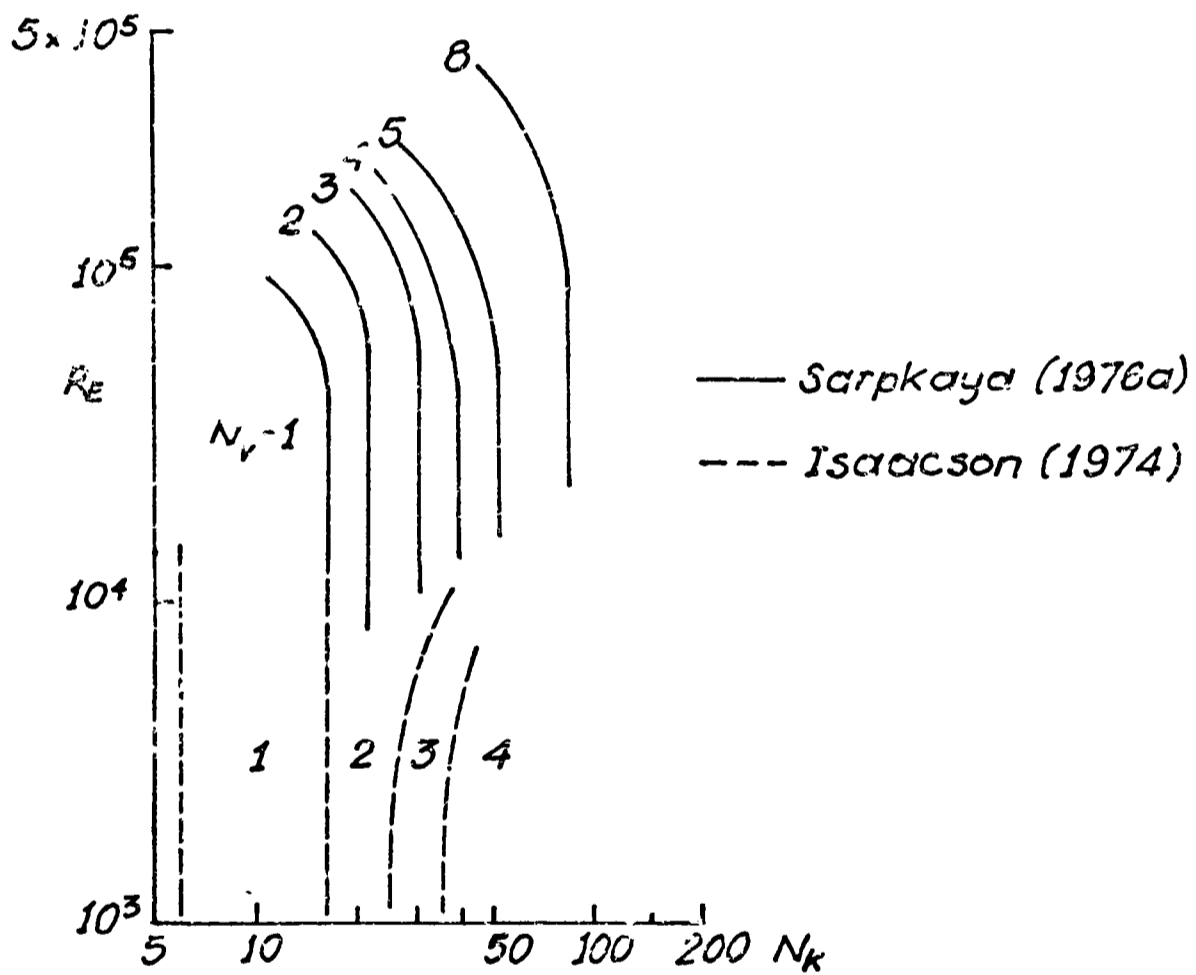
CORRELATION OF C_D & C_M
FIGURE (1.16)

(FIGURES (1.15 - 1.17) FROM: SARPKAYA & GARRISON (1963))



TYPICAL VARIATION OF UNSTEADY
STROUHAL No. WITH N_k FOR PLANAR
OSCILLATORY FLOW
 (FROM: SARPKEYA (1976a))

FIGURE (1.17)

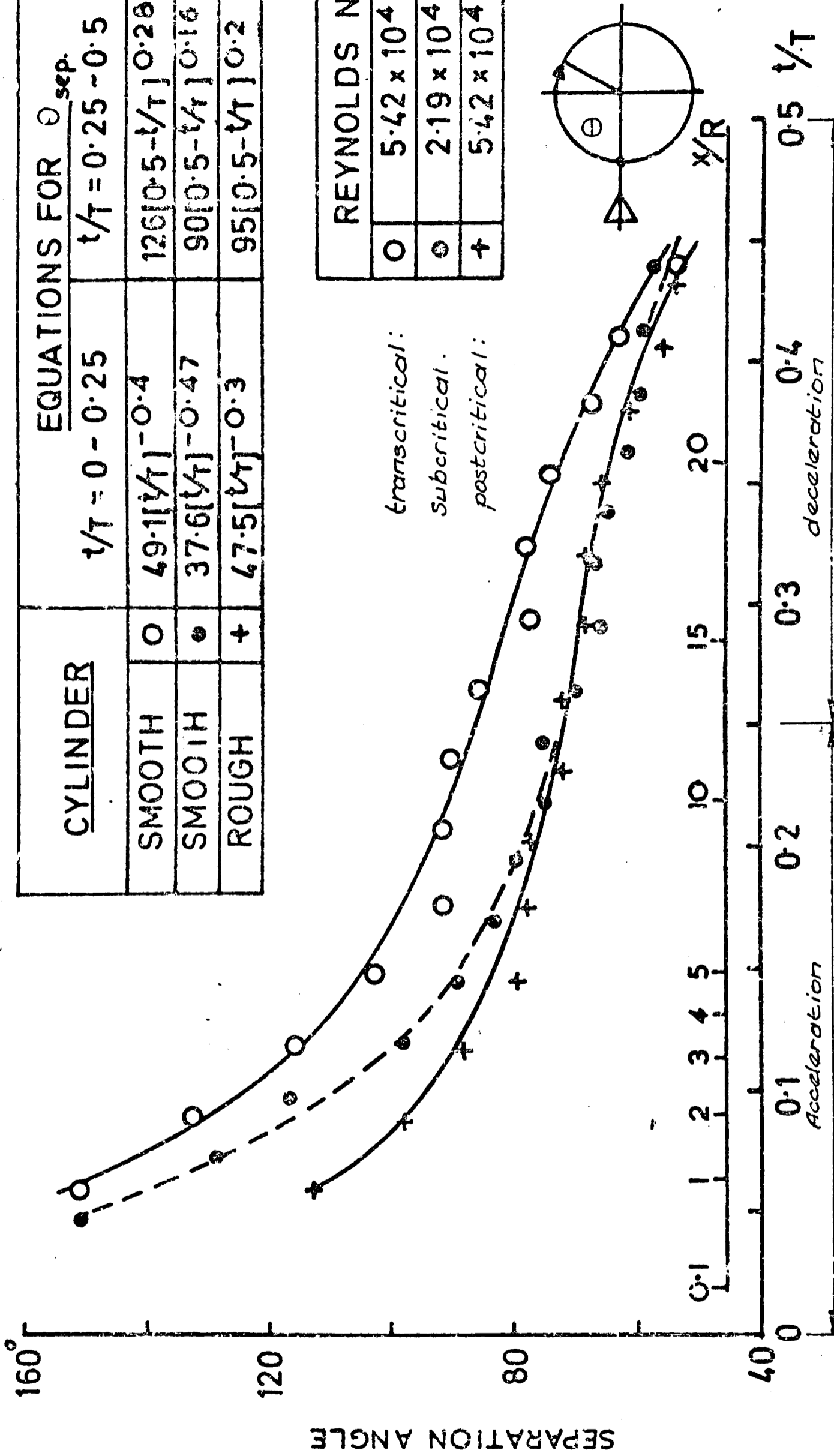


NUMBER OF VORTICES SHED PER
SEMI-CYCLE OF PLANAR OSCILLATORY
FLOW

FIGURE (1.18)

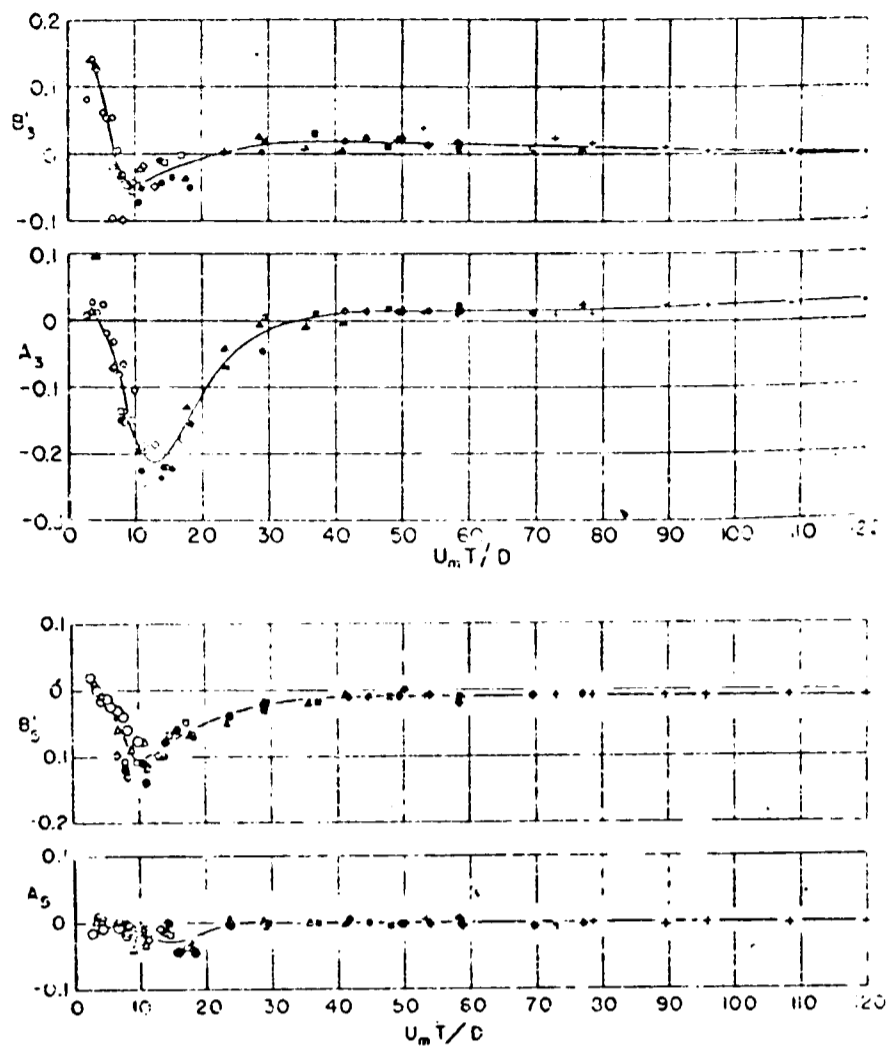
CYLINDER	EQUATIONS FOR $\theta_{sep.}$	
	$1/T = 0 - 0.25$	$1/T = 0.25 - 0.5$
SMOOTH	$49.1[1/T]^{-0.4}$	$126[0.5 - 1/T]^{0.28}$
SMOOTH	$37.6[1/T]^{-0.47}$	$90[0.5 - 1/T]^{0.16}$
ROUGH	$47.5[1/T]^{-0.3}$	$95[0.5 - 1/T]^{0.2}$

REYNOLDS NO.	
O	5.42×10^4
●	2.19×10^4
+	5.42×10^4



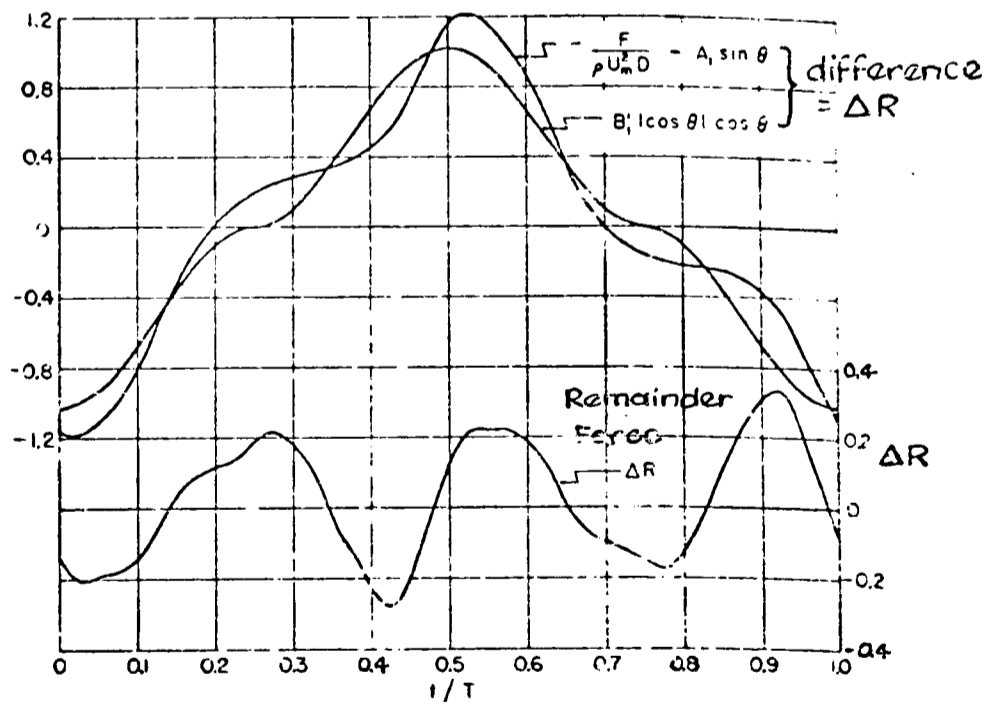
VARIATION OF SEPARATION ANGLE THROUGHOUT A SEMI-CYCLE OF PLANAR OSCILLATORY FLOW FOR $N_k=38$ (FROM: GRASS & KEMP(1978))

FIGURE (1.19)



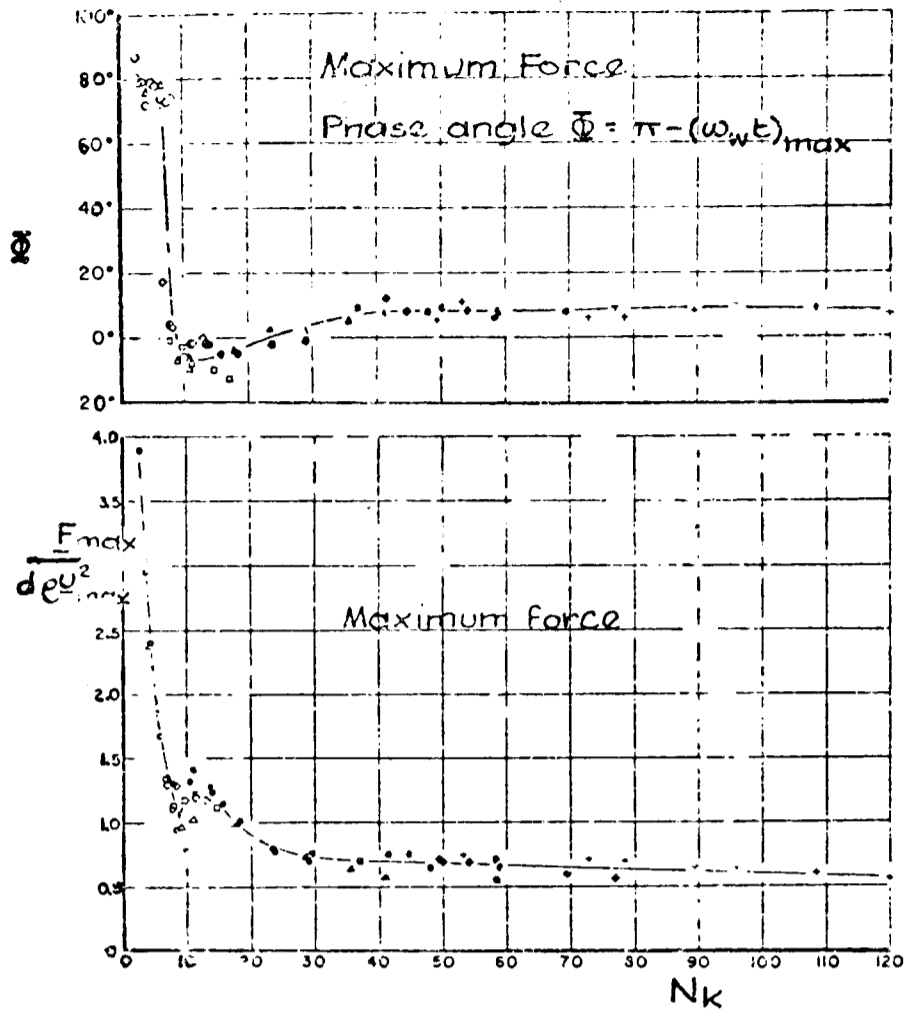
Remainder Force constitution

$$\Delta R = A_3 \sin 3\omega t + A_5 \sin 5\omega t + B_3' \cos 3\omega t + B_5' \cos 5\omega t$$



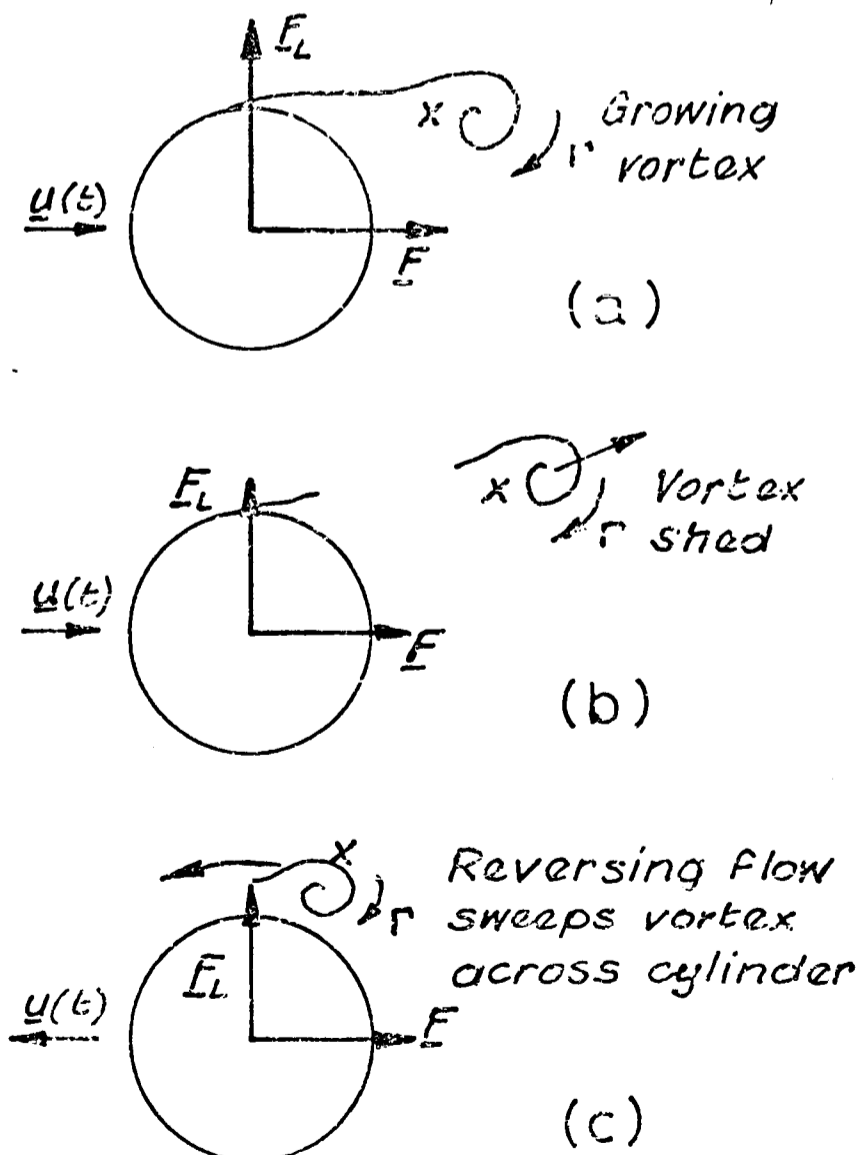
THIRD HARMONIC DOMINANCE OF REMAINDER FORCE FOR $N_k = 15.6$ FROM KEULEGAN & CARPENTER (1958)

FIGURE (1.20)



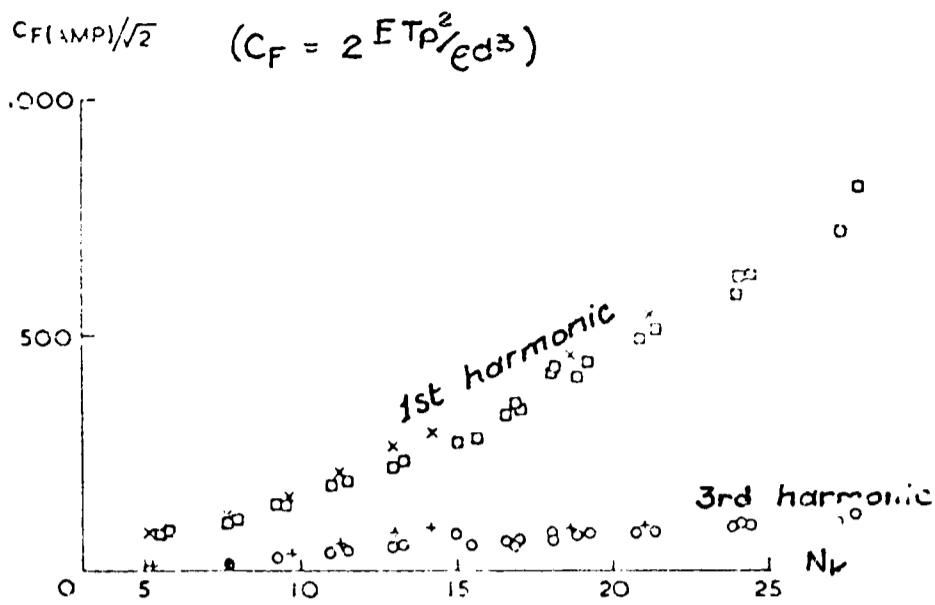
MAXIMUM FORCE MAGNITUDE & PHASE FROM KEULEGAN & CARPENTER (1958)

FIGURE (1.21)



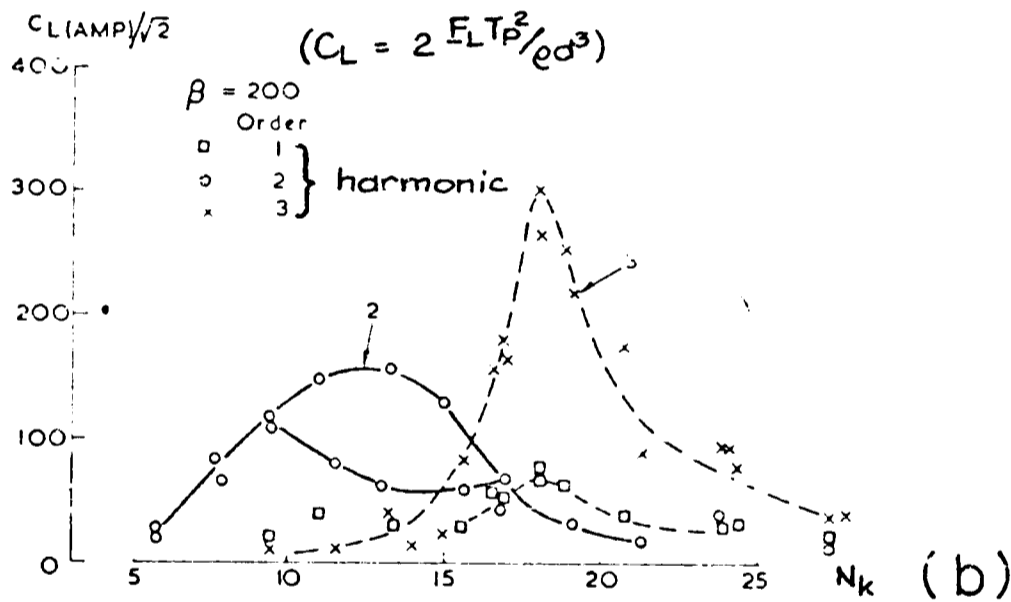
FORCES ASSOCIATED WITH VORTEX BEHAVIOUR

FIGURE (1.22)

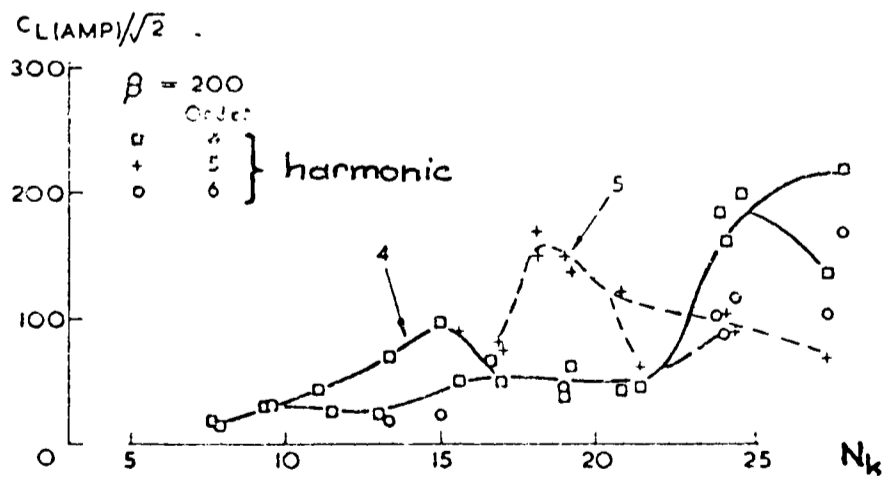


IN-LINE FORCE

(a)



(b)



LIFT FORCE

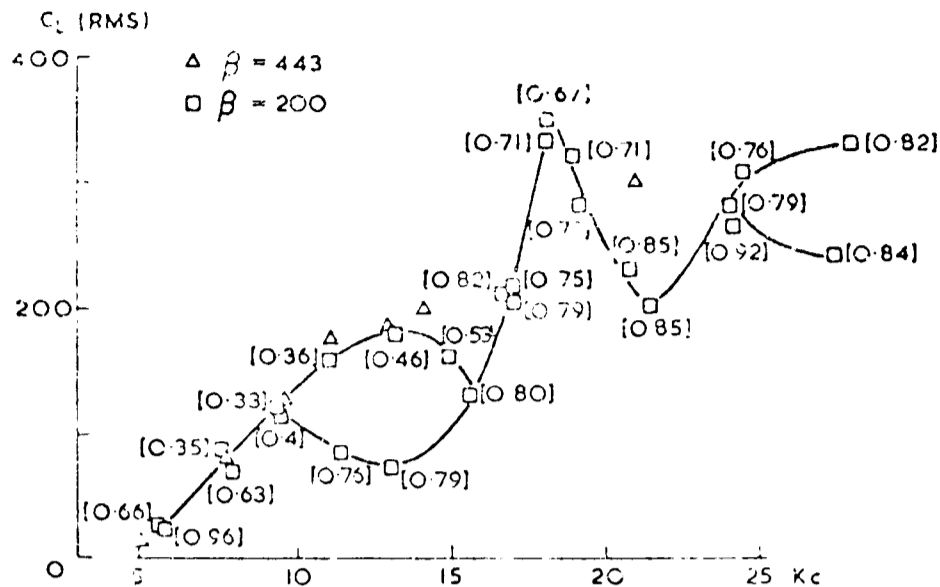
(c)

HARMONIC CONTENT OF FORCES IN PLANAR OSCILLATORY FLOW

(FROM: MAULL & MILLINER (1978))

FIGURE (1.23)

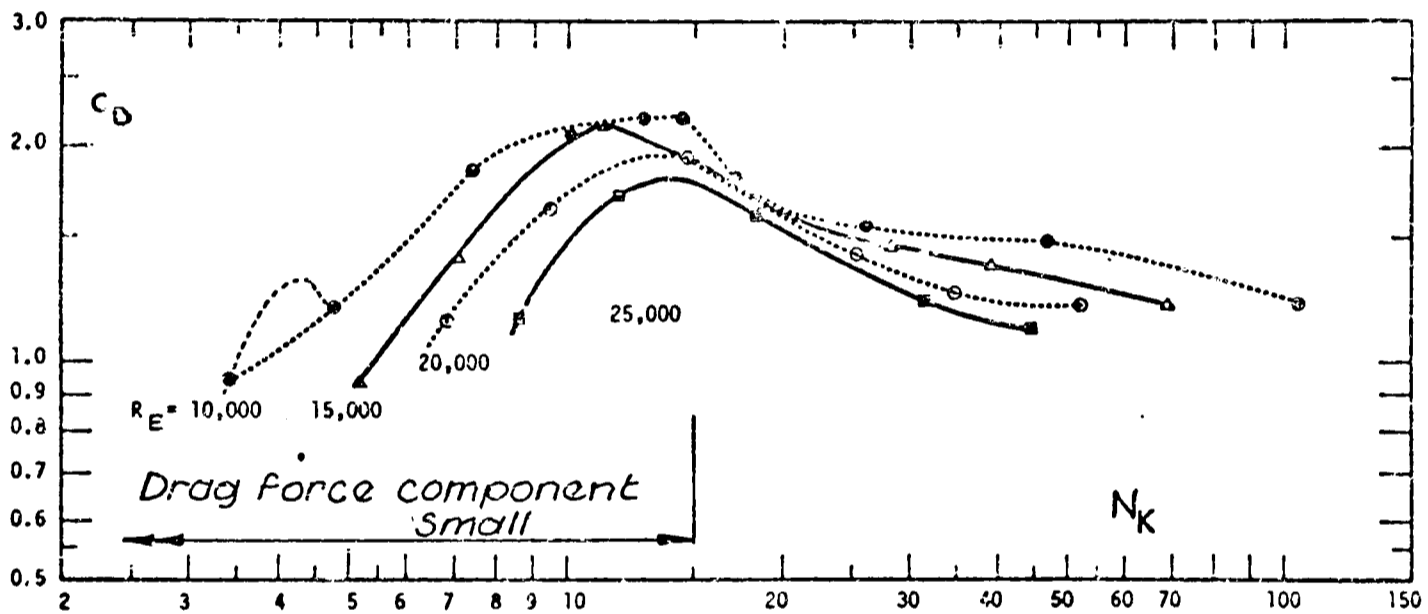
[] Fraction of time force stays above range (-0.2 → 0.2)
of maximum



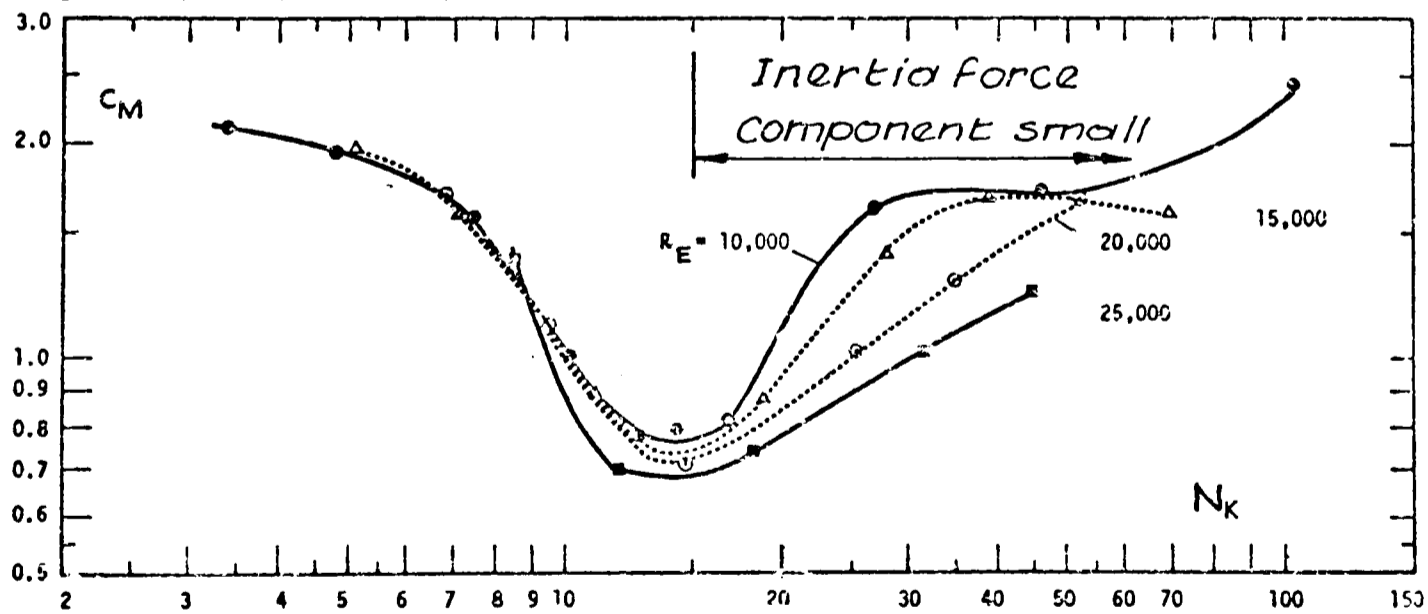
C_L RMS VARIATION WITH N_k - PLANAR OSCILLATORY FLOW

(FROM: MAULL & MILLINER (1978))

FIGURE (1.24)



(a)

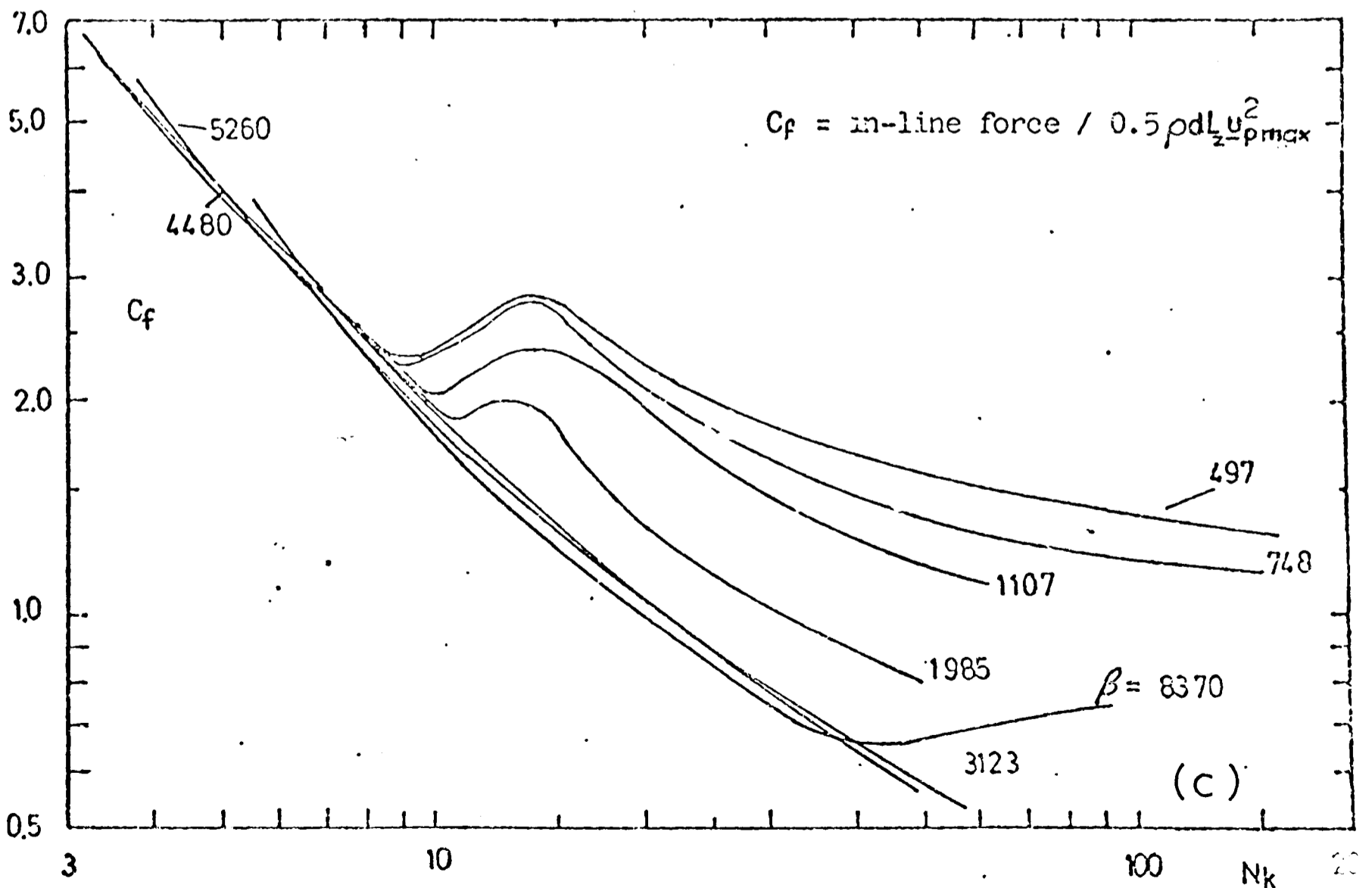
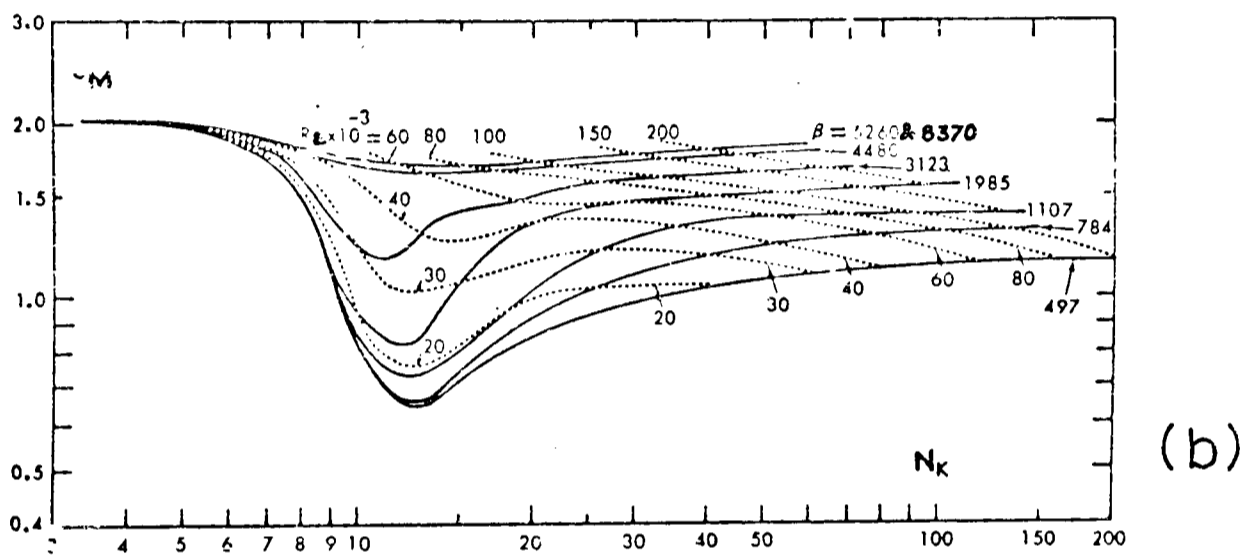
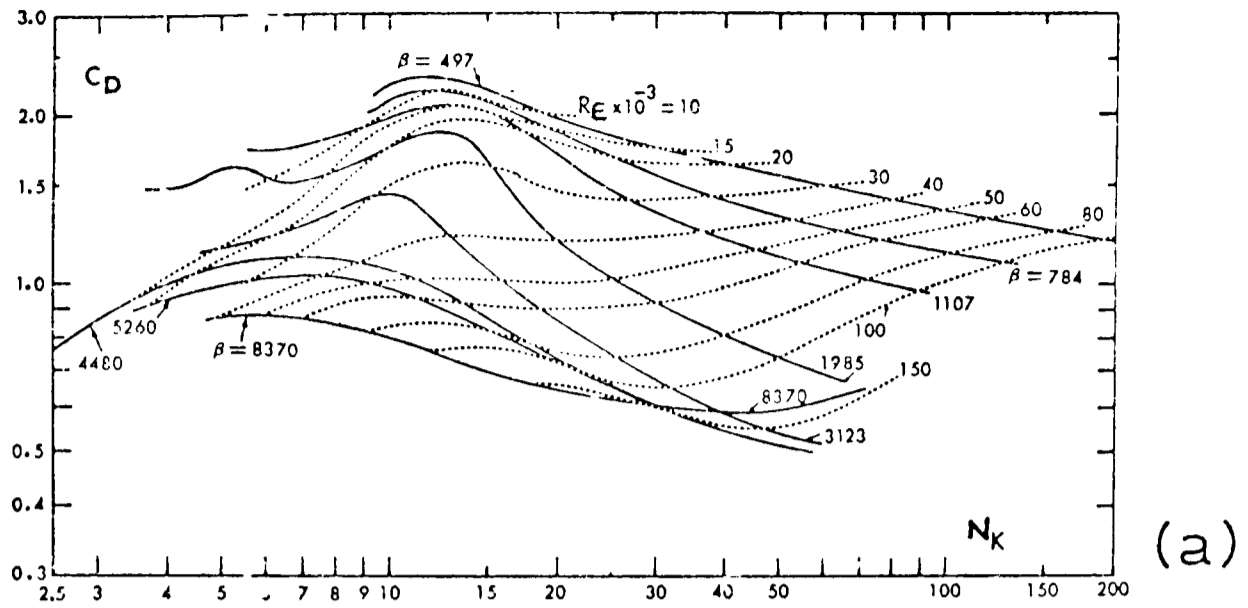


(b)

DEPENDENCE OF C_D & C_M UPON N_k & R_E - RESULTS OF KEULEGAN & CARPENTER

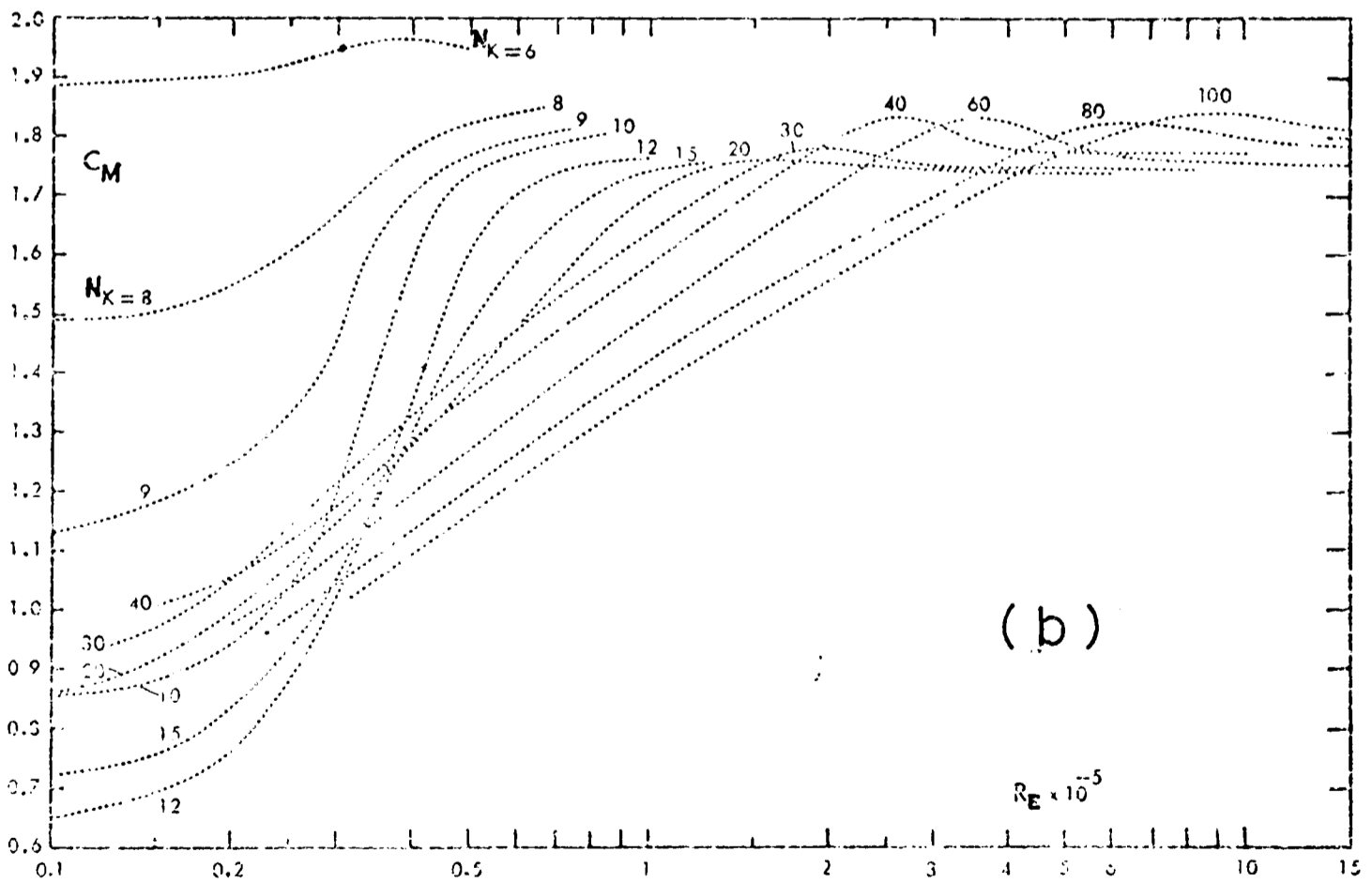
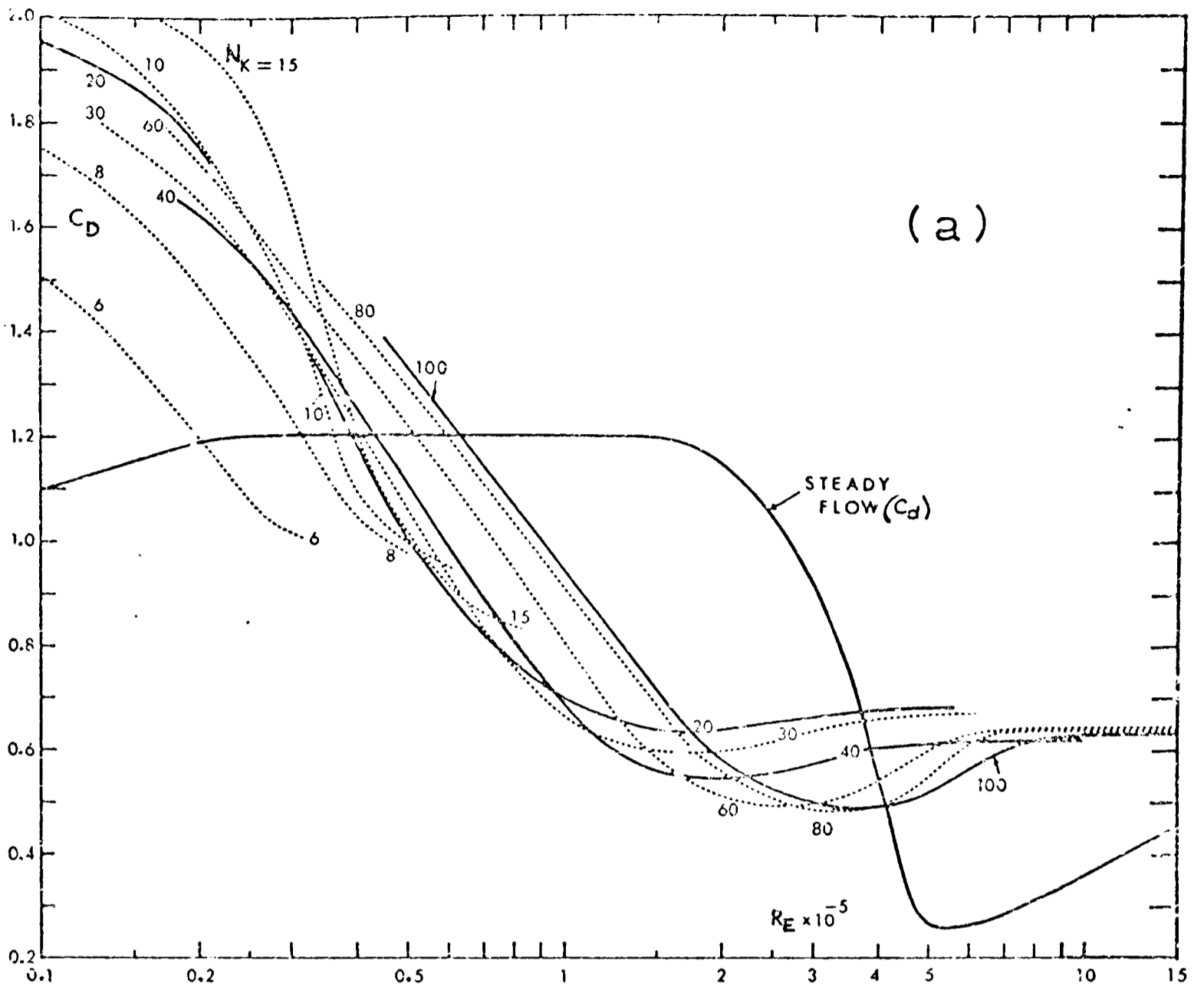
(FROM: SARPKAYA (1976a))

FIGURE (1.25)



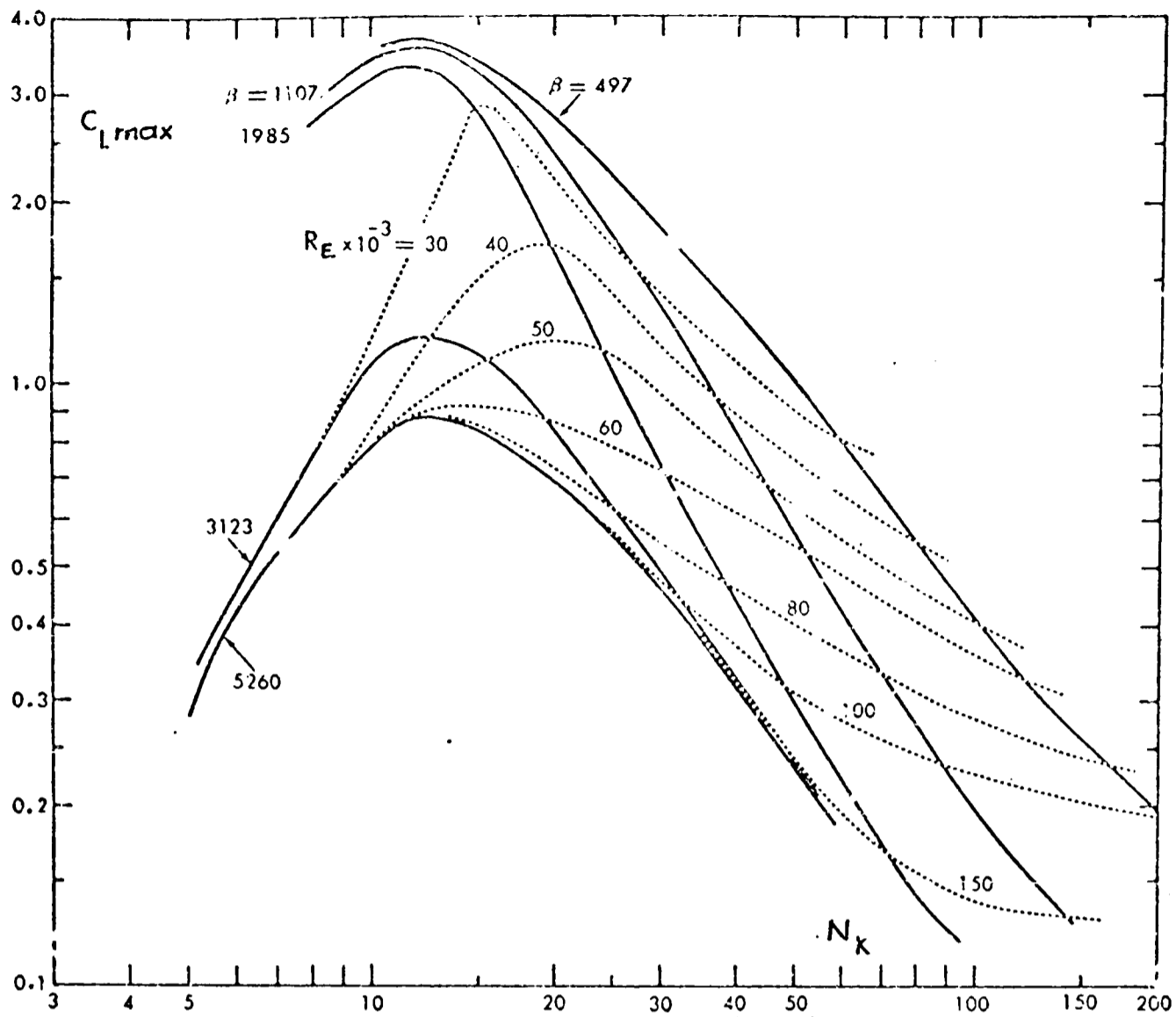
DEPENDENCE OF C_D , C_M & C_f UPON β AND N_k
 (FROM: SARPKAYA (1976a))

FIGURE (1.26)

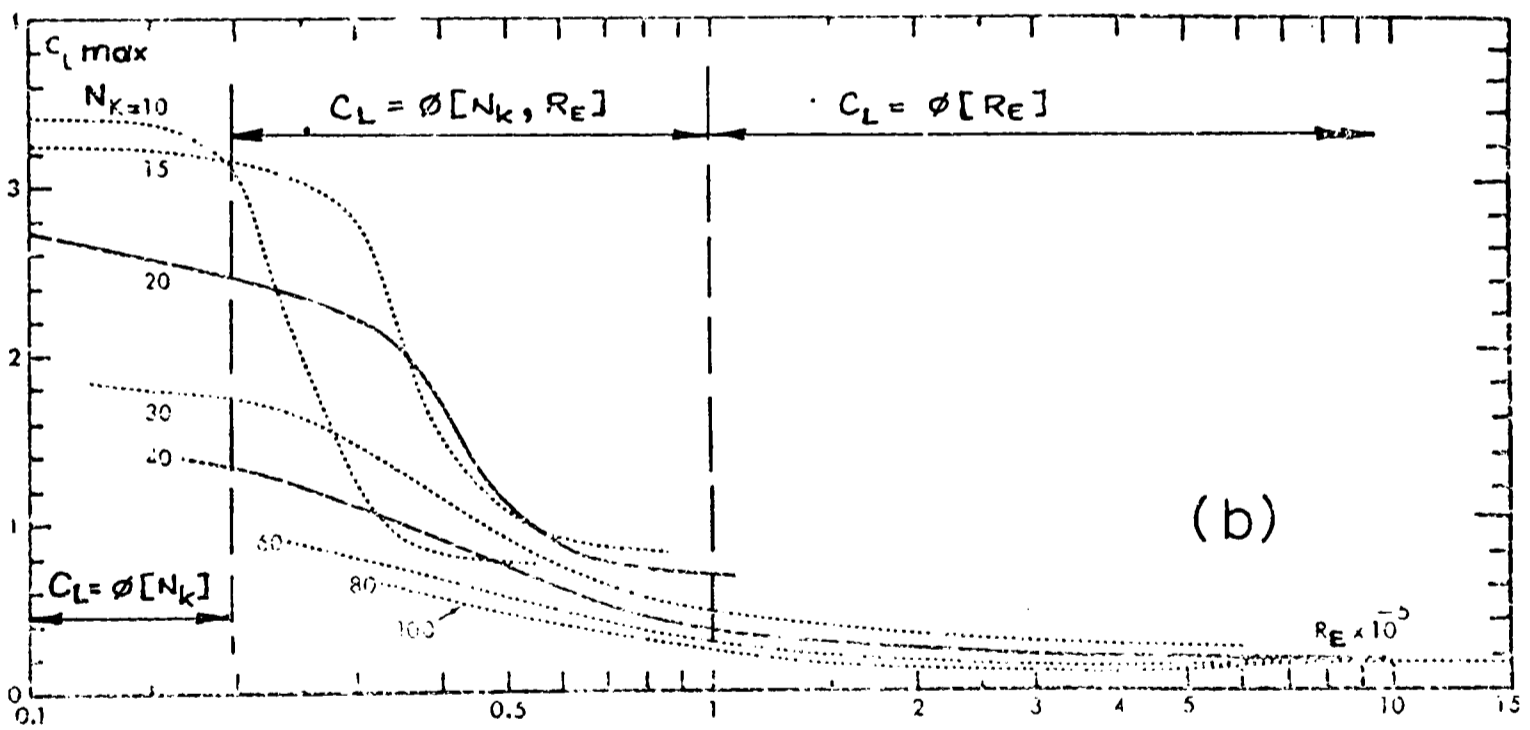


C_D & C_M DEPENDENCE UPON R_E FOR CONSTANT N_k
(FROM: SARPKEYA (1977c))

FIGURE (1.27)



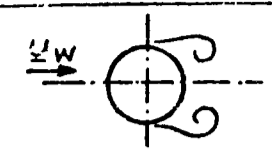
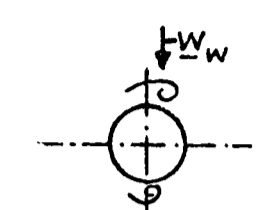
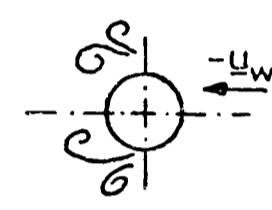
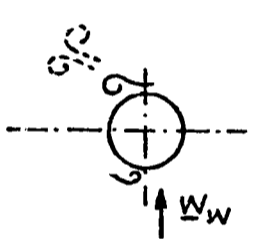
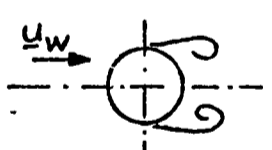
(a)



(b)

VARIATION OF C_{Lmax} WITH R_E & N_k
(FROM: SARPKEYA (1977a))

FIGURE (1.28)

WAVE	FLOW PATTERN	COMMENTS
Crest		Symmetric vortices - upper having greatest circulation
Surface level falling		Asymmetric flow pattern due to quicker decay of lower vortex
SWL		Reversing flow moves original vortices around cylinder
Surface level falling		Stronger upper vortex assists rapid formation of new adjacent one
Trough		Similar, weaker vortex pair also on the other side of the cylinder
Surface level rising		Decreasing velocity - upper and lower vortex pairs shed, new vortices start to form
SWL		Newly formed vortices disappear as flow reverses
Surface level rising		New vortices formed similar to previous semi-cycle, but on other side of the cylinder
Crest		Ditto

Falling surface compresses vortices - increasing circulation
 Rising surface decreases circulation

VORTEX SHEDDING PATTERN FOR A VERTICAL SURFACE PIERCING CYLINDER IN WAVES: $N_k - 5.4$

(FROM: Zdravkovich & Namork (1977))

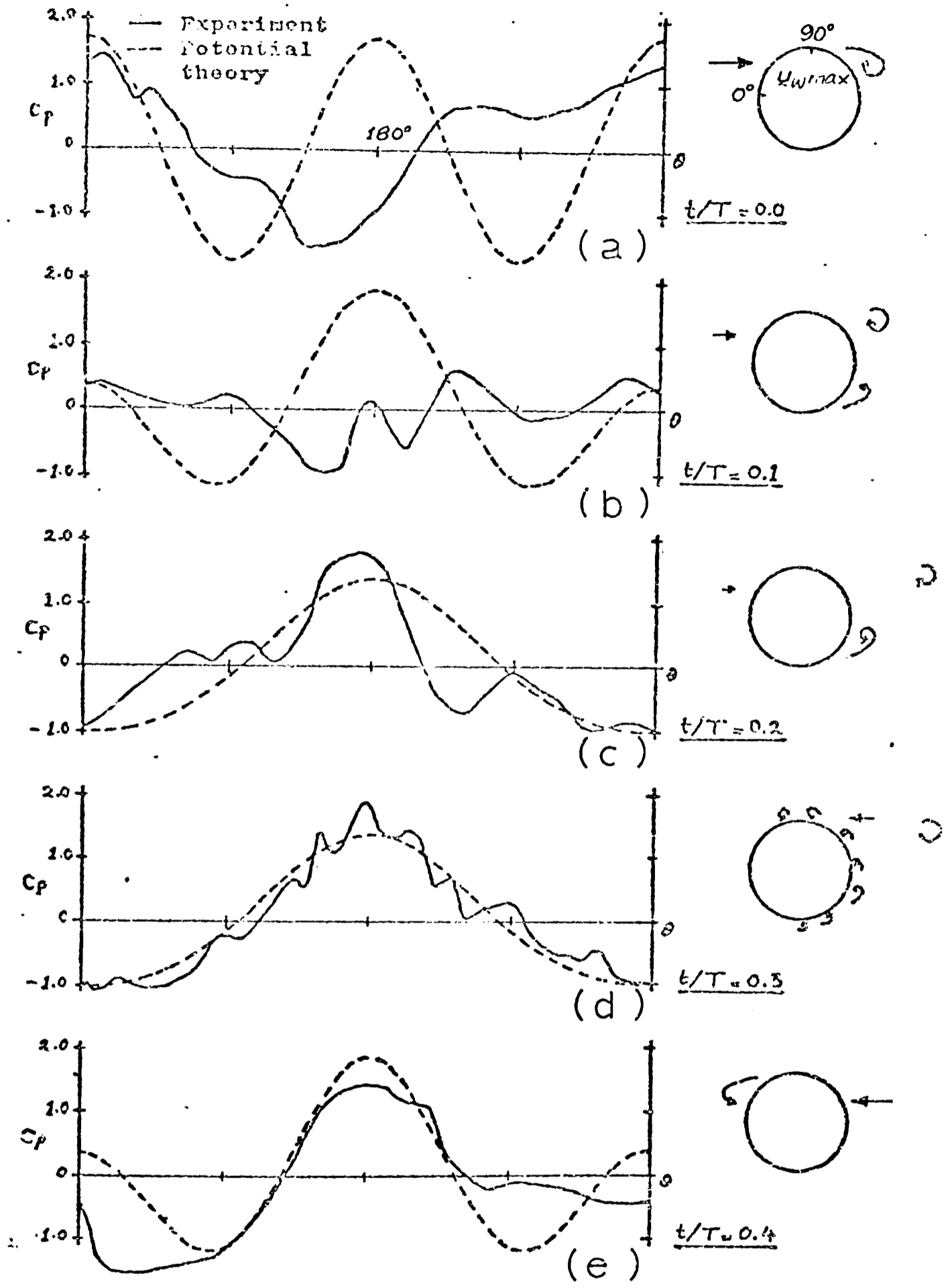
FIGURE (1.29a)

WAVE	FLOW PATTERN	COMMENTS
Crest		Vortex pair on one side of cylinder - smaller vortex on the other
Surface level falling		Lower vortex pair shed
SWL		Shed vortex pair more persistent than at lower N_k - new vortices begin to form
Surface level falling		Upper vortex moved around cylinder by reversing flow
Trough		Inverted picture of crest condition above
Surface level rising		Upper vortex pair shed
SWL		Conditions similar to previous semi-cycle, but on other side of the cylinder
Surface level rising		Vortex growth
Crest		As crest above

VORTEX SHEDDING PATTERN FOR A VERTICAL SURFACE PIERCING CYLINDER IN WAVES: $N_k = 9.3$

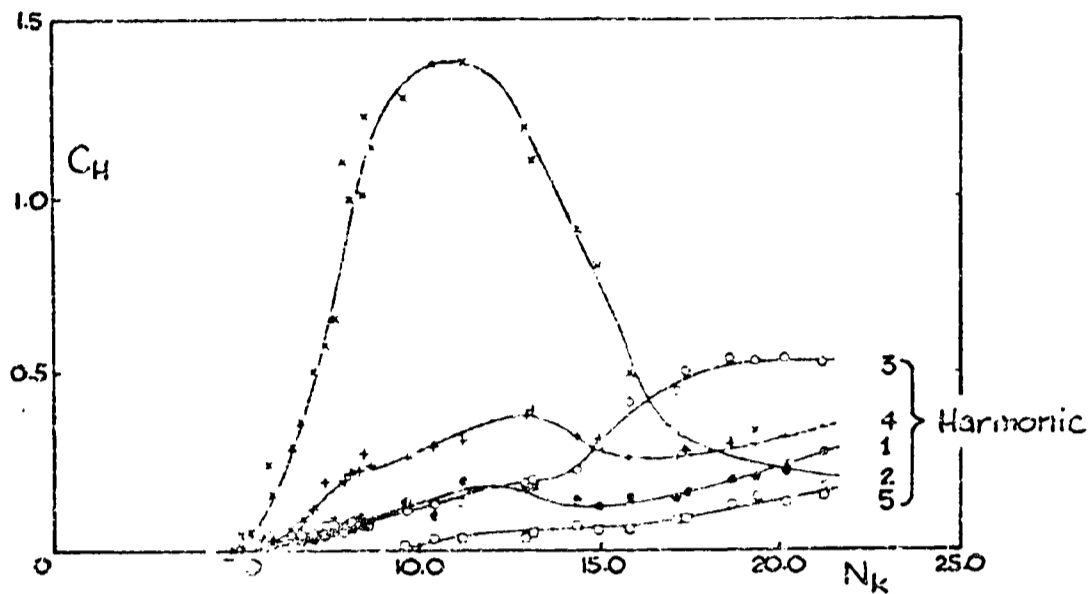
(FROM: Zdravkovich & Namork (1977))

FIGURE (1.29b)



PRESSURE COEFFICIENT & VORTEX
BEHAVIOUR IN WAVES FOR $N_k=10$
 (FROM: ISAACSON (1974))

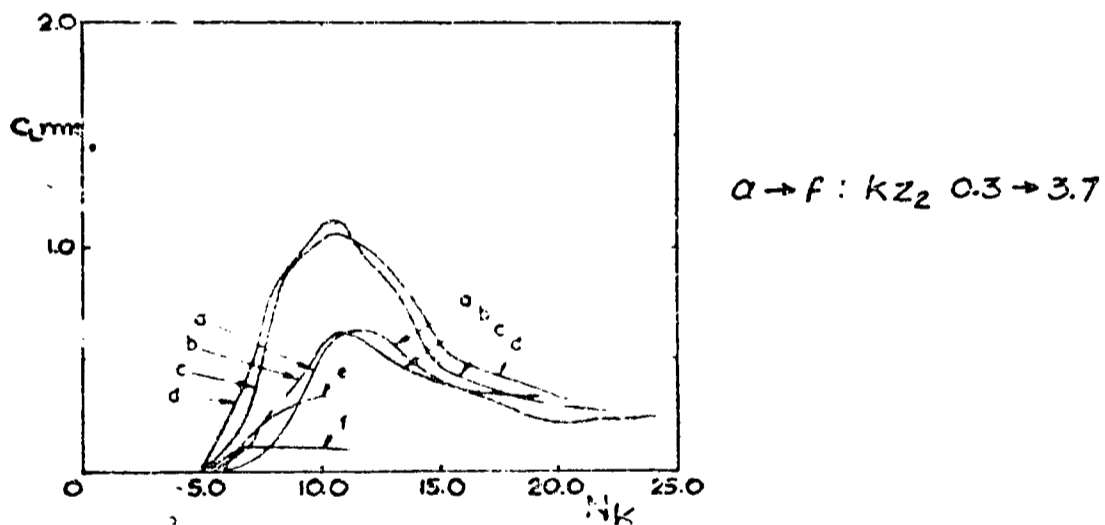
FIGURE (1.30)



FOURIER HARMONIC COMPONENT OF LIFT FORCE - VERTICAL CYLINDER IN WAVES

(FROM: ISAACSON (1974))

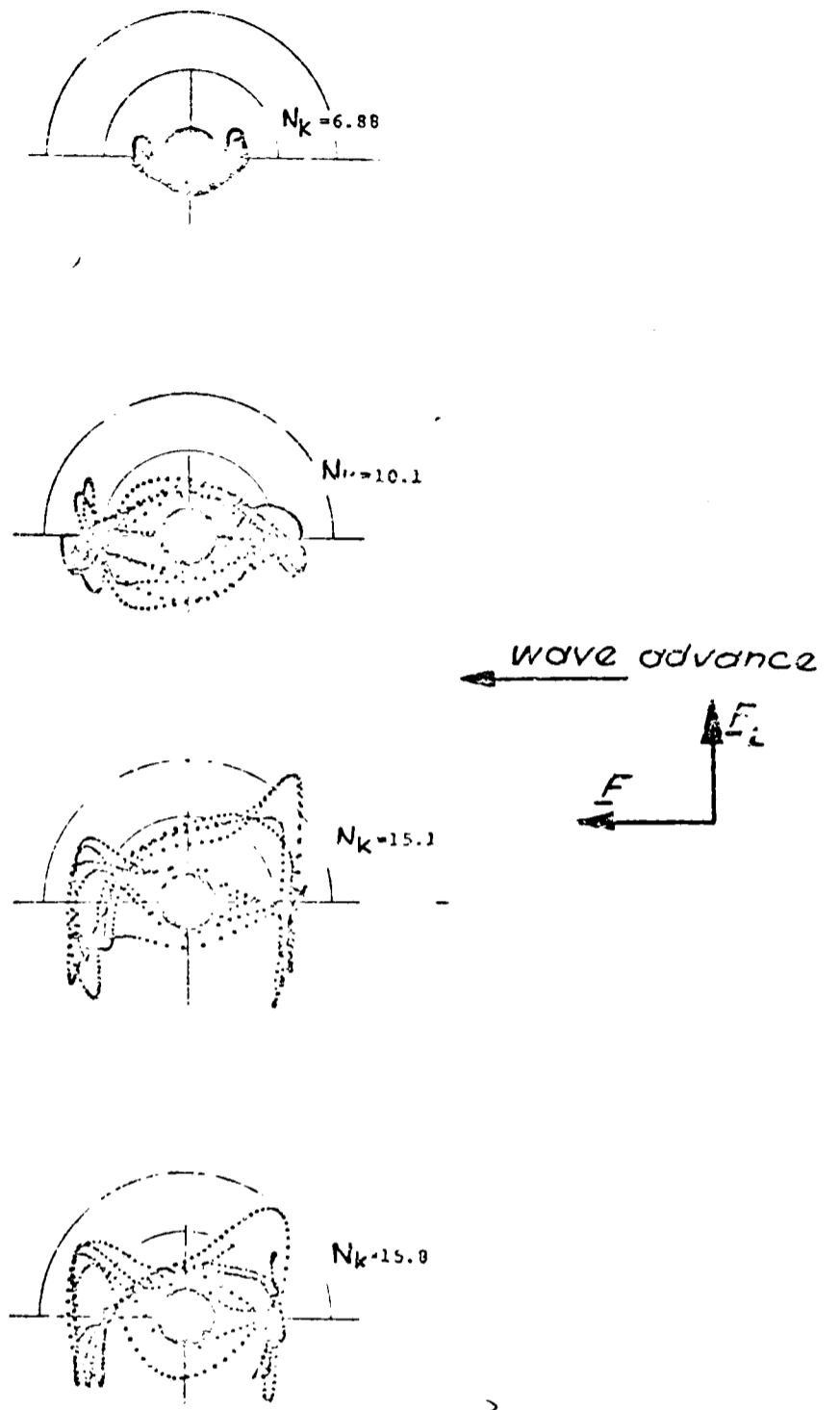
FIGURE (1.31)



EFFECT OF $k z_2$ UPON C_{Lrms} IN WAVES

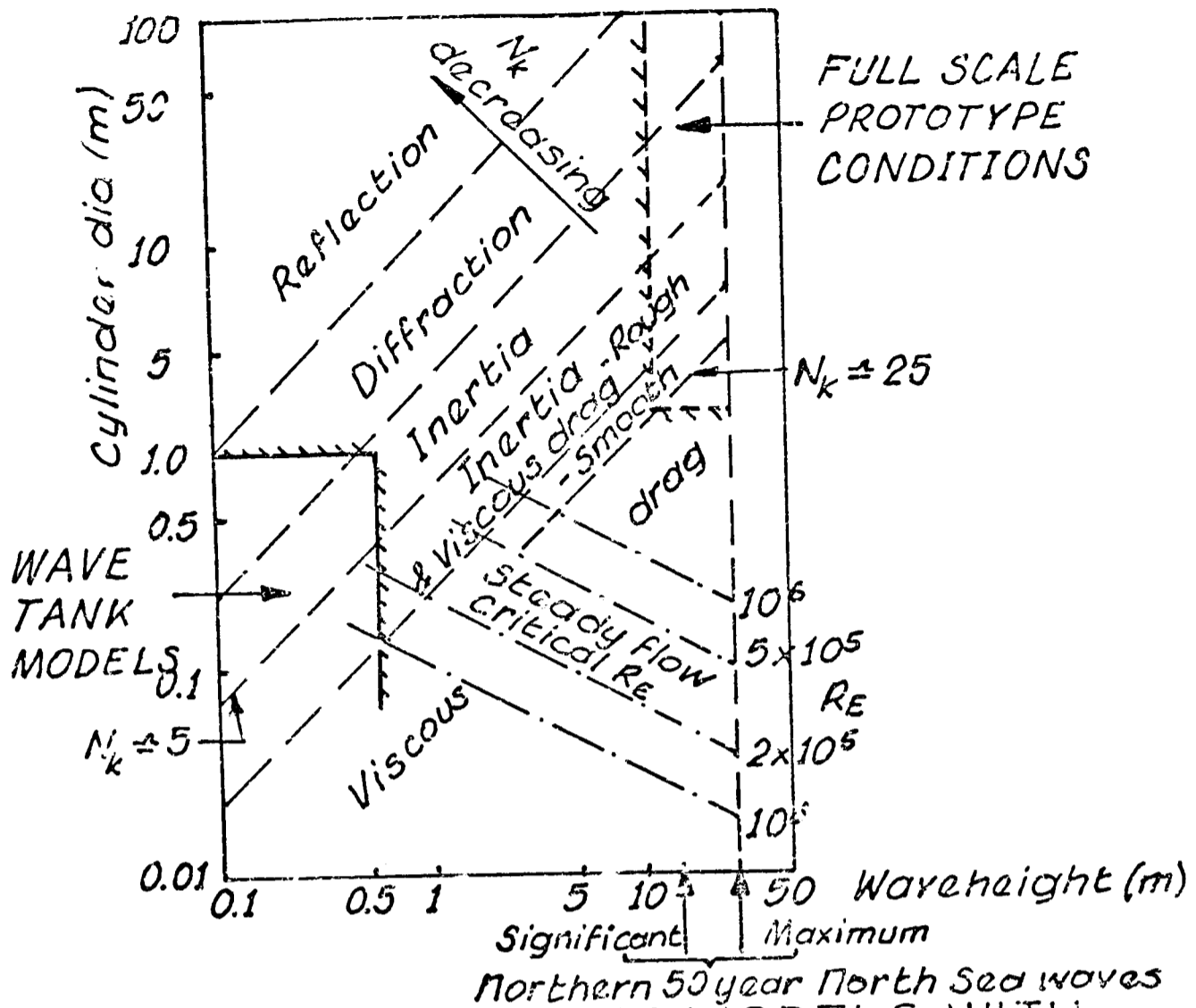
(FROM: ISAACSON (1974))

FIGURE (1.32)



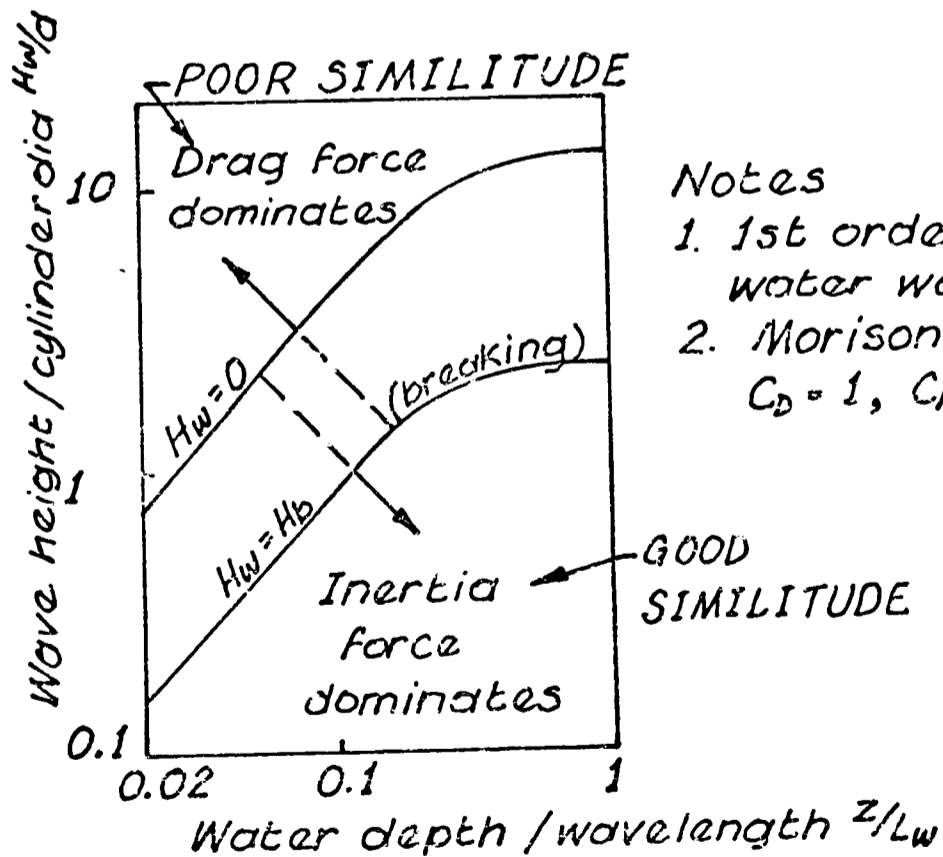
VARIATION OF RESULTANT FORCE VECTOR FOR A SERIES OF WAVES
 (FROM: CHAKRABARTI et al (1976))

FIGURE (1.33)



COMPARISON OF WAVE MODELS WITH FULL SCALE

FIGURE (2.1)



Notes

1. 1st order, deep water waves
2. Morison equation
 $C_D = 1, C_M = 2.$

WAVE TANK MODEL VALIDITY

FIGURE (2.2)

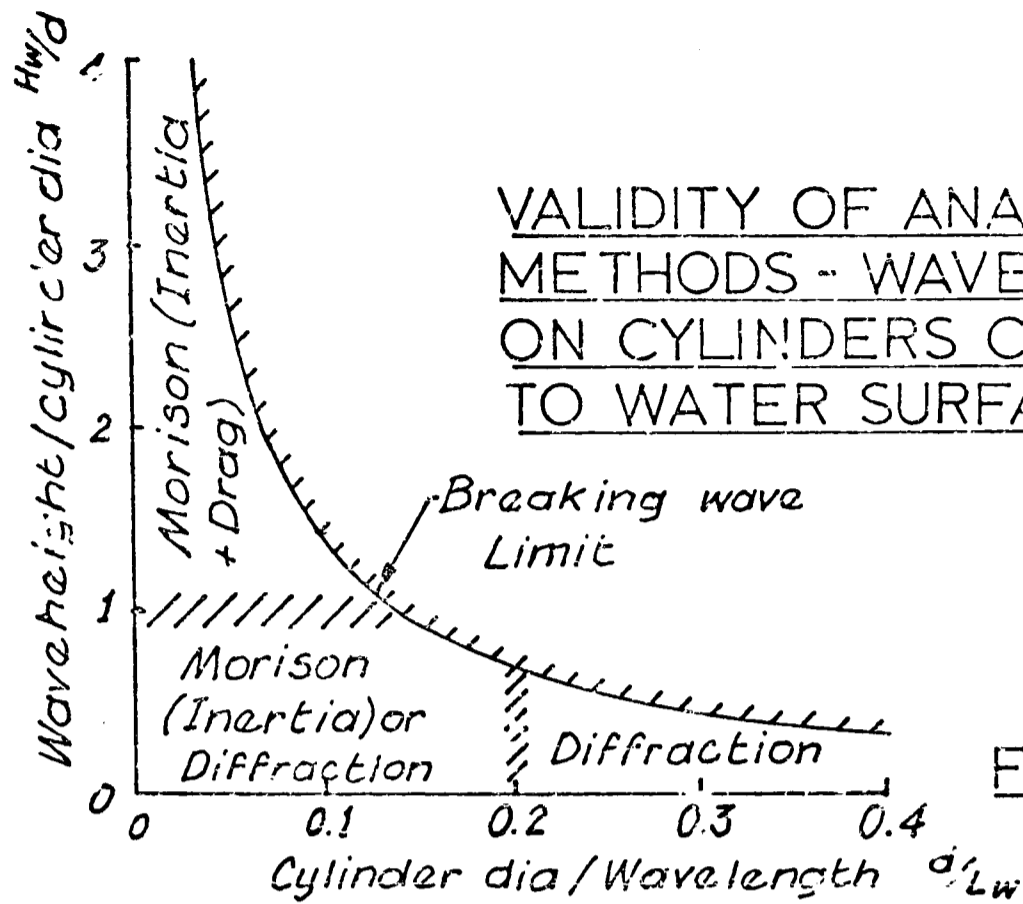
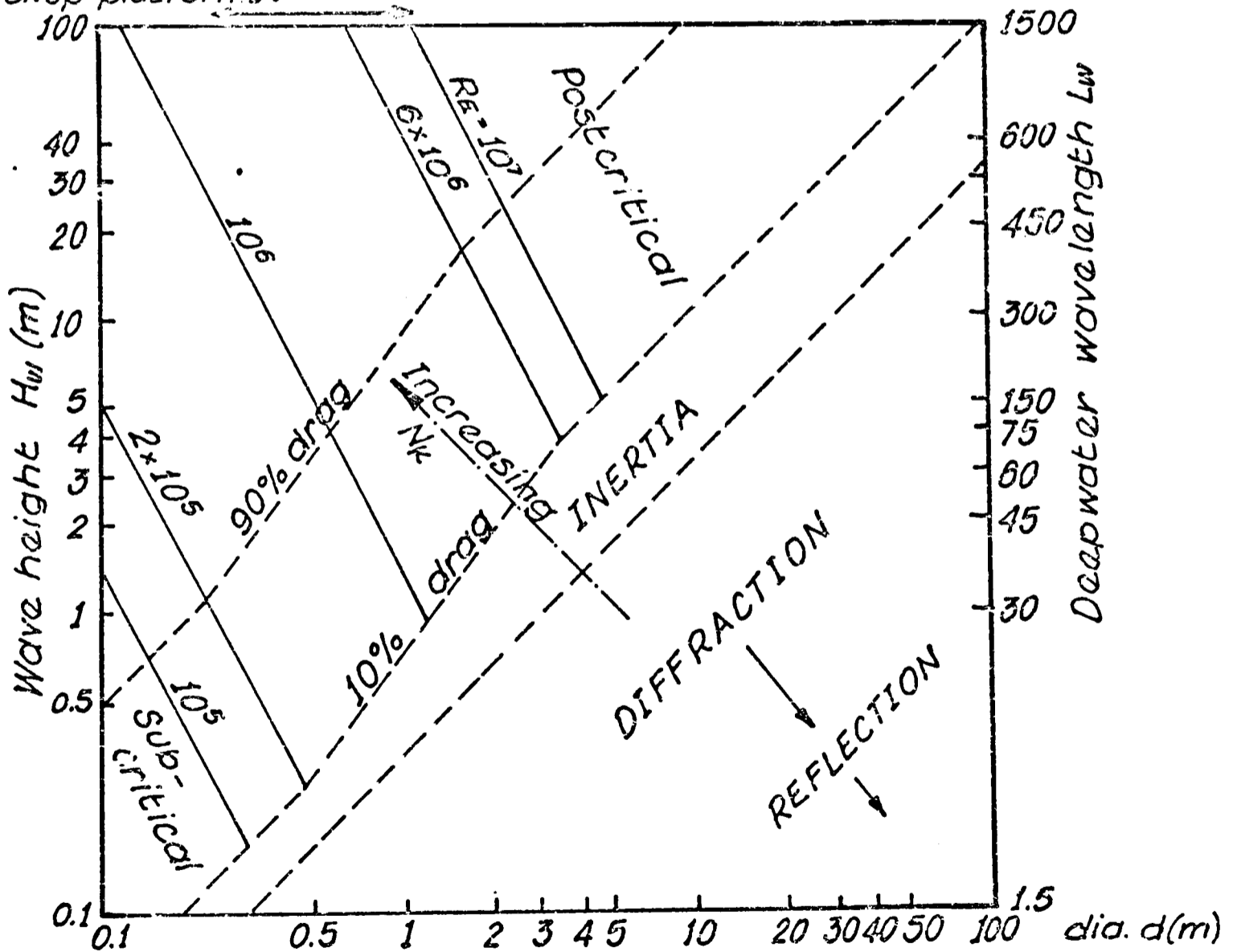


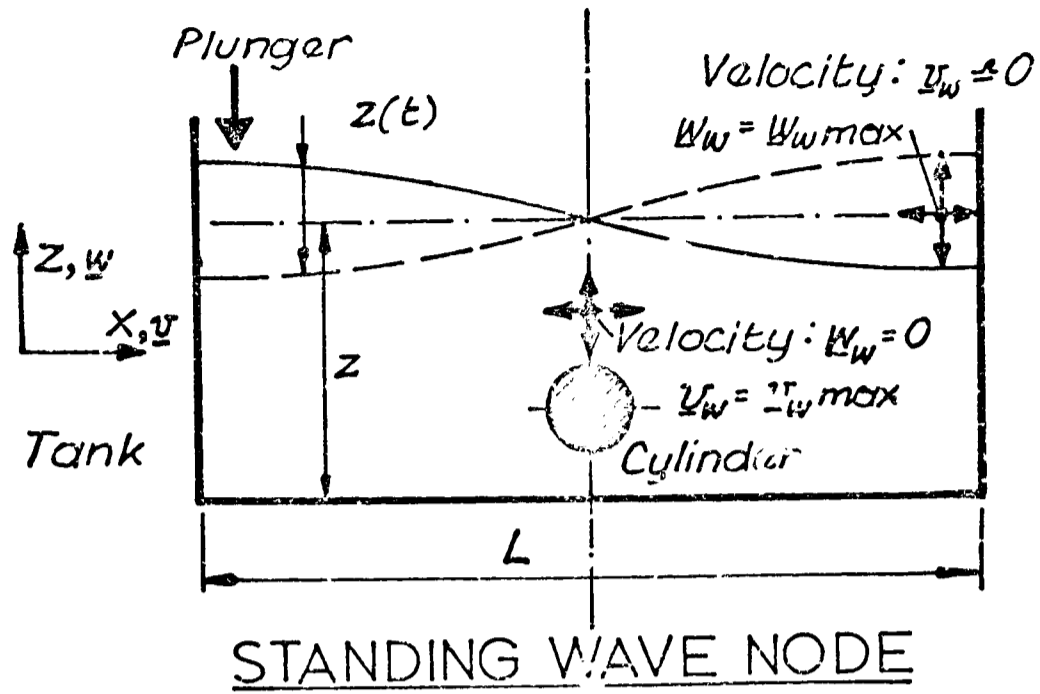
FIGURE (2.3)

Gravity structures & TBPs:
 Semi-submersibles:
 Jacket structures:
 Jackup platforms:

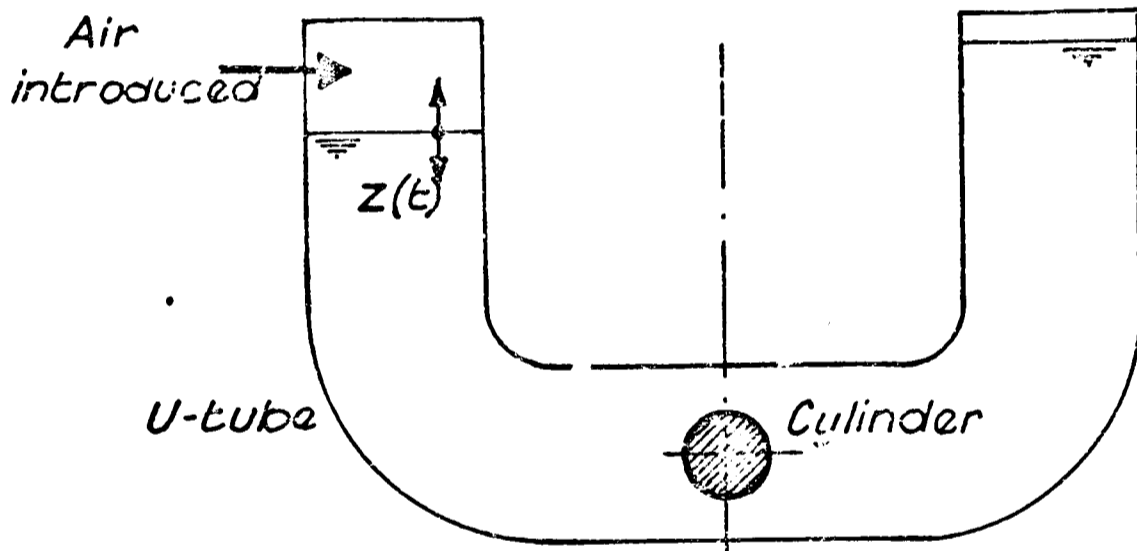


RELATIVE PROPORTION OF WAVE FORCE COMPONENTS AT SURFACE

FIGURE (2.4)



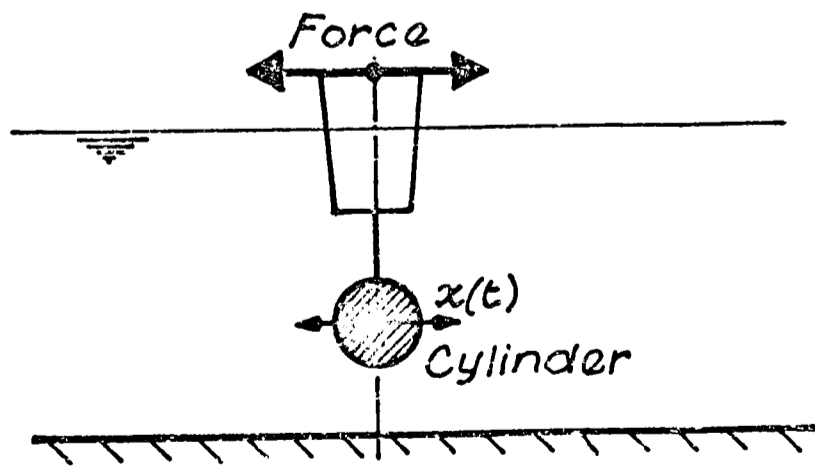
(a)



U - TUBE

(b)

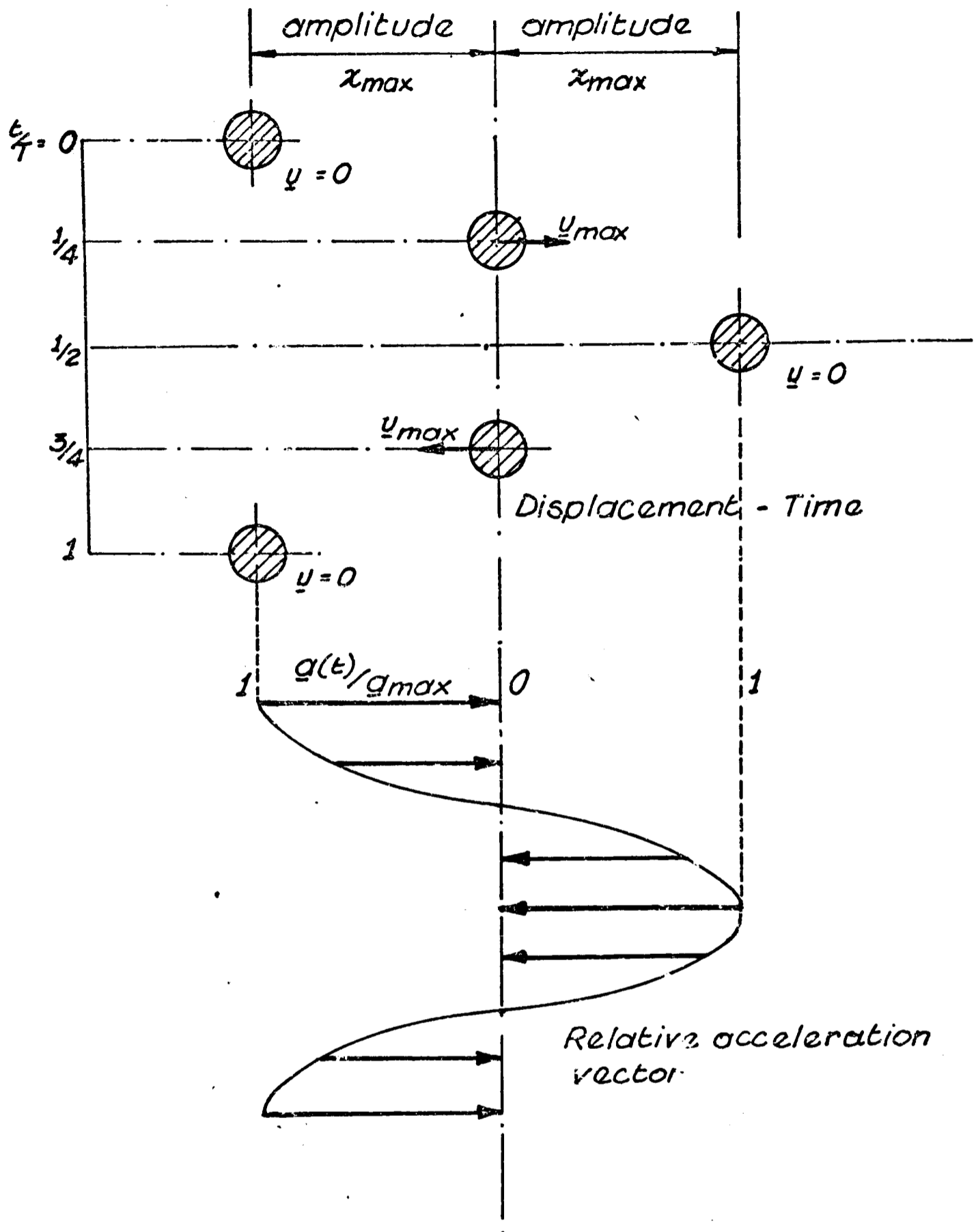
N.B. Cylinder size exaggerated



OSCILLATING CYLINDER

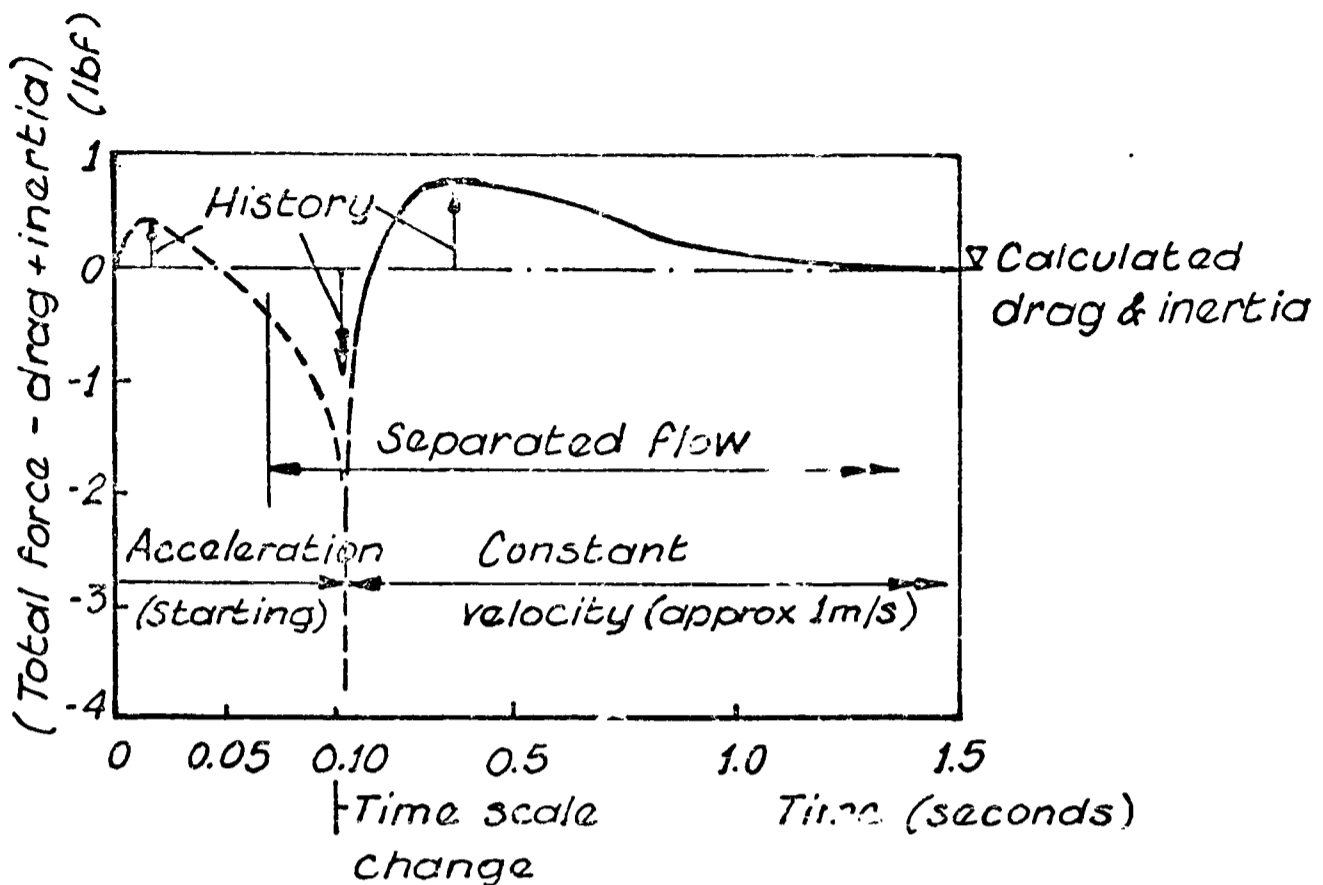
(c)

EXPERIMENTAL PRODUCTION OF PLANAR OSCILLATORY FLOW FIGURE(3.1)

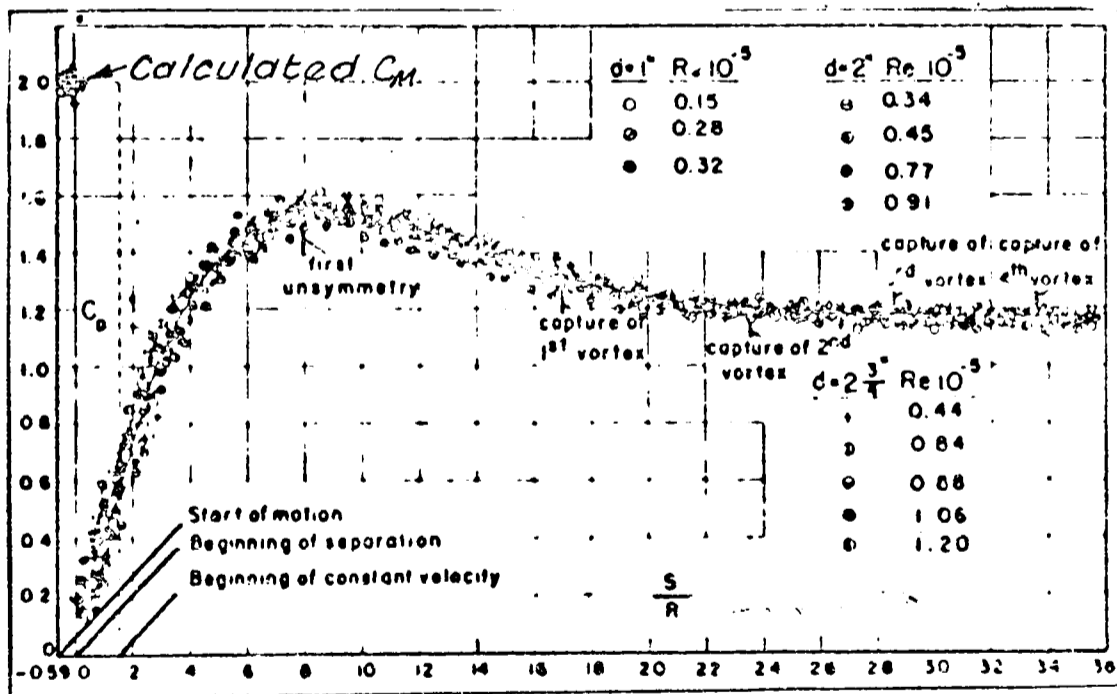


RELATIVE PLANAR OSCILLATORY
MOTION BETWEEN A FLUID
AND CYLINDER

FIGURE (3.2)

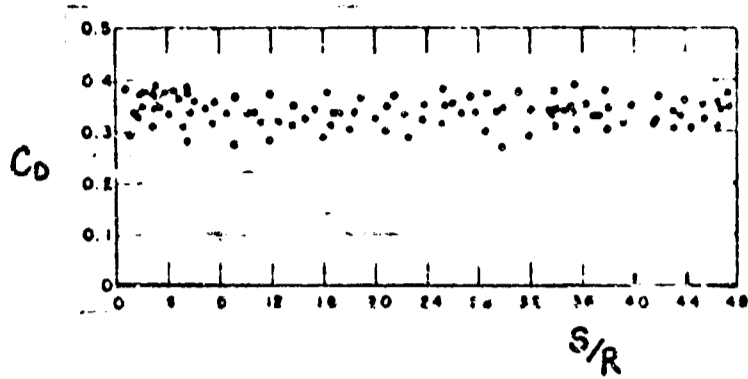


HISTORY FORCE TERM FOR A STARTING FLOW FIGURE (3.3)
 (From HAMILTON (1972))

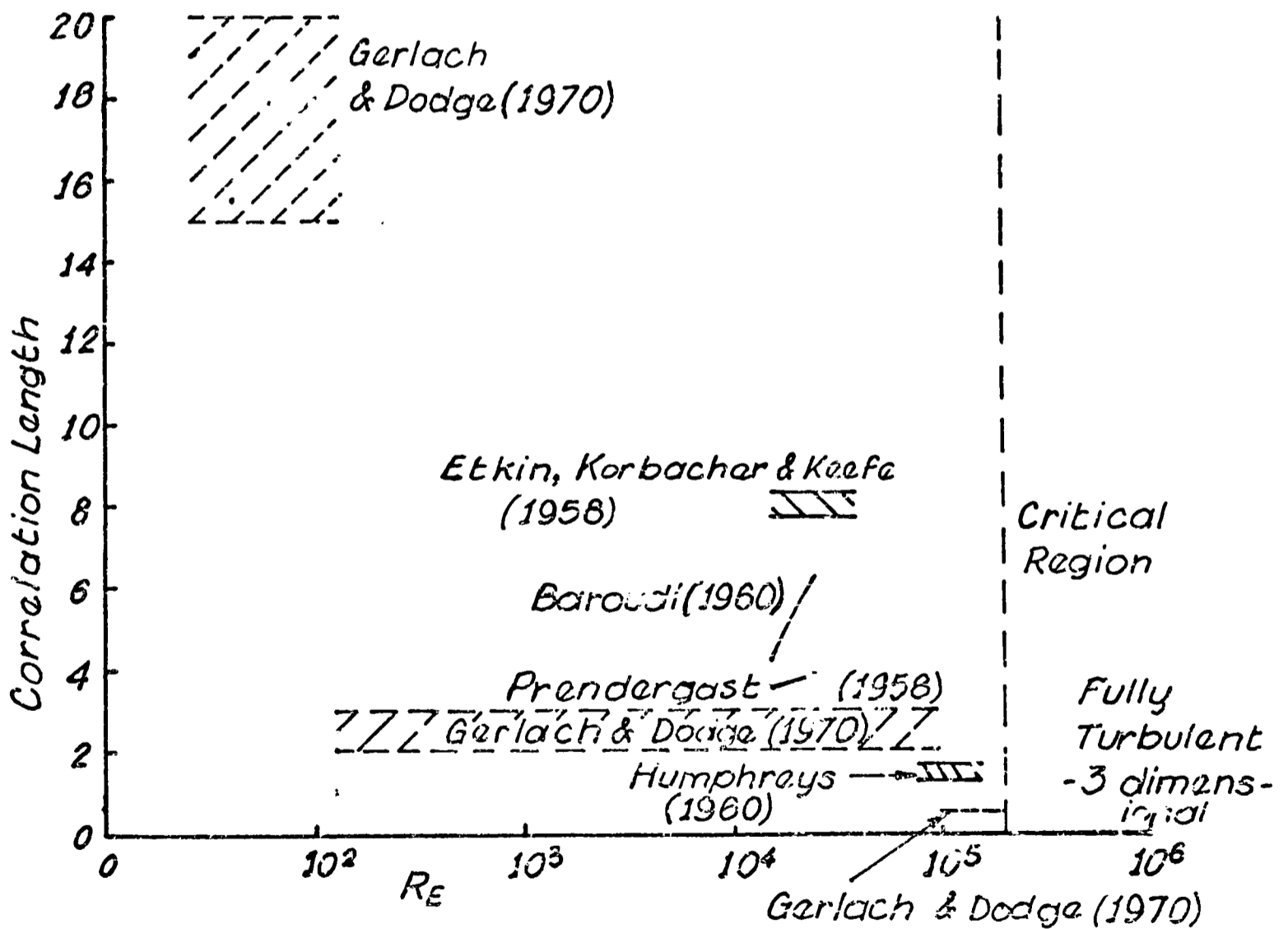


C_D FOR IMPULSIVELY STARTED LAMINAR FLOW FIGURE (3.4)
 (From SARPKEYA (1966))

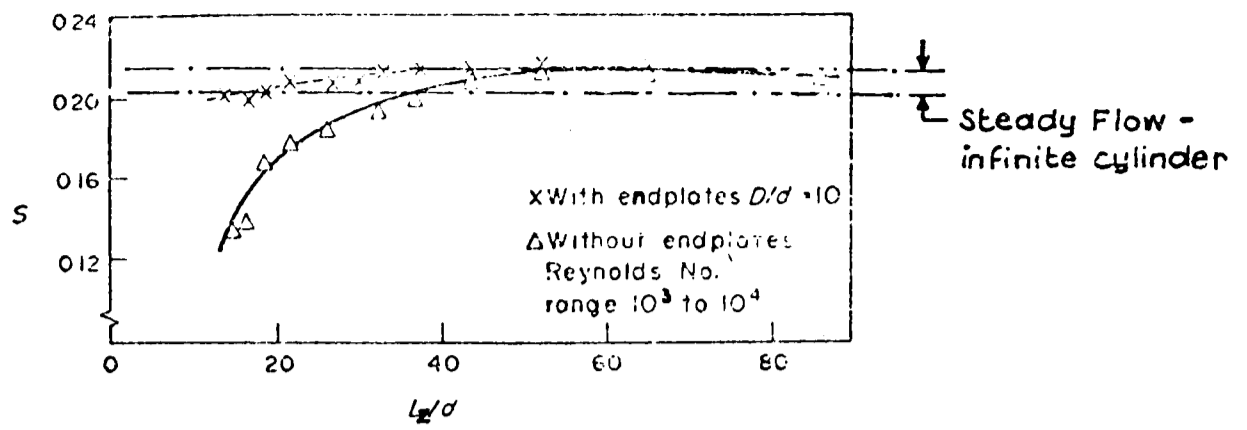
N.B. $C_M = 4F_i / \rho a d^2$ subtracted from C_{Dc} to give C_D for acceleration period



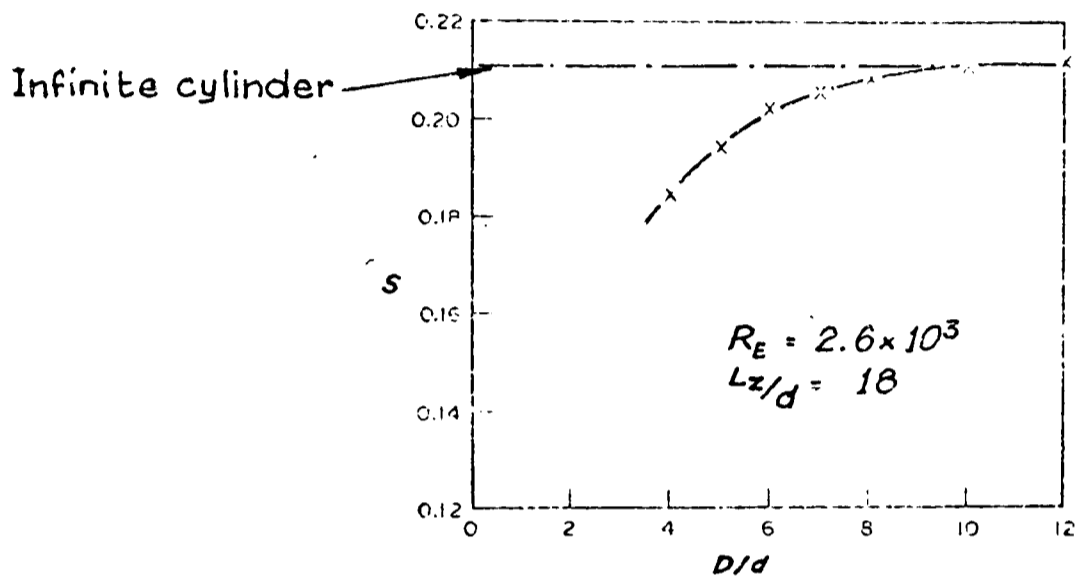
C_D FOR IMPULSIVELY STARTED
TURBULENT FLOW FIGURE (3.5)
(From SARPKEYA (1966))



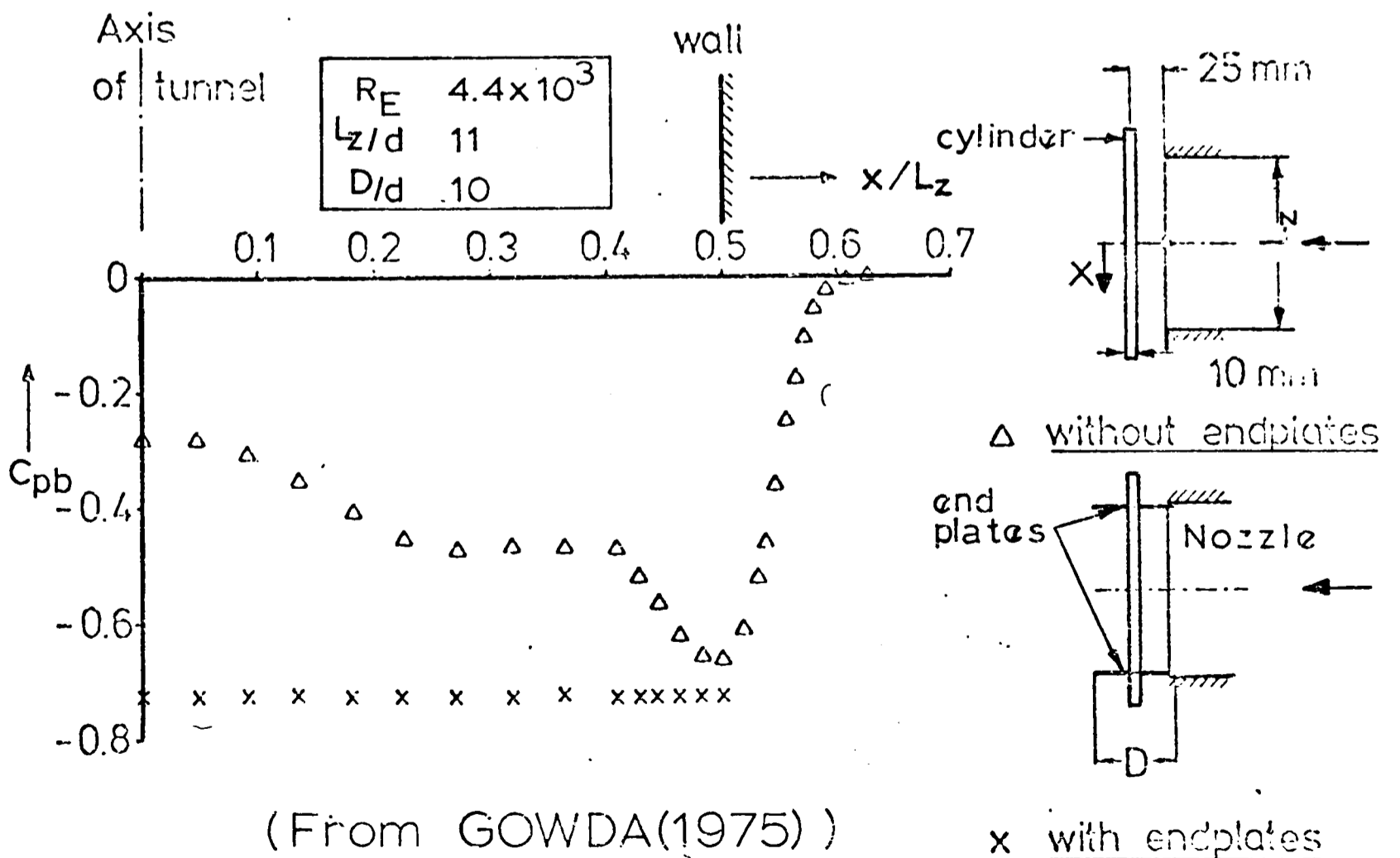
CORRELATION LENGTH - Re RANGES
(From GLENNY (1966) & KING (1977)) FIGURE (3.6)



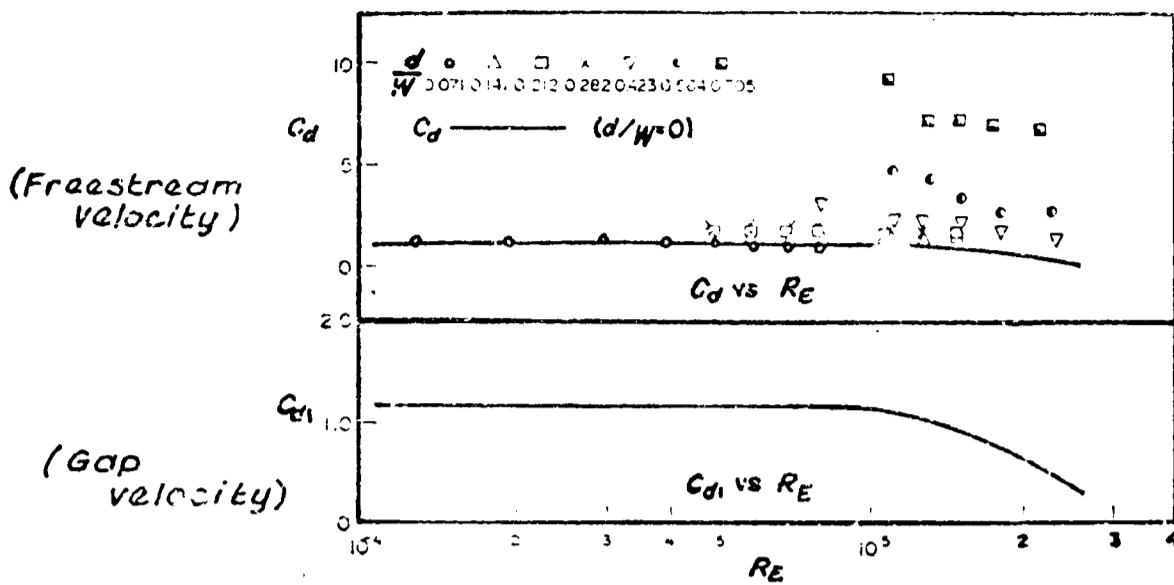
VARIATION OF STROUHAL No. WITH ASPECT RATIO (From GOWDA(1975)) (a)



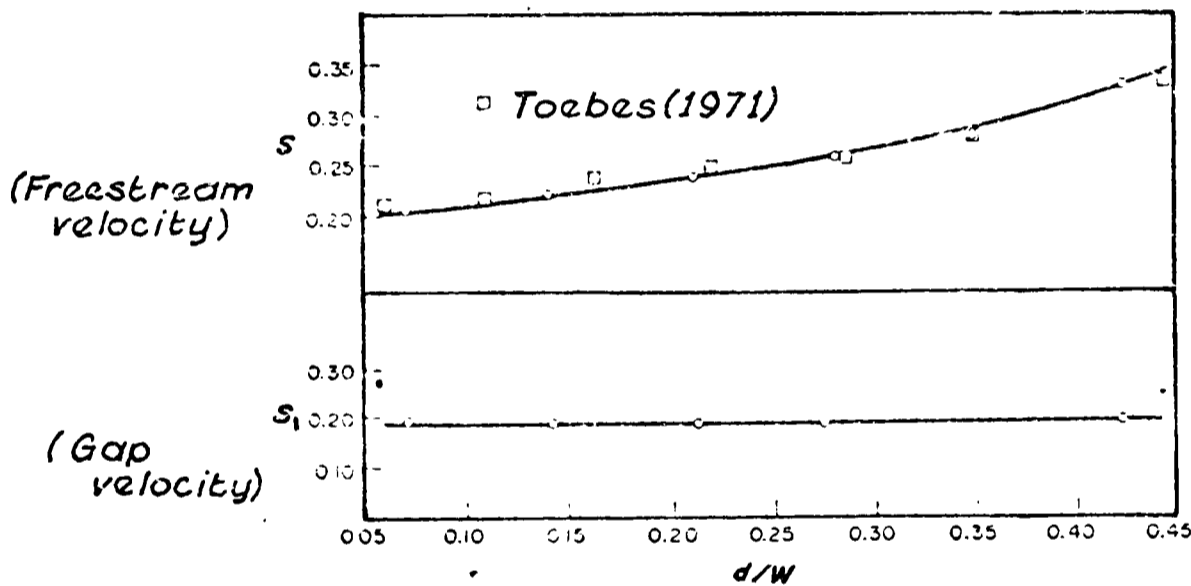
VARIATION OF STROUHAL No. WITH SIZE OF END PLATE (From GOWDA(1975)) (b)



(From GOWDA(1975)) VARIATION OF BASE PRESSURE COEFFICIENT WITH RELATIVE SPAN (c) FIGURE (3.7)



VARIATION OF DRAG COEFFICIENT WITH BLOCKAGE RATIO (a)



VARIATION OF STROUHAL No. WITH BLOCKAGE RATIO (b)

(From KING(1977))
 FIGURE (3.8)

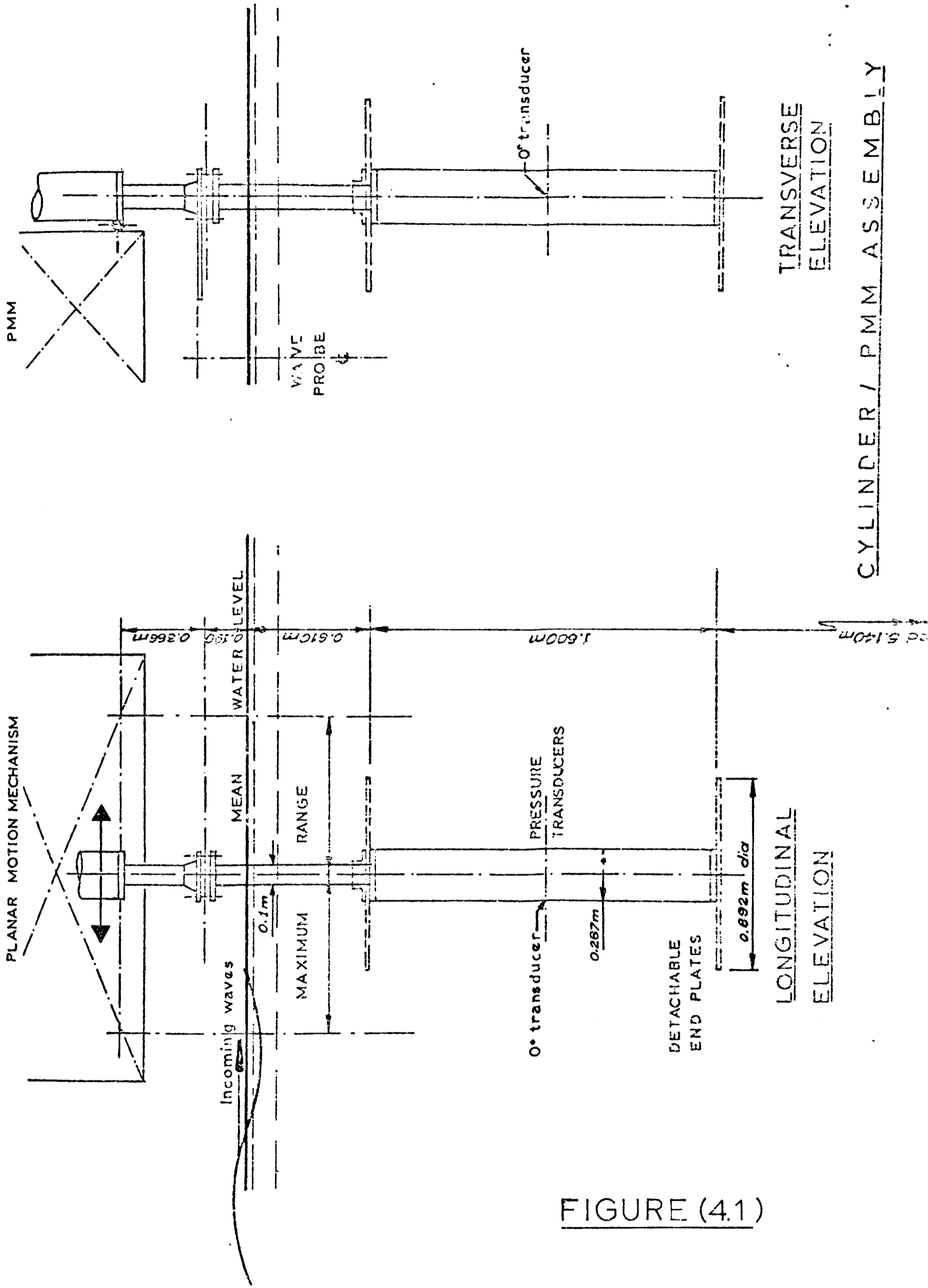
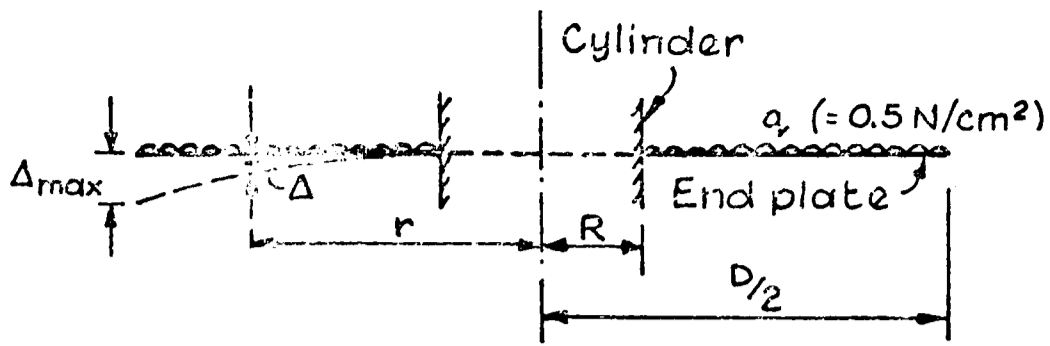


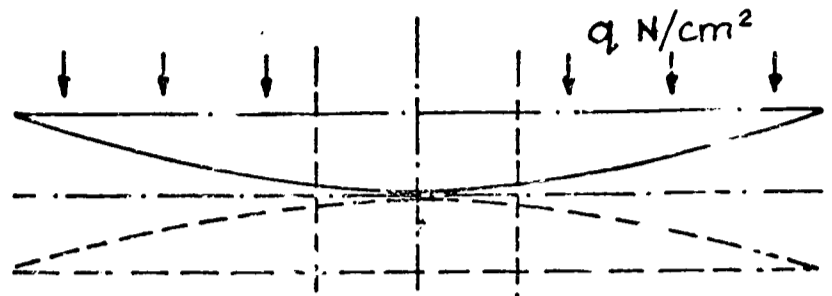
FIGURE (4.1)

CYLINDER / PMM ASSEMBLY



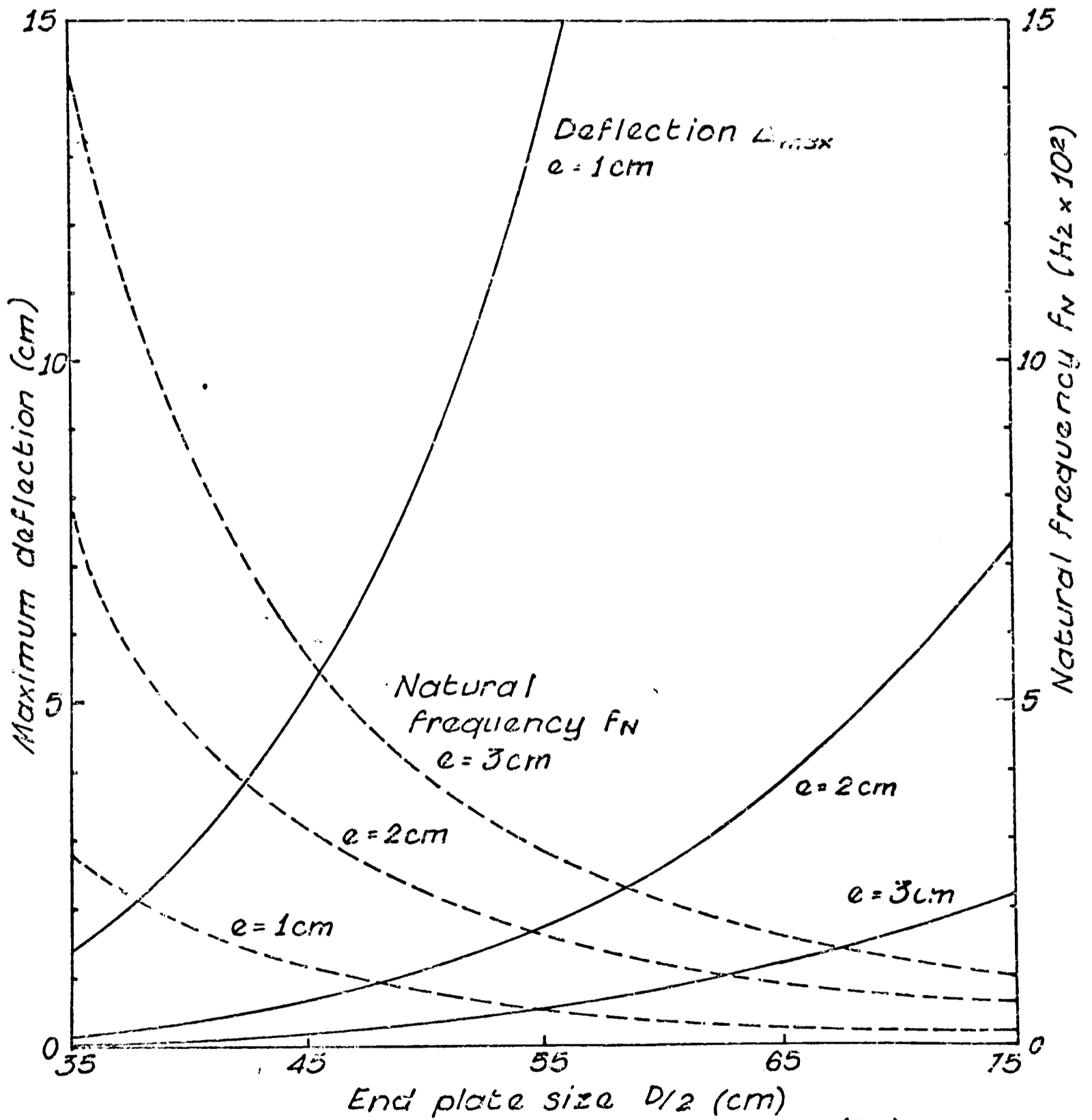
DEFLECTION OF END PLATE

(a)



FREQUENCY ANALYSIS

(c)



(b)

END PLATE DESIGN

FIGURE (4.2)

```

    R=.5
    PY=2.14159
    RHO=.341
    E=278212.
    V=.3
    DO I=20 J=35,75,110
    A=FLOAT(J)
    P=A
    P=A**2.*(A/(3.*PY))
    P1=12.5
    A2=A**2
    A4=A**4
    P2=P**2
    P4=P**4
    A3=A**3
    P3=P**3
    EA=ALOG(A)
    EP=ALOG(P)
    ADD=(A3-P3)*PY**2./3.
    DO I=1,3
    T=FLOAT(I)
    D=E*(T**3)/(12.*(1.-(V**2)))
    C1=-2*A2/(2.*D)
    V1=1.-V
    V2=1.+V
    C2A=2*R4/(16.*D*A2)
    C2B=C1*R2*(EP-.5)/(2.*A2)
    C2C=C1/4.
    CA=V1*(C2A+C2B+C2C)
    C2D=2*A2/(16.*D)
    C2E=C1*EA/2.
    CB=V2*(C2D+C2E)
    CC=R2*(V-1.)/(2.*A2)
    CC1=V2/2.
    C2=(CA+CB)/(CC-CC1)
    C3A=2*R4/(16.*D)
    C3B=C1*R2*(EP-.5)/2.
    C3C=C2*R2/2.
    C3=-(C3A+C3B+C3C)
    C4A=2*R4/(64.*D)
    C4B=C1*R2*(EP-1.)/4.
    C4C=C2*R2/4.
    C4D=C3*EP
    C4=-(C4A+C4B+C4C+C4D)
    RP4=R**4
    RP2=R**2
    EEP=ALOG(R)
    W1=2*RP4/(D*64.)
    V2=C1*RP2*(EEP-1.)/4.
    V3=C2*RP2/4.
    V4=C3*EEP
    W=W1+V2+V3+V4+C4
    WRITE(30,11)W,T,A
    PV=1.3*T*PY*(A2-R2)*.5
    TW=(ADD+PV)*RHO
    S=P/W
    F1=S/PV
    F=(SQRT(F1))/(2.*PY)
    WRITE(30,13)F
100 CONTINUE
11 FORMAT(4HF = ,F3.4,3Y,4HT = ,F3.1,3Y,4HA = ,F4.1)
13 FORMAT(4HF = ,F3.4)
    STOP
    END

```

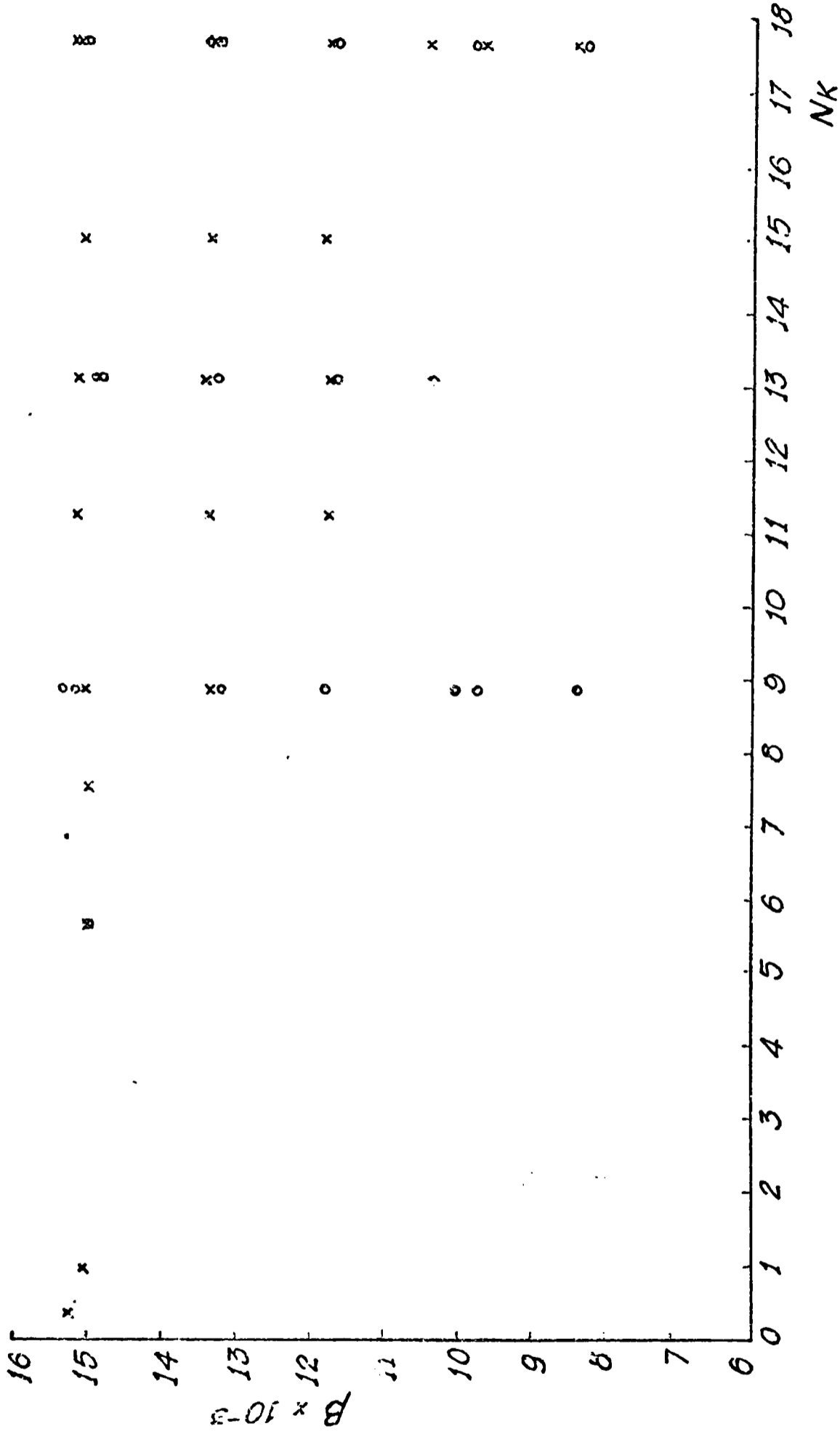
SOLUTION OF THIN
PLATE EQUATION
FOR END PLATE
DESIGN

FIGURE (4.3)

- x with end plates
- o without end plates

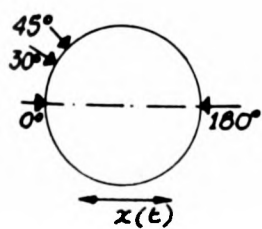
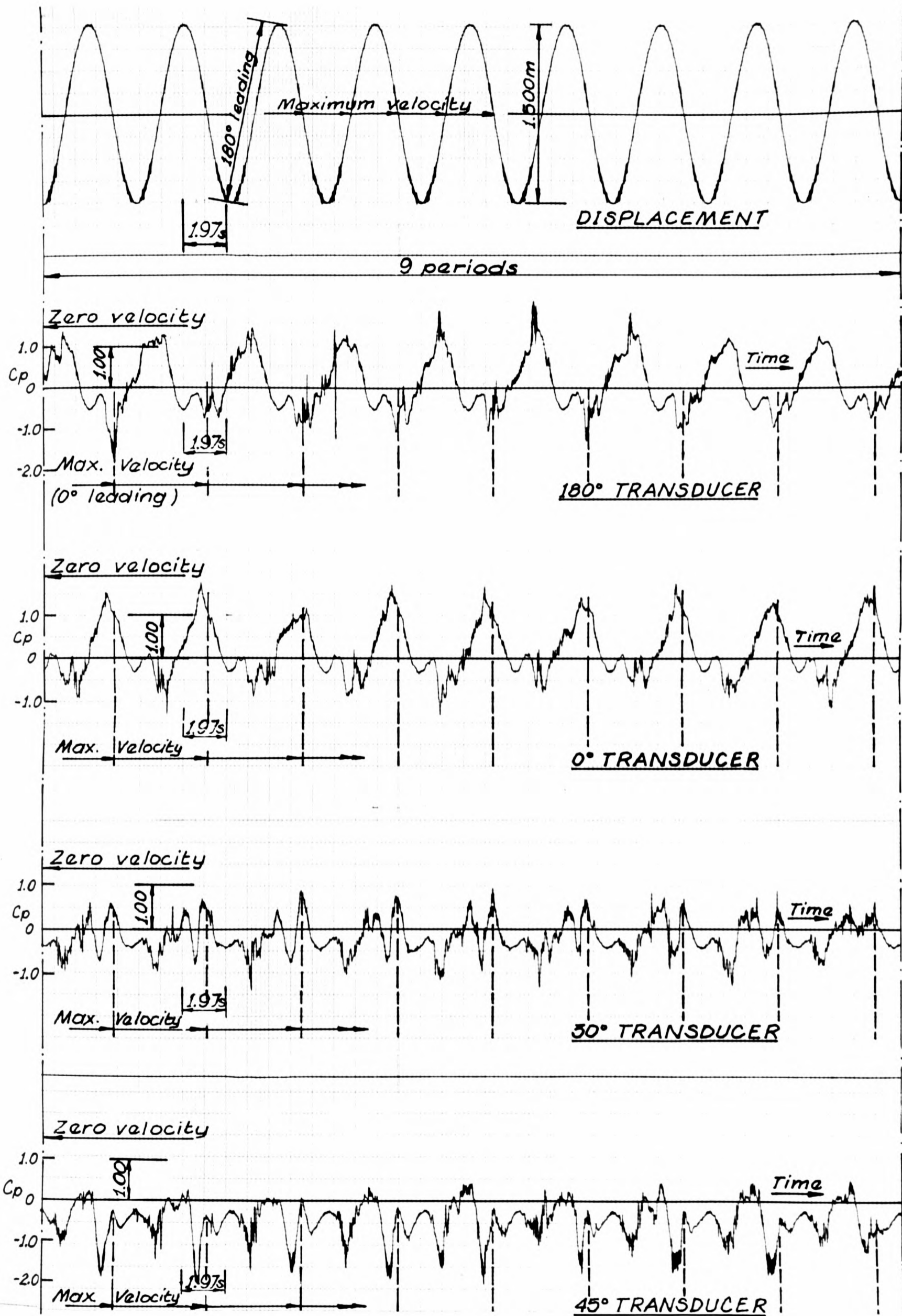
Delta versus Keulegan Carpenter number

PLANAR MOTION ALONE



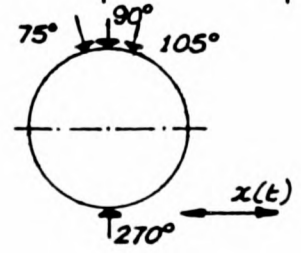
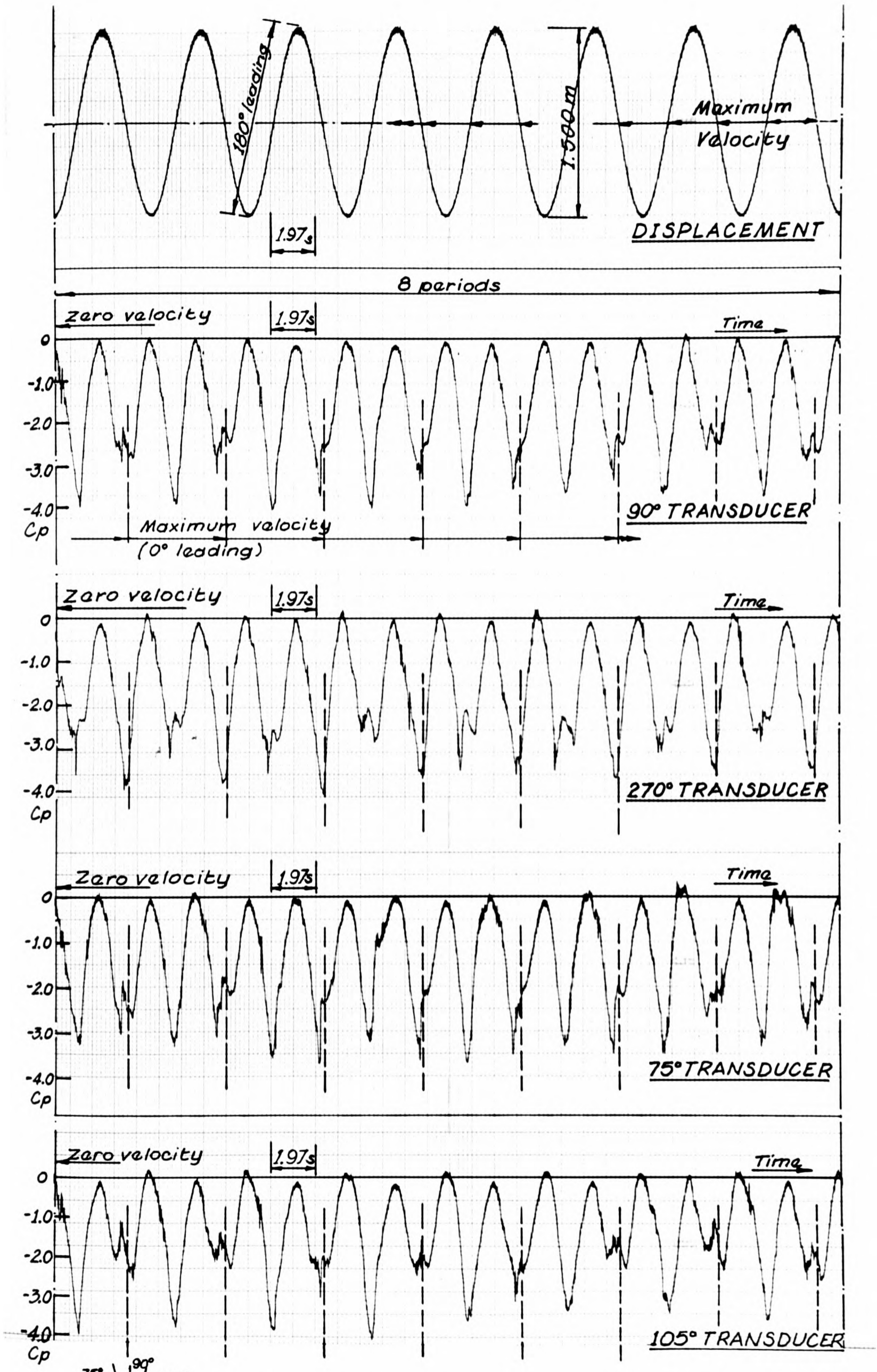
EXPERIMENTAL RANGE COVERED BY FMM

FIGURE (4.4)

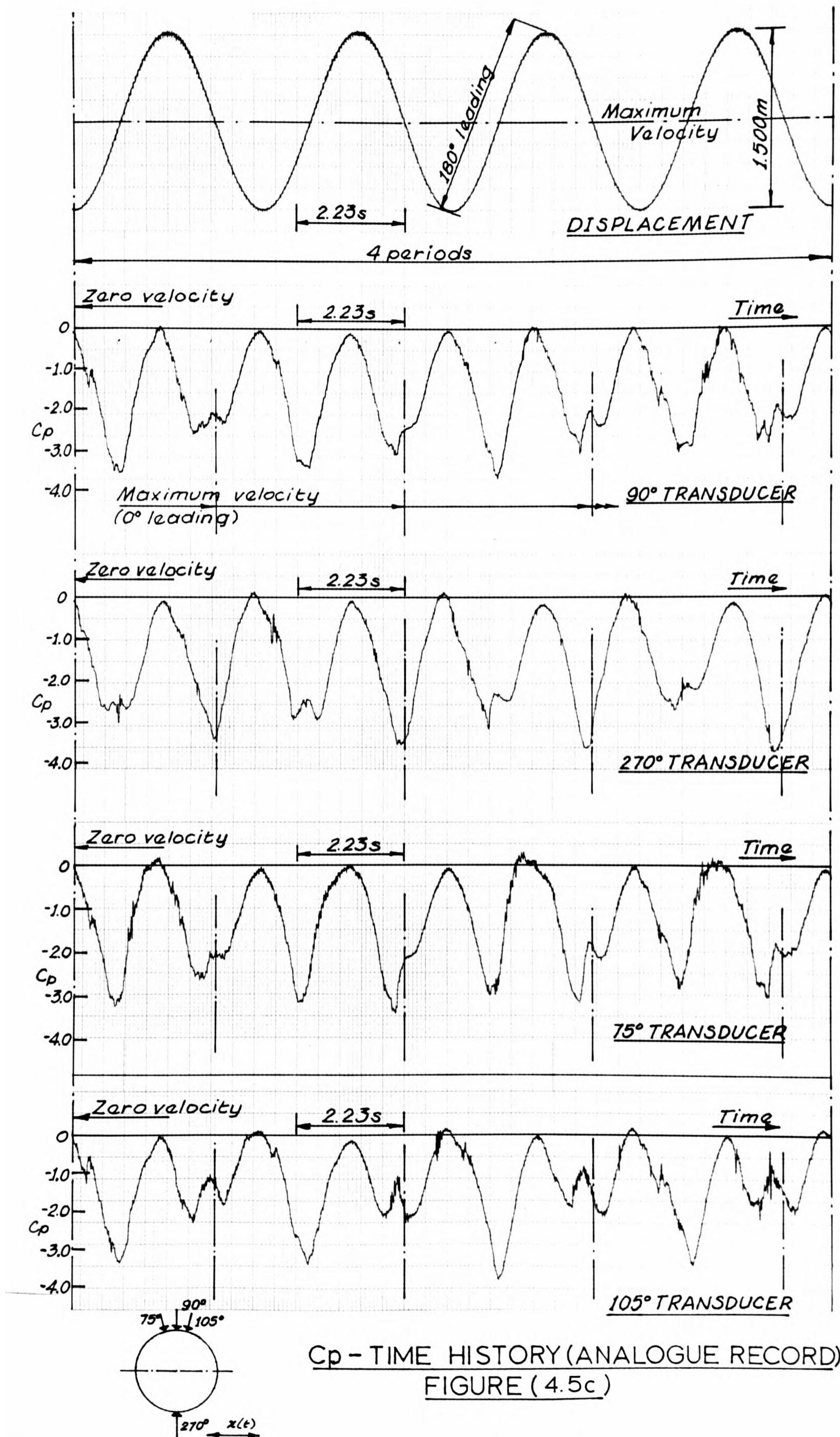


C_p -TIME HISTORY (ANALOGUE RECORD)

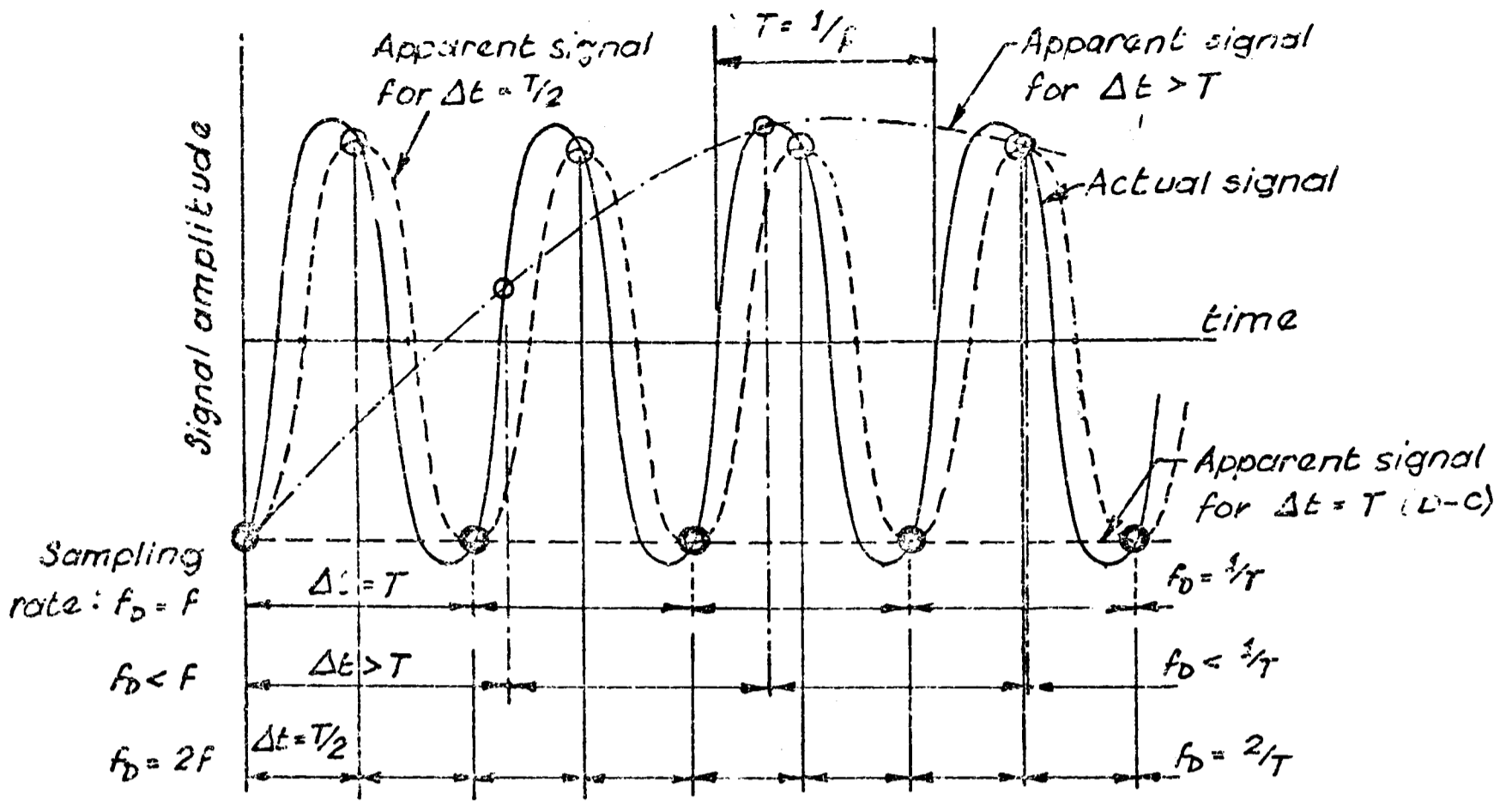
FIGURE (4.5a)



Cp - TIME HISTORY (ANALOGUE RECORD)
FIGURE (4.5b)



Cp - TIME HISTORY (ANALOGUE RECORD)
FIGURE (4.5c)

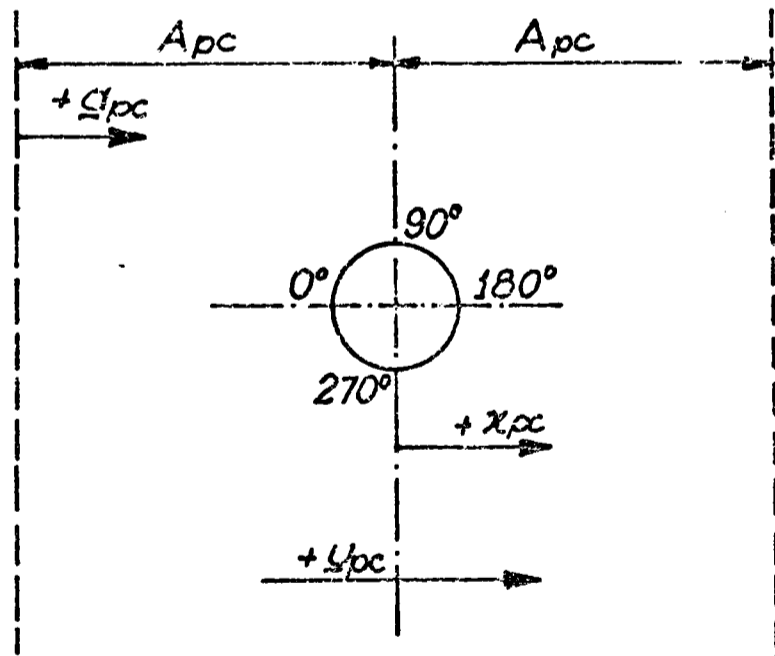


o - sampled points

Minimum sampling rate necessary to detect frequency f must be $2f$, i.e. $\Delta t = T/2$ maximum. N.B. Frequency correct, but more points necessary to detect the correct amplitude ($\Delta t < T/2$)

ALIASING DUE TO AN INADEQUATE SAMPLING RATE

FIGURE (4.6)



SIGN CONVENTION - PMM EXPERIMENT

FIGURE (4.9)

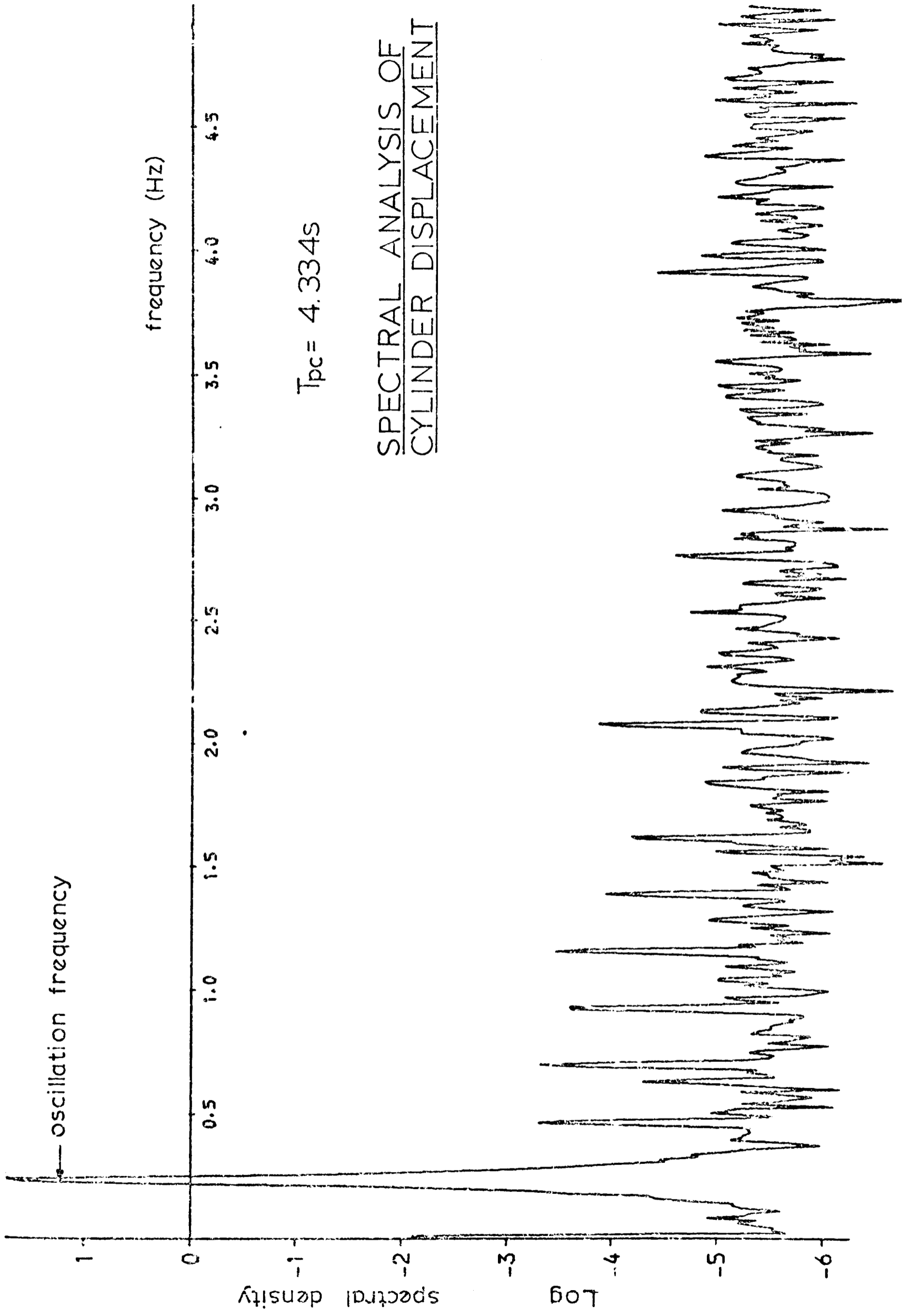
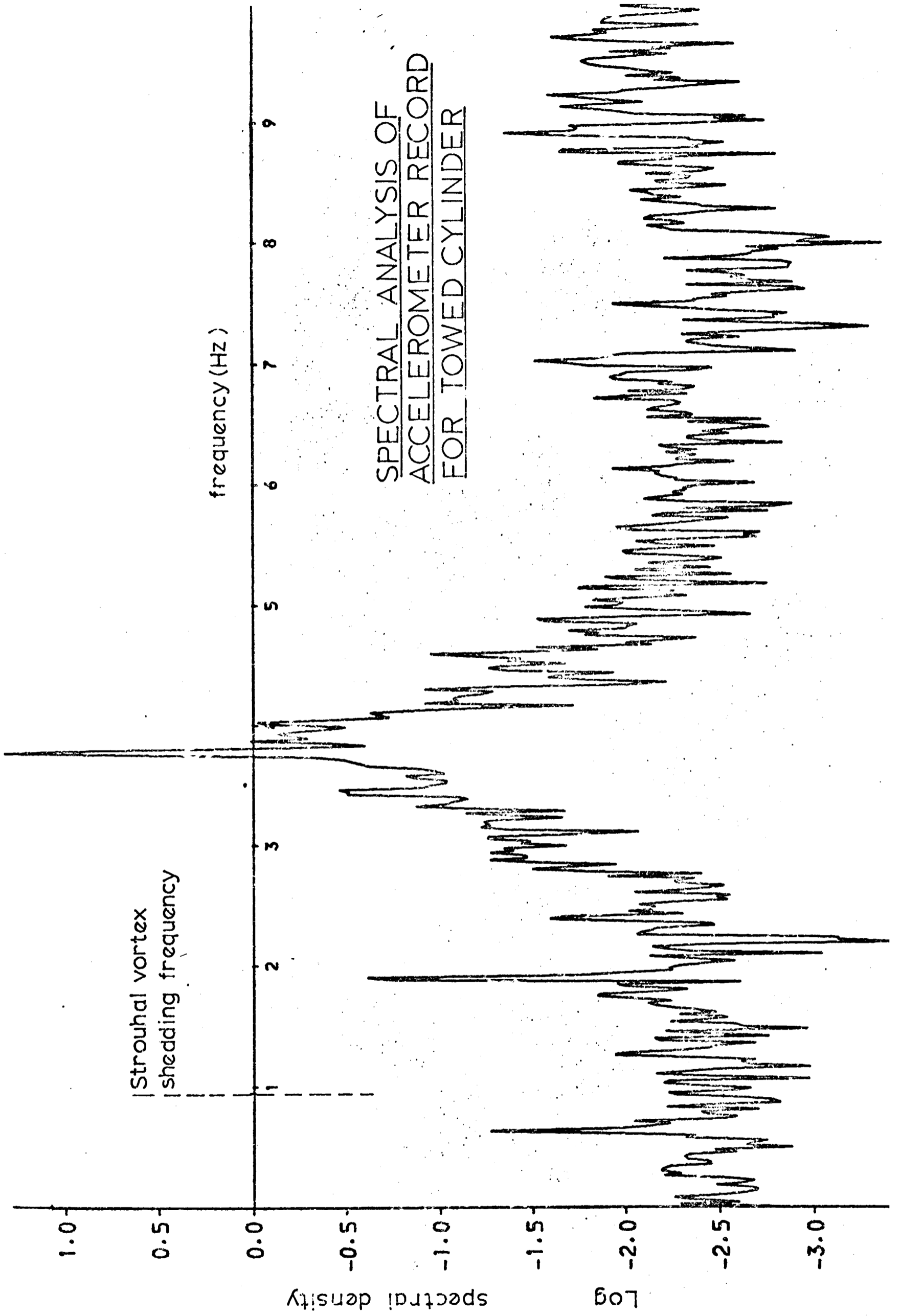
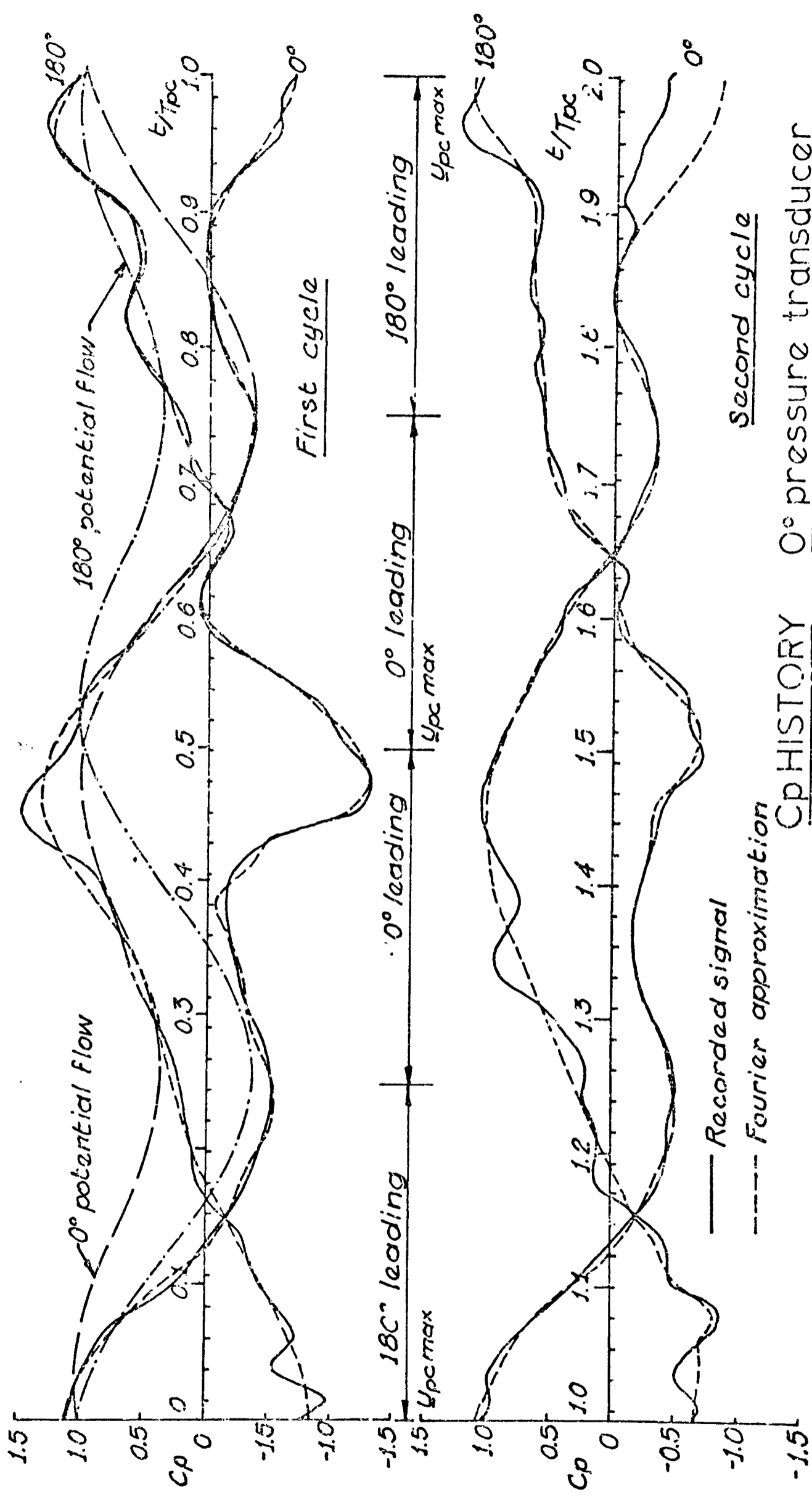


FIGURE (4.7)



SPECTRAL ANALYSIS OF
ACCELEROMETER RECORD
FOR TOWED CYLINDER

FIGURE (4.8)



Cp HISTORY 0° pressure transducer
 & 180° pressure transducer

FIGURE (4.10a)

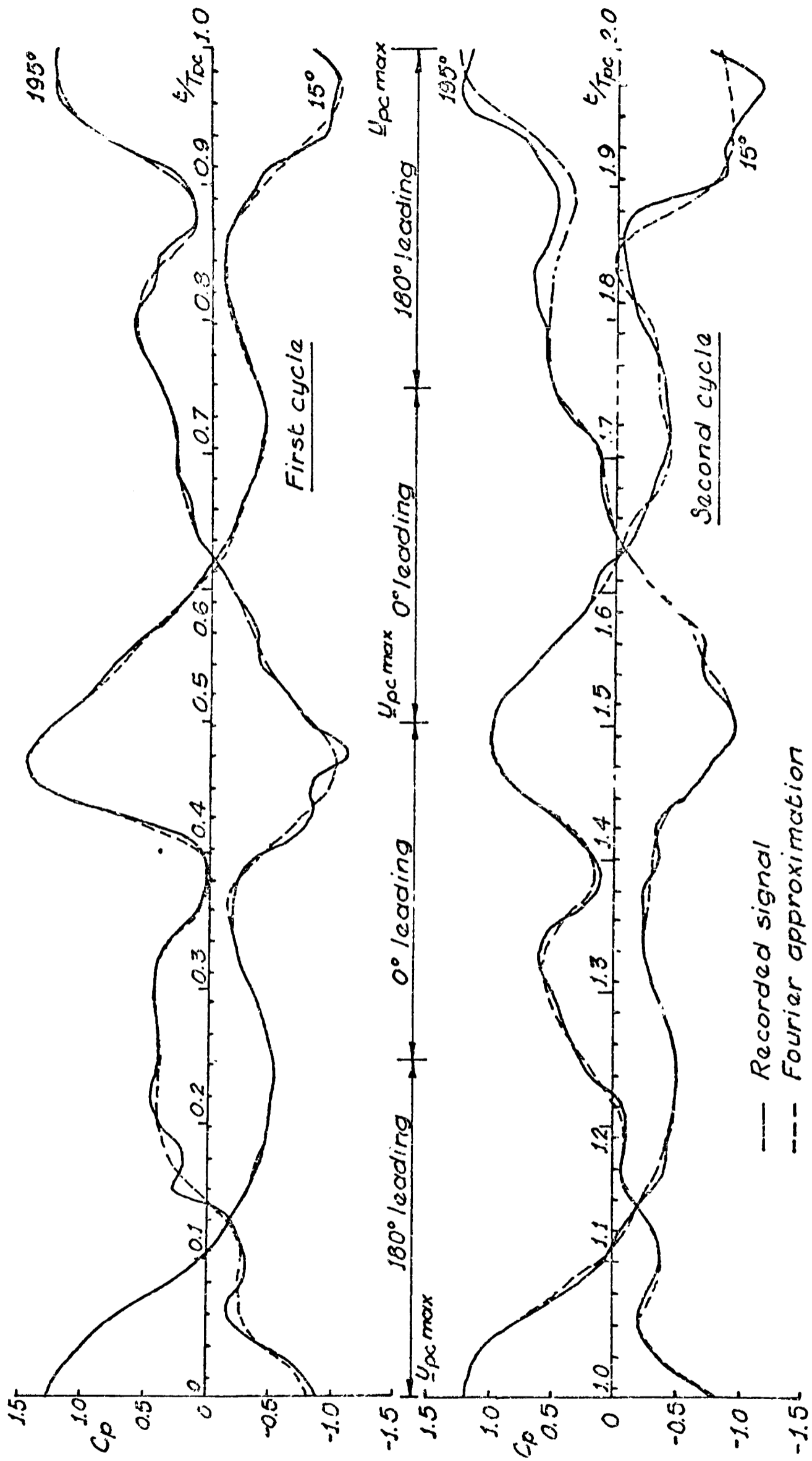
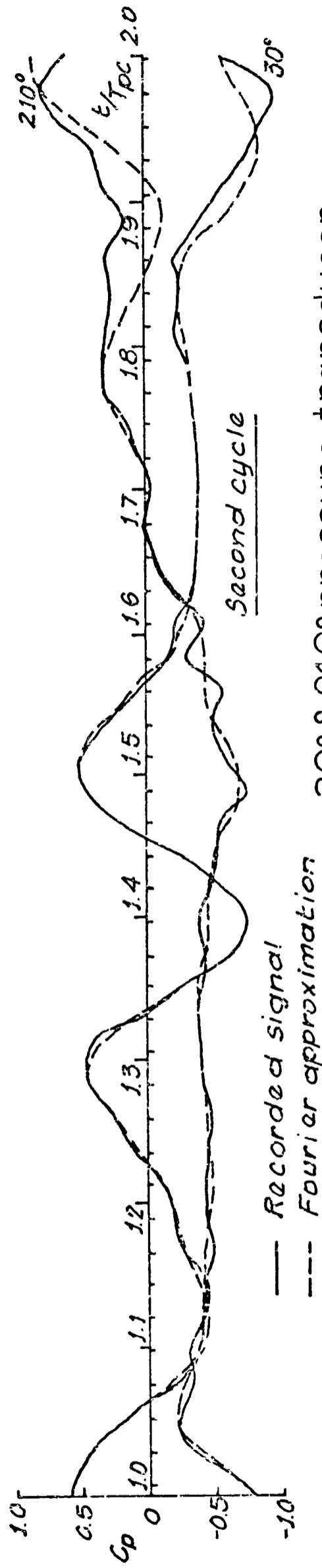
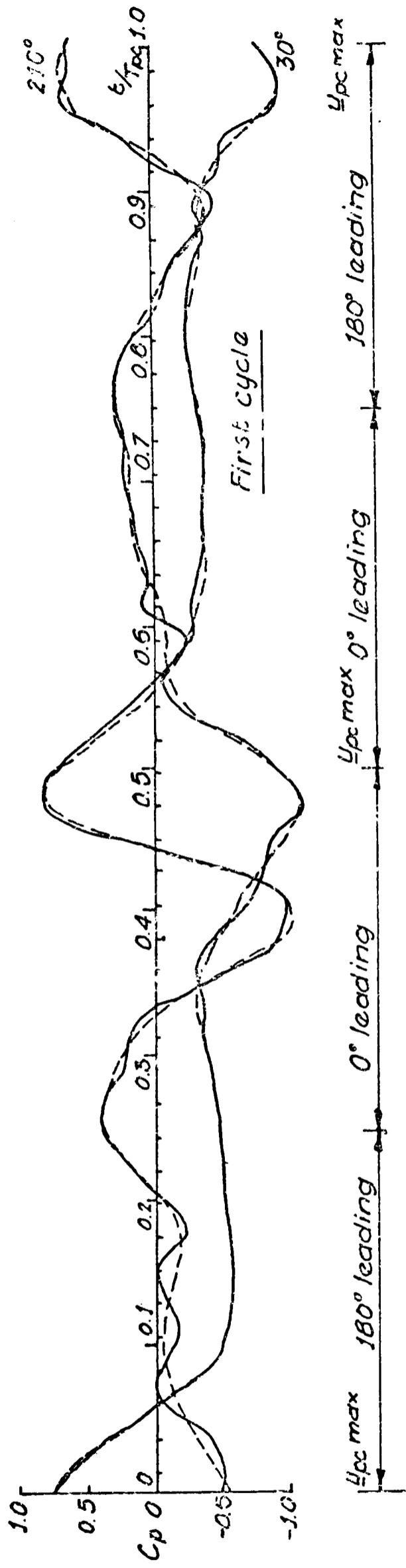


FIGURE (4.10b)

15° & 195° pressure transducer
Cp HISTORY



— Recorded signal
--- Fourier approximation

30° & 210° pressure transducer

Cp HISTORY

FIGURE (4.10c)

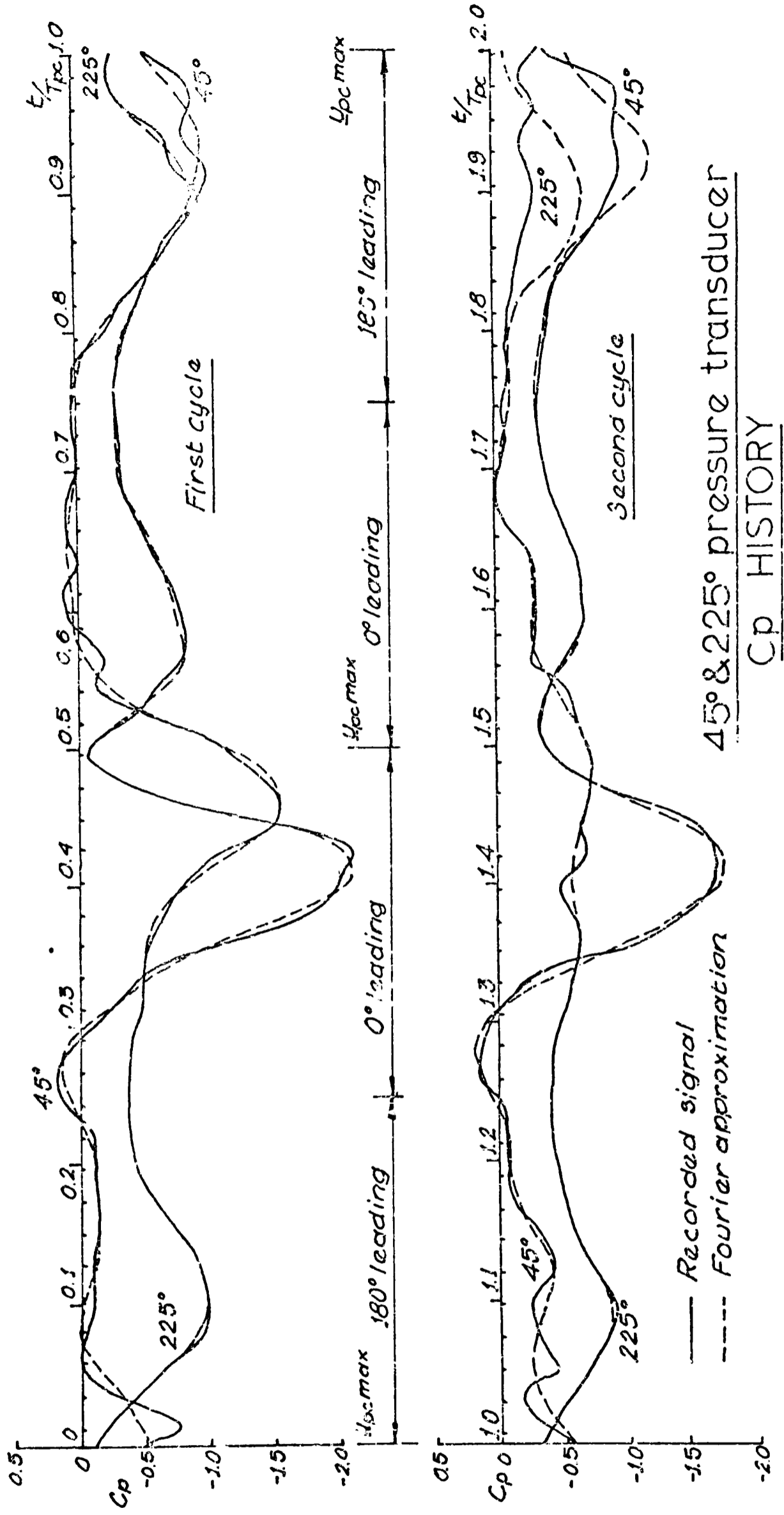
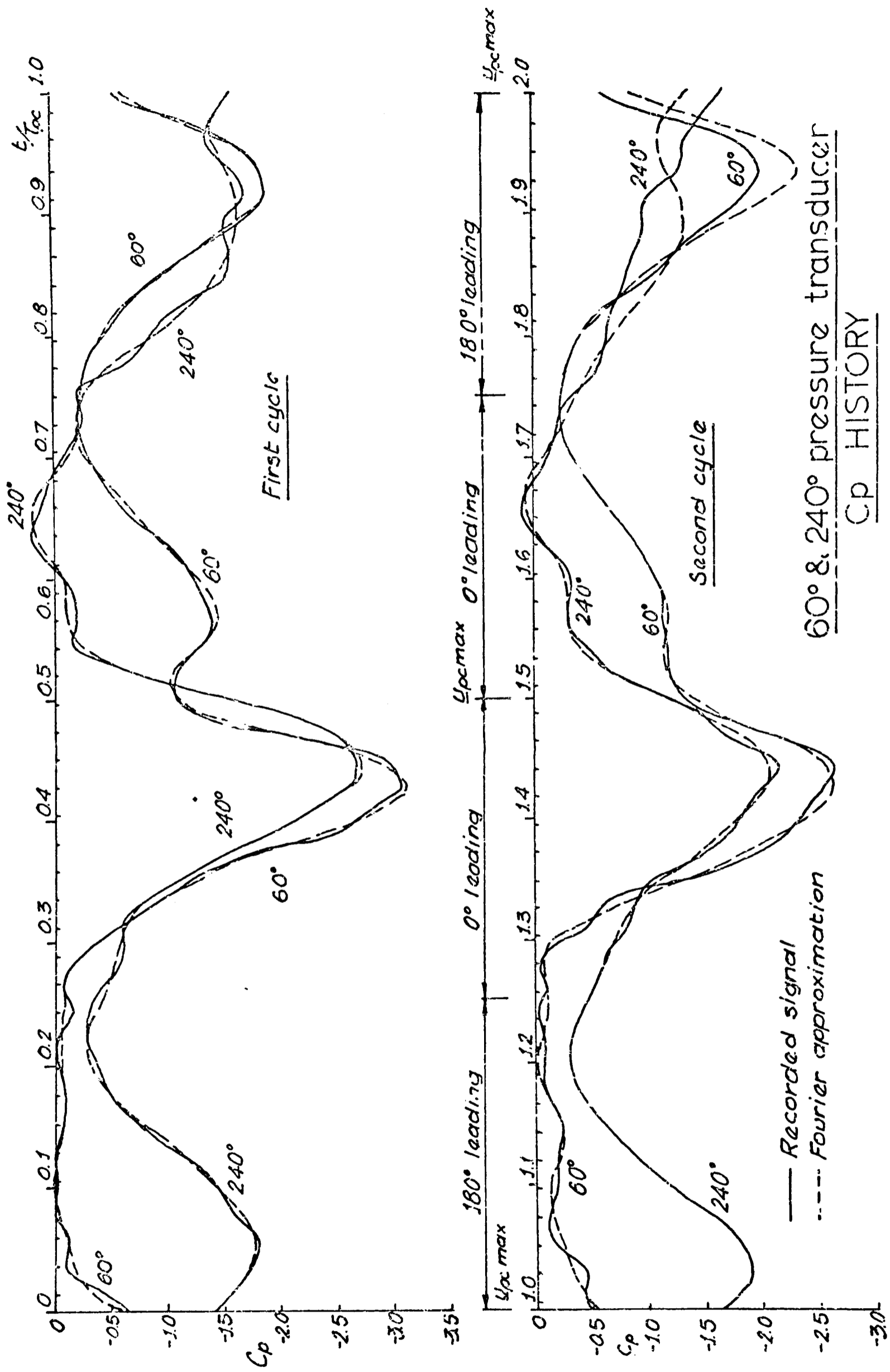


FIGURE (410d)

45° & 225° pressure transducer
Cp HISTORY



60° & 240° pressure transducer
 Cp HISTORY

FIGURE (4.10e)

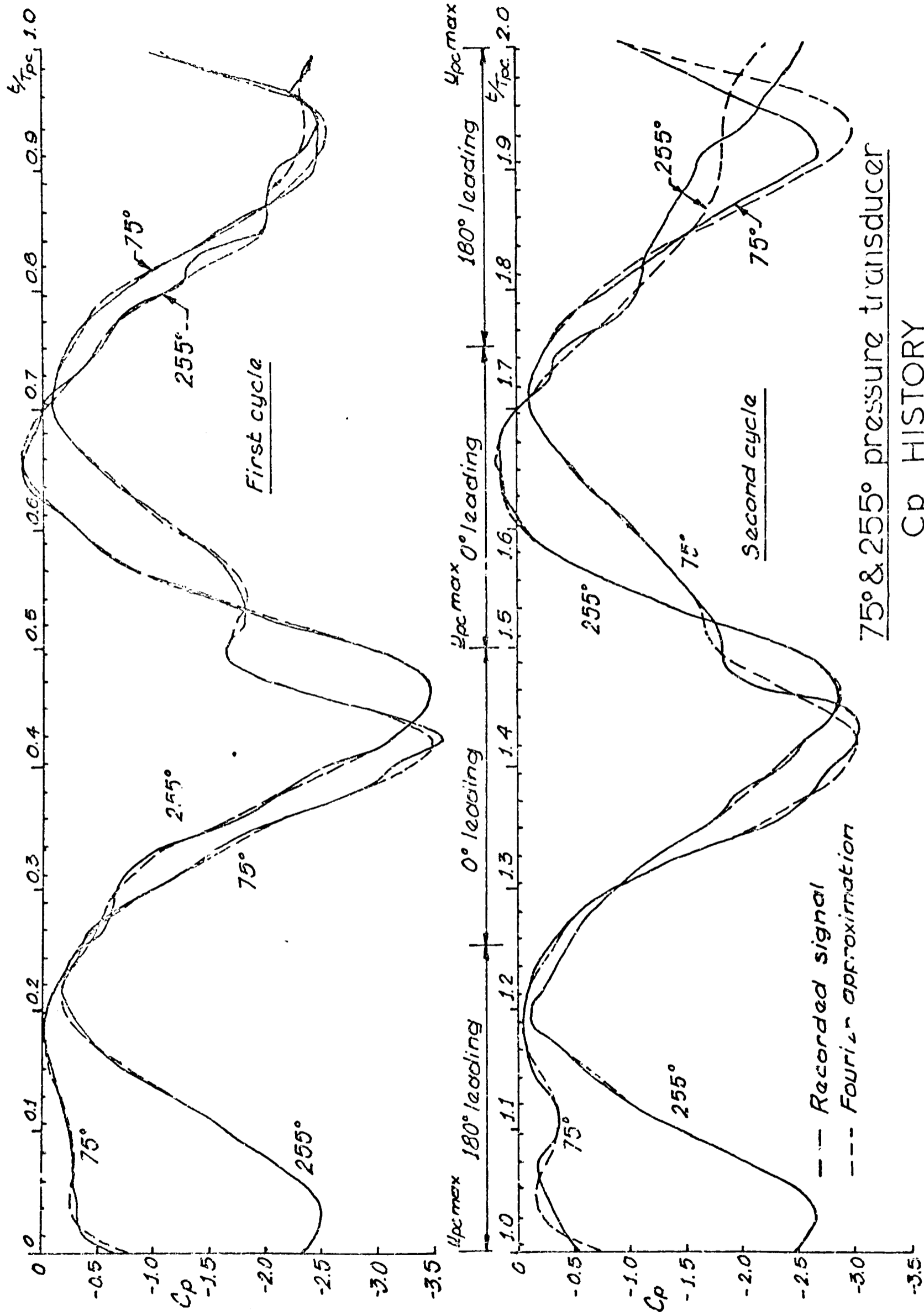


FIGURE (4.10f)

75° & 255° pressure transducer
Cp HISTORY

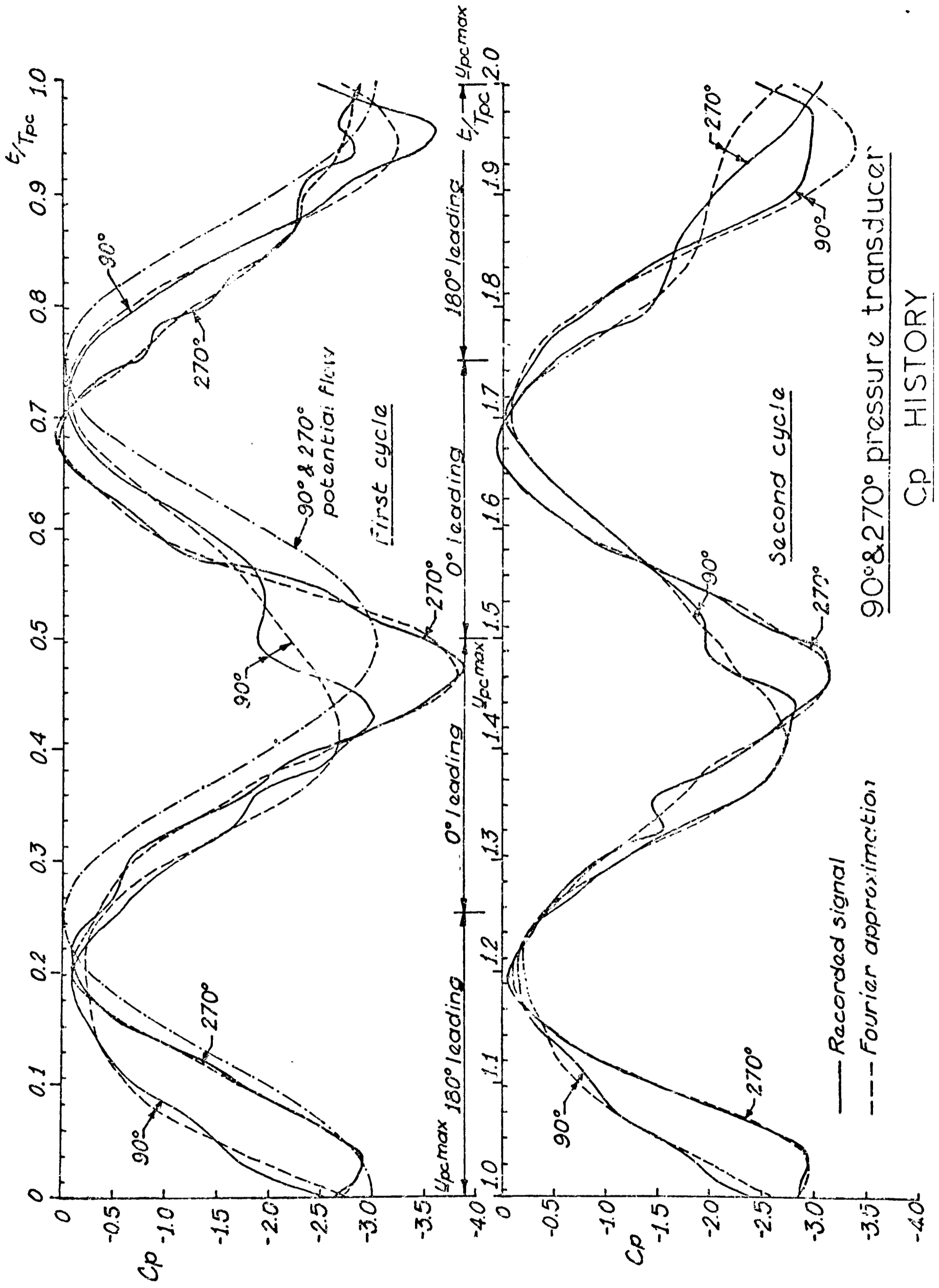
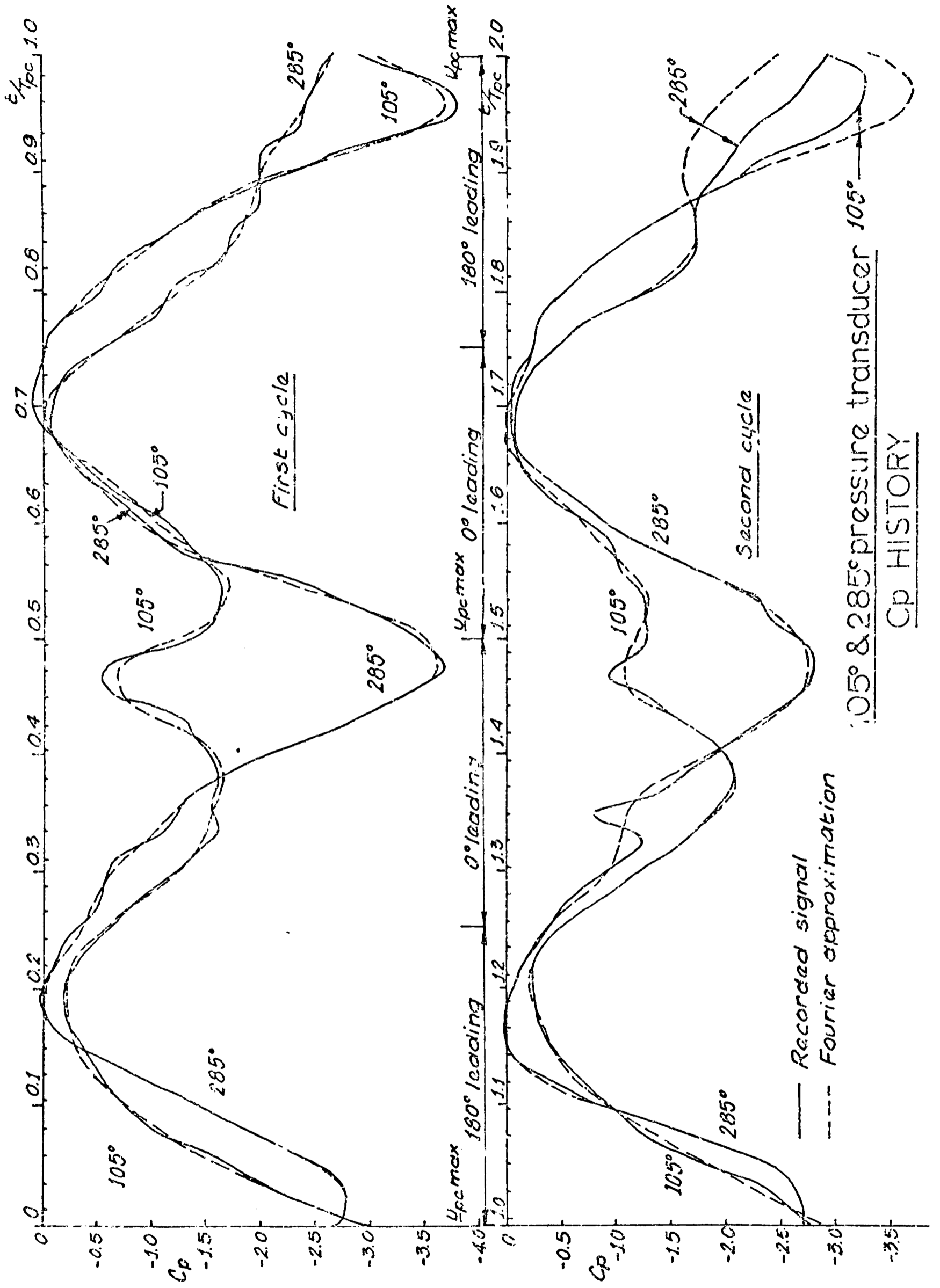


FIGURE (4.10g)

90° & 270° pressure transducer

Cp HISTORY



105° & 285° pressure transducer 105°
Cp HISTORY

FIGURE (4.10h)

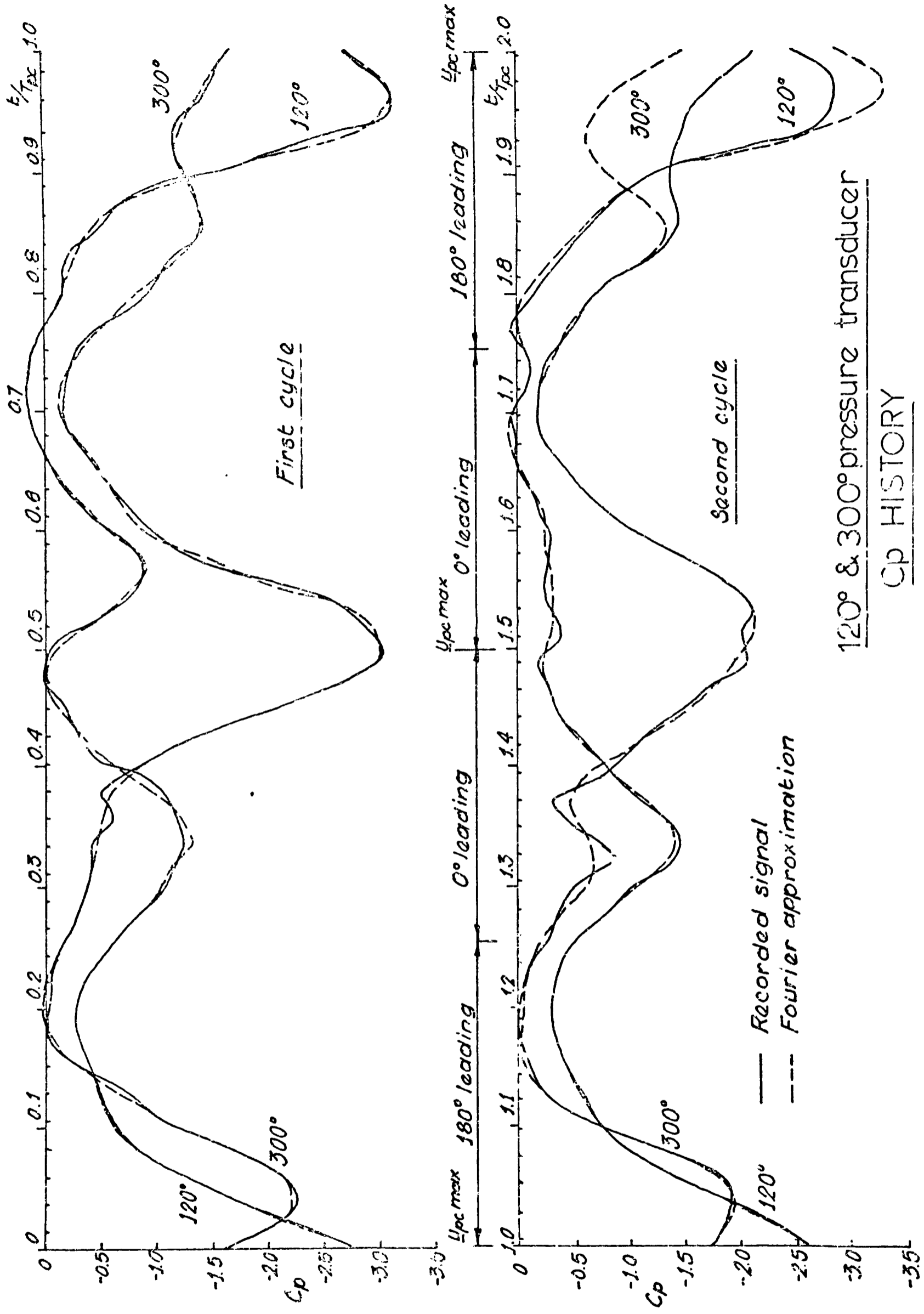


FIGURE (4.10i)

120° & 300° pressure transducer
Cp HISTORY

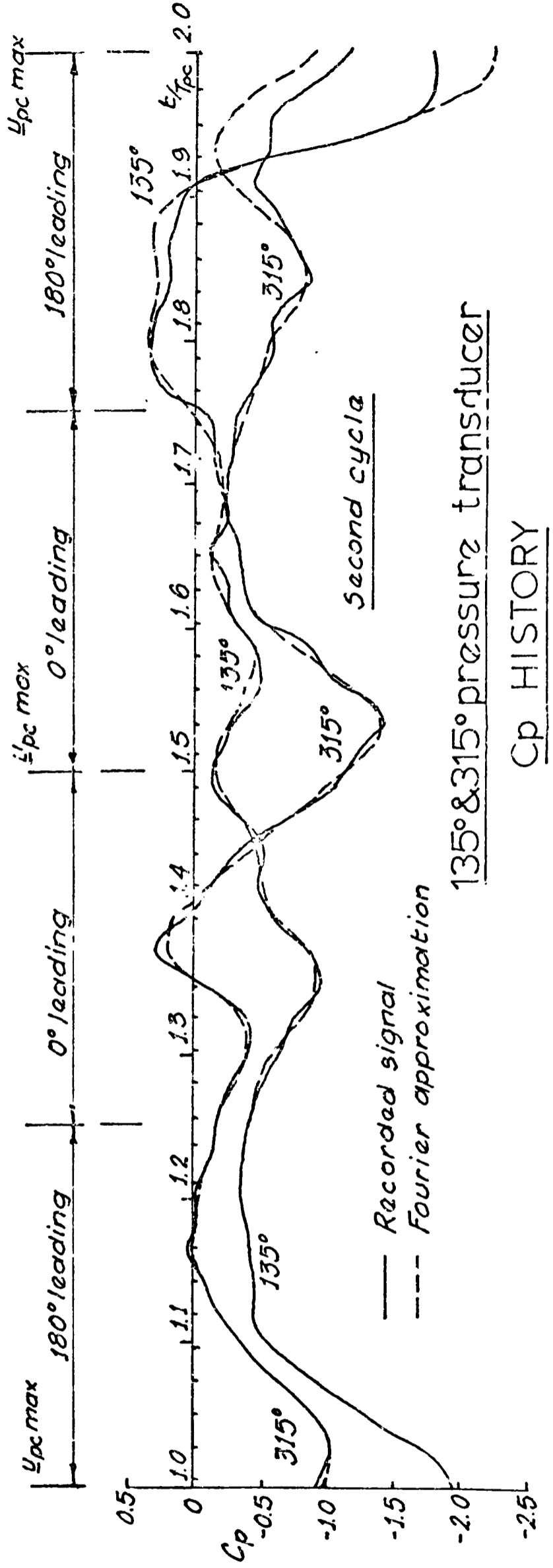
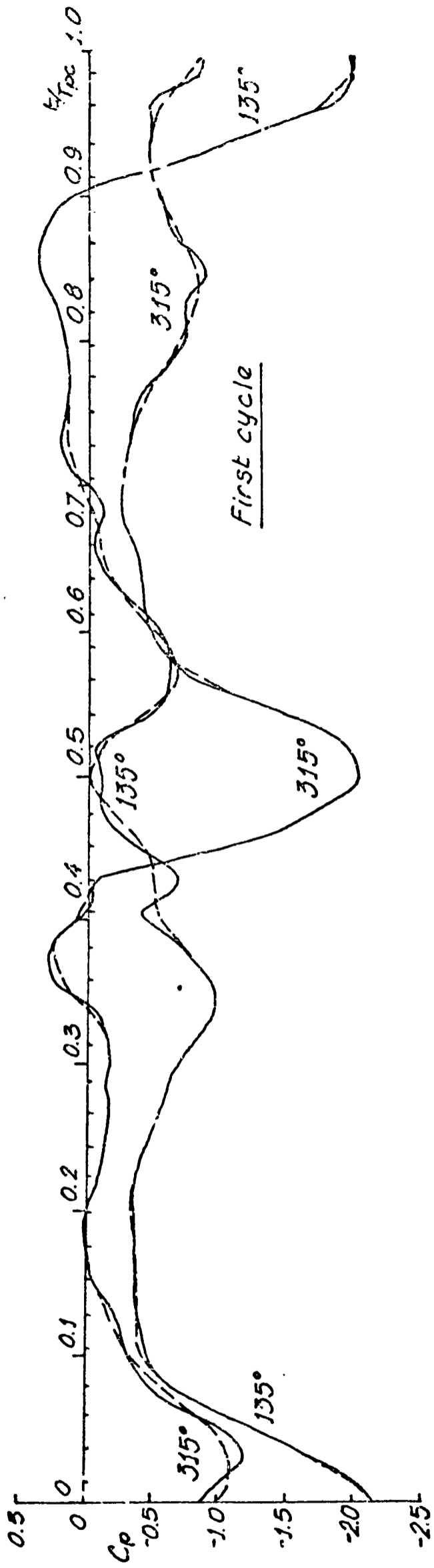
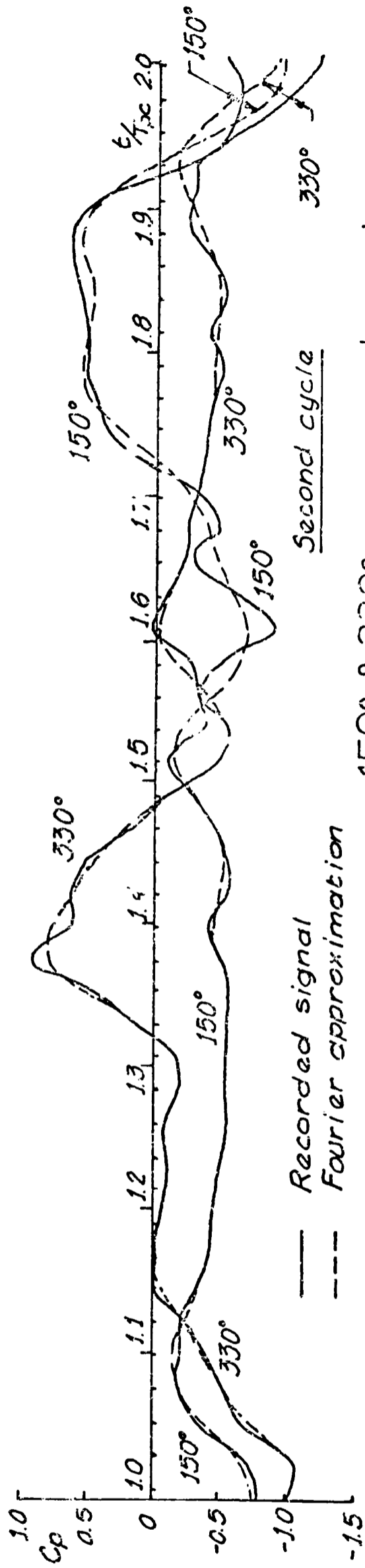
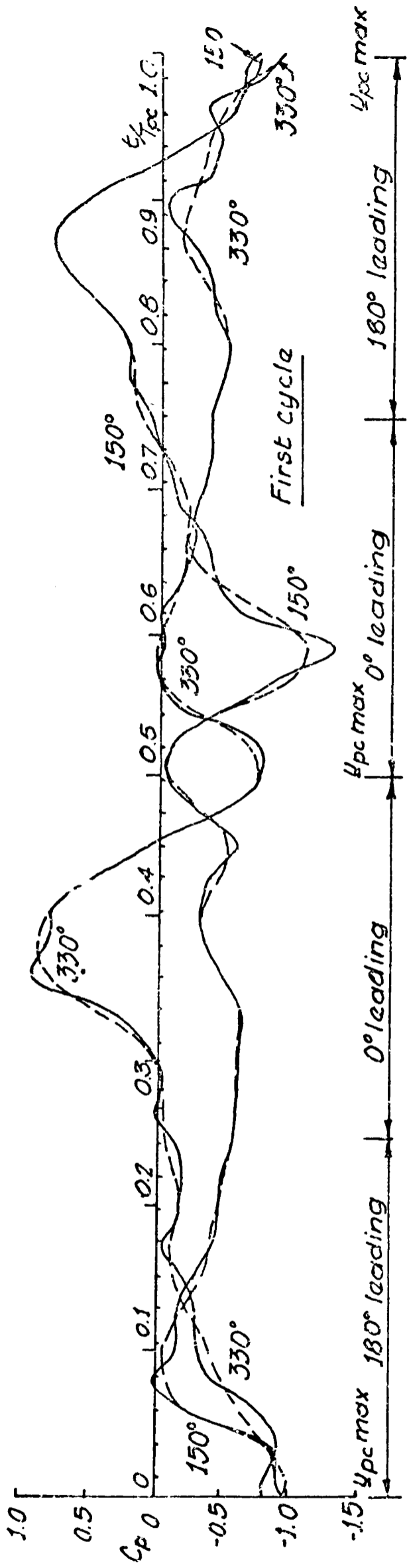


FIGURE (4.10j)

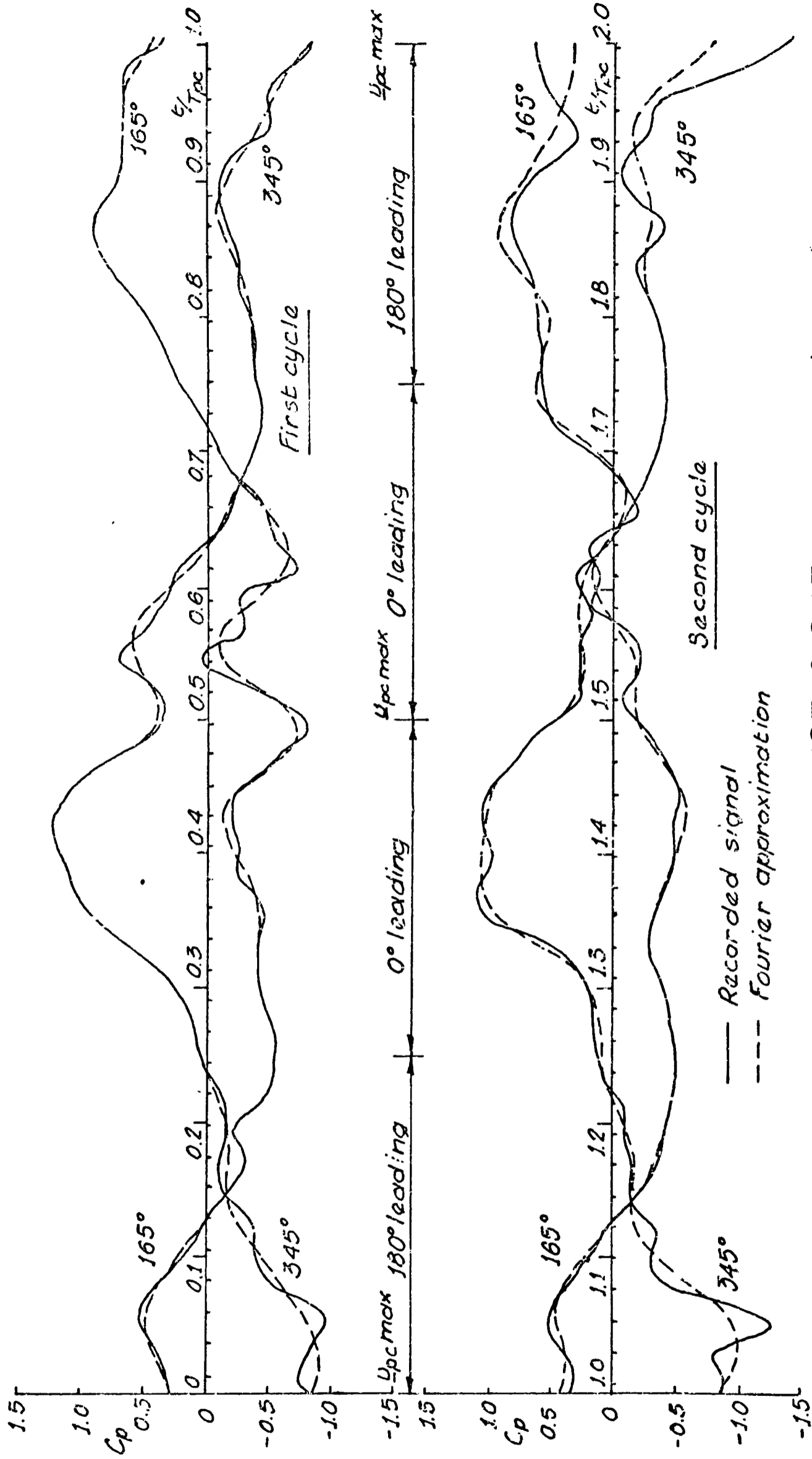
135° & 315° pressure transducer

Cp HISTORY



150° & 330° pressure transducer
Cp HISTORY

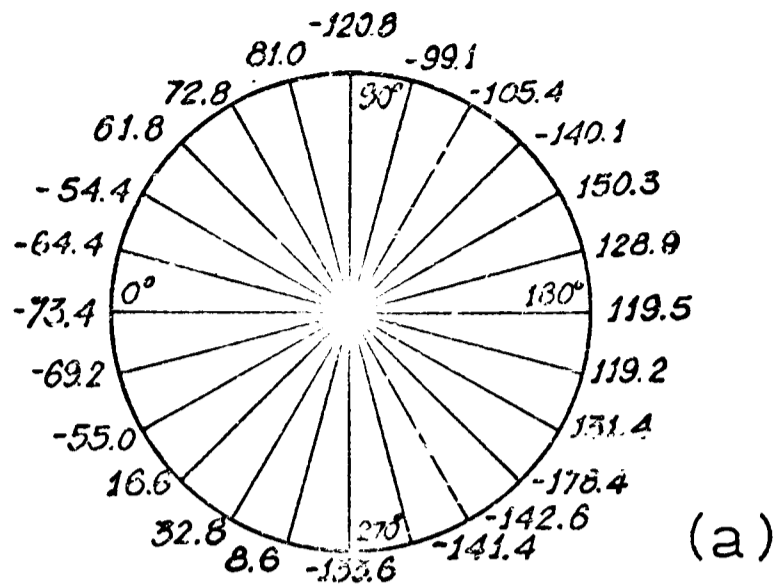
FIGURE (4.10k)



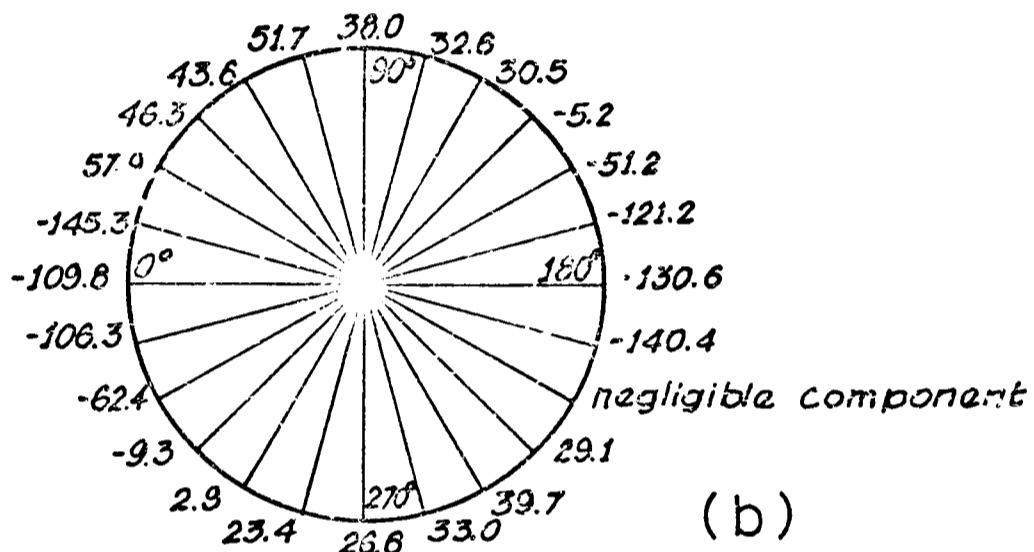
165° & 345° pressure transducer

Cp HISTORY

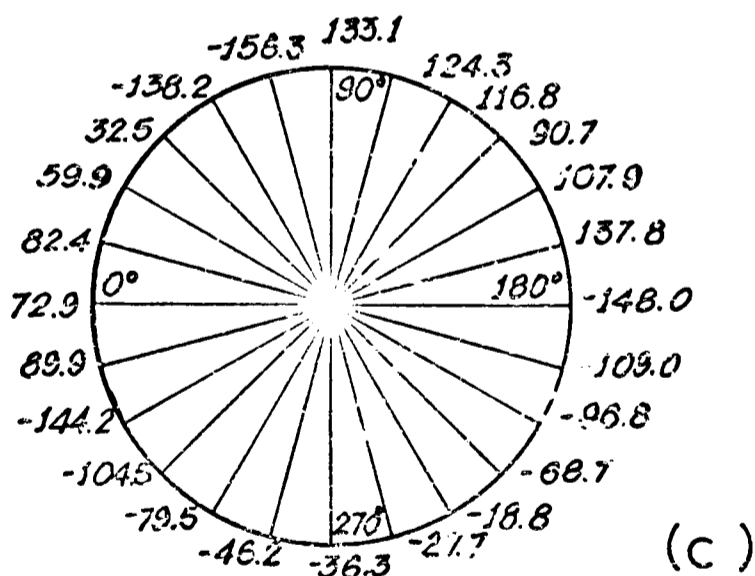
FIGURE (4.10 l)



(a)
1st Harmonic
(Relative to displacement transducer)



(b)
2nd Harmonic
(Relative to displacement transducer²)



(c)
3rd Harmonic
(Relative to displacement transducer³)

All phase angles in degrees adjusted in the range $\pm 180^\circ$

RELATIVE PHASES OF Cp 1st, 2nd & 3rd HARMONICS

FIGURE (4.11)

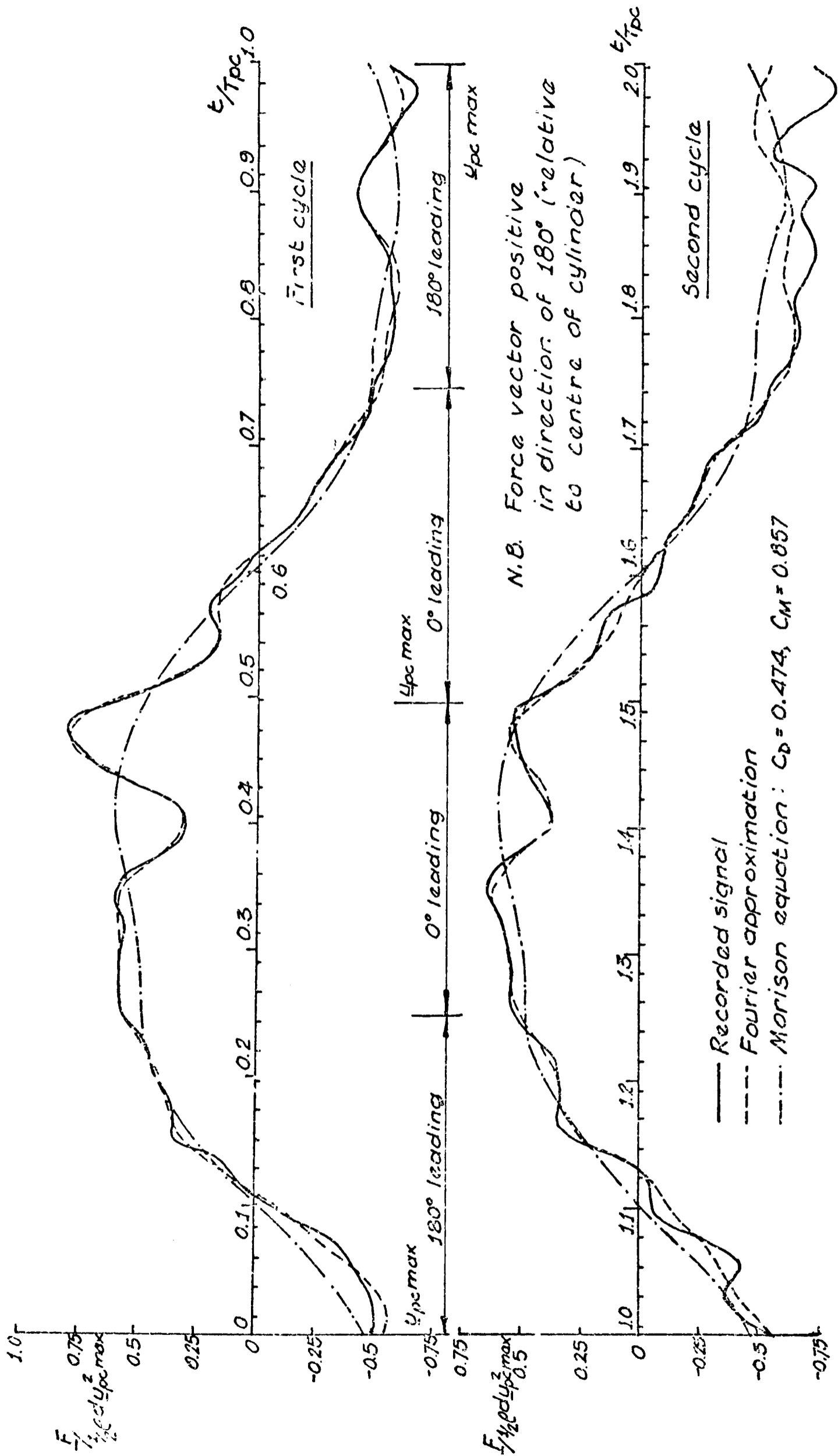
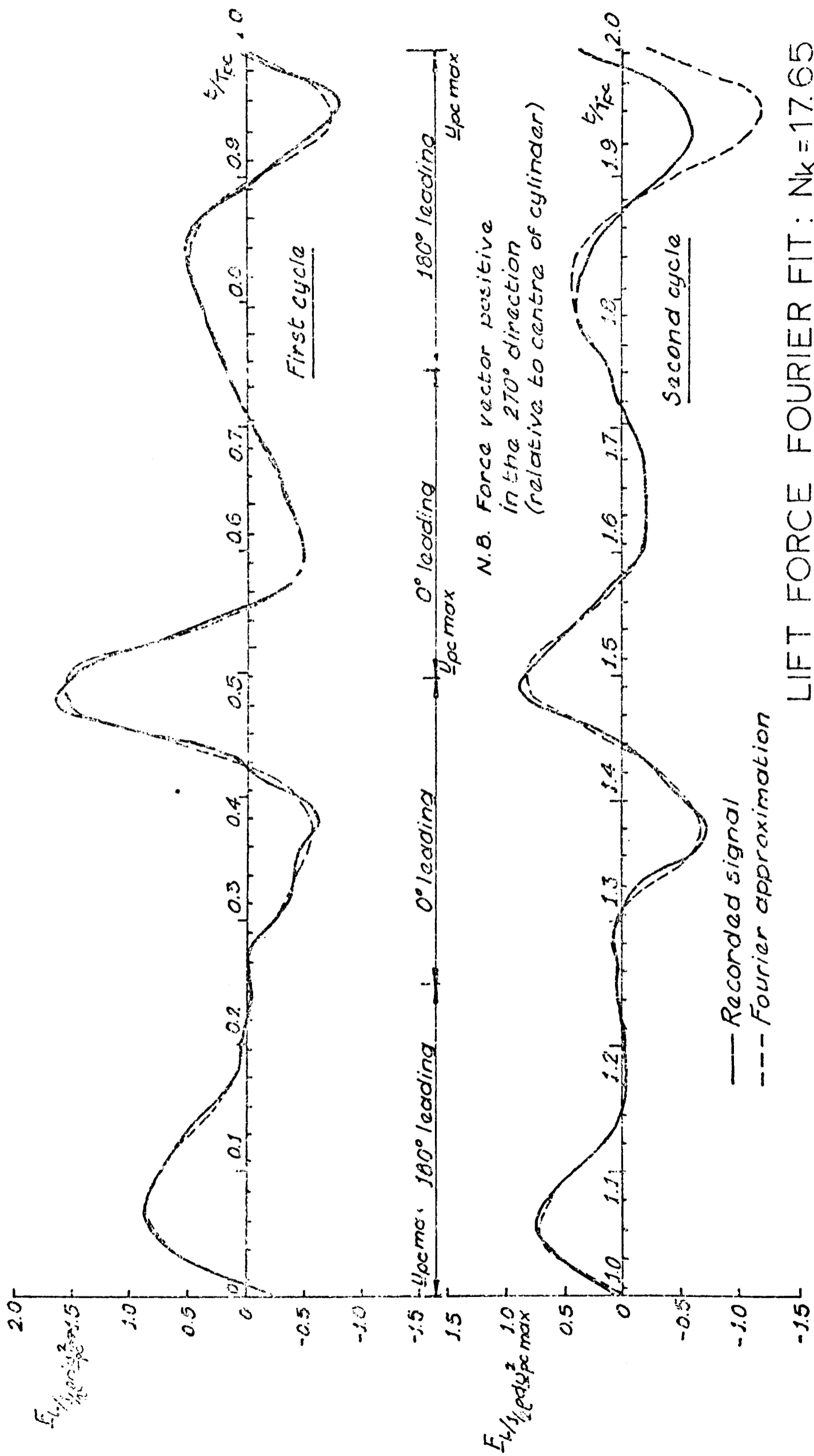


FIGURE (4.12)

IN-LINE FORCE FOURIER & MORISON
 EQUATION FIT: $N_k = 17.65$



N.B. Force vector positive in the 270° direction (relative to centre of cylinder)

LIFT FORCE FOURIER FIT: $N_k = 17.65$

FIGURE (4.13)

- Notes:
1. C_p origin cylinder surface.
 2. 1 dimensionless force unit = 2 cm

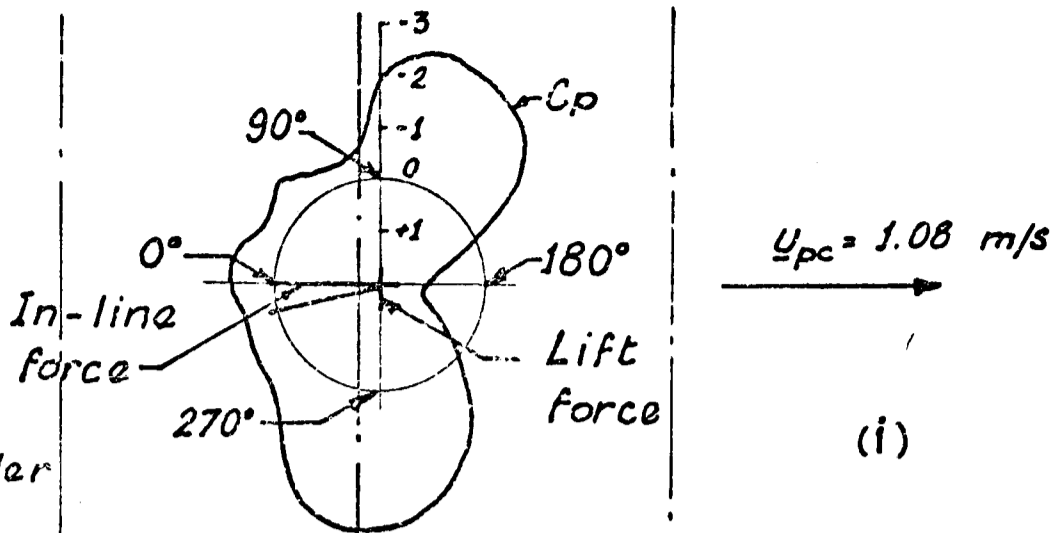
$t/T_{pc} = 0.02$

$t/T_{pc} = 0.08$

$t/T_{pc} = 0.18$

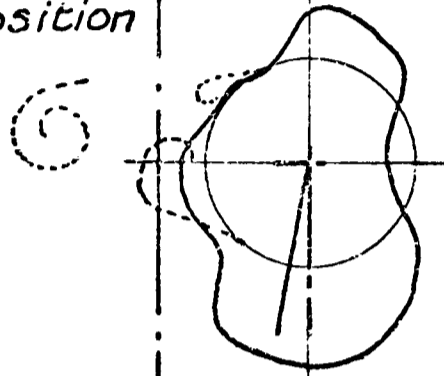
$t/T_{pc} = 0.24$

$t/T_{pc} = 0.34$



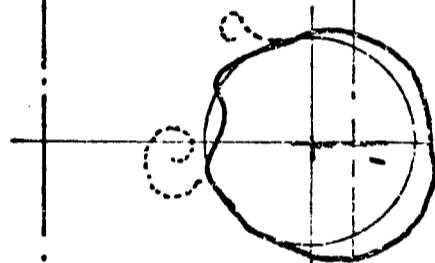
(i)

Mean position

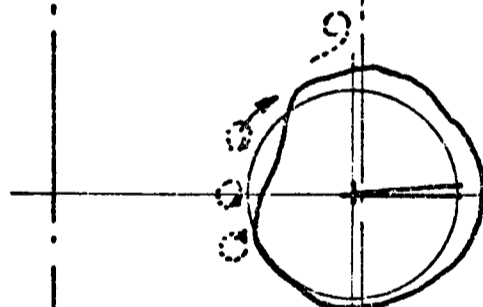


(ii)

A_{pc} A_{pc}

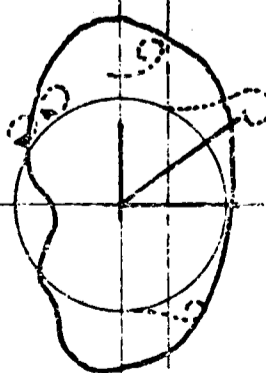
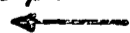


(iii)



(iv)

$U_{pc} = 0.57$ m/s

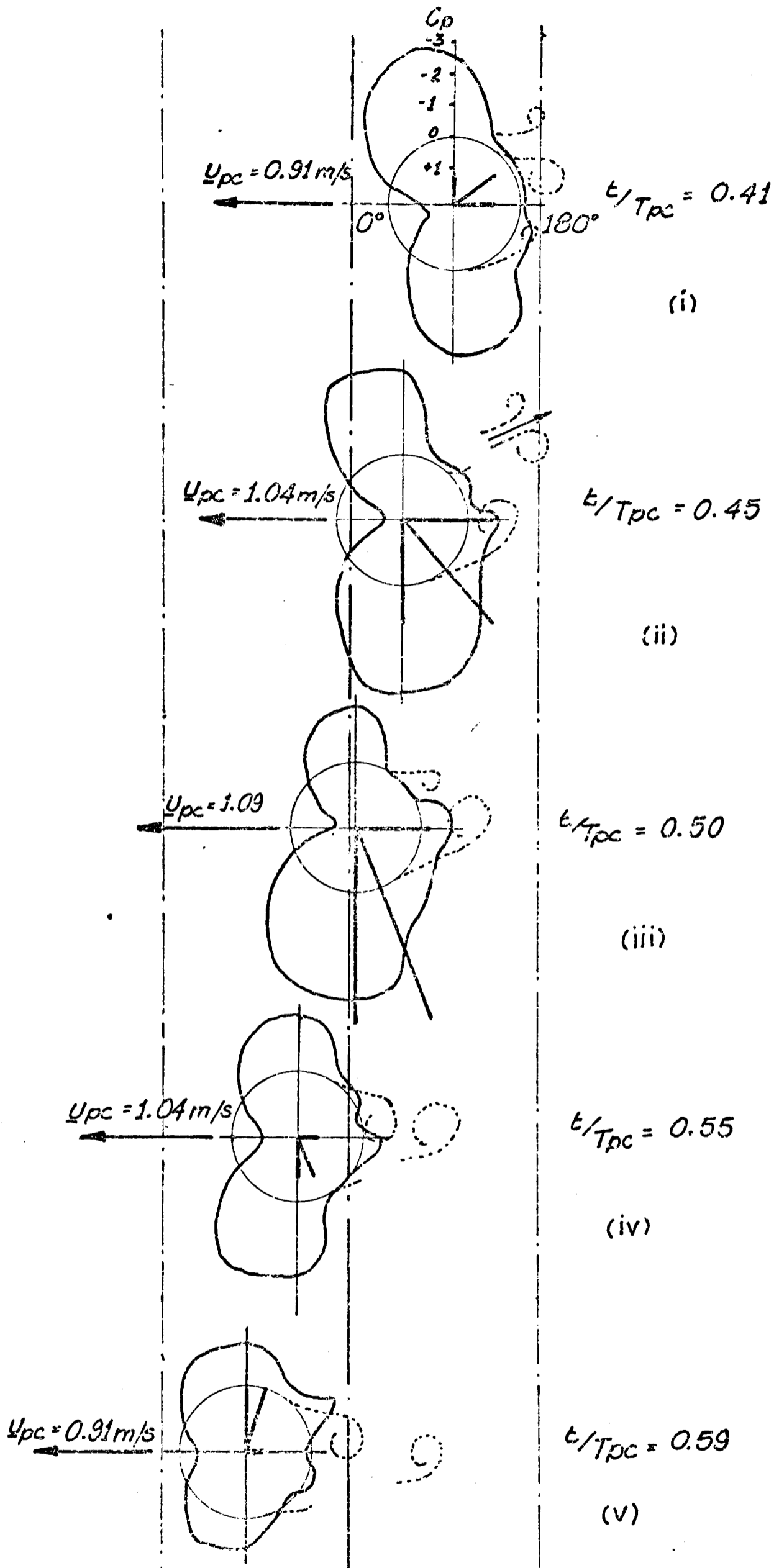


(v)

INSTANTANEOUS C_p DISTRIBUTION

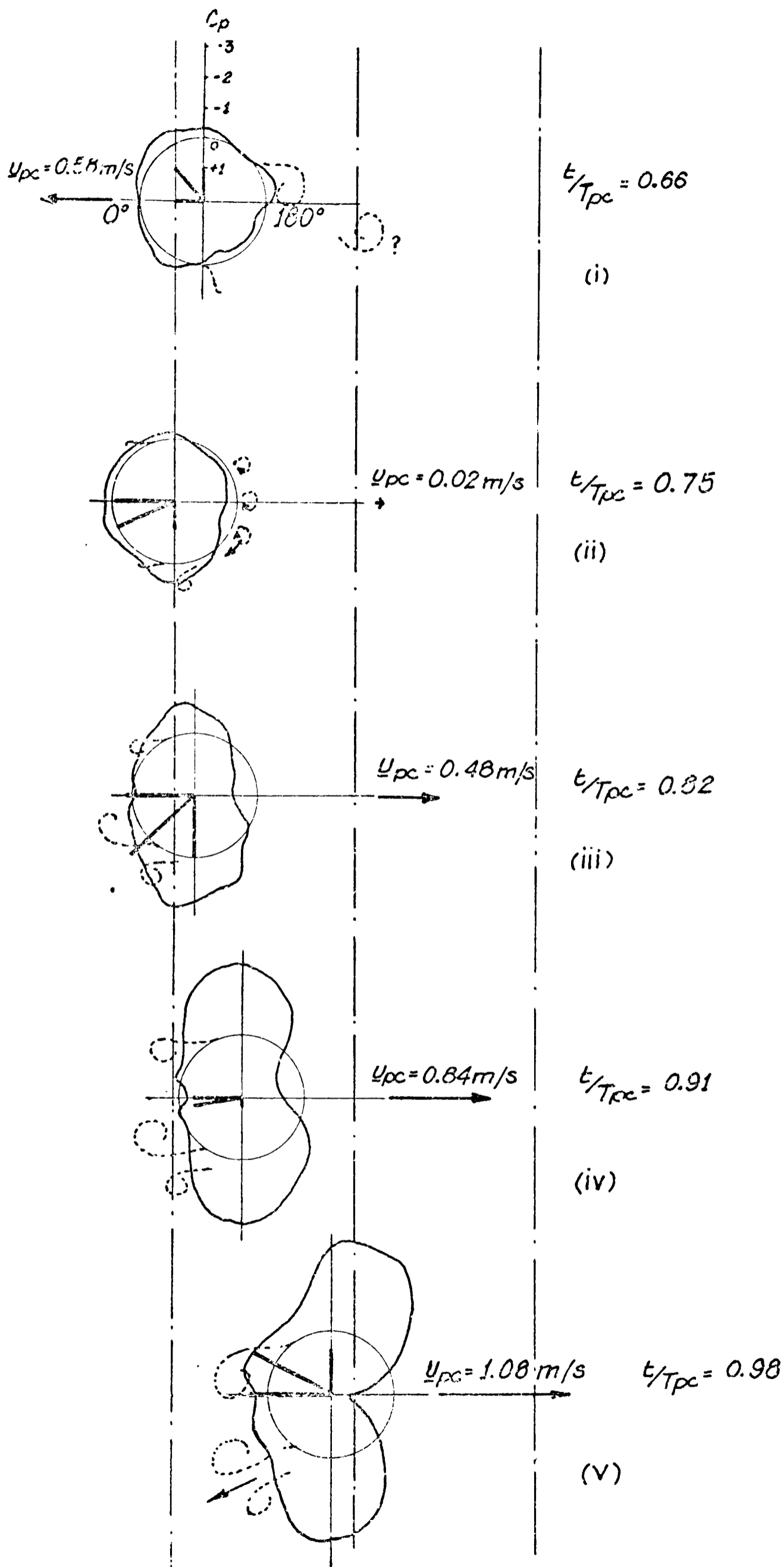
$N_k = 17.65$ - FIRST CYCLE

FIGURE (4.14a)



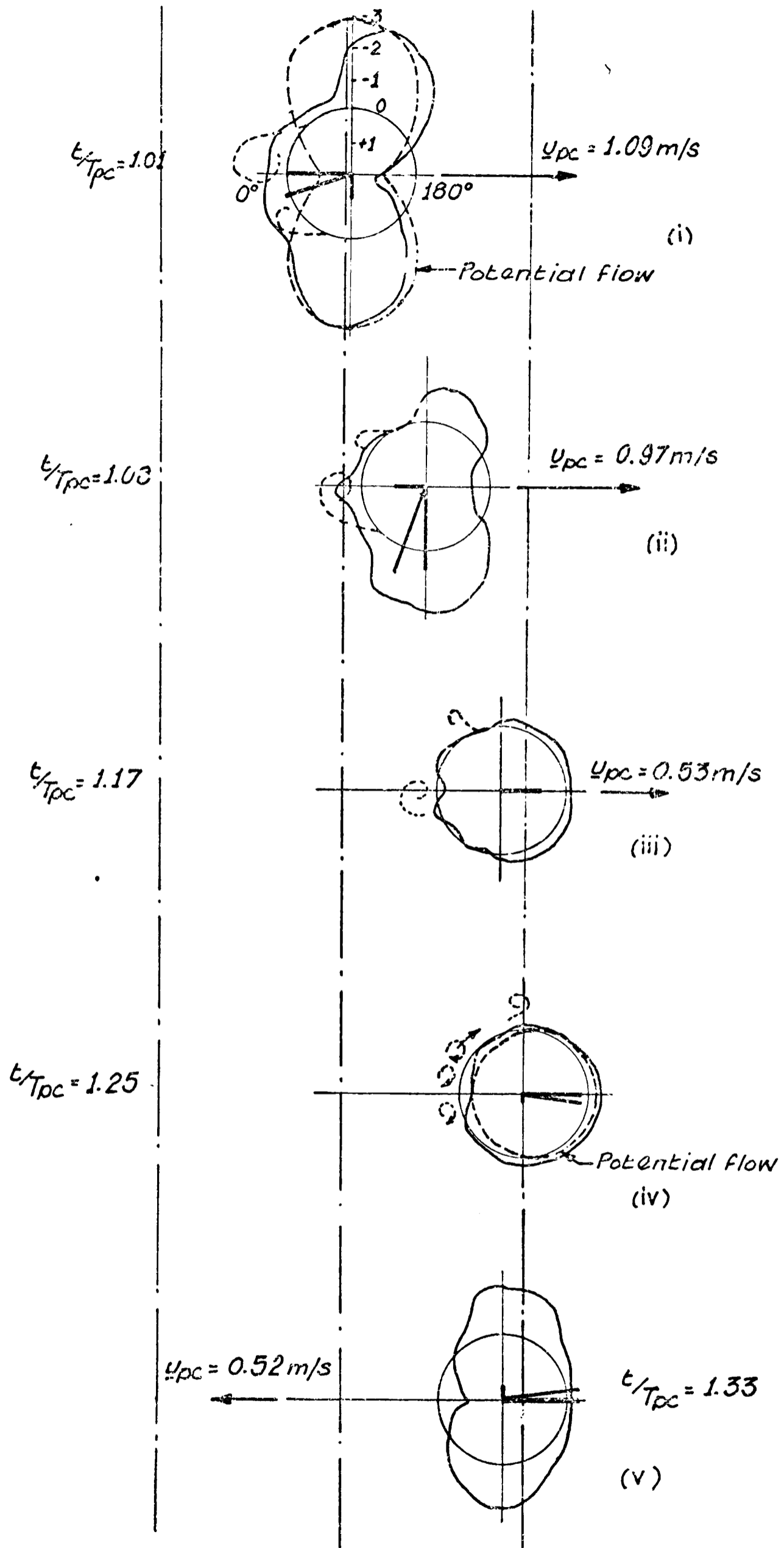
INSTANTANEOUS C_p DISTRIBUTION
 $N_k = 17.65$ - FIRST CYCLE

FIGURE (4.14b)



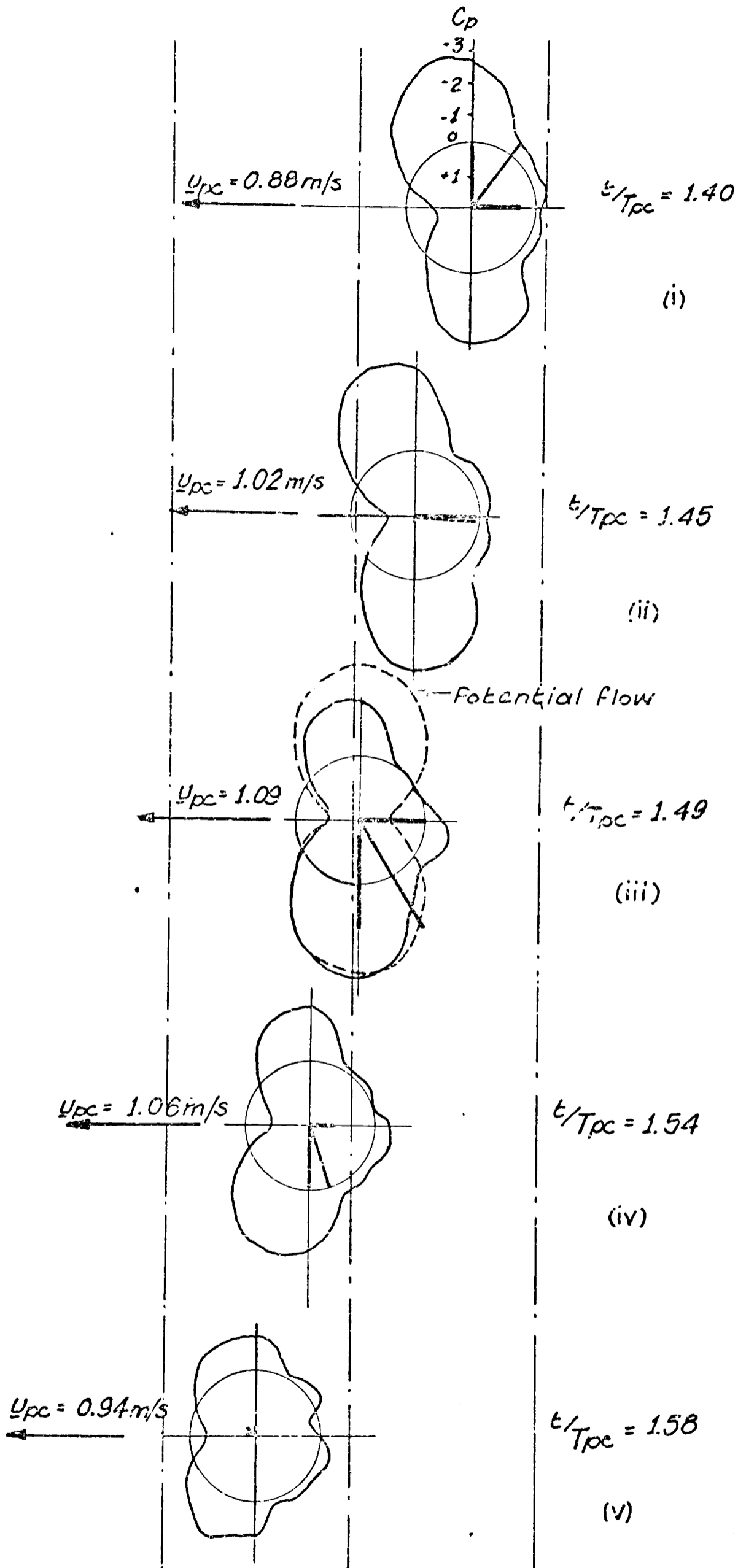
INSTANTANEOUS C_p DISTRIBUTION
 $N_c = 17.65$ - FIRST CYCLE

FIGURE 4.14c



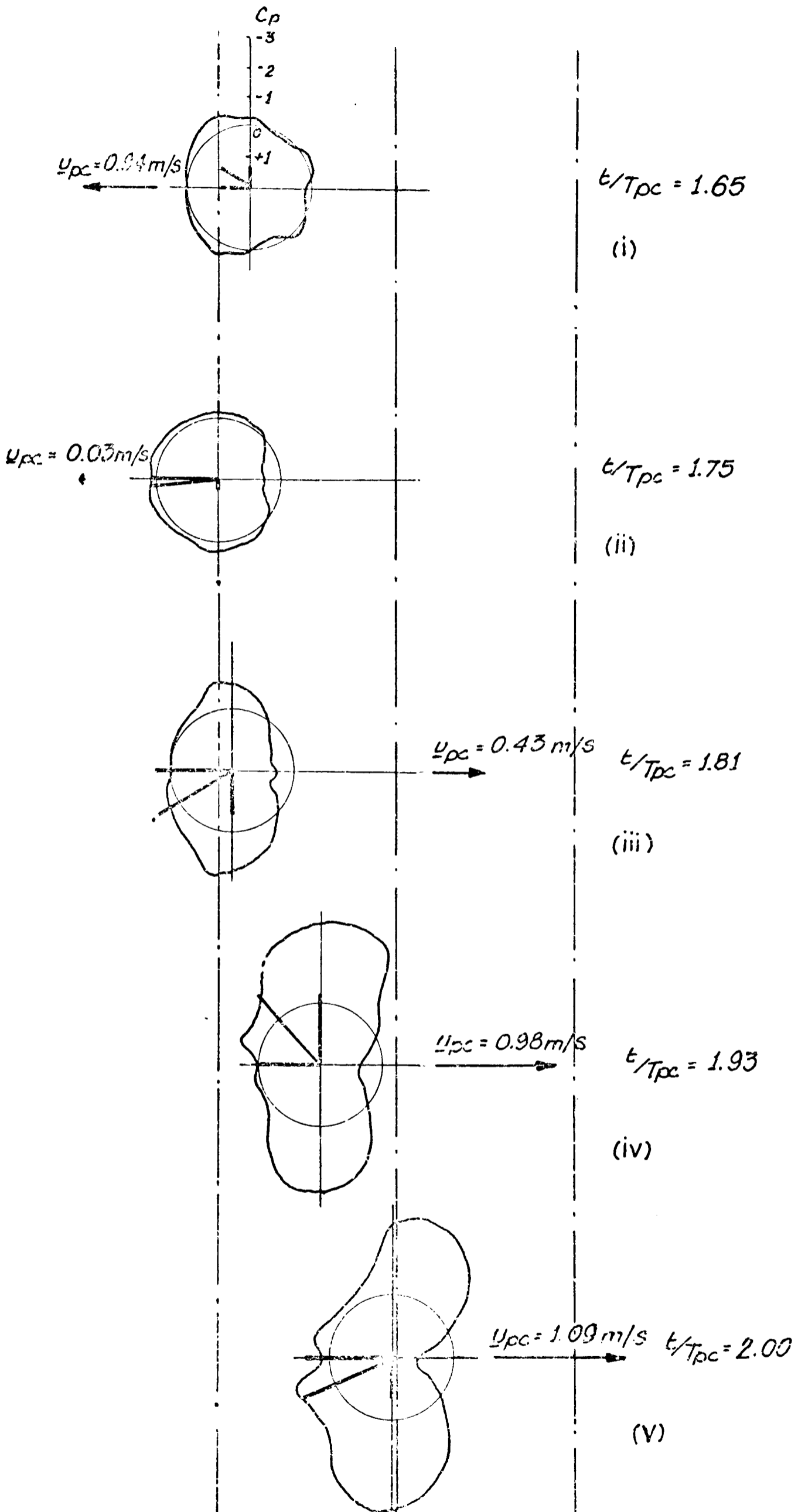
INSTANTANEOUS C_p DISTRIBUTION
 $N_k = 17.65$ - SECOND CYCLE

FIGURE (4.15a)



INSTANTANEOUS C_p DISTRIBUTION
 $N_k = 17.65$ - SECOND CYCLE

FIGURE (4.15b)



INSTANTANEOUS C_p DISTRIBUTION
 $N_k = 1765$ - SECOND CYCLE

FIGURE (4.15c)

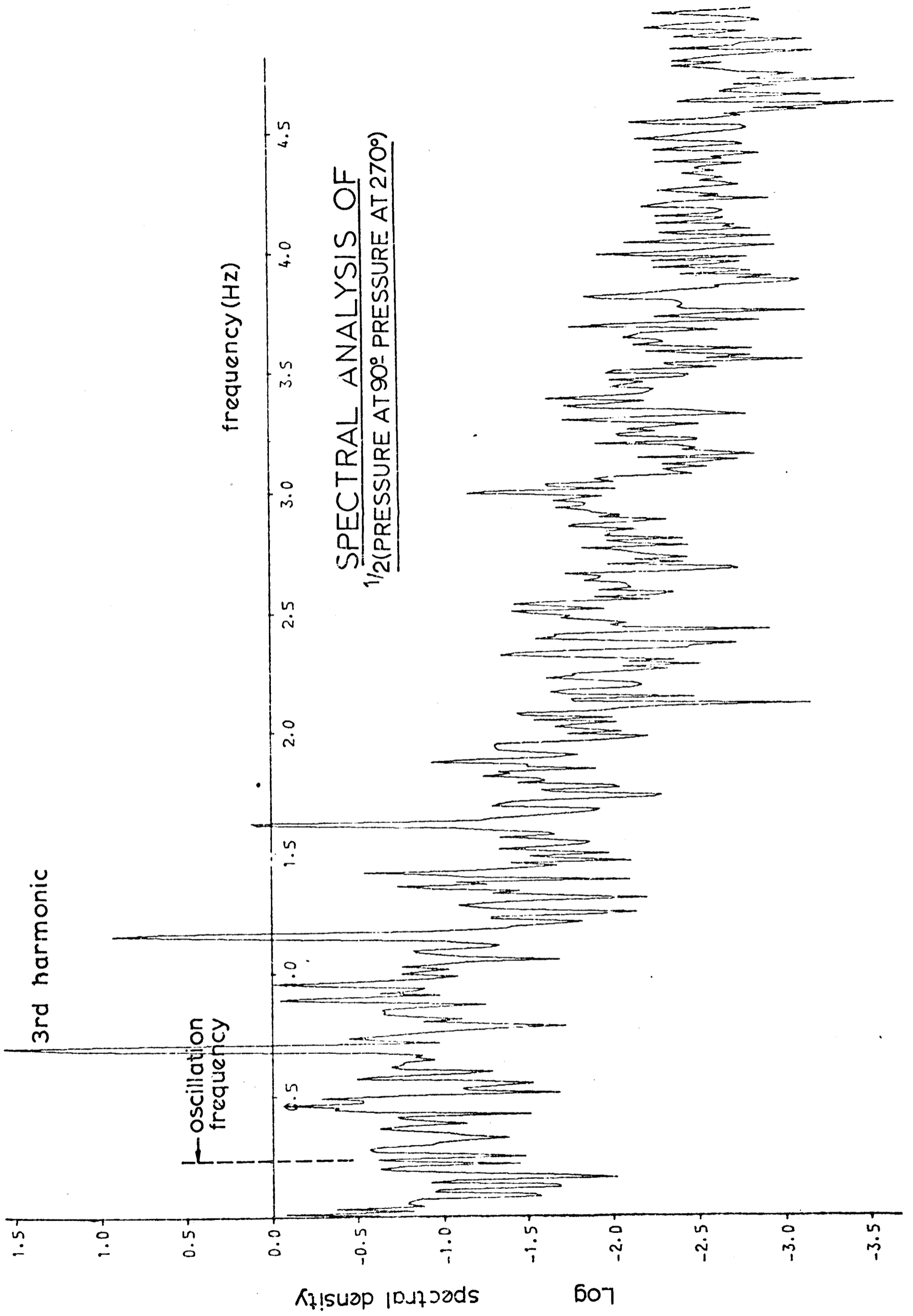


FIGURE (4.16)

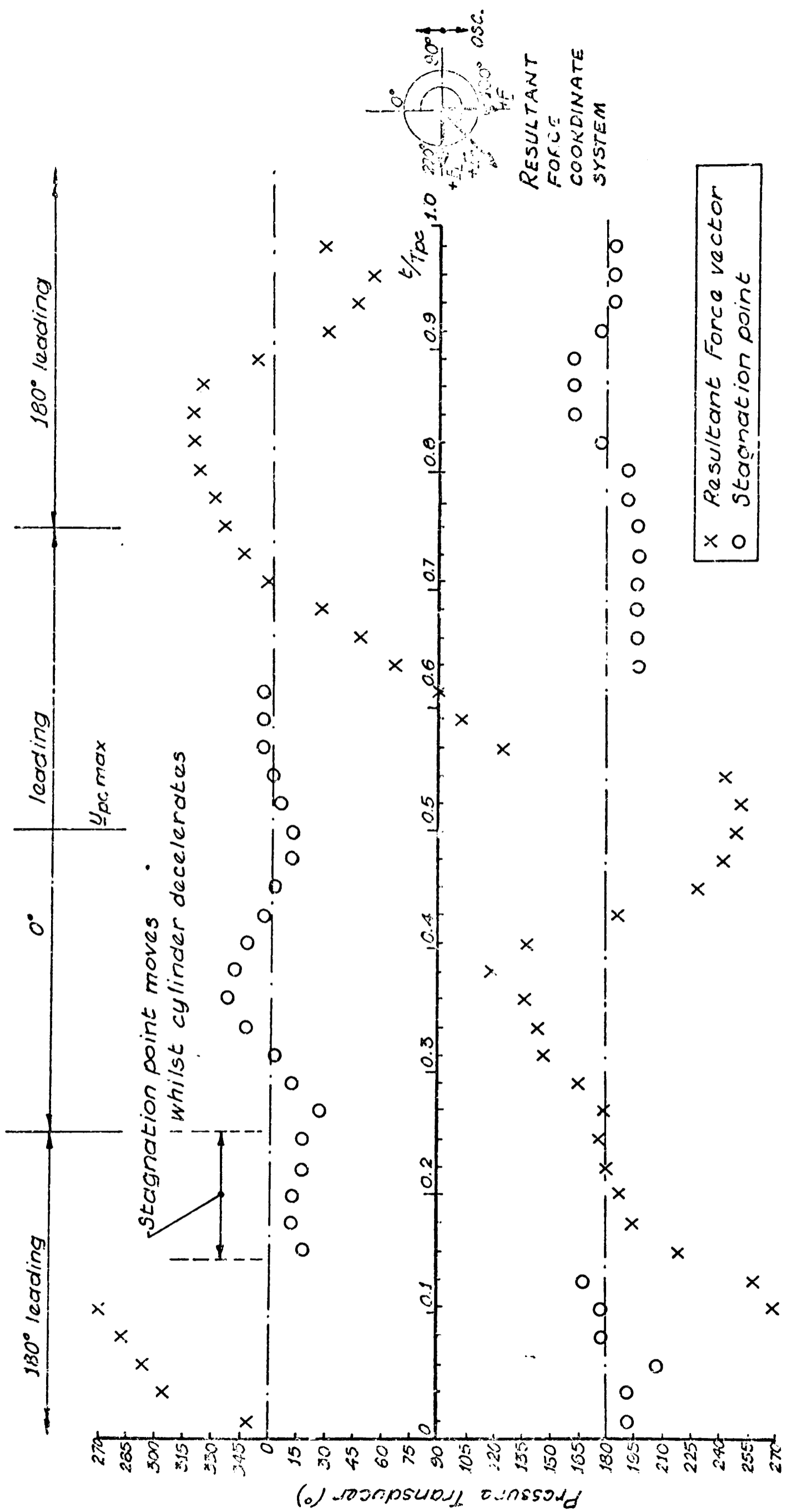


FIGURE (417a)

MOVEMENT OF STAGNATION POINT AND DIRECTION OF RESULTANT FORCE DURING THE FIRST COMPLETE CYCLE

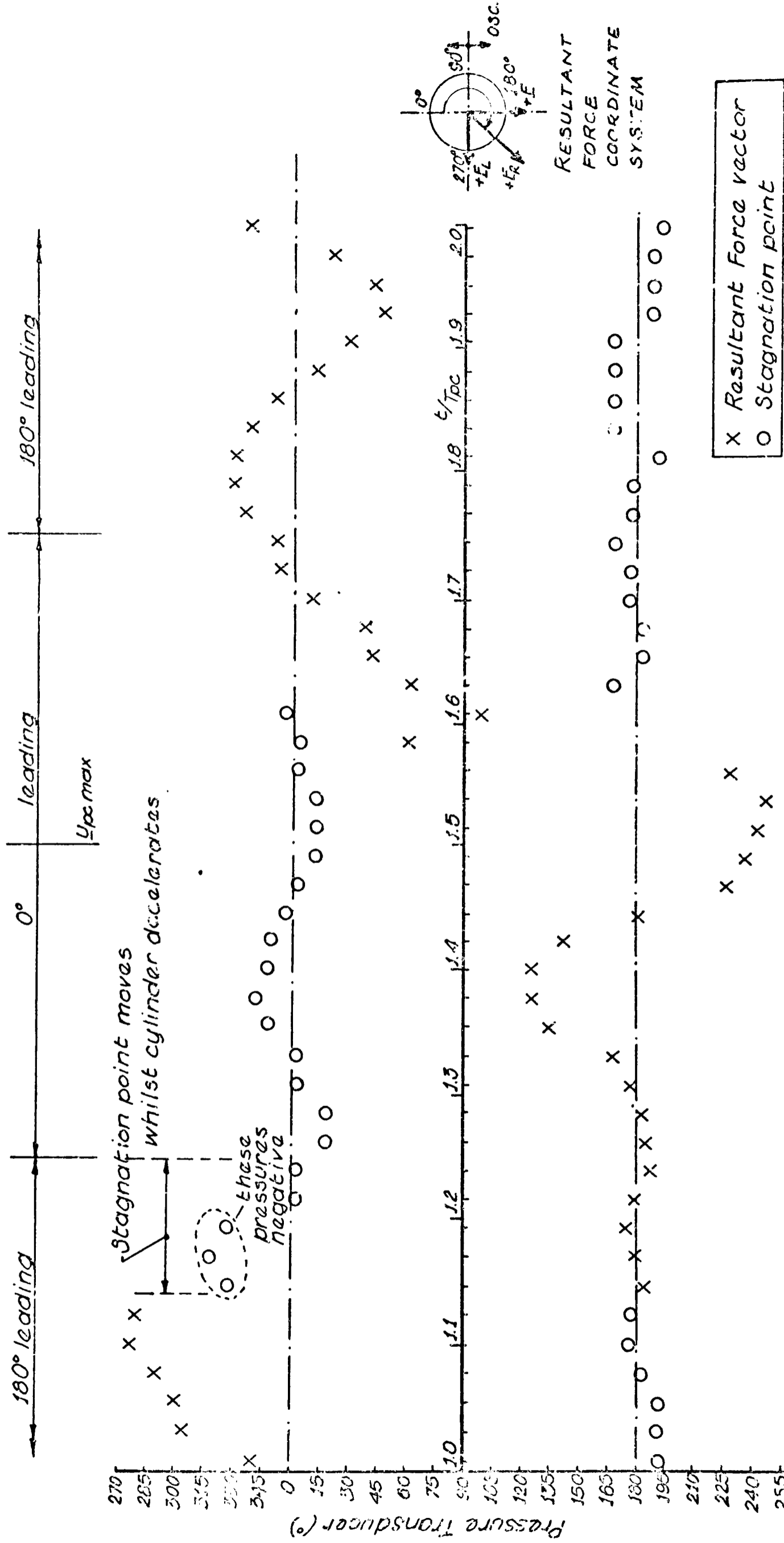
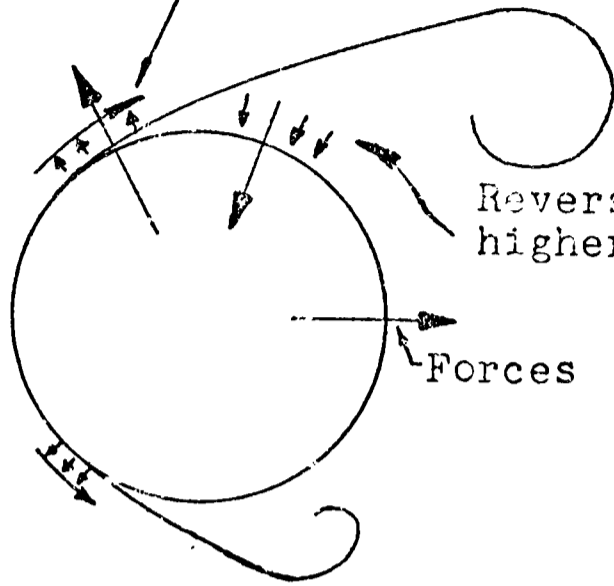


FIGURE (4.17b)

MOVEMENT OF STAGNATION POINT AND DIRECTION OF RESULTANT FORCE DURING THE SECOND COMPLETE CYCLE

Circulation - creates low pressure



Combination of effects results in lift force in either direction

Reverse flow - creates higher pressure

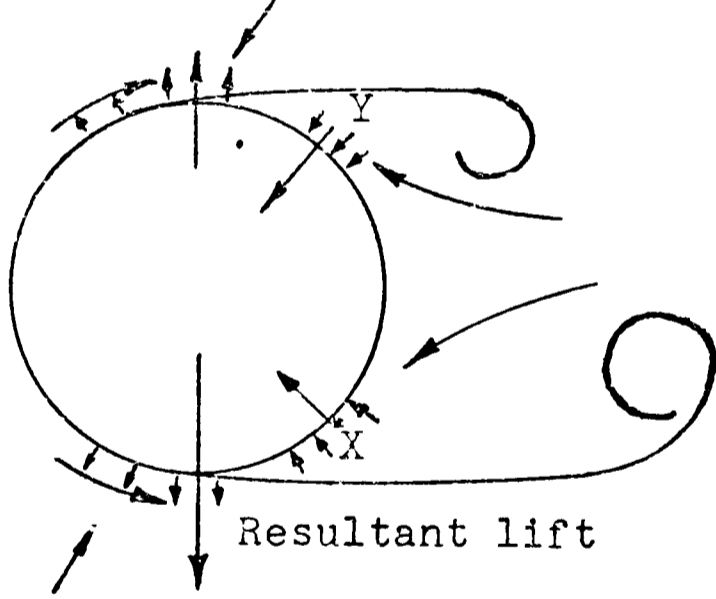
Forces

As the largest vortex is shed the pressure increases on that side as the circulation reverses

LOW RE

(a)

Smallest circulation - low pressure



Increased pressure at Y due to the proximity of the smaller developing vortex. The increased pressure at the point X is smaller because the larger vortex is further from the cylinder; this higher pressure is also farther back on the cylinder influencing the lift force less. The resultant lift is therefore toward the largest vortex. As the vortex is shed the effects reverse.

Largest circulation - lowest pressure

HIGH RE

(b)

POSSIBLE LIFT FORCE MECHANISM

FIGURE (4.18)

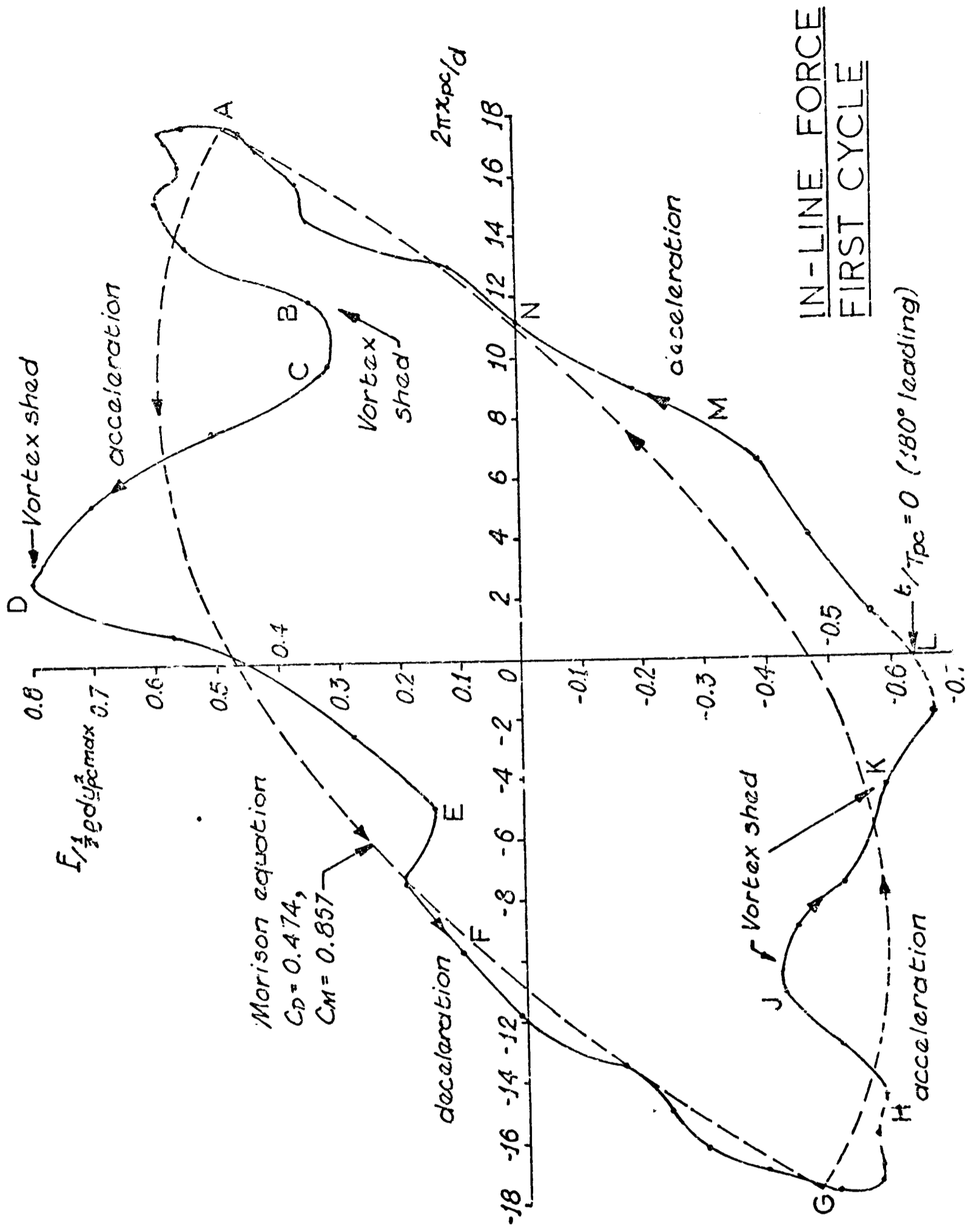
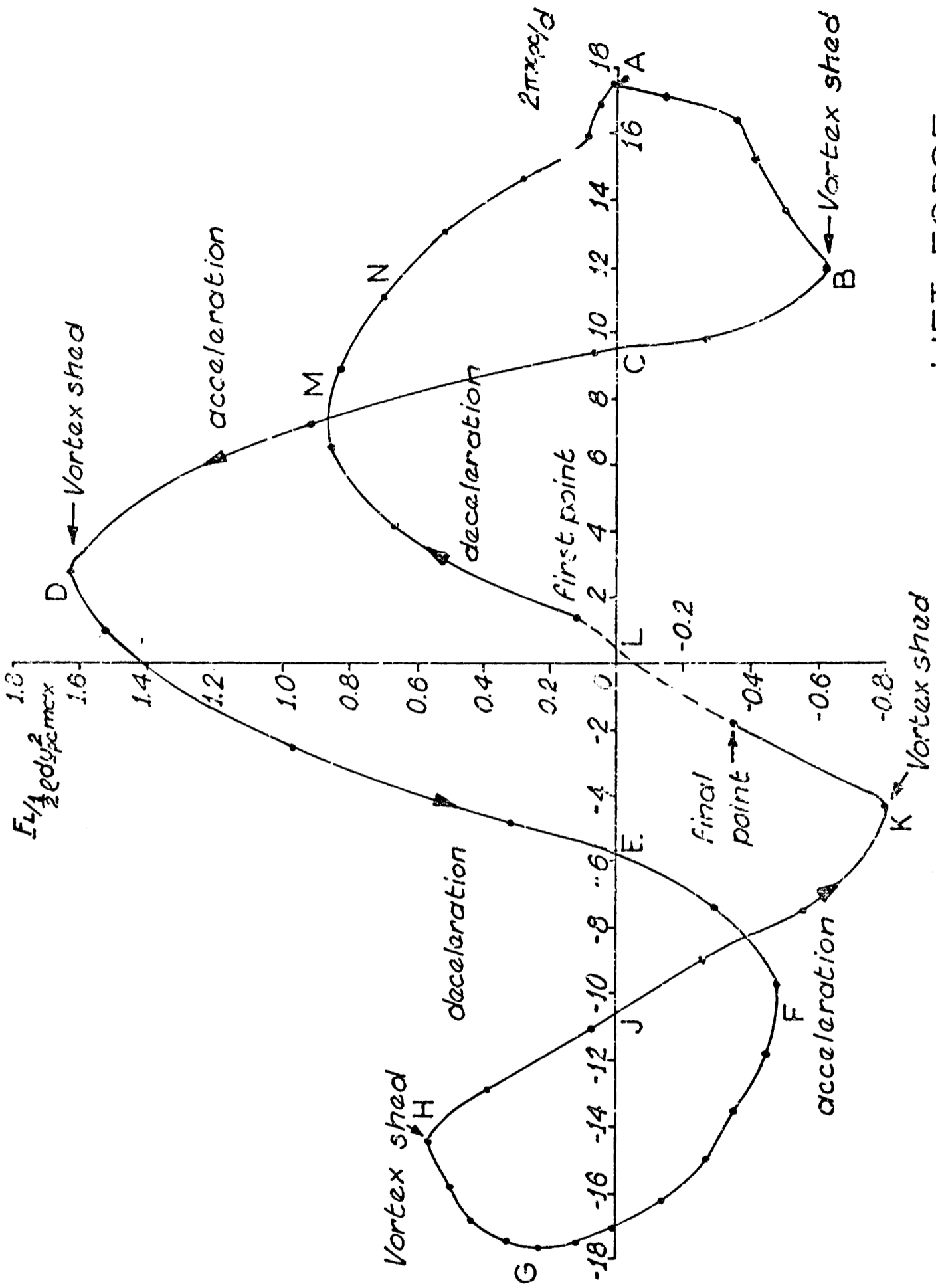
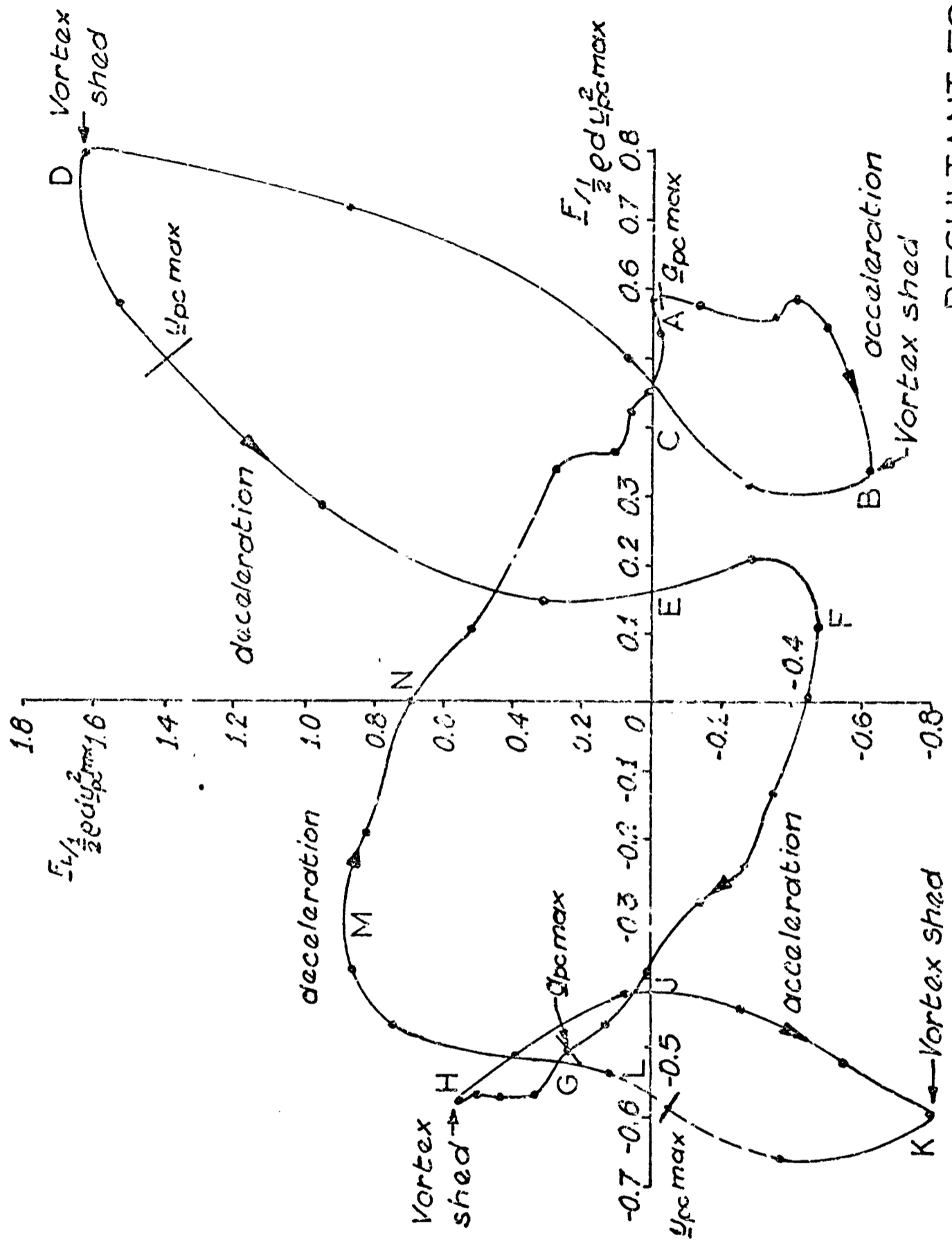


FIGURE (4.19a)



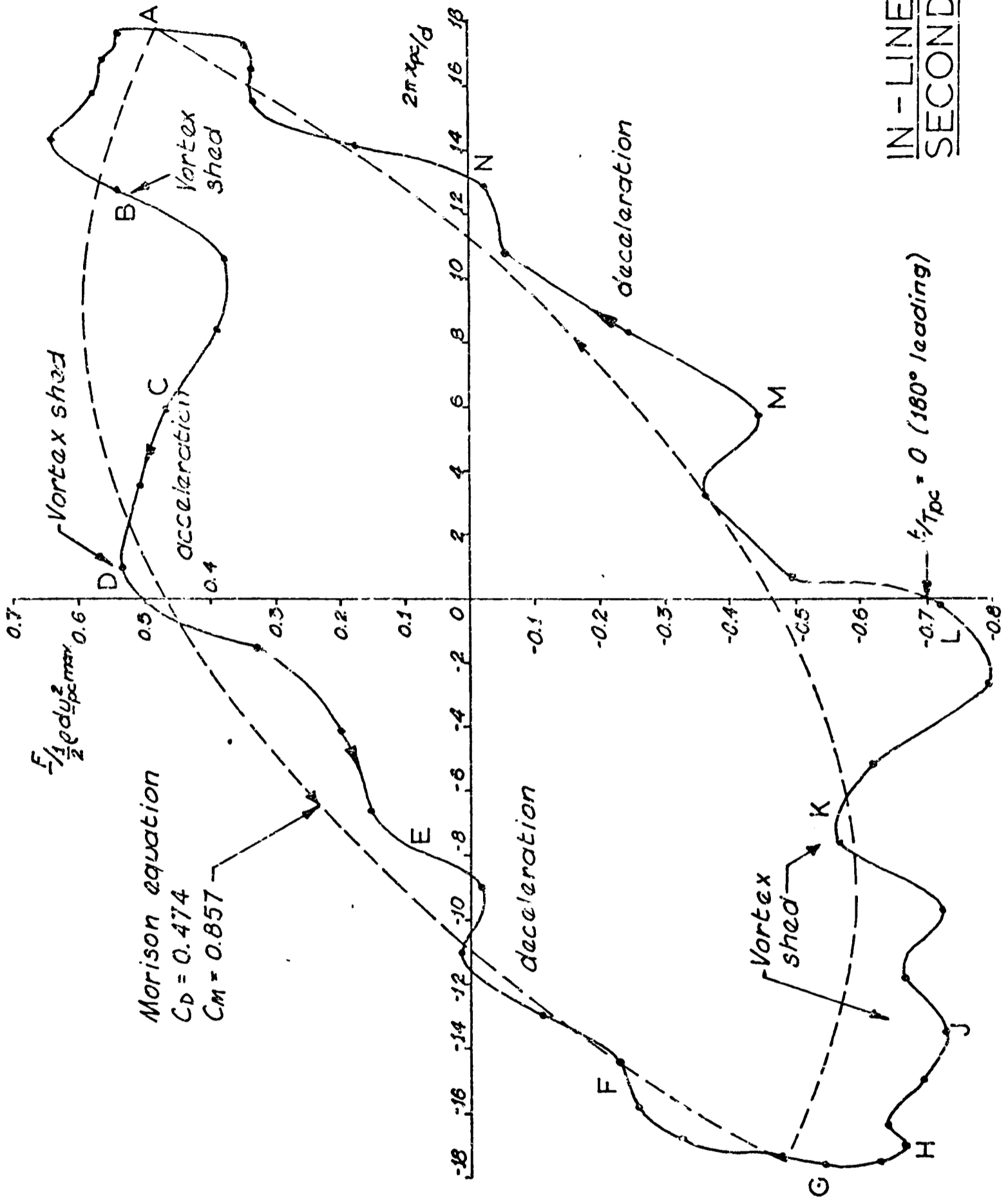
LIFT FORCE
FIRST CYCLE

FIGURE (4.19b)



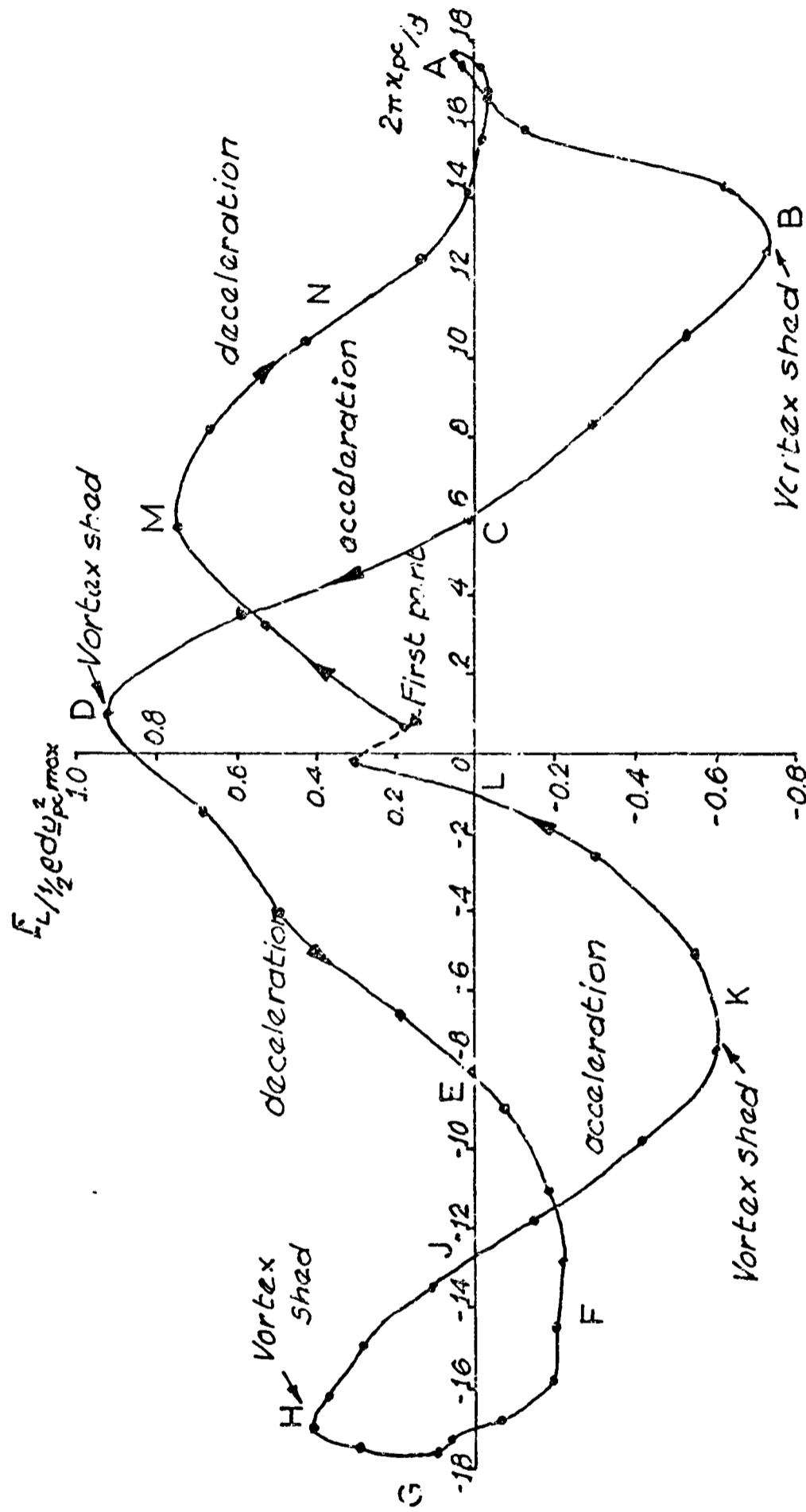
RESULTANT FORCE
FIRST CYCLE

FIGURE (4.19c)



IN-LINE FORCE
SECOND CYCLE

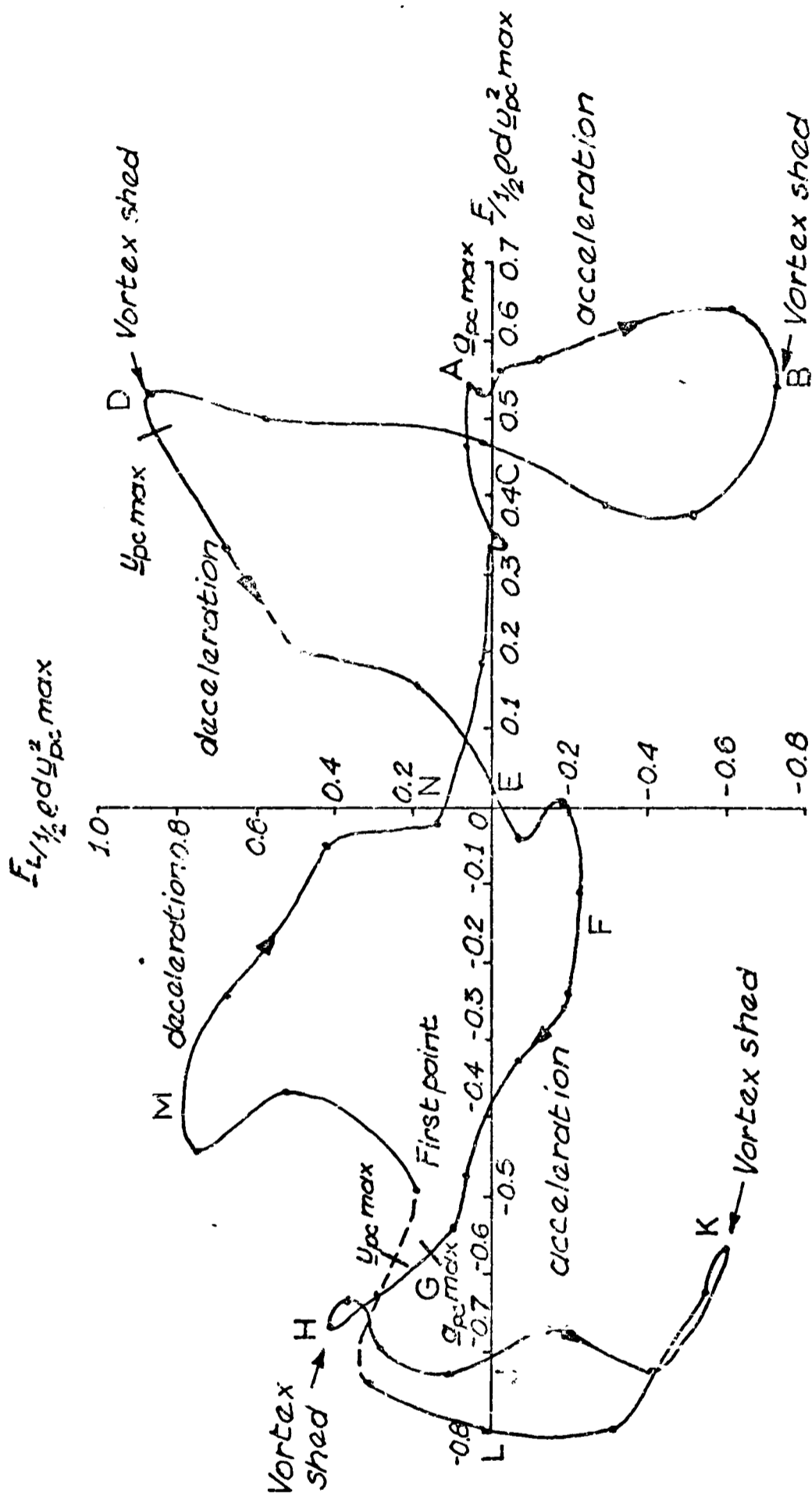
FIGURE (4.20a)



N.B. Comparison of final point in this cycle with that in previous (Figure 4.19b) indicates a significant change

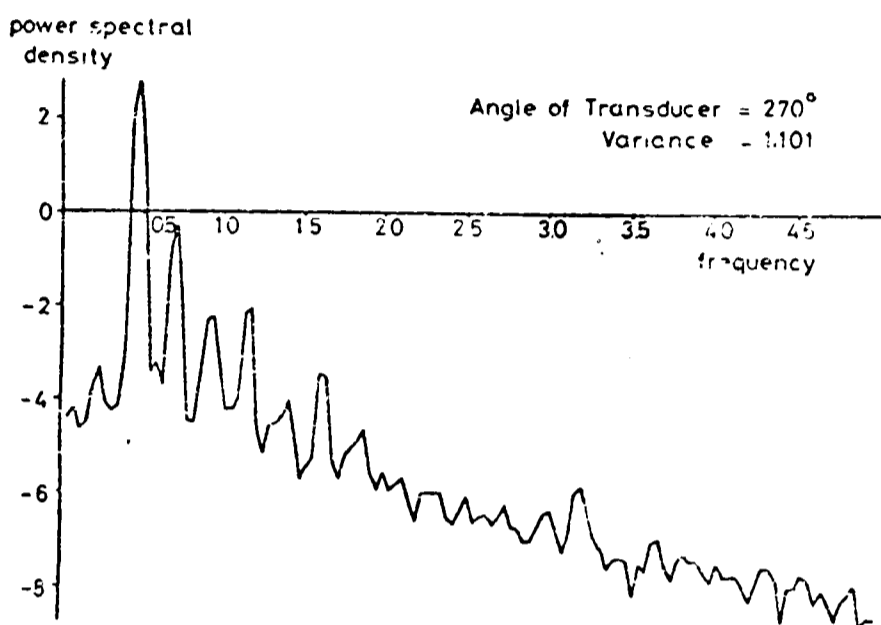
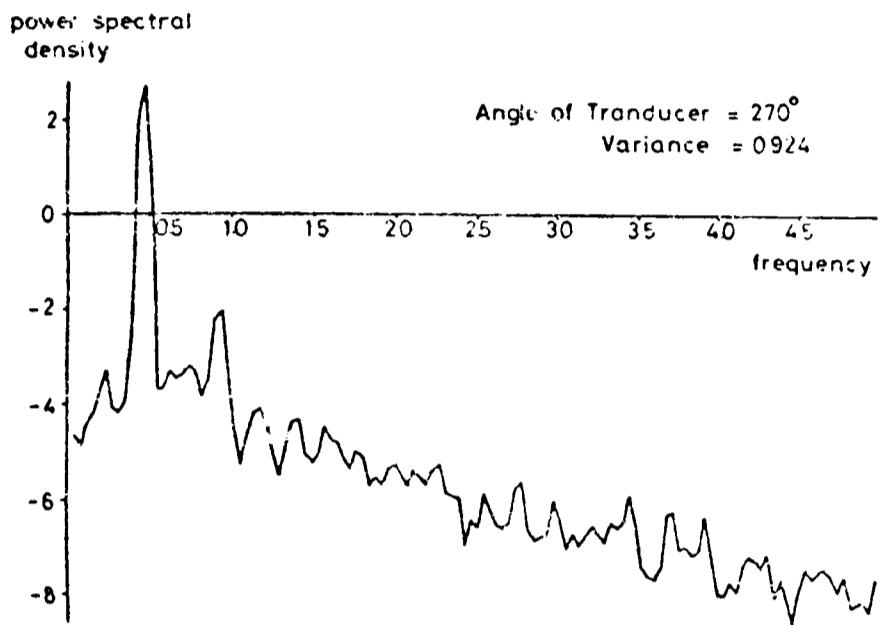
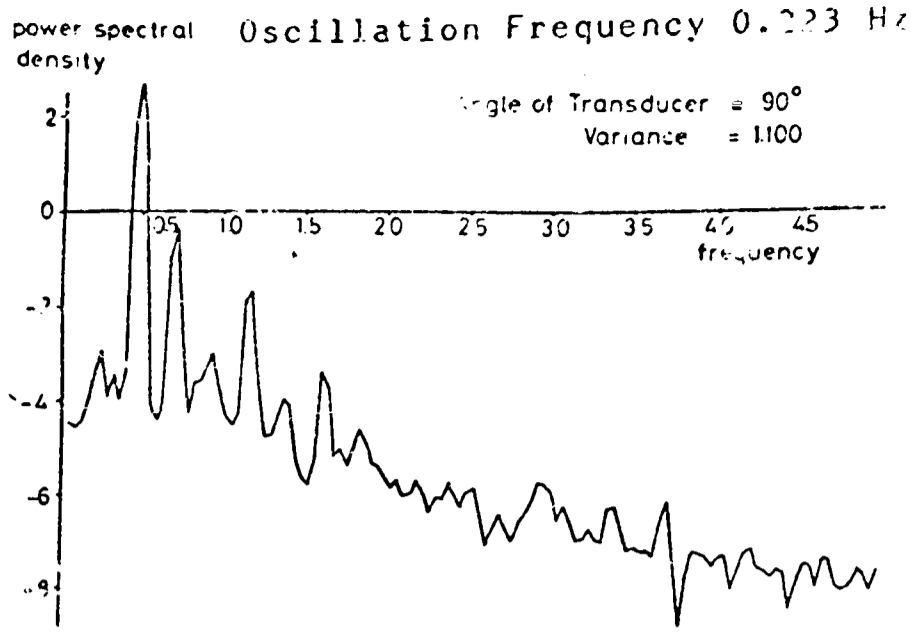
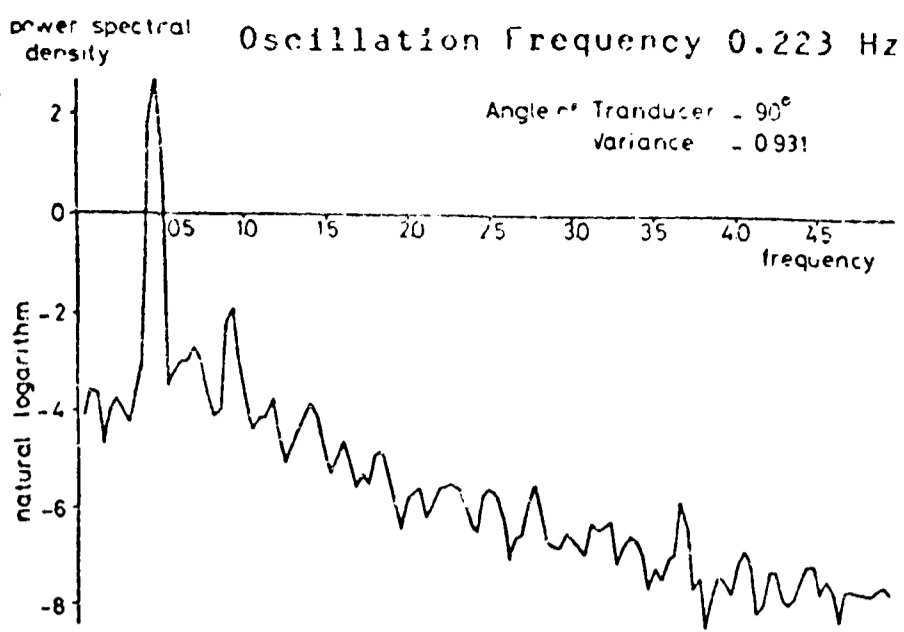
LIFT FORCE
SECOND CYCLE

FIGURE (4.20b)



RESULTANT FORCE
SECOND CYCLE

FIGURE (4.20c)



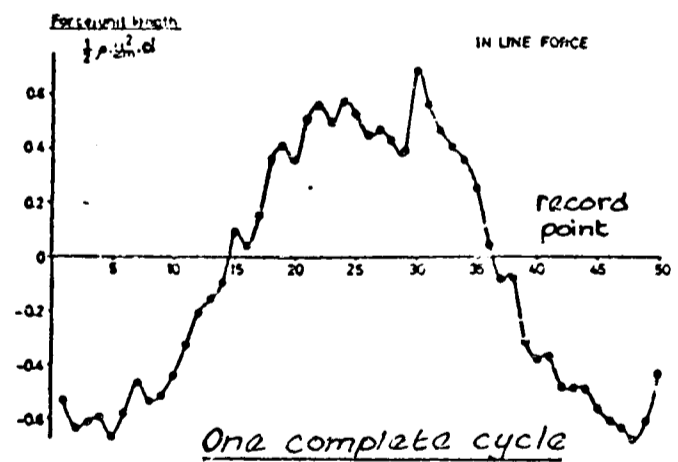
End plates removed

End plates attached

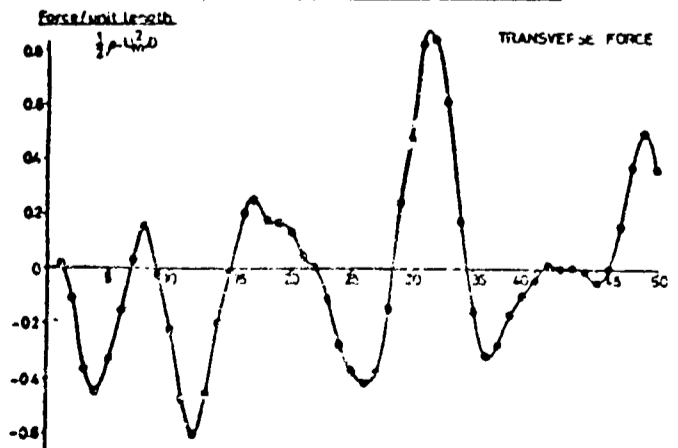
EFFECT OF END PLATES UPON 90° & 270°
PRESSURE SPECTRA

FIGURE (4.21)

BOTH FIGURES
FROM: MATTEN,
HOGBEN &
ASHLEY (1978)



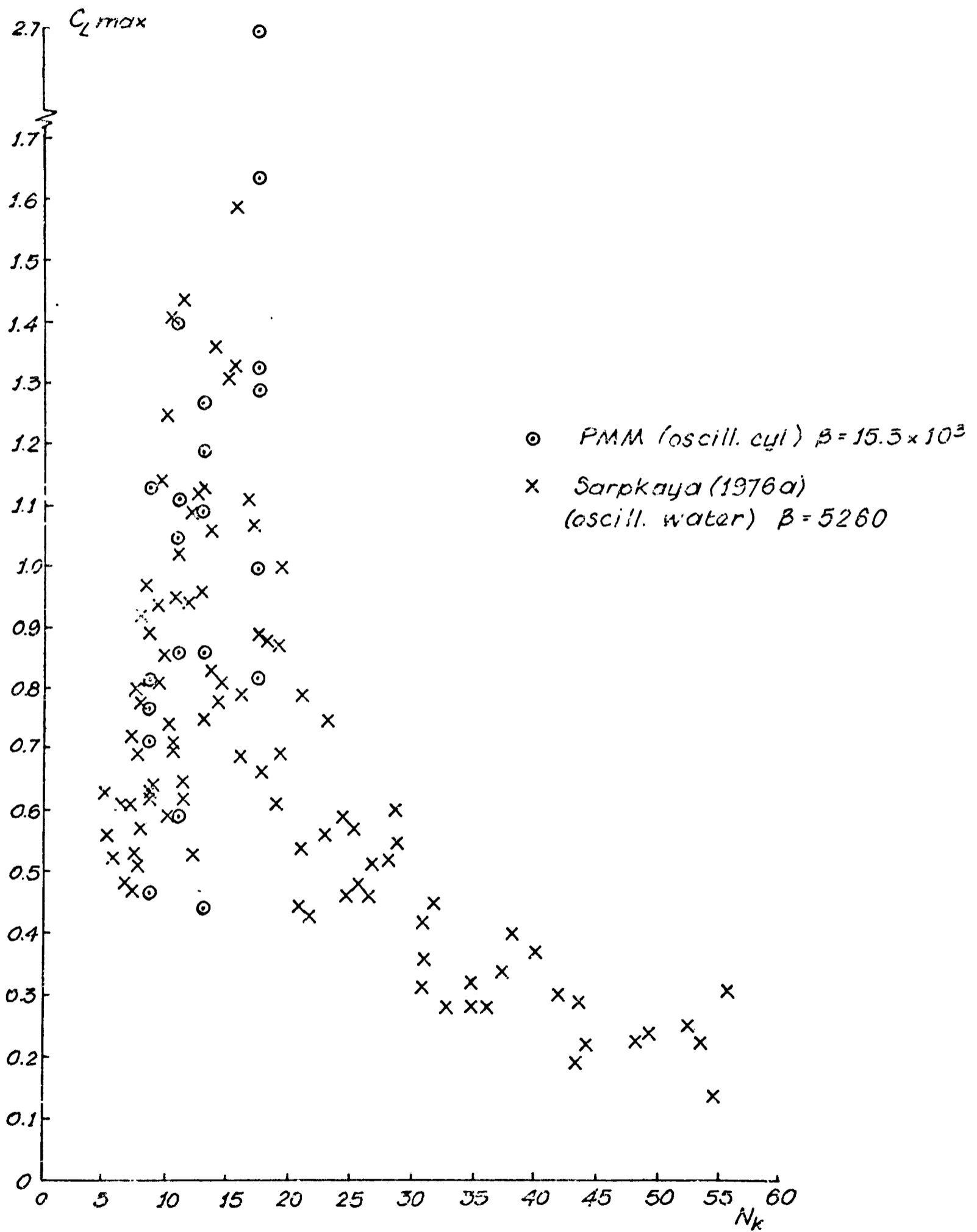
(a)



(b)

IN-LINE AND LIFT FORCES FOR AN OSCILLATING
CYLINDER WITH AXIAL FLOW (NO END PLATES)

FIGURE (4.22)



COMPARISON OF OSCILLATING CYLINDER AND WATER: C_{Lmax} VS N_k

FIGURE (4.23)

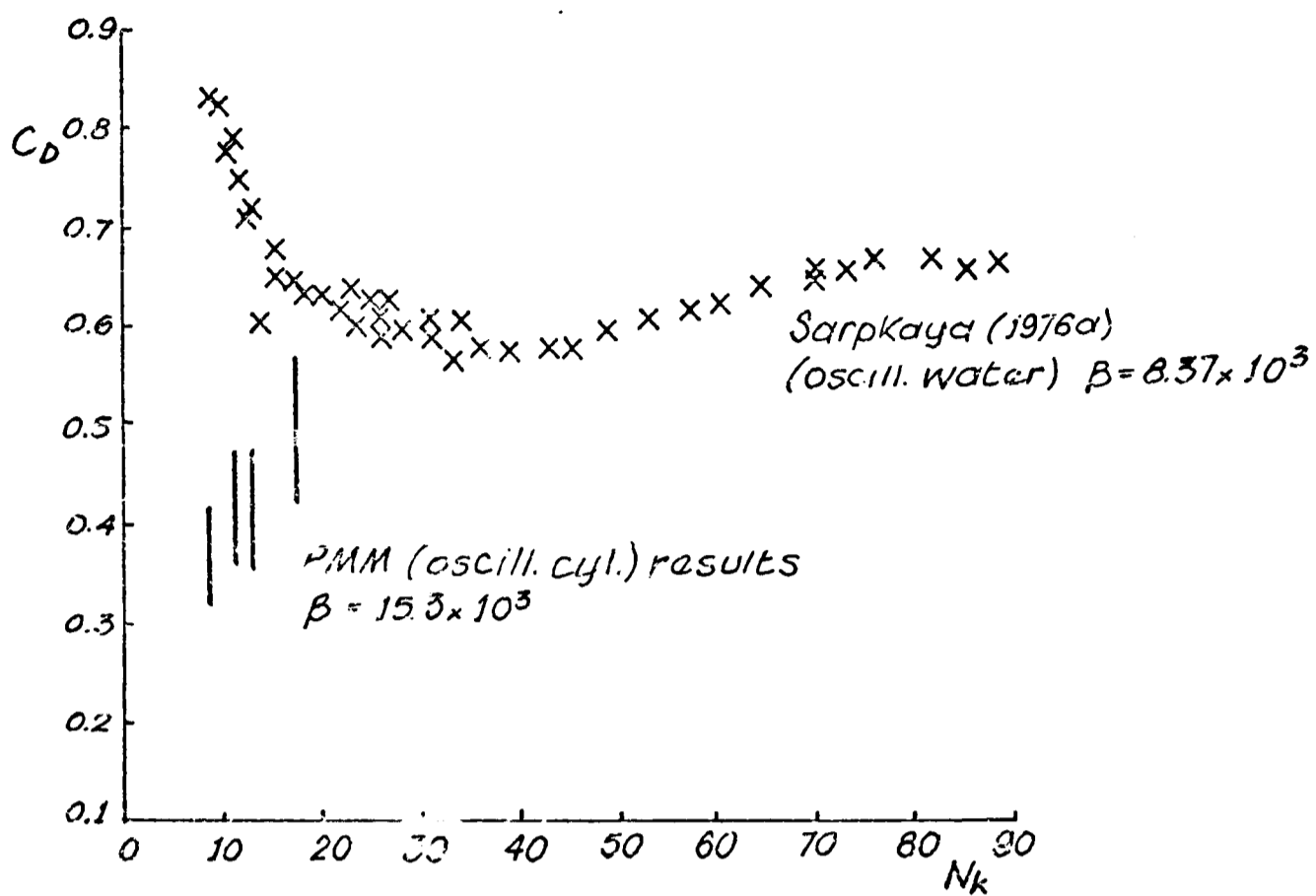


FIGURE (4.24)

COMPARISON OF OSCILLATING CYLINDER
AND WATER RESULTS: C_M & C_D VS N_k

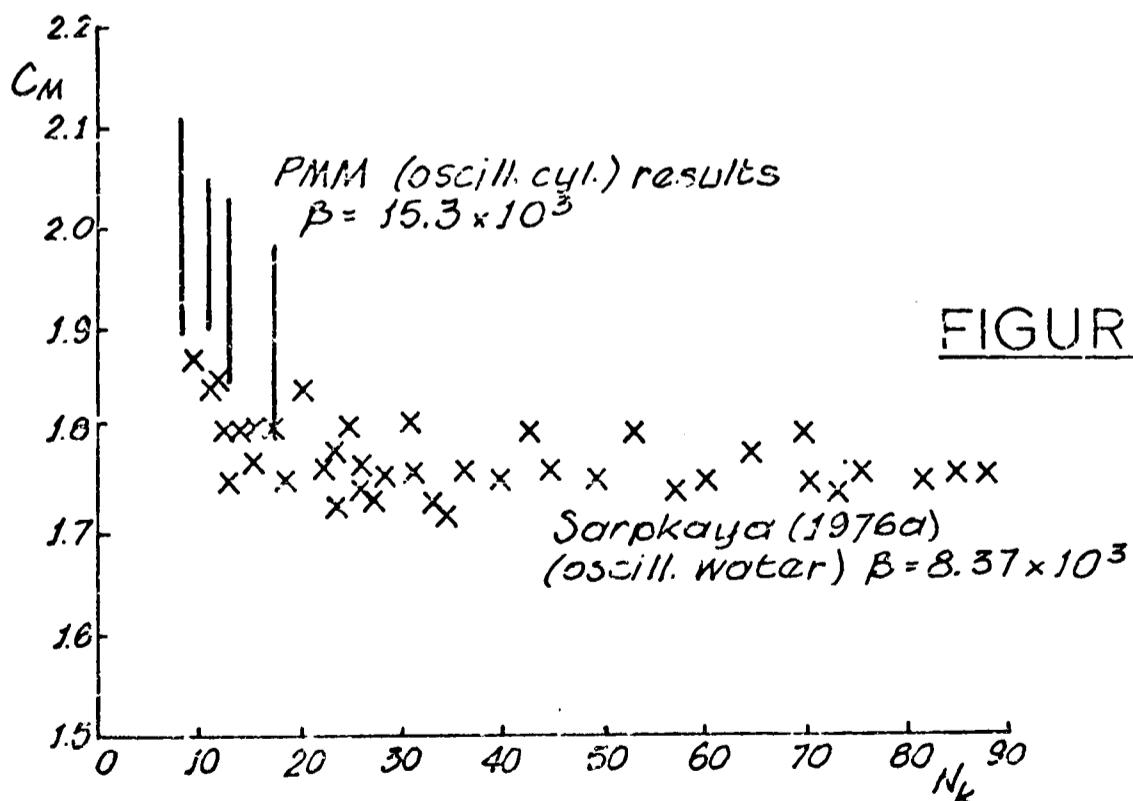
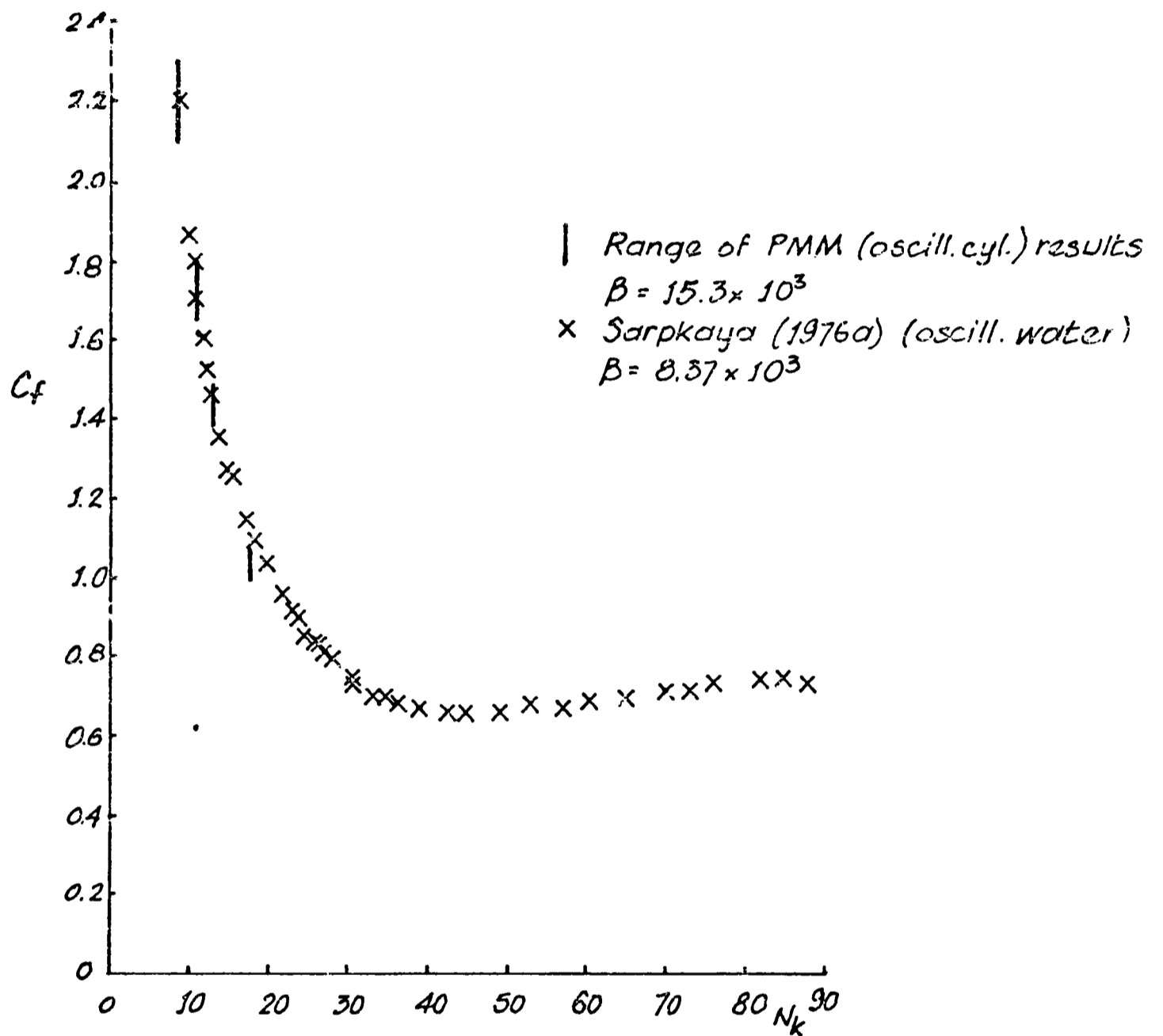
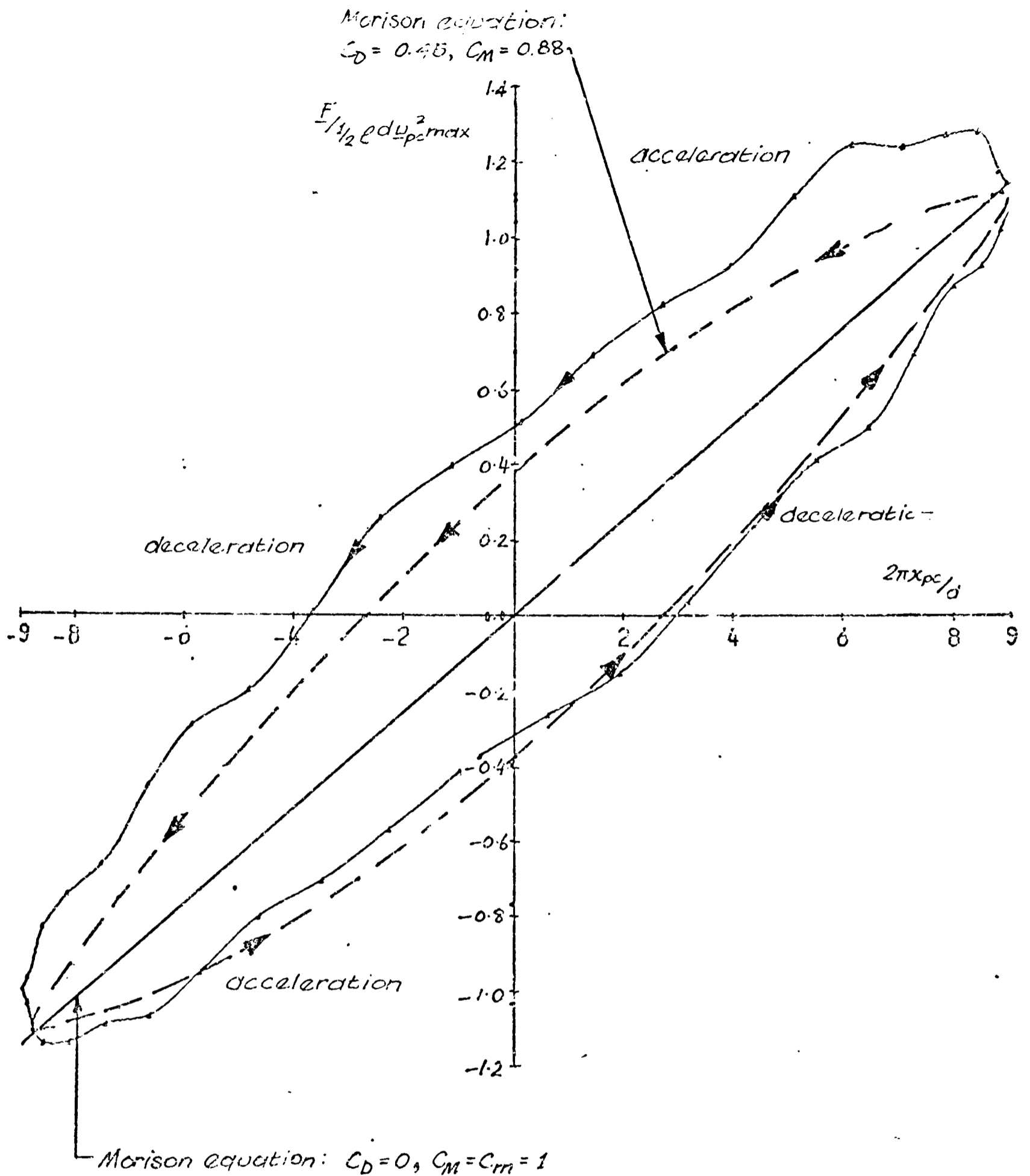


FIGURE (4.25)



COMPARISON OF OSCILLATING CYLINDER WITH
WATER RESULTS: COMBINED IN-LINE FORCE
COEFFICIENT C_f VS N_k

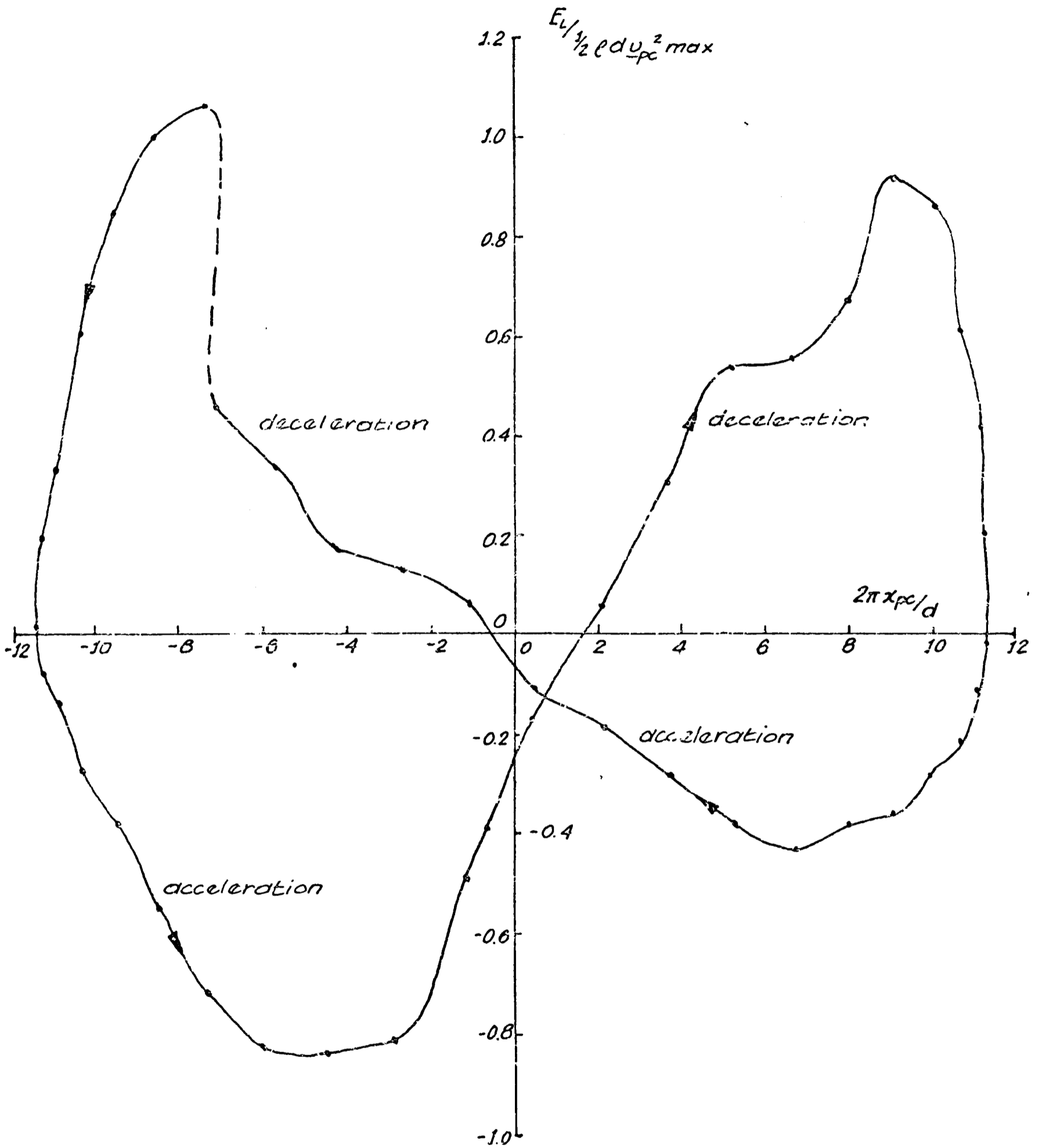
FIGURE (4.26)



AVERAGE IN-LINE FORCE CYCLE FOR $N_k = 8.85$
OSCILLATING CYLINDER

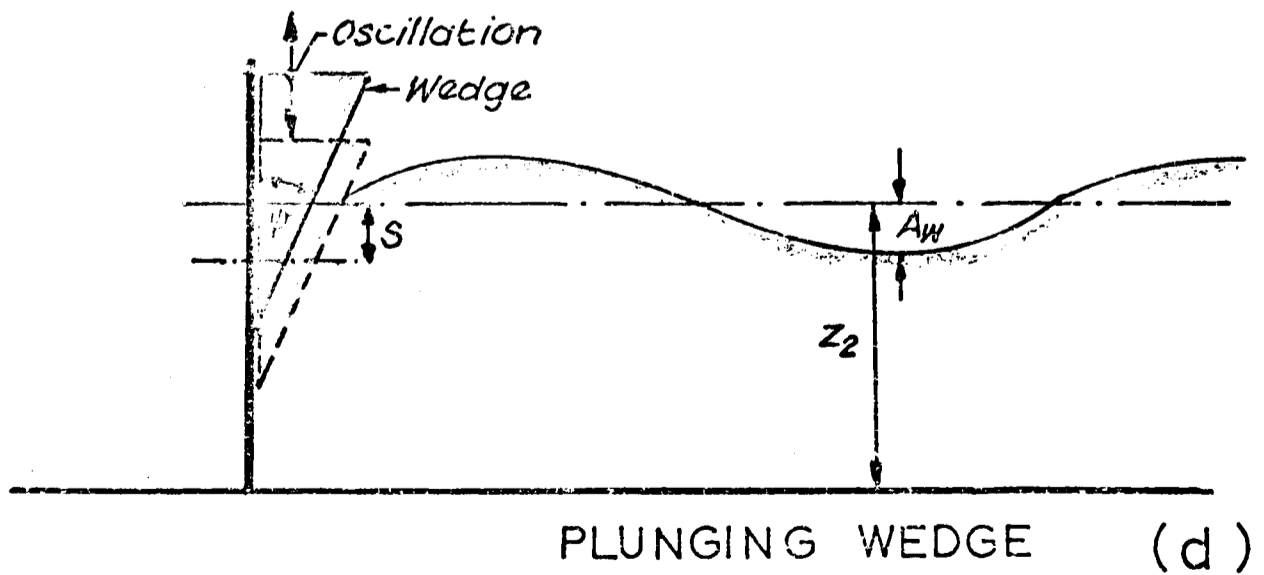
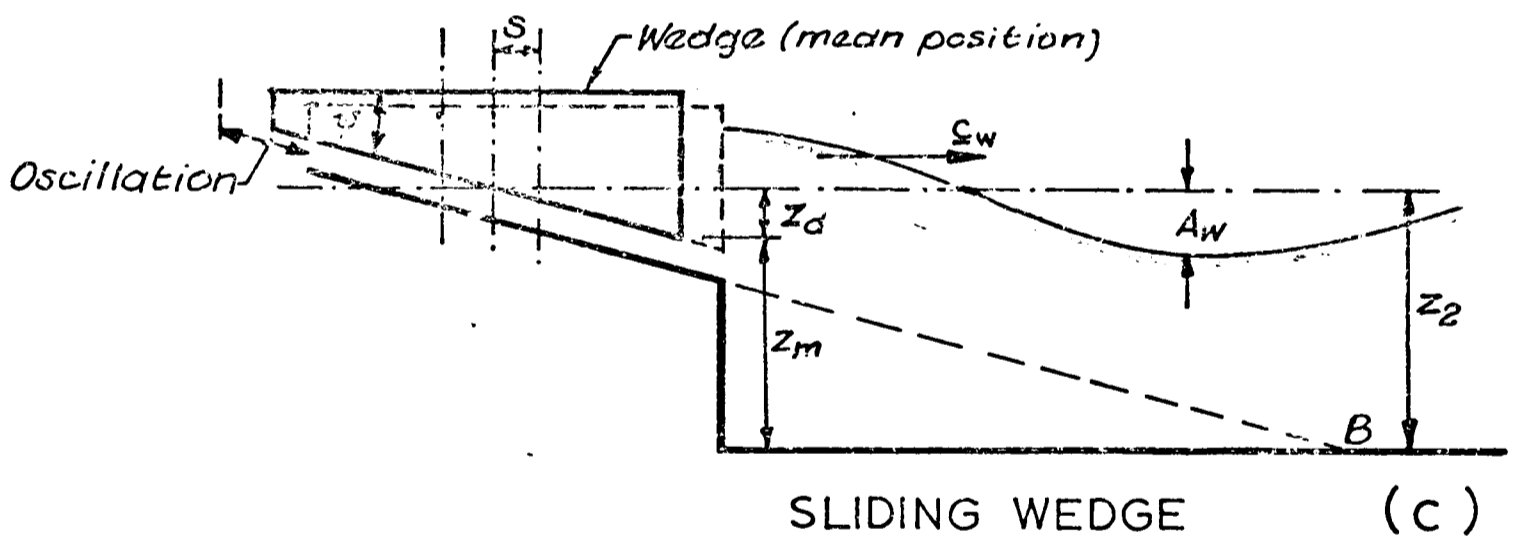
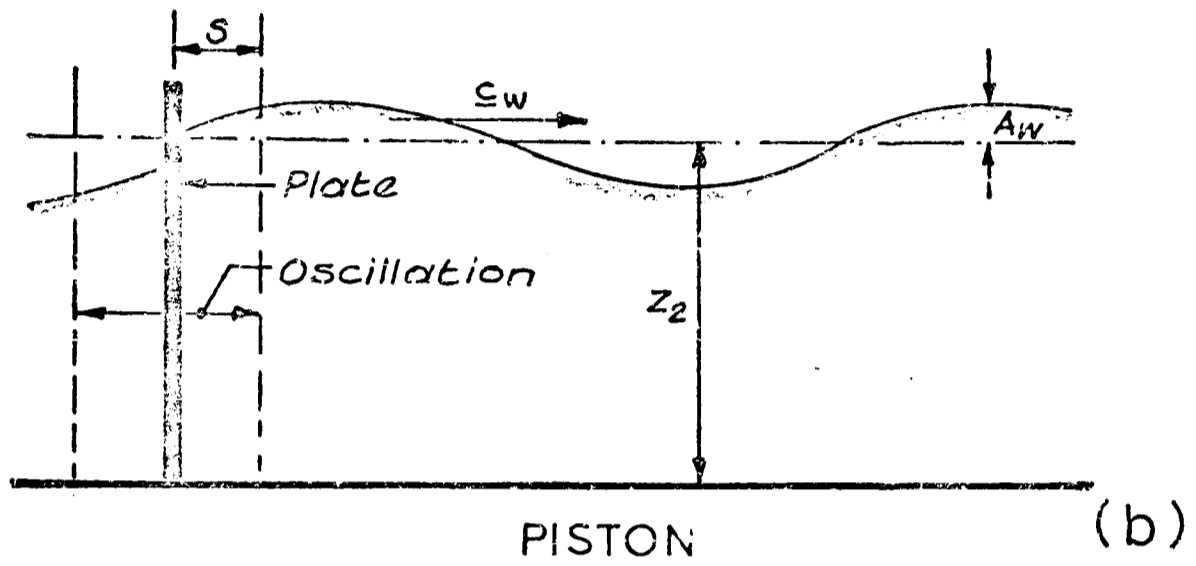
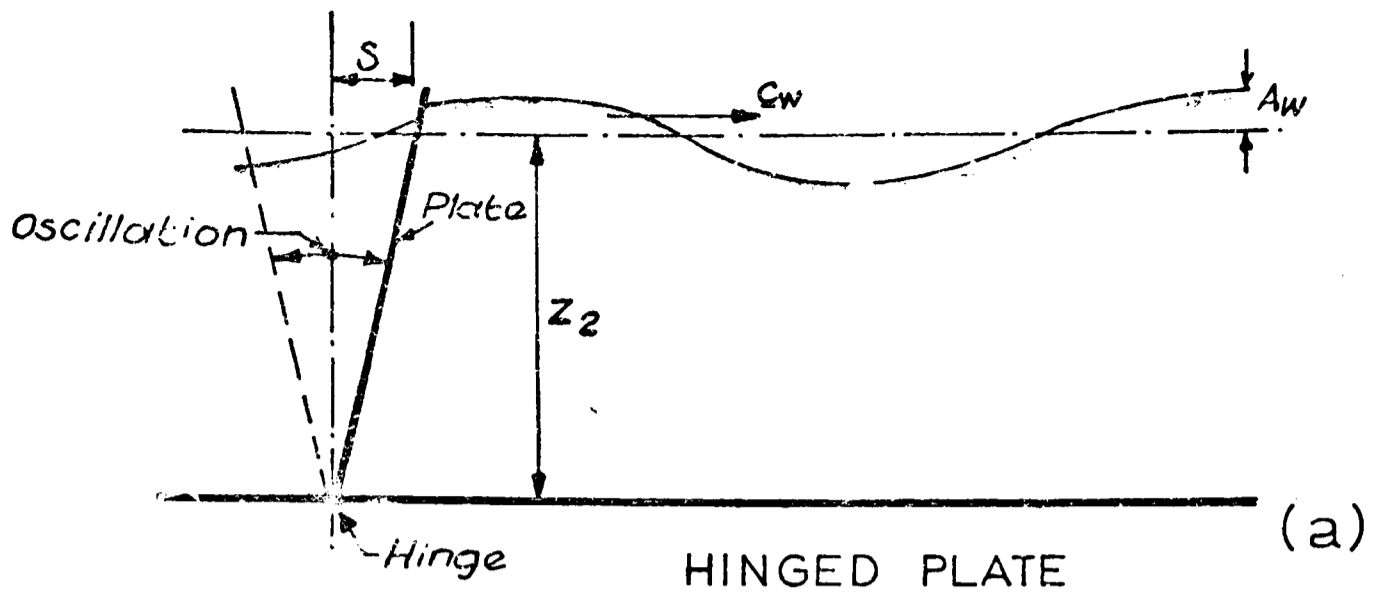
(From: MATTEN (1979))

FIGURE (4.27)



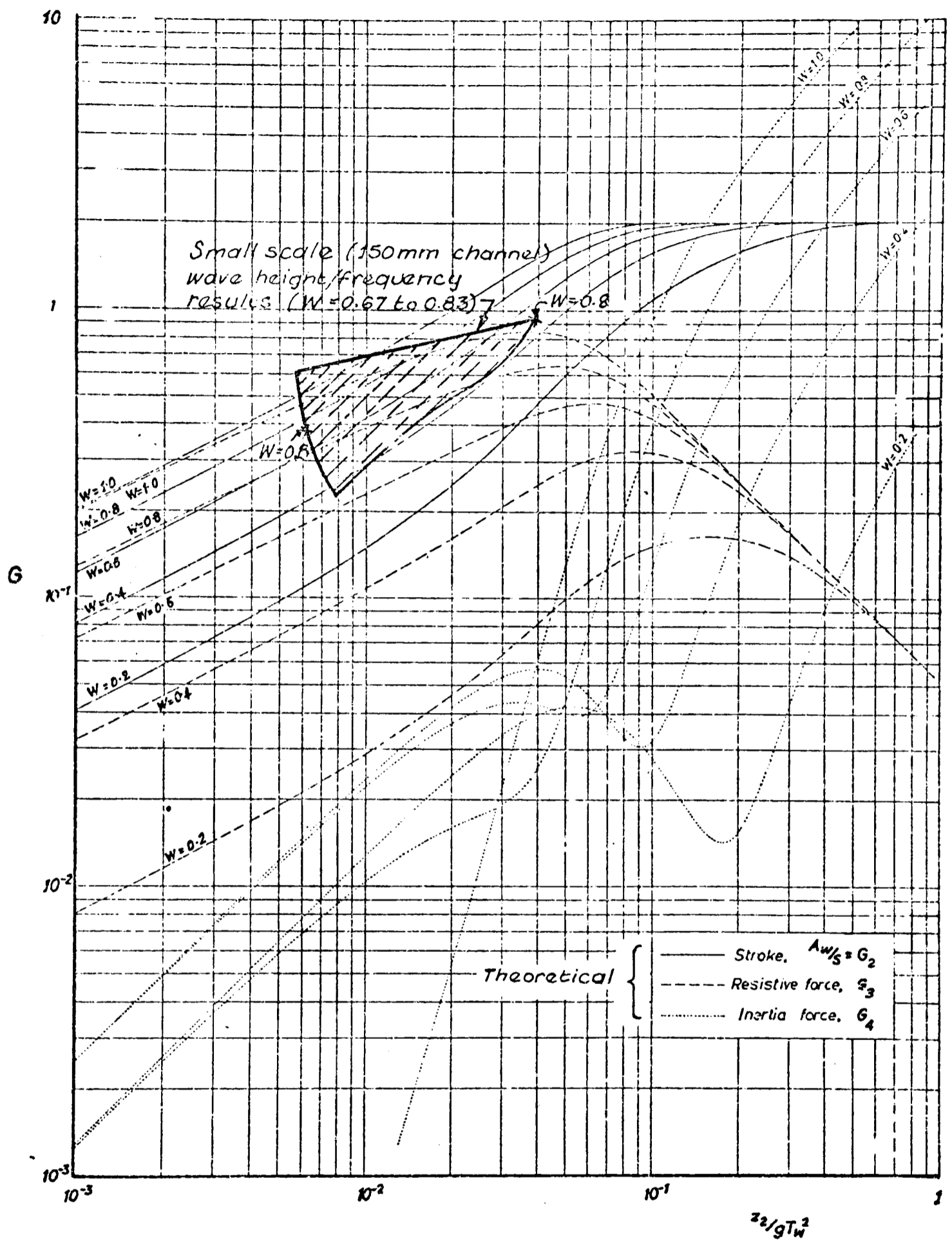
TYPICAL LIFT FORCE CYCLE $N_k = 11.3$
OSCILLATING CYLINDER (From: MATTEN (1979))

FIGURE (4.28)



PRINCIPAL TYPES OF WAVE GENERATOR

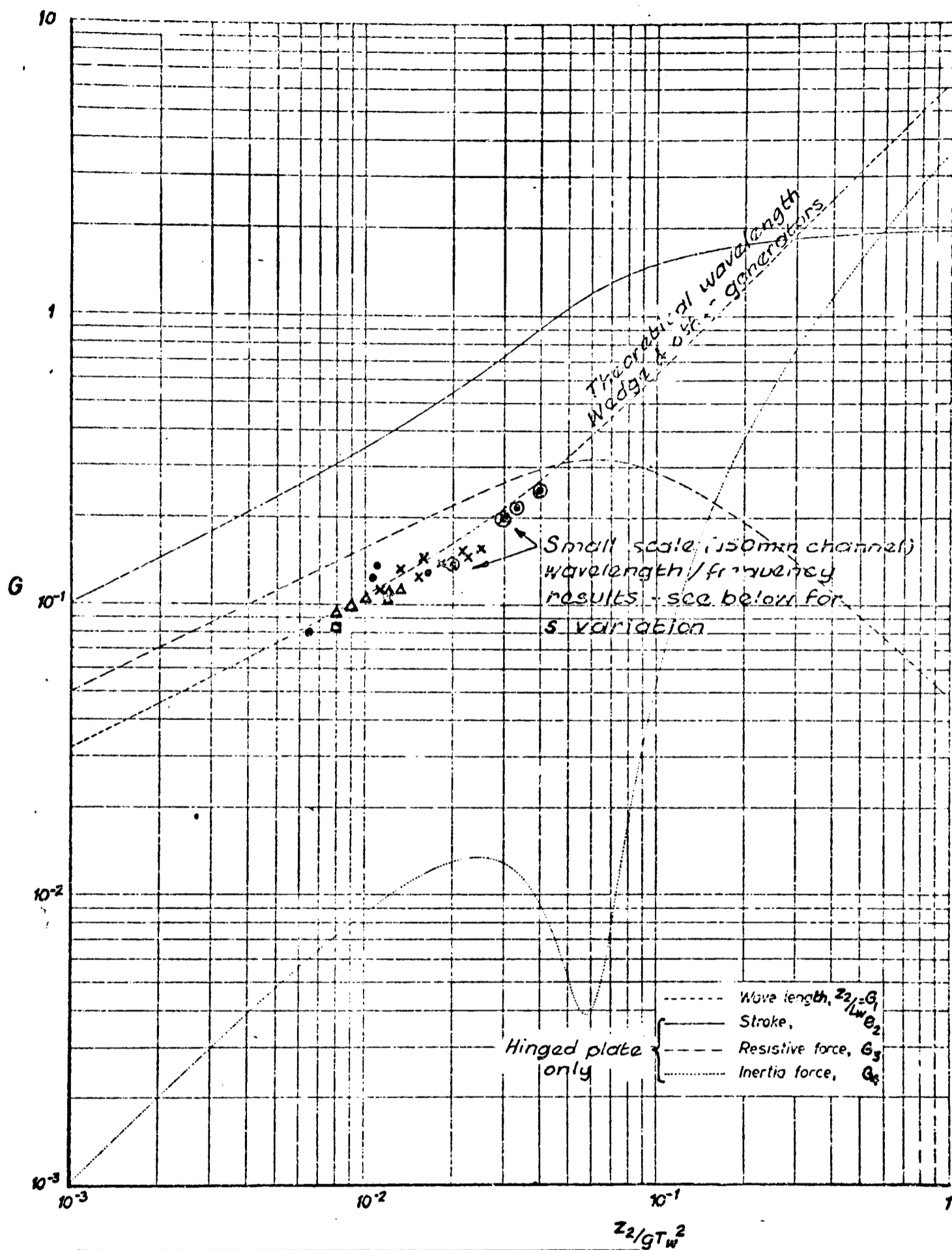
FIGURE (4.29)



WAVE AMPLITUDE & WEDGE THRUST
FOR VARYING STILL WATER DEPTH
AND FREQUENCY

(From: GILBERT et al (1977))

FIGURE (4.30)

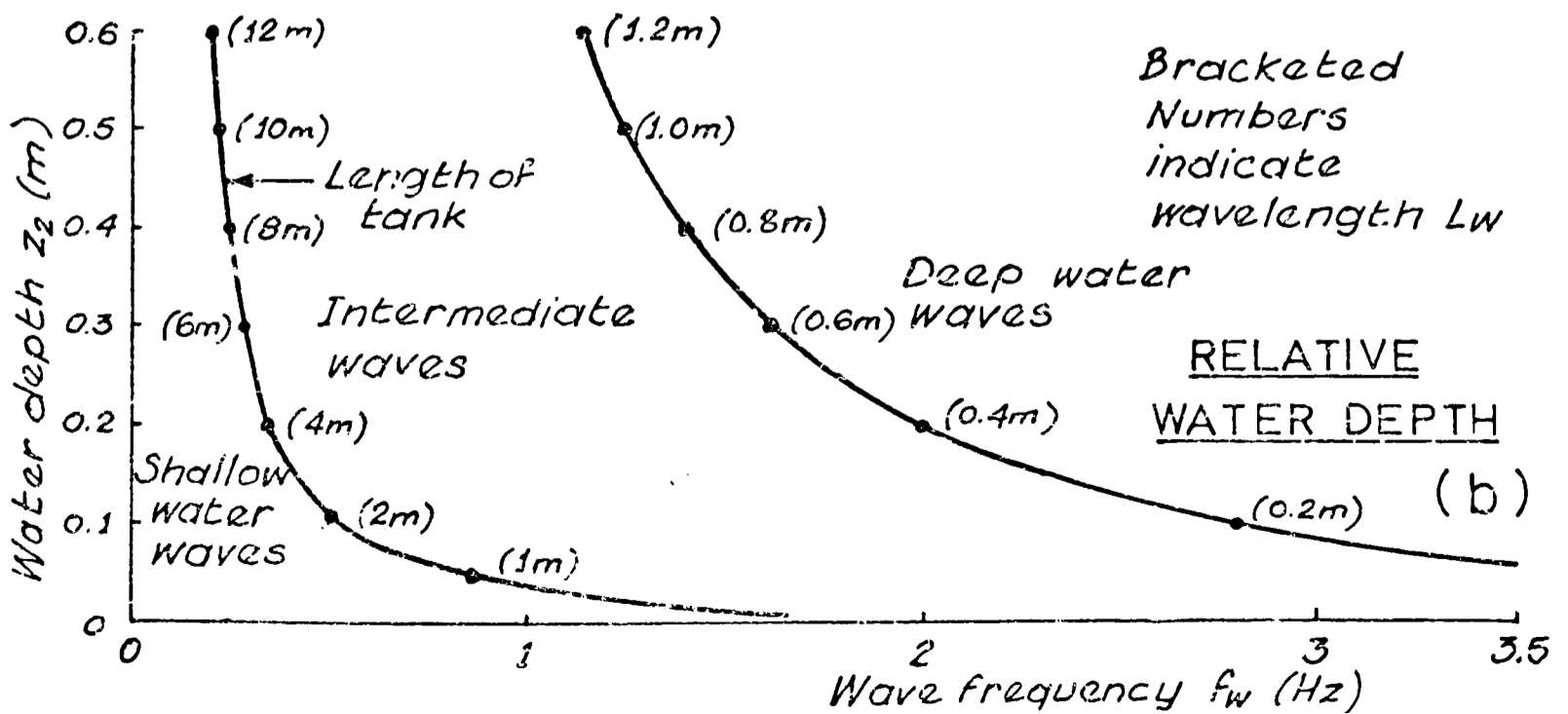
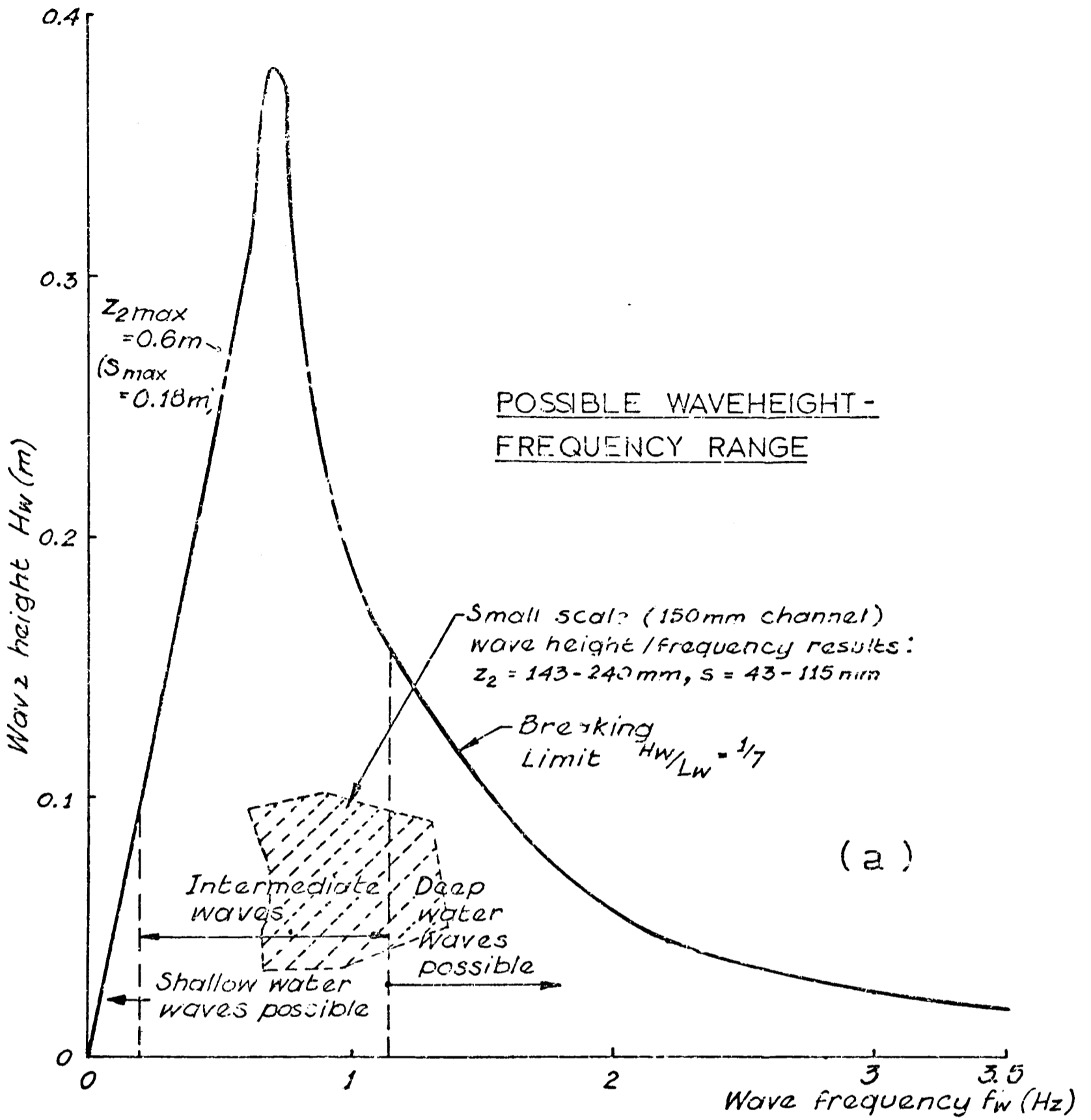


EXPERIMENTAL RESULTS				
LEGEND:	x	$s = 43 \text{ mm}$	⊙	$s = 47 \text{ mm}$
	•	$s = 75 \text{ mm}$	Δ	$s = 79 \text{ mm}$
	□	$s = 90 \text{ mm}$		

WAVELENGTH FOR VARYING STILL WATER
 DEPTH & WAVE FREQUENCY

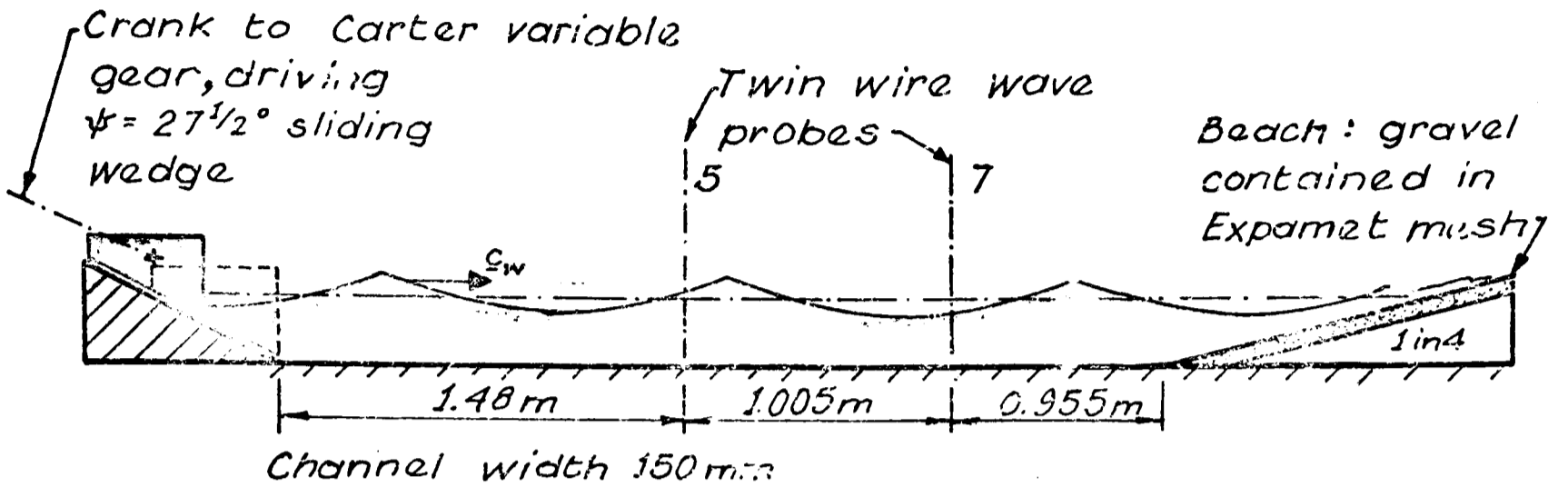
(From: GILBERT et al (1977))

FIGURE (4.31)

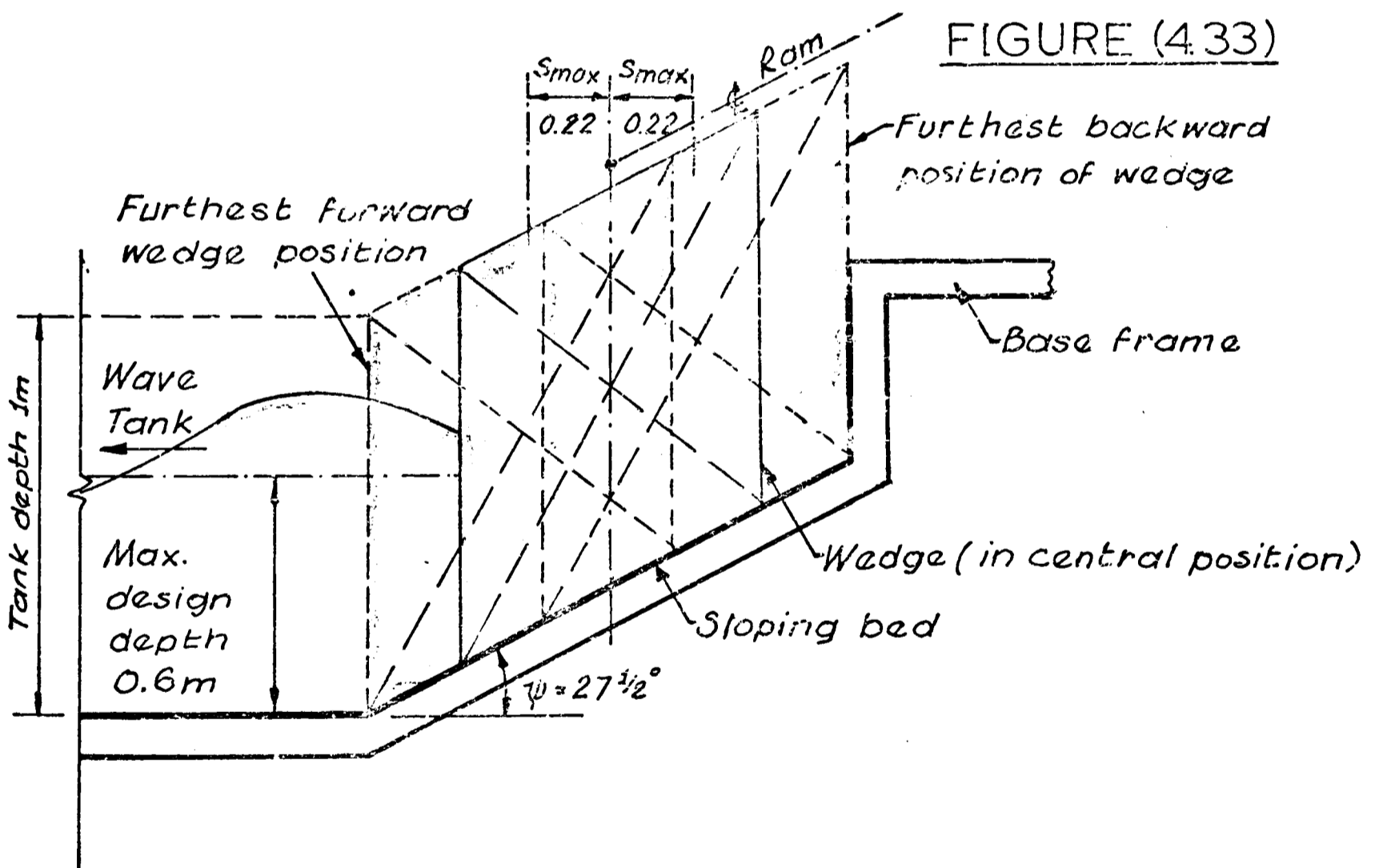


THEORETICALLY OBTAINABLE WAVES -
SLIDING WEDGE $\psi = 27.5^\circ$

FIGURE (4.32)



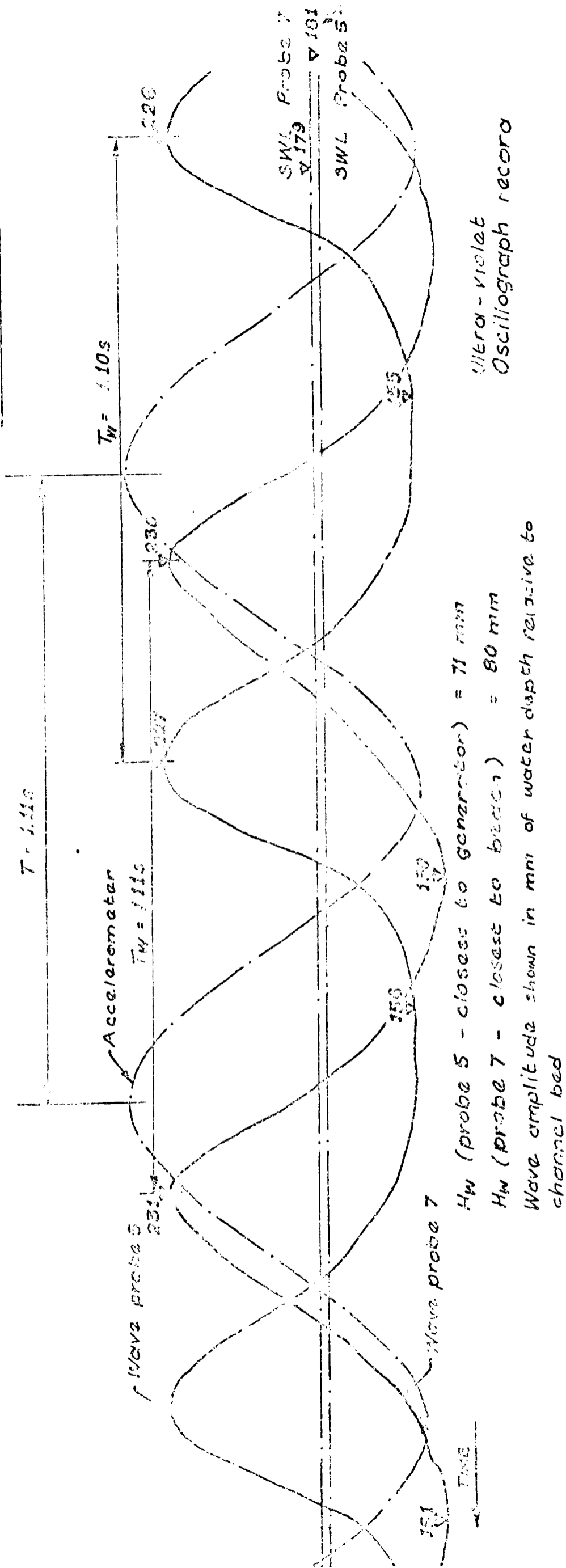
SMALL SCALE SLIDING WEDGE EXPERIMENT



PROTOTYPE SLIDING WEDGE (DIAGRAMMATIC)

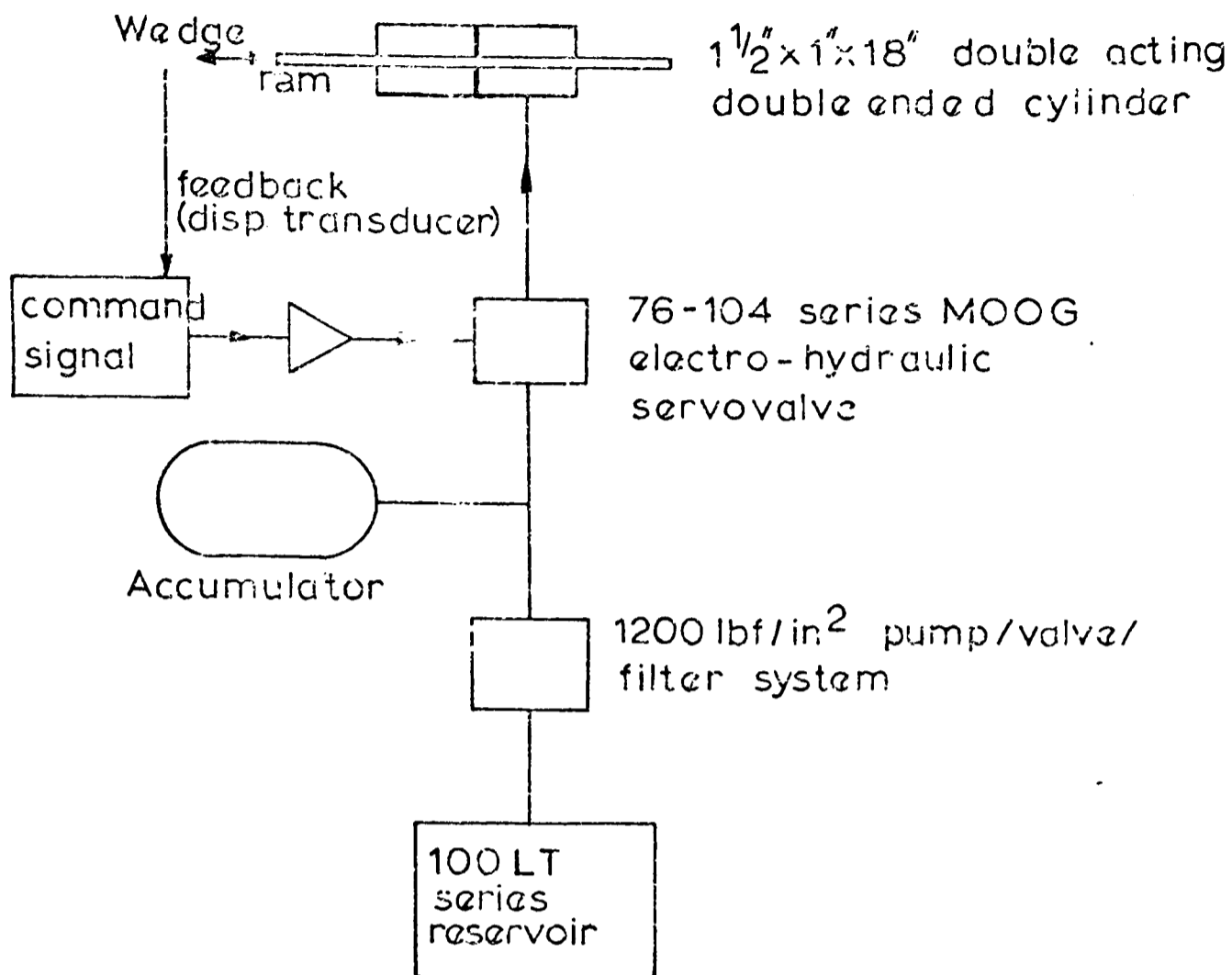
FIGURE (4.35)

RUN No. 2.2



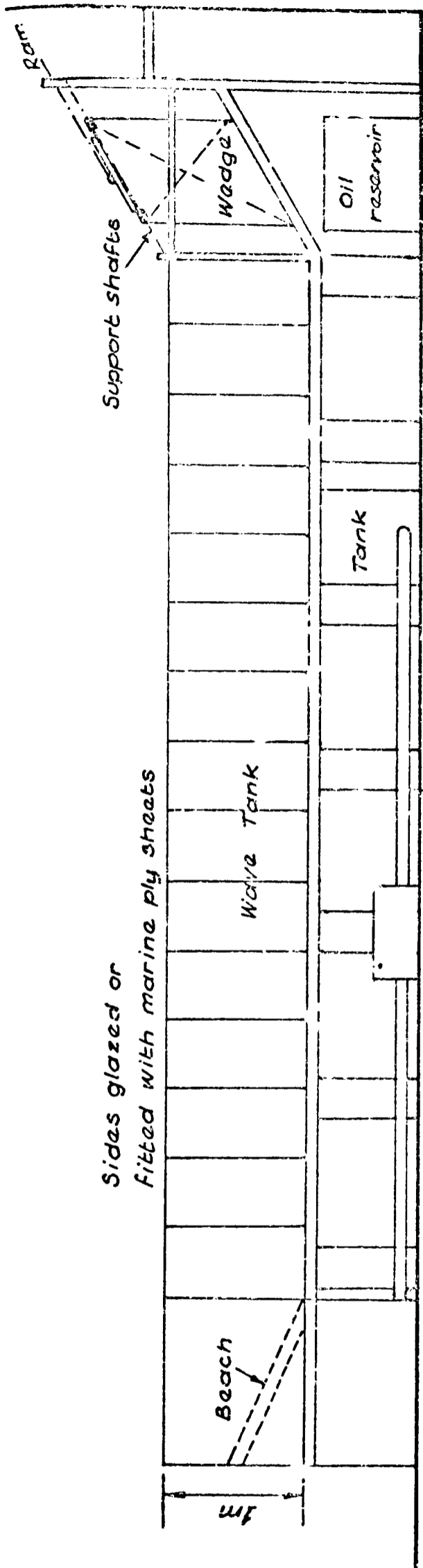
TYPICAL SMALL SCALE WAVE GENERATION

FIGURE (4.34)

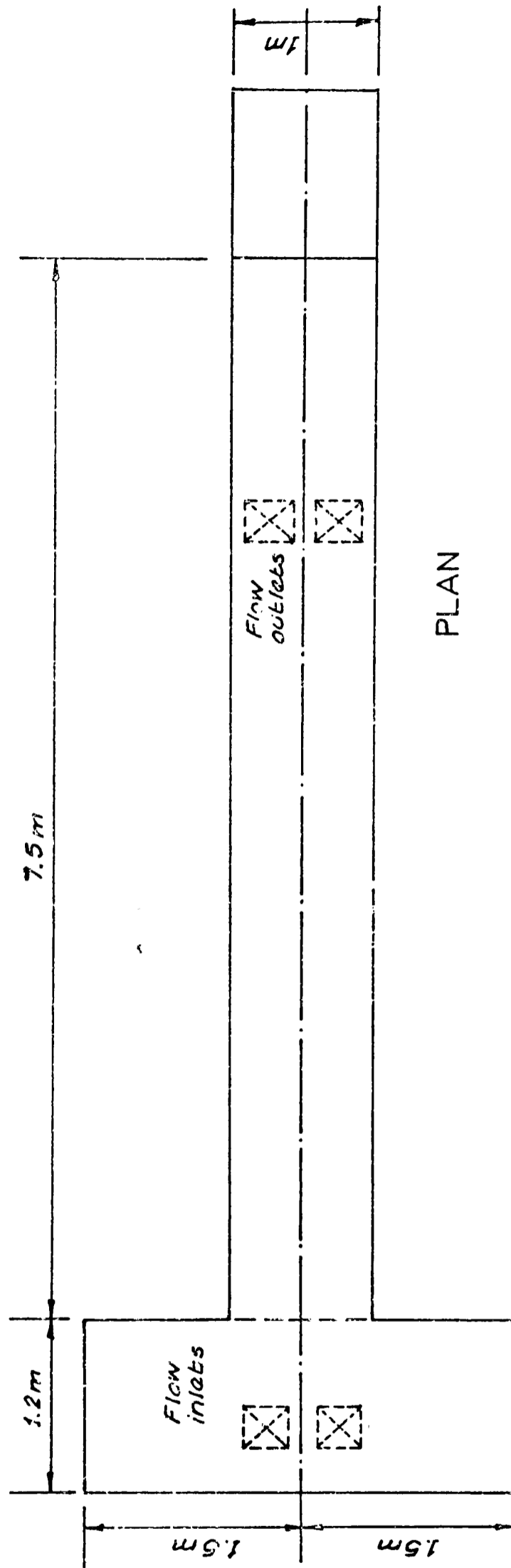


SCHEMATIC LAYOUT OF WAVE GENERATOR POWER AND CONTROL SYSTEM - AS SUPPLIED BY HI-POWER LTD.

FIGURE (4.36)



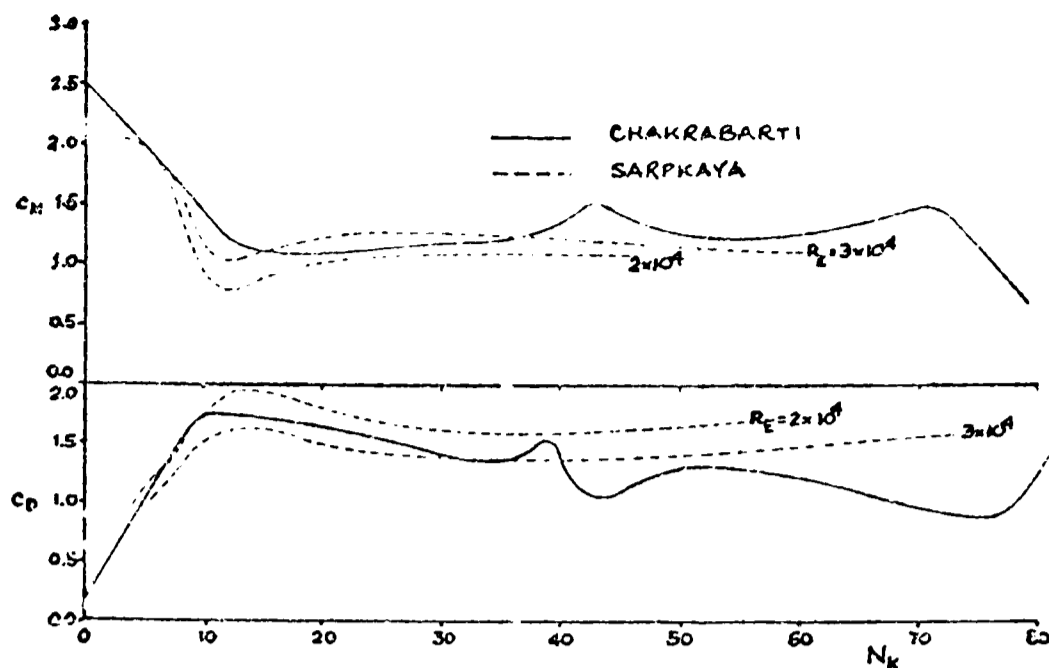
ELEVATION



PLAN

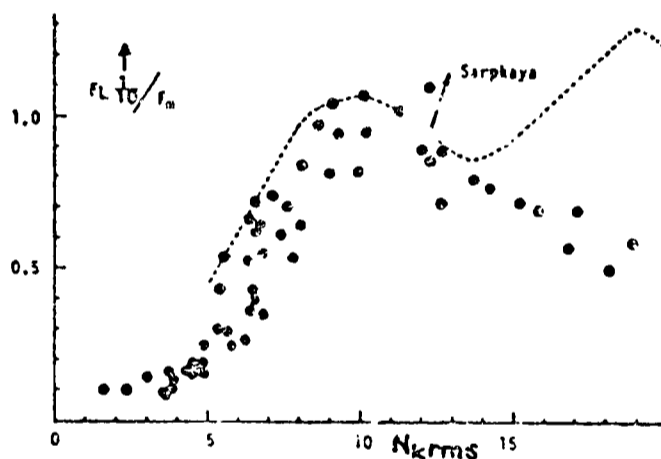
SKETCH OF THAMES POLYTECHNIC WAVE TANK

FIGURE (4.37)



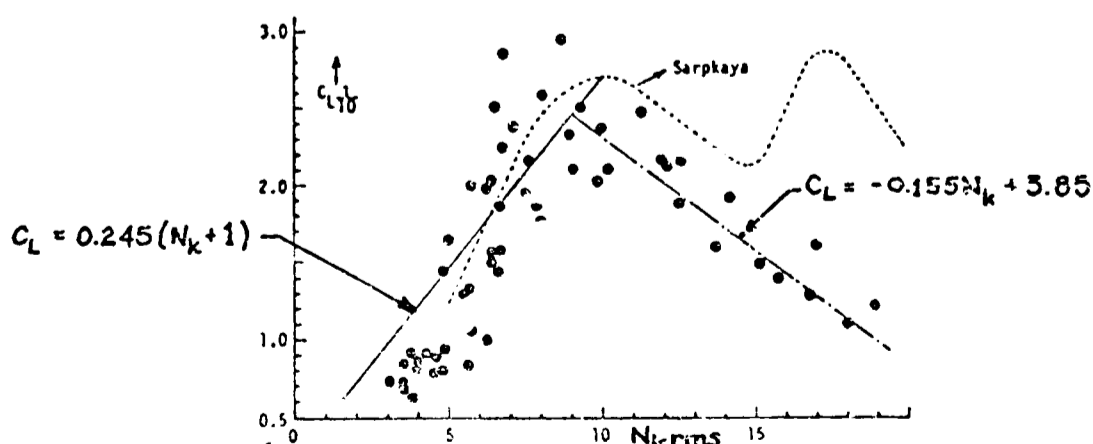
COMPARISON OF WAVE FLOW RESULTS WITH PLANAR OSCILLATORY: C_M & C_D VS N_k
 (From: CHAKRABARTI (1980))

FIGURE (5.1)



$1/10$ SIGNIFICANT F_L / E_{max} FOR RANGE OF $N_{k rms}$

(a)

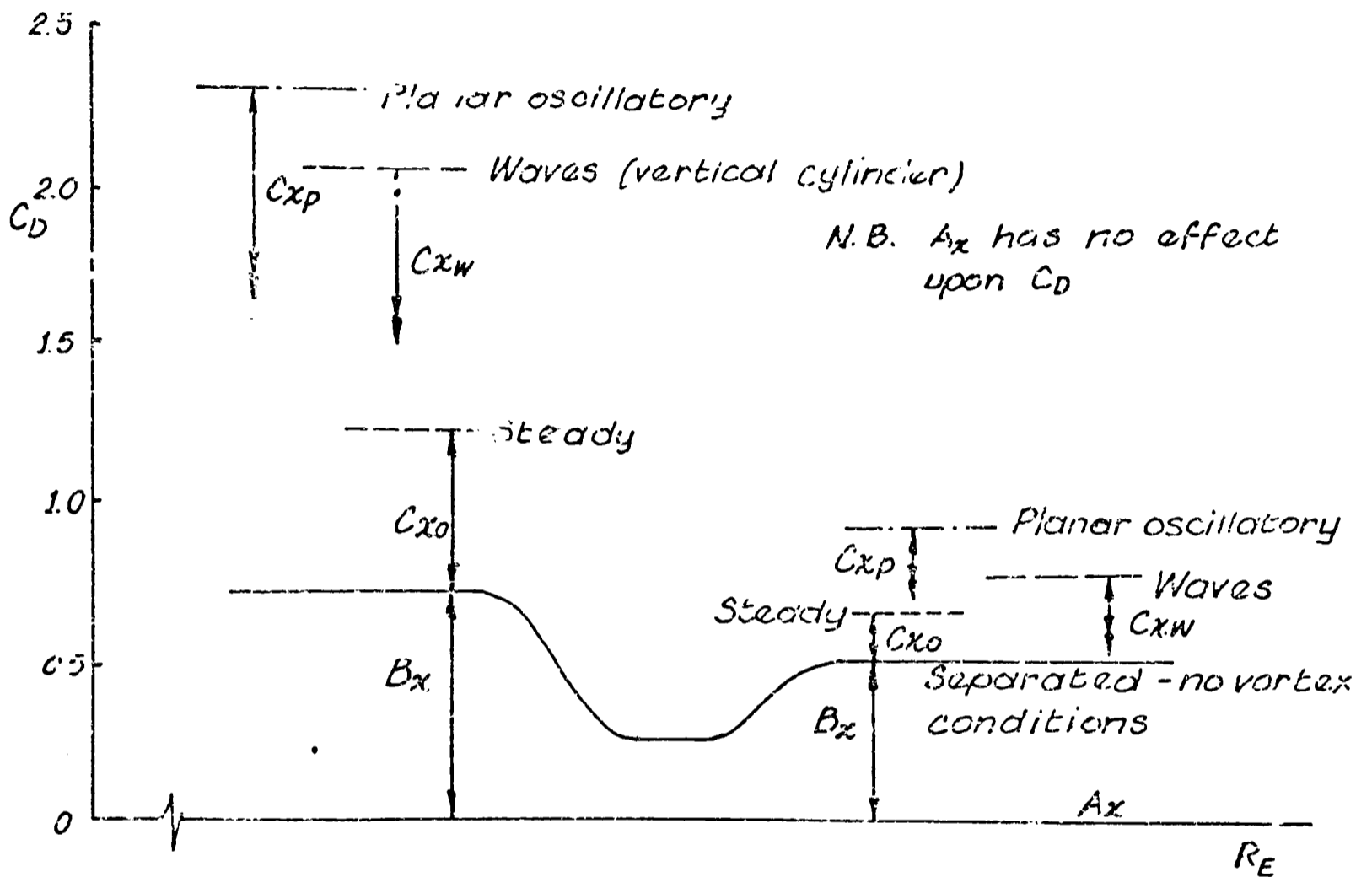


$1/10$ SIGNIFICANT C_{Lmax} FOR RANGE OF $N_{k rms}$

(b)

COMPARISON OF WAVE FLOW RESULTS WITH PLANAR OSCILLATORY
 (From: SAWARA et al (1976))

FIGURE (5.2)

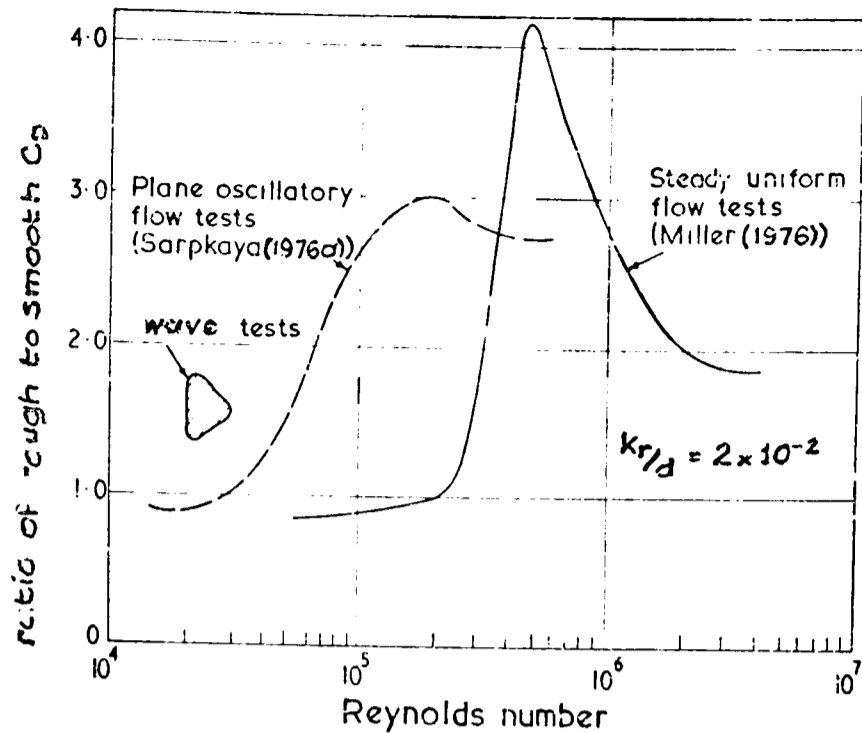


Total in-line force = $A_x + B_x + C_x$
 where: A_x is potential flow component
 B_x is separated steady flow (splitter plate) conditions
 C_x is discrete vortex effect

COMPOSITION OF DRAG COMPONENT OF IN-LINE FORCE FOR VARIOUS KINEMATIC CONDITIONS

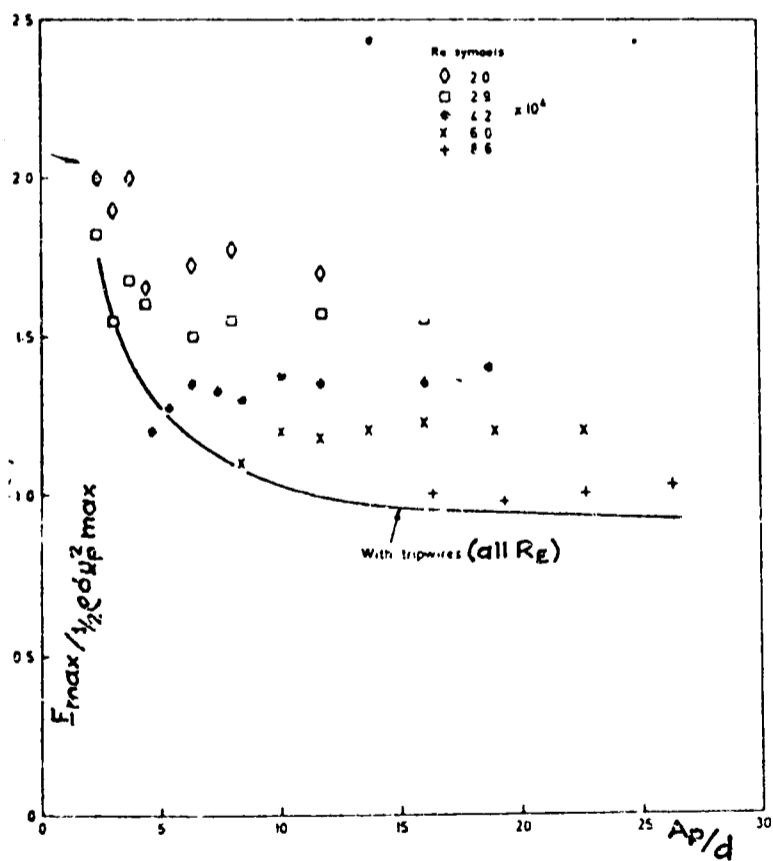
(From: PEARCEY (1979))

FIGURE (5.3)

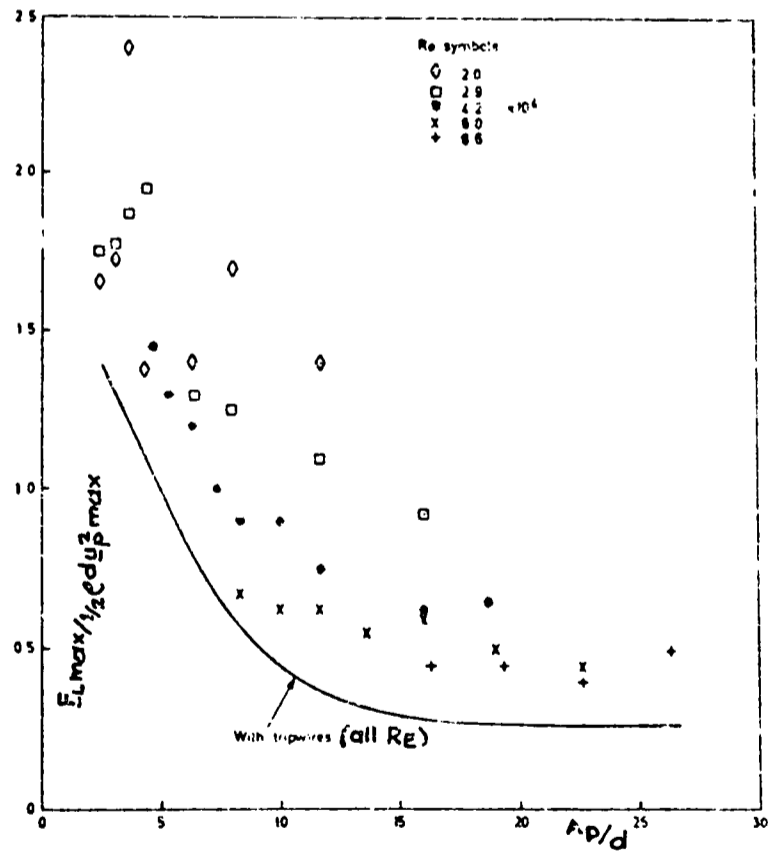


COMPARISON OF EFFECTS OF ROUGHNESS
IN WAVE, PLANAR OSCILLATORY & STEADY
FLOWS (From: MATTEN(1977))

FIGURE (5.4)



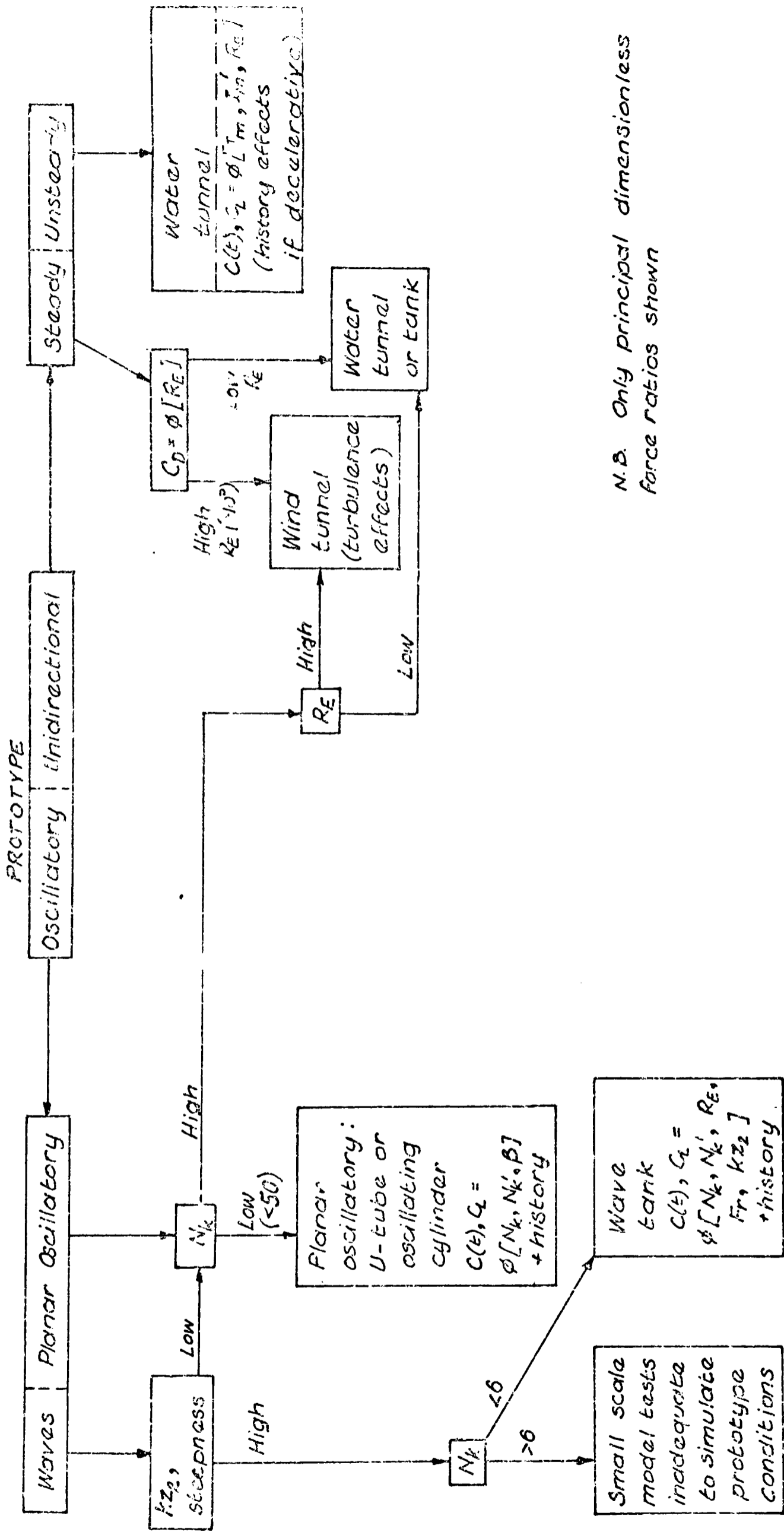
IN LINE FORCE (a)



LIFT FORCE (b)

EFFECTS OF TRIP WIRES IN PLANAR OSCILLATORY
FLOW (From: BUSHNELL(1977))

FIGURE (5.5)



N.B. Only principal dimensionless force ratios shown

FIGURE (5.6)

MODELLING OF A PROTOTYPE - STUDY OF FLUID DYNAMICS